Digital Signal Processing for Structural Health Monitoring of Buildings

A thesis submitted for the degree of Doctor of Philosophy

by

Fragkiskos P. Pentaris

College of Engineering, Design and Physical Sciences

Dept. of Electronic and Computer Engineering

Brunel University London

Date: 03/11/2014

Abstract

Structural health monitoring (SHM) systems is a relatively new discipline, studying the structural condition of buildings and other constructions. Current SHM systems are either wired or wireless, with a relatively high cost and low accuracy.

This thesis exploits a blend of digital signal processing methodologies, for structural health monitoring (SHM) and develops a wireless SHM system in order to provide a low cost implementation yet reliable and robust. Existing technologies of wired and wireless sensor network platforms with high sensitivity accelerometers are combined, in order to create a system for monitoring the structural characteristics of buildings very economically and functionally, so that it can be easily implemented at low cost in buildings.

Well-known and established statistical time series methods are applied to SHM data collected from real concrete structures subjected to earthquake excitation and their strong and weak points are investigated.

The necessity to combine parametric and non-parametric approaches is justified and to this direction novel and improved digital signal processing techniques and indexes are applied to vibration data recordings, in order to eliminate noise and reveal structural properties and characteristics of the buildings under study, that deteriorate due to enviromental, seismic or anthropogenic impact.

A characteristic and potential harming specific case study is presented, where consequences to structures due to a strong earthquake of magnitude 6.4 M are investigated. Furthermore, is introduced a seismic influence profile of the buildings under study related to the seismic sources that exist in the broad region of study.

Contents

ABSTRACT ..... **I**
CONTENTS ..... **II**
LIST OF FIGURES ..... **IX**
LIST OF TABLES ..... **XXII**
ABBREVIATIONS ..... **XXIII**
ACKNOWLEDGMENTS ..... **XXIV**
CHAPTER 1. INTRODUCTION **1**
1.1 THE BACKGROUND OF THIS THESIS 1
1.2 AIMS AND OBJECTIVES OF THIS STUDY 2
1.3 METHODOLOGY 2
1.4 SELECTION OF THE STUDY REGION 3
1.5 THESIS OUTLINE 4
1.6 CONTRIBUTION TO KNOWLEDGE FROM THIS RESEARCH: 5
1.7 SUMMARY 7
CHAPTER 2. LITERATURE REVIEW **8**
INTRODUCTION 8
2.1. LITERATURE REVIEW IN STRUCTURAL HEALTH MONITORING 8
2.1.1. Definition of damage *8*
2.1.2. Methods of damage identification *9*
2.1.3. Frequency changes for detection of damage *12*
2.1.4. Non-Parametric methods for damage identification *13*
2.1.5. Wavelets in structural health monitoring *15*
2.1.6. HVSR approach in buildings *20*
2.1.7. Parametric methods for damage identification *21*
2.1.8. Neural networks for structural damage detection *24*
2.1.9. Limitations and weaknesses of the structural health monitoring methods *25*
2.1.10. Discussion on SHM literature *26*
2.1.11. Conclusions in SHM literature *28*
2.2. LITERATURE REVIEW IN WIRED AND WIRELESS STRUCTURAL HEALTH MONITORING SYSTEMS ... 29

2.2.1. Introduction 29

2.2.2. MEM Sensors 30

2.2.3. Wireless Sensor Networks 30

2.2.4. Autonomy in wSHMs 31

2.2.5. Data synchronization in Wireless SHM systems 33

2.2.6. Data rate analysis 35

2.2.7. Summary from wSHMs literature 36

2.2.8. Conclusions from wSHMs literature 37

2.3. LITERATURE REVIEW IN DIGITAL SIGNAL PROCESSING 38

2.3.1. Introduction 38

2.3.2. Signal processing 38

2.3.3. Digital signal processing 39

2.3.4. Domain 41

2.3.5. Methods and techniques of digital signal processing. 43

2.3.6. Filters in DSP 45

2.3.7. Wavelets 46

2.3.8. Summary of DSP methods literature 48

2.4. CONCLUSIONS OF LITERATURE REVIEW 49

CHAPTER 3. DESIGN OF A HYBRID WIRED AND WIRELESS SHM NETWORK. 50

3.1 WIRED STATIONS 50

3.1.1 Introduction 50

3.1.2 Case study infrastructures 50

3.1.3 Define the best placement of accelerometers 52

3.1.4 Technical Characteristics and specifications of the wired SHM system 53

3.1.5 Acceleration recordings from the wired SHM network on both buildings 55

3.1.6 Seismic activity 55

3.1.7 Strong wind activity 59

3.1.8 Manmade activity 61

3.1.9 Results from the correlation of wired SHM recordings in two buildings 62

3.2 WIRELESS STRUCTURAL HEALTH MONITORING STATIONS (WSHMS)..... 62
3.2.1 Introduction..... 62
3.2.2 Key-Features of wSHMs..... 63
3.2.3 Autonomy of a wireless SHM system..... 63
3.2.4 Data transmission & synchornization..... 64
3.2.5 Data rate and resolution..... 66
3.2.6 Cost of implementation on metropolitan scale..... 66
3.2.7 Sensor Platform..... 67
3.2.8 Data Resolution..... 69
3.2.9 Wireless Communication..... 69
3.2.10 Configuring wSHMs..... 70
3.2.11 wSHMs setup: a hybrid network..... 72
3.2.12 Optimum deployment of accelerometers in a building..... 73
3.2.13 Data collection..... 74
3.2.14 Pilot comparative study of the developed wSHMs..... 75
3.2.15 Conclusion on wSHM network..... 79
3.3 RAW DATA RECORDED BY WIRED AND WIRELESS SHM NETWORK..... 80
3.3.1 Seismic Acceleration Recordings..... 81
3.3.2 High magnitude earthquake (6.4M)..... 86
3.3.3 Waspmotes recordings from 6.4 earthquake..... 88
CHAPTER 4. DIGITAL SIGNAL PROCESSING METHODS 90
4.1. INTRODUCTION 90
4.2. NON-PARAMETRIC METHODS PSDS, FRFS, COHERENCES, HVSR, WAVELETS 91
4.2.1 Power Spectral Densities..... 91
4.2.2 Frequency Responce Functions..... 93
4.2.3 Coherence diagram..... 94
4.2.4 Horizontal to Vertical Spectral Ratio (HVSR)..... 95
4.3. PARAMETRIC MODELING METHODS AR, ARX, ARMAX..... 96
4.3.1 Parameter time series methods..... 96

4.3.2 Parametric modeling 96

4.3.3 Autoregressive models 98

4.3.4 Class of parametric modeling 99

4.3.5 The choice of model – ARX model 100

4.4. STRUCTURAL IDENTIFICATION AND DAMAGE DETECTION METHODOLOGY 102

4.4.1 Non-Parametric Identification of the Healthy Structure Dynamics 102

4.4.2 Parametric Identification of the Healthy Structure Dynamics 104

4.4.3 Damage Detection based on a Statistical Time Series Method 105

4.5. SUMMARY OF METHODS 106

CHAPTER 5. DATA ANALYSIS OF SHM RECORDINGS WITH NON-PARAMETRIC METHODS 107

5.1 FREQUENCY CHANGE METHOD 107

5.1.1 Introduction 107

5.1.2 Description of the proposed DSP method on SHM application 107

5.1.3 Application of the proposed-index in SHM data 109

5.1.4 Recordings of acceleration for both buildings 110

5.1.5 Discussion 112

5.2 HORIZONTAL TO VERTICAL SPECTRAL RATIO 113

5.2.1. Instrumentation for HVSR recordings 114

5.2.2. Comparison of velocimeter and accerelometer sensors for HVSR Method 115

5.2.3. Recordings of acceleration for both buildings 117

5.2.4. Analysis of HVSR with specific processing software 117

5.2.5. Data Analysis 121

5.2.6. Results 124

5.2.7. Description of the proposed index 125

5.2.8. Discussion 127

5.2.9. Conclusions 127

5.3 DATA ANALYSIS BY POWER SPECTRAL DENSITY METHOD 128

5.4 DATA ANALYSIS BY FREQUENCY RESPONSE FUNCTION METHOD 130

5.5 NON-PARAMETRIC STATISTICAL TIME SERIES ANALYSIS OF FREQUENCY RESPONSE FUNCTIONS 131

5.6 DATA ANALYSIS BY COHERENCE DIAGRAMS 134

5.7 WAVELETS 137

5.7.1 Wavelets families in acceleration recordings from the established wired SHM 138

5.7.2 Haar Wavelet 140

5.7.3 Data Analysis with wavelet families 141

5.8 CONCLUSIONS OF NON-PARAMETRIC METHODS 142

CHAPTER 6. DATA ANALYSIS OF SHM RECORDINGS WITH PARAMETRIC METHODS 145

6.1 INTRODUCTION 145

6.2 DATA COLLECTION 146

6.3 DATA ANALYSIS BY ARX MODELING 147

6.4 CONCLUSIONS FROM PARAMETRIC METHODOLOGY 152

CHAPTER 7. DISCUSSION 153

7.1 INTRODUCTION 153

7.2 COST EFFECTIVE WIRELESS STRUCTURAL HEALTH MONITORING NETWORK 153

7.3 DSP METHODS FOR PARAMETRIC AND NON-PARAMETRIC MODELING AIMING TO DAMAGE IDENTIFICATION 154

7.3.1 FRF and HVSR indices of structural vulnerability 155

7.3.2 Application of wavelets families in SHM recordings 156

7.3.3 ARX to ARMAX modeling 157

7.4 STATISTICAL TIME SERIES ANALYSIS FOR SHM 161

7.5 NOVEL PROCEDURE OF DSP METHODOLOGIES TO BE APPLIED FOR SHM 161

7.6 NOVEL MAP THAT CORRELATES SEISMIC ACTIVITY WITH EPICENTER DISTANCE AND STRUCTURES SEISMIC ACCELERATION 163

7.7 COMPARISON OF REAL STRUCTURES WITH ARTIFICIAL AND LABORATORY MODELS 167

7.8 HOW MUCH THE AIMS AND OBJECTIVES HAVE BEEN ACHIEVED 167

7.8.1 When a building or a structure is inadequate 167

7.8.2 How is it possible to identify this deficiency 168

7.8.3 What system is needed and what features should be that there is the ability to easily and cost-effectively monitor the structural condition of buildings 168

7.8.4 How could DSP techniques be combined in order to present a robust methodology to identify SHM faults in real structures 168

CHAPTER 8. CONCLUSIONS – FUTURE WORK 170

8.1 CONCLUSIONS 170

8.2 FUTURE WORK 171

REFERENCES 173

APPENDIX A: PUBLICATIONS DERIVED FROM THIS RESEARCH 187

APPENDIX B: PROGRAMMING OF WASPMOTES 188

AT mode 192

API mode 193

Error rate AT mode 193

Use of array to store measurements 194

Final program code (First version) 195

Final program code (Second version) 198

APPENDIX C: FREQUENCY CHANGE METHOD ANALYSIS 201

APPENDIX D: HVSR ANALYSIS 207

One hour time duration HVSR recordings of ambient noise during noon and midnight 209

Measurements with Lennartz seismometer. 211

Laboratory validation 214

APPENDIX E: PSD, FRF, COHERENCE ANALYSIS 219

APPENDIX F: WAVELET ANALYSIS 224

Daubechies Family Wavelet 224

Symlets Family Wavelet 227

Coiflets Family Wavelet 228

Biorsplines Family Wavelet 229

ReserveBior Family 230

APPENDIX G: PARAMETRIC ANALYSIS 232

ARX ANALYSIS COMPARED TO AR ANALYSIS. 233

ONE DIMENSION MODELING WITH ARX (EVENT SELECT) 236

Filtering *238*

Search for optimum model order *241*

BIC, AIC and RSS/SSS criteria *242*

Verification of the selected model by ACF of residuals between model and RAW data *243*

Bode plot of the system *244*

ONE DIMENSION MODELING WITH ARMAX 244

BIC, AIC and RSS/SSS criteria *246*

ONE DIMENSION MODELING WITH ARMAX AND OPTIMIZATION OF NOISE PARAMETER 247

BIC, AIC and RSS/SSS criteria *249*

MULTIDIMENSIONAL MODELING WITH ARX 251

BIC, AIC and RSS/SSS criteria *259*

FREQUENCY COHERENCES BETWEEN HORIZONTAL COMPONENTS 261

MULTIDIMENSIONAL MODELING WITH ARX IN A CELL 264

ANALYSIS OF ALL ARX MODELS 265

Comparison of both plots with 6.4 M earthquake. *267*

APPENDIX H: ACCELERATION RECORDINGS BEFORE EARTHQUAKE OF 6.4 M 268

APPENDIX I: ACCELERATION RECORDINGS AFTER EARTHQUAKE OF 6.4 M 272

APPENDIX J: AMBIENT NOISE RECORDINGS 276

APPENDIX K: PHOTOS OF INSTRUMENTATION & INSTALLATION 280

APPENDIX L: ANALYSIS OF SEISMIC EVENTS WITH NON-PARAMATRIC METHODS 281

APPENDIX M: ANALYSIS OF SEISMIC EVENTS WITH PARAMETRIC METHODS 291

List of figures

Figure 1.1 *Broad region of Chania, Western Crete [6]* 4

Figure 2.1. *Damage Detection Study of the I-40 Bridge over the Rio Grande in New Mexico, USA. Left figure: electric saw cutting cause damage in the bridge girder right figure: The levels of introduced damage in the girder (the shaded area is the reduced cross-section, Sohn et al. [10].* 9

Figure 2.2. *The change of fundamental frequency on I-40 Bridge related to the damage levels presented in figure 2.4, Sohn et al. [10]* 9

Figure 2.3. *Wavelet Scalogram with ridge (initial wavelet ridge is the line,selection region of wavelet coefficient is the dashed line)[42]* 17

Figure 2.4. *Typical component energies of a model , WPT is the wavelet packet energy (a) Without free span damage (b)with free span damage [44]* 18

Figure 2.5. *Suggested de-noising algorithm based in entropy by Beenamol et al.[45]* 19

Figure 2.6. *Analog to digital processing schematic[171]* 40

Figure 2.7. *S-plane and the z-plane relationship[176].* 42

Figure 2.8. *Fourier representation of signals [177]* 43

Figure 2.9. *Wavelet translation (left) and dilation with translation (right) [187]* 48

Figure 3.1. *Location of Technological Educational Institute of Crete at the city of Chania (35°31'9.30"N, 24° 2'34.35"E) [194]* 51

Figure 3.2. *The old (left) and new (right) building of Technological Educational Institute of Crete at the city of Chania* 51

Figure 3.3. *(Left) Schematic diagram of the wired SHM deployment in the old and new building, (right) Schematic plan of the TEI buildings at Chania. The location of the sensors is presented on each building.* 52

Figure 3.4. *Schematic diagram of the wired SHM deployment in the old and new building* 54

Figure 3.5. *Schematic diagram of the SHM system data flow* 55

Figure 3.6. *RTCC Display presents the characteristics of each remote wired accelerometer.* 55

Figure 3.7. *Epicenter of the earthquake with magnitude M 2.3 that occurred on 10/12/2012 at 06:11:32 UTC 16 km Northwest from the city of Chania [201]* 56

Figure 3.8. Recordings of the earthquake with magnitude M 2.3 that occurred on 10/12/2012 at 06:11:32 UTC 16 km Northwest from the city of Chania, from the accelerographs of the wired SHMs 57

Figure 3.9. Fast Fourier Transform on new building of the earthquake with magnitude M 2.3 that occurred on 10/12/2012 at 06:11:32 UTC 58

Figure 3.10. Fast Fourier Transform on old building of the earthquake with magnitude M 2.3 that occurred on 10/12/2012 at 06:11:32 UTC 59

Figure 3.11. FFT from the acceleration recordings to the old and new building (3^{rd} and 2^{nd} floors) under the affect of strong wind gusts on 8 November 2012..... 60

Figure 3.12. Acceleration recordings to the old and new building (3^{rd} and 2^{nd} floors) under the affect of strong wind gusts on 8 November 2012..... 61

Figure 3.13. FFT from the manmade event (explosion type) on 26 September 2012 10:40 UTC 20 km north from city of Chania Crete recorded from the third floor of the old building of TEI. 62

Figure 3.14. Time stamping of the acceleration data in the main computer..... 65

Figure 3.15. Waspmote Top side (up) and bottom side (down) [205] 68

Figure 3.16. RF Modules XBee & XBee-PRO 802.15.4 [42]..... 70

Figure 3.17. Special construction with metal base, spirit level, and plastic cover. 72

Figure 3.18. (up) Schematic diagram of wSHMs hybrid network setup in a building (down) Schematic diagram of wSHMs network setup in a metropolitan scale..... 73

Figure 3.19. Left: Schematic diagram of the wSHMs hybrid network setup in pilot mode at the two buildings of TEI of Crete (Chania premises). Right: Google Earth ^{TM} satellite composite image of Crete Island depicting the location of the Chania premises of TEI of Crete. The seismicity (Mag $\geq$ 3.0) of the period Jan 2013 – Jan 2014 for the broad area N34.4-36.2deg, E22.5-27.3deg is presented (earthquake data extracted from Euro-Mediterranean Seismological Centre). 74

Figure 3.20. RefTek 130-SMA (left) and Waspmote (right) installed (with screwing) on the second floor of the old building of TEI of Crete at Chania. 75

Figure 3.21. Earthquake epicenter map and information provided by the European Mediterranean Seismological Centre concerning the strongest event of the last three years in the very active seismogenic region of Greece[201]. 76

Figure 3.22. Earthquake Intensity map of the M 6.4 event on October 12, 2013, provided by the Euro-Mediterranean Seismological Centre. 77

Figure 3.23. Comparison of the horizontal components of acceleration, recorded during the M 6.4 earthquake on October 12, 2013, by the non-wireless sensor network based on RefTek 130-SMA and the developed wSHMs based on Waspmote platform respectively, installed on the second floor of a 18 years old building at Chania premises of TEI of Crete. 79

Figure 3.24. Acceleration recordings for the seismic event of 3.9M on 2013-03-09 07:41:49 GMT (Lat 23.43 Lon 23.31). The list code number is b1 from the table 3.3. 83

Figure 3.25. Acceleration recordings for the seismic event of 4.3M on 2013-10-1214:05:50 GMT (Lat 35.37 Lon 23.29). The list code number is a1 from the table 3.3. 84

Figure 3.26. Recordings of 20 minutes time duration of ambient noise inside TEI buildings from table 3.3.4 (2013 10 13 22:00 UTC event). Local time is 11:59:59 pm 85

Figure 3.27. Seismic event of 2013-10-12 13:11:54 UTC 6.4M (lat 35.56 Lon 23.31)[201] 86

Figure 3.28. Acceleration recordings in both buildings during 6.4 M earthquake 87

Figure 3.29. Acceleration recordings from Waspmote accelerometer with code BC, in the old building, during 6.4 M earthquake 88

Figure 3.30. Acceleration recordings from Waspmote accelerometer with code C9, in the new building, during 6.4 M earthquake 89

Figure 4.1. Experimental Identification schematic [50] 97

Figure 4.2. Statistical analysis by PSD F distribution [103] 102

Figure 4.3. Statistical analysis of FRF by Gaussian distribution[103] 103

Figure 5.1. Low and high dispersion of fundamental frequency of a structure 108

Figure 5.2. Seismicity of South Aegean in the period 2007-2010 recorded by the stations of the Seismological Network of Crete (M>=3.5) and location of Technological Educational Institute of Crete in the city of Chania (35°31'9.30"N, 24° 2'34.35"E) 109

Figure 5.3. The 2012/11/23 02:08 UMT earthquake (left column), the 2012/12/05 06:54 UMT earthquake (mid column), 2013/01/05 02:04 UMT earthquake (right column), all recorded at 3rd floor of new building (3NB) accelerometer, North-South component (NS) 9F8E accelerometer, analyzed with Wavelet Transform, WV family db (level 2). In lower row data are denoised. 111

Figure 5.4. FFT based PSDs for the previous events (Figures 5.3 left and right & Figure 5.4) 112

Figure 5.5. Case study buildings location is indicated. This map presents frequency of recorded HVSR for the broader area of Chania[213] 114

Figure 5.6. Data of Guralp velocimeter (left graph) and REFTEK accelerometer SMA 130 (right graph), analyzed with HVSR technique for a recording of 60 minutes length on the Ground floor, of the Old Building of TEI Chania. 115

Figure 5.7. HVSR analysis of Lennartz LeD/5s velocimeter, for recording of 60 minutes length, on the Ground floor of Old Building of TEI Chania. 116

Figure 5.8. 10 minutes recording of ambient noise on the 2nd floor of the new building of TEI Chania. 118

Figure 5.9. The time window (up) of 25 seconds for the previous recording with the HVSR result (down). Different colours corresponding in different time windows. Grey background colour presents the automatic recognition of fundamental frequency of the Geopsy program [217]. 119

Figure 5.10. The time window of 25 seconds for the above recording(left) with the HVSR result (right). Different colors corresponding in different time windows. Grey background color presents the automatic recognition of fundamental frequency of the geopsy program. 120

Figure 5.11. The 2013/04/28 16:33 UMT time seismic event at 37.45 (Latitude) 22.70 (Longitude) 58.0 Km (Depth)[201] 121

Figure 5.12. HVSR recordings on 2013/04/28 16:33 UMT (2013/04/28 19:33 local time) on the old (up) and new (down) building of TEI in Chania for the above seismic event. 122

Figure 5.13. HVSR recordings from the on 2013/03/09 07:43 UMT time seismic event (Blue line), the 2013/03/12 midnight recording (red line) and the 2013/03/12 noon recording of the old (up) and new (down) building of TEI in Chania 126

Figure 5.14. Power Spectral Densities of the old building 1rst floor(upper row), 2nd floor (mid row) and 3rd floor (lower row). Left column refer to East-West component, mid column to North-South component and right column to Vertical component. The seismic event is with name code b1 from table 5 (09/03/2013 3.9M 67km) 129

Figure 5.15. Frequency Responce Functions of the old building lower floor(input) in relation with outputs: 1rst floor(upper row), 2nd floor (mid row) and 3rd floor (low row). Left column refer to EW input with EW output , mid column refer to NS input with NS output and right column to Vertical input with Vertical ouput. The seismic event is with name code b1 from table 3.3 (09/03/2013 3.9M 67km) 131

Figure 5.16. Seismic events with name codes b1 & b2 (table 3.3)..... 132

Figure 5.17. Seismic events with name codes b2 (blue) & b3(red) from table 3.3..... 133

Figure 5.18. Seismic events with name codes b3 (blue) & b4 (red) from table 3.3..... 134

Figure 5.19. Coherences diagrams of the old building lower floor(input) in relation with outputs: 1rst floor(upper row), 2nd floor (mid row) and 3rd floor (low row). Left column refer to EW input with EW output , mid column refer to NS input with NS output and right column to Vertical input with Vertical ouput. The seismic event is with name code b1 from table 3.3 (09/03/2013 3.9M 67km) 135

Figure 5.20. Frequency coherence diagrams of excitation due to response for each component of input related to each component of output during seismic event of 6.4M 137

Figure 5.21. The epicenter of the earthquake 2013-04-28 16:31:04.0 UTC at 37.45 N ; 22.70 E [201] 138

Figure 5.22. The seismic acceleration of the "2013-04-28 16:31:04.0 UTC at 37.45 N ; 22.70 E" seismic event in the old building 139

Figure 5.23. The seismic acceleration of the "2013-04-28 16:31:04.0 UTC at 37.45 N ; 22.70 E" seismic event in the new building 139

Figure 5.24. Haar wavelet scaling function function phi and wavelet function psi. In the decomposition (mid) and reconstruction (down) low and high pass filters. 140

Figure 5.25. Haar wavelet original details coefficients (left) the original signal and the original coefficients (right). 141

Figure 6.1. The region of interest. The earthquakes and their magnitude are depicted on the figure: Baseline events are denoted with green color, inspection events with yellow and the strong earthquake in denoted with red color 146

Figure 6.2. Excitation-response signals from the old building for an event before the strong earthquake: (a) East-West excitation (xew), (b) North-South excitation (xns), (c) first floor East-West response (y1ew), and (d) second floor North-South response (y2ns). (a,c) EW direction, (b,d) NS direction. Subscript denotes direction and superscript floor number. 148

Figure 6.3. ARX identification results (old building, xew=y1ew signal pair, sixth event before the strong earthquake): (a) Percentage RSS/SSS, (b) BIC criterion (the square box indicates the criterion's minimum for na = 38), and (c) frequency stabilization diagram fo various ARX (na; na) models [the blue line indicates the model-based FRF of the ARX (60, 60) model]. 150

Figure 6.4. ARX (60, 20) validation: Actual response –□– and one-step-ahead model-based predictions –x–, (b) normalized autocorrelation function of the ARX (60, 20) model-based residuals (the horizontal lines indicate statistical significance at the α = 0.95 level). 150

Figure 6.5. Damage detection results based on the characteristic quantity $x\theta 2$: (a) Old building EW direction, (b) old building NS direction, (c) new building EW direction and (d) new building NS direction. 152

Figure 7.1. Proposed algorithm for SHM on real structures 162

Figure 7.2. EW component of seismic acceleration (green) in relation with increasing EQ magnitude (blue) and EQ distance (red) recorded on the 2nd floor of the old building of TEI of Crete at Chania city. 165

Figure 7.3. Earthquake influence map, by means of the EW component of seismic acceleration (color code from green-lower to red-higher), from the 2nd floor in the old building for year 2013 EQ epicenters having magnitudes (circle size) that affected the building located in Chania. 166

Figure C.1. 2012/11/23 02:08 UMT seismic event (left) and 2012/12/05 06:54 UMT seismic event (right), recorded at 3rd floor old building (3OB) accelerometer, North-South component (NS) A392 accelerometer, analyzed with Wavelet Transform, WV family db (level 2) 201

Figure C.2. 2013/01/05 02:04 UMT seismic event, recorded at 3rd floor old building (3OB) accelerometer, North-South component (NS) A392 accelerometer, analyzed with Wavelet Transform, WV family db (level 2) 201

Figure C.3. FFT based PSD for the previous events (Figures 9. & Figure9.2) 202

Figure C.4. FFT based PSDs for the previous events (up 2012/11/23 02:08 UMT, middle 2012/12/05 06:54 UMT and lower 2013/01/05 02:04 UMT) for the old building (Vertical component) 203

Figure C.5. FFT based PSDs for the previous events (up 2012/11/23 02:08 UMT, middle 2012/12/05 06:54 UMT and lower 2013/01/05 02:04 UMT) for the new building (Vertical component) 203

Figure C.6. FFT based PSDs for the previous events (up 2012/11/23 02:08 UMT, middle 2012/12/05 06:54 UMT and lower 2013/01/05 02:04 UMT) for the old building (East-West component) 204

Figure C.7. FFT based PSDs for the previous events (up 2012/11/23 02:08 UMT, middle 2012/12/05 06:54 UMT and lower 2013/01/05 02:04 UMT) for the new building (East-West component) 204

Figure C.8. Spectrogram for the previous events (up 2012/11/23 02:08 UMT, middle 2012/12/05 06:54 UMT and lower 2013/01/05 02:04 UMT) for the old building (East-West component) 205

Figure C.9. Spectrogram for the previous events (up 2012/11/23 02:08 UMT, middle 2012/12/05 06:54 UMT and lower 2013/01/05 02:04 UMT) for the new building (East-West component) *205*

Figure D.1. Four seismic events with code names 1(up left), 2(up right), 3(down left) and 4(down right) [201]. *207*

Figure D.2. HVSR analysis of seismic events with code names 1(left) and 2(right). *208*

Figure D.3. HVSR analysis of seismic events with code names 3(left) and 4(right). *209*

Figure D.4. Programmed 30 minutes HVSR recordings on 2013/05/08 10:00 UMT (2013/05/08 13:00 local time) on the old building of TEI. On the right is the presentation of 25 seconds time duration windows which are extended in the whole length of the recording. *210*

Figure D.5. Programmed 30 minutes HVSR recordings on 2013/05/07 22:00 UMT (2013/05/08 01:00 local time) on the old (left) and new (right) building of TEI. On the right is the presentation of 25 seconds time duration windows which are extended in the whole length of the recording. *210*

Figure D.6. HVSR analysis of ambient noise recording with time duration of 1 hour *211*

Figure D.7. HVSR plots of outside area (left figure) and inside building of TEI on the lower floor (right figure) *212*

Figure D.8. HVSR plots of acceleration recordings for lower floor old building (up left figure), ground floor old building (up right figure), 1rst floor old building (down left figure) and 2nd floor old building (down right figure). *212*

Figure D.9. HVSR plots of acceleration recordings for lower floor new building (left figure), ground floor new building (mid figure) and 1rst floor old building (right figure) *213*

Figure D.10. HVSR plots of acceleration recordings for second floor new building (left figure), and third floor new building (right figure) *213*

Figure D.11. HVSR plots of acceleration recordings for lower floor of TEE building (left figure), ground floor of TEE building (mid figure) and 1rst of TEE building (right figure) *213*

Figure D.12. Metallic dexion model *214*

Figure D.13. HVSR analysis of ambient noise recording, for undamaged scenario 1 of the metallic model *215*

Figure D.14. HVSR analysis of ambient noise recording, for undamaged scenario 2 of the metallic model *216*

Figure D.15. HVSR analysis of ambient noise recording for damaged scenario 1 of the metallic model 217

Figure D.16. HVSR analysis of ambient noise recording for damaged scenario 2 of the metallic model 218

Figure E.1. PSDs of seismic event is with name code b2 from table 3.3 (31/03/2013 4.3M 62km) 219

Figure E.2. PSDs of the strong motion seismic event with name code 13 from table 3.3 (12/10/2013 6.4M 65km) 219

Figure E.3. PSD of seismic event with name code a4 from table 3.3 (22/12/2013 3.8M 60km) ... 220

Figure E.4. FRFs of seismic event with name code b2 from table 3.3 (31/03/2013 4.3M 62km) .. 220

Figure E.5. FRFs of the strong motion seismic event with name code b13 from table 3.3 (12/10/2013 6.4M 65km) 221

Figure E.6. FRFs of seismic event with name code a4 from table 3.3 (22/12/2013 3.8M 60km) 221

Figure E.7. Coherence diagrams of seismic event with name code b2 from table 3.3 (31/03/2013 4.3M 62km) 222

Figure E.8. Coherence diagrams of the seismic event with name code name code b13 from table 3.3 (12/10/2013 6.4M 65km) 222

Figure E.9. Coherence diagrams of seismic event with name code a4 from table 3.3 (22/12/2013 3.8M 60km) 223

Figure F.1. DB wavelet (order of N is 2) scaling function phi and wavelet function psi. In the middle decomposition low and high pass filters and below the reconstruction low and high pass filters. 224

Figure F.2. DB N=2 wavelet original details coefficients (left), the original signal and the original coefficients (right). 225

Figure F.3. DB N=2 wavelet original details coefficients (left), the original signal, the original coefficients and the thresholded coefficients (right) 226

Figure F.4. Sym wavelet (order of N is 3) scaling function phi and wavelet function psi. In the middle decomposition low and high pass filters and below the reconstruction low and high pass filters. 227

Figure F.5. Sym order N=3 wavelet original details coefficients (left), the original signal, the original coefficients and the thresholded coefficients (right) 227

Figure F.6. Coiflets wavelet (order of N is 1) scaling function phi and wavelet function psi. In the middle decomposition low and high pass filters and below the reconstruction low and high pass filters. 228

Figure F.7. Coiflets order N=1 wavelet original details coefficients (left), the original signal, the original coefficients and the thresholded coefficients (right). 229

Figure F.8. Biorthogonal wavelet (order of N is 3.1) scaling function phi and wavelet function psi. In the middle decomposition low and high pass filters and below the reconstruction low and high pass filters. 229

Figure F.9. Biorthogonal wavelet (order of N is 3.1) t original details coefficients (left), the original signal, the original coefficients and the thresholded coefficients (right). 230

Figure F.10. ReserveBiorthogonal wavelet (order of N is 3.1) scaling function phi and wavelet function psi. In the middle decomposition low and high pass filters and below the reconstruction low and high pass filters. 230

Figure F.11. Reserve Biorthogonal wavelet (order of N is 3.1) t original details coefficients (left), the original signal, the original coefficients and the thresholded coefficients (right). 231

Figure G.1. Power Spectral Densities of b Seismic event. 233

Figure G.2. Power Spectral Densities of c (left) and d (right) Seismic events. 234

Figure G.3. Frequency Response Functions of seismic events b 235

Figure G.4. FRF of c Seismic event. 235

Figure G.5. FRF of d Seismic event. 236

Figure G.6. Raw data(left), mean removal(mid) and transform in mg (right) of seismic event with codes f. Upper raw line refers on 3rd floor old building TEI, below refers to 2nd, under this is 1rst floor and at the bottom line is lower floor of the old building. 237

Figure G.7. PSDs (left) and non-parametric FRF (right) of seismic event with cofe f. Frequency range up to 62.5 Hz. 238

Figure G.8. Filter frequency response (magnitude up, phase down) 239

Figure G.9. Recording data filtered at 20 Hz (left acceleration waveforms, centre PSDs, right FRFs). Frequency range after filtering is up to 20 Hz. 240

Figure G.10. Stabilization diagram of ARX modeling from 10-100 model order. Frequency range is up to 20 Hz (level of filtering) 241

Figure G.11. Model order selection criteria (RSS/SSS, AIC and BIC). 242

Figure G.12. Autocorrelation function of the "model to data" residuals 243

Figure G.13. Model fitting on the data waveform. Red color is the recording. Blue color is the designed ARX model. 243

Figure G.14. Bode plot of the designed system model (red line) in comparison to raw data (blue line) 244

Figure G.15. Stabilization diagram of ARMAX modeling from 10-68 model order 245

Figure G.16. Model order selection criteria (RSS/SSS, AIC and BIC) 246

Figure G.17. Autocorrelation function of the "model to data" residuals of the ARMAX model with model order 34 246

Figure G.18. Model fitting on the data waveform for the ARMAX(24,24,24,1) model 247

Figure G.19. Bode plot of the designed system model ARMAX (34,34,34,1) (red line) in comparison to raw data (blue line) 247

Figure G.20. Stabilization diagram of ARMAX (34,32,x,1) modeling with 1<x<42. 248

Figure G.21. Model order selection criteria (RSS/SSS, AIC and BIC) for the ARMAX (34,32,x,1) model, with 1<x<42 249

Figure G.22. Autocorrelation function of the "model to data" residuals for the ARMAX (34,32,15,1) model 249

Figure G.23. ARMAX (34,32,15,1) model fitting on the data waveform 250

Figure G.24. Bode plot of the designed system model ARMAX (34,32,15,1) (red line) in comparison to raw data (blue line) 250

Figure G.25. Recording data with mean removal and transform in mg at all components on every floor. left column presents east-west component, mid column North-South and right is vertical component. Horizontal axe are the samples with sampling rate 125 Hz. Vertical axe is acceleration in mg. 252

Figure G.26. Power spectral densities for every recording at every floor and component 253

Figure G.27. Frequency response functions of every floor with the lower floor (for the same component) 253

Figure G.28. Frequency coherences of every floor with the lower floor (for the same component) 254

Figure G.29. Chebyshev filter frequency reqsponce (magnitude up, pahse down) with Low Pass filtering at 10.5 Hz 255

Figure G.30. PSD (left) and FRF (right) analysis of the filtered data. On PSD graphs (left side), up line is 3rd floor, mid is 2nd floor and lower line is lower floor of the old building TEI. FRF graphs (right side), up line is lower floor EW,NS & V components due to 2nd floor EW.

Mid line is lower floor EW,NS & V components due to 2nd floor NS component, and lower line is lower floor EW,NS & V components due to Vertical component of 2nd floor. 256

Figure G.31. Frequency coherence and STFT diagrams of the filtered data 256

Figure G.32. 3D plots of the STFT data to reveal the amplitude of accelerations in time and space 257

Figure G.33. Stabilization diagram of multi-component ARX modeling from 10-70 model order 258

Figure G.34. Model order selection criteria (RSS/SSS and BIC) 259

Figure G.35. Autocorrelation function of the "model to data" residuals of the designed ARX (40, 40, 1) model 259

Figure G.36. ARX (40, 40, 1) model fitting on the data waveform 260

Figure G.37. Bode plot and phase of the designed system model ARX (40, 40, 1) 260

Figure G.38. Bode plot of the designed system model ARX (40, 40, 1)(red line) in comparison to raw data (blue line) 260

Figure G.39. Frequency coherence diagrams of excitation due to response for each component of input related to each component of output for seismic event code 2(before 6.4 M earthquake) 261

Figure G.40. Frequency coherence diagrams of excitation due to response for each component of input related to each component of output during seismic event of 6.4M 262

Figure G.41. Frequency coherence diagrams of excitation due to response for each component of input related to each component of output for seismic event code 4 (after 6.4 M earthquake) 262

Figure G.42. Frequency coherence diagrams of excitation due to response for each component of input related to each component of output for seismic event code 2 263

Figure G.43. Frequency coherence diagrams of excitation due to response for each component of input related to each component of output during seismic event of 6.4M 263

Figure G.44. Frequency coherence diagrams of excitation due to response for each component of input related to each component of output for seismic event code 4 264

Figure G.45. Sum of bode plots for each floor and component for the old building before the earthquake (6.4M earthquake is indicated with bold black line) 265

Figure G.46. Sum of bode plots for each floor and component for the old building after the earthquake (6.4M earthquake is indicated with bold black line) 266

Figure G.47. Sum of bode plots for each floor and component for the new building before the earthquake (6.4M earthquake is indicated with bold black line) *266*

Figure G.48. Sum of bode plots for each floor and component for the new building after the earthquake (6.4M earthquake is indicated with bold black line) *267*

Figure H.1. Seismic acceleration recordings from 2013-04-06 11:26:22 UTC earthquake *268*

Figure H.2. Seismic acceleration recordings from 2014-04-28 00:43:04 UTC earthquake *268*

Figure H.3. Seismic acceleration recordings from 2014-04-28 04:37:25 UTC earthquake *269*

Figure H.4. Seismic acceleration recordings from 2014-05-22 14:29:42 UTC earthquake *269*

Figure H.5. Seismic acceleration recordings from 2014-06-16 21:39:37 UTC earthquake *270*

Figure H.6. Seismic acceleration recordings from 2013-09-09 07:42:01 UTC earthquake *270*

Figure H.7. Seismic acceleration recordings from 2014-03-31 16:28:24 UTC earthquake *271*

Figure H.8. Seismic acceleration recordings from 2014-07-23 05:16:37 UTC earthquake *271*

Figure I.1. Seismic acceleration recordings from 2013-10-19 02:19:34 UTC earthquake *272*

Figure I.2. Seismic acceleration recordings from 2013-12-22 21:55:29 UTC earthquake *272*

Figure I.3. Seismic acceleration recordings from 2014-01-02 05:29:07 UTC earthquake *273*

Figure I.4. Seismic acceleration recordings from 2014-01-08 18:06:11 UTC earthquake *273*

Figure I.5. Seismic acceleration recordings from 2013-10-12 14:06:02 UTC earthquake *274*

Figure I.6. Seismic acceleration recordings from 2013-10-13 17:44:04 UTC earthquake *274*

Figure I.7. Seismic acceleration recordings from 2013-11-29 13:24:49 UTC earthquake *275*

Figure I.8. Seismic acceleration recordings from 2013-11-07 19:41:22 UTC earthquake *275*

Figure J.1. 20 minutes ambient noise recording at 2013-11-20 21:59:59 UTC *276*

Figure J.2. 20 minutes ambient noise recording at 2013-05-07 21:59:59 UTC *276*

Figure J.3. 10 minutes ambient noise recording at 2013-12-13 12:33:00 UTC *277*

Figure J.4. 10 minutes ambient noise recording at 2013-12-13 12:51:00 UTC *277*

Figure J.5. 10 minutes ambient noise recording at 2013-12-15 16:19:00 UTC *278*

Figure J.6. 10 minutes ambient noise recording at 2013-12-15 16:47:00 UTC *278*

Figure J.7. 10 minutes ambient noise recording at 2013-12-15 18:04:00 UTC *279*

Figure K.1. Wired accelerometers *280*

Figure K.2. Wireless accelerometers *280*

Figure K.3. Instrumentation for ambient noise recordings 280

Figure L.1. For the earhquake with code name b1 (table 3.3) the acceleration recordings for lower, 1rst, 2nd & 3rd floor old buidling (up) and STFT (down) 281

Figure L.2. For the earhquake with code name b1(table 3.3) the PSD for lower, 1rst, 2nd & 3rd floor old buidling (up) and FRF (down) 282

Figure L.3. For the earhquake with code name b2 (table 3.3) the acceleration recordings for lower, 1rst, 2nd & 3rd floor old buidling (up) and STFT (down) 283

Figure L.4. For the earhquake with code name b2 (table 3.3) the PSD for lower, 1rst, 2nd & 3rd floor old buidling (up) and FRF (down) 284

Figure L.5. For the earhquake with code name b3 (table 3.3) the acceleration recordings for lower, 1rst, 2nd & 3rd floor old buidling (up) and STFT (down) 285

Figure L.6. For the earhquake with code name b3 (table 3.3) the PSD for lower, 1rst, 2nd & 3rd floor old buidling (up) and FRF (down) 286

Figure L.7. Earhquakes with code names b4 & b5 (table 3.3). Comparison of PSD (up left), FRF (up right), FRF coherence diagrams (mid row left and right) and statistical analysis of FRF deviation (low graph) with "a risk level"(red line). 287

Figure L.8. Comparison of earhquake with code names b5 &b6 (table 3.3). 287

Figure L.9. Comparison of earhquake with code names b6 & b7 (table 3.3). 288

Figure L.10. Comparison of earhquake with code names b7 & b8 (table 3.3). 288

Figure L.11. Comparison of earhquake with code names b8 & b9 (table 3.3). 289

Figure L.12. Comparison of earhquake with code names b9 & b10 (table 3.3). 289

Figure L.13. Comparison of earhquake with code names b10 & b11 (table 3.3). 290

Figure L.14. Comparison of earhquake with code names b11 & b12 (table 3.3). 290

Figure M.1. Parametric analysis of earquake with code names b1 (table 3.3). Stabilization diagram(up), RSS/SSS, BIC & AIC critiria (mid) and bodeplot (down). 291

Figure M.2. Parametric analysis of earquake with code names b2 (table 3.3). Stabilization diagram(up), RSS/SSS, BIC & AIC critiria (mid) and bodeplot (down 292

Figure M.3. Parametric analysis of earquake with code names b3 (table 3.3). Stabilization diagram(up), RSS/SSS, BIC & AIC critiria (mid) and bodeplot (down 293

List of tables

TABLE 3.1. CHARACTERISTICS OF THE TECHNOLOGICAL INSTITUTE BUILDINGS AT CHANIA 50
TABLE 3.2. SEISMIC EVENTS CATALOG, RECORDED BY WIRED SHM NETWORK OF TEI 81
TABLE 3.3. EARTHQUAKES RECORDED BY WIRED SHM NETWORK OF TEI BEFORE THE HIGH MAGNITUDE SEISMIC EVENT OF 6.4M (LEFT COLUMN) AND AFTER (RIGHT COLUMN). LEFT COLUMN IS "B" CODE EVENTS AND RIGHT IS "A" CODE EVENTS. 82
TABLE 3.4. DATE AND TIME (UTC) OF HVSR RECORDINGS INSIDE BUILDINGS ON EACH FLOOR 82
TABLE 6.1. EARTHQUAKES WITH THEIR GEOLOGICAL DETAILS. BASELINE AND INSPECTION PHASES 147
TABLE 6.2. SELECTED MODELS 149
TABLE 7.1. EXAMPLE OF THE RICH DATABASE OF EARTHQUAKES AND CORRESPONDING STRUCTURAL SEISMIC ACCELERATION USED IN THE ANALYSIS 164

Abbreviations

ASD	Auto Spectral Density
ANN	Artificial Neural Network
ACF	Auto Correlation Function
AR	Autoregressive
ARMA	Autoregressive Moving Average
ARMAX	Autoregressive Moving Average with Exogenus input
ARX	Autoregressive with Exogenus input
CCF	Cross Correlation Function
CWT	Continuous Wavelet Transform
CSD	Cross Spectral Density
DI	Damage Identification
DFT	Discrete Fourier Transform
DoF	Degree of Freedom
DWT	Discrete Wavelet Transform
EMA	Experimental Modal Analysis
FDD	Frequency Domain Decomposition
FDI	Fault and Damage Identification
FE	Finite Element
FEM	Finite Element Model
FFT	Fast Fourier Transform
FT	Fourier Transform
FRF	Frequency Response Function
HVSR	Horizontal to Vertical Spectral Ratio
IDFT	Inversr Discrete Fourier Transform
IRF	Impulse Response Function
LS	Least Squares
MAC	Modal Assurance Criterion
MEMs	Micro Electro Mechanical Systems
OE	Output Error
OMA	Operational Modal Analysis
OMAX	Operational Modal Analysis with exogenous input
PDF	Propability Density Function
PEM	Prediction Error Method
PP	Peak Peaking
PSD	Power Spectral Density
RC	Reinforced Concrete
SHM	Structural Health Monitoring
SSI	Subspace System Identification
STFT	Short Time Fourier Transform
TEI	Technological Eduational Institute
TF	Transfer Function
wSHMn	wireless Structural Health Monitoring network
WSN	Wireless Sensor Network

Acknowledgments

I would like to express my gratitude to a number of people who contributed in completion of this thesis.

Initially I would like express my gratitude to my first supervisor Professor John Stonham for his guidance, support and advices. He teached me, looking for the “why”, behind all things.

Also I would like to thank my second supervisor, Professor Filippos Vallianatos for his continuous support and guidance at various stages of this thesis.

Many thanks to my Professor and Mentor John P. Makris, for his guidance throughout the course of my thesis.

Special thanks to Assistant Professors George N. Fouskitakis and John S. Sakellariou, for their valuable guidance on the field of parametric analysis and data processing.

Thanks to Klaas Pluvier, Tim Langouche, Cappelle Thomas and Vernier Kevin for their contribution in the programming part of Waspmotes and ADXL accelerometers.

Many thanks to Dr. Despoina Kalisperi, for her help on the structure of this thesis and to Dr. Ilias Papadopoulos for his help on HVSR field.

I am grateful to the National Foundation of Scholarships in Greece (IKY), for the financial support during this research.

I owe a big thank to my parents for their support and encourage.

At last but not at least I would like to thank my wife Gina, who encouraged, inspired, helped and supported me, during this thesis. Her contribution, moral and spiritual, is invaluable.

To my son Pantelis

Chapter 1. Introduction

1.1 The background of this thesis

Safety is the most important factor in any human activity. Ensuring the safe use of buildings and constructions ensures personal safety and implies structural integrity. Monitoring buildings can detect possible structural errors or defects, to warn or even ban, if necessary, the use by people in the case of serious infrastructure damage, and also inform on possible refurbishment requirements. Environmental conditions, natural hazards and human activities can affect the structural state and behavior of a construction. Buildings could experience loading conditions that put them in strong motion, such as human made explosions, strong winds, and big earthquakes which may cause small or large structural damages. These damages could change the structural characteristics of buildings or affect the integrity and the strength of building materials and increase the possibility of collapse. Thus buildings require continuous monitoring of the structural characteristics and parameters in order to prevent or fix possible structural problems that exist or have been created through specific events or aging. An area where the buildings and constructions are subject to significant seismic activity is the island of Crete, southern Greece located at the fore-arc of the Hellenic Subduction Zone (HSZ). Therefore, the development of a system for monitoring structural condition of buildings deemed necessary and of great importance.

Author Rytter [1] defines four discrete damage factors for Structural health monitoring (SHM).

- Damage identification in a structure
- Determination of damage location or locations
- Damage severity level
- Life prediction issues

This thesis is concerned with the identification of damage, using digital signal processing methodologies (parametric and non-parametric) for damage detection. Furthermore these DSP techniques should be combined with a very cost effective Structural Health Monitoring system (SHM) implementable on a metropolitan scale.

1.2 Aims and objectives of this study

The overall aim of this thesis is:

The design and evaluation of a structural health monitoring system, in a highly seismic region that contains many old public buildings. Also the application of advanced DSP methods, for effective SHM and damage identification of real structures, for reliable structural damage identification.

The primary questions of this research thesis are:

- When a building or a structure is inadequate?
- How is it possible to identify this deficiency?
- What system is needed and what features should be measured in order to achieve cost-effective monitoring of the structural condition of buildings?
- How could DSP techniques be combined in order to present a robust SHM methodology to identify faults in real structures?

1.3 Methodology

Recording data (in terms of acceleration) will be analyzed by DSP methods, novel algorithms and techniques to achieve an efficient monitoring of structural health of buildings under study. This study presents in detail all the technological features of a system that was fully designed, installed and implemented within the aforementioned thesis. Also this thesis analyzes data and records of the above system, monitors buildings and applies various techniques of digital signal processing in these recordings.

These methods are:

- An approach for SHM which measures the fundamental frequency deviation of a structure and correlates it with the extent of structural faults.
- A procedure in which several wavelets families are applied in the SHM recordings in order to reveal the ability of each family, to present more clearly, changes in frequency spectrum of specific seismological recordings.
- Horizontal to vertical spectral ratio (HVSR) technique is applied in the buildings under study and a novel index is defined, which correlates the increase or the change of the HVSR from floor to floor (inter-floor drift) with the structural vulnerability of a building.

- Non-parametric methods such as power spectral densities (PSDs), frequency response functions (FRFs), coherences diagrams, and parametric methods such as Autoregressive (AR), Autoregressive with exogenous input (ARX) and Autoregressive Moving Average with exogenous input (ARMAX), using parameter model based modeling, are applied in this research. The vibration response of the structures under seismic and environmental noise excitation, reveals linear and non-linear characteristics or differences in models which will signify structural damage and reduction of mass and/or stiffness.
- The identification procedure of the concrete buildings, which is based on scalar ARX models while their parameters are used for damage detection via proper statistical hypothesis testing procedures. The results of the study - though at a preliminary stage - indicate that ARX modeling is sufficient for representing the structure's dynamics. Nonetheless the previous non-parametric methods are required in order to define specific parameters such as the energy distribution, the frequency spectrum and coherence between excitation and response.

The above methods are used since they are efficient in computation and reveal information concerning damage sensitive parameters, such as fundamental frequency response, building internal drift and modal parameters.

1.4 Selection of the study region

Chania is located in the western part of Crete (figure 1.1). The broad region excibits high seismic activity, because it is located in a subduction zone. The African plate subducts beneath the European plate, creating shallow and intermediate earthquakes and volcanoes [2-4]. The population of the city of Chania is 60000 residents and the wider area of the prefecture of Chania, is approximately 150000 inhabitants, which increase by a factor of 2-3 during summer time [5]. Within the city there are many public buildings, which are old and have an urgent need for structural health monitoring.

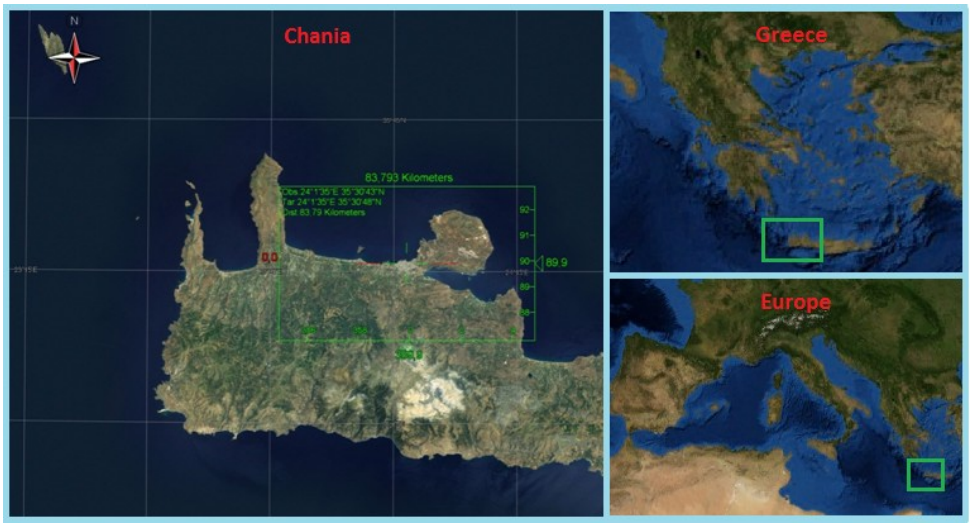

Figure 1.1 ***Broad region of Chania, Western Crete [6]***

1.5 Thesis outline

This work consists of 8 chapters.

The introduction chapter refers to the aims and objectives of the thesis, the geographic location of the deployment and the thesis outline.

The 2nd chapter is a detailed literature review on structural health monitoring. Monitoring systems in the last decade are evaluated, and their evolution of SHM is assessed. The theory that governs these systems and the shortcomings, are reviewed. The limitations that may exist and the state of the art on these systems, are presented. Also the advantages and disadvantages of various works done on SHM and how they have contributed to SHM are considered. Finally digital signal processing methodologies relevant to SHM are evaluated in order to contribute to enhance building monitoring.

The third chapter describes the instrumentation, the design, the features of wired and wireless SHM system and the main reasons that these were selected. Also the key points of this instrumentation are listed, and address installation and data collection issues. It presents the programming and development of the wireless SHM systems.

The fourth chapter introduces non-parametric methods that will be used in this thesis, namely Power Spectral Densities (PSDs), Frequency Response Functions (FRFs), Coherences diagrams, Horizontal to Vertical Spectral Ratio (HVSR). Also, parametric techniques along with parametric identification procedures are presented.

In fifth chapter data analysis with non-parametric methods on acceleration recordings data sets from wired and wireless SHM network is developed. Digital signal processing techniques namely PSDs, FRS, coherence diagrams are applied on recordings of the SHM system that has been installed in buildings used as case studies for this research. Novel approaches of digital signal processing for structural health monitoring like frequency deviation, and HVSR index, are evaluated on data obtained from these test sites.

Chapter six addresses the application of parametric identification of vibration based data sets. Also statistical analysis of results for damage identification is presented.

In chapter seven there is the discussion of all the above chapters, correlation of the results and comparison of analyzed data. Also it presents the results of the aims and objectives of this thesis.

Chapter eight summarizes the most important findings of the research, and suggests future work at specific scientific areas.

1.6 Contribution to knowledge from this research:

I. The contribution from wireless SHM, is that a system very cost effective, has been programmed and developed, able to record acceleration of buildings in high data rate, high sensitivity up to 2 mg (optimum for strong motion accelerations in buildings), send the data wireless to the base (gateway) and it is able to function as network to more than one buildings. Compared with other commercial and scientific wireless SHM systems, the developed system achieves high quality recordings with the minimum cost. As a result it can be implemented in many buildings, as SHM system with the minimum cost.The contribution is that how a low cost system is able to function like the expensive systems for SHM. Such to increase the safety of more buildings through the ability of lower cost systems to more buildings.

II. The contribution of the wired SHM is that it has been established and developed a very sensitive and accurate SHM system which is able to monitor and record, very low amplitude acceleration measurements, like environmental noise, low structure accelerations etc. This system enable us to study digital signal processing methodologies for structural health monitoring which have not been applied yet in buildings (HVSR), to compare DSP methodologies in order to reveal how a

method could be more effective in fault detection etc. Conclusively to increase the safety of buildings through the better detection of a probable fault.

III. The contribution of the frequency deviation index (Π index) is that it correlates the maximum fundamental frequency deviation of a building, with the reduce of structural stiffness. It uses this frequency deviation change as damage indicator and quantifies this change.

IV. The contribution of "HVSR Rise Index" is that it can reveal when the differential acceleration from floor to floor in a building is higher than specific thresholds, under which conditions it could happened (environmental noise, earthquake activity, or man-made activity) and how high is this value, correlate simultaneously the probable vulnerability of the structure in the specific floors. Monitoring the vulnerability of a structure also contributes to the maximization of the safety of a structure for the people who use it.

V. The contribution of ARX and ARMAX modeling of both building in TEI Chania is that parametric identification is applied on seismic acceleration of low amplitude earthquakes, in real structures data (time series), in order to reveal the modal characteristics before and after major seismic shocks. The buildings are studied not as structures but as systems with input (ground), system transfer function (building transfer function) and output (floor responses). This enables to study the modal parameters of structures, find out if they change during time or after major earthquake shocks and finnaly overpass the limitation of different input dynamical parameters on every seismic event.

VI. The contribution of wavelet approach is that, it presents the advantages and disadvanages of wavelet transform in seismic acceleration of real structures, under real conditions. Acceleration recordings of a real structure SHM system, excited by earthquakes, are processed in order to reveal the efficiency of non-parametric wavelet analysis in damage identification. Wavelet transform is very efficient to reveal much clearer in wavelet plane (space and time) specific waveforms that connected with frequency content of real structures under vibration, but only under stable and determined specific dynamical parameters. When these parameters change in every seismic event the results are chaotic and wavelet approach becomes inefficient in identification analysis.

VII. Characterization of seismic regions and determination of specific geographical zones of South Hellenic Arc, according with the seismic acceleration on case study buildings, and creation of a novel-prototype map which correlates magnitude of earthquakes, their distance with case stuby buildings and seismic acceleration that effect these case study buildings for every seismic event. This map presents the seismic vulnerability of buildings under study, for specific areas and specific metropolitan areas. It demonstrates an earthquake influence map on a building, by means of the recorded acceleration, that reveals directional characteristics as well as the effect of the epicentral distance and offers a first approach to identify seismic areas to which the building is more vulnerable.

VIII. The contribution of the novel proposed algorithm in this thesis (section 7.10) is that it is able to reveal the same frequency response function, such the same way of structural response and modal characteristics, under different dynamical parameters excitation. Overcomes the limitation of the laboratory experiments where FRF is stable only when the dynamical parameters of the excitation are stable and determined. Conclusivelly model bodeplot's significant change (in terms of amplitude or graph form) is related with the change of dynamical parameters of the structure under study. Existance of damage is verified by model parameter vector distribution studied under a statistical manner (chapter 6.3).

1.7 Summary

The first chapter of introduction highlights the aim and objectives of this research. Provides general information about the area of Chania, the seismicity of the region and summarizes chapter contents. Also it presents the importance and necessity of this research and the methods that will be used to this direction. Finnaly presents the contribution to knowledge from this research.

Chapter 2. Literature review

Introduction

Chapter two has three subsections of literature review:

- Structural health monitoring, in order to reveal the key points of damage detection.
- Wireless structural health monitoring systems, in order to present state of the art in systems of SHM.
- Digital signal processing methodologies, in order to study the advantages and disadvantages of various DSP methods.

2.1. Literature review in Structural health monitoring

2.1.1. Definition of damage

With the term “Structural health monitoring” (SHM) it is defined the integrated procedure for the detection and characterization of damage to structures or buildings. Worden et al. [7] define damage as the change in either the material (mass of the construction) or the characteristics and structural properties of a structure (damping or stiffness of construction). These changes could affect the structural acceleration response of a construction, when there is excitation (vibration-acceleration excitation in construction). In above [7] it is suggested that damage identification is a sum of four parts which conclude "the existence of damage, the damage locations, the types of damage, and the damage severity". The damage of a structure could have linear or non-linear result in the structural response, such that after damage the structural response remains linear and elastic or alternatively the system has a non-linear and inelastic response [8]. Kim et al. [9] state that the purpose of damage detection is to find any probable structural damage and to identify its location and severity in a structure. Sohn et al. [10], correlate the structural damage (cracking) in a structure with the variation of the mechanical part of the construction (change of construction mass), the change of the geometry of the structure at this point (change of center of gravity and center of mass) and the change in rigidity of the construction (change in structural stiffness). The above studies highlight the statement, that almost all vibration based damage detection methods are based on observational study of changes in stiffness, mass, and also the change of properties of energy distribution (how the energy of excitation distributes on the frequency spectrum of response of a construction), and all above are related to the measured dynamic response of the system. In [10] it is stated that while the fundamental

frequency of a structure is related with its stiffness, any change in frequency reveals change in stiffness. As indicative example, refering to figures 2.1 and 2.2, where in the experiment of I-40 Bridge over the Rio Grande in New Mexico, USA, there is change in fundamental frequency related to the reduced stiffness.

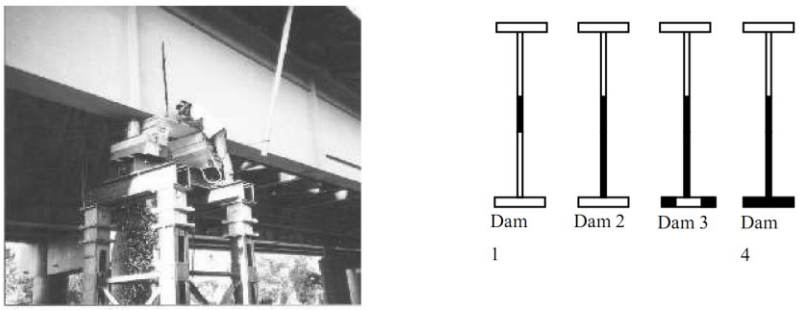

Figure 2.1. Damage Detection Study of the I-40 Bridge over the Rio Grande in New Mexico, USA. Left figure: electric saw cutting cause damage in the bridge girder right figure: The levels of introduced damage in the girder (the shaded area is the reduced cross-section, Sohn et al. [10].

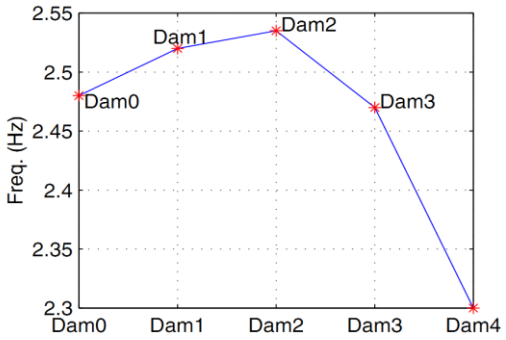

Figure 2.2. The change of fundamental frequency on I-40 Bridge related to the damage levels presented in figure 2.4, Sohn et al. [10]

Generally damage could be defined as the change of a structure's behavior through structural change that has impact on mass, stiffness of damping of the structure.

2.1.2. Methods of damage identification

SHM can be achieved by measuring kinematic characteristics (e.g. acceleration), strain, displacement and environmental characteristics (e.g. temperature, wind, moisture, saltiness and emitting gasses). These parameters affect the structure and cause corrosion or damage. According to Gong et al. [11] System Identification (SI) is a general term for the description of algorithms and computation tools, which construct dynamical models from

vibration recordings (data sets). A review of methods to identify damage in structures, by studying the vibration response of buildings or other mechanical systems, is presented by Doebling et al., [8]. They categorized the identification methods, initially based on the data type being collected and secondly the analysis technique adopted to identify the damage from the measurements. They use the method of frequency change, where the damage detection is based on the shifts and changes of fundamental frequency of structures of systems. The methods study the changes in mode shape (determination of mode shapes before and after damage) where there is the ability of localization of structural damage. A different approach to mode shapes is to study the mode shape curvature derivatives. The author refers to beams that are related with curvatures and strain with the relation:

$$\varepsilon = \frac{y}{R} = ky \qquad (2.1)$$

where the strain is ε, the curvature radius R and k the curvature.

Doebling et al. [8] also present other methods for damage identification by vibration response analysis, such as the "based on dynamically measured flexibility method", "matrix update method", "non-linear method" and "neural-network based method". In modal analysis in order to achieve accurate results (for structural health monitoring) many tests and experiments are required [12], in order to describe efficiently the dynamic characteristics of a construction (damping, mass, stiffness). Modal analysis therefore studies the physical characteristics of the structure. Modal analysis methods are operational modal analysis (OMA), where there is study of modal properties under operating conditions (without external or artificial excitation, only ambient noise). Next is the experimental modal analysis (EMA), where there is study of modal properties under artificial excitation. The experimental modal analysis of a structure requires the description of the dynamic properties of the structure, using the fundamental frequencies, the damping ratio and the way these parameters vary throughout the construction. Furthermore there is OMAX which is operational modal analysis with external forces [13].

Vibration based SHM, has attracted significant attention in recent years due to its ability to monitor and identify structural characteristics from global monitoring of a structure (vibration data could be measured from any point and location of the structure). This ability overcomes limitations, in terms of access and recording, of other non-destructive SHM techniques (acoustic and ultrasonic waves, thermography, x-rays etc). Vibration based methods detect changes in structure stiffness and are strongly related to the dynamic response of a

structure. Such monitoring vibration-acceleration data of a construction can reveal possible change in its dynamic properties. These modal parameters are natural frequencies, damping ratios and mode shapes [14].

Methods for damage identification are also referred by Sohn et al., [10] highlighting the same techniques as above (resonant frequencies, mode shapes, dynamic flexibility etc.) but also present methods based on damping (change of damping of the structure), anti-resonance (comparison of measured frequencies with frequencies predicted from finite element model "FEM"), ARMA model (autoregressive moving average), wave propagation, autocorrelation function and empirical mode decomposition.

Damage detection is based on correlation and study of the modal and dynamical parameters (resonance frequencies, damping ratios, mass and stiffness) of a structure system over time. The changes of these parameters define possible change in structural properties of an infrastructure. System identification (SI) is again defined as the analysis, calculation and process of these data with specific methods and techniques [15]. In case of SHM with SI, buildings are affected by environmental or manmade activity that is the system input. This excitation causes specific building responses depending on its own dynamical characteristics. The response of building under this excitation is the system output. Dynamical characteristics of a structure which simultaneously reveal damage are parameters like displacement, its first derivative with respect to time (speed) and second derivative (acceleration), in relation with force as excitation of system [15].

Xu et al. [16] face the measurements errors and modeling in SHM damage detection methods by a stochastic method where they calculate before and after the damage the probability density functions (PDFs) of stiffness in a structure, and they compute a specific probability function with the measured PDFs in order to present the damage location and severity. They find the stiffness parameters of PDFs in a structure with and without damage occurrence, and compute the probability function:

$$\mathrm{P}\{(\mathrm{K}^{\mathrm{u}} - \mathrm{K}^{\mathrm{d}}) \geq \mathrm{a} \times \mathrm{K}^{\mathrm{u}}\} \qquad (2.2)$$

where K^{u} the stiffness before damage and K^{d} stiffness after damage and a index which takes values from 0% until 100%, in order to detect the location and the extent of damage. Another method much faster for the revealing of cracks in beams is referred by Lee et al. [17] where the problem is inversed and the solution is given by the application of Newton-

Raphson technique. A crack is modeled as a rotational spring and using finite element method they relate the crack with a stiffness matrix, and finally iterate the location and size of the crack by the above method. According to [17] the real and the modeled cracks are quite similar in terms of severity and location. Finite element model is also used by Goldfeld et al., [18] with the combination of vibration frequencies and modes in order to locate and quantify damage. Although the prediction of mode shapes and bending stiffness is presented as reliable, they underline that theory differs from reality, and many mode shapes are needed in order to reliably define stiffness distribution (to determine damage in real constructions).

2.1.3. Frequency changes for detection of damage

The methods of measuring the changes in resonance frequency of a structure are very efficient, due to the high reliability of the results and the fast process of the recordings. The minimization of natural frequency indicates the reduction of stiffness whereas high frequency reveals higher stiffness of a structure [19]. Salawu et al. [19] present scale models and real structures with cracks, structural failures, overloads that caused damage. For all cases, change in fundamental frequencies is included, compared with the undamaged status. The ease of measurement and the characteristic of global parameter of the eigen frequency on a structure, was supported by Sayyad and Kumar [20], where they assess the location and size of crack on a beam. They study the natural frequencies on an un-damaged and a damaged beam, with the method of finite element model (FEM), in order to define the crack size and location by an inverse approach. They present that a crack could be defined like a spring, which connects the parts of the beam and they apply a model to correlate natural frequencies with crack characteristics. The predicted crack's location is very close to the real one, but this concern an experimental model, which differs from the characteristics of real buildings [20]. Application to real structures to evaluate the technique is stil pending. Frequency response function methodology (FRF) is computed for assessment and estimation of damage and/or fault detection, with applications in structural health monitoring, system identification and model updating. Mao and Todd [21] apply experimental (data driven) and analytical (mathematical approach) FRF, and propose a statistical model based on Gaussian bivariate, in order to reduce the possibility of false alarms from dispersion of FRF evaluation. Results are verified for laboratory and simulation models, but not for real structures (buildings etc), where the structural responses and/or coherences of input-output may differ significantly. Frequency response functions (FRFs) have been also applied by Salehi et al., [22] using two methods: a) the independent component analysis (ICA) which

separates a mixed signal to a set of source signals, and b) operational deflection shapes (ODSs), a method of visualizing the vibration pattern of a structure under external force excitation, in order to detect and localize damage. They prove that, except the FRFs data of the pre-damage and damage structure, there isn't the need of analytical model, in order to localize damage. A frequency-based technique is presented by Esfandiari et al. [23] where they consider that eigen frequency is related with stiffness reduction. For verification of results they use mode shapes of a structure in intact and in damaged state. They claim that the mode shape changes through the proposed algorithm are efficient without the need of undamaged state. But these results refer only to specific laboratory experiments and under specific supervised damage identification. Vibration frequencies of damaged and undamaged states used by Goldfeld and Elias [24] proposing a “direct identification procedure” for changes and dispersion of rigidity of a beam. They identify the problem of high number of unpredictable coefficients and face it with specific polynomial and the exact element method. The proposed procedure, although reveals the damage distribution in a beam, is verified only under specific excitation conditions.

2.1.4. Non-Parametric methods for damage identification

Digital signal processing enables to analyze and distinguish signals in discrete recordings. Despite the big evolution yielded the last decades in parts of data processing, wireless protocols, autonomy and data rate analysis, Structural Health Monitoring (SHM) is an open issue which exhibits many technological and scientific challenges, like sensors which will be able to detect damage, low cost, high scalability [25-28]. Revealing possible structural damage from recordings requires appropriate algorithm which will be able to extract reliable information determining the response of the structure under excitation, and discard useless man-made or environmental noise.

The methods of detection and location of damages in buildings are discussed in detail by Doubling et al. [8]. They analytically present a methodology based on the frequency change (frequency shift of the natural frequency response of a structure), mode shape changes and mode curvature/strain changes, methods based on dynamically measured flexibility, matrix update methods, non-linear methods and neural network-based methods.

According to the study of Mojtahedi et. al [13] in a platform model, the eigen frequency study is associated with the flexibility and stiffness. The study applies 5 different damage scenarios and studies two methods for detecting damage. The measurements carried out

indicate that the damage or the presence of structural change loss of integrity is associated with the change of frequency.

SHM methods are presented by Sohn et al. [10], where the sensing parameters, like strain, displacement, acceleration, are presented, as well as the feature that each method uses for SHM, like resonant frequencies, frequency response functions, modal shapes, damping, non-linear features etc. They indicate that the dependency on pre-defined analytical models has significant uncertainties and are not fully validated by the experimental data. In addition, no one of the reviewed research verified the numerical models or quantified the associated uncertainties in order to employ these models for damage detection. A key-problem to deal with, is how the damage identification can be achieved over operational and environmental variability as well as when non-linear response introduced into the system. Approaches like statistical process control or simple hypothesis testing identify the existence and location of damage but cannot identify the type and the magnitude of the damage.

Hou et al. [29] analyze vibration signals with non-parametric Wavelet Transform (WT) method. They investigate the noise intensity and damage severity of a building but they don't locate the point of the damage. Even when the severity of the damage is referred they cannot argue on which degree this reduces the stiffness of a building and affects its integrity or response. But they point out the need of further study to justify the results.

At a next publication, Hou et al. [30] apply again wavelets and they present the application of a model in non-linear, time-variant systems but there is no discussion on the localization of damage in a complex structure , or the detection of local change-lack of stiffness of a structure. Xing et al. [31] use WT to study a bridge model and investigate the extent and time occurrence of pounding (for each frequency) in the specific tests, but they clearly indicate the need of further experimental studies on more practical (real) cases.

Fast Orthogonal Search (FOS) has been applied by El Shafie et al. [32] where they apply this method to the IASC-ASCE SHM benchmark structure. They suggest that FOS is a non-linear modeling technique which provides high resolution spectral analysis and is able to reveal functional expansions in SHM data. FOS is able to detect critical frequencies in spectra better than FFT when the time-window of the data is less than 10 sec but for bigger time-windows in data analysis there are detection limitations. Thus, for small window analysis, FFT cannot reveal the frequencies that FOS does. On the other hand, FOS

limitation is that background noises being removed sometimes could contain critical frequency information.

Performance of mono-bit DFT and quantization of the time signal have been examined by Penny et al. [33], in order to minimize data analysis requirements in Wireless Sensor Network (WSN) systems, but they refer that more work is needed in order to develop these methods to be efficient. Also the sampling rate they use is very high (1600 Hz) in order to evaluate it in a WSN system and it is unknown if the same computational approximations could be achieved with a much lower sampling rate of e.g. 200 Hz per sensing node.

Power spectral densities have been discussed by Fassois and Sakelariou [34] as method for damage detection, identification and also definition of damage severity/level, through small or large scale changes in auto-spectral density function. They clarify that the method is applicable when there is no information about excitation of a vibrating structure and the only available data is the response data. Then damage determination is based on changes of one or more frequencies of the auto-spectral density function of the structure. A number of different measurements are necessary in order to validate the results statistically. Due to the fact that frequency changes are sensitive to environmental conditions the method functions properly when environmental but also excitation parameters are stable (temperature, amplitude of vibration and distributed energy).

2.1.5. Wavelets in structural health monitoring

From literature it is known that for every specific application we can introduce an appropriate wavelet in order to present the desired signals's characteristics that we are interested for. Yan et al. [35] discusses fault detection by continuous and discrete wavelet transform (DWT), wavelet packet transform and wavelet transform of second generation. They indicate challenges in wavelet fault detection, the property that as wavelet function comes closer to the shape of the signal, so the optimum will be the extracted characteristics of the transform. As a result they suggest that the creation of wavelet that will be similar or match in high level to the desired signal characteristics is a very important issue but they apply wavelet transforms only in rotary machine damage detection and they do not suggest any new type of wavelet that could match to the related characteristics of the signals.

A review on the application of wavelets in SHM is presented by Kim et al., [9]. They indicate that in some situ conditions, wavelet methods are not efficient for damage detection, but the developments in the field promise results in the future. They highlight the ability of wavelets

to de-noise response signals and in such a way to achieve better performance in identification of damage location and time of occurence. Finally they point out that measurement of damage severity with wavelets is still an open issue and this could be treated by artificial neural networks (ANN), but the disadvantage is the high computational requirements (necessary iterations) that are needed for on-line SHM by ANN.

Non-linear filtering with the application of wavelet transform has also been applied by Chun [36] where they process the whole spectrum of probability density functions recursively by DWT, they overpass the high frequency data with the multi-resolution analysis and the proposed algorithm presents higher accuracy by the Kalman filter. Non-linear filtering by WT is also studied by study Pazos et al., [37] with application on seismic recordings. They underline that the minimization of noise effect by linear filters decreases the signal bandwidth and suggest that with time-frequency localization every coefficient is related to a specific window on the wavelet plane. Such any disturbance affects only the frequency and time of the specific window. Finally they propose three levels, starting with minimization of periodic noise, the elimination of spikes and at the end non-linear filtering of the data. Discrete Wavelet Transform is also applied by Zhang et al., [38] in one component seismograms in combination with auto-pick of Akaike information criteria (AIC) method. AIC is an index of the relative good adaptation of a statistical model (how accurate or complex is a model). They correlate the AIC recordings with the detection of P-wave signals at specific time windows. Author states that wavelet picking with AIC method is more efficient in noisy environment and there is more clearly P-wave detection instead of conventional method of band-pass filtering.

Seismic estimation through wavelet method is studied also from Wang et al. [39] where they indicate the catalytic role of wavelet in inversion of wave impedance together with the forward modeling, defining the main fields of statistical and deterministic wavelet estimation. They used autoregressive moving average (ARMA) model in order to reveal seismic signals, calculating AR variables (order and parameters) with a total least squares technique and the singular value decomposition (SVD) from a selected matrix calculated with autocorrelation and conclusively suggest a novel model through correlation of "higher-order cumulant method" along with the "information theoretic criteria method".

Wavelets have also been used for fault detection with piezoelectric technologies by Xu et al. [40] and Filho et al. [41] with the first to install piezoceramic sensor in steel tube filled from concrete and analyze the recordings of artificial de-bond by wavelet packet analysis, and the

second to apply wavelet transform in two discrete levels of variation in electromechanical impedance of piezoceramic wafer which are used for structural health monitoring. Wang et al. [42] presents continuous wavelet transform in order to detect instantaneous frequency data in constructions and buildings where data are time varying. Minimization of the noise is achieved by inserting specific function and implementation of dynamic optimization is used in order to reveal instantaneous frequencies through the wavelet ridges. Below figure 2.3 presents the typical example of this analysis.

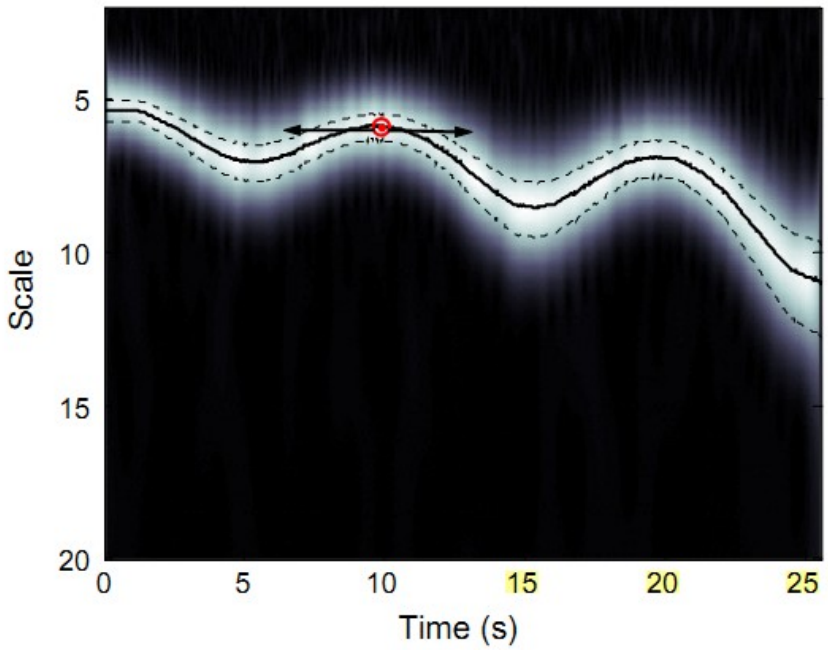

Figure 2.3. Wavelet Scalogram with ridge (initial wavelet ridge is the line,selection region of wavelet coefficient is the dashed line)[42]

Fault indicator is suggested by Peng et al. [43, 44] calculated from wavelet packet transform in order to detect and define possible damage in models of sub-sea pipelines. In [43, 44] proposed the so-called Average Wavelet Packet Energy Change Rate (WPECR) in order to compare the damage and undamaged data, by means of the wavelet energies and the Rate (WPECR). Although authors claim efficiency in damage localization, the proposed model differs from real structure subsea pipelines, the scale model cannot simulate real structure 100 percent and also in small scales the distances the attenuations, the response of waves is completely different related with real subsea pipelines. Figure 2.4 presents this typical energy distribution of the model without and with damage.

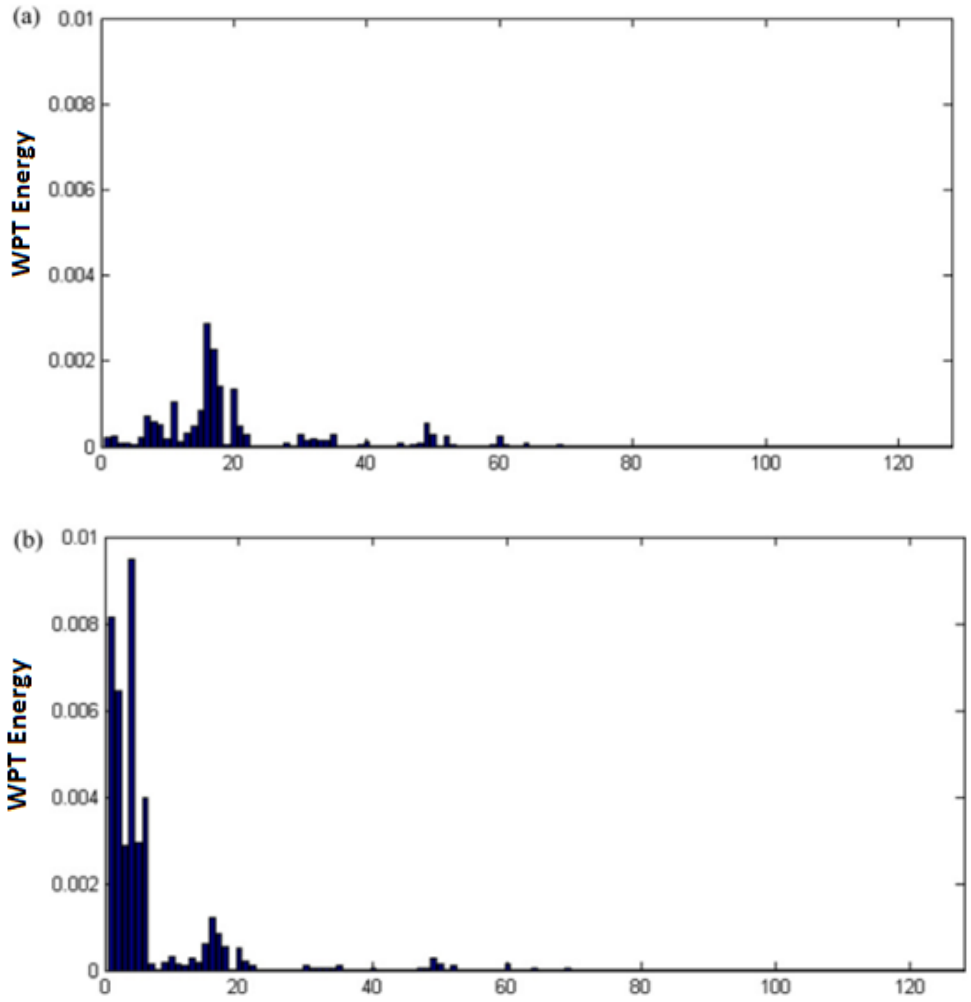

Figure 2.4. Typical component energies of a model , WPT is the wavelet packet energy (a) Without free span damage (b)with free span damage [44]

Seismological records always contain noise which has to be removed before the data are used in seismic applications [45]. The wavelet methods are very efficient in the removing of noise. The right level of threshold is vital for high Signal to Noise Ratio (SNR). In [45] it is suggested specific thresholds for wavelet de-noising techniques in SHM data, based in Shannon entropy and Tsallis entropy and compares them with other thresholdings that already exist, like normal shrink and visu. The below thresholds (equation 2.3 & 2.4) are suggested as more efficient in wavelet denoising procedure. Shannon entropy is given by the type:

$$\text{Shannon} = \sum_{j=1}^{m} p_j \log_2\left(\frac{1}{p_j}\right) \qquad (2.3)$$

where the probability is p_j, m is the number of system possibilities. Tsallis entropy is an expansion of Shannon Entropy with an extra parameter given by the below equation:

$$\text{Tsallis} = \frac{1-\left(\sum_{j=0}^{m} p_j^q\right)}{q-1} \qquad (2.4)$$

where q is the entropic index (real number)

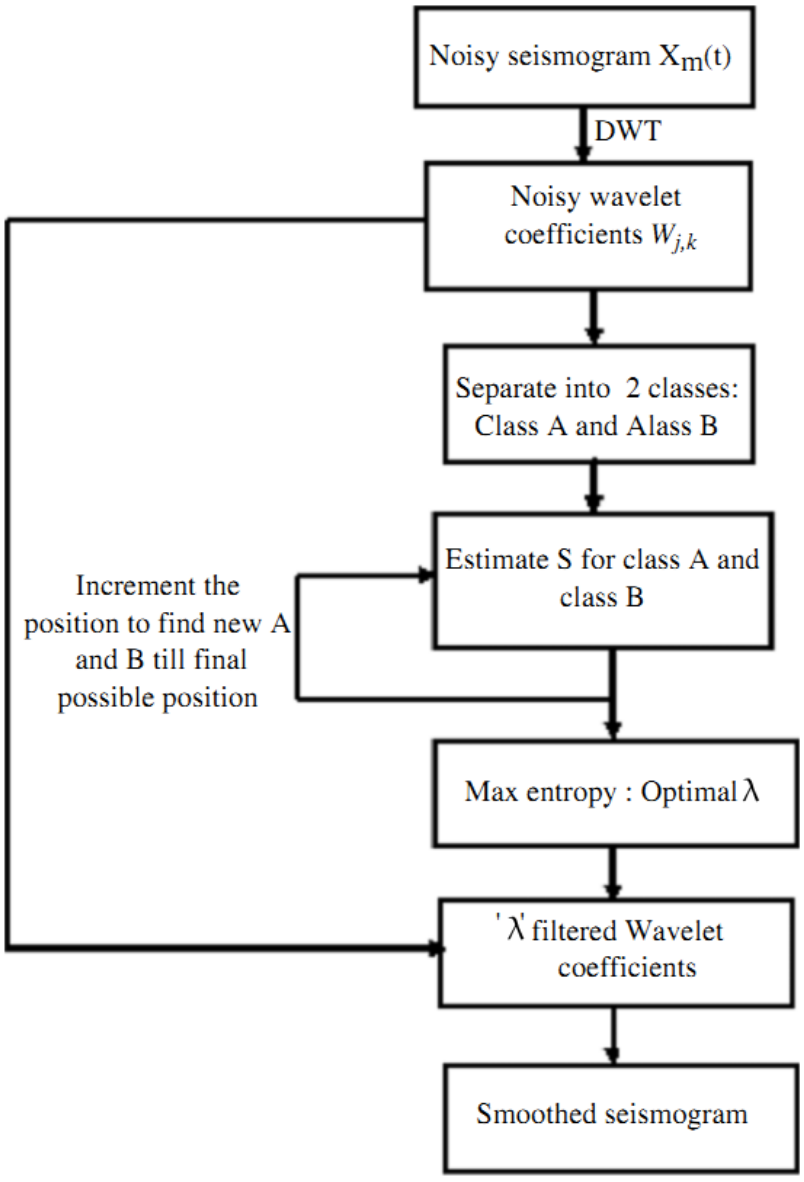

Figure 2.5. Suggested de-noising algorithm based in entropy by Beenamol et al.[45]

Also author [45] propose an algorithm for denoising of noisy seismograms (figure 2.5) based on filtering of specific wavelet coefficients.

2.1.6. HVSR approach in buildings

Mucciarelli et al. [46] refers that study of microtremors and weak motion provides fast and reliable data for site amplification and structure vulnerability compared with other traditional methods, and the correlation of damage and structural integrity is with physical parameters and not normalized dimensional indeces. Furthermore they propose a technique (filtering of the signals to diminish noise effects like wind and traffic) based in empirical method to estimate the structural vulnerability of buildings under seismic excitation, by HVSR methodology.

Triwulan et al. [47] refer that geological characteristics of a region, structural characteristics of a building and also their correlation can be described by the application of HVSR approach on data recorded on the ground of the building and inside the building. It studies fundamental frequency, the amplification factor of the ground as well as indeces of vulnerability of buildings and ground.

Luo et al. [48] uses ambient noise of a concrete reinforced building in Beijing, caused by subway trains, and present the resonance frequencies of the building on each one of 7 floors. They study the range of the building's fundamental frequency (around 2.4 Hz), the frequency which is generated by the nearby traffic on the building (around 10 Hz) and the geological fundamental frequency of the region that the building is located (around 2-3 Hz). They indicate that although the amplification of the site is critical for the specific building, its dumping ratio of 0.17 is very effective on structural integrity.

Hong and Hwang [49] refer that the fundamental frequency of a structure, is estimated theoretically using the matrices of stiffness and a mass model, and experimentally from real structure recordings. Furthermore an empirical equation, based on length and width of case study buildings, is used:

$$\mathrm{T} = 0.0294 \times \mathrm{Y}^{0.804} \qquad (2.5)$$

where Y is the height of the building and T is the period.

According to the above author our case study buildings have height almost 14 meters, such the fundamental frequency of the structures period is 0.24 sec or around 4.20 Hz. These

hypotheses are almost close to the real fundamental frequencies of case study buildings of this research (TEI), found experimentally, which around 5,5 Hz.

2.1.7. Parametric methods for damage identification

Mojtahedi et al. [13] point out the great importance of detecting damage to offshore platforms due to the fact that these platforms are in very harsh environments (sea waves, winds etc.). They describe a model of an offshore construction and they are testing it under various damage scenarios. They present two methods of analysis, the first method studies the modal parameters in the frequency domain (with fuzzy logic) and the second is studying the features extracted from the data series and stochastic self-regression to test them, and the effectiveness of each method in conditions of damage . It is studied the effectiveness of detection uncertainties and nonlinear operation of the construction. The method of fuzzy logic although has proven effective for diagnosing damage in this experiment the author refers that is not very effective in detecting of damage. The second method is based on studying stochastic self-regression moving average with exogenous input. The great advantage of this method is that data can be analyzed directly without change from the time domain to the frequency domain (the first method). The second method is much less computationally compared with the first. But in both cases there was not damage detection under all scenarios. Also the specific algorithms that are proposed are applied in the specific model without being bound if they are equally effective in actual construction or other construction models.

Advantages of parametric identification compared with non-parametric methods, are referred by Fassois [50], where author indicates parsimony of data, accuracy and resolution, analysis flexibility, and high detection of system dynamic, as key advantages of parametric techniques.

Cazzulani et al. [51] studied the detection of damage in a machine arm. They apply an algorithm to model that arm, to detect cracks of the arm, by measuring the change in the frequency of the system. They also use an overload detection algorithm in order to detect when there is overloading of the mechanic arm. They present that techniques based on modal analysis and armax models, require computational time and preprocessing of data which makes it difficult to detect damage in real time. Kalman filter overpass this limitation and can be applied in real time. Two algorithms named FVD (frequency variation detection) and OLD (overload detection algorithm) based on Kalman Filtering are applied in the

research. The FVD method is studying the change in frequency of the arm (for the detection of loss) and the OLD studying the overload of the arm. The experimental measurements do show clearly overload and damage detection.

In the study of Bao et. al [52] modal functions like resonance frequencies, mode shapes and damping are parameters that describe the physical properties of a building like the damping ratio, the change in stiffness or the mass of a structure. Furthermore author refers three main disadvantages of time series methods. Time series are affected by operational or environmental alterations. The noise disrupts the accuracy of time series methods and also the creation of index which characterizes the building damage, has large dispersion and flexibility in values. In their study they apply an algorithm for damage detection in subsea pipeline system. They employ normalization to data to cut off loading conditions, auto-correlation to solve noise effect, partial autocorrelation to define optimum ARMA model and a damage indicator based on Mahalanobis distance to detect and localize damage.

Cui et al. [53] apply acoustic emmition method for SHM of aircraft parts. They study ARMA and SVM (support vector machine) models, by building ARMA model and extracting its parameters to define vector. This SVM vector is used for damage detection. They claim that method is able to detect cracks in aircraft effectively.

Autoregressive moving average (ARMA) model applied by Bao et al., [52] for monitoring the structural health of a subsea pipeline. They analyze acceleration signals from the located on the pipeline sensors, normalize the data and apply auto-correlation function for reducing the noise effect. They also use partial autocorrelation function (a method for the identification of the lag in an autoregressive model (AR)) in order to define the best AR model order. The produced AR coefficients reveal the damage induced in the system. The method is applied in submarine pipelines under the effect of the force of waves and the author presents interesting results in the detection and localization of damage, but this is a specific system and a subsea system is different from a building or other structures, and the same principles (wave forces) may not occur in other states of structures like buildings (also the earthquake activity is completely different of the ambient wave force). Fassois [54] suggests a method of linear multi stage ARMAX with application in systems of multi-input multi-output (MIMO) data. Author presents the computing of LMS parameters, ARMAX vector, the model order selection and analysis of digital dispersion, suggesting that this approach solves many difficulties from simple MIMO ARMAX models, in terms of accuracy model and algorithm stability, compute complexity. As a result the proposed method is able for higher-

dimensional systems with low damping ration, extraction of precise modal parameters and effective determination of different structural modes.

In a following part [54] of the research [55] the LMS-ARMAX method in comparison with ARX and Eigensystem realization Algorithm (ERA) one, applied in aircraft's model. They present that LMS ARMAX method is appropriate in model dynamics identification. ARX model is presented effective as well, with only drawback the need for higher order modeling and such an added number of 'unrelated or extraneous' modes. The ERA is shown less effective in identification of structure and higher frequency modes.

Stochastic methods (Prediction Error Method, Two stage least square, Linear multi stage, Instrumental variable) and deterministic methods (Least squares, Prony Method, Eigensystem Realization Algorithm) are discussed by Petsounis et al. [56] in order to reveal the ability to identify the characteristics from stochastic excitation in vibrating structures. Non-parametric methods represent frequency or impulse response whereas parametric method (based on models) have parameterized data which represent differential equations or modal models[56]. The above methods are studied in areas like model order and parameter estimation, simulation and sensitivity, and expertise of user.

ARX and ARMAX parametric methods of system identification are applied to dynamical characteristics of structures such as resonances frequencies, damping and stiffness in order to indicate possible damage in buildings through change of these parameters by Jekikj [15]. Author presents that, time increase damping ratio in contrast with minimization of stiffness and resonance frequency and that this procedure can be accelerated by strong motion events (like earthquakes greater than 5 M) that affect the structures, and also that dynamic parameters of a structural system are mode shapes, damping ratio and natural frequencies.

Natural frequencies as index for structural damage have been studied by Yang and Wang [57] where they apply two methods named "natural frequency vector (NFV)" and "NFV with assurance criterion" in an 8-story shear frame model triggered by an external exciter. Although numerical results reveal that natural frequencies can be estimated by high accuracy with and without noise effect, the disadvantages are the necessity of a finite element model of the structure, impractical for real buildings cases, the inability of detecting small structural damages through natural frequency and also that this method functions for the specific type of simple structures (without near space modes).

2.1.8. Neural networks for structural damage detection

Methods based in neural networks demand a phase of training and recognition. Fang et al., [58] study damage detection through neural network, uses data of frequency response functions (FRFs) and tests training algorithms named dynamic steepest descent (DSD), Fuzzy steepest descent (FSD) and tunablesteepest descent (TSD). Author claims that although DSD and FSD present high learning speed, disadvantage in the optimum choice of parameters and strategy controls, and suggests that TSD is more efficient in convergence speed. Lin and Qun [12] study variation of statistical parameters of vibration signals in time-domain, in order to achieve damage diagnosis with artificial neural network. Their experiment is on data monitored by bridge artificially excited. The architectures TNN (task negative network) and TDNN (time delay neural network) were tested with TDNN having better performance in terms of time and training process. Although they found some interesting results, they need specific statistical parameters (in which their efficiency is depentent and specific network architecture, for the prediction of damage in the tested bridge. In the same direction of neural network approach for structural health monitoring Shi et al., [59] study ANN in the model structure of IASC-ASEE. They created response data from the finite element models of the specific structure, and they compare them with various SHM systems. They de-noise the data with wavelet transform (with specific thresholds) and these data are used as inputs to the neural network. The ANN applies pattern recognition in order to detect possible fault in the structure. Their results present high accuracy in damage detection, but the specific ANN needs both states of the structure (damage and un-damaged) in order to complete the learning procedure, and another one disadvantage is that this accuracy is for the specific structure and we don't know if the same procedure of ANN can be used for other structures or if it will have to complete a learning procedure again. Combination of two methods of ANN namely radial basis function (RBF) and probabilistic neural network (PNN) with HVSR method has been tested by Yaghmaei-Sabegh and Tsang[60] for site classification in the wide area of Taiwan. The data of ANN were compared by known data in order to extract the accuracy of the system in the identification and estimation of site amplification. Authors claim that the specific technique would be effective in states and regions with stations of strong motion where the site condition is unavailable.

Taha et al. [27] examine wavelet transform, wavelet multi-resolution analysis and wavelet packet transform in analysis of signals from structures under excitation. They claim that although above methods provide damage detection, when these methods are combined with

ANN the results are improved. ANN have been discussed by Fang et al. [58] where they implemented and compared Dynamic Steepest Descent (DSD), Fuzzy Steepest Descent (FSD) and Tunable Steepest Descent (TSD) learning rate algorithms demonstrating their limitations and merits. Although damage detection is enabled, these algorithms were applied in model structures and not real ones. Furthermore the system needs training in order to be effective, which means that it would learn in a real damage of a structure in order to be able to reveal possible damage in the future.

ANN and WT have also been addressed by Shi et al. [59] where they discuss and apply a hybrid wavelet - neural network method to a benchmark structure. They use WT as neural network input achieving to reduce noise, and with ANN (pattern recognition) damage detection is performed in the lab. The damage detection has high accuracy (95 to 96% for the damage patterns under test) but this is not repeated with real structures, or with more damage patterns.

A major drawback of artificial neural network (ANN) approach is the necessity of training, damage data should be as input and also that in every case study there is different approach and need for specific training.

2.1.9. Limitations and weaknesses of the structural health monitoring methods

Literature [7, 8, 10, 19, 27, 30-33, 59] reveals that there are major drawbacks in the existing SHM methods. First of all, it is required a data history before the damage of the structure in order to be compared with the data after the damage. This is very important because usually the time of damage occurrence is unpredictable, so as to distinguish the data before and after the damage.

Literature does not define the exact deployment and the number of sensors in a structure. This issue is under research and in every structure a careful examination should take place to find the optimum sensor deployment, but even in that case there is no guarantee that rich data will be captured. Another important constrain is that almost every known method is applied to linear structural models. In contrast, when structural damage occurs there is non-linear behavior, so there is possibility not to be able of reveal the specific structural response.

Equally important is the issue concerning the difficulty to discriminate noise from data that reveal damage. The sensitivity of the sensors is an open challenge since the literature has

not define yet specific minimum and maximum levels of data and noise respectively, or there is not a clear method to identify the valuable data in the noise when the level of signal is very low. Moreover, it is very difficult to discriminate statistical variation from low level damage SHM recordings. Furthermore, the majority of SHM tests, methods and research is conducted in laboratories and models differ from real structures.

2.1.10. Discussion on SHM literature

Identification and localization of damage has been widely studied by many authors and institutes [8-10, 16, 17, 20, 22, 61-67]. Until nowadays every method solves or contributes to specific problems referred to specific structures. No method can be applied for all structures and problems. Damage detection and/or localization require previous tests and application of models in order to compare with the current structural status and assess for damage. Linearity is necessary for the majority of methods in order to evaluate damage detection. The tests and studies applied in laboratories or in artificial models differ sometimes a lot with real life applications. One dimensional problem could not be applied with success in multidimensional problems.

Structure and building safety is of great importance for urban areas. Structural health monitoring (SHM) is referred in effective monitoring of the structural integrity of infrastructures and the ability to identify possible damage or fault. The procedure of damage identification includes also localization and quantification of damage, along with estimation of remaining life of case study structures. The literature presents high amount of studies related on general topic of SHM [8, 10, 26, 68, 69]. Vibration based methods are used for two main advantages in comparison with other know damage detection techniques (x-rays, sound waves etc). They are global, which means that they are able to be measured from every point of a structure while they are also covering the whole response of the structure. The second advantage is the ability for automatic analysis of the recording data. Both advantages contribute to very low cost in relation with other methods of damage identification. There are works that study vibration based damage identification on finite element models (FEM), small and large scale laboratory models, and real structures (buildings, bridges etc). The above studies try to find out structural damage from changes on frequency and damping ratio, mode shape and Eigen-frequencies.

Literature presents a large scale studies on FEM [13, 20, 32, 57, 62, 63, 70-79]. Many authors apply analytical modeling of beams, bridges, buildings, skyscrapers etc. The main

disadvantage and limitation on all these studies is that on real world structures and more generally real life differs a lot from these models. Many analytical algorithms function right, under specific models with specific degree of freedom (DoF), and under specific input (excitation) and output (response) scenarios [16, 80-89]. When all these scenarios are transferred in real world dimensions many parameters are not the same, with the simplest or smallest experimental laboratory model to present many more DoF than a designed FET model, and such even the analytical modeling of a simple beam requires parameters that most sophisticated FEM until nowadays do not include. A simple FEM of a metallic beam includes usually basic parameters of length, weight and its material [20, 24, 62, 73]. But the same beam on real world may include rust from moisture, which changes its structural integrity, probable different rates in the mix of materials that is constructed, which could also affect its elasticity and stiffness, and this procedure could be aggravated and intensified through time and age. Such a simulation FEM should be not only much more sophisticated but also to be able to recognize and compute all these factors in order to be efficient. This kind of FEM is still a scientific challenge.

Laboratory experimental analysis for damage identification overpass many of the limitations that inherent on FEM. Studies on small scale laboratory models present damage identification, localization and on specific studies quantification is much more effective [13, 14, 23, 31, 57, 59, 80, 90-100]. But also small scale models induce in SHM procedure many specific requirements that usually do not exist in real world structures. In laboratory the excitation is controlled and such the response is also the expected [91, 94, 97, 101-104]. Furthermore in laboratory there is the ability to control the level of amplitude of excitation and its specific form. Laboratory dynamical parameters can be determined with high accuracy. This is much different than real world structures where the level of excitation and its form is unpredictable, and also each experiment, excitation or just triggering contains different dynamical parameters. Most important is that in the laboratory the level of excitation is much higher in analogy with the dimensions of the model than in real world. Laboratory models are tested at high amplitude levels related their dimensions. Such there is triggering of frequencies and mode shapes on specific frequencies bands (usually higher than real world structures). In other words coherency between input and output differs a lot from real world structures, where the excitation is much lower level of amplitude (related the specific dimensions of structures), frequencies and mode shapes are in a very low range and also the coherence between excitation and response remains in a very low window, and low

band, frequency range. This reveals a completely different vibration response of between laboratory models and real structures.

Application of fault and damage identification on real structures has the advantage that overpass many limitations of designed FEM and laboratory models in terms of DoF, coherence and structural parameters that a designed and/or scale model and system cannot describe or include [11, 27, 105-111].

Literature presents damage identification on real structures excited either by ambient noise, low seismicity, strong motion seismicity, and human made affect (impulsive or explosion type excitation) [15, 74, 76, 112-120]. Each type of motion-excitation reveals different characteristics of dynamical parameters of case study buildings or structures. Ambient noise effect on a specific frequency range of structures, low seismicity creates a different frequency response and strong motion seismicity cause again a different frequency spectrum of structures. Works that study ambient excitation on real structures could be found in [76, 113, 116, 117, 121], works that study low seismic activity and other works that study high seismic events are addressed by [11, 27, 74, 109, 114, 115, 119, 121]. There are studies that use historical events recorded from past years on buildings in order to evaluate models for damage identification [85, 89, 118, 122-128]. Also there are studies of ambient or seismic or human made excitation in real building. Furthermore there are studies of damage identification through parametric modeling on real structures.

Vibration based methods will be used in this thesis for two main advantages that present compared with NDT methods [129]. They are global, which means that they are able to be measured from every point of a structure, and also they cover the whole response of the structure. The second advantage is that there is the ability for automatic analysis of the recording data. Both advantages contribute to very low cost in relation with other methods of damage identification.

2.1.11. Conclusions in SHM literature

Conclusively according to the above literature review, there is lack in comparison of structural response from buildings of different ages, that have the same structural characteristics, (dimensions, structural code), and are in the same seismic region. Also there is lack in parametric modeling of concrete buildings continuously, first at low seismic excitation, secondly during strong motion event, and at last under low seismic excitation again [7, 25, 130-132]. This will enable to study the structural response of real concrete

buildings before and after major structural shocks, and reveal the ability of parametric modeling to illustrate possible existence of structural integrity change on case study buildings.

Such in this thesis the vibration response of real world buildings will be studied, through low seismicity excitation before a strong motion seismic event, the vibration response at the event, and after the event. A structural health monitoring system, with very high sensitivity accelerometers, able to record from ambient noise of level of μg acceleration, until strong motion, records excitation of two different age, 3 floor concrete buildings, where both are located on a high seismicity broad region (beside each other). The specific analysis of structural response, from low magnitude earthquakes, before, during and after a strong motion seismic event, on two different aged concrete buildings, in accordance with the parametric damage identification and statistical time series analysis is novel.

2.2. Literature review in wired and wireless Structural health monitoring systems

2.2.1. Introduction

Structural health monitoring systems are being implemented into the cities at an increasing rate [102, 130, 133-138]. More and more buildings and other structures (e.g. bridges, highways etc) are deployed with monitoring systems in order to minimize the possibility of structural hazards through the continuous control and monitoring of structural damages and changes. Kurata et al. [138] refers that as systems (computers, sensors etc) are developed (smaller, smarter, cheaper) the interesting in wireless sensor networks becomes greater and impacts on almost every part of society.

Research indicates that this trend will continue in the near future [25, 26, 28]. Jinping et al.[26] refers the increased number of SHMs in railways, buildings, bridges and various other structures in China. Lynch et al. [28] refers that there is an increasing interest in application of sensing technologies in structures, for structural health monitoring. The catastrophic events which effect in the structural health of buildings and could be mitigate by SHM systems are presented by Aygun et al. [25] who indicate that evolution in WSN and MEMs boost the implementation of wSHMs in large scale in the societies.

Many researchers address that wireless sensor networks provide more efficient data collection for SHM, than traditional conventional wired SHM systems [25, 28, 102, 139-142],

due to ease of installation, low cost, and small size of wSHMs. High cost of wires in wired SHM systems and limitation in installation, design flexibility and cost is referred by lynch et al. [142] and Harms et al.[141]. Minimization of design and cost of a SHM system by wireless sensor networks in also presented by Sazonov et al. [140] where they recognize the continuous raised popularity in the specific scientific field of SHM.

Although there is significant evolution in wireless structural health monitoring, in many cases, monitoring by itself is not enough to indicate when a structure becomes inappropriate and/or unsafe for use, and the damage or low durability of a structure cannot be revealed [101, 137]. Several features and specifications of WiSHMs like wireless sensor networking, reliability and autonomy of sensors, algorithms of data transmission and analysis should still be evolved and improved in order to increase the predictive effectiveness of the SHM [26, 143] . On the other hand, low cost MEMs systems are not able to record low level ambient vibrations due to the low resolution [139]. Accuracy and reliability are crucial factors in wireless SHM systems [144], in order to be able to measure in detail and continuously the state of a structure.

Wireless SHM systems are deployments which generally measure acceleration, the recordings are sent wirelessly to a central computer server for analysis and storage. Wireless SHM are being introduced into cities and big infrastructures at an increasing rate. This trend probably will continue in the future by covering small and large buildings, bridges and structures [10, 25, 26, 28].

2.2.2. MEM Sensors

Micro-Electro-Mechanical Systems (MEMS) dominate in wireless sensor networks systems especially for SHM [145, 146]. Miniaturized highly integrated sensors have low cost, tiny size, and very low power consumption, such giving a significant boost to the evolution of wireless SHM systems. Their main disadvantage is that they do not yet have the high sensitivity of an analog accelerometer [143, 147, 148].

2.2.3. Wireless Sensor Networks

Wireless SHM systems are monitoring systems in which the sensors are remote nodes connected wirelessly with the central database (or the central PC) where the data are collected). The term Wireless Sensor Network (WSN) describes the architecture, the

protocols and the rules that exist in order a wireless connection to be established. Also it defines the routing of the data packets [25, 149, 150].

Sivrikaya et al. [151] present the main characteristics of the WSN and discuss about synchronization, energy, storage, bandwidth of a WSN. They refer that each of those parameters is a limitation for high number of wireless nodes and to increase the nodes, each parameter should increase in order the WSN to function properly. WSN are also proposed by Jeongyeup et al. [88, 152] highlighting the advantages in fast and ease deployment with high flexibility, along with the low maintenance needs and the low installation costs. Interesting is the presentation of Kim et al. [153] where they indicate that with WSN there is no affection at all in the operation of a structure (no need for cables, supports of cables etc). Characteristics of WSN like network topology, communication routing and protocols, power management are discussed by Lewis et al. [154] emphasizing in challenges in hierarchy of a WSN like selection of the nodes, the monitoring and collection of the data, the assessment and evaluation of the information, being produced. Authors indicate that the variety of the parts of WSN systems many times make a challenge for a WSN to be stable, reliable and with high sensitivity for a long time period. In WSN each protocol of communication (Bluetooth, Wi-Fi, ZigBee, UWB) has different characteristics in terms of power consumption, bandwidth and distance from peer to peer [150]. Major advantage of WSN is that they are able to monitor heritage buildings, in which there are strong limitations in deployment of wired SHM systems due to low level of integration (most of them are very old structures) [135]. Although WSN are deployed with high efficiency in many applications (military, aircraft, security etc) in the part of SHM, there is the challenge that high rate vibration measurements, yield high communication load that has to be transferred wirelessly from the wireless nodes to the central server efficiently [155]. Problems and challenges of WSN in SHM are discussed in detail from Wang et al. [156] presenting compatibility challenges (due to different sensors), the required sampling frequency, possible problems with communication and transmitting bandwidth. Also they address that topology choice, data fusion methods and the variety of energy consumption in the parts of a WSN system, are key points which need further investigation and evolution.

2.2.4. Autonomy in wSHMs

The importance of autonomy of wireless structural health monitoring systems is addressed by several researchers [141, 157-160]. Autonomy relies on the relationship of the energy

consumed under working state, versus the ability to store energy. A relationship that proxies this concept is:

$$A \propto \frac{E_b}{E_f} \qquad (2.6)$$

where E_b is the energy that battery can store and E_f is the energy that the system needs to function. If energy harvesting is also considered, then this relationship becomes:

$$A \propto \frac{E_b + E_h}{E_f} \qquad (2.7)$$

where E_h is the energy which is added in the system, by charging the batteries, through solar panels, wind turbines or other means of charging.

The energy harvesting obviously could provide high autonomy in the SHM system (since it can supply energy for long time through battery charging). Many papers, address the issue of autonomy in wireless sensor networks for structural health monitoring as a key point due to the fact that it determines the reliability of a system (continuous uninterrupted power supply ensures continuous system operation and uninterrupted measurements) [157-159]. Generally accelerometers which is the main sensor for monitoring the structural motion, consume higher energy than other SHM sensors (temperature, moisture, pressure) due to the need of continuous high resolution measurement instead of much lower data sampling in other physical measurements [135].

A SHM system consists of many electronic parts that consume electrical energy thus forming the total energy consumption of the SHMs. The main parts are the sensor (accelerometer), which transforms the structure acceleration movement to electric signal, the analog to digital converter (ADC) the microcontroller, which controls the data flow, local storage and/or transmission (for wireless systems), the transmitter which sends the data to the central node (or retransmits data from other remote nodes in case of full mesh network). The resulting total power consumption should be kept low in order the system to be cost effective (higher energy consumption means more batteries, bigger systems of power harvesting all these result to higher cost). Furthermore comparison of commercial wireless sensor node platforms named MICA and MICA 2, reveals that energy transmitting consumption is analogous with the range of the data transmission [138]. The transmission range should be in specific limits in order to satisfy moderate power requirements. More distance between wireless nodes requires more transmitting power for each node.

A way to minimize power consumption is by turning to sleep mode when the system is not triggered [153]. Sleep mode has also been applied for efficient use of energy consumption for the commercial wireless sensor platform Imote2 by Rice et al. and Jo et al. [113, 158], where inactive nodes turn to sleep mode. Other way of reducing energy is the local process for reducing the transmitting energy [137] but this requires high processing abilities for each sensor node. On the other hand, minimization of power consumption should not affect the quality of the measurement and functionalities of a SHM system [136]. Low noise sensors require of stable and clean power supply. The output signal can be affected by the noise of power supply and this could be confronted by low-noise low dropout linear regulator [147]. Wireless sensor network platforms which use Zigbee protocol are characterized by much lower power consumption than other commercial platforms [157] but Zigbee protocol can achieve transmission rate 250 kbs and range no more than 100 m (instead of WiFi protocol with 54 Mbit and range more than 100 m) [150].

Almost all available today WiSHM systems have elevated energy consumption, low batteries capacity and almost no-one wireless node has autonomy more than one year [141]. Consequently energy harvesting is necessary in order to charge the batteries before being discharged under a voltage threshold). Furthermore the sleep mode of inactive nodes is generally approved method for energy efficiency. Nodes could minimize the overall power consumption so as wireless nodes batteries live more than one year. But in this case a number of sensor turn to sleep and the system sensitivity reduces. The energy harvesting of solar panels and wind turbines could improve energy efficiency and batteries life but such solutions can be applied only in open constructions (eg bridges). A suitable algorithm which will control the sleep mode, the triggering mode and the record mode of the accelerometers, combined with sophisticated process of transmitting data to the central node could provide high autonomy to a wireless SHM system.

2.2.5. Data synchronization in Wireless SHM systems

Many researchers were concerned with time synchronization issue of wireless sensor networks (WSN) [134, 140, 144, 151, 161-163]. SHM collects data from several points around a structure. All these data is very important to arrive to the central data base synchronized in order to be able to analyze. Data synchronization is an important aspect for SHM systems as it is responsible for the communication of the peers with the main gateway to the database. Literature reveals problems like clock errors, interferences, data losses and conflicts and presents solutions like time stamping, specific synchronization algorithms for

the communication between wireless nodes in SHMs. Wireless network sensors are more prone to delays due to interferences and problems due to clock errors [161].

Sazonov et al. [140] discusses time synchronization in WSN, indicating that a beacon signal is a way of synchronization in order to satisfy scalability and proposes an hierarchical architecture with internal cluster beacon signal by using GPS time reference. Although GPS has very high accuracy (almost 200nsec relative to UTC), has been addressed as unsuitable for time synchronization, due to high cost and the need for clear sky [163]. Uchimura et al. [134] and Jeongyeup et al. [152] suggest time stamping of the packets but this method requires all nodes to be synchronized, difficult to maintain in a long time period, due to variation of temperature, applied voltage and the added electronic tolerances [164].

Data synchronization is an open challenge [153], as sampling should be performed simultaneously in all nodes even if there is drift at the local clocks. Furthermore data follow different routes and demand processing time. On the other hand, a wireless sensor network should be able to support a big number of nodes [137]. The latter requires bigger bandwidth, in order a node to be able to transmit its data and retransmit other node's data simultaneously (full mesh network), and sophisticated communication algorithm, in order to apply full mesh networking effectively.

Modal analysis and identification algorithms require synchronized acceleration data from different points of a structure [136], otherwise the result may be corrupted due to delayed data. High accuracy (of the order of 1 msec) in time synchronization of a wireless sensor network, especially in case of seismic activity data, is a fundamental aspect, in order to have a real time view of seismic acceleration impact on a structure [135, 165]. Timer-counter of the microcontroller has been proposed by Katsikogiannis et al. [165], in order to succeed time synchronization between the nodes, by calculating the differences of each node timer's value, but it is not easy to define in any WSN the internal clock drifts or the clock differences between the nodes because these events are random and unpredictable. Indicative example is the application of wireless sensor network in metallic bridge by use of Imote2 sensor platform, where the steel elements and dense foliage cause communication problems due to interference [106].

Developers of wSHMs use many techniques, in order to mitigate the time differences i.e., microcontrollers, re-sampling protocol and beacon signals in wireless sensors. The time delays between wireless nodes and base station can be minimized in some tens of μsec,

whereas the time threshold for seismic data should be less than 1msec, and is depended from the time synchronization technique. Any WiSHMs should satisfy this requirement in order to be effective.

2.2.6. Data rate analysis

Important research is also performed in the field of data-rate and data-analysis of the wSHMs [83, 88, 101, 108, 152, 160, 166, 167].

Data rate of accelerometer sensor is key-aspect that determines the quality of a measurement for SHM. High data rate results on many samples per second and the sensor can record high frequency accelerations of the structure. This is vital because structural response is reflected in a band of frequencies, and most of the constructions damp the disturbance of their structure in less than a second, thus higher sampling rate is necessary.

Jo et al. [139] refer that relatively low resolution result to weakness in low-level ambient vibrations measurement. Sampling frequency should be analogue to the attenuation of a structure [152]. But the definition of the attenuation and the definition of the new attenuation after a structural damage remain a challenge. Jeongyeup et al. [152] discuss the necessary sampling frequency in a SHM system. They point out that typical frequency response band is 0-20 Hz. Satisfyng the Nyquist sampling frequency more than 50 Hz support the reliable detection of such a response. For structures depicting high damping coefficient, structural vibrations strongly decay in less than half a second. In such cases 50 Hz sampling frequency, eventually provides very few samples for performing spectral analysis, so higher sampling rates should be exercised for SHMs deployed in civil structures [152].

Wireless Mica2 and MicaZ implemented by Kurata et al. [138] measure with 100 Hz sampling rate with maximum possible record up to 200 sec (with 512 kB flash memory) . Kim et al. [153] use in research project mica2 with 38 kbps in 433 MHz. Fundamental eigen frequencies of the structure should be lower than 10 Hz otherwise structure depicts high stiffness. Also they suggest that sampling frequency should be higher than 200 Hz and sampling jitter effect lower than 250 μsec in order to minimize the spectral jitter (undesired frequency signals around the central frequency) and the noise (random jitter).

An alternative to achieve the mitigation of the large amount of data transfer could be by the transmission of the frequency spectrum instead of time series [168].

A prototype system [136] uses the MaxStream 9XCite transceiver where central server is able to collect data from up to 24 wireless sensors with real time sampling frequency of 50 Hz for each sensor. If the communication bandwidth is constrained and higher frequency is desired, the available number of the nodes is reduced (12 nodes for 100 Hz). Constrained bandwidth limits the sampling frequency and the number of the nodes, as each node requires a part of the total available bandwidth.

High sensitivity acceleration board developed for the wireless sensor platform Imote2 by Jo et al. [147]. Imote2 platform supports 250 Kbps data rate, with onboard at 2.4 GHz wireless communication but without sensor. A separate sensor board ITS400 comprises a 3 axes digital accelerometer and 560 Hz sampling rate is used for 14 sensor boards. The resolution of the digital accelerometer is 0.98 mg which is not enough to measure ambient vibrations. In contrast to ITS400 Lu and Lo et al. [143] present a very sensitive acceleration sensor (VSE-15D) which is able to detect low amplitude vibration motion up to 0-70 Hz. Prieto et al. [108] present a 17-story steel moment frame factor building is instrumented with 72 channel array of accelerometers. The array records 100 samples per second using a 24 bit digitizer of the horizontal acceleration (north-south and east-west directions).

All the wireless SHMs mentioned above as well as of the commercial wireless systems still have poor acceleration response compared to the wired SHM systems, worse identification of modal shapes and and suffer from loss of wireless synchronization [101]. Frequency response is an index to quantify damage in a mechanical system, but solely natural frequency of a structure cannot reveal possible local damage, and a sensor network able to detect local damages is still a challenge [26].

2.2.7. Summary from wSHMs literature

Recent years many manufacturers have presented applications for wireless SHM. Imote platforms (also Imote2) have been widely investigated for structural health monitoring scientific applications. Large amount of on-board memory and high speed processor is ideal for high data-rate analysis like SHM but the disadvantage of Imote is the high energy consumption which reduces drastically the autonomy. A way to harvest energy could be solar panels or wind turbines but this is available only in outdoor applications (like bridges) and not at indoor (like buildings). Very interesting platform is Waspmote manufactured by Libelium. Based on Zigbee protocol has low power consumption and is able to measure acceleration and ambient parameters (temperature, moisture) depended on the extra

peripheral sensor board but the disadvantage is that it hasn't as high data throughput as Imote, which is a basic requirement for acceleration measurements. Zigbee technology has also been used by Harms et al [141], where there is low power consumption, high autonomy and reliability but also low data rate ability (lack of high frequency vibration analysis). Wireless sensor node "Telos" by Berkeley [157] has also low power consumption, and high data throughput but it features slow read-write process due to external flash memory.

A wireless SHM system presented by Wang et al. [136], exhibits low power consumption fast and cheap deployment and offers multiple data receiving but it needs better filters for de-noising, higher data rates, sampling rates and better algorithms for more efficient data management. The problem of clock drifting and loss of synchronization is solved by Katsikogiannis et al. [165] by using the timer counter of the microcontroller, but remains the problem of high power consumption and the need of data-analysis algorithm for better detection of seismic activity. One from the solutions to overcome low data rate analysis suggests the use of high sensitivity accelerometer board able to capture weak motion caused by ambient noise [147], at the cost to require special noise removal algorithms and filters. In the same context Prieto et al [108] suggest that instead of recording shaking due to earthquakes, the wireless SHM monitors ambient noise vibrations by applying impulse response function (IRF). The benefits are more data for analysis and more buildings being monitored.

Furthermore the technique of FRFCM is presented [169], where each wireless unit transmits spectrum of frequencies (close to structure frequencies) instead of whole spectrum. Also units perform FFT transform with result spare in bandwidth energy and autonomy. This way there is less requirement in transmitted frequency spectral but the time information (time series) is being lost. The absence of synchronization and the low resolution of commercial wireless SHM systems in respect to with wired SHM systems, is indicated in Ramos et al. [101].

2.2.8. Conclusions from wSHMs literature

Previous sections discussion on wSHM literature reveals that further research and improvement is essential for extended and reliable use of wSHMs. In autonomy there is still the need for less power consumption of the accelerometer, as well as of the ADC microcontroller and transmitter in order the total power supply to be less than up to now implementations. This will damp down the requirements concerning batteries expocity and

the energy harvesting system and will reduce the cost. In a wireless sensor network, there is the need for data synchronization and minimization of data losses between remote nodes and central node, as well as clock error or clock drifts handling. Accelerometer sensors should be enough sensitive, featuring high data rate to be able monitor the frequencies that reveal probable structure damages. In acceleration data analysis there is great need for algorithms able to reliably reveal possible structural problems in buildings from the recorded data. As an overall conclusion, structural health monitoring lacks a cost effective wSHM systems that will be able to deploy in metropolitan scale with very low cost.

2.3. Literature review in digital signal processing

2.3.1. Introduction

In this section of the literature review will be presented the fundamental DSP characteristics that are going to be used in the thesis. Digital signals are used by the accelerometer sensors (digital sensors are used), convolution is going to be used in the section 5 of DSP, but also is the core of wavelet transform, Fourier analysis and fast Fourier transform is going to be used also in chapter 5 in analysis of the measurements, wavelets families and wavelet transform is applied wide in the records in order to reveal critical information through signal. Below there is an introductive presentation of all these parts of DSP analysis that are used in the thesis.

2.3.2. Signal processing

Signal processing is the conversion of a signal from its physical form to a form that can be recorded and analyzed. The signal processing is included in almost all disciplines of applied sciences as mathematics, industry, electronics and engineering. The signals in the nature (along with artificial) include various different forms. Speed, acceleration, conductivity, resistance, voltage etc. are just some of the forms that a signal may have. Depending on what form we use there are two signal formats. Proakis et al. [170] defines the meaning of signal as a varying in time, space or other variable physical quantity, and states some examples which a signal could be described mathematically as function of one signal or variable (for example $y(x)=x$), more variables in the same plane (for example $y(x,z)=1x+2xz+3z$) or as a sum of more independent variables. Analogue signals, where the recorded values are continuous and theoretically start from infinity and going to infinity, and digital signals, where the recorded values listed are discrete and finite in number. Analogue signals, which appeared in real life, in order to be processed by computers and digital

microprocessors, need to be transform in digital form [171]. About linearity of a system author Tan [171] refers that a system is linear when a system has superposition, such the output of a sum of two inputs a and b is the same as the sum of two outputs where the first output has input a and second output has input b.

About time invariance in a system in [171] refers that a system is time invariant when the output shifting (for example n) in that system is the same as the input shifting (n) that system has, in terms of time amount. A system has causality when the output is defined only by current and/or previous values of input and not future values of output[171].

For each signal format (analogue or digital form) there is the corresponding signal processing sector. For analogue signals is analogue signal processing which includes electronic systems which process continuous signals and convert them into another format suitable for processing, storage or transmission [172]. Generally there are four different types of signal in terms of time and value that they could have [170]. Signals continuous in time and in value they could have. They can be described by continuous variable and they called analogue signals. The value could have any value from -∞ to +∞. Signals discrete in time and continuous in the value they could have. The value could also have range from -∞ to +∞ but the time are in specific intervals. Signals continuous in time but discrete in the values they could have. The value could be only at specific levels. Signals discrete in time and in the value they could have. The value is only at specific levels and in specific time intervals.

2.3.3. Digital signal processing

Discrete time signals are signals where the time of the data are in discrete time of equal time period, but the amplitude -magnitude of the signals are not discrete [171]. Digital signal processing is the category where the signals are recorded in discrete time and can take certain fixed values (discrete and finite). This enables digital storage, transmission, analysis methods with advanced digital signal processing methods available only when there are digital data [173]. Most signals in the physical world have analog values (continuous) and also our senses in order to understand and feel these signals, need to be in such an analogue form. To be able to record, storage, process, send these data over analog signal processing needed to convert analog data into digital and vice versa.

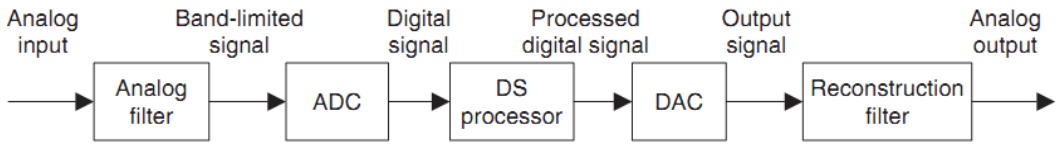

Figure 2.6. Analog to digital processing schematic[171]

In order to transform a signal from analogue form to digital form and again to analog form it needs first to filter the analog signal, only the desire signal pass, convert the analog signal to digital with an analog-digital converter (ADC), process the digital signal through a digital processor, convert again the digital signal to analog signal with a digital to analog converter and at the end filter again the output signal with a filter that will reconstruct the analog output to the initial analog input signal (or will be close to the initial analog signal). In digital signal processing the data are finite and with specific time space between the data. The rate of the data called data rate and it refers on how many data there are in each second.

Sampling in a common form is a sequence of samples $x[k]$ taken by a continuous-time signal $y(t)$ by obtaining values at equally time-interval points. Sampling is defined by the relation:

$$x[k] \triangleq y(t)x[n]\,|_{t=kT} = y\,(kT) \qquad -\infty < n < \infty \qquad (2.8)$$

where T is the sampling period (time between samples). Sampling frequency or sampling rate is the fraction:

$$f = \frac{1}{T} \qquad (2.9)$$

A digital signal has specific sampling.In sampling is critical the theorem of Nyquist-Shannon stating that the sampling frequency must be at least twice the maximum occurring frequency in a signal. This exemplified as follows. When the sampling frequency is twice the maximum frequency of valuation frequency of the signal then there is the ability to sample the positive part and the negative part of the maximum frequency in a signal. Suchall the included signals (until that frequency) are sampled. Also in an analog signal after sampling and quantization, its accuracy is limited to the margins of the finite values. There are methods of reconstruct the analog form but it is very close to that form and not exactly the same [174]. A discrete-time signal $y(x)$ is an independent variable function of an integer. The discrete-time signal between the samples cannot be defined [170].

2.3.4. Domain

The digital signal processing is determined by the domain where the measurements are performed and analyzed. Domain can be either based on time, where measurements are presented based on the time (time series), or based on the frequency domain (frequency spectral), where measurements are presented as spectralbased on the frequency that occurs each measurement. Furthermorethere iswavelet domain, wheremeasurements are presented in the three-dimensional, time, the frequency spectral content and strengthening of each measurement [131, 171, 172].

There is also the domain of Z plane and Splane where measurements are presented as arguments of the base e and lne. Z-transform is of great importance in the analysis of discrete – time signals. Proakis et al. [170] refers that "in Z-domain the convolution of two time-domain signals is equivalent to multiplication of their corresponding Z-transforms". Also they present how this characteristic contributes in the analysis of an LTI system along with other signals. Zero-pole locations of Z-transform describe an LTI system and its response under various signals.

If there is a discrete-signal $y(k)$ the Z -transform is the power series:

$$Y(z) = \sum_{k=-\infty}^{\infty} y(k) z^{-k} \qquad (2.10)$$

where z is a complex variable, and the time-domain signal $y(k)$ is transformed to its complex-plane form $Y(z)[170]$.

Mertins et al. [175] refers about z-transform that although time index k is a discrete value, z is a continuous value and complex even when y(k) is real. Also they state that for the $z = e^{j\omega}$ the Z-transform is the same as the discrete-time Fourier transform. The same is referred by smith et al. [176] where they present that Laplace transform for the designing of analog filters is similar of Z-transform used for the designing of recursive digital filters. The author states that Laplace and z-transform are similar techniques, which could work parallel.

Smith et al. [176] also presents that Laplace transform can turn to Z -transform in three actions. Initially transform signals from continuous to discrete, by replacing the variable of time t in a number of samples n. Next step is to change the exponential form, to a form that will contain real and imaginary part. Last stage is the replacing of the variables of radius r and angle speed ω, with the variable z.

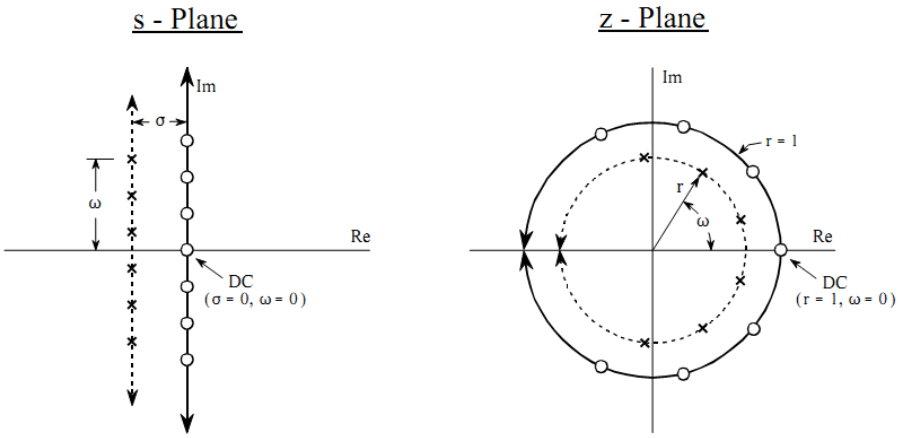

Figure 2.7. S-plane and the z-plane relationship[176].

The S-plane is a rectangular coordinate system which the real part is expressed in horizontal axis, and imaginary part is expressed in vertical axis. Z-plane is isa polar form, where r is the distance to the origin, and the angle is measuredto the positive horizontal axis. Vertical lines in the S-plane are in circles in the Z-plane [176].

The properties of Z-transform, which give the ability to solve in linear digital systems the output responses with constant coefficients could briefly presented as linearity (Z-transform is a linear transform), shifting (ability to shift the sequence in time or other variable), convolution, time inversion, scaling and derivation [171, 175].

Z-transform is also referred by Manolakis et al. [177] as a different representation of a sequence. In [177] also presented the properties of Z-transform, that z-transform is a linear operator, the time could shifted in Z-transform, that the multiplying of two sequences is equivalent with the convolution of these two sequences.

Inverse Z transform of a function is defined as:

$$y(k) = Z^{-1}(Y(z)) \qquad (2.11)$$

where Z^{-1} is the operator of te inverse Z -transform[171].

Manolakis [177] refers that recovery of a sequence from its Z-transform could be also done by the formula:

$$x[k] = \frac{1}{2\pi j}\oint_C X(z)z^{k-1}\,dz \qquad (2.12)$$

Which involves the complex integration by residues method.

2.3.5. Methods and techniques of digital signal processing.

There are many techniques which are applied in digital signal processing. With these techniques the data are presented in an appropriate form to reveal the necessary information, in order to extract valuable conclusions. Literature presents many books that refer methods in digital signal processing [131, 171-174, 178-183]. Bilinear transform called the method used to convert the analogue signal into discrete digital and vice versa. During the implementation of the transformation a continuous sequence of data is transformed into discrete and finite data.

A signal could be expressed as a sum of sinusoid signals. This is the main idea of Fourier transform (FT). Fourier analysis presents all signals into a sum of sinusoidal components or complex exponential components. The characteristic of a signal in terms of time (continuous or discrete) or periodicity defines the form of its Fourier representation [177]. In FT any change or perturbation in coefficient affect the whole recording of the signal [37]. The determination of the signal from the spectrum and the reverse is presented below along with the exact mathematical equation. Discrete Fourier transform is the method of converting a sequence of data from the time domain to the frequency domain. The method converts a finite time series data or a sequence of numbers in a set of coefficients. These coefficients are combined arguments of sines which are determined by the frequency of each sample.

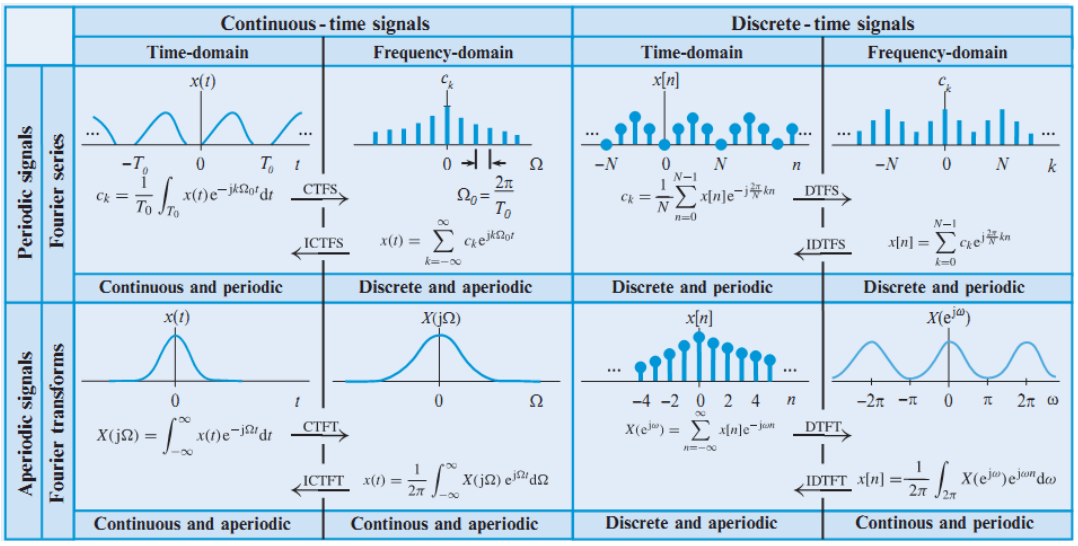

Figure 2.8. Fourier representation of signals [177]

Fourier transformation is one of the most basic components of digital signal processing. The main drawback is the high processing power required to implement in most cases. The discrete Fouriertransformation requires N^2 operations where N is the set of samples of the transformations. The fast Fourier transform contributes that turns the required volume of operations to a $N \log_2 N$ operations [184].

Tan [171] also refers efficiency of FFT algorithm for estimating the DFT coefficients and the minimization of computational complexity, highlighting that in a sequence with 1024 data points the DFT application would require 1024×1024=1.048.576 complex multiplications, instead of the FFT, which requires only (1024/2) $\log_2$ (1024) = 5120 complex multiplications. There are many ways-algorithms for calculating faster the Discrete Fourier Transform and they are called fast Fourier transforms (FFT). Some of themare Prime-factor FFT algorithm, Bruun's FFT algorithm, Rader's FFT algorithm, and Bluestein's FFT algorithmwith the most recognized the Cooley –Tukey algorithm.

Duhamel et al. [182] refers that Fourier transform along with linear filtering belong to the basic functions of digital signal processing. They indicate that convolution and discrete Fourier transform require high volume of operations in their direct computation (more specific on the order of N^2 with N the filter length of the size of the transform), highlighting that Cooley-Tukey FFT solves this complexity problem with the order of operations at $N \log_2 N$.

Z transform transforms a discrete value from the time domain to the frequency domain, a single value to a complex. This transform creates also the Z plane a domain in which the values represented as a complex number in a 2 dimensional plane. Like Z plane there is S plane which is created by Laplace transform on the initial data. This plane is a different presentation of Z transform (instead of a circle in horizontal and vertical direction). Windowed Fourier was first introduced by Gabor [185] for measuring the frequency variations of sound signals [186].

A symmetric and real window $h(t) = h(-t)$ has a dilation of a and a modulation of a frequency f:

$$h_{a,f}(t) = e^{ift} h(t - a) \qquad (2.13)$$

After normalization of $\|h\| = 1$, the $\|h_{a,f}\| = 1$ for any $(a, f) \in \mathbb{R}^2$.

The windowed Fourier transform result $b \in L^2(\mathbb{R})$:

$$Sb(a,f) \quad = \langle b, h_{a,f} \rangle = \int_{-\infty}^{+\infty} b(t)h(t-a)\, e^{-ift}dt \qquad (2.14)$$

The above transform defined as the short time Fourier transform. The term $h(t-a)$ integrate Fourier transform in the area of $t-a$. The energy density plot, called spectrogram, computes the energy of the function $b(t)$, at the specific time-frequency area (a,f) defined by the Heisenberg box $h_{a,f}$ as follows [186]:

$$P_s b(a,f) = |Sb(a,f)^2| = \left| \int_{-\infty}^{+\infty} b(t)h(t-a)e^{-ift}dt \right|^2 \qquad (2.15)$$

2.3.6. Filters in DSP

Filters in digital signal processing, have a crucial role. Filters limit the range of frequencies in the desired value, they form the signal phase, and generally they set the desired parameters in the digital signal. Manolakis [177] refers that filter as a term is used for linear time invariant systems which transform their input signals in a defined way. The digital filters have many characteristics that define them and their operation. Filters that determine the allowable frequencies are low pass, high pass, band-pass, band-stop, filters that strengthen or weaken frequencies bands in specific value. Filters that are able to change the phase of the input signal in a desired value (delay or proceed). Digital filters are divided in two main categories, finite impulse response (FIR) filters and Infinite impulse response (IIR) filters. FIR filters have a finite duration impulse response (after finite time they turn to zero). They do not contain internal feedback. The duration of the impulse response of an Nth order discrete time FIR filter is $N+1$ samples before it turn again to zero[177]. FIR filters are divided in continuous or discrete time. Also another one discrimination is according with the form of the signal they filter (analog or digital) [171]. FIR filter is a finite impulse response filter which is defined by the below equation:

$$y(k) = \sum_{n=0}^{M} a_n x(k-n) =$$

$$= a_0 x(k) + a_1 x(k-1) + a_2 x(k-2) + \cdots + a_k x(k-M) \qquad (2.16)$$

where a_n is the FIR filter coefficient and $M+1$ is the FIR filter length. The application of Z-transform in the above equation has the below result:

$$Y(z) = a_0 X(z) + a_1 z^{-1} X(z) + \ldots + a_k z^{-M} X(z) \qquad (2.17)$$

The factoring of $X(z)$ and its dividing in both sides leads to the transfer function which presents the FIR filter and is defined as [171]:

$$H(z) = \frac{Y(z)}{X(z)} = a_0 + a_1 z^{-1} + \ldots + a_k z^{-M} \quad (2.18)$$

2.3.7. Wavelets

Wavelet is a wave that its amplitude start from zero, increases to a maximum value and then reduces again to zero. The mean value of a wavelet is zero. A wavelet function $y(t)$ is a zero average function:

$$\int_{-\infty}^{+\infty} y(t)d(t) = 0 \quad (2.19)$$

Function $y(t)$ has dilation a and translation b:

$$y_{a,b}(t) = \frac{1}{\sqrt{a}} y\left(\frac{t-b}{a}\right) \quad (2.20)$$

In Fourier transform, the decomposition function is only a sinusoidal wave; in contrast with wavelet transform where in analogy with the signal characteristics, the basis function could have specific shape and form, from specific wavelet shape. In wavelet analysis the two fundamental components which define the basis function are the scale and translation.

Misiti et al., [187] refer for wavelets that is a relatively new signal processing tool which gives the ability of analysis of complex signals in many timescales and also is able to reveal non-stationary signals hidden in the initial data. In [187] the three main characteristics that make wavelets a powerful and high very efficient technique, summarizes as:

- Wavelets are able to be localized in time and frequency, at the same time, and supply a set of functions with dilate in scale and translate in time, thus wavelets are able to describe the characteristics of a signal in different timescales.
- Wavelets can estimate a function and de-noise a signal. They are able to reveal valuable information from a noisy signal. Each de-noising method is connected with specific wavelet representation. In a recorded signal, after wavelet transforms, the coefficient could change in order to reveal signal in contrast with noise, and again apply inverse transformation, in order to recover the initial signal de-noised.
- Wavelets are very efficient in compressing of data. The WT presents very sporadic the wavelet representations, such there is the ability for high condensation of the data.

Mother wavelet is the basis function used for wavelet transform. Misiti et al. [187] discuss the most common and well known families of wavelets, illustrating their aspects, similarities and differences among them. Authors refer that wavelets with orthogonal and biorthogonal shape, not only give the ability of discrete decomposition by FFT but also computed by their dedicated filters. The types of wavelet families are many and differ in properties. Some of the principal characteristics that determine the properties are the symmetry, the number of zero moments of wavelet function, the regularity, scaling function existence, orthogonality and/or biorthogonality and also computation convenience. Properties of wavelet families could be found in by Misiti et al. [187].

The simplest wavelet form is Haar wavelet. It was first proposed by Alfred Haar [188] where he presented square functions which could be dilated and translated, in order to generate orthonormal basis of $L^2(\mathbb{R})$. It is not continuous and such not differentiable. Haar mother wavelet $y(t)$is described by:

$$y(t) = \begin{cases} 1 & 0 \le t < 1/2 \\ -1 & 1/2 \le t < 1 \\ 0 & \text{anywhere else} \end{cases}$$

Morlet wavelet is a complex mother wavelet created by the modulation of Gaussian function [189] and defined as:

$$z(t) = e^{j\omega_0 t} e^{\frac{-\beta^2 t^2}{2}} \qquad (2.21)$$

Daubechies wavelets are defined with an N order (dbN wavelet) [190]. They have the highest number A of vanishing moments, for specific width $N=2A$. For db1 is the Haar wavelet. Symlets were proposed by Daubechies and are a modification of dbN with high symmetry. Coiflets wavelets have $2N$ zero moments and its scaling function has $2n\text{-}1$ zero moments with integral value to 1. Morlet et al. [191, 192] introduced wavelet transform in order to process and estimate earthquake data, in the early eighties. All these years many types and applications of wavelet transforms have been applied and developed. Discrete wavelets transform (DWT) and integral wavelets transform (IWT) are some very popular applications. Wavelet transform could be defined as the convolution of a signal $f(t)$ with a wavelet or a mother wavelet signal $z(t)$. The equation of the continuous wavelet transform of the$f(t)$:

$$(Wf)(a,b) = \frac{1}{\sqrt{a}} \int_{-\infty}^{+\infty} f(t) z\left(\frac{t-b}{a}\right) dt \qquad (2.22)$$

Where a is the dilation and b the translation parameters [189].

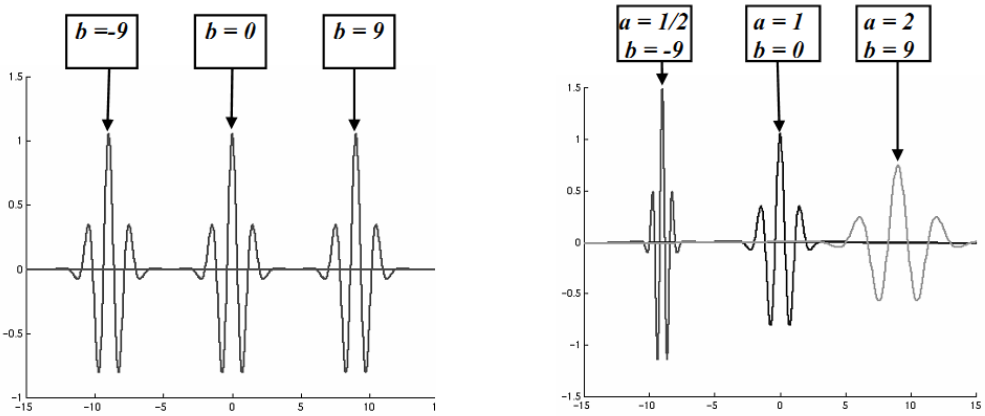

Figure 2.9. Wavelet translation (left) and dilation with translation (right) [187]

Kim and Melhem [9] state that wavelet analysis presents much more information and details for signals non-stationary compared with the traditional Fourier analysis.

The signal to which wavelet analysis is separated into two signals A1 and D1. This is the decomposition stage. In this stage A1 is the term approximation signal, showing the low part of frequencies while the term D1 is the term of the detail of the signal showing the high part of the frequencies in this range. At each decomposition data length is halved. This process continues for the other decays to A2 A3 D2 D3 etc. In wavelet analysis the details appear in the low levels which have the high frequency while approximations appear in the high level where it presents the low frequency of the signal [193]. Reconstruction of the decomposed signal becomes in the same number of levels as decomposition. Data from approximation coefficient of the last level of decomposition sampled and then filtered with a low pass filter. Also data from the details coefficient of the last level decomposition sampled and filtered. Transfer functions of low and high pass filters create the appropriate conditions for reconstruction of the signal. These filters are called absolute filters when they have the ability to reconstruct the signal in its original form[193].

2.3.8. Summary of DSP methods literature

Summarizing on the literature review of DSP methods it is observed that there is no DSP method that is able to function effectively alone (in terms of revealing valuable information from damage sensitive parameters) for structural health monitoring. Every DSP method is able to support specific characteristics from a signal. In order to detect, de-noise and further

study an acceleration recording in a building (thesis case study) it is required to apply a combination of DSP methods. By this way the advantages of each method will overcome the disadvantages of other DSP methods.

2.4. Conclusions of literature review

From the literature review in structural health monitoring, in wired and wireless SHM systems and in Digital Signal Processing, it is apparent that there are limitations in designing effective SHM. In order to improve SHM performance and contribute to a better understanding of SHM in urban areas, these limitations were addressed in above sections 2.1, 2.2 and 2.3, and below there are specific quidelines for study. These parameters are referred in SHM system networks, in damage detection, on presentation of increased building vulnerability and in combined algorithms for effective (fast and computational efficient) SHM. The parameters that are going to be evaluated and developed in this thesis are:

- Low cost SHM wireless SHM network in a metropolitan scale. A novel SHM network is going to be developed, programmed, and installed in a metropolitan scale, able to monitor the strong motion seismic acceleration of buildings under study.
- Very high sensitivity wired SHM network implemented in specific concrete buildings (same designed code RC buildings but of different age). This network will be able to monitor continuously from extremely low seismic and ambient excitation until strong motion , in order to compute statistically the effect of vibrations in real structures and the changes that may introduced by time.
- Application of a simple but powerful index that will not compute only the change of the fundamental frequency in a structure but also the total deviation of this change. In other words this index will penalize (in damage terms) the range of Freq. dispersion for damage detection.
- Application of a simple but powerful method, used widely for site amplification, in SHM in order to produce a novel index for structural vulnerability which will connect this index with vulnerability of building (HVSR analysis).
- Combination of several DSP techniques (non-parametric and parametric methods) with application in real structures, for low magnitude earthquake data for a long time period, in order to reveal the specific requirements of real buildings (and not laboratory models). Also the creation of an algorithm that will be able to extract information for structural integrity of real world structures.

Chapter 3. Design of a hybrid wired and wireless SHM network.

3.1 Wired stations

3.1.1 Introduction

This chapter deals with the deployment of this study, presenting in detail instrumentation and its specifications. Seismographs and accelerometers are nessecary in earthquake engineering technology [45]. Wired and wireless accelerometers are applied, tested and combined in order to study both advantages and disadvantages and establish a network which will be able for efficient and economical SHM.

3.1.2 Case study infrastructures

Case study includes two different university buildings, which are attached to each other on one side. They have different construction material, and different year of construction. In more detail, the two buildings host the Chania branch of the Technological Institute of Crete. Building (A) is built on the west side in 1995, with concrete, glass and steel, while building (B) is built on the east side in 2007 with concrete. Table 1, presents characteristics for both buildings, and figure 3.1 illustrates schematic diagram of the two buildings, showing the sensor's location. On each building, one accelerometer is deployed-located on each of the three floors. The structures are located in Chania, Crete, Hellas a region characterized by high seismicity (figure 3.1). Figure 3.2 presents the old and the new building and figure 3.3 the plan of both buildings.

Building Code	Age (years)	Size(m)	Shape (Direction)	Floor height	Number of rooms	Number of floors
A	19	30,62×18,03	Rectangle (NS)	3.65	7	4
		11.29×43.30	Rectangle (EW)	3.65	5	4
B	7	51.55×21.85	Rectangle (NS)	3.67	15	4

Table 3.1. Characteristics of the Technological Institute buildings at Chania

Sensors recorded data at various instances throughout a day, in order to study the effect of human activity during day and night.

Figure 3.1. Location of Technological Educational Institute of Crete at the city of Chania (35°31'9.30"N, 24° 2'34.35"E) [194]

Figure 3.2. The old (left) and new (right) building of Technological Educational Institute of Crete at the city of Chania

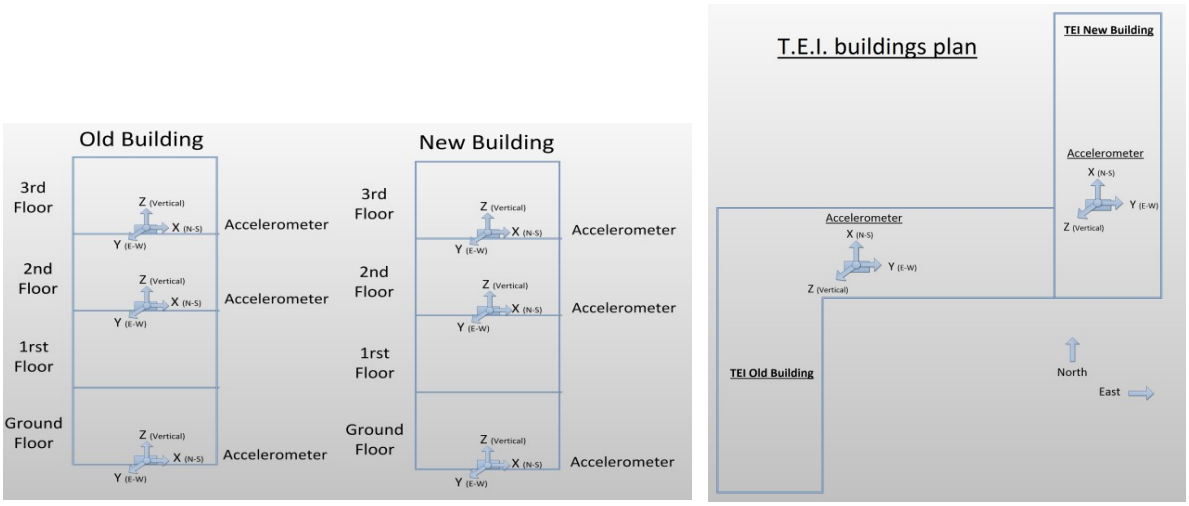

Figure 3.3. (Left) Schematic diagram of the wired SHM deployment in the old and new building, (right) Schematic plan of the TEI buildings at Chania. The location of the sensors is presented on each building.

3.1.3 Define the best placement of accelerometers

The selection and placement of each accelerometer in a structure is critical. In order a measurement to be effective, the location of the accelerometers should be in specific places of a structure, able to record the dynamic response of a building under seismic force [166, 195-197]. Optimal sensor placement is presented by Yi et al., [82, 84] using multiple methods, propose an algorithm for the optimal sensor location for SHM in a structure. Huang et al. [198] discuss the available instrumentation models in order the system to be able to record the ground motion, the building basement motion, the lateral and torsional floor motion.

In order to determine the best place on the deployment, Power Spectral Densities (PSDs) of acceleration recordings were studied at various positions in order to identify where the primary frequencies are monitored is a clearly way. The symmetric points of the buildings were avoided and the sensors were finally placed at key points such joints of floor plates and joints of plate beams with columns. Measurements on the highest floors of the buildings, found to be absolutely necessary. Generally natural frequencies and damping ratio of a structure are global properties, without any variation along a structure [69, 199]. These parameters can be computed from any, frequency response recording, on the structure, except the locations in which the amplitude of mode shapes is presented on the lowest value.

3.1.4 Technical Characteristics and specifications of the wired SHM system

The accelerometers of wired SHM netwrok are 24 bit strong motion accelerographs (model 130 SMA by Reftek) [200].

The sampling frequency band of the accelerometers has been programmed at 125 Hz, in order to be able to present the frequency spectrum (up to 60 Hz) of the seismic acceleration of the case study buildings and such reveal the energy distribution across the frequency spectrum [153]. The majority of the structures have primary frequencies below 10 Hz. Higher frequency represents extremely high stiffness. Nyquist theorem increases the sampling rate at least to the double. Also in order to reduce the effect of noise there is the need to multiply the sampling frequency with an average number X, where this number will indicate how much the noise will be decreased (with a factor of the square root of X).

The duration of each measurement has been programmed to last 90 seconds. The pre-triggering time is 30 seconds and measurement is completed 60 seconds after the first triggering. This time allocation is able to present the whole seismic acceleration response of the buildings.

To reduce the total volume of recorded data, the system is triggered, only if the acceleration signal is higher than the threshold of the 200 μG. Thus acceleration due to earthquake activity or manmade strong accelerations is being recorded. The SHM provides the acceleration data in real time mode.

Each measurement point is synchronized with the other ones and the central data server by GPS. Every node synchronizes with the others nodes and the central data server with external GPS with accuracy +-10 μsec (with GPS locked). Also the power supply has high redundancy using 220 V power supply and a transformer which also charges a 12 V 65 A battery. Each node is able to measure and collect data with the battery for more than 4 days. The communication with the central data server is by Ethernet cable (IP protocol). The accelerometers are 24 bit. At the central data server, runs RTPD software where the network recordings are collected in real time. SMA 130 has an operating power consumption of 2W which can reach 3W (with input voltage 12 V) that imposes the use of battery charger and reveal low autonomy.

The A/D converter is 24 bit resolution and the sample rates vary from 1 Hz up to 1000 Hz (with the chosen sample rate in the experiment to be 125 Hz). The communication is

established by ethernet cable. The triggering is in Level type. The SMA130 has the ability to measure from 100 μG up to 4 G. In the specific experiment the measurement level is selected 200 μG for every node. The sensitivity of the internal accelerometer is at 2.5 V/g which is very high and accurate with linearity up to 0.03% at full scale. The above technical specifications of 130 SMA reveal a sensor recorder that has high fidelity and accuracy but its installation is not cost, time, space efficient and effective for SHM. Conclusively the case study wired structural health monitoring system has high accuracy and reliability, but the main disadvantage is the low scalability due to high cost and the low autonomy.

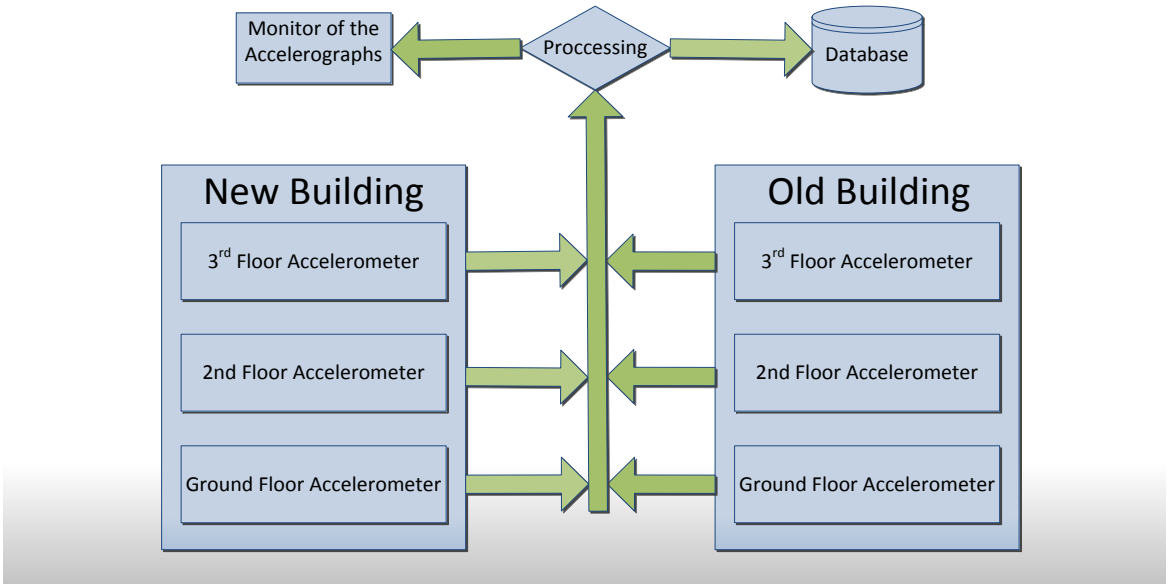

Figure 3.4. Schematic diagram of the wired SHM deployment in the old and new building

Figure 3.4 present the schematic diagram of the wired SHM network. In order to measure ambient noise the system should be able to record accelerations less than 1 mg [139]. Measurements present that the level of 100-150 μG is the minimum threshold where there is cut off of the environmental noise on the specific structures. The system is able to record very low level earthquake acceleration signals. The amount of transmitted data has been greatly reduced, with trigger mode recording. Control of the accelerometer stations is achieved by the RTCC program [200]. Figure 3.5 presents the data flow of the wired SHM network and figure 3.6 presents the RTCC display.

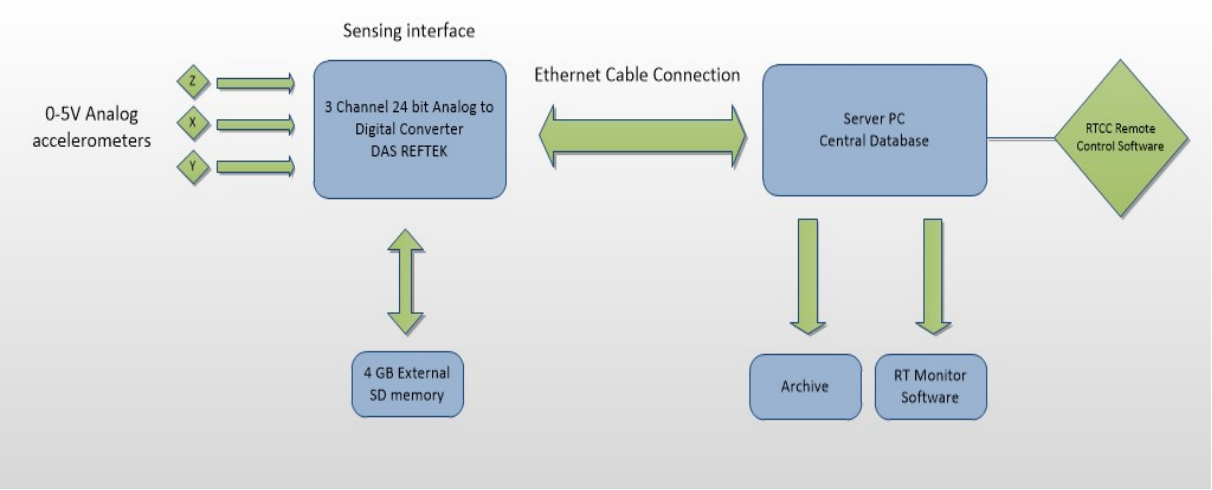

Figure 3.5. Schematic diagram of the SHM system data flow

Das Discovery Page (RTCC version - 13JUN2007)

Host IP address: 127.0.0.1 | Host PORT address: 2543 | Connection type: Rtpd | DAS-DISCOVERY

DasId	Host	Port	Type	Action
9F8E(3ORN)	127.0.0.1	2543	Rtpd	Status/Control Parameters Remove From List (ID)
A388(YPGN)	127.0.0.1	2543	Rtpd	Status/Control Parameters Remove From List (ID)
A389(2ORN)	127.0.0.1	2543	Rtpd	Status/Control Parameters Remove From List (ID)
A390(YPGP)	127.0.0.1	2543	Rtpd	Status/Control Parameters Remove From List (ID)
A391(1ORP)	127.0.0.1	2543	Rtpd	Status/Control Parameters Remove From List (ID)
A392(2OFP)	127.0.0.1	2543	Rtpd	Status/Control Parameters Remove From List (ID)
A763(ORFS)	127.0.0.1	2543	Rtpd	Status/Control Parameters Remove From List (ID)

Figure 3.6. RTCC Display presents the characteristics of each remote wired accelerometer.

3.1.5 Acceleration recordings from the wired SHM network on both buildings

The experimental wired SHM set-up is able to record acceleration on both buildings caused from natural hazards (i.e. seismic activity), weather conditions (wind gusts) and manmade activity (explosion type). Below there is detailed analysis of these recordings in order to reveal and present the recording abilities of the experimental wired SHM system.

3.1.6 Seismic activity

Figure 3.7 presents the epicenter of the earthquake that occurred at 06:11:32 UTC on 10/12/2012 16 km northwest from the buildings in Chania.

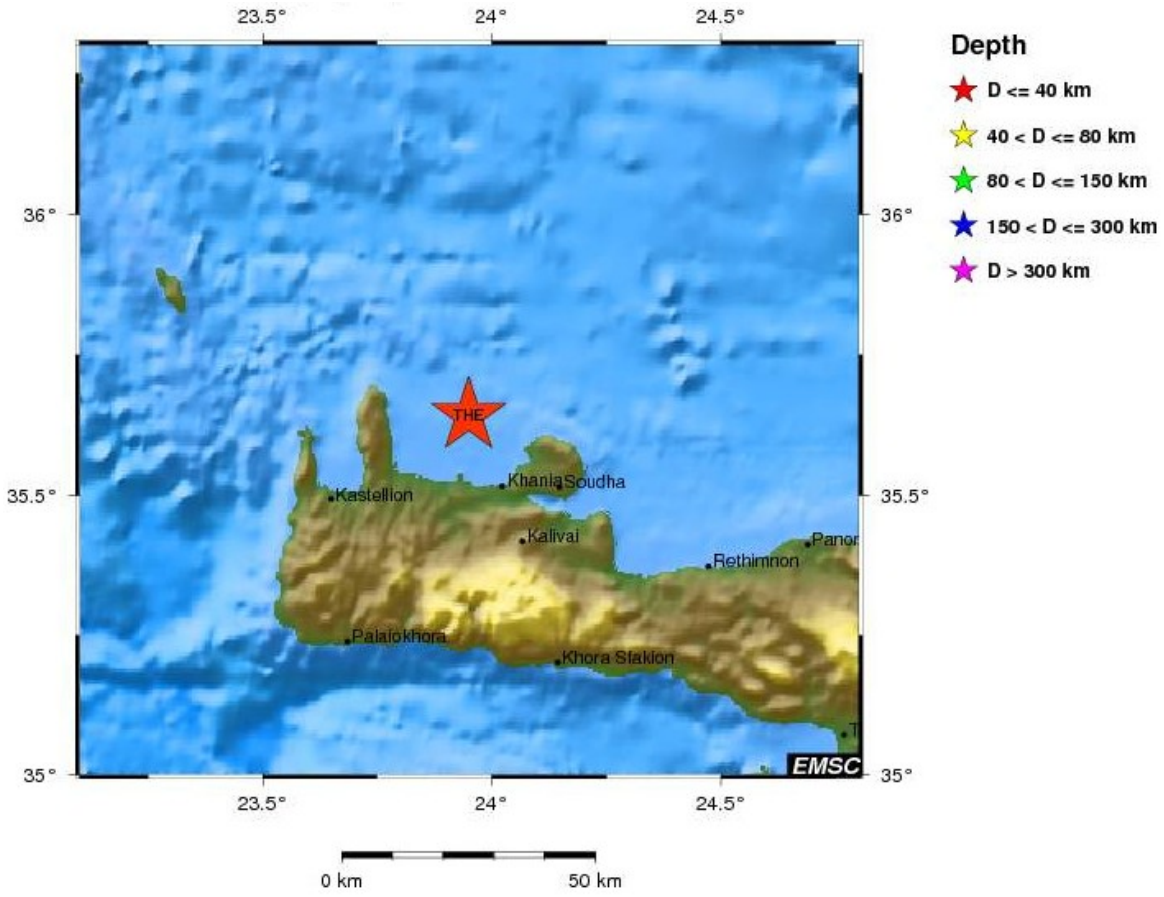

Figure 3.7. Epicenter of the earthquake with magnitude M 2.3 that occurred on 10/12/2012 at 06:11:32 UTC 16 km Northwest from the city of Chania [201]

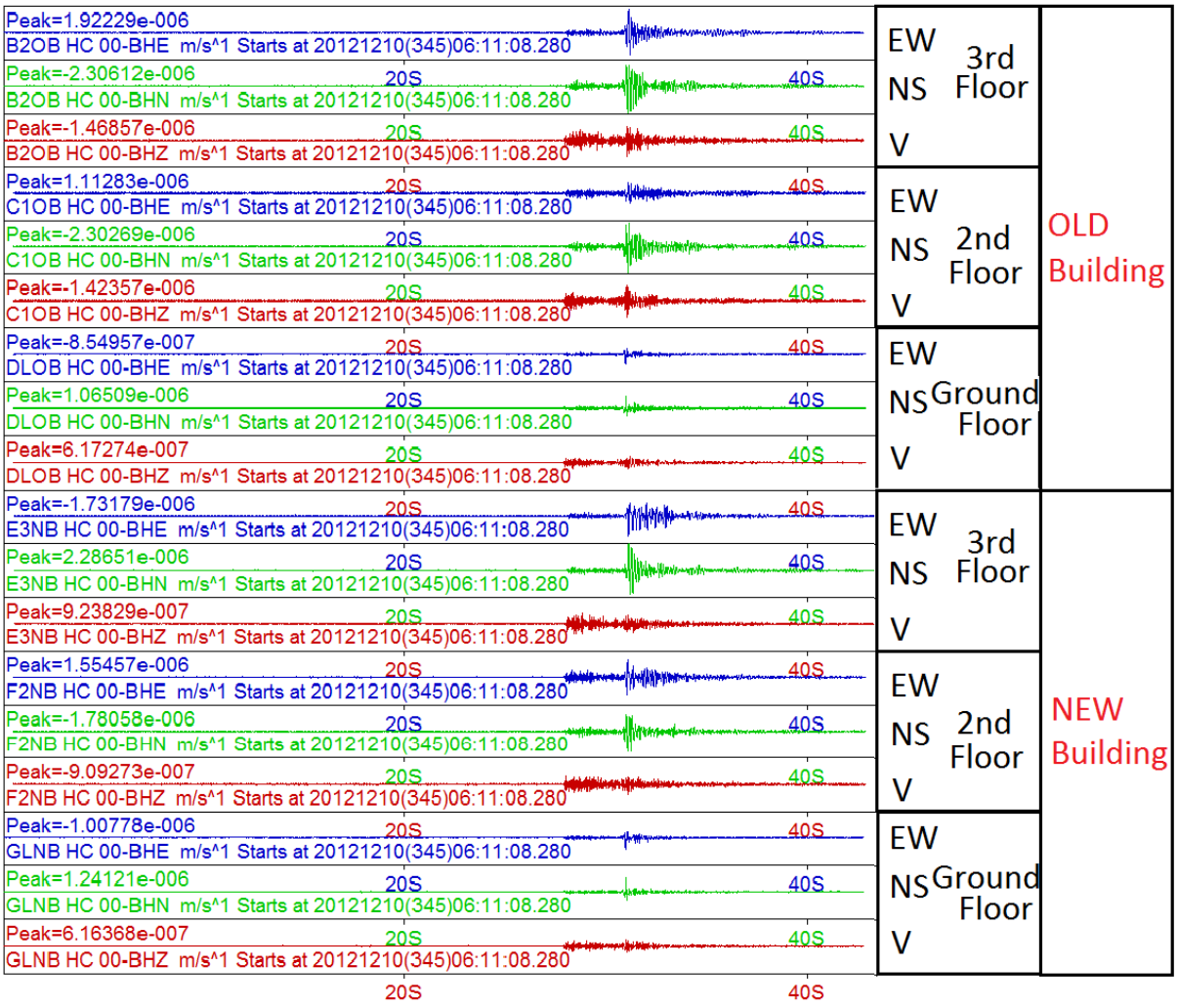

Figure 3.8. Recordings of the earthquake with magnitude M 2.3 that occurred on 10/12/2012 at 06:11:32 UTC 16 km Northwest from the city of Chania, from the accelerographs of the wired SHMs

Figure 3.8 presents the recordings from the accelerographs for this. It is obvious that seismic acceleration has higher amplitude for the higher floors. Also the seismic acceleration amplitude is almost the same for the new and the old building, for each floor respectively. The direction of the earthquake can be revealed from the analysis of amplitude on recordings (the north-south component has higher amplitude than the east-west). The vertical recordings have lower amplitude from other two components. Figures 3.9 and 3.10 present the PSD created by FFT from the accelerographs of the new and the old building for the event. The PSDs reveal that the principle frequency responses of the new and the old building, are almost the same, and around 7-8 Hz (the primary frequency response of both buildings with the higher amplitude), for all components (Vertical, NS and EW).

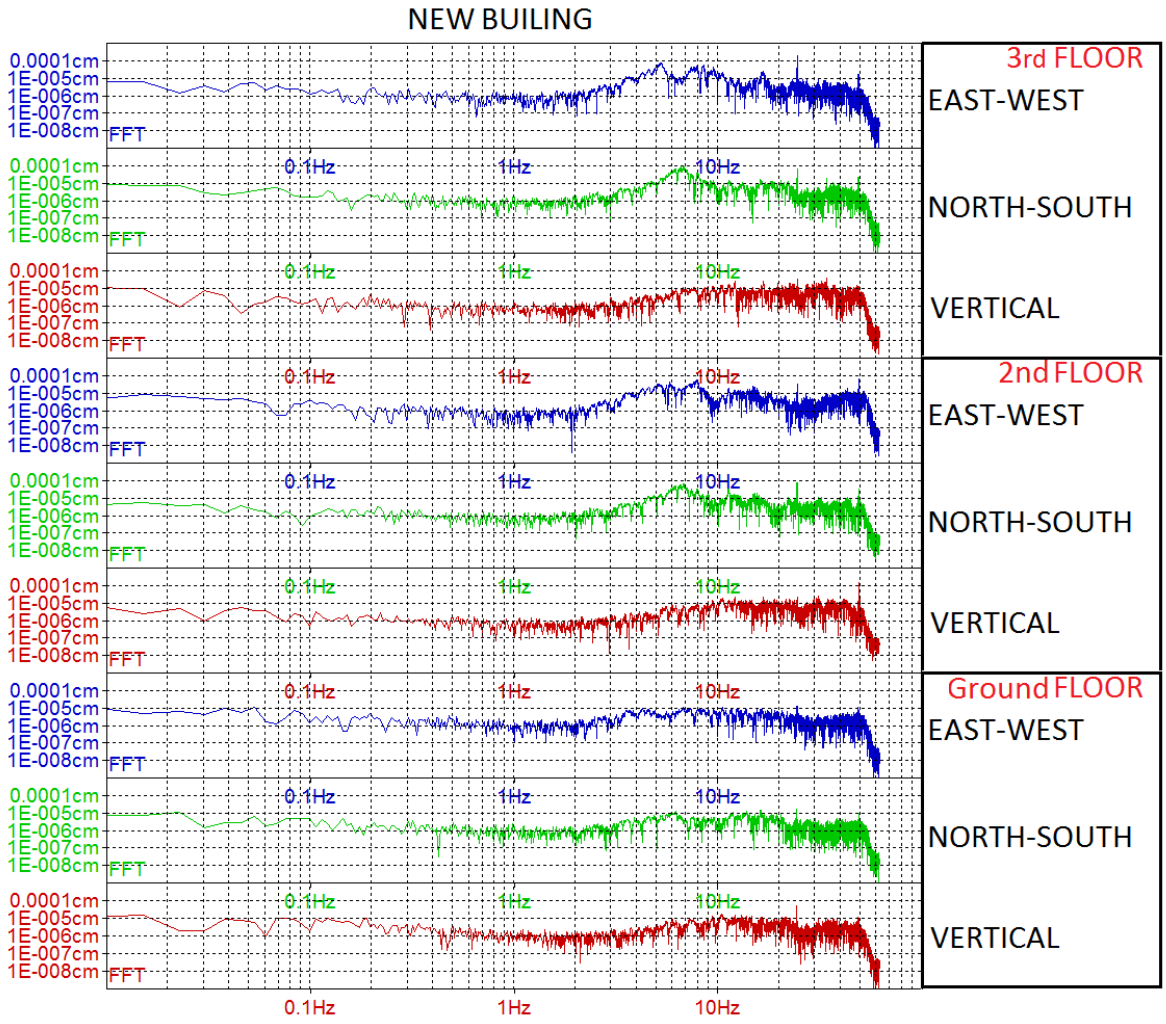

Figure 3.9. Fast Fourier Transform on new building of the earthquake with magnitude M 2.3 that occurred on 10/12/2012 at 06:11:32 UTC

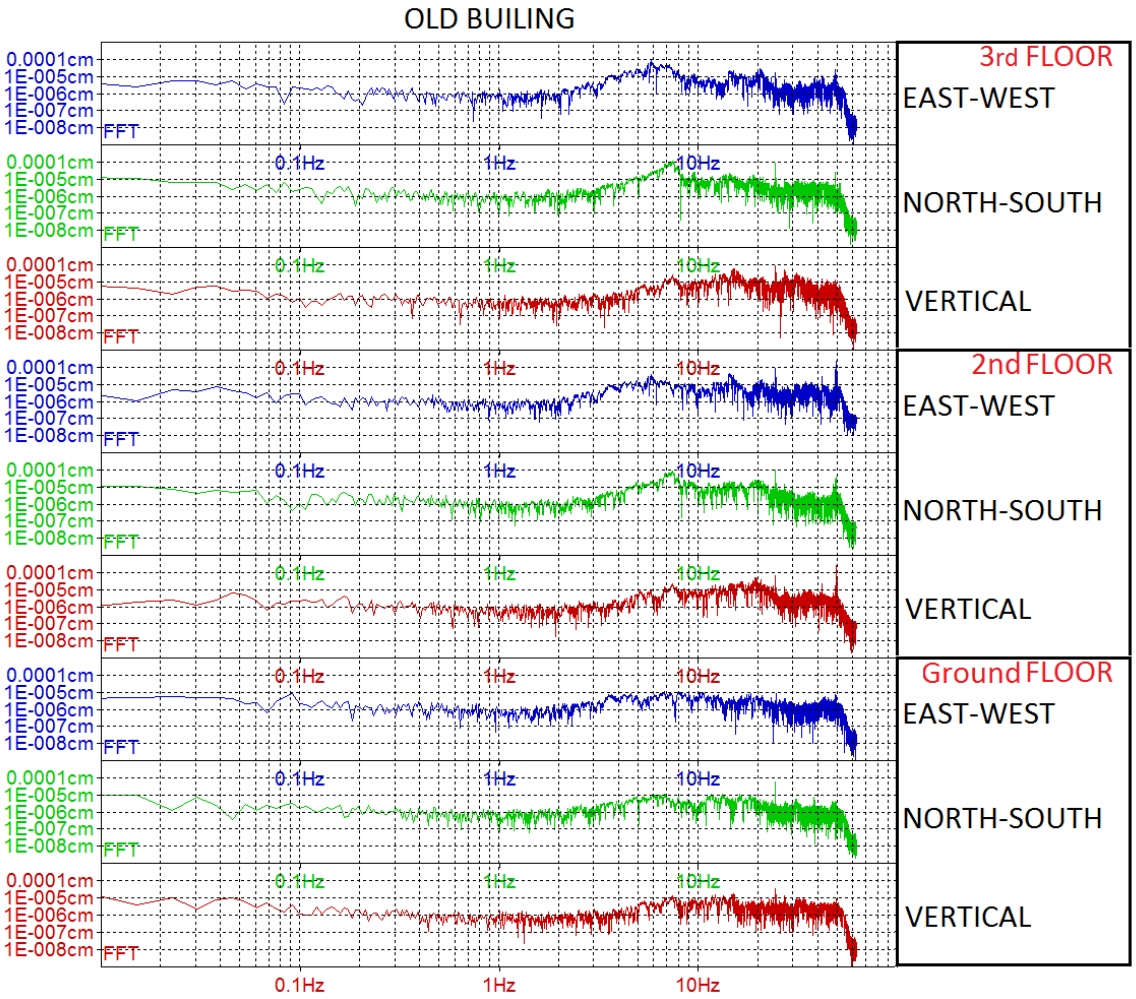

Figure 3.10. Fast Fourier Transform on old building of the earthquake with magnitude M 2.3 that occurred on 10/12/2012 at 06:11:32 UTC

3.1.7 Strong wind activity

On 08/11/2012 at the town of Chania very strong winds were observed on the broad area. The wind gusts blew from north direction with average strength of 8 Beaufort scale. The gusts of wind acting on the building reached up to 10 Beaufort scale. Acceleration recordings (under wind gusts excitation) at the old and the new building of TEI have been recorded and analyzed.

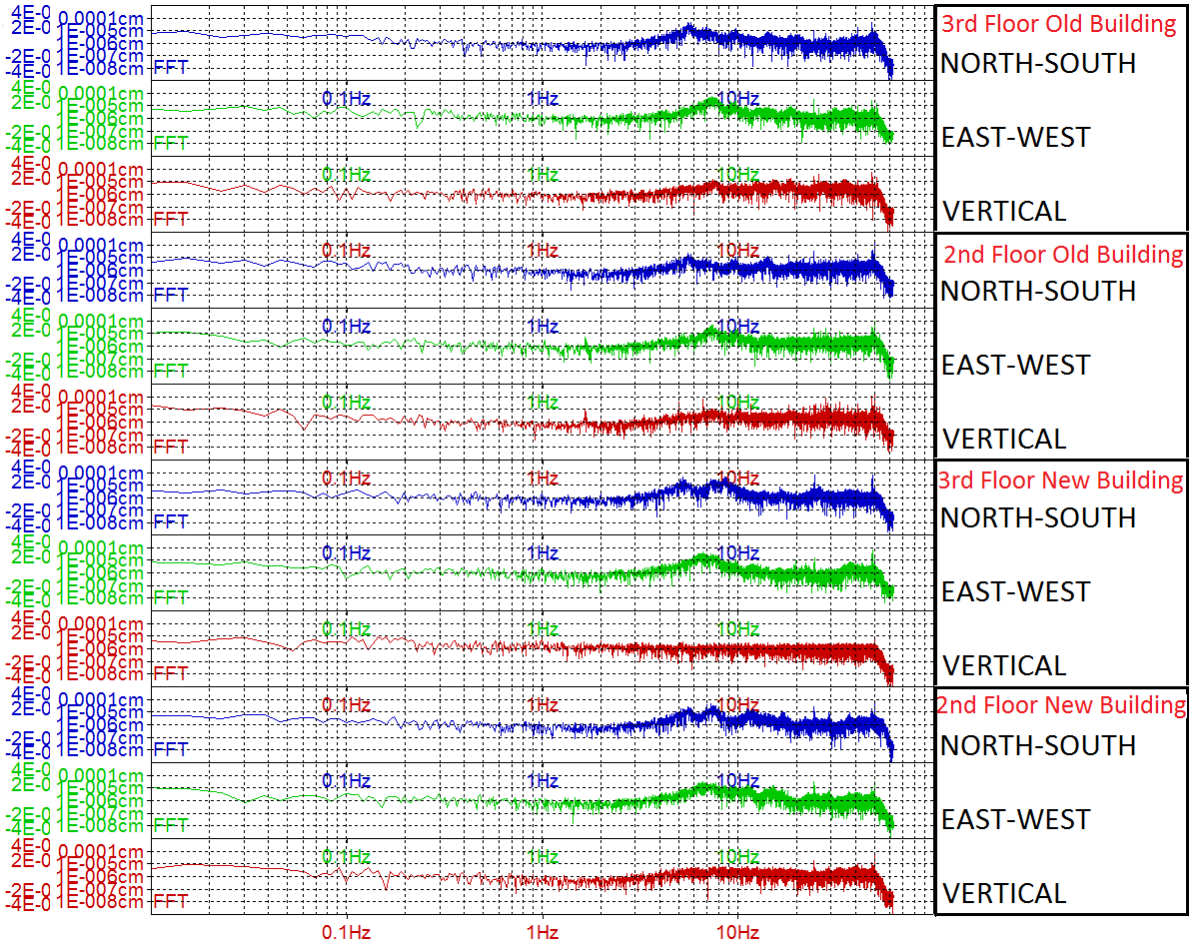

Figure 3.11. FFT from the acceleration recordings to the old and new building (3rd and 2nd floors) under the affect of strong wind gusts on 8 November 2012

These wind gusts affected mainly the upper floors as expected (only 3rd floor of new and old building, and sometimes the 2nd floor). The amplitude in 3rd floor was higher than the 2nd. In figure 3.12 the top three recordings present the acceleration component (vertical, NS, EW, respectively) of the third floor of the new building, the next three those of the second floor of the new building, the next three recordings present again the accelerations of the second floor of the old building and the bottom three of the third floor of the old building.

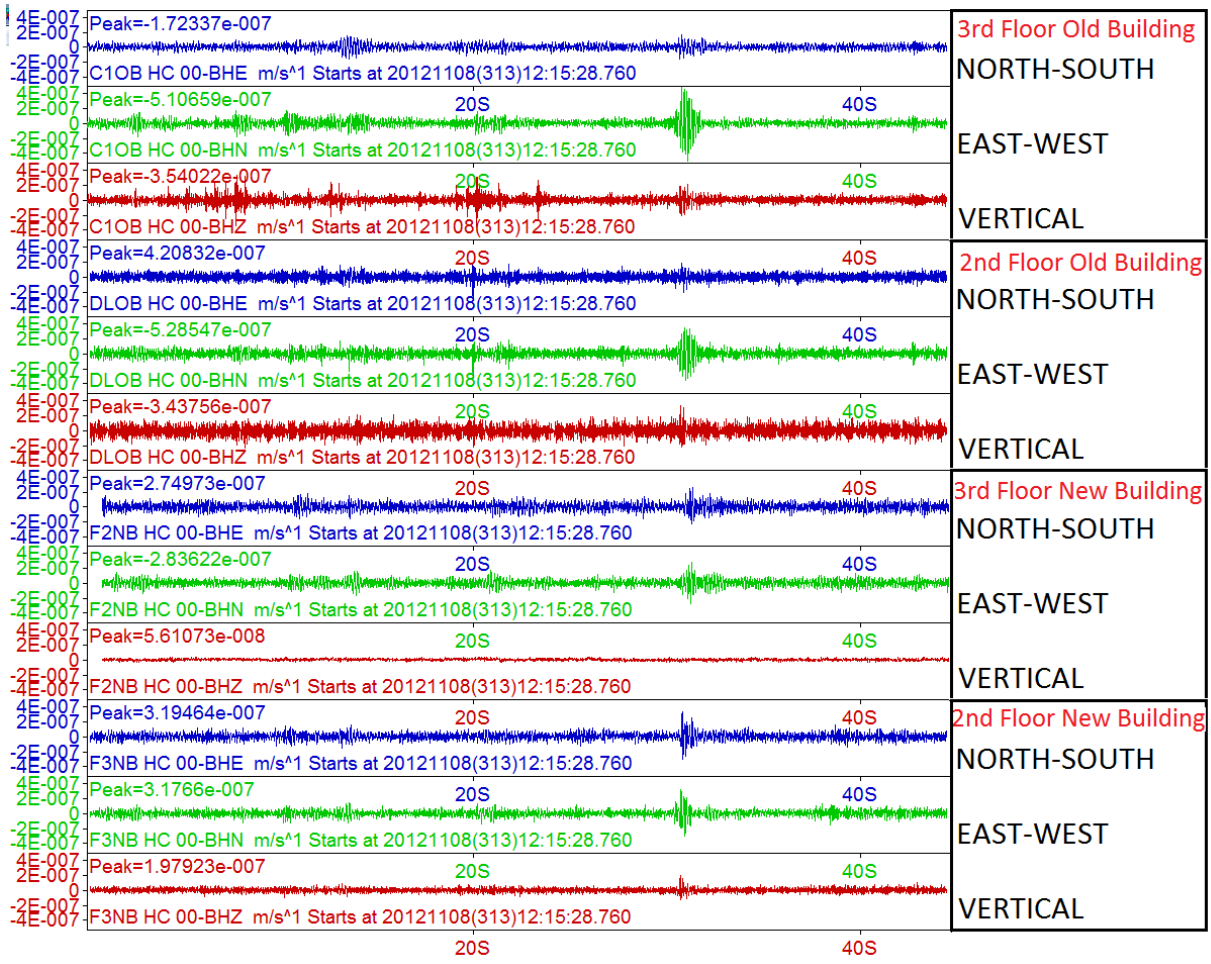

Figure 3.12. Acceleration recordings to the old and new building (3rd and 2nd floors) under the affect of strong wind gusts on 8 November 2012

3.1.8 Manmade activity

An unknown manmade activity of explosion type was recorded in the broad region of city of Chania on 26th of September 2012, 10:00 UTC. This activity affected strongly the two buildings of TEI of Crete at Chania. The manmade activity generated structural vibrations with frequencies up to 50 Hz with high amplitude in contrast to earthquakes and strong wind which generated shaking of the old building with frequencies up to 7, 8 or 9 Hz. That period is hadn't been deployed yet the accelerometers in the new building, thus there isn't any recording for the new building.

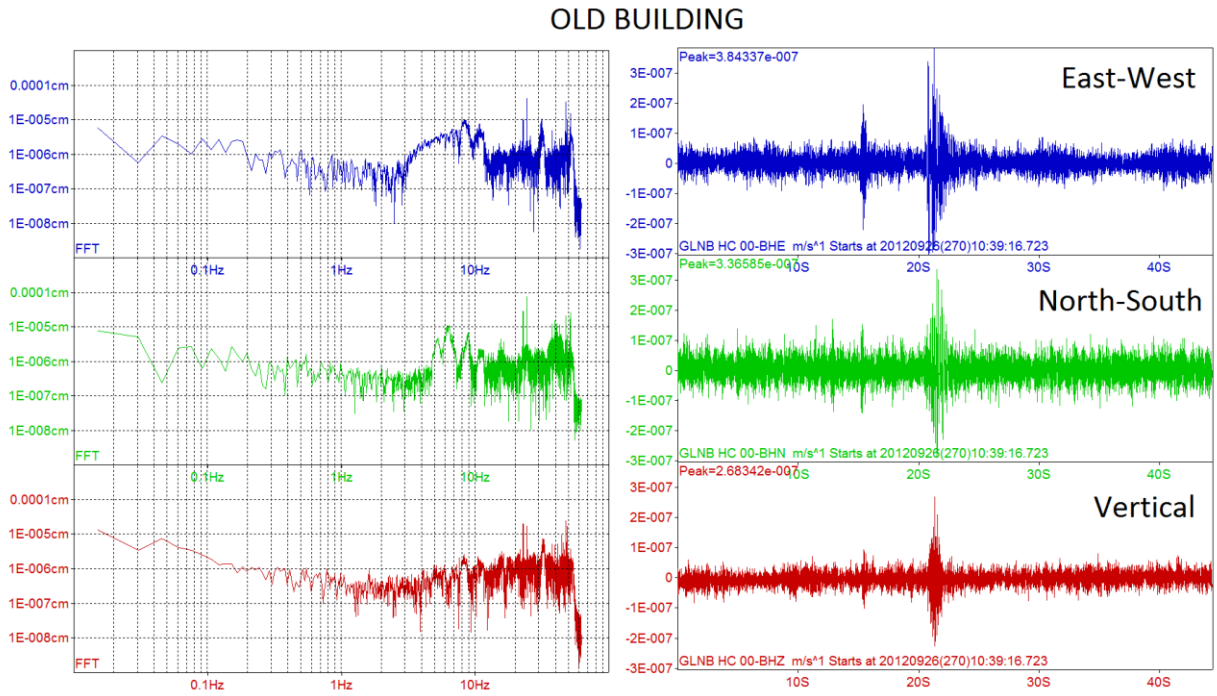

Figure 3.13. FFT from the manmade event (explosion type) on 26 September 2012 10:40 UTC 20 km north from city of Chania Crete recorded from the third floor of the old building of TEI.

3.1.9 Results from the correlation of wired SHM recordings in two buildings

By comparing the accelerations in the old and the new building of TEI it is observed similar behavior for both buildings for the respective floors. The same holds for small magnitude earthquakes (up to 4 on the Richter scale). The manmade activity (explosion type) created high amplitudes in the area of 8 Hz but also in 25 Hz and 50 Hz, and a different spectral frequency density on the old structure, than the earthquake and the wind affection. The earthquake activity created a primary frequency response around the frequency of 7-8 Hz for the floors, almost similar with the wind gusts response, and the rest of the frequency spectrum remains with low amplitude. The experimental results show that wired SHM system is able to record with high accuracy and sensitivity enviromental and artificial accelerations that affect both case study buildings.

3.2 Wireless Structural Health Monitoring Stations (wSHMs)

3.2.1 Introduction

There is a long list of efforts to develop wireless Structural Health Monitoring systems in order to monitor the structural condition of buildings [68, 83, 102, 105, 133, 144, 168, 202,

203]. The large scale implementation cost of SHM systems (many buildings in a metropolitan area) is quite high, even for wireless systems, and this is a significant drawback to overcome. On the other hand, there is an increasing demand for monitoring the structural health of buildings in order to maximize safety and security in the cities, especially at earthquake prone areas [102, 130, 133-138]. SHM systems are installed on bridges, highways, special structures and buildings in order to improve the capacity of damage detection. Although the cost of monitoring with wireless SHM systems is much lower than that of the wired ones, it still remains too high for the overall instrumentation necessary to cover many buildings [25, 28, 102, 139-142]. Literature depicts that this trend will continue rising in the future [25, 26, 28]. In this part of the study it is presented a wireless sensor network, fast to install, more economical (concerning the application on many buildings) than the majority of wireless SHM systems and much more efficient than conventional wired SHM systems in terms of cost, installation, size, number of sensors, and ease of use.

3.2.2 Key-Features of wSHMs

Key-features for wireless monitoring of the structural condition, and thus the structural safety, of buildings are the autonomy and continuous/real-time operation, the wireless connectivity of remote nodes to the central node, data rate and resolution and the whole system cost. Below it is discussed in detail these key-features, presenting the parameterization of the proposed system along with solutions to problems that arise.

3.2.3 Autonomy of a wireless SHM system

Autonomy is a very important aspect as it determines the capability of the system to operate continuously for a long time, in the absence of an external power supply [141, 157-160]. In particular, wireless systems is not expected to connect to external power supply, thus high autonomy can be achieved mainly by low power design of the system [157-159]. In terms of autonomy, the design principles followed for the wSHMs were:

System configured with low power consumption modules concerning both operating and idle state.

Data communication protocol with low power consumption (XBee protocol has been selected against other much more intensive protocols e.g., WiFi protocol).

Triggered recording (trigger mode) in order to consume energy only when the acceleration is above a certain threshold.

Optional power harvesting adaptive to the specific application environment. Taking into account that in most cases, the systems will be installed within buildings, it has been chosen constant feedback and battery charging using the powering of each building. Furthermore, overload battery protection is present to protect the batteries and prolong their lifetime.

3.2.4 Data transmission & synchornization

Data transmission and synchronization is a key-issue in wireless sensor networks [134, 140, 144, 151, 161-163, 204]. For reliable structural health monitoring, the network gateway must collect acceleration data wirelessly from several points of the structure without any loses or conflicts. Moreover, synchronized data is a requirement of great importance in order to be able to analyze them effectively to produce structure models for fault estimation [13, 52, 125]. Two basic principles have been adopted to achieve reliable data transfer and maximum synchronization of wireless nodes:

The transmitters from wireless nodes should send data with specific transmittion power amplitude, related with the distance between nodes, in order to reach the central node (which collects all the data) without any data loss.

The wireless SHM system should record real time synchronized data. Thus, when there is excitation, its microprocessor sends the data through the transmitter to the network gateway attached to the local microcomputer. The latter synchronizes its clock through GPS and performs data stamping with UTC time labels to each line of data records (figure 3.14). Data are sent to gateway as arrays with specific sampling rate. Such for the same local time there is a number of data from each Waspmote to the gateway. Central PC program stamps these data with the same time. Every one second there are totally 40 recordings (40 Hz sampling rate).

LOCAL TIME	Waspmote ID	N-S	E-W	Vertical
2014.02.26 08:24:40.562	BC	-3	-12	1046
2014.02.26 08:24:40.625	BC	-1	-13	1041
2014.02.26 08:24:40.640	BC	-5	-16	1043
2014.02.26 08:24:40.671	BC	0	-6	1038
2014.02.26 08:24:40.703	BC	0	-11	1038
2014.02.26 08:24:40.718	BC	0	-13	1041
2014.02.26 08:24:40.750	BC	1	-14	1042
2014.02.26 08:24:40.812	BC	-1	-11	1040

LOCAL TIME	Waspmote ID	N-S	E-W	Vertical
2014.07.24 12:10:17.109	C3	16	-8	1024
2014.07.24 12:10:17.171	C3	18	-8	1024
2014.07.24 12:10:17.234	C3	19	-2	1027
2014.07.24 12:10:17.296	C3	15	0	1024
2014.07.24 12:10:17.359	C3	23	-2	1023
2014.07.24 12:10:17.389	C3	22	-3	1024
2014.07.24 12:10:17.402	C3	14	-4	1019
2014.07.24 12:10:17.421	C3	18	0	1027

LOCAL TIME	Waspmote ID	N-S	E-W	Vertical
2014.08.14 12:30:44.877	C9	55	-6	1016
2014.08.14 12:30:44.803	C9	76	-16	1012
2014.08.14 12:30:44.939	C9	58	-4	1035
2014.08.14 12:30:44.969	C9	0	-73	1044
2014.08.14 12:30:45.002	C9	16	-83	1039
2014.08.14 12:30:45.032	C9	58	-61	1032
2014.08.14 12:30:45.064	C9	38	-21	1001
2014.08.14 12:30:45.127	C9	83	86	996

Figure 3.14. Time stamping of the acceleration data in the main computer

3.2.5 Data rate and resolution

To reveal all the resonance frequencies of the monitoring structures, high quality acceleration recordings must have adequate frequency range [83, 88, 101, 108, 152, 160, 166, 167]. High data rate ensures recording of high frequency accelerations of the structure, and also many samples before completeattenuation of the seismic response of a building. Structural response is reflected in a band of frequencies. Nevertheless, many authors refer that commercial wireless SHM systems still depict low levels of acceleration response, identification of modal shapes and analysis [26, 101]. Consequently, data rate and resolution principles for the proposed wSHMs are as follows:

a) Sampling rate should be able to reveal all the fundamental acceleration frequencies of a structure subject to earthquake or anthropogenic shaking.

b) Low trigger threshold in order the system to be sensitive in strong but also weak motion (acceleration) of the building.

c) Adequate recording time-window to record the complete seismic or man-made excitation. If the duration of the acceleration event is longer than the nominal time-window, then the recording time should be extended.

d) Sampling rate and sensitivity threshold of the system should be programmable, in order to be determined according to specific building characteristics (attenuation, stiffness etc).

3.2.6 Cost of implementation on metropolitan scale

The economic cost of a SHM system widely deployed on a metropolitan scale becomes a fundamental parameter. On the other hand, existing robust SHM systems featuring great sensitivity and reliability have prohibitive cost for multiple implementations. Thus, there is a crucial trade-off between wSHMs's effectiveness and cost saving. Consequently, a system optimization to attain the highest possible measurement quality at the lowest possible implementation cost has been performed. This enabled the pilot implementation of wSHMs in two neighboring buildings, which demonstrates its feasibility to implement it on metropolitan scale, at relatively tolerable cost.

Cost-saving principles followed:

a) Low-cost accelerometer

b) Low-cost wireless platforms

c) Low-cost operating system

d) Exploit existing internet connections.

3.2.7 Sensor Platform

In accordance to the design principles expounded in the previous section, Waspmote platform manufactured by the Spanish company Libelium [41] was carefully selected for the pilot implementation of the wSHMs (figure 3.15). The performance characteristics of this platform, namely autonomy, synchronization with other remote nodes and gateway, data rate, were studied and compared with other commercial systems. Waspmote is a low cost wireless system for monitoring buildings. The platform has an onboard accelerometer and is based on the microprocessor Arduino, and is designed for wireless networks. Data transmission is performed wirelessly via various communication protocols like WiFi, ZigBee, 3G, GPRS, but can be also wired (via USB cable). The on board three-axis linear accelerometer (LIS331DLH) is connected with the microprocessor through I2C or serial peripheral interface (SPI). Three measuring ranges of acceleration are offered (±2g, ±4g and ±8g dynamically selectable full-scale) with 16bits ADC resolution. Sampling rate is customizable up to 1 kHz and the data output is a 16bits word.

Waspmote's powering lies between 2.16V and 3.6V, and the low power consumption is met in all four possible operating modes:

a) On: 15mA

b) Sleep: 55μA

c) Deep Sleep: 55μA

d) Hibernate: 0.6μA

There are two independent programmable interrupt generators for free-fall and motion detection. The shock tolerance, provided by the manufacturer, is very high (10000g) and this minimizes vulnerability of the sensor.

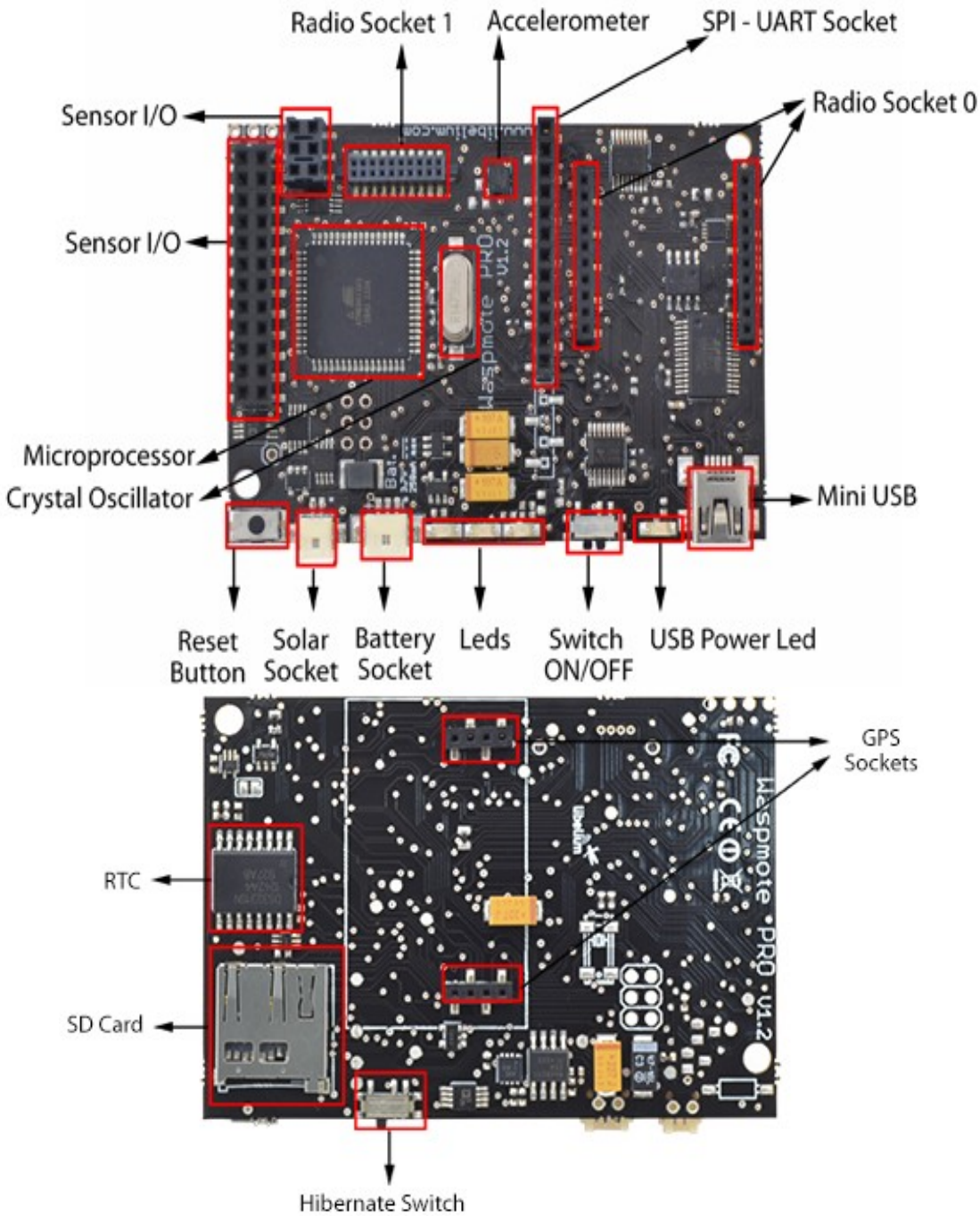

Figure 3.15. Waspmote Top side (up) and bottom side (down) [205]

Following, are summarized the important specifications of the Waspmote platform:

- Microcontroller: ATmega1281
- Frequency: 14MHz
- SRAM: 8KB
- EEPROM: 4KB (1KB reserved)
- FLASH: 128KB
- SD Card: 2GB
- Weight: 20gr
- Dimensions: 73.5 x 51 x 13 mm
- Temperature Range: [-10 º C, +65 º C]
- accelerometer range: at ±8g
- USB port communication: 115200 bps
- SPI connection availability
- Serial Number chip with unique ID for each board
- Programming of Waspmote Pro without unplugging XBee

3.2.8 Data Resolution

Waspmote's triggering acceleration threshold is 16mg and its sensitivity (resolution) reaches down the 2mg, acceleration levels much lower than the response of a building under strong excitation (50-300 mg). On the other hand, the system is insensitive to ambient vibration acceleration (0.1-0.3 mg). Many authors address that typical response of a building has a spectrum up to 20 Hz [83, 88, 101, 108, 152, 160, 166, 167]. Furthermore, a structure with fundamental frequency higher than 10 Hz is characterized by very high stiffness. Based on the above facts and satisfying the Nyquist-Shannon theorem, a sampling rate of 40 Hz was selected and considered to be sufficient for recording structural response.

3.2.9 Wireless Communication

There is a variety of available communication protocols in Waspmote: 802.15.4 (XBee), ZigBee, WiFi, Bluetooth, GPRS, RFID, NFC, 868 MHz, and 900 MHz. The XBee Protocol (802.15.4) was selected for three reasons: (i) low power consumption communication protocol that supports acceptable deployment range of the system; (ii) data transfer rate 250 kBps, sufficient to transmit data with sampling rate up to 50 Hz from 10 platforms with no data loss nor data collision; (iii) straightforward programming of point to point data routing compared to other communication protocols.

XBee is cost effective platforms which provide inter- connectivity between the nodes [42]. Waspmote platform uses an XBee module for wireless data transfer (figure 3.16).

Figure 3.16. RF Modules XBee & XBee-PRO 802.15.4 [42]

Initially, 1 mW XBee modules were tested on the wSHMs. In terms of data loss and synchronization the communication between remote node and gateway was satisfactory only for short distances, i.e., inside a room, but the experiments revealed that for inside distances longer than 30 meters, i.e., different rooms or floors, in a building, the data loss reached unacceptable levels (e.g. 30 % of data packets).

Consequently, the 1 mW XBee modules were replaced with others having much higher transmission power (63 mW) and data transmission experiments were repeated. The new tests revealed almost zero data loss for adjacent rooms, and less than 0.1% data loss for the case of different floors using a sampling frequency of 40 Hz. This increase of transmitting power creates a slight reduction of the total autonomy of each wireless node, because the recording is not continuous but in trigger mode, i.e., the wireless system sends data only when the acceleration exceeds the threshold of 16 mg (under strong motion excitation). This way, autonomy of two months, without any power harvesting, was achieved during tests, by considering four recordings per day (artificial excitation).

3.2.10 Configuring wSHMs

By means of configuration software (X-CTU) the basic parameters of XBee are defined to communicate with the wireless network, and also with the sensor platform that is connected. These parameters are related with Networking and security (Channel ID, PAN ID, Scan channels etc), RF interface (transmitting power level, CCA threshold), Serial interface (interface data rate, parity etc), Diagnostics and AT command options.

Waspmotes are also programmed (via Waspmote IDE software) in order to meet the specific requirements of the wSHM application. Programming the wireless nodes demands to carefully configure recording and communication interdepended parameters: sampling rate, triggering recording mode, length of the data packet, level of the triggering threshold. The trigger mode functions in three dimensions North-South (x), East-West (y) and vertical (z). If any of these components exceeds the defined acceleration threshold then the accelerometer starts to record and send the data through the XBee to the Gateway.

There are two available modes for data and command transfer, namely Application Programming Interface (API) and transparent mode (AT). API is a frame-based mode which allows the user to send or receive data via the radio's serial UART. Data are packed in frames in order to establish a data stream without loss of data. Minimization of data loss makes this option safer in comparison to the basic AT mode, which functions without data frames [206].

On the other hand, API mode provides extremely low throughput resulting to a sampling frequency not higher than 3 Hz. This main drawback constrained us to the AT mode (default mode). In AT mode the XBee module acts as a serial line replacement. The unframed data are sent wirelessly without any additional information. But in the networking scheme (multipoint to point) it is necessary to add information in the data package to identify the module from which the data has been sent. Thus, every data packet contains an ID and one measurement of the X (North-South), Y (East-West) and Z (vertical) axis. To avoid collision of data packets, a buffer stores multiple measurements (array). The array can be read out later and multiple measurements can be sent to the gateway at once. That enables a much higher sampling rate (40 Hz). Data rate of Gateway is much higher (250 kbps) than that of the sensor platforms. The configured wSHMs can be composed of up to 10 sensors, recording 40 samples/sec and wirelessly networked, without any data collisions, to a central microcomputer or simple PC with internet connectivity.

Each sensor node is contained into a special case (figure 3.17). The sensor platform is screwed onto a metal base which contains spirit level for accurate sensor leveling and it can be bolted to a ground screw (for maximum sensitivity). The plastic cover protects sensor node from moisture and dust and provides space for an optional battery.

Figure 3.17. Special construction with metal base, spirit level, and plastic cover.

3.2.11 wSHMs setup: a hybrid network

Inside a building under monitoring, the installed wSHMs's network consists of wireless links between the deployed sensor nodes and a wireless gateway attached to a local microcomputer or standard PC that collects the data from the sensor platforms. The local computer performs time stamping on raw data using GPS synchronization and provides temporary data storage for redundancy (figure 3.18 a). Exploiting existing wireline or wireless broadband connections (ADSL, VDSL, Satellite, WiMax) in the building, the local computer transmits the SHM data to the Data Analysis and Storage Center using internet (cloud). This setup can be a straightforward implementation at many important buildings and structures of a metropolitan area, thus creating a wireless Structural Health Monitoring system that will operate cost effectively in a metropolitan scale (figure 3.18 a & b).

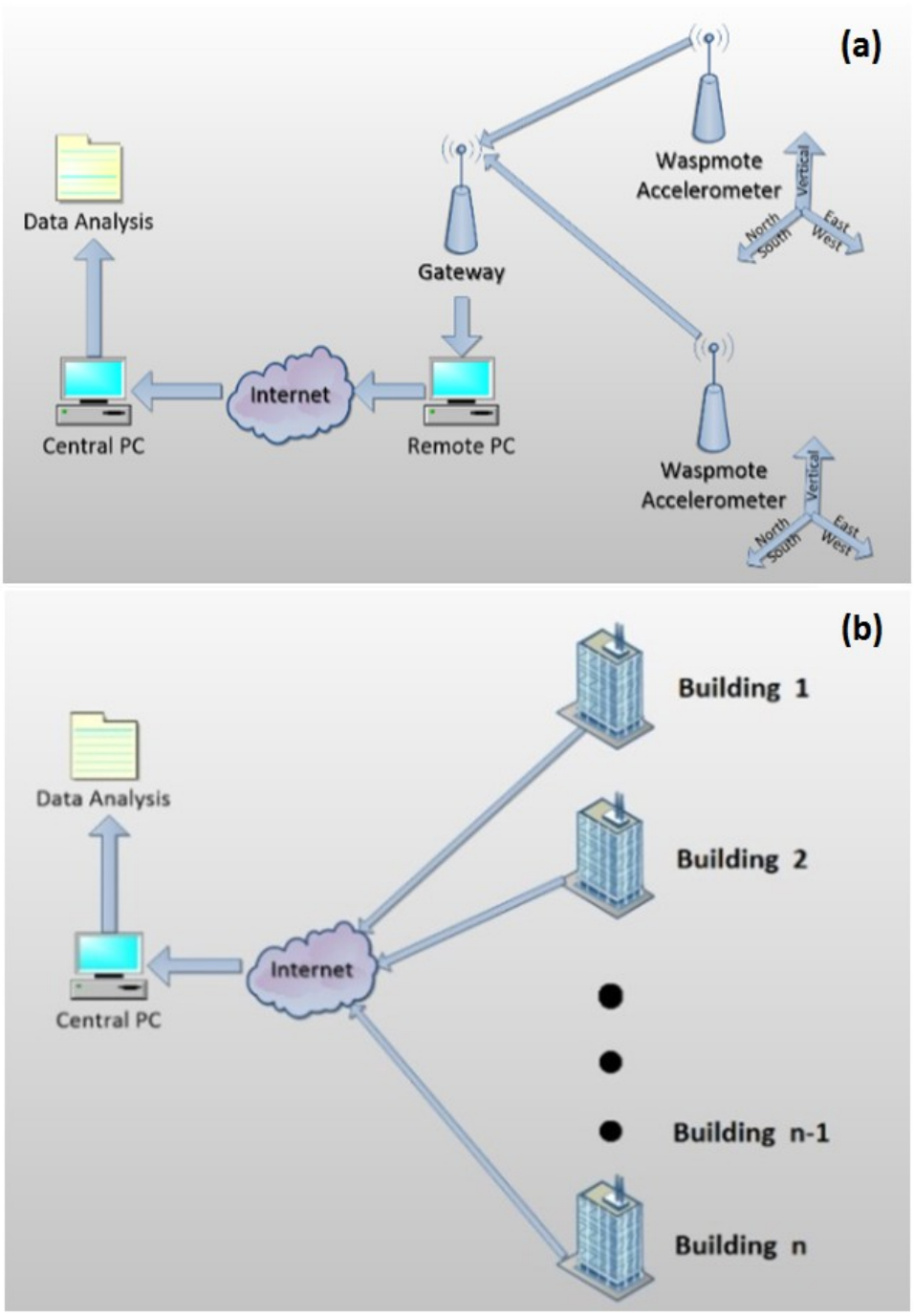

Figure 3.18. (up) Schematic diagram of wSHMs hybrid network setup in a building (down) Schematic diagram of wSHMs network setup in a metropolitan scale.

3.2.12 Optimum deployment of accelerometers in a building

The proper installation of the accelerometers in a structure is of great importance. In order to effectively measure the dynamic response, or the excitation in a structure, from seismic activity, the location of the accelerometers should be in specific places [166, 195-197]. Many

authors have addressed sensor placement [82, 84, 198] proposing algorithms for the optimal sensor installation for SHM in a structure, or discussing the available instrumentation models in order the system to be able to record the ground motion, the building basement motion, the lateral and torsional floor motion, and even more the floor and wall shear and motion. As a general rule, the study of the power spectral density of the acceleration recordings from many locations in a building, is an efficient way to determine where the resonance frequensies are revealed unambiguously. Such key-locations are joints of floor plates and/or joints of plate beams with columns. Furthermore, sensors should be placed in the higher floors because the shock response of the structures is the highest [155, 196].

3.2.13 Data collection

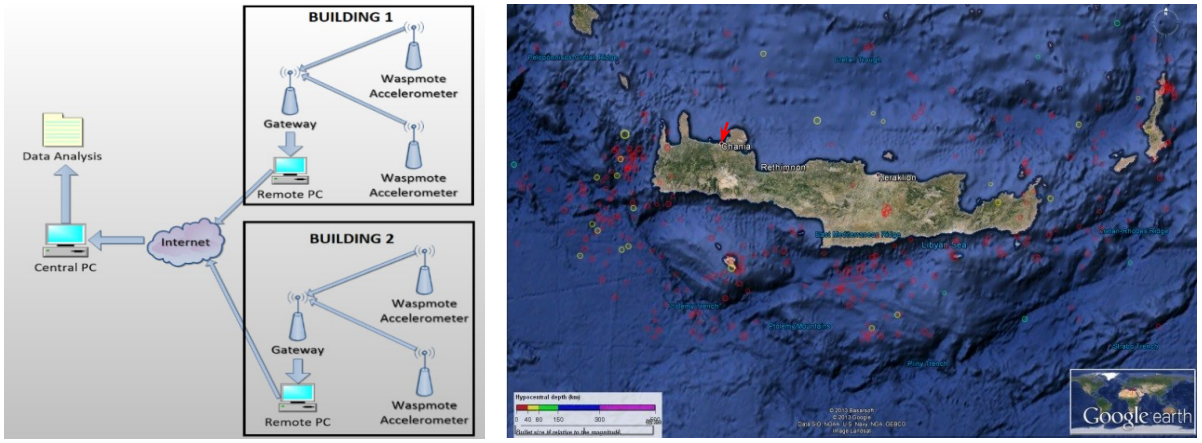

Figure 3.19. Left: Schematic diagram of the wSHMs hybrid network setup in pilot mode at the two buildings of TEI of Crete (Chania premises). Right: Google Earth ™ satellite composite image of Crete Island depicting the location of the Chania premises of TEI of Crete. The seismicity (Mag ≥ 3.0) of the period Jan 2013 – Jan 2014 for the broad area N34.4-36.2deg, E22.5-27.3deg is presented (earthquake data extracted from Euro-Mediterranean Seismological Centre).

In the event of an excitation that exceeds the acceleration trigger level (2mg), the data from the remote wireless sensor platforms are sent in real time and collected through a wireless gateway to a local microcomputer. The serially received data is checked on its ID, and sorted to correspond to each wireless node by means of a commercial software “DataloggerSuite” [207]. After time stamping, the acceleration data stream is saved to an event file.

3.2.14 Pilot comparative study of the developed wSHMs

The wireless sensor network, wSHMs, was designed and installed in pilot mode to evaluate its functionality and efficiency. The installation took place in an eighteen years old three floor building and an adjacent six years old three floor building [208]. At each building was deployed one wireless accelerometer on the third floor and one on the second floor, in order to record strong motion (under anthropogenic or earthquake excitation). The two buildings under SHM are the premises of Technological Educational Institute (TEI) of Crete at Chania, Crete.

Figure 3.20. RefTek 130-SMA (left) and Waspmote (right) installed (with screwing) on the second floor of the old building of TEI of Crete at Chania.

For comparison, a parallel accelerometer network operated using local intranet [209]. The latter sensor network comprises of very reliable and sensitive (100μg resolution) accelerometers 130-SMA by RefTek [200] but orders of magnitude more expensive. Both sensor networks were operated in trigger mode (60sec trigger time) having different trigger levels (2mg for Waspmote, 0.2mg for 130 SMA), while the 130-SMA has the ability of saving pre-trigger data (30sec pre-trigger time), recording the complete event.

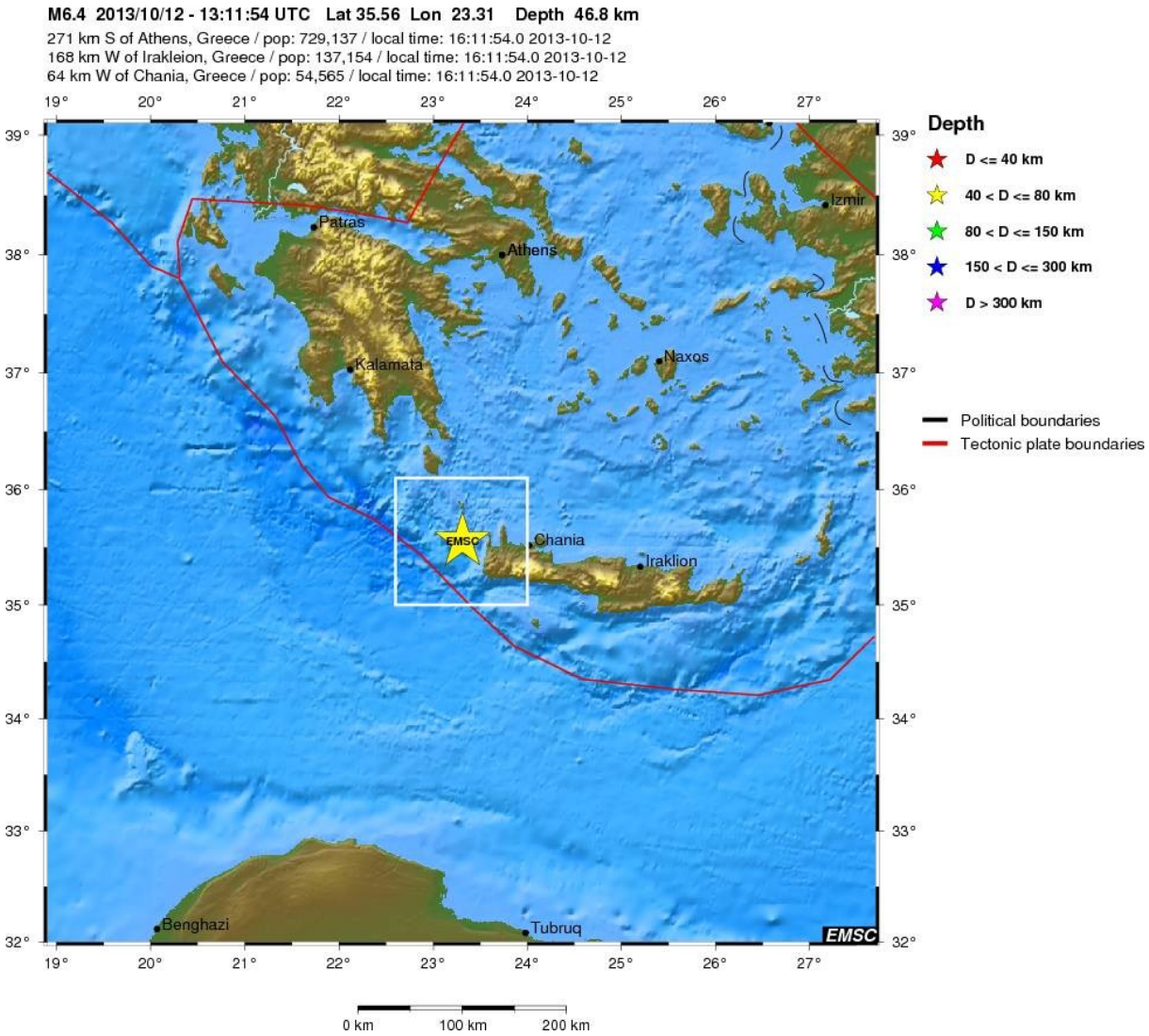

Figure 3.21. Earthquake epicenter map and information provided by the European Mediterranean Seismological Centre concerning the strongest event of the last three years in the very active seismogenic region of Greece [201].

A comparative study of the operation of the two sensor networks in the event of a nearby strong earthquake is presented. On 12 of October 2013 at 13:11:54 UTC, occurred a very strong earthquake with epicenter (N35.56deg, E23.31deg) approximately 65 km west of Chania (figure 3.21). The M6.4 earthquake was the strongest event that occurred the last three years in Greece (and in the last 30 years on the local region). In the broad region is taking place more than 80% of the seismic activity in Europe. This earthquake affected with moderate strong motion the structures in the city of Chania and was largely felt as it is revealed by its intensity map (figure 3.22).

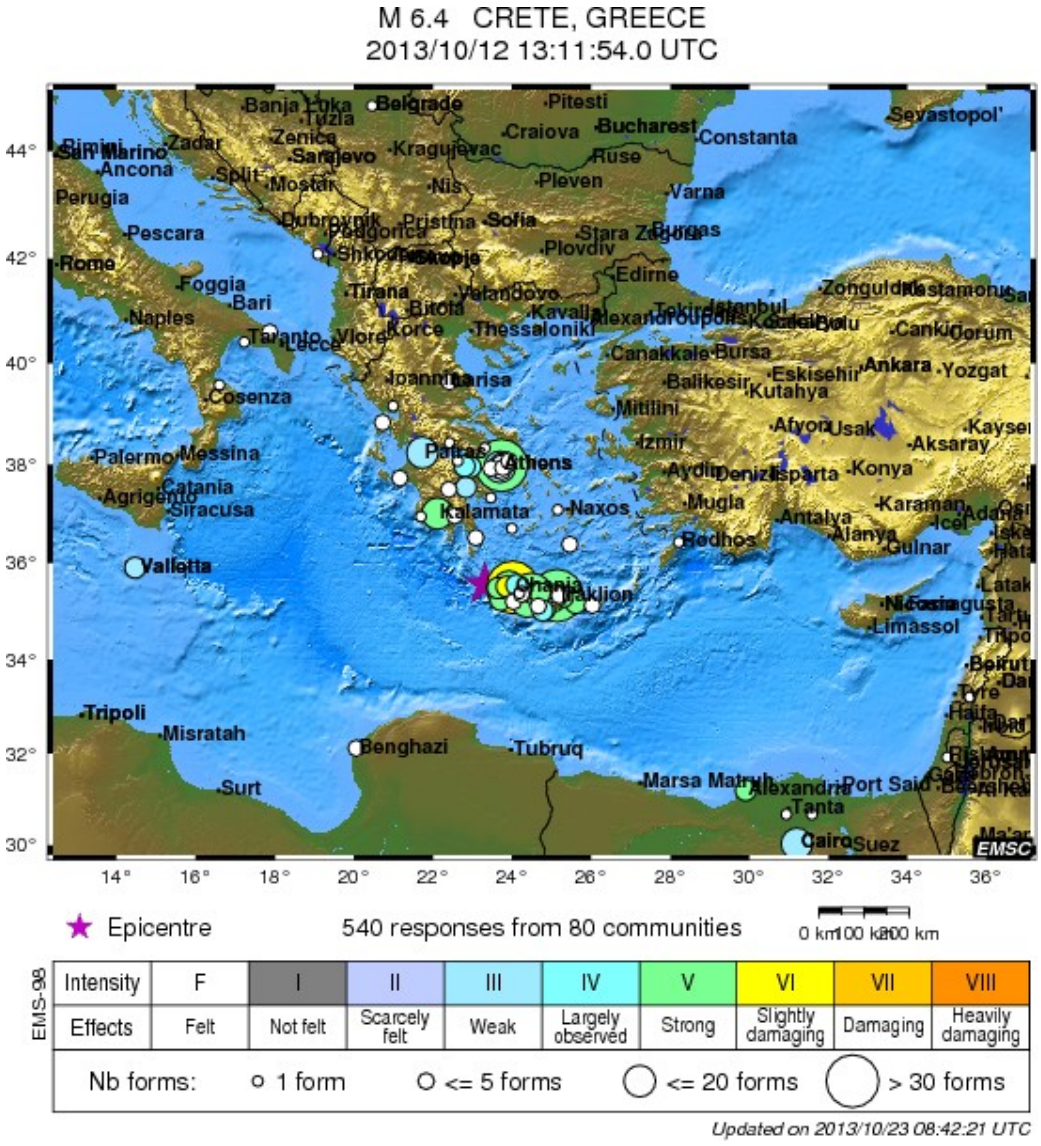

Figure 3.22. Earthquake Intensity map of the M 6.4 event on October 12, 2013, provided by the Euro-Mediterranean Seismological Centre.

The strong motion of the two buildings under SHM was recorded from both sensor networks. The RefTek strong motion accelerographs recorded the complete vibration, due to the pre-trigger recording. Waspmotes were triggered after the arrival of the S-waves.

Figure 3.23 depicts that both accelerometers installed on the second floor of the old building recorded similar acceleration. The maximum of almost 80mg p-p is present in the recordings of the NS-component of 130-SMA and Waspmote respectively. By inspecting the corresponding Power Spectral Densities (PSD) it is observed comparable spectrum, taking into account that the pre-trigger record is absent for Waspmote. Furthermore, it is revealed a resonance frequency of excitation around 1 Hz as well as the resonance frequency of the 19 years old building's second floor around 7 Hz, but with much lower amplitude. Analogous results were obtained from the comparative study of the strong motion recordings of the two SHM systems, recorded on the third floor of the buildings of different age, thus of different state of health. These results demonstrate the efficiency of the developed wSHMs in monitoring the vibration of buildings and structures subjected to strong excitation.

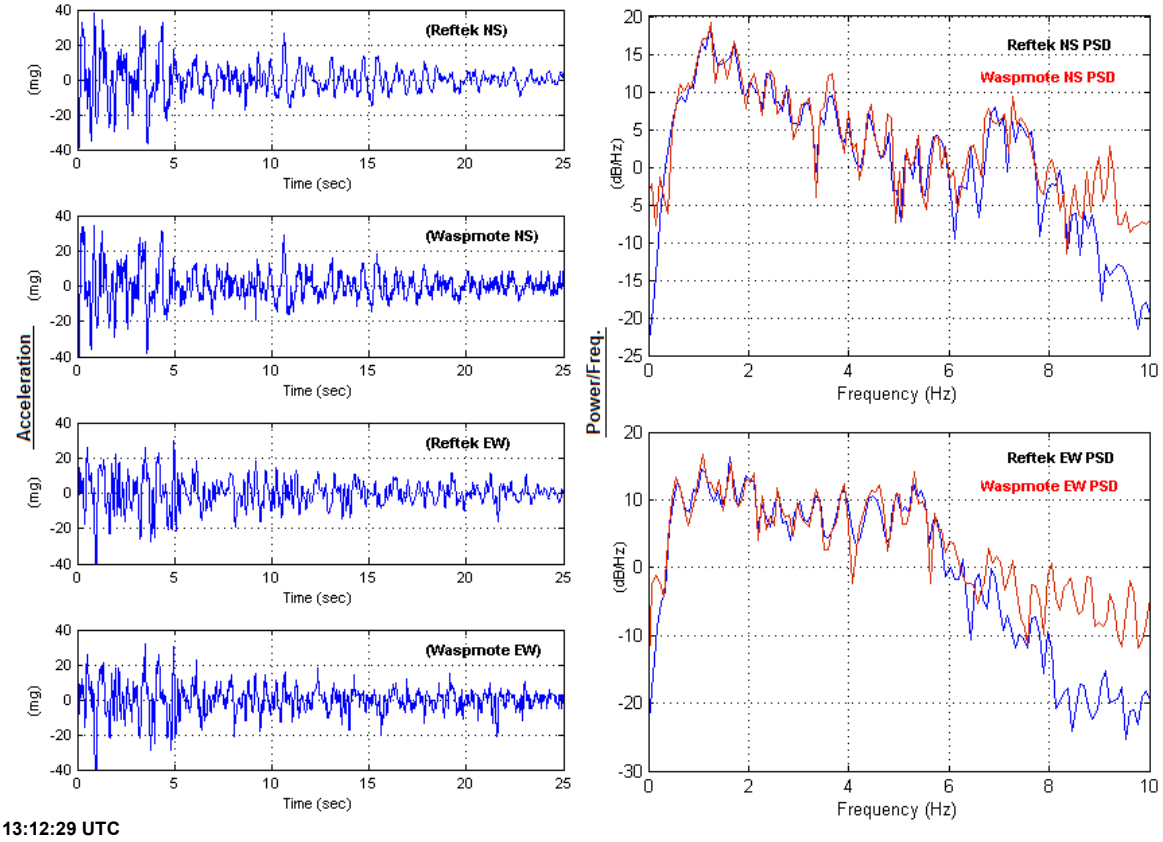

Figure 3.23. Comparison of the horizontal components of acceleration, recorded during the M 6.4 earthquake on October 12, 2013, by the non-wireless sensor network based on RefTek 130-SMA and the developed wSHMs based on Waspmote platform respectively, installed on the second floor of a 18 years old building at Chania premises of TEI of Crete.

3.2.15 Conclusion on wSHM network

At this chapter is presented the design, programming and pilot implementation of a cost effective wireless Structural Health Monitoring system (wSHMs) that monitors the strong motion of buildings. Key-features for wireless monitoring of the structural condition of buildings, namely, autonomy, continuous / real-time operation, data rate, resolution and synchronization, wireless error free connectivity and implementation cost have been analyzed and addressed in the design and configuration of the developed wSHMs. Hybrid networking combines a wireless sensor network with the exploitation of existing wire lines or wireless broadband connections in the building making possible to implement the wSHMs in WAN mode to cover many remote structures and buildings, on metropolitan scale.

The efficiency of the wSHMs was tested through a pilot comparative study of the operation in two neighboring buildings of different age in an earthquake prone area (Chania, Crete,

Greece). The comparison was made against a far more expensive, high sensitivity, low level triggering, accelerometers network installed in parallel using local intranet. The real performance of both sensor networks in the case of a strong earthquake (M 6.4) occurred close to Chania region on October 2013, demonstrated that the developed wSHMs is capable to record the acceleration caused by strong excitation, reveal the resonance frequencies and thus to monitor the structural health of the buildings being installed. In the near future, the wSHMs is going to expand in the city of Chania covering high importance public buildings, heritage buildings etc. Furthermore, a more sensitive acceleration sensor will be added.

Conclusively in terms of instrumentation design, an optimum stategy for design a SHM network that will be able to record effectively seismic and vibration data from buildings and infrastructure, is proved to be a combination of technologies. Wireless communication is addressed necessary for fast and low cost deployment. Sensitive accelerometer sensors should have low noise threshold. Utilization of existing technologies and technological infrastructures, such as internet connections in buildings, reduce the cost of development and implementation. The ability to store and analyze the recorded data from remote locations, improves the cost and analysis efficiency.

3.3 Raw Data recorded by wired and wireless SHM network

This section presents the raw data, recorded from the wired accelerometer network (Reftek 130 SMA) of both buildings in TEI (old and new building). Also it is presented the data from wireless SHM network of building in TEI and TEE, from the wireless systems of Libelium (Waspmotes). Recording data are from several seismic events that affected case study buildings and also from ambient noise during day and night. The specific recordings have an added value due to the fact that they present the seismic acceleration caused from seismic activity of a very active seismic region of Hellenic Arc on two buildings (real structures and not laboratory models), for a long time period (more than 2 years). This enables to study the structural response under real excitation scenarios and due to time. Table 2 presents the seismic events recorded for a time period more than two years.

3.3.1 Seismic Acceleration Recordings.

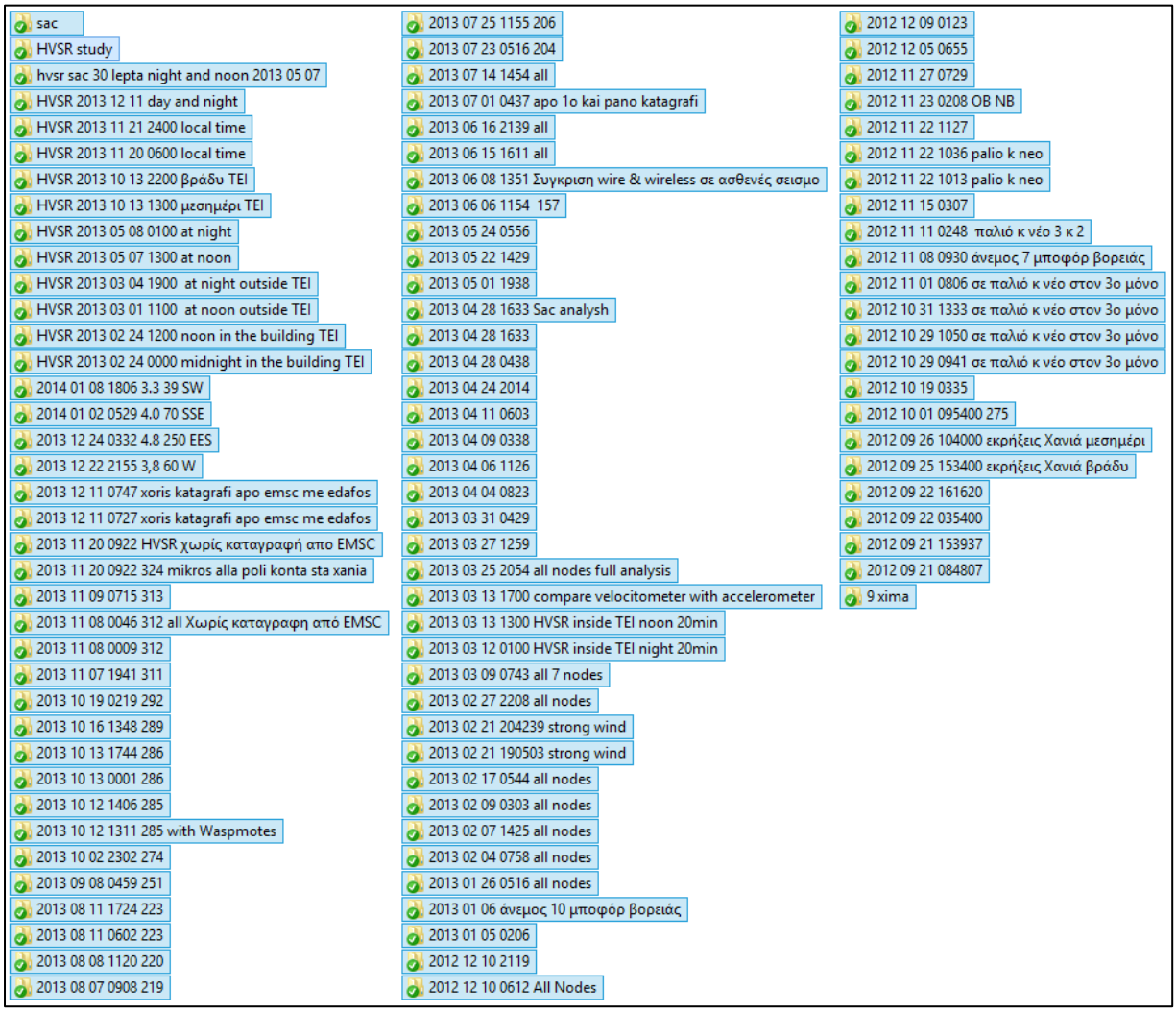

Table 3.2. Seismic events catalog, recorded by wired SHM network of TEI

"b" events from 1-21
1 9-3-2013 3.9M 67km
2 31-3-2013 4.3M 62km
3 6-4-2013 5.2M 80km
4 11-4-2013 3.6M 52km
5 28-4-2013 3.4M 36km
6 22-5-2013 4.1M 98km
7 16-6-2013 5.8M 160km
8 23-7-2013 3.4M 64 Km
9 25-7-2013 3.7M 55 km
10 8-8-2013 3.2M 35km
11 9-8-2013 5M 100km
12 14-07-2013 2.6M 55km
13 12-10-2013 6.4M 65km
14 10-12-2012 2.3M 16km
15 05-01-2013 3.5M 55km
16 26-01-2013 4.3M 100Km
17 04-02-2013 4,4M 80km
18 07-02-2013 3.9M 150km
19 09-02-2013 3.5M 50Km
20 25-03-2013 4.3M 55km
21 27-03-2013 3.7m 58km

"a" events from 1-18
1 12-10-2013 4.3M 70km
2 13-10-2013 4.0M 100km
3 19-10-2013 4.5M 97km
4 22-12-2013 3,8M 60 km
5 02-01-2014 4.0M 70 km
6 08-01-2014 3.3M 39 km
7 09-11-2013 4.4M 84 km
8 07-11-2013 3.4M 35 km
9 13-10-2013 3.8M 65km
10 16-10-2013 3.5M 52km
11 15-01-2014 3.5M 94 km
12 11-01-2014 3.5M 72km
13 08-01-2014 3.0M 88km
14 07-01-2014 3.5M 64km
15 06-01-2014 3.7M 65 km
16 05-01-2014 3.7M 77km
17 31-12-2013 4.1M 113kr
18 29-11-2013 4.4M 84km

Table 3.3. Earthquakes recorded by wired SHM network of TEI before the high magnitude seismic event of 6.4M (left column) and after (right column). Left column is "b" code events and right is "a" code events.

Table 3.3 presents specific earthquakes before and after the earthquake of 6.4 M. All seismic events of this table are up to 100 Km away from case study buildings and with magnitude higher than 3 M. Table 3.4 presents ambient noise recordings inside case study buildings. Recordings have time duration of 20 minutes, 30 minutes and one hour. Data have been recorded in buildings on each floor.

HVSR 2013 05 07 1300
HVSR 2013 05 08 0100
HVSR 2013 10 13 1300
HVSR 2013 10 13 2200
HVSR 2013 11 20 0600
HVSR 2013 11 21 2400
HVSR 2013 12 11 1200
HVSR 2013 12 11 2400

Table 3.4. Date and time (UTC) of HVSR recordings inside buildings on each floor

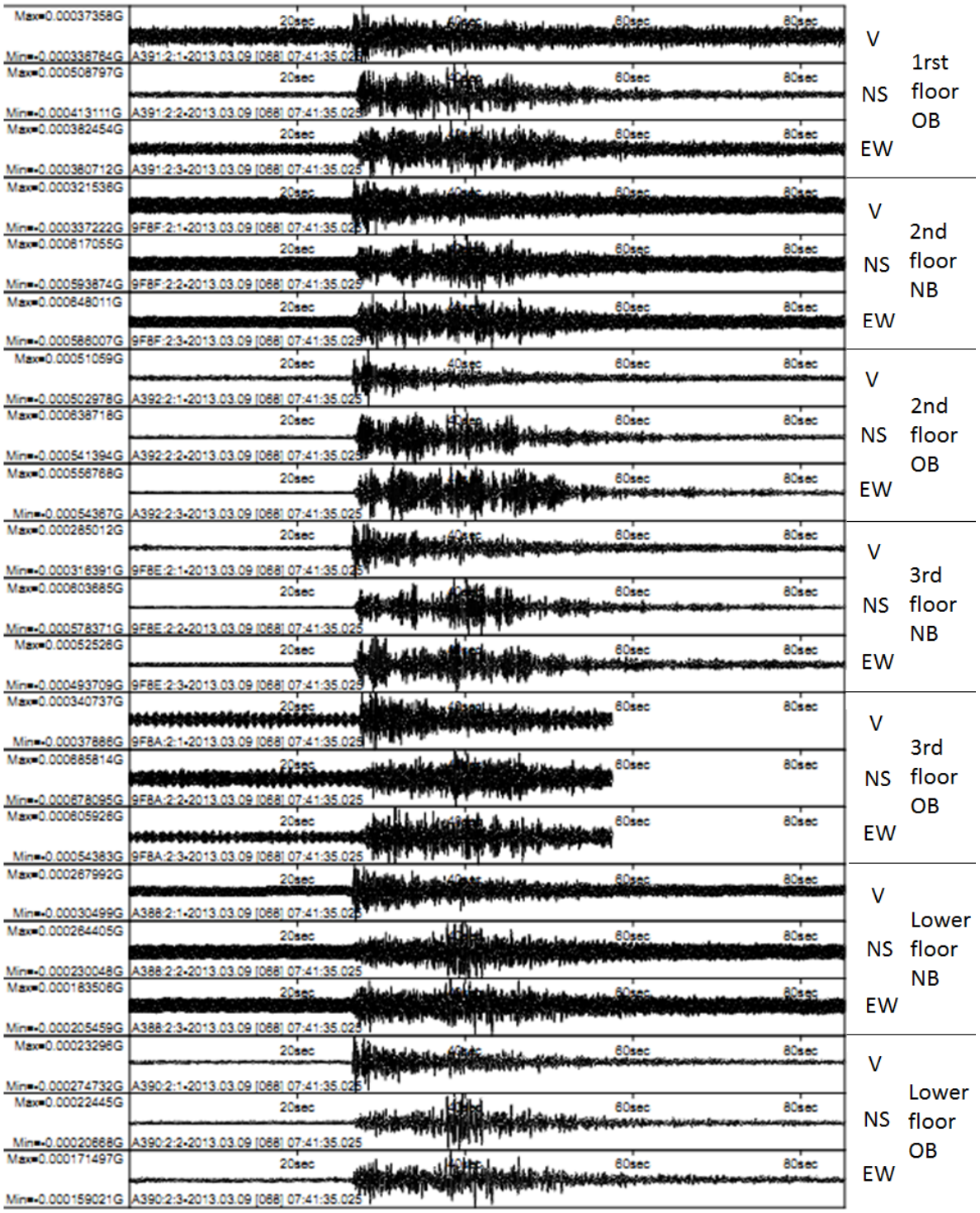

Figure 3.24. Acceleration recordings for the seismic event of 3.9M on 2013-03-09 07:41:49 GMT (Lat 23.43 Lon 23.31). The list code number is b1 from the table 3.3.

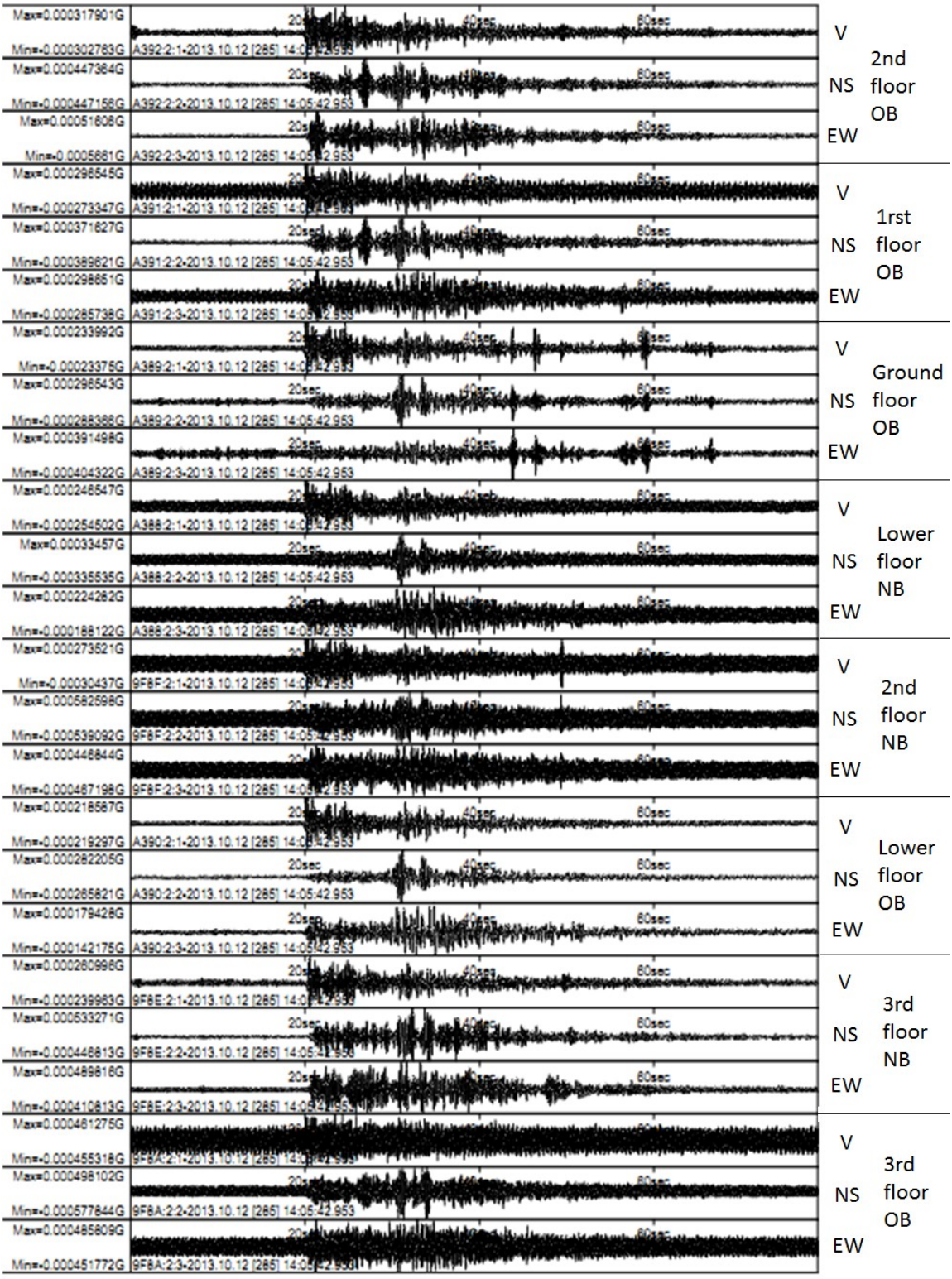

Figure 3.25. Acceleration recordings for the seismic event of 4.3M on 2013-10-1214:05:50 GMT (Lat 35.37 Lon 23.29). The list code number is a1 from the table 3.3.

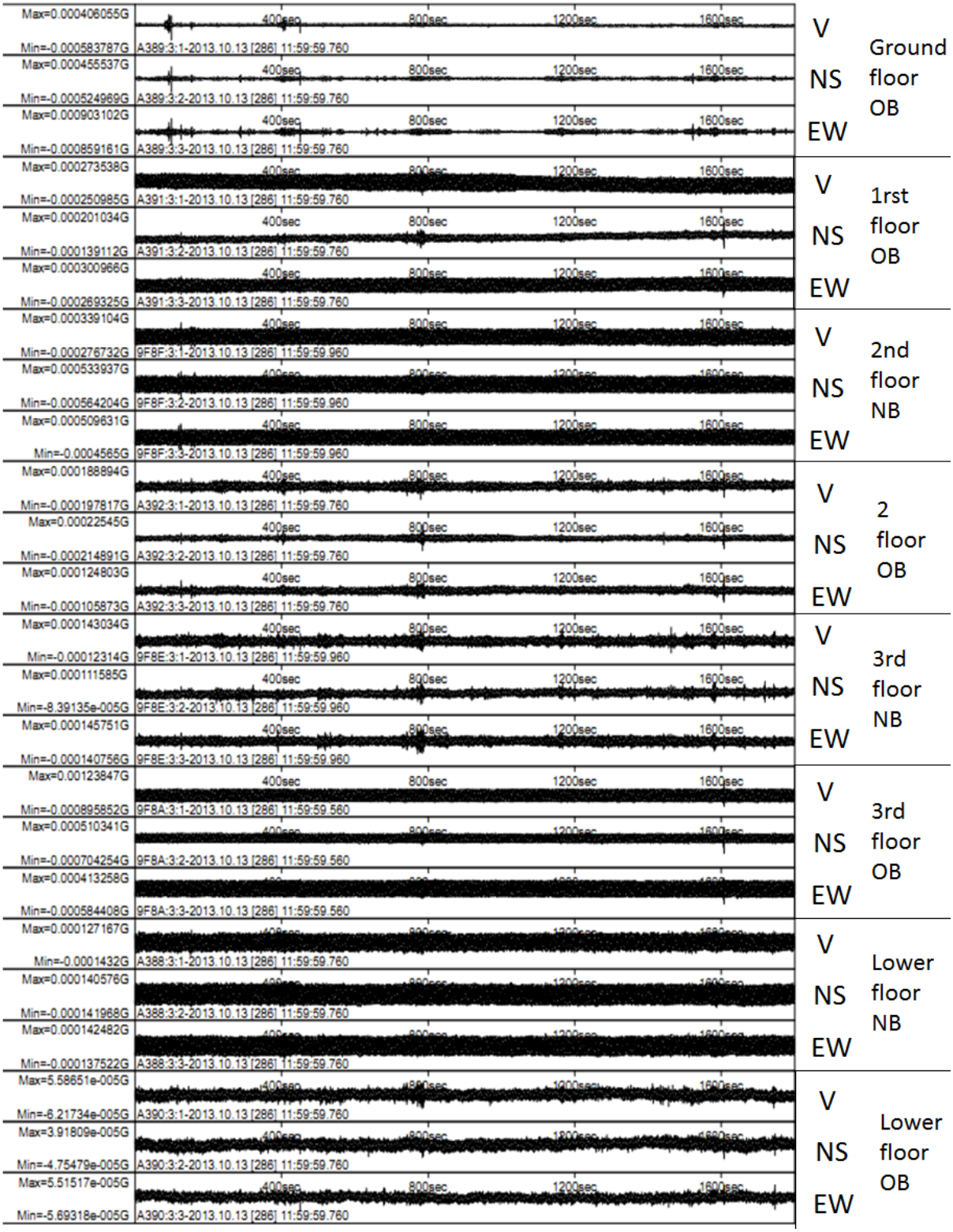

Figure 3.26. Recordings of 20 minutes time duration of ambient noise inside TEI buildings from table 3.3.4 (2013 10 13 22:00 UTC event). Local time is 11:59:59 pm

The components and the floor of each accelerometer are indicated on the right side of the recordings. The rest of the acceleration recordings from event b2 until b21 on table 3.3, are in **Appendix H**. The rest of the acceleration recordings from event a2 until a18 on table 3.3, are in **Appendix I**. The rest of ambient noise recordings on buildings from table 3.4, can be found in **Appendix J.**

3.3.2 High magnitude earthquake (6.4M).

The earthquake that affected both buildings is presented on below figure 3.27. The recordings of seismic acceleration is presented on below figure 3.28. The distance from case study buildings was approximately 64 km. The maximum seismic acceleration recorded on the 3rd floor of the old building was almost 88 mg, and on the new one was almost 84 mg (see figure 3.28).

Figure 3.27. Seismic event of 2013-10-12 13:11:54 UTC 6.4M (lat 35.56 Lon 23.31)[201]

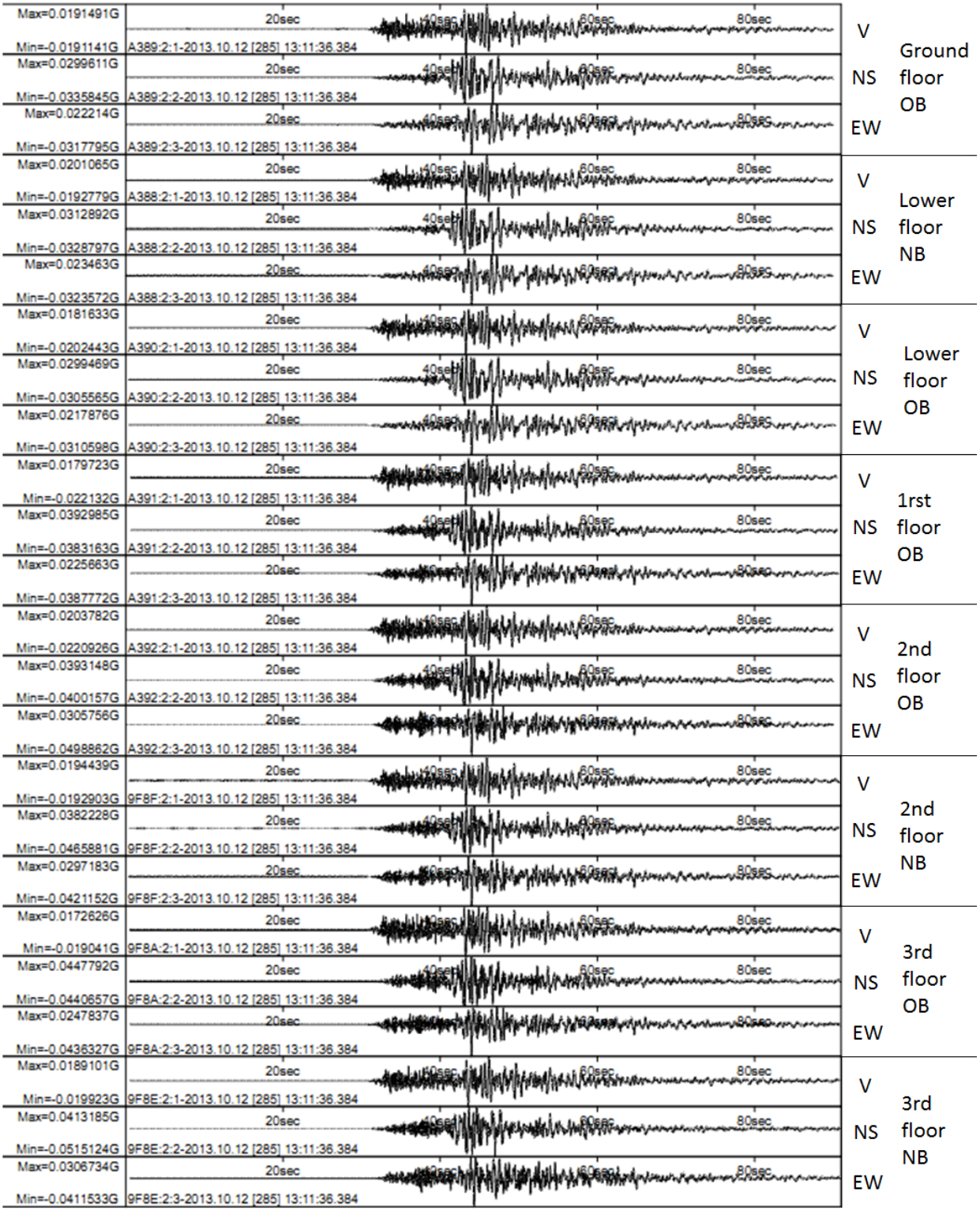

Figure 3.28. Acceleration recordings in both buildings during 6.4 M earthquake

The components and the floor of each accelerometer are indicated on the right side of the recordings. The seismic acceleration of both buildings is increased, as floor gets higher.

3.3.3 Waspmotes recordings from 6.4 earthquake.

The installed Waspmotes accelerometers on both TEI buildings, recorded the 6.4 M earthquake. Figure 3.29 depicts seismic acceleration in the old building from accelerometers with code names "BC". Figure 3.30 depicts the seismic acceleration on the new building recorded by "C9".

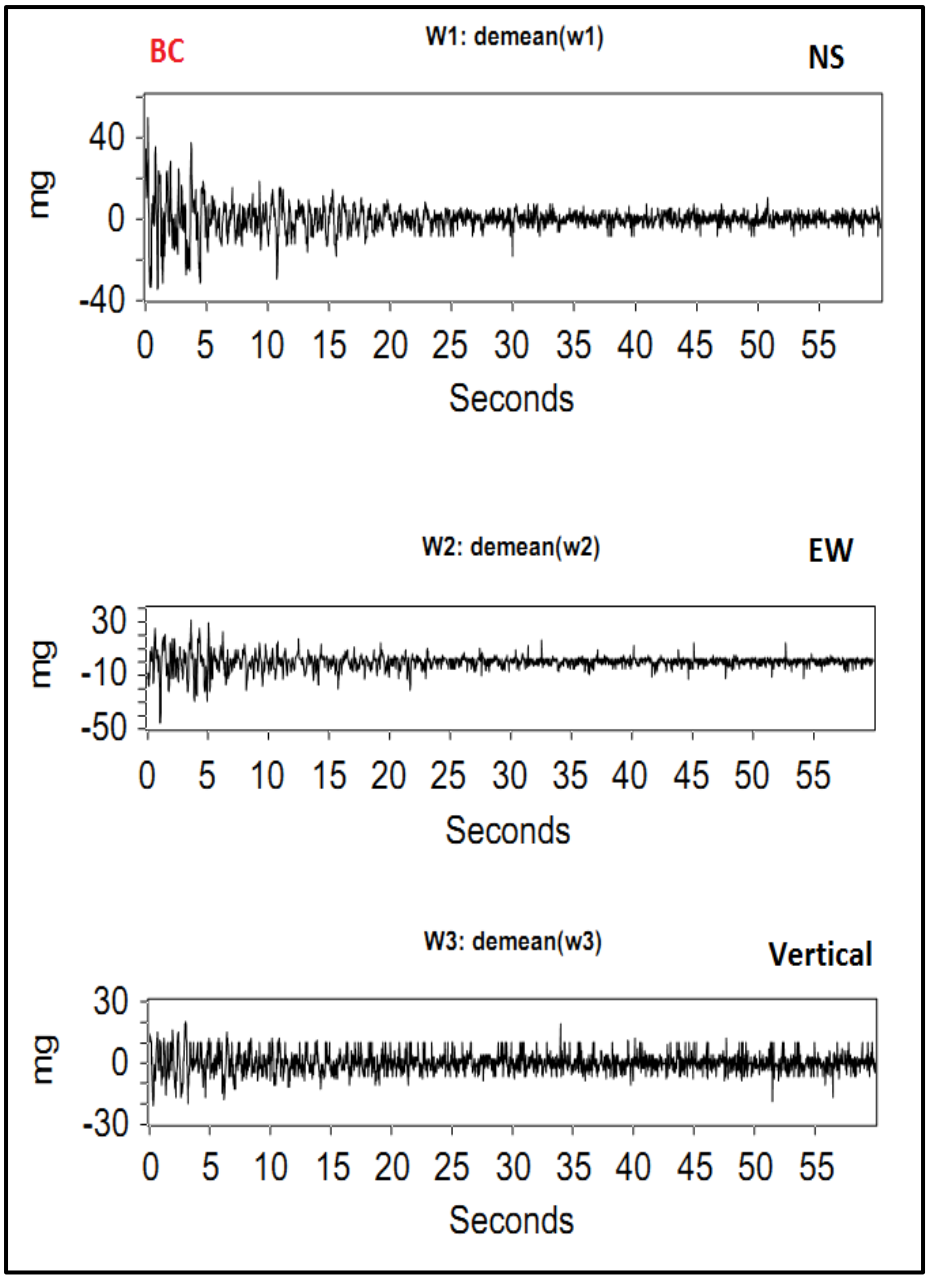

Figure 3.29. Acceleration recordings from Waspmote accelerometer with code BC, in the old building, during 6.4 M earthquake

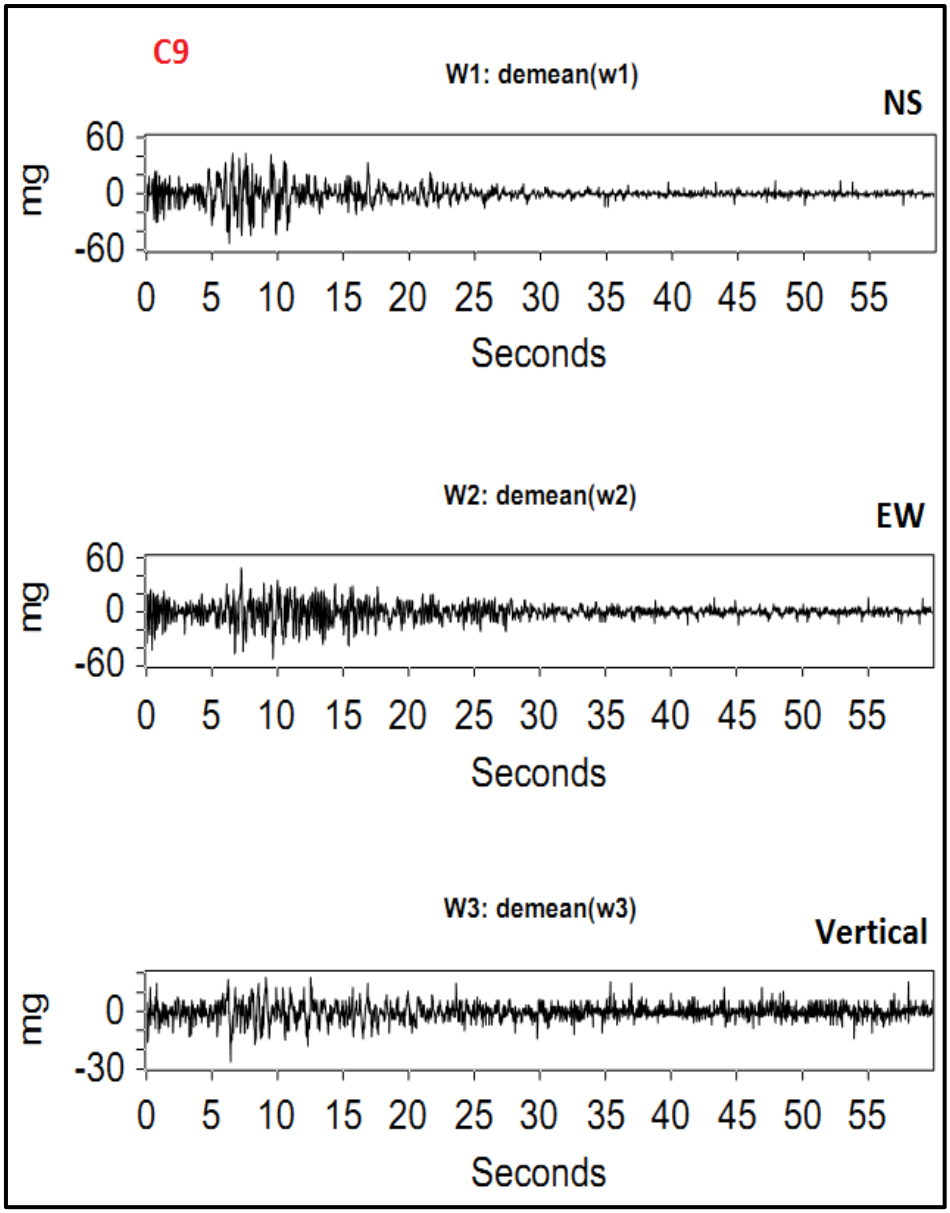

Figure 3.30. Acceleration recordings from Waspmote accelerometer with code C9, in the new building, during 6.4 M earthquake

Chapter 4. Digital Signal Processing Methods

4.1. Introduction

This chapter presents the theoretical background, of digital signal processing methodologies presented on chapter 2 (literature review) and applied on chapters 5 and 6 (data analysis).

Second section (4.2) deals with non-parametric methods, namely non-parametric Power Spectral Densities (PSD), Frequency Response Function (FRF), Coherences, Horizontal to Vertical Spectral Ratio (HVSR). Third section (4.3) deals with parametric methodologies, namely autoregressive with exogenus input (ARX) and autoregressive moving average with exogenous input (ARMAX). Fourth section (4.4) presents structural identification methodology that utilizes statistical time series methods, for effective SHM (applied in chapter 6).

Non parametric methods create non parametric results in terms of frequency and/or impulse response functions. These methods do not create any parametrized model, neither any differential equation that could relate data observations with specific assumptions. They have low computational complexity and the results do not depended with specific procedures or data sets. In contrast parametric methods related recording data with differential equations and parametrized models. They have much higher computational complexity than non-parametric and require used expertization, but they have presentation parsimony in results and also the created parametric models could be directly related with dynamic properties of a structure such as stiffness, mass or damping.

Both families of methods are required in specific thesis. Although parametric method could efficiently reveal possible dynamic change in case study constructions, non-parametric methods are necessity in order to define parameters such as energy distribution, frequency spectrum and coherence between excitation and response.

4.2. Non-parametric methods PSDs, FRFs, Coherences, HVSR, Wavelets

4.2.1 Power Spectral Densities

Signal's spectrum is the real-positive function of frequency that is correlated with a deterministic or stochastic function in time-plane. The dimensions are energy and/or power per herzt. A stochastic signal is decomposed in to various contained frequencies and presented at specific scales. Acceleration recordings are vibrations of waveforms. The power spectral density of these waveforms could be computed by multiplication of spectral density of signal with specific-appropriate function (sinusoidal), giving the power or energy of the waveform, for every frequency range. This energy is the Power spectral density (PSD) of the recording, in watts per hertz (W/Hz).

The term that describes the energy of a recorded time series is:

$$\int_{-\infty}^{+\infty}|x(t)|^2dt \quad (4.1)$$

on signals, with discrete values such with finite energy, the expression is given by the Fourier expression: $\hat{x}(f)$

$$\int_{-\infty}^{+\infty}|x(t)|^2dt = \frac{1}{2\pi}\int_{-\infty}^{+\infty}|\hat{x}(f)|^2df \qquad (4.2)$$

where f is the angular frequency. Integral describes the energy on frequency f. Respectively the energy of the whole spectral of a recording $x(t)$ is given by:

$$S_{xx}(f) = \left|\int_{-\infty}^{+\infty}|x(t)|e^{-ivt}dt\right|^2 \quad (4.3)$$

the overall power contained in a signal $x(t)$ for specific time T is the average value of:

$$P = lim_{T\to\infty}\frac{1}{2T}\int_{-T}^{+T}|x(t)|^2dt \quad (4.4)$$

Fourier transform (FT) can be used in order to analyze the frequency spectrum of a signal $x(t)$. If the FT cannot be applied to a signal (if the signal is not integrated on its whole length), then there is the ability to apply FT in specific limits of a signal (in specific finite time interval 0-T) where there is integration only between these limits.

Such:

$$\hat{x}_T(f) = \frac{1}{\sqrt{T}} \int_0^T x(t) e^{-ift} dt \qquad (4.5)$$

in this case spectral density is determined as:

$$S_{xx}(v) = lim_{T\to\infty} E\,[|\hat{x}_T(v)|^2] \quad (4.6)$$

where E, is the energy spectral density.

Power spectral density of a signal could be computed by autocorrelation of this signal:

$$x(\tau) = \{X(t)X(t-\tau)\} \quad (4.7)$$

PSD is also presented by Fourier analysis of signal $X(t)$:

$$S_{xx}(f) = \int_{-\infty}^{+\infty} \delta(\tau) e^{-if\tau} d\tau = \hat{\delta}(f) \qquad (4.8)$$

Characteristics of PSD:

- Real numbers frequency spectrum are even process:

$$S_{xx}(-f) = S_{xx}(f) \quad (4.9)$$

- PSD is the computation of the energy distribution of a signal over frequency:

$$Dis(Xm) = \delta(\tau) = 2 \int_0^{+\infty} S_{xx}(f) df \quad (4.10)$$

- Fourier transform can compute PSD of a continuous stochastic signal and Inverse Fourier transform can compute the autocorrelation function of this signal.

Cross spectral density of two signals $n(t), m(t)$ is defined by the computation of Power spectral densities of these signals $S_{nn}(f)\, S_{mm}(f)$ given by:

$$S_{nm}(f) = lim_{T\to\infty} E\,\{[F_n^T(f)] \times F_{\mathrm{m}}^T(f)\} \qquad (4.11)$$

Where F_n^T the Fourier is transform for signal $n(t)$ and F_m^T is the Fourier transform of signal $m(t)$. Such cross power spectal density is equal with the Fourier transform of cross correlation of both signals at a time limit 0 to T. Conclusively cross-covariance of two signals present the cross spectral density of these signals, for example $S_{nm}(f)$ and power spectral density of a signal could be a specific case where $n(t)$ is equal to $m(t)$, such instead of cross-correlation there is auto-correlation (or convolution) of this signal $n(t)$ with itself.

PSD is used for damage detection as non-parametric method. Author Fassois and Sakelariou [34] present that methods based on spectral density functions, try to detect damage, and quantify possible magnitude of this damage, through identification of specific changes on PSDs functions. The PSDs are from recorded acceleration vibrations from output only (cases where only the response of a vibrating system is available).

According to [34] fault detection is based on verification of high scale statistic deviations on PSDs before and after specific events (which could indicate healthy and damaged cases).

4.2.2 Frequency Responce Functions

Frequency Response Function (FRF) indicates the quantitive relation, of the response spectrum of an output and/or response of a system (model, building, equation etc), with respect to the input and/or excitation of the same system. FRF identifies the dynamical characteristics of a system, where it characterises the phase and magnitude of the response in relation to the excitation of the case study system.

In linear systems the magnitude and phase of output is analog with the signal input. Any increase or decrease of input signal will cause corresponding change whether in magnitude or phase at the frequency spectrum of the output. Frequency response function on a system remains stable in case where the system is time-invariant.

Methodology based on frequency response function (FRF) is an extension of PSD based methodology. It used both input and output (or excitation and response) power spectral densities. The magnitude of FRF is estimated by the quotient of Welch [34] cross-correlation of input with output divided by the auto-correlation of input. Damage estimation is based on changes of FRF magnitudes (in one or more frequencies).

FRF magnitude is computed from cross spectral density of input-output of a system, with the auto spectral density of input:

$$\left|\hat{H}(jf)\right| = \frac{|\hat{S}_{nm}(jf)|}{\hat{S}_{nn}(jf)} \qquad (4.12)$$

where $\hat{H}(jf)$ is the transfer function of the system (or frequency response function of the system), $\hat{S}_{nm}(jf)$ is the cross spectral density of input-output, and $\hat{S}_{nn}(jf)$ the auto spectral density of input.

FRF is also non-parametric based method (structural health monitoring damage identification field), and fault detection is determined by the identification of important deviations of FRFs of a system between recorded events (healthy and damage cases) [34].

4.2.3 Coherence diagram

Coherence diagram or coherence spectral is the relation between two recordings or time-series under a statistical manner. In structural health monitoring damage detection, spectral coherence is reffered on frequency spectrum content relationship of excitation (as input is considered the lower floor of building) with response(as output is considered the 1^{rst}, 2nd and 3rd floor of case study building). The computation of coherence is performed by power spectral densities of input and output, where system linearity is requirement.

Type of conherence diagram is given by:

$$\hat{C}_{nm}{}^{2} = \frac{|\hat{S}_{nm}|^{2}}{\hat{S}_{nn}\hat{S}_{mm}} \qquad (4.13)$$

where S_{nm} is the input-output cross spectral density, S_{nn} the autocorrelation function of input and S_{mm} the autocorrelation function of output of the system. $|S_{nm}|$ denotes the magnitude of cross-spectral density. Value range of coherence C_{nm} is higher to 0 and lower to 1. Optimum value of coherence $C_{nm} = 1$ leads to a system where every frequency amplitude is also presented at the output with the same amplitude.

Fassois [34] refers that under specific experimental and/or environmental parameters coherence should be the same and reduces by damage occurance. Fault introduce or increase, to a system or a structure, non-linear characteristics where they affect the frequency content of input and /or output, and such they change the spectral relation of excitation and resonance. More generally methodology of damage identification, based on coherence measuring, relays in the theory that faults or damages induced in a system effect

the overall coherence of the input-output (excitation and response) of a structure. Coherence of frequency spectrum decreases as damage affects a structure. Coherence is equal with the quotient of Welch power spectral densities of output with input. Damage detection is based on identification of important decrease of coherence under a statistical manner (between events of healthy and damaged scenario cases).

4.2.4 Horizontal to Vertical Spectral Ratio (HVSR)

Seismic noise is called the low level vibration of the ground caused by ocean waves, traffic, wind, environmental parameters and also human made like traffic industry etc. Generally seismic noise or ambient noise enables to study ground characteristics and parameters. Horizontal to vertical spectral ratio method (or HVSR) is user friendly, fast, and computational efficient method to study ground properties such as fundamental frequency of the ground and site amplification. HVSR method is related to ambient vibration data and also to three other techniques:

- Resonance frequencies related to the analogy of several types of waves on environmental noise
- Phase of the Love waves
- Rayleigh ellipticity peak

The values of these methods are almost the same, such for specific ground HVSR could function as an accurate method for assessment of fundamental frequency of a site. For grounds where the resonance frequency f is correlated with the S waves velocity, and the depth of the ground layer under study is D , then is given:

$$f = \frac{S_u}{4D} \qquad (4.14)$$

where there is correlation of the sediment depth with S-wave parameters and fundamental frequency.

HVSR method is low cost, does not affect buildings or structures and does not impact changes in the structure integrity. It is appropriate for study urban regions and with small quantity of data could reveal valuable information. Ditomamso et al. [112] uses HVSR method to estimate with with cost and time efficiency resonance frequencies of specific structures. HVSR has also been studied by Luo et al. [48] where referred that H/V spectral method has been widely used for estimation of site amplification from microtremors and the

relation with the amplification that can be presented through strong motion events. In addition in [48] HVSR value on ground and on buildings to reveal the both eigenfrequencies were presented. Triwulan et al. [47] uses HVSR to demostrate that there is the ability to record: Geological parameters, Structures parameters and Relation of structure and local geology parameters. This thesis is going to correlate HVSR method with differential acceleration between floors (building internal drift) and characterize structural vulnerability of structures.

4.3. Parametric Modeling Methods AR, ARX, ARMAX

4.3.1 Parameter time series methods

Parametric time series methods could be classified in model parameter-based (PB) methods, residual based method (RB) and functional model based method (FB) [103]. This thesis deals only with model parameter-based methods, since the other two groups of methods are very sensitive (in terms of parameters assesement) when system parameters change (every earthquake induce different dynamic parameters on case study buildings). RB and FB methods are very efficient and accurate under stable and specific input-excitation (the input parameters do not change). In laboratory experiments where there is control of excitation characteristics this is efficient. There is an initial parametric model, and the rest of inspection models are compared with the residuals of the specific initial model. But in real world applications (like buildings under earthquake excitation) every seismic event has different frequency, amplitude and direction characteristics. Such different magnitude, distance and severity earthquakes affect both case study buildings, introducing different dynamical parameters in the system of both buildings. This is the main reason that residuals based methods are inappropriate for this real world study. In contrast, group of model parameter-based methods, computes in every seismic event new parameters of the system, ignoring the past model parameters, such it is highlighted as appropriate for the specific study.

4.3.2 Parametric modeling

Parametric modeling on the field of damage identification is based on creation of models parametrized on a finite base, from data acquired from excitation and response recordings on buildings and/or structures. The vibration response of the structure could be measured either in acceleration, velocity or displacement, whereas the induced excitation is an acceleration maze.

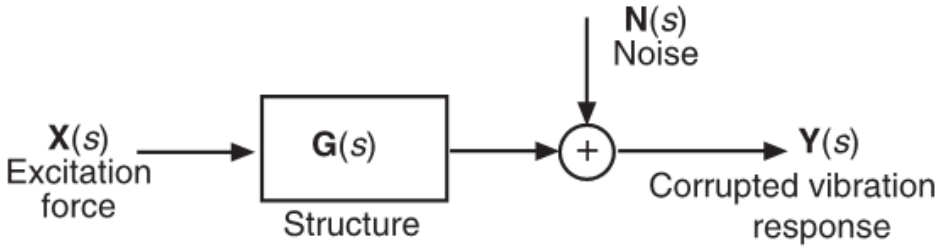

Figure 4.1. Experimental Identification schematic [50]

In figure 4.1 indicated the Laplace transform of an excitation $x(t)$, $G(s)$ is the transfer function of the system (or equally Laplace transform of impulse response function of the structure), $N(s)$ is the stochastic parameter that is induced in the system (could be noise, artificial or environmental procedures that could not be determined), and finally $Y(s)$, the Laplace result of the response of the structure $y(t)$. It is used the S plane (presented on section 2.3.4), because instead of solving a differential equation between input and output, the ouput could be just the algebric result of $X(s), G(s)\ and\ N(s)$ and the response could be just computed with the inverse FFT of Laplase output $Y(s)$.

Parametric methodology creates parametric models in terms of differential equations and/or modal approaches which overcome limitation of non-parametric methods. Models finitely parametrized present advantage of strong correlation with physical characteristics of case study structures, high frequency analysis and optimized accuracy, low number of parameter able to simulate dynamical characteristics of complex systems [50]. Combination of above advantages leads to ability of effective analysis, simulation, prediction and damage detection. The main disadvantage is that model is strongly related with the way that assesses the parameters of a system and also high computation demands.

In order to apply parametric methodology in vibration based techniques, it is necessary to follow specific procedure which determines every parameter for efficient identification.

These steps include:

- Determination of characteristics of recording data.
- Appropriate class of model.
- Methodology to assess model parameters.
- Technique to verify the created model and definition of damage or fault detection from designed model results.

Characteristics of data recordings can be distinguished to continuous or discrete mode recoding, with unique excitation and response, or several excitations and responses. Also type of data could be separated to either ambient or human made, and impermanent or guided by external factor. Class of model defines if the data will be non-linear or linear, random or deterministic, and if they could be determined by a transfer function, a complex exponential or a state space approach. The assessment of model parameter, defines the method that will determine the parameters of the designed identification model. This can be discritized in either absolute type of estimation, where the recording is computed one time in order to extract model parameters, either in dynamic type of estimation, where model parameters are computed every time there is new recording. Furthermore type of recording set; along with model class and model parameters estimation define a parametric identification techique.

The data sets of acceleration recordings, of instrumentation applied on this thesis, consist of simple input (excitation) multiple output (responses) signals. They are discrete acceleration recordings (vibration signals), with specific sampling rate (at 125 Hz). The data set consist of both ambient recordings (transient), and forced (seismic excitation). Experimental studies on buildings reveal that both ambient and forced excitation, is able to excite only a specific frequency range (0-10 Hz) on real structures (concrete 3 floor buildings). In the experimental instrumentation the reliable frequency identification up to 62,5 Hz (from Niquist theorem 125/2=62.5 Hz), much higher than the required frequency range. This enables a study of the response of the structures up to 62,5 Hz and indicate the effective frequency content of both case study structures. It is nessecary to remove the DC component from acceleration recordings data sets.

4.3.3 Autoregressive models

The Auto-Regressive (AR) model is a representation of a process where the output variable output depends linearly on the previous values. In an autoregressive model of order p, the value χ_ι is the linear equation of n previous values of the series with a term for the error β_ι. Time series data are considered as:

$$\chi_\iota = \alpha_0 + \alpha_1\chi_{\iota-1} + \alpha_2\chi_{\iota-2} + \cdots + \alpha_\nu\chi_{\iota-\nu} + \beta_\iota \qquad (4.15)$$

Where $\alpha_0, \ldots, \alpha_\nu$ are the weights which are required to be defined, β_ι is normalized to zero mean and dispersion in σ^2.

Moving average is a method used in statistics and calculates the average of the data for specific time series (moving average term). It can be seen as a finite response FIR filter which processes data and returns the average for a particular amount of data. Mathematically the moving average acts as convolution and therefore can be considered as low-pass filter for signal processing.

4.3.4 Class of parametric modeling

The class of a parametric model could be characterized by a complex exponential function, when noise affectes the output. In case the input-output system could be characterized by a transfer function then the parametric model class could be provided by a polynomial namely: ARX, ARMAX, Output Error and Box Jekins. Also in case the Kalman gain matrix is also available along with the input, output and prediction error parameters, then the state space class of model could be used. In the experimental procedure it is used ARX and ARMAX methodology because both buildings could be characterized as systems with specific transfer functions, both methodologies have low computation demands (computationally efficient), but with powerful results (lead to parametric models related with the dynamical parameters of the case study systems) and also the necessary data could be provided by the specific experimental instrumentation. Assessment of model parameters in identification techniques could be classified in 4 categories based on:

1. Methods based on prediction error
2. Methods based on least square
3. Methods based on subspace
4. Methods based on correlation

Prediction Error Method (PEM) is based on decrease of prediction error for one-step-ahead between design model and recording data set. Parameters of the model are created upon this necessity. Least Square (LS) techniques overpass complexity and initial definition of parameters value disadvantages of PEM, sacrificing high accuracy of PEM methods. Methods of subspace estimate model parameters through linearity and state space computations. Eigensystem Realization Algorithm (ERA) is known method of such kind. At last correlation techniques compare prediction error of specific models with past data set in order to create a function of correlation vectors.

Model order of an estimated parametric model, reveals and computes the number of the past data recorded on a data set, in order to create specific parametric model for these data

sets. Author Fassois [50] refers that model order is of great importance for parametric identification, as it defines the available degrees of freedom of a structure. In theory, model order determines the number of structural degrees of freedom, such optimum model order computation is requirement for efficient identification.

The optimum model order is defined in terms of fitting by criteria like Residual Sum of Squares (RSS), Output Error (OE) and Bayesian Information Criteria (BIC) [56].

RSS computes the quality of fit between stochastic model and data, but suffers from continuously decrease as order increase. BIC overpass this limitation by penalizing model increase and complexity through an added term:

$$BIC(\theta) \triangleq ln\left[\frac{RSS(\theta)}{N}\right] + dim\ \theta \times \frac{lnN}{N} \qquad (4.16)$$

Where ln is the natural logarithm, N the data record length and dim the vector dimensionality. The optimum model order is defined with the minimum BIC value.

Validation of designed parametric model is based upon, the comparison of the real data set, with the parametric model data set, and the computation of the residuals between them. An autocorrelation function of these residuals should not reveal any structure or high value of residuals. Such designed parametric model will contain all important imformation of recorded data set, and the residual of model and data will have totally uncorrelated information.

Each estimated parametric model represents a structural mode. In order to separate false modes from real modes, there are methods such as modal amplitude coherence, stabilization diagrams and dispersion diagrams. In the experimental analysis frequency, stabilization diagrams are used because they reveal effectively the real structural frequencies (stabilized on the diagram), instead of false frequencies which are unstabilized in the stabilization diagram.

4.3.5 The choice of model – ARX model

Autoregressive modeling with exogenous input (ARX) belongs to parametric identification modeling methods and it is very simple (related other parametric identification methods), powerful and common used. ARX is a single-input single-output technique (SISO). ARX modeling is a linear equation that calculates weighted past data from the system output with

system input. These data could provide the calculation of dynamic characteristics of a building. Below is the expression of ARX model:

$$a(x)y(t) = b(x)u(t) + e(t) \qquad (4.17)$$

where $a(x)$ is the polynomial of output $y(t)$ of the system, $b(x)$ is the polynomial of the input $u(t)$, x is the model order and $e(t)$ is the system residual error. The quotient of polynomial $\frac{b(x)}{a(x)}$ is the dynamic system transfer function.

$$y(t) = \frac{b(x)}{a(x)}u(t) + \frac{1}{a(x)}e(t) \qquad (4.18)$$

Autoregressive moving average modeling with exogenous input (ARMAX) is an extension of ARX modeling with simulation of the noise of the system with a polynomial $c(t)$ that applies moving average in the white noise of the system.

$$a(x)y(t) = b(x)u(t) + c(t)e(t) \qquad (4.19)$$

ARMAX model is a time series model studied and applied by American and British statisticians GEP Box G M Jenkins during the decade of 70s. The time series model ARMAX (p,q) has the below form:

$$x_t - a_1 x_{t-1} - \cdots - a_p x_{t-p} = y_t - \beta_1 y_{t-1} - \cdots - \beta_q y_{t-q} \qquad (4.20)$$

The real part parameters $a_j(1 \le j \le p)$named autoregressive coefficients and the real part parameters $\beta_j(1 \le j \le q)$ named moving average coefficients and $\{y_t\}$is the white noise parameter. Equation (4.20) is denoted by ARMAX (p,q) and called Moving Average Model of p autoreggresive order and q moving average order.

ARX model is effective in systems where noise is generally negligible, unlike ARMAX model which is suitable for stochastic systems with unpredictable noise level [54]. ARMAX form has a transfer function of noise which is able to reveal the variation of types of noise with the appropriate MA polynomial [56].

4.4. Structural Identification and damage detection methodology

According to Fassois and Sakelariou [103] statistical time series techniques for effective SHM include initially random signals which could be acceleration, velocity or displacement). Next is the design of statistical model, which includes non-parametric or parametric statistical models that depict the buildings on each structural state (healthy or damaged state). Last stage is the design of a statistical S quantity that compares the structural state for every event-case.

For non-parametric time-series analysis the statistical quantity S is based on non parametric models such as frequency based PSD, FRFs and coherence diagrams.

4.4.1 Non-Parametric Identification of the Healthy Structure Dynamics

The statistical quantity S, for the PSD based method, is the PSD vibration response signal. The PSD of the healthy state P_o is compared with PSD of current phase P_c. Damage detection is based on significant distribution of PSD in current phase related with PSD on healthy state. This PSD distribution is quantified by an index F equal with the normalized quotient:

$$F = \frac{\hat{P}_0/P_0}{\hat{P}_c/P_c} \qquad (4.21)$$

where $\hat{P}_0$ and $\hat{P}_c$ are the estimated PSDs of healthy and current states, P_0 and P_c the PSDs of healthy and current state. The specific limits where F is in healthy state, are determined by a propability $a-1$ where a is adressed as risk level and limits are $\left[f_{\frac{a}{2}}, f_{1-\frac{a}{2}}\right]$. More details could be found in Fassois and Sakelariou [103].

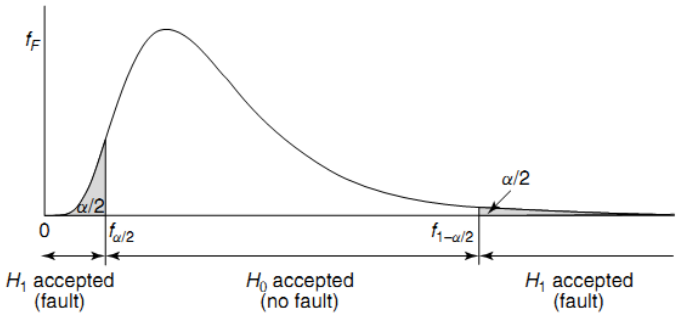

Figure 4.2. Statistical analysis by PSD F distribution [103]

The statistical quantity S, for the FRF based method, is the same as PSD with the addition that response and excitation signals are utilized as statistical quantity. Current structural state FRF magnitude $|H_c(j\omega)|$ is compared with healthy state FRF $|H_{co}(j\omega)|$ in order to reveal possible variance between magnitudes

$$v_o^2(\omega) = var\left[\left|\hat{H}_o(j\omega)\right|\right] \qquad (4.22)$$

Variance $v_o^2(\omega)$ is unknown and estimated from the FRFs of healthy state and below equation:

$$var\left[\left|\hat{H}_o(j\omega)\right|\right] \approx \frac{1-\gamma^2(\omega)}{\gamma^2(\omega)2K}|1-\gamma^2(\omega)|^2 \qquad (4.23)$$

Statistical analysis utilizes the “a” risk level to assess the similarity of the FRF magnitudes through the equation:

$$Z = \frac{|\delta|\hat{H}_o(j\omega)||}{\sqrt{2v_o^2(\omega)}} \qquad (4.24)$$

$$Z \leq Z_{1-\frac{a}{2}} \rightarrow H_o \text{ reveals healthy structure}$$

$$\text{Else} \rightarrow H_1 \text{ reveals damage}$$

$Z_{1-\frac{a}{2}}$ is the normal distribution. $1-\frac{a}{2}$ is the critical value (determines damage). Figure 4.3 presents the statistical FRF analysis of damage detection. More details could be found in [103]

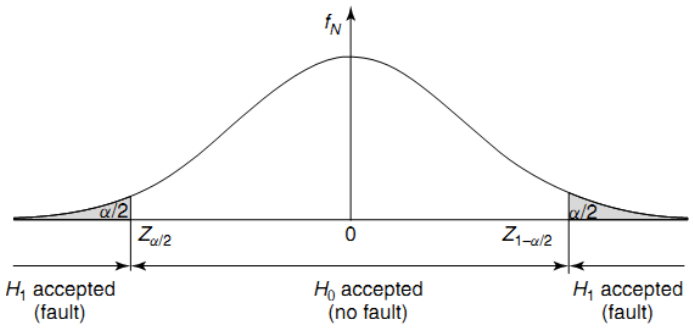

Figure 4.3. Statistical analysis of FRF by Gaussian distribution[103]

4.4.2 Parametric Identification of the Healthy Structure Dynamics

Suppose that h[t] designates the discrete-time impulse response function describing the relation between an excitation and a vibration response signal (figure 4.1). Let x[t] represent the excitation and y[t] the noise-corrupted response signal. The excitation and response signals are related via the convolution summation plus noise expression [103]:

$$y[t] = h[t] \times x[t] + n[t] = \sum_{\tau=0}^{\infty} h[t] \times x[t-\tau] + n[t] \qquad (4.25)$$

with × designating discrete convolution. Alternatively, using the backshift operator B (defined such that $B^j y[t] = y[t-j]$), the above may be re-written as:

$$y[t] = H(B) \times x[t] + n[t] \; with \; H(B) = \sum_{\tau=0}^{\infty} h[t] \times B^{\tau} \qquad (4.26)$$

Various parametrizations of equation (4.21) may lead to a number of models, including the AutoRegressive with eXogenous excitation (ARX) that is presently utilized [50, 210, 211]. A scalar ARX model is thus of the form:

$$A(B) \times y[t] = B(b) \times x[t] + w[t] \qquad (4.27)$$

with

$$A(B) = 1 + \sum_{j=1}^{na} a_j \times B^j \quad B(B) = b_0 + \sum_{j=1}^{nb} b_j \times B^j \; (4.28)$$

with w[t] designating the model's one-step ahead prediction error (residual) sequence, (aj, bj) the AR and X model parameters and (na, nb) the AR and X orders, respectively.

The parameter estimation of an ARX model is achieved by minimizing a quadratic criterion of the prediction error that leads to a typical Least squares (LS) estimator, [50, 210, 211]. Model structure selection, which refers to the determination of the model orders (na, nb) includes the successive fitting of ARX models of increasingly higher order until a suitable model is selected. Model order selection may be based on the model Residual Sum of Squares (RSS) [often normalized by the Series Sum of Squares (SSS)] as well as on the Akaike Information (AIC) and the Bayesian Information (BIC) which are statistical criteria that penalize model complexity (order) as a counteraction to a decreasing quality criterion such as the RSS [50, 210, 211]. Other tools such as the modal frequency "stabilization diagrams" which represent the estimated modal parameters (usually frequencies) as a function of increasing model order, the residual's autocorrelation function, the residual cross-correlation

with the excitation and the Sample Per (estimated) Parameter (SPP) that must be maintained sufficiently high, may be also combined for final model structure selection and validation.

4.4.3 Damage Detection based on a Statistical Time Series Method

The model parameter based method [103] for damage detection is employed in the present study. This method consists of two phases: (a) the baseline phase which includes the modeling (via identification) of the healthy structure and the method's training based on different measurements from the healthy structure, and, (b) the inspection phase that may be performed periodically or on demand for the detection of a potential damage as the structure is in an unknown structural state. It is noted that in the present study the baseline phase refers to the period before the strong earthquake where both buildings are assumed to be in their "healthy state".

More specifically, the identification of the healthy structure is initially achieved in the baseline phase based on ARX modeling as described in the previous subsection. Then, a characteristic quantity, say $Q = f(\theta)$, which may be a function of the model parameters or part of them (typically= θ) is extracted and a critical threshold is determined based on the measurements of the baseline phase.

Damage detection is then achieved in the inspection phase based on proper comparison between the parameter vectors θ_o and θ_u that correspond to the healthy and current (unknown) state of the structure through the following hypothesis testing procedure:

$$H_o : \delta\theta = \theta_o - \theta_u = 0 \text{ (null hypothesis-healthy structure)} \qquad (4.29)$$

$$\mathrm{H_1} : \delta\theta = \theta_o - \theta_u = 0 \text{ (null hypothesis-healthy structure)} \qquad (4.30)$$

under the null ($\mathrm{H_o}$) hypothesis is:

$$\delta\hat{\theta} = \hat{\theta}_o - \hat{\theta}_u \sim \mathrm{N}(0, 2P_0) \qquad (4.31)$$

(Bold-face upper/lower case symbols designate matrix/column-vector quantities, respectively)

where the hat designates estimator/estimate and Po designates the covariance matrix that corresponds to θ_o which is replaced by its corresponding estimate.

then the quantity:

$$X_{\theta}^{2} = \delta\hat{\theta}^{T} \times \hat{\delta}P^{T} \times \delta\hat{\theta} \quad (4.32)$$

follows a χ^2 distribution with d (parameter vector dimensionality) degrees of freedom. Full details are reported in [103]. Based on the above the following test is constructed at the α risk level:

$$\chi_{\theta}^{2} \leq \chi_{1-\alpha}^{2}(d) \rightarrow H_o \text{ is accepted (healthy structure)}$$

$$\text{Else} \rightarrow H_1 \text{ is accepted (damaged structure)}$$

with $\chi_{1-\alpha}^{2}(d)$ designating the χ distribution's $(1-\alpha)$ critical point.

4.5. Summary of methods

Summarizing in this chapter was presented the theoretical background of non-parametric methods PSD, FRF, Coherence digram and Horizontal to Vertical Spectral Ratio (HVSR). Also parametric methodologies ARX and ARMAX were presented along with the structural identification methodology that uses statistical time series methods, for effective SHM. All DSP methods are required on the next chapters 5 and 6, in order to test, apply, correlate, verify and validate the recording data, with possible change of dynamical parameters of case study buildings.

Chapter 5. Data analysis of SHM recordings with non-parametric methods

5.1 Frequency change method

5.1.1 Introduction

In this part of the thesis, it is studied the resonance frequencies shift, of the spectrum from acceleration recordings of case study buildings through time and seismic events. Findamental frequency shift is a fast computationally approach and does not require user expertation. In this direction it is applied a combination of digital signal processing methods to specific SHM data, namely FFT along with Wavelet Transform (WT) and Short Time Fourier Transorm (STFT), and also it is proposed an index of fundamental frequency deviation. Main aim is to reveal possible changes of fundamental frequency of case study buildings, in frequency plane but also in wavelet plane. FFT enables to define the fundamental frequency changes in frequency domain, STFT presents the frequency spectrum in space and time and WT presents frequency changes in wavelet plane. Above results give the ability to reveal the deviation of the building's fundamental frequency.

5.1.2 Description of the proposed DSP method on SHM application

A method is proposed, towards an adequate yet fast Digital Signal Processing method which attempts to improve the comparison of the previous (before damage) data with new (after damage) data without any prerequisite. It calculates only the current fundamental frequency spectrum deviation and presents its difference in undamaged and damaged state. The proposed method relies on the principle that stiffness of a structure is strongly related with the fundamental frequency of the specific structure [7, 8, 10, 212]. The main idea is that a system has very small limits of deviation of its fundamental (natural) frequency when no damage has occurred, and this deviation enlarges as the damage becomes higher. Figure 5.1 presents an example where the fundamental frequency of a structure changes by time denoting changes of the construction stiffness. The deviation of fundamental frequency gets higher as the mean value of the frequency gets lower and also the stiffness of the structure is reduced.

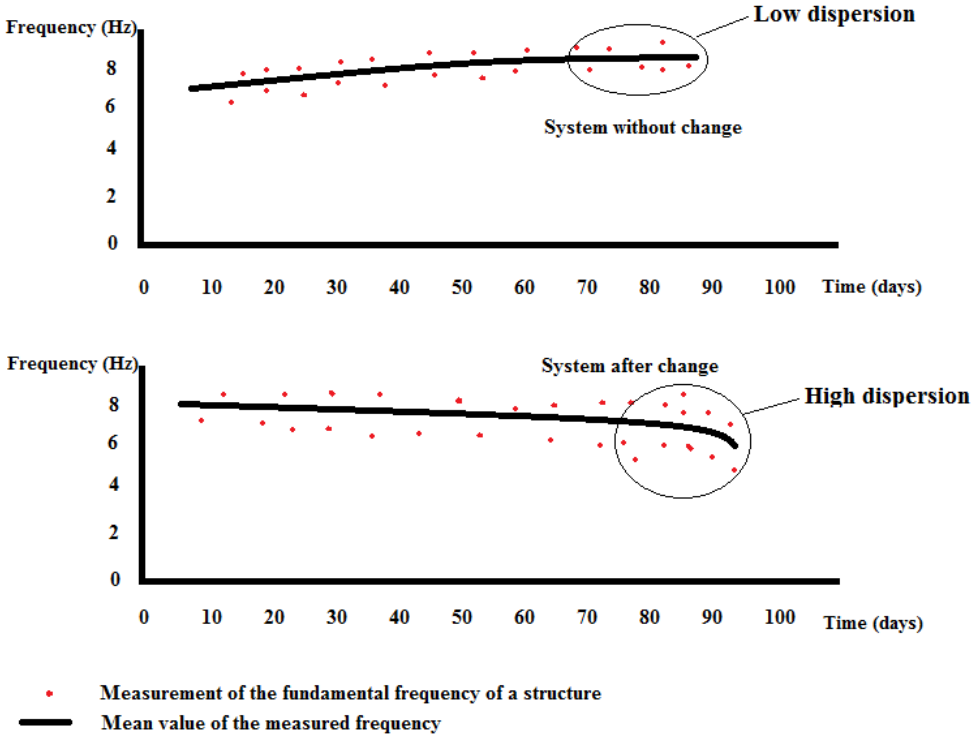

Figure 5.1. Low and high dispersion of fundamental frequency of a structure

The proposed method is used to measure the stiffness of a structure and the loss of stiffness. It applies the principle that natural frequency is damage sensitive parameter, so if there is a change in modal parameters, e.g., in stiffness, in dynamic response of the structure, the frequency parameter depicts this change. Frequency is the result of response, so any change has influence in fundamental frequency. The proposed formulation has as follows:

$$\mathbf{\Pi} = 1 - \frac{f_{max} - f_{min}}{f_{mean}} \qquad (5.1)$$

where **Π** is the proposed normalized index, f_{max} is the maximum fundamental frequency that appears in the spectrum, f_{mean} is the mean of fundamental frequency value of all the fundamental frequencies that have been measured (the whole variation of fundamental frequency) and f_{min} is the minimum frequency that appears in the spectrum

The suggested method has a major advantage as concern the problem of historical data of SHM. In the literature, the majority of FDI methods require SHM data of the structure before damage in order to compare them with the inspection phase data. In equation (5.1) it is used the maximum and the minimum recorded fundamental frequency and not the conventional variance, because the important is the maximum difference of highest and lowest frequency

(whenever it has occurred) and not the conventional variance of a specific measurement. With this method, the knowledge of past (before damage) data is not necessary. If there is damage the **Π**-index will have different value than undamaged state, due to the fact that in a healthy structure the frequency deviation will be small. Furthermore, if there is already damage of the structure the **Π**-index will have completely different value (lower than 1). As the damage increases the index will become lower, closer to zero.

5.1.3 Application of the proposed-index in SHM data

Π-index is implemented in the data of the wired SHM system of both case study university buildings.

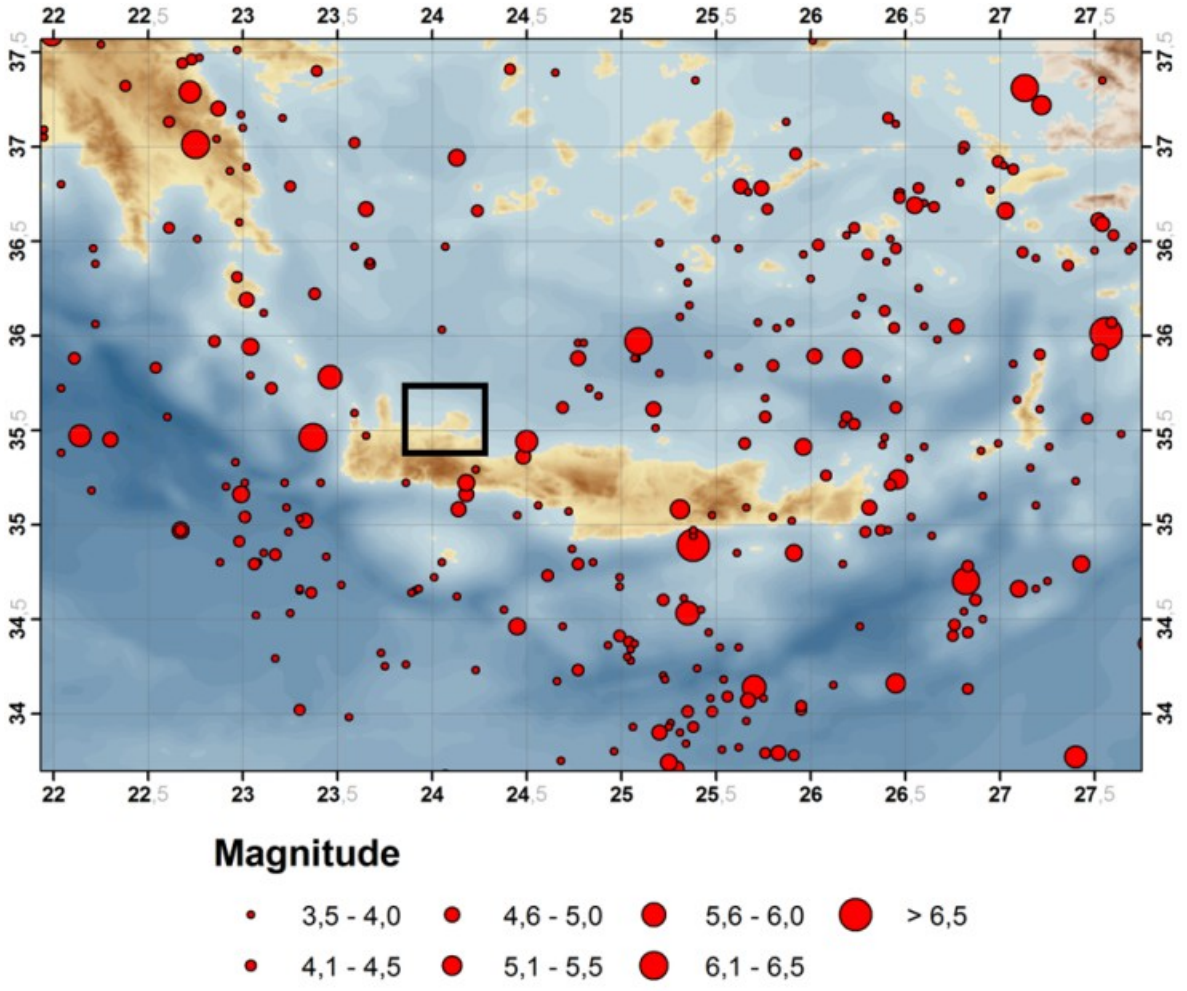

Figure 5.2. Seismicity of South Aegean in the period 2007-2010 recorded by the stations of the Seismological Network of Crete (M>=3.5) and location of Technological Educational Institute of Crete in the city of Chania (35°31'9.30"N, 24° 2'34.35"E)

Main characteristics could be addressed in:

- Computationally efficient and fast analysis of the recording data.
- Low process requirements.
- No need for data knowledge before damage (no need for comparison with historical data).

It is assumed that in case of damage on a structure, the differences between f_{max} and f_{mean} as well as between f_{mean} and f_{min} are larger than the difference without damage. Thus, measuring the deviation of fundamental frequency enables to address the damage on the structure.

5.1.4 Recordings of acceleration for both buildings

During the deployment of the wired SHM network in the two case study buildings of the TEI of Crete in Chania, PSDs (Power Spectral Densities) from accelerometer recordings have been studied at various locations in order to identify where the fundamental frequencies are monitored more clearly from the accelerometers. The experimental SHM set-up records seismic acceleration of both buildings for more than 24 months. The data are recorded and analyzed by applying FFT in order to present the frequency spectrum. Fundamental frequencies of both buildings are being monitored and **Π**-index is calculated from SHM records. Then WT is being applied to the measurements in order to depict possible frequency deviation wavelet plane, of each building (figure 5.3).

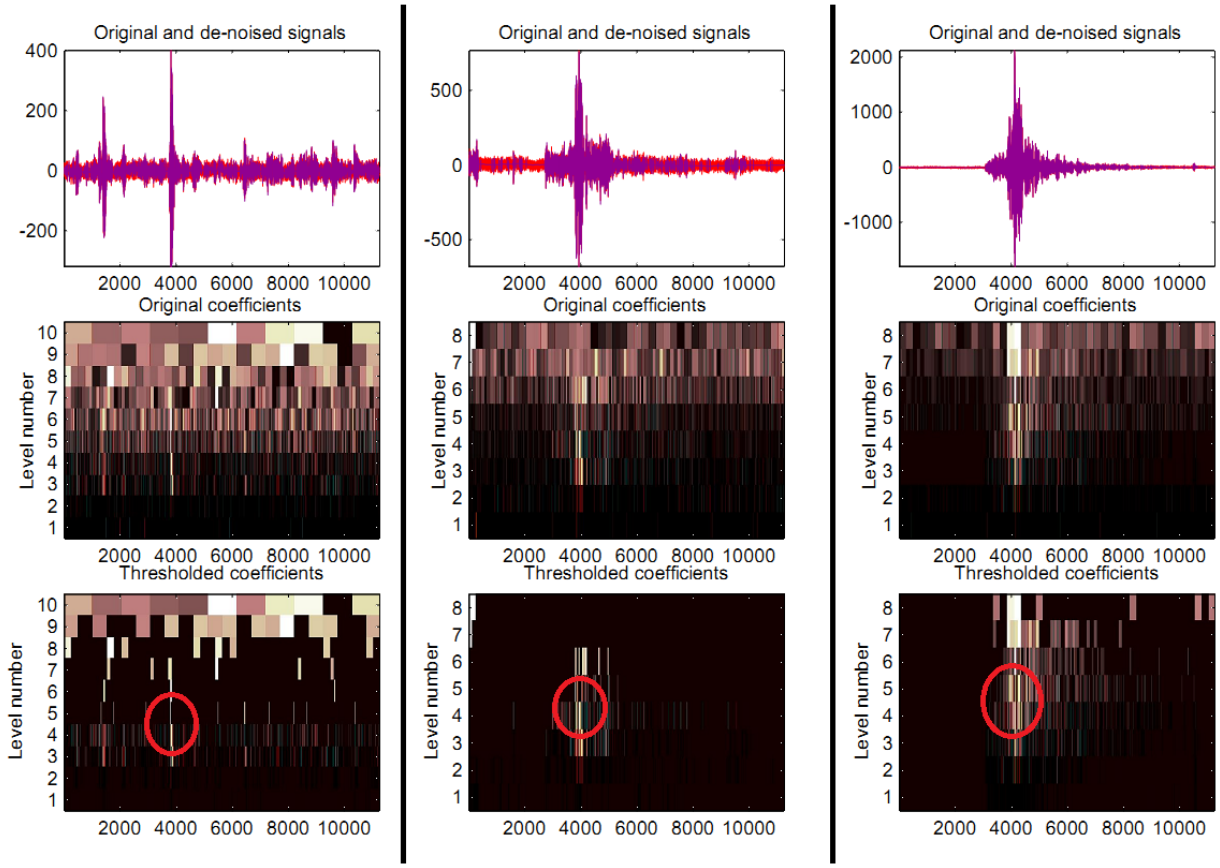

Figure 5.3. The 2012/11/23 02:08 UMT earthquake (left column), the 2012/12/05 06:54 UMT earthquake (mid column), 2013/01/05 02:04 UMT earthquake (right column), all recorded at 3rd floor of new building (3NB) accelerometer, North-South component (NS) 9F8E accelerometer, analyzed with Wavelet Transform, WV family db (level 2). In lower row data are denoised.

For the case of figure 5.4 (up row), the signal is very weak (the spectrum and distribution of energy from the earthquake on building is low) and therefore many frequencies are observed (the fundamental frequency of the new building can not be revealed). In figure 5.4 (mid row) the seismic acceleration recording has very clear spectrum and the fundamental frequency of the new building is 6.62Hz. Figure 5.4 (lower row) depicts fundamental frequency 6.5 Hz.

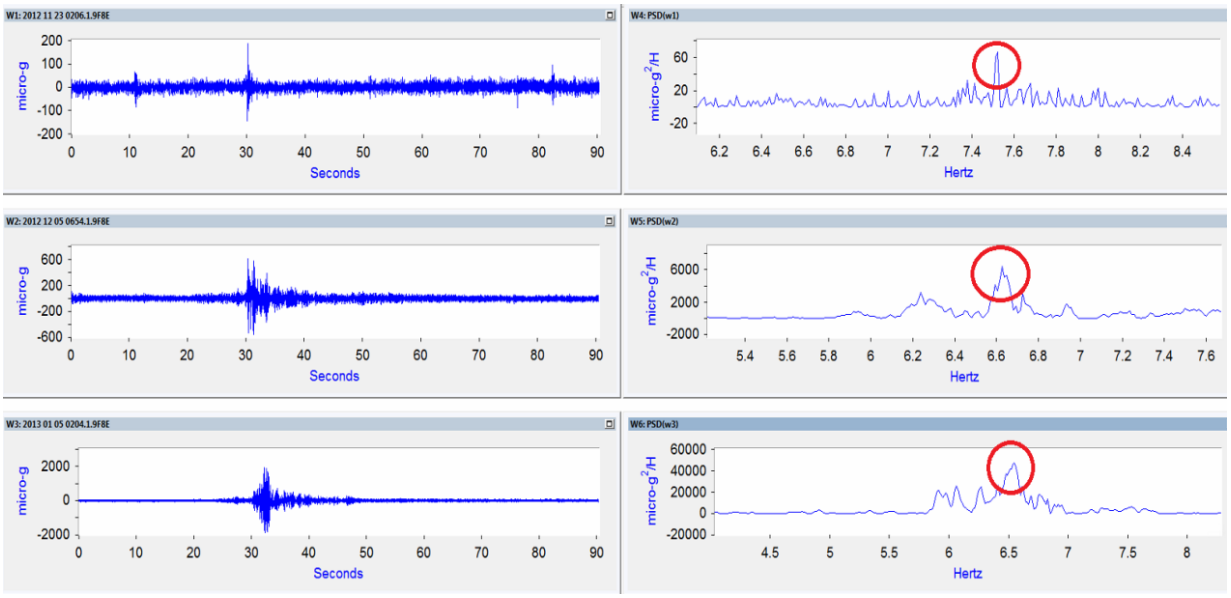

Figure 5.4. FFT based PSDs for the previous events (from figure 5.3)

Thus, there is a frequency deviation of 0.09 Hz in fundamental frequency. Consequently, **Π**-index of the new building is calculated:

$$\mathbf{\Pi} = 1 - \frac{f_{max} - f_{min}}{f_{mean}} = 1 - \frac{6.62 - 6.53}{6.57} = 1 - 0.013 = 0.987 \qquad (5.2)$$

5.1.5 Discussion

More data analysis by frequency deviation can be found in **Appendix C**. On analyzed data, fundamental frequency of case study buildings presents specific frequency deviation for each building, defined by the maximum and the minimum recorded frequency. Fundamental frequency changes exist for both buildings. Also the old building (19 years old) has higher frequency deviation than the new building (6 years old) and this indicates that, although the buildings have the same structural characteristics, the old one has suffered more damage than the new one mainly due to seismic activity all these years. As frequency change increases, it can alert about possible damage in buildings, but since results are not stable, more data required. Proposed index tries to quantify this frequency change, but it is not enough for the determination of damage, as this index changes in every new set of data. Such frequency change and Π Index are damage sensitive parameters but they should be correlated with other DSP methods (presented below) for efficient FDI.

5.2 Horizontal to Vertical Spectral Ratio

At next step, it is applied also a fast computationally, cost effective method which does not require high user expertization. Ambient noise is studied on buildings, for the purpose of structural health monitoring. The HVSR technique is widely used by geophysicist to study the resonance frequency of sediments over bedrock, while its usage inside buildings is limited. This study applies HVSR inside the two university buildings. Also there is HVSR application in another one, much older building, with visible cracks on its structure. Sensors have been installed on every floor of the two university buildings and recordings have been acquired for both ambient noise and earthquakes. Resonance frequencies for every floor of every building are calculated, from both noise and earthquake records, using the HVSR technique for the ambient noise data and the Receiver Function (RF) for the earthquake data. HVSR amplitude is correlated with the differential acceleration between floors, for every building, and this also is related with the vulnerability of the buildings. Results indicate that HVSR process on acceleration data proves to be an easy, fast, economical method for estimation of fundamental frequency of structures as well as an assessment method for building vulnerability estimation. Comparison between HVSR and RF technique show an agreement at the change of resonance frequency as we move to higher floors.

HVSR method is applied in every floor of the buildings in order to discover the effect of floor amplification on each floor and the similarities which may exist under seismic and ambient noise. The approach of studying the HVSR on each floor in a building, under seismic activity, and ambient noise and correlate the increase of HVSR value with the building internal drift, is done for first time. In this context this work proposes an index which is correlated with HVSR changes from floor to floor in a building and could probably present the vulnerability of a building (under excitation) on every floor. Below, figure 5.5 presents a map of the HVSR frequency for the broad region of the city of Chania. Case study buildings are located on the geographical region where recorded HVSR frequency is on the range of 0.49-0.69 Hz. The HVSR amplitude for the area close and on the case study university buildings is on the range of 0.40-0.54.

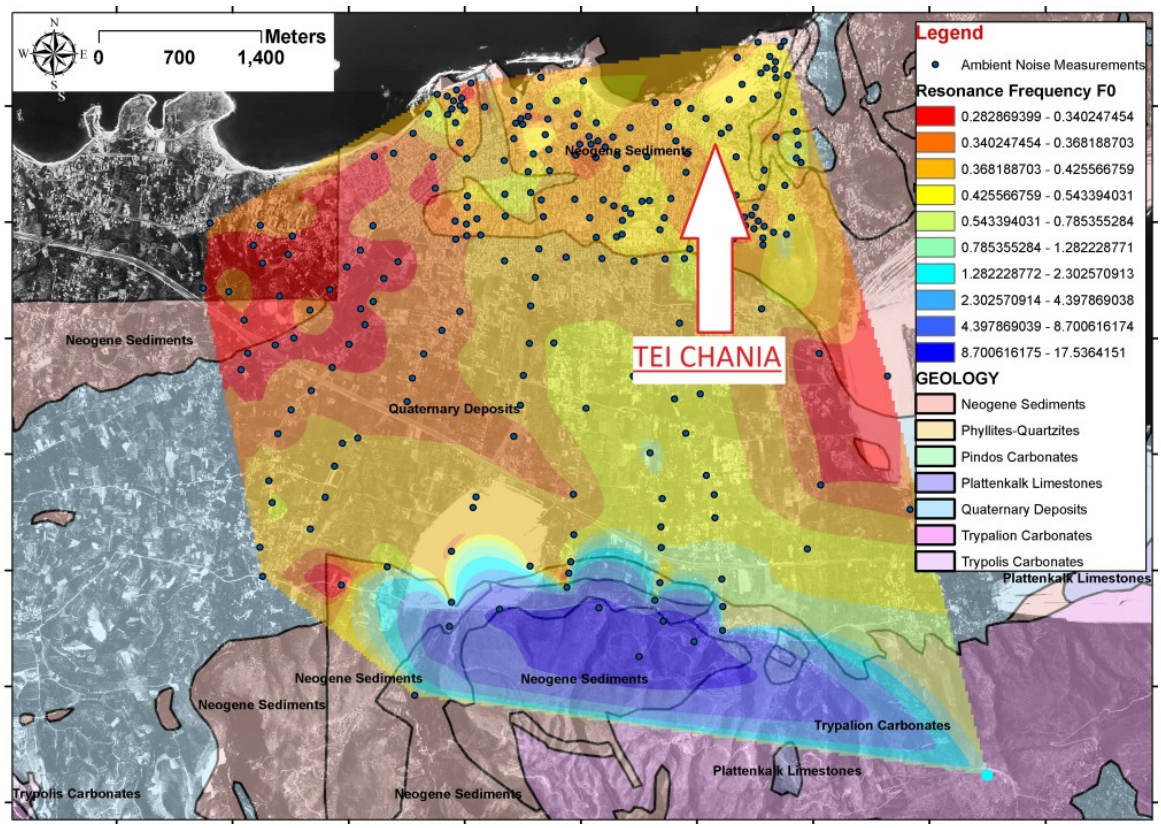

Figure 5.5. Case study buildings location is indicated. This map presents frequency of recorded HVSR for the broader area of Chania [213]

The instrumentation that is used in this work is from the wired SHM system which is deployed in the Technological Educational Institute of Crete, Chania, with accelerometers of high sensitivity, sample rate at 125 Hz, and configured in triggered mode [209].

5.2.1. Instrumentation for HVSR recordings

In this study three kinds of sensors are used, in order to present the recording capabilities of each approach. Initially a Reftek accelerometer 130 SMA is used with a scale range of +-4g, dynamic range of 112 dB @ 1Hz and a sensitivity of 1.6 V/g/m. The frequency response is from flat DC up to 500 Hz. More information about Reftek accelerometer SMA 130 can be found in Reftek [200]. Next a Guralp CMG-3ESP velocimeter is used, which is a broadband seismometer with response from 0.016 Hz until 50 Hz, sensitivity 2 x 1000 V/ms^{-1} and dynamic range higher than 140 dB. More details about Guralp Seismometer are on Guralp [214]. Also HVSR is studied by seismometer “Lennartz Le3D/5s”. The sensitivity is 400 V/m/sec with a frequency spectrum from 0.2-100 Hz. The sensitivity of the seismometer is

flat between 0.4- 100 Hz. Details about the ground velocity sensor “Lennartz LeD/5s” could be found in Lennarzt-electronic [215].

5.2.2. Comparison of velocimeter and accerelometer sensors for HVSR Method

HVSR is applied in seismometers and accelerometer, in order to study if they have the same sensitivity the same levels of electronic noise, and if the recorded data have the same ability to reveal the HVSR data. The recording of the ambient noise will be divided in specific length segment and will be processed by Fourier transform, presenting the frequency spectrum with the resonance frequencies.

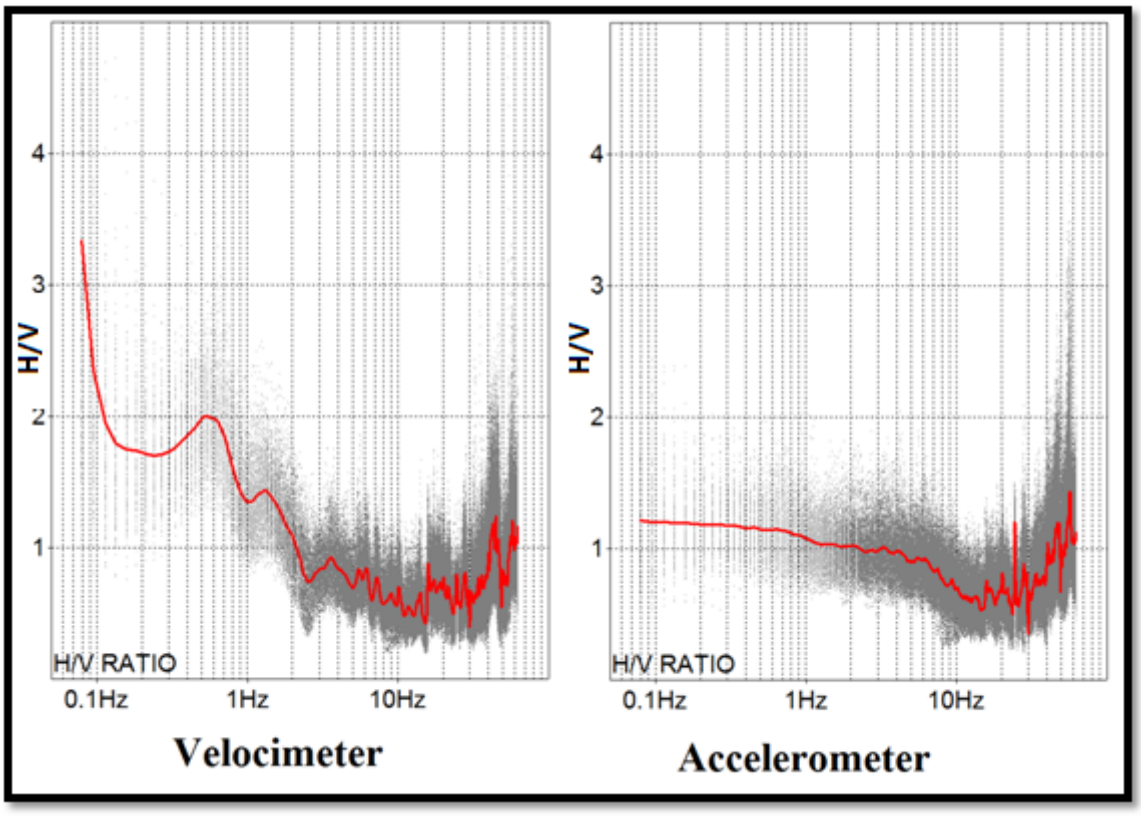

Figure 5.6. Data of Guralp velocimeter (left graph) and REFTEK accelerometer SMA 130 (right graph), analyzed with HVSR technique for a recording of 60 minutes length on the Ground floor, of the Old Building of TEI Chania.

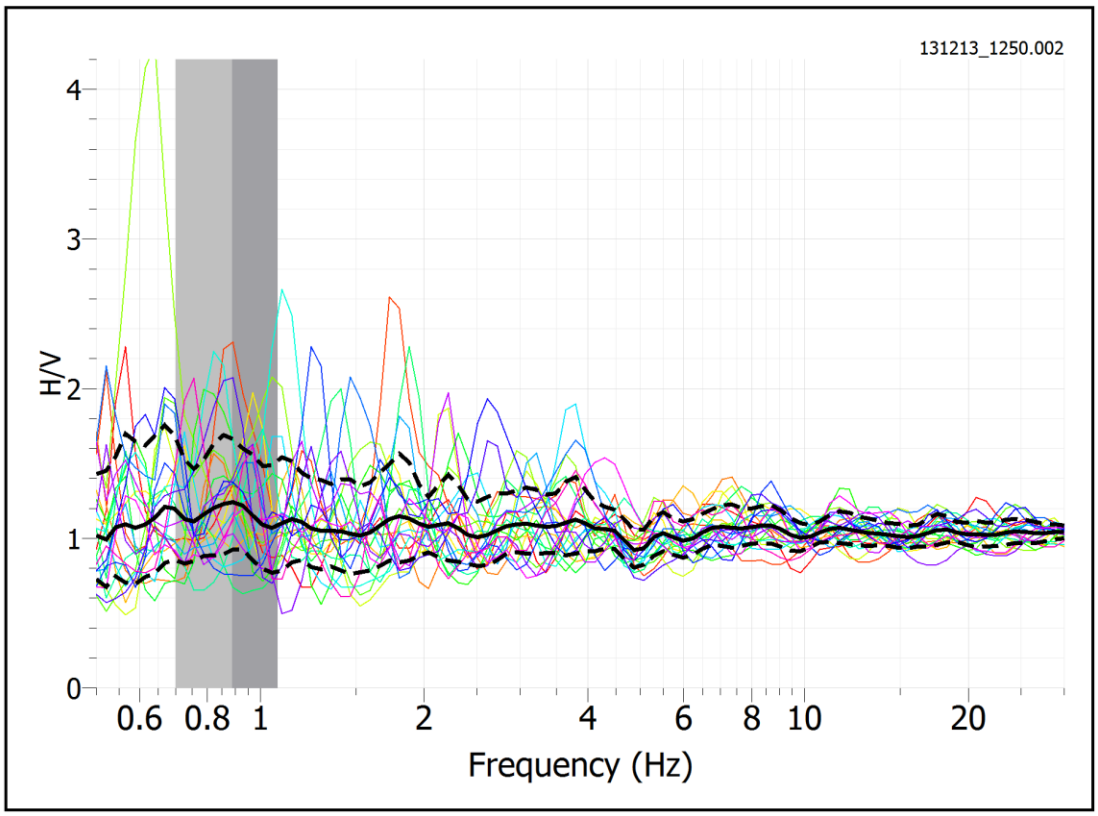

Figure 5.7. HVSR analysis of Lennartz LeD/5s velocimeter, for recording of 60 minutes length, on the Ground floor of Old Building of TEI Chania.

Figures 5.7 and 5.8 agree with the findings of Chavez et. al [216], where both instrumentation present the same characteristics for frequency higher than 2 Hz. Also the HVSR frequency and amplitude, from figures 5.7 and 5.8, recorded on the ground floor of old building of TEI at Chania, and for frequency spectrum higher than 2 Hz, is strongly related with the recorded HVSR frequency and amplitude of the surrounding area of TEI buildings (see figure 5.6 which presents the HVSR map of the broad region and show HVSR frequency close to 0.5-0.6. The lower HVSR amplitude (2.0) on the ground floor of TEI, (related with the HVSR amplitude of 2.5 for the surrounding open field of TEI) is expected as building functions like a filter-with specific transfer function, where energy of ambient noise is slightly weakens, from the open field to the building infrastructure.

In the case study experiment the fundamental frequency of both new and old building is much higher than 2 Hz (around 5.5 Hz). Fundamental frequency was computed from fast Fourier transform FFT of acceleration recordings at every floor of both buildings. HVSR method through specific accelerometers can function properly for the suggested approach of HVSR in SHM. The fundamental frequency of almost 5.5 Hz was recorded in every floor of

the building. From the recordings of seismometers in both buildings, the FFT reveals that below 2 Hz the seismic acceleration has very low amplitude. As a result in the specific structures the accelerometers that have an Eigen-frequency of 1 Hz and are able to measure frequencies higher than 1 Hz, are very efficient for studying HVSR method at these buildings. Other measurements that applied in the surround area outside the buildings of TEI Chania (with accelerometer) presented that HVSR resonance frequency is very close with the values of frequency spectral of velocimeter for frequencies higher than 2 Hz (figure 5.7).

5.2.3. Recordings of acceleration for both buildings

In this work, recordings from high sensitivity accelerometers are going to be analyzed with HVSR method. The recordings are from earthquakes that occurred in the wired area of the buildings and affected them, from midnight and noon recordings of ambient noise (each of 20 minutes recording duration). Each recording has been captured from every wired accelerometer (in every floor) of the new and the old building. The analyzed data are discussed in detail in order to present similarities and differences. HVSR data are studied, from earthquakes, midnight ambient noise and midday ambient noise, all recorded from the accelerometers of the wired structural health monitoring system of Technological Educational Institute in the city of Chania. One measurement of each kind for each sensor is presented. The analysis of all recorded data proves that there are very few and low range disturbances in the measurements and almost all the amplitudes and resonance frequencies are the same in HVSR graphs, for each kind of measurement.

5.2.4. Analysis of HVSR with specific processing software

Analysis of data with HVSR method is achieved by specific software (GEOPSY) [217], developed in the frame of SESAME program (Site Effects assesment using Ambient Excitations). The data proccess enquires specific procedures. Initially there is mean removal in the recordings. Then there is the specification of time.This section includes band pass filtering of the data in the frequency spectrum 0.5-30 Hz, range that it in the range of interest for in structural health monitoring (this frequency range includes the majority of resonance frequencies for structures and buildings), application of time window of 25 seconds according with the minimum frequency measured (0.5 Hz), no overlap of the windows and finnaly computation of frequency spectrum with fourier transform for the components North-Sout, East-West and Vertical and every time window.

The next process part is referred in the parameters of smoothing of data. The Ohmachi and Konno smoothing method is applied with smoothing constant value at 40 and cosine taper width at 5 %. Finnaly there is computation of horizontal to vertical ratio for every time window with log step of 100 number of samples and presentation of HVSR results. The horizontal componet is computed by the geometric mean of NS and EW component for every time window with the relation $H(t)=\sqrt{NS(t) \times EW(t)}$. In case study recordings all time windows are kept (even if they present very high amplitudes) in order to reveal the effect that they have in the structures. There is interest also for microtremors (human made excitation) and not only for microseismicity (enviromental noise) because both effect in the structura lcharacteristics of a structure. Below, figure 5.19 presents the three components of a 10 minutes duration recording. (Vertical component is "Z", North-South is "N" and East-West is "E"). As figure reveals, some noises-excitations are presented on three components and other only on two or one.

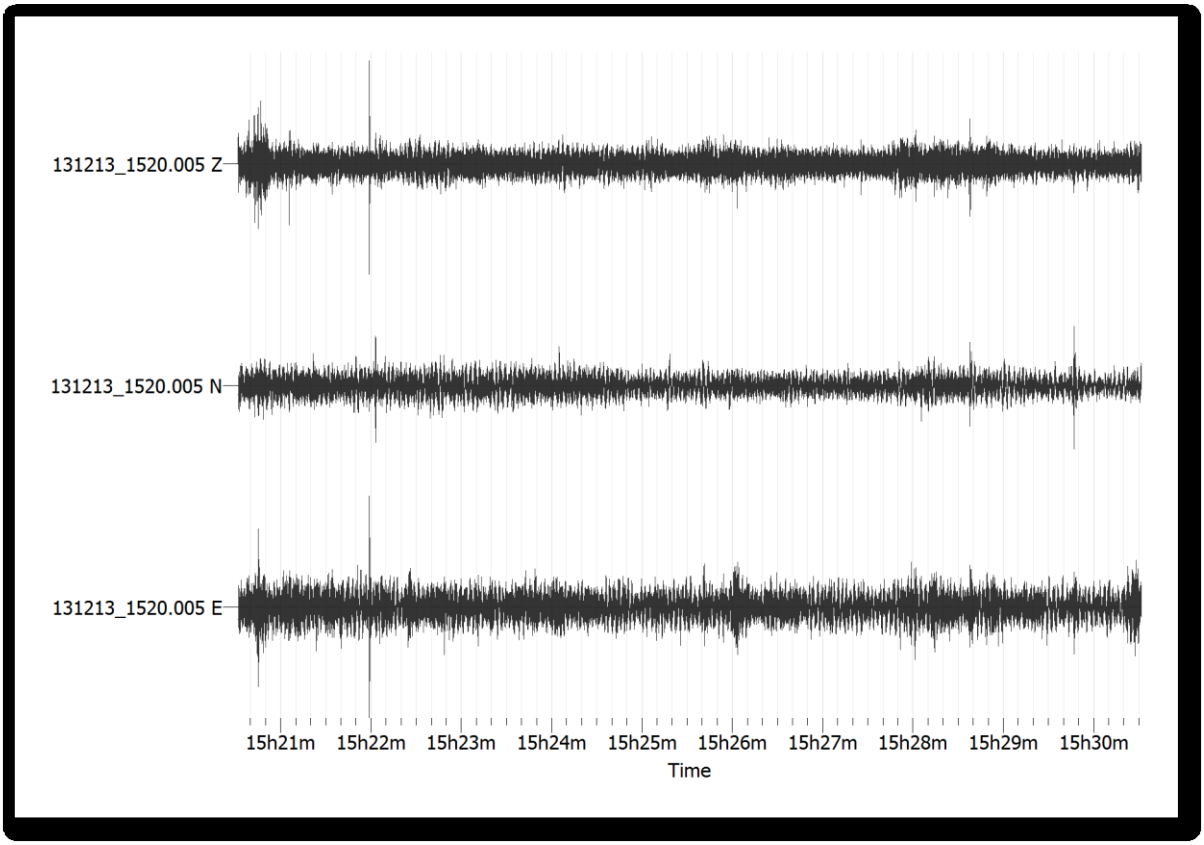

Figure 5.8. 10 minutes recording of ambient noise on the 2nd floor of the new building of TEI Chania.

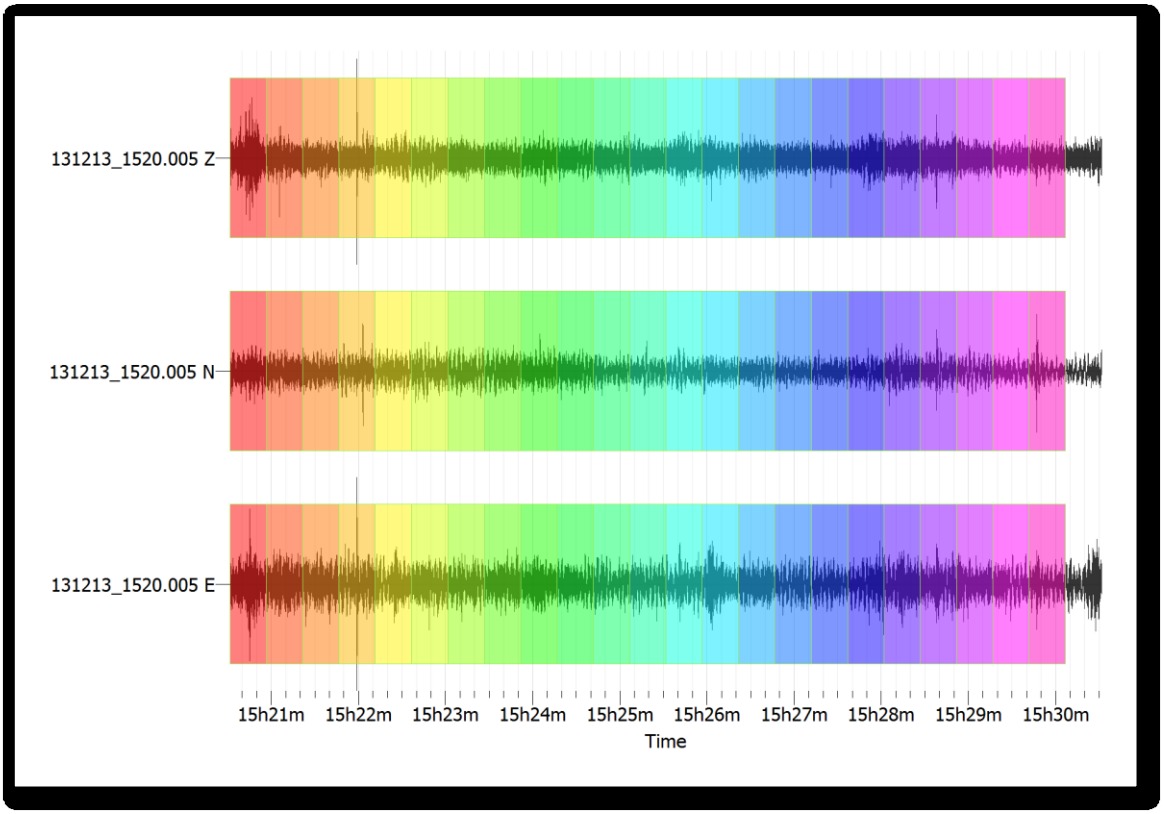

Figure 5.9. ***The time window (up) of 25 seconds for the previous recording with the HVSR result (down). Different colours corresponding in different time windows. Grey background colour presents the automatic recognition of fundamental frequency of the Geopsy program [217].***

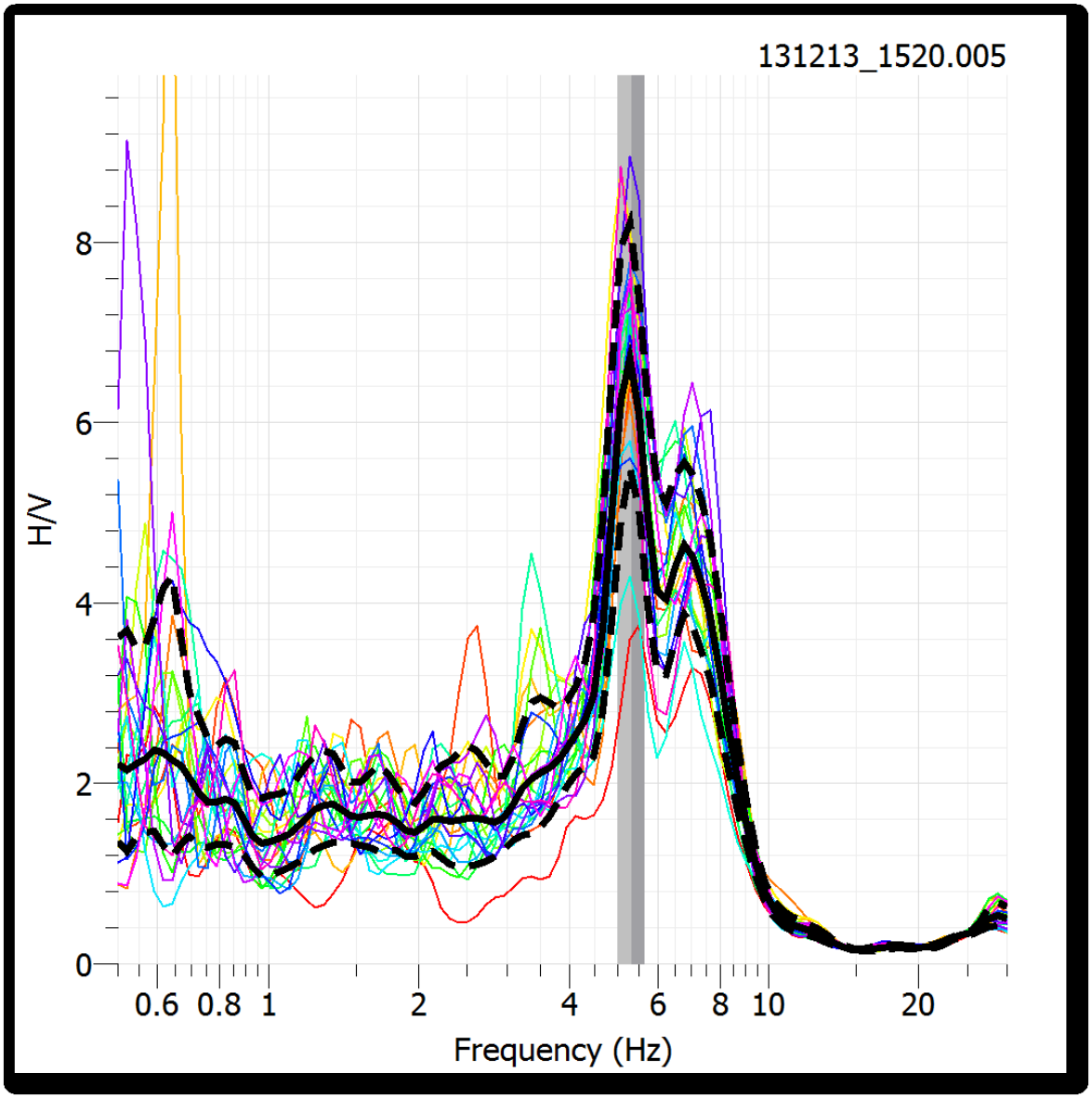

Figure 5.10. The time window of 25 seconds for the above recording(left) with the HVSR result (right). Different colors corresponding in different time windows. Grey background color presents the automatic recognition of fundamental frequency of the geopsy program.

Figure 5.9 presents the same recording (with figure 5.8) of ambient noise acceleration on three components, windowed with specific length of 25 sec (with different colour each time window), in order to separate specific time durations of the recording signal and analyze it with HVSR technique. Figure 5.10 presents the HVSR of the corresponding time window (for each colour). Such figure 5.10 presents the sum of HVSR plots of all the time windows of 25 seconds duration. The highest amplitude of HVSR plots is indicated with grey bold line on the background of graph in figure 5.10. The specific frequency is presented for the highest amplitude arround 5.5 Hz. The corresponding amplitude reach up to 9. There is a dispersion

on amplitudes because each time window (of figure 5.9) contains different ammount of energy. Artificial noises that induces in case study recordings, contain more energy. Such in order to approximate the real HVSR value there is a statistical approach of many time windows in order to indicate the contianing artificial noises and minimize their effect.

5.2.5. Data Analysis

In this part of study there is proccess analysis of an earthquake that occured at 28 april 2013 at 16:31 UTC 250 km away from the buildings at TEI chania, with a magnitude of 4.7 M. Data were recorded by SMA 130 instrumentation. On figure 5.11 is depicted the map epicenter of the case study earthquake.

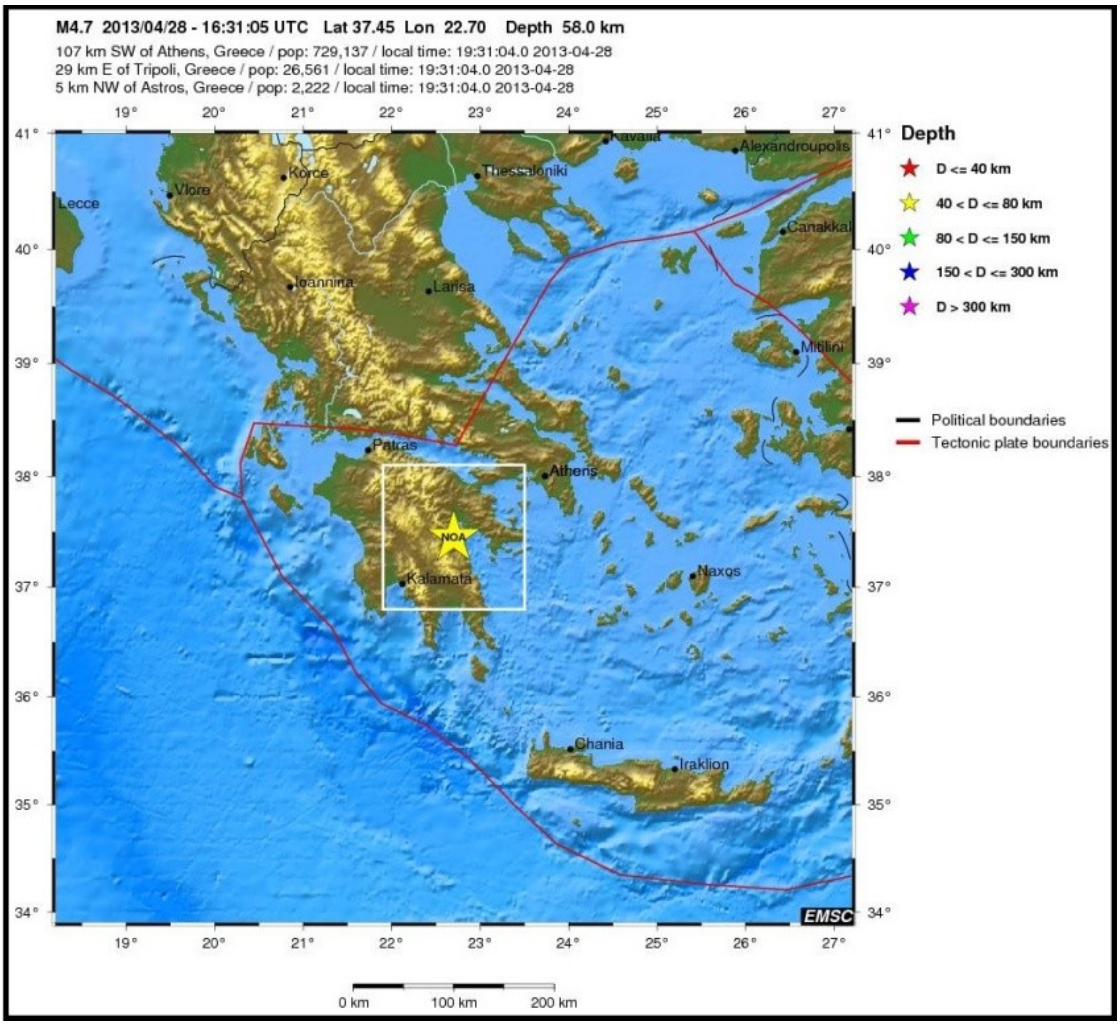

Figure 5.11. The 2013/04/28 16:33 UMT time seismic event at 37.45 (Latitude) 22.70 (Longitude) 58.0 Km (Depth)[201]

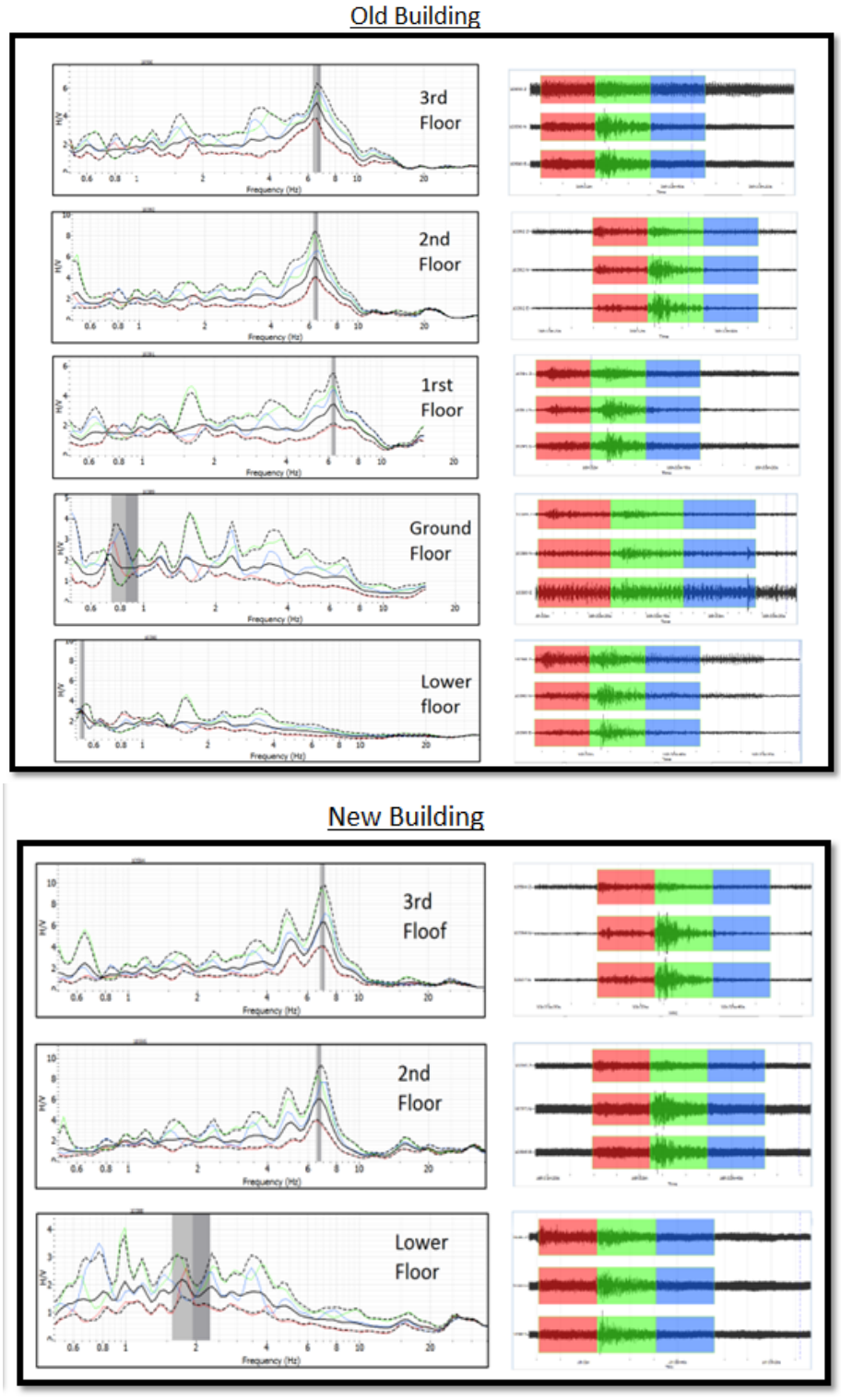

Figure 5.12. HVSR recordings on 2013/04/28 16:33 UMT (2013/04/28 19:33 local time) on the old (up) and new (down) building of TEI in Chania for the above seismic event.

Figure 5.12 reveals the HVSR analysis of the seismic event of figure 5.11, as it was recorded by the SMA accelerometers on TEI buildings at Chania (old and new building). The acceleration time series have been separated in three time duration zones (red, green and blue) with 25 seconds time duration, each time window. Red window contains the "primary wave" of the earthquake, green the "secondary wave" and blue the "after the secondary wave". Figure presents that the amplitude of HVSR plot is higher as the energy is getting higher. Such the HVSR amplitude plot of P-wave is much lower than the S-wave plot. Also the HVSR amplitude rises as the floor rises.

In **appendix D**, there are another four seismic tests that reveal if the HVSR remains stable due to different parameter seismic excitation on both case study buildings. Also there are HVSR tests with ambient noise and under earthquake excitation for the old and the new building.

From data analysis it is concluded that resonance frequencies of both buildings remain stable for each floor and also the amplitude remains the same for each corresponding frequency. Furthermore, the increase of the amplitude for old and new building follows the same pattern. For the old building, on the 3rd floor, the first resonance frequency is on the range of 6 Hz and second at 8 Hz. The same resonance frequencies are reveal on the 2nd floor and 1rst floor with lower HVSR amplitude, during noon and midnight. On the ground floor and lower floor of the old building the energy of the ambient noise is so low, that there is no effect from the transfer function of the building, and the ambient noise of the surround area is revealed on the lower floors of the building (the HVSR outside TEI is on the range of 0.55-0.65 Hz). For the new building on the 3rd floor the first resonance frequency is presented on the range of 5.7 Hz and the second on the range of 8 Hz. On the 2nd floor the value of HVSR lower. On the lower floor of the new building the energy of ambient noise is again so low, that it is not able to excite the resonance frequencies of the building and such the HVSR plot is almost a smooth curve, highlighting the HVSR value of the area outside TEI.

Data analysis reveals that, in every HVSR measurement in the old and new building, HVSR rises with higher rate in the old building and with lower in the new building. Under earthquake excitation or under ambient noise , old building, which has been effected by much more load from seismic and human made ecxitation but also from the time (as it is much older than the new building), presents higher HVSR rise, from floor to floor. Also the TEE building which is a very old building, with many visible cracks on its structure presents

much higher HVSR rise than the two buildings of TEI. HVSR rise could function as an indicate from possible high vulnerability of a structure. From the above recordings, it is observed that in both earthquakes the FR was almost the same for the old and the new building for each floor. As the floor goes higher the FR also goes higher. The windows that include S waves have much higher FR than the windows with P waves and the windows after S waves. In the programmed recordings of 30 minutes at noon and night the hvsr is much more lower at every floor but it also rises as the floor gets higher with a much more low rate that in seismic events.

5.2.6. Results

Accelerometers present lower HVSR than seismometers. This is expected as acceleration is the derivative of speed. The HVSR recordings of accelerometers are the derivative of HVSR of seismometers. The resolution of accelerometers, from frequency spectrum higher than 2 Hz is very high, compared with resolution of seismometers, presenting all the resonance frequencies of the structures with great detail. For buildings that fundamental frequency is higher than 2 Hz accelerometers could be used of HVSR measurements. As the floor gets higher the amplitude of the HVSR index rises in the range of resonance frequencies. This indicates that the differential acceleration from floor to floor increases and such increase the vulnerability of the structures as the getting higher. (There is specific threshold of differential acceleretion from floor to floor that indicates damage when the value operpass this threshold).

HVSR plots of ambient noise of old and new TEI buildings, for each floor reveal that:

- Analysis of acceleration recordings under seismic activity present the same frequency spectrum under FFT analysis and under FR analysis.
- Proccessing of ambient data with HVSR method and earthquake data with FR method, present almost the same analogy of amplitudes increase, for the same frequencies.
- Old building of TEI, is revealed to have higher RF under earthquake excitation, but also higher HVSR under night and day ambient noise.

Conclusively ambient noise analysed with HVSR method could present the amplitudes that affect each floor of a structure and also present an index (see figure 5.13) of effect of seismic acticity in each floor of a building. This index is the tilt of the graph from floor to floor in each building for each kind of measurement and presents how the HVSR rises as the floor

gets higher in each condition (under earthquake excitation, and/or under ambient noise during night and noon).

5.2.7. Description of the proposed index

The specific index presents the change of HVSR of the fundamental frequency of the structure from one floor to another. In ideal conditions this index should be stable. As the HVSR increase the influence of site amplification in the specific structure increases. And if the HVSR increase on higher floors it indicates that there is higher vulnerability of the structure in higher floors. The fundamental frequency of HVSR recordings at each floor is being measured and there is comparison of the increase of the value of HVSR, and it is correlated this rise with the increase of probably vulnerability of the structure. On figure 5.13 presents the rise of HVSR maximum amplitude value, for the three case scenarios (night, noon and under seismic excitation) for the old and the new TEI building respectively.

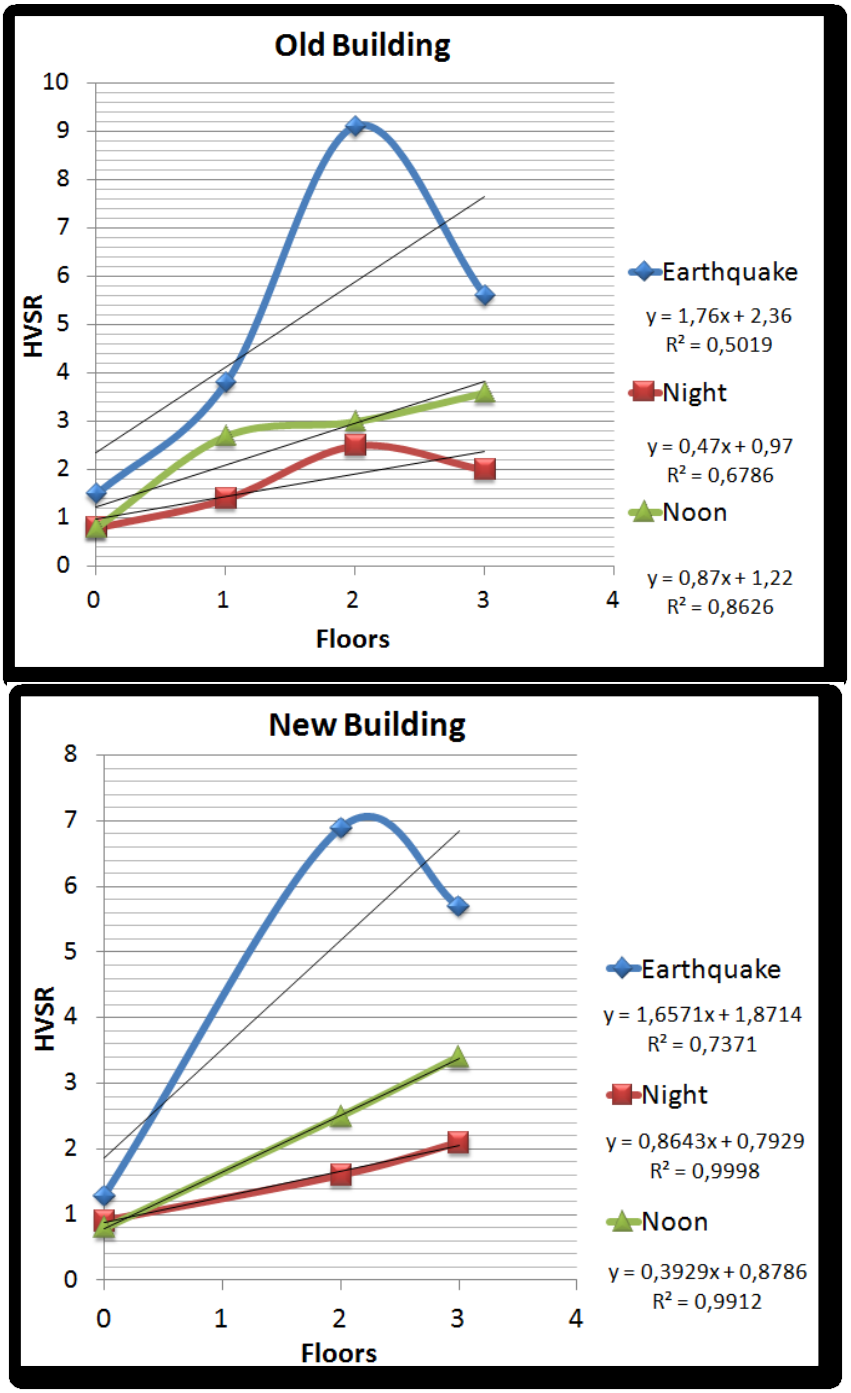

Figure 5.13. HVSR recordings from the on 2013/03/09 07:43 UMT time seismic event (Blue line), the 2013/03/12 midnight recording (red line) and the 2013/03/12 noon recording of the old (up) and new (down) building of TEI in Chania

There is effort to approach this index from the field of digital signal processing rather than the civil engineering, and correlate the increase of HVSR with the increase of the amplitude of structure accelaration of the building. This approach is instead of a simple value of horizontal to vertical spectral rations to study the rate of increase or decrease of this value

as the floor gets higher or lower. The RF under seismic excitation, as well as the HVSR under night and day ambient noise, is higher for the old building in relation with the new one.

5.2.8. Discussion

HVSR technique has been used in order to present the impact of seismic activity in two building (different age), and how it differs from floor to floor. In this work there is a novel approach of HVSR method in SHM recordings. SHM data gathered from wired SHM system are analyzed by HVSR method. These data present the effect of ambient noise in the ground floor, the second and the third of two university buildings and also present the effect of amplification site which could define vulnerability of each floor and the whole building. This work uses HVSR technique to compare ambient noise in both buildings (19 years old and a new 7 years), search the site amplification in ground floor, 2nd and third and try to find out if these recordings extract interesting findings in terms of site amplification. Also is trying to find out possible differences and similarities in the structural response of both buildings under seismic and ambient excitation. From the earthquake data it is observed that HVSR is much higher in every floor than the programmed time measurements and also that these values follow the pattern of the seismic acceleration of the building (the transfer function of the building) where the amplitude of seismic acceleration of the second floor is higher than the amplitude of the third floor.

5.2.9. Conclusions

Horizontal to vertical spectral ratio and Receiver Function (RF) methods, have been applied in microtremors and earthquake acceleration recordings, in order to study the resonances frequencies and their spectral amplitude, that exist in two concrete buildings, in a high seismogenic region. These frequencies are in the range 5,5-6,5 Hz. The site amplification on the area that case study buildings are located, is much lower (arround 0.7 Hz). The HVSR rise as floor gets higher. In this study the increase of HVSR is strongly related with the age of the buildings and the visible cracks in the beams. HVSR also indicates higher differential acceleration from floor to floor and such higher structural vulnerability. This work presents for first time an approach of HVSR by implementation of the method for structural health monitoring. More specifically it applies HVSR in each floor of buildings, finds out the different HVSR values and suggests a new index which compares and analyses the HVSR of the fundamental frequency in each floor of a building and how this value changes. Also it searches the possibility of correlation of this value with the vulnerability of a building and

presents that as HVSR rises as floor gets higher the vulnerability of the building could rise for these floors.

Analysis of building vulnerability provided by HVSR and/or RF method is a very cost effective and fast method which uses simple acceleration recordings and provides information for structural vulnerability. The data results of this study reveal that earthquake excitation follow the same analogy of RF rise (as the floor rises) as the HVSR of ambient noise excitation. This could indicate the way that a structure could response under strong seismic excitation, by recording simple environmental noise (microtremors). HVSR index could also indicate higher vulnerability for a concrete building, but since values are not stable (change for every seismic event), they should be correlated with other DSP methods, in order to apply effectively FDI in buildings.

5.3 Data analysis by power spectral density method

Next, Power Spectral Densities (PSD) of acceleration recordings on both new and old building at TEI Chania are analyzed and presented. These data analysis reveal the frequency content of structural acceleration caused by seismic activity, at every floor of both buildings.

Figure 5.14 presents the PSDs of seismic acceleration of TEI old building, for the earthquake of with code name b1 from table 3.3 (09/03/2013 3.9 M 67 km). On the upper row are the three components (East-West, North-South and Vertical) for the 1^{rst} floor. On the mid row are the 3 components for the 2nd floor. On the lower row are the 3 components of the 3rd floor. It is observed that PSD in EW component presents almost the same spectrum for every floor. Respectively NS and vertical components has the same spectrum on every floor. This reveals that specific energy spectrum is applied on every component on the building, due to seismic acceleration, and this spectrum is different for every component.

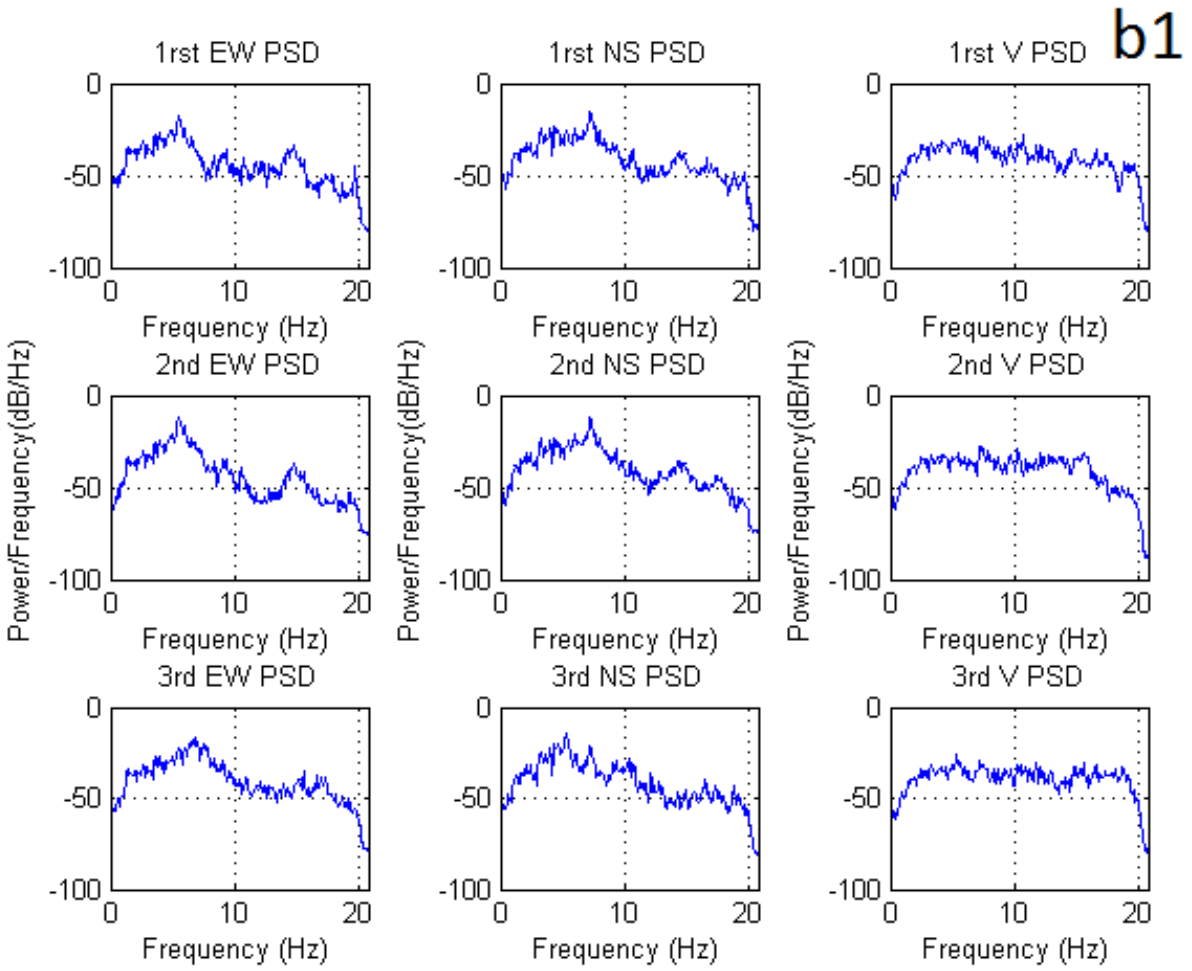

Figure 5.14. Power Spectral Densities of the old building 1rst floor(upper row), 2nd floor (mid row) and 3rd floor (lower row). Left column refer to East-West component, mid column to North-South component and right column to Vertical component. The seismic event is with name code b1 from table 5 (09/03/2013 3.9M 67km)

More PSDs analysis could be found in **Appendix E.** PSDs have been applied for more the 20 events before the 6.4 M seismic event and more than 15 seismic events after the 6.4M event, in order to have a statistical number of events able to indicate important changes in frequency content of structures under seismic excitation. PSD analysis indicates resonance frequencies and power spectrum effectively, but there is a big disadvantage. If we consider that building is a system with input (the basement) and output (1rst, 2nd and 3rd floor) then the PSDs of the outputs that we study are strongly affected by the changes and uncertainties of input for every seismic event. Every earthquake induces different energy on both buildings and this is presented on PSDs. Such although PSD presents more information from the frequency shift (presented in 5.1) and HVSR rise (presented in 5.2), it is also not enough, there are uncertainties and also PSD is not stable for different seismic event. In order to

overpass this limitation and eliminate the effect of input in analysis, we will study output in accordance with input (of seismic acceleration of case study building) for the same earthquakes. Section (5.4) there is Frequency Response Function analysis. Since PSD analysis presents so high distribution (in graphs) in structure's response PSD P_c, it is not applied PSD statistical time series analysis based on PSD (presented on section 4.3.1), because results would be inaccurate (the effect of input-excitation is very high in the output-response of the case study system-building).

5.4 Data analysis by frequency response function method

In this section there is data analysis with frequency response functions of acceleration recordings on both new and old building at TEI Chania. Data analysis reveals the frequency content of structural acceleration caused by seismic activity, at 1^{rst}, 2nd and 3rd floor (output-response) in correlation with frequency content on the lower floor (input-excitation) on each building. FRFs of seismic event are presented for the same events as above, in order to reveal how much is the amplitude of frequency response function (or the transfer function) of both buildings, the changes from event to event and also the limits of these correlations.

Figure 5.15 shows the FRF output (1rst, 2nd and 3rd floor) in relation with the input (basement floor). The upper row is output of 1rst floor related with basement and respectively mid row is 2nd floor output related with basement and lower row is the 3rd floor output related the basement. Each column refers to either NS component or EW or vertical. For the EW component (left column) it is observed that spectrum is almost the same for every floor. Respectivelly NS and vertical components present almost the same spectrum for each floor, but EW related to NS and to vertical component present different spectrum. This reveals that seismic acceleration is different for each component (as presented also in PSD analysis in section 5.3) but on the same component remains the energy is almost the same spectrum. More FRF plots of other earthquakes could be found in appendix E in order to reveal the changes of FRF between different earthquakes with different energy spectrums. Although every earthquake induces different dynamic parameters in the system (case study building) the FRF plot is much more stable than the PSD plots, in terms of frequency amplitude and frequency shift.

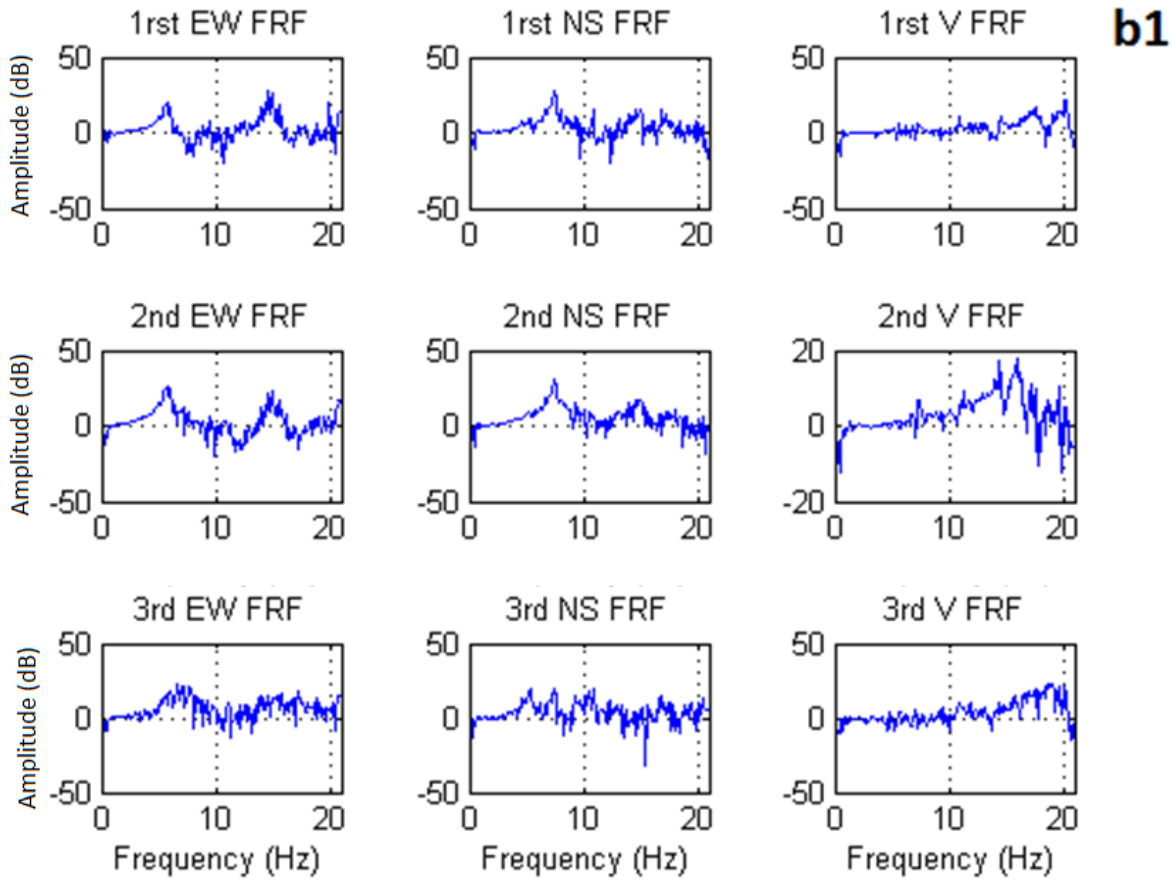

Figure 5.15. Frequency Responce Functions of the old building lower floor(input) in relation with outputs: 1rst floor(upper row), 2nd floor (mid row) and 3rd floor (low row). Left column refer to EW input with EW output , mid column refer to NS input with NS output and right column to Vertical input with Vertical ouput. The seismic event is with name code b1 from table 3.3 (09/03/2013 3.9M 67km)

More FRF graphs could be found in **Appendix E.** FRFs have been applied for more the 20 events before the 6.4M seismic event and more than 15 seismic events after the 6.4M event, in order to be a statistical number of events able to indicate important statistical changes in the correlation of frequency content of structures, between excitation (lower floor) and response (1^{rst}, 2nd and 3rd floor) under seismic excitation.

5.5 Non-parametric statistical time series analysis of frequency response functions

In data analysis of seismic acceleration FRF is much more stable than PSD under different earthquakes on case study buildings, because the effect of input on output is eliminated. In order to reveal possible changes in FRF plots there is the need of high amount of events

(non-parametric analysis) in order to assess possible change in dynamic parameters of the system. In order to reveal structural changes it is applied statistical analysis of FRF changes from FRF plot to FRF plot. The FRF of one seismic event is compared with FRF of another seismic event. The distribution of FRFs cases are analyzed under a statistical manner according to the methodology presented in chapter 4.3 (FRF statistical analysis). A threshold defined by user (the "a" risk level) determines the accepted FRF distribution limits, indicating healthy state or possible damage through FRF analysis.

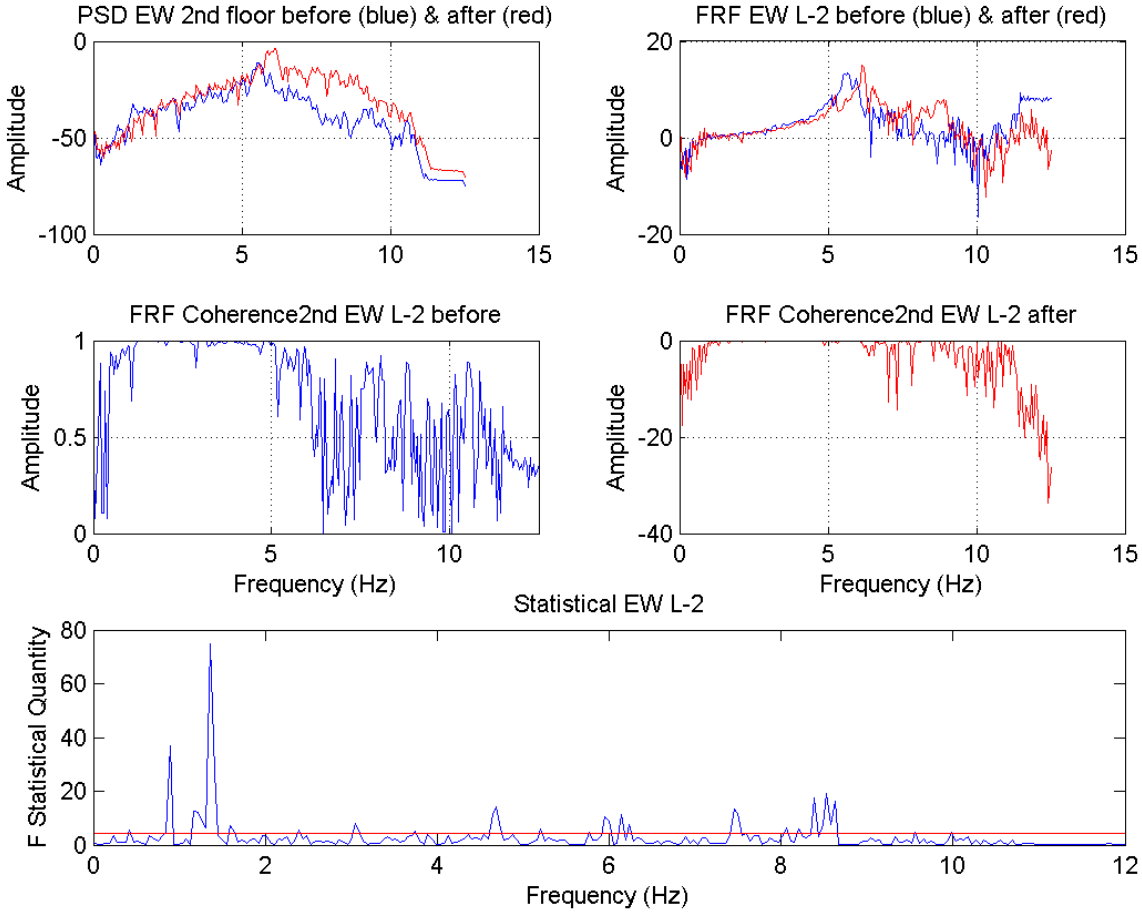

Figure 5.16. Seismic events with name codes b1 & b2 (table 3.3)

Figure 5.16 presents two earthquakes (blue line the earthquake with code b1) and (red line the earthquake with code b2) from the table 3.3 (section 3.3.1). On up left graph are the PSD diagrams of EW component of 2nd floor old building. On up right graph there are the FRFs of both earthquakes. On mid row there are the coherences diagrams of seismic event b1 (left) and seismic event b2 (right) between lower floor and 2nd floor on EW component, of the old building. At the bottom there is statistical time series analysis based on FRF between earthquake 1 and earthquake 2. The statistical quantity ("a" risk level) with red line, on the

bottom graph, is produced from the equation 4.24 that computes the distribution of each frequency parameter between these to FRF plots. It is revealed that different earthquakes produce seismic acceleration which creates different FRF on case study buildings. The FRF changes are much lower than PSD changes (between different earthquakes) but they are still enough high in order to prevent an effective FDI analysis on buildings, through statistical time series analysis. Frequency shift and deviation in spectrum graphs are so high, that the statistical analysis penalizes these changes, such giving false alarms. Although risk level a is minimized, the dynamic parameters of each earthquake change so much that do not allow accurate results for damage identification.

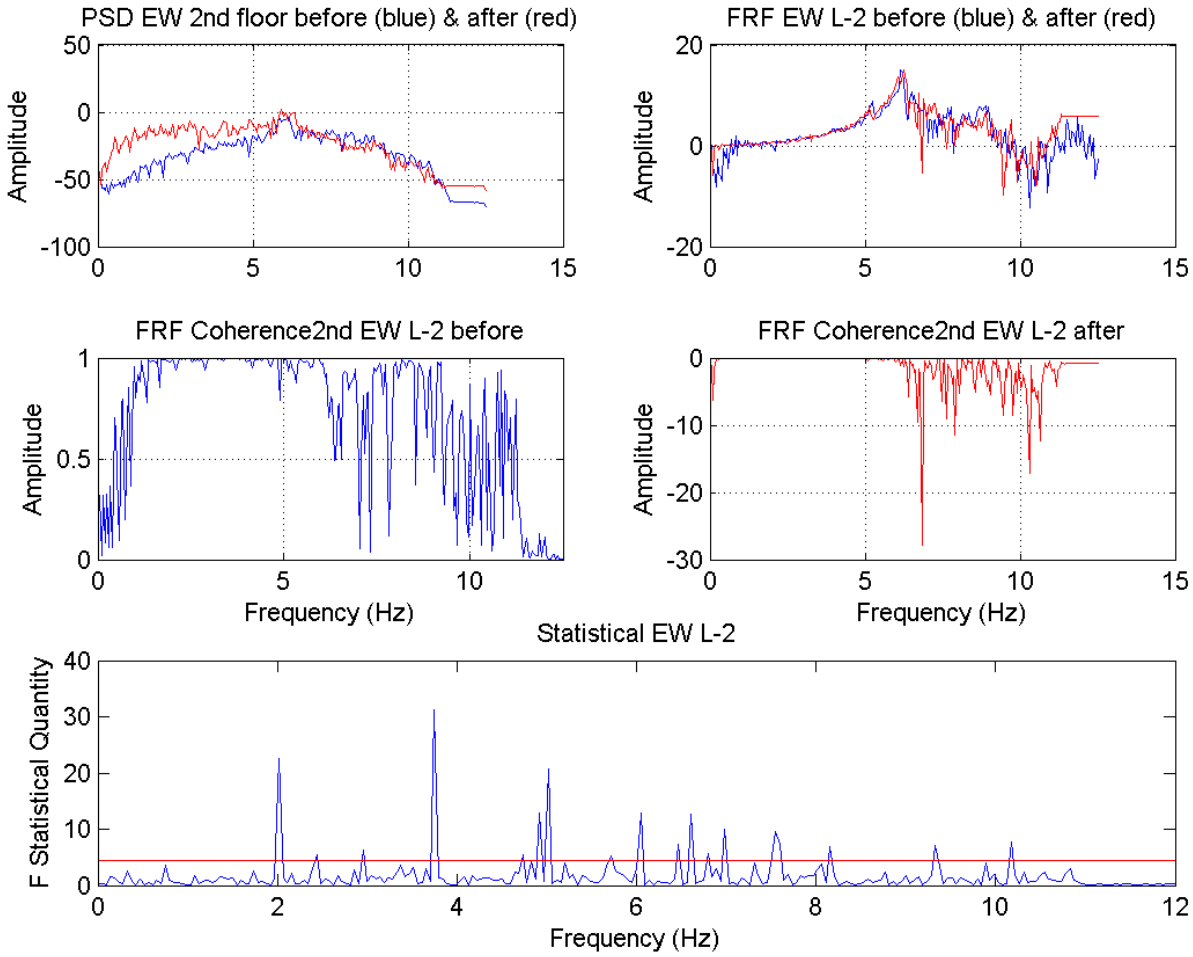

Figure 5.17. Seismic events with name codes b2 (blue) & b3(red) from table 3.3

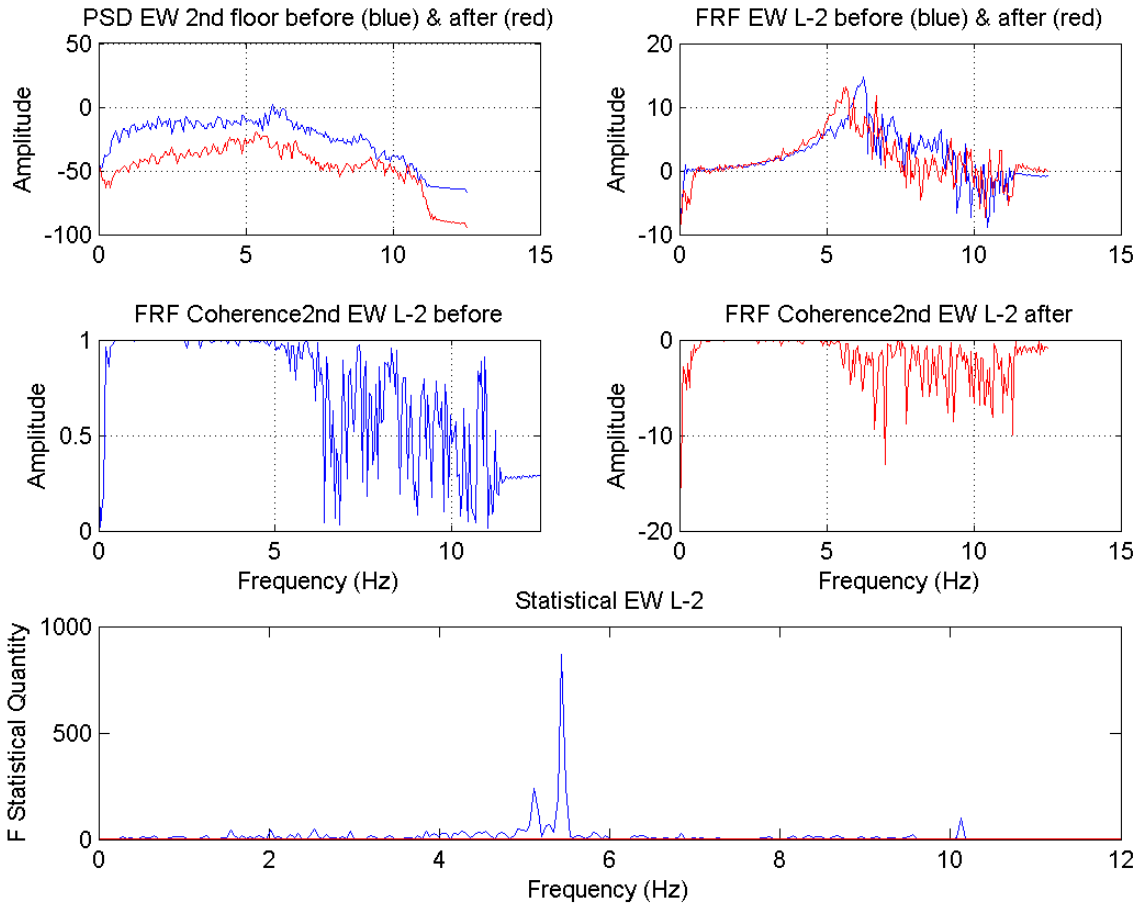

Figure 5.18. Seismic events with name codes b3 (blue) & b4 (red) from table 3.3

The rest of diagrams for other seismic events are in **Appendix L**.

From the graphs in figures 5.16, 5.17 & 5.18, it is revealed that statistical time series analysis based on non-parametric FRF could function as damage indicator but only under excitations where dynamical parameters remain stable. If the excitation has stable spectrum, then FRF statistical analysis is able to indicate very effectively FRF changes of the system. But if we study different earthquakes, FRF are also sensitive in input changes, such non-parametric FRF analysis is not enough. Below it is presented coherence diagram analysis of recording data.

5.6 Data analysis by coherence diagrams

Coherence analysis for above seismic events is applied on acceleration recordings on both new and old building at TEI Chania. Data analysis present the coherence of frequency spectrum from lower floor to 1^{rst}, 2nd and 3rd corresponding floor. Coherence diagram of seismic event with code name b1 is presented below figure. Coherence diagram reveals

how the frequencies of input (lower floor) pass through the specific transfer function of systems (buildings) to the response (higher floors). In other words how transfer function of both buildings changes from seismic event to event and also the changes of this coherence under a statistical manner. Below graphs present coherences diagrams between lower floor and 2nd floor of the TEI old building, for every couple of components. Left column is EW component of excitation, mid column is the NS component of excitation and right column is the vertical component of excitation. Respectively every row refers to specific component of output. Upper row refers to EW component of response, mid row is for NS component of response and lower row is for vertical component of response.

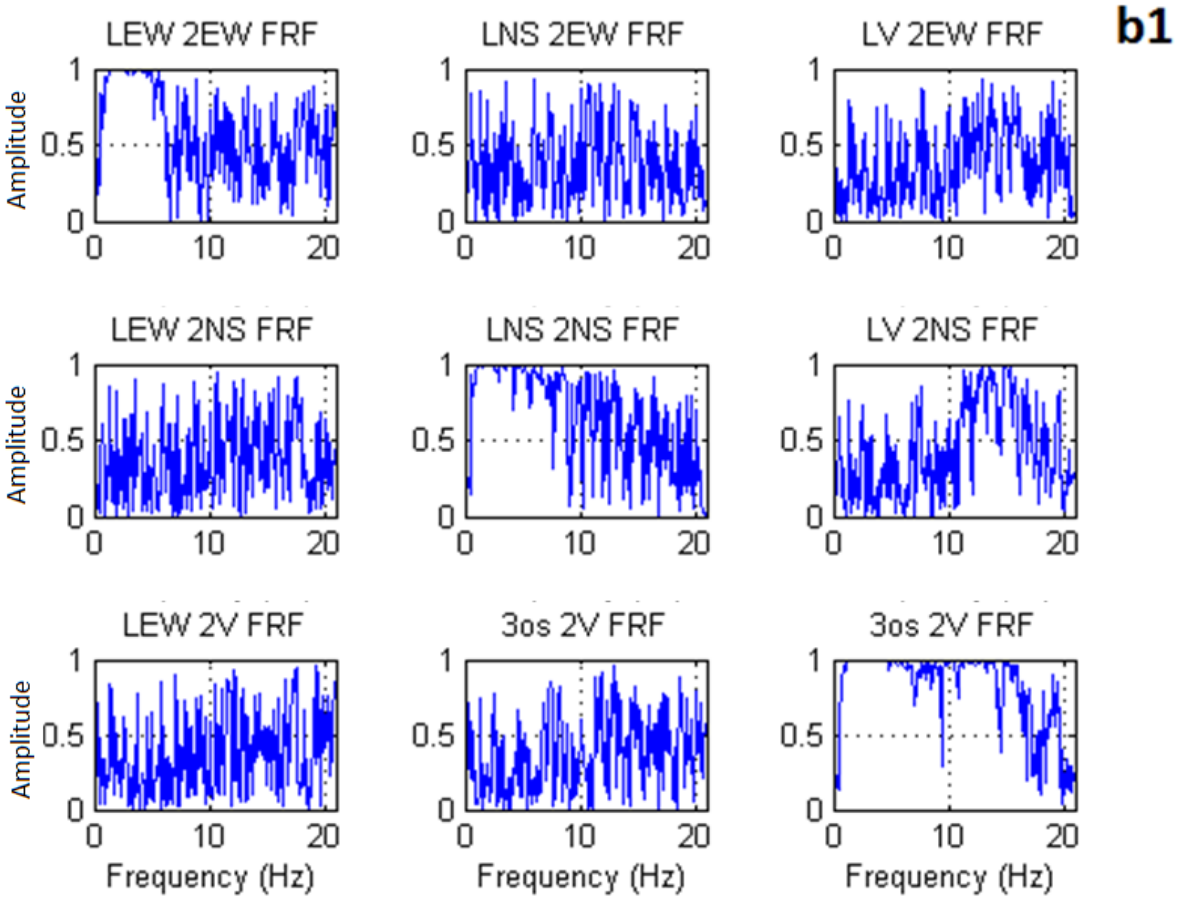

Figure 5.19. Coherences diagrams of the old building lower floor(input) in relation with outputs: 1rst floor(upper row), 2nd floor (mid row) and 3rd floor (low row). Left column refer to EW input with EW output , mid column refer to NS input with NS output and right column to Vertical input with Vertical ouput. The seismic event is with name code b1 from table 3.3 (09/03/2013 3.9M 67km)

Coherence diagrams of figure 5.19 presents high coherence between the same component of excitation and response. The value of **y** axe is normalized amplitude value. Coherence between the same components (ie EW input –EW output, NS input-NS output & V input-V output) is very high for frequencies up to 6 Hz. Between other components there is no coherence. This indicates that building has specific movement and there is no torsion modes, under the specific seismic excitation. More coherence diagrams from other low magnitude earthquakes are presented in **Appendix E**. Coherence diagrams have been applied for more the 20 events before the 6.4M seismic event and more than 15 seismic events after the 6.4M event, in order to apply a statistical number of events able to indicate important changes of coherence in the transfer function of both buildings, with respect to time and events. Coherence diagrams are able to reveal structural characteristics of buildings parameters, such as the frequency spectrum that there is coherence between input and output, and also to reveal torsional modes. Coherence diagram presents valuable information, but it is not able alone to function as damage indicator.

Below figure 5.20 reveals that 6.4 M earthquake affected the old building of TEI with severity and caused torsional modes. The frequency coherence between different horizontal components is very high. North-South of lower floor related East-West of the 2nd floor, EW of lower floor related with NS of 2nd floor are presented with high coherence up to 3-4 Hz (red circles point it out in figure 5.20). This indicates torsional modes at this direction during 6.4M earthquake. In RC constructions torsional modes may cause reduce in coherence between concrete and steel in beams. Such this type of torsional movement could cause structural damage and reduce of stiffness. In **Appendix G** (section: **Frequency coherence between horizontal components**) could be found detailed coherence analysis of the old and new building, before, during and after 6.4 M earthquake, which presents that both buildings had torsional modes on horizontal axes, during the strong motion earthquake.

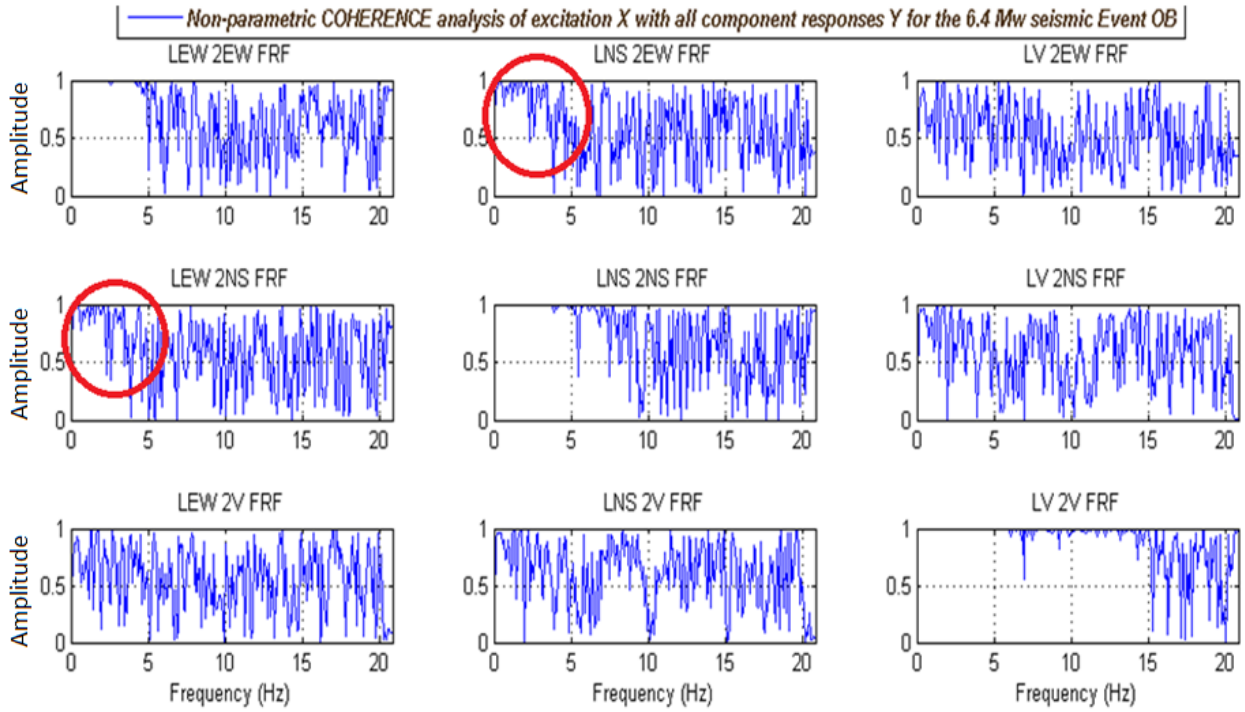

Figure 5.20. Frequency coherence diagrams of excitation due to response for each component of input related to each component of output during seismic event of 6.4M

5.7 Wavelets

In section 2.3.7 it was discussed the basic theory of wavelets, the variety of wavelet families, their usefulness and also the damage detection methods that have been used with wavelets. Wavelets are categorized in non-parametric analysis technique aiming to identify specific frequency changes in wavelet plane. From literature it is known that for every specific application it is required appropriate wavelet and analysis of the signal is determined by this chosen wavelt. In SHM wavelets could be used to identify specific frequency changes along time and time, in a structure. Multi resolution method of wavelet transform provides the ability to calculate variation of frequencies in many scales of resolution. Wavelet transform is the convolution of a signal (in the specific case the seismic acceleration recordings of 3 floor concrete buildings) with a specific wavelet families. If the wavelet shape comes very close to the seismic activity signal then the convolution will reveal much more efficiently the earthquake signal even if it has very low amplitude. In case of buildings damage identification, an optimum wavelet will be able to reveal the affection of seismic activity at specific frequencies due to space and time much more effectively.

5.7.1 Wavelets families in acceleration recordings from the established wired SHM

In this part of the thesis a variety of wavelets will be applied in specific SHM recordings in order to find out similarities and limitations of existing wavelets to reveal important information and to present de-noising abilities of the recorded data. This information will present advantages of wavelet families in non-parametric damage identification on vibration based methods in terms of frequency change. Wavelet families will be applied in the "2013/04/28 16:31 UTC 37.45 N; 22.70 E" seismic event that effected both buildings in TEI Chania.

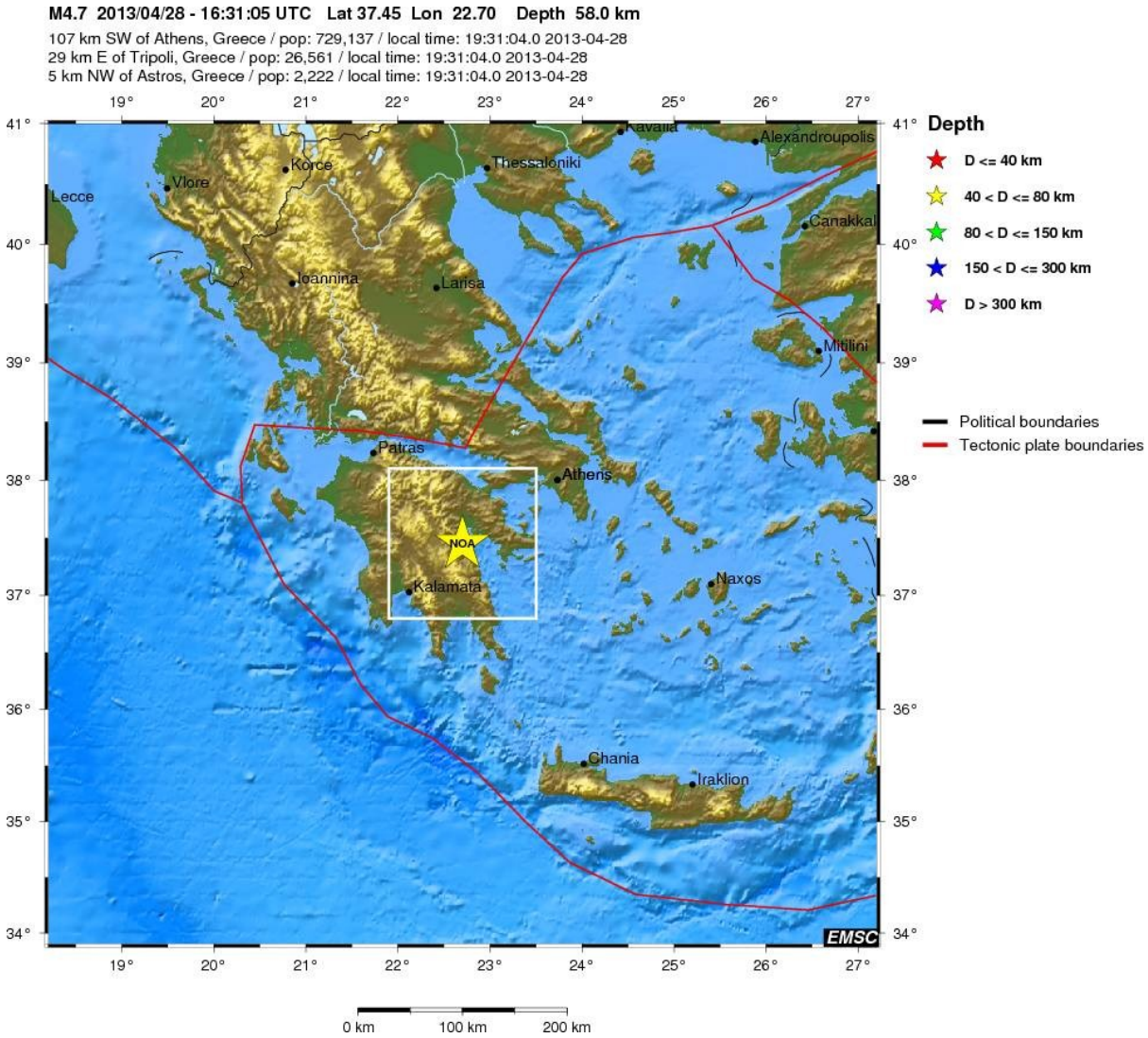

Figure 5.21. The epicenter of the earthquake 2013-04-28 16:31:04.0 UTC at 37.45 N ; 22.70 E [201]

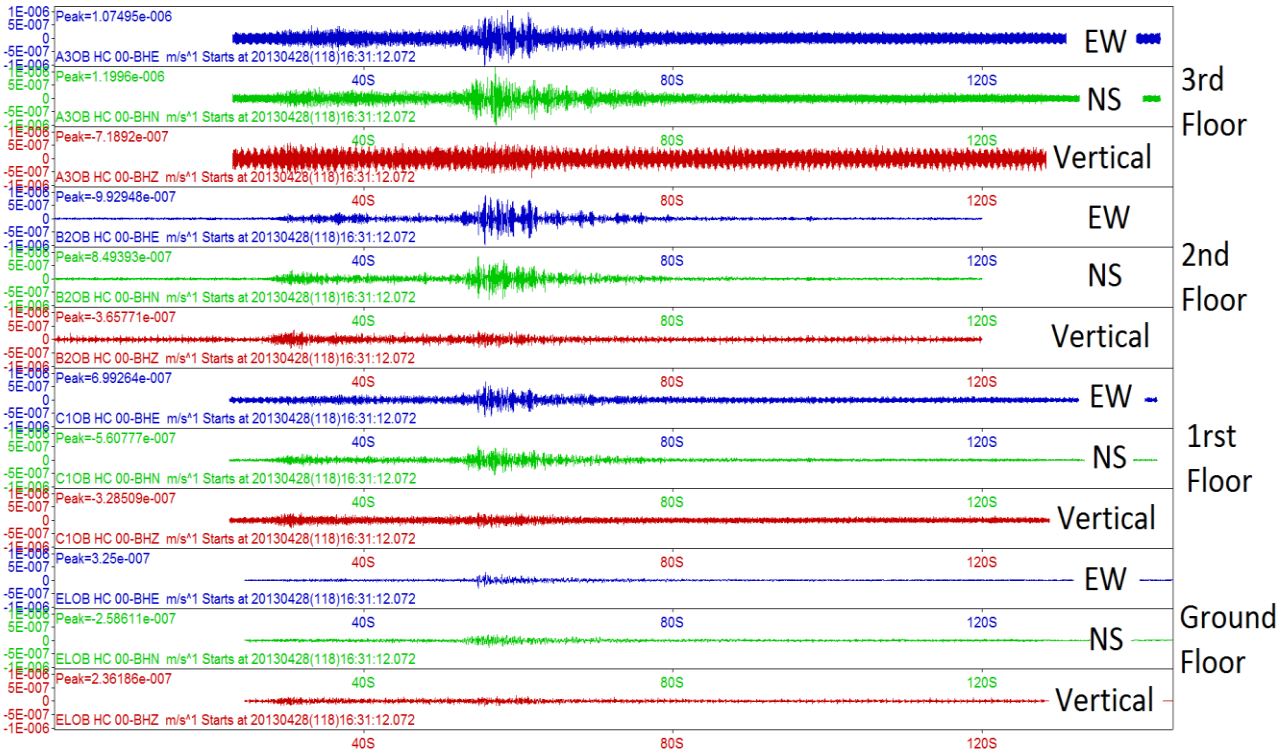

Figure 5.22. The seismic acceleration of the "2013-04-28 16:31:04.0 UTC at 37.45 N ; 22.70 E" seismic event in the old building

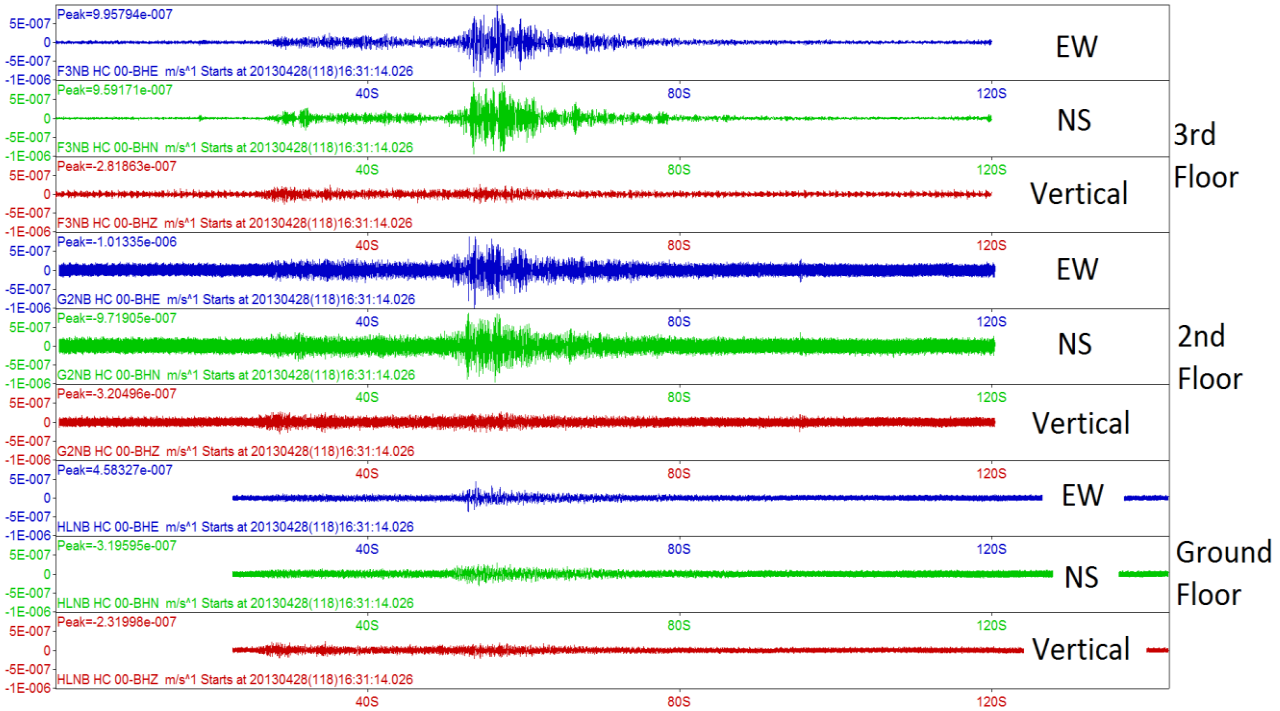

Figure 5.23. The seismic acceleration of the "2013-04-28 16:31:04.0 UTC at 37.45 N ; 22.70 E" seismic event in the new building

Wavelet transform is applied at the recording of North-South on the 3rd floor of the new building due to the fact that the amplitude of that recording is high and there is the maximum affection of the earthquake at the structure there. It is analyzed the results of these of wavelet families' at that specific recording and how every wavelet is approaching the shape or the form of a acceleration measurement.

5.7.2 Haar Wavelet

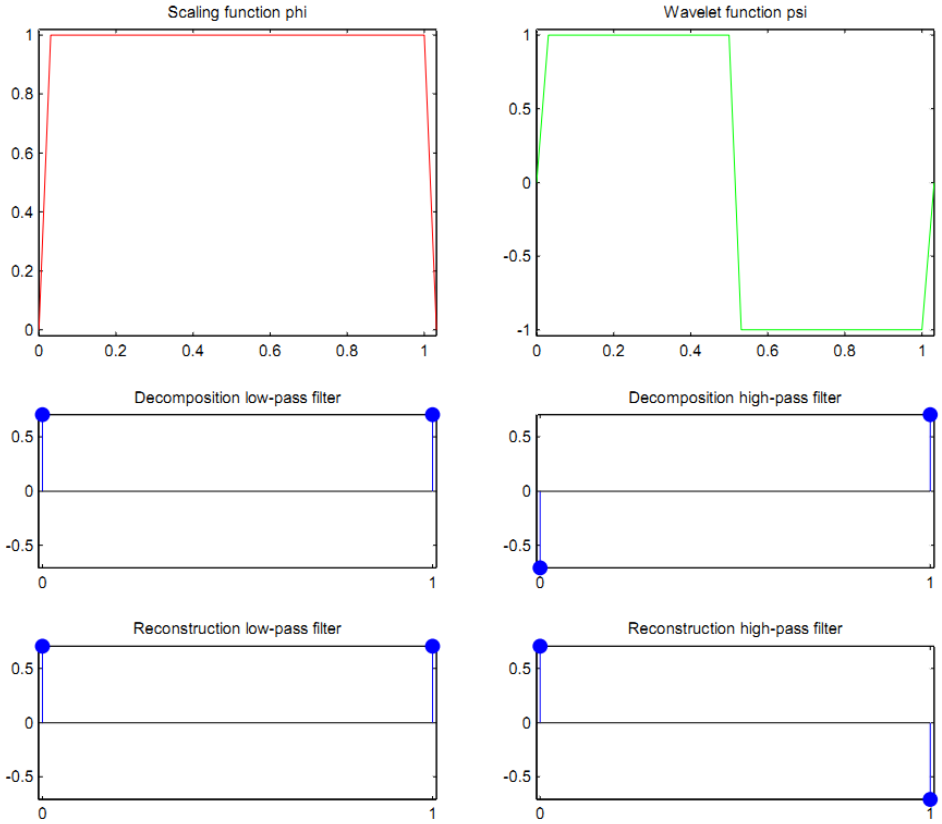

Figure 5.24. Haar wavelet scaling function function phi and wavelet function psi. In the decomposition (mid) and reconstruction (down) low and high pass filters.

Figure 5.24 presents the scaling function and the wavelet function of the Haar wavelet. At the bottom on the same figure, there are four filters for the computation of the coefficients. The left column consist the filters of the scaling function and the right column consist the filters of the wavelet.

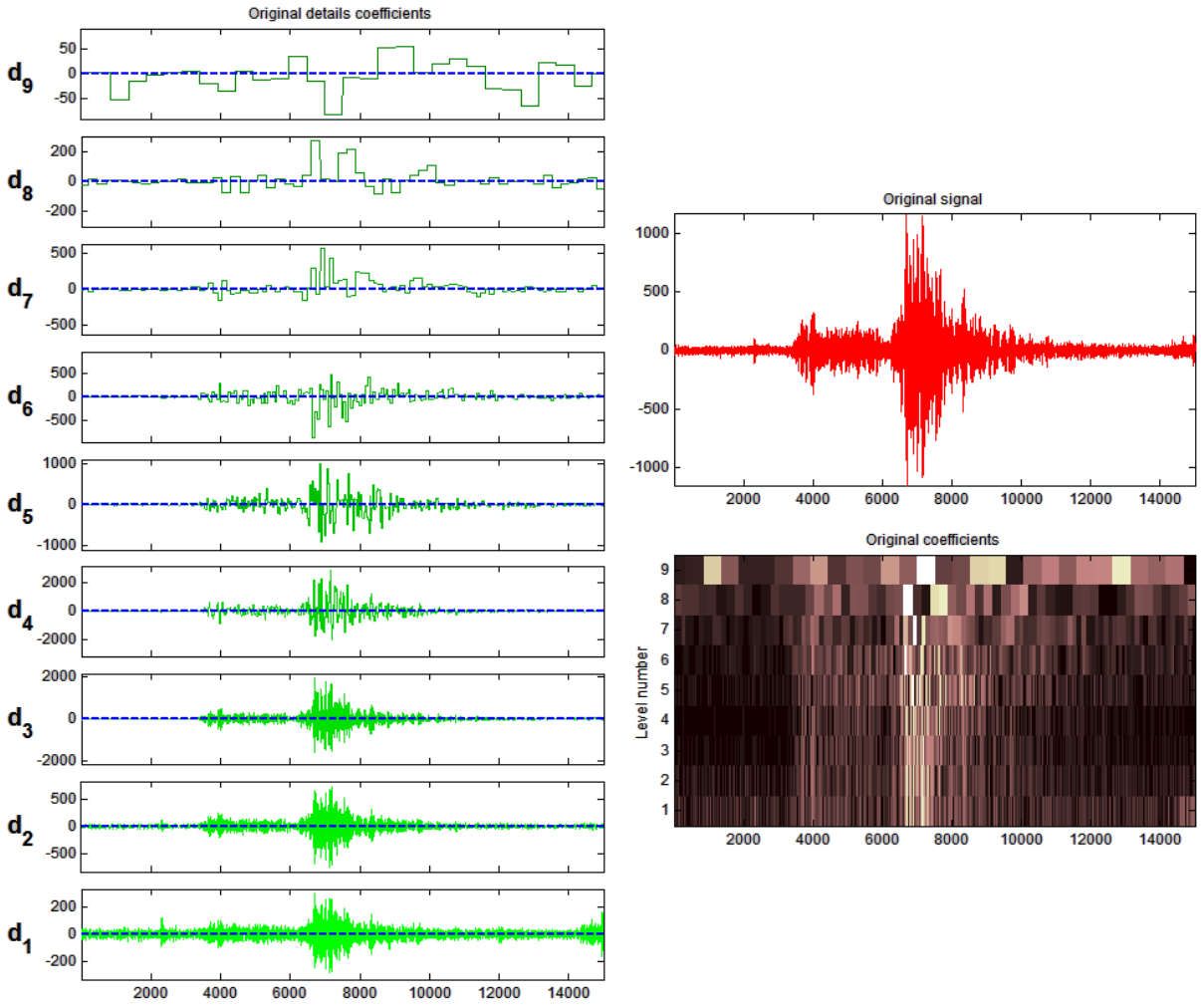

Figure 5.25. Haar wavelet original details coefficients (left) the original signal and the original coefficients (right).

In the level details d_1 it is observed that the noise is presented in the whole length of the recording. In levels d_2 until d_6 the signal of earthquake is presented in clear. Again in levels d_7 until d_9 the coefficients present also noise of the recording. The data analysis, of seismic acceleration recordings, by other wavelet families is presented in **Appendix F**.

5.7.3 Data Analysis with wavelet families

The study of the wavelet graphs reveals that analysis gives the ability to estimate outliers which are detected in a non-parametric manner. Wavelet analysis could indicate specific frequency ranges under a statistical manner of several recordings. Change in dynamical characteristics of a structure could be indicated by change in form or frequency content of case study recordings. In the denoising procedure details level 1 (d1) contains the majority of noise which its amplitude is low in normal states. Almost every wavelet is able to reveal

specific coefficients in every SHM recording, and all of the case study wavelets reveal almost the same data characteristics. The main differences in denoising analysis are addressed on the determinition of specific thresholds defined in the denoising process. By adjusting the thresholds in specific levels there is the ability to de-noise the acceleration SHM signals much more efficiently in terms of detection frequency content in space and time. Still there is an important issue related wavelets analysis for SHM damage identification in real structures. Seismic events induce different dynamical parameters in case study buildings for every different seismic event. This indicates different frequency content in response and excitation of buildings for every earthquake. Such wavelet analysis reveals change of frequency values and form of seismic waveforms, although there isn't change in structural condition of case study buildings. Conclusively wavelet analysis is appropriate for laboratory experiments, where excitation and response parameters are known and stable. In lab conditions every change in wavelet plane indicates damage or fault. In contrast in real structures under real seismic excitation, where there are uncertainties induced in input of the system, wavelet analysis is inappropriate and even if there is statistical analysis of results of wavelet analysis, outliers could not detect or being related with changes in dynamical characteristics of structure, since there are significant changes in every earthquake event.

5.8 Conclusions of Non-parametric methods

Non-parametric methods, namely frequency deviation, HVSR, Wavelets, PSD, FRF and coherence diagrams were applied in section 5. On these methods, damage detection is based in non-parametric time series representations, where the fault detection is based on significant statistical deviations of measured quantities from recorded seismic events. From non–parametric analysis it is obvious that every seismic event has different dynamical parameters and induces these different parameters in the system of structures. PSD is not appropriate for this kind of analysis (real world scenarios), because for each seismic event the power spectrum has completely different spectrum. FRF of input and output have much more stabilized plots, but the non-parametric analysis of these FRFs is also unstable in changes of input parameters. The statistical approach reveals high percentage of false alarms (peaks over the red line). With specific calibration of alarm threshold (red line level), this non-parametric statistical approach is able to reveal important changes in dynamical characteristics of case study structures. Such supervised identification (comparison undamaged with damaged scenarios), is very effective under a statistical manner.

Furthermore coherence diagrams are able to reveal where there is significant change in transfer function of both buildings, caused by specific seismic events, such could function as indicator in damage intentification.

In this chapter there are three new contributions:

Initially time series statistical analysis is applied on non-parametric FRF data. These data are seismic acceleration recordings, of low magnitude earthquakes, from the excitation and response of real buildings. Such low amplitude seismic acceleration of real structures, is analyzed under a statistical manner (methodology of statistical analysis and threshold of risk level is described on section 4.3 on section “FRF statistical analysis”.

Then a fast, computational efficient index is proposed. The frequency deviation index (Π index) penalizes not only the fundamental frequency change but also the maximum frequency deviation (maximum to minimum value) and correlates it with the reduce of stiffness of the structure.

The third contribution is a fast computational efficient index named "HVSR Rise Index" which correlates the rise of HVSR (from floor to floor), with the increase of building internal drift, under environmental noise, earthquake activity, or man-made activity. Such it reveals structural vulnerability of the structure on specific floors.

Conlusively non-parametric methods are fast, computational efficient and able to give results without specific user expertization. The main disadvantage is that the results could not be connected directly with dynamic parameters of a structure and damage or fault identification could only be applied under a large number of experiments and supervised mode (comparison of several undamaged cases with several damaged cases).

Nonetheless, non-parametric methodologies are necessary and very important in damage identification because they enable to determine the appropriate frequency spectrum for analysis, the filters applied, the required resampling of data series. Furthermore they contributed to define all the important parameters in order either to apply a non-parametric analysis, either to apply a parametric analysis. PSDs reveal the frequency spectrum of acceleration data series. FRFs present the frequency relation between input and output of a system. Coherence diagrams reveal the coherence between input and output (how the frequencies of the input pass to the output of the system). The entire above are required in order to apply effective damage identification and to understand the dynamic parameters of

a structural system. The two proposed novel approaches function supplementary with the above non-parametric methods, and contribute to a faster and computational more efficient damage identification.

PSD, FRF and coherence analysis contribute to assess and estimate the response signal scale, the different excitation levels of the specific case study and also the coherence of the system. Such they are necessary parameters in statistical time series analysis, even if only parametric analysis is utilized for damage identification, because the offer important imformation about the characteristics of the case study systems.

Chapter 6. Data analysis of SHM recordings with parametric methods

6.1 Introduction

On previous chapter non-parametric analysis presented specific limitations in acceleration recordings of real structures, in terms of the requirement of high number of data and of no-direct correlation between non-parametric model and structure dynamic parameters. Considering these shortcomings, this chapter applies, parametric vibration based damage detection of the case study reinforced concrete buildings under real earthquake excitations, based on a statistical time series method. Ljung [210] refers three basic parameters for an efficient system identification methodology. Data collection, a number of appropriate designed models and specific directions which assess and estimate the optimum model, according to the recording data, are the three key points addressed by the above author. Based on these directions, is applied system identification procedure on chapter 6 and also on **Appendix G**.

For presentation parsimony, on this chapter there is comprehensive presentation of parametric methodoly and statistical analysis, applied in this thesis. Detailed presentation of parametric data analysis (parametric procedure along with the detailed steps of analysis before the parametric analysis of chapter 6) could be found on **Appendix G**. More specifically the vibration acceleration responses of the two RC buildings of the School of Applied Sciences, Technological Education Institute of Crete, measured under low level earthquakes, are initially used for the structural identification of the buildings through AutoRegressive with eXogenous excitation (ARX) models [210]. In the sequel and after the strong earthquake of magnitude 6.4 M the dynamic behavior of the buildings is reinvestigated and the detection of a potential damage is pursued through the parameter based method [103], which compares via an appropriate hypothesis testing procedure the parameter vectors of ARX models that correspond to the healthy and the unknown, potentially damaged, state of the buildings. It is noted that the structural identification and the training (baseline phase) of the parameter based method as well as damage detection after the strong earthquake is based on a number of excitation (earthquakes) and vibration response acceleration signals from both buildings provided by the seismological network of Crete [218]. These signals are measured by appropriate seismographs established at the basement (structure's foundation) and presently considered as the ground's acceleration, and at all floors of the buildings (lower and ground floor, 1st floor, 2nd floor and terrace). The results of the study, although they are in a preliminary stage, indicate that the effects of the strong earthquake did not lead to a permanent damage in the considered buildings.

6.2 Data Collection

The data collection consists of vibration excitation-response acceleration signals obtained from each storey (from both buildings, see Chapter 3 figure 3.2) due to relatively low amplitude earthquakes with epicenter close (within a “circle” of radius equal to approximately 100 km, see figure 6.1) to the buildings under study, before and after a strong earthquake of magnitude 6.4 M [209]. Earthquakes with magnitude greater than 3 M are currently considered. Such earthquakes are selected since they are capable of sufficiently exciting both buildings above the level of ambient noise, while also being below the level of “strong” (high-amplitude) earthquakes that could impose damages. Thus, the study focuses on the “every-day” structure’s vibrational behavior. In addition, for purposes of damage detection, the structural characteristics are compared before and after the strong earthquake. The data base consists of 8 events before the strong earthquake, the strong earthquake and 9 events after the strong earthquake. The earthquakes and their geological details are summarized in Table 5 and depicted in figure 6.1.

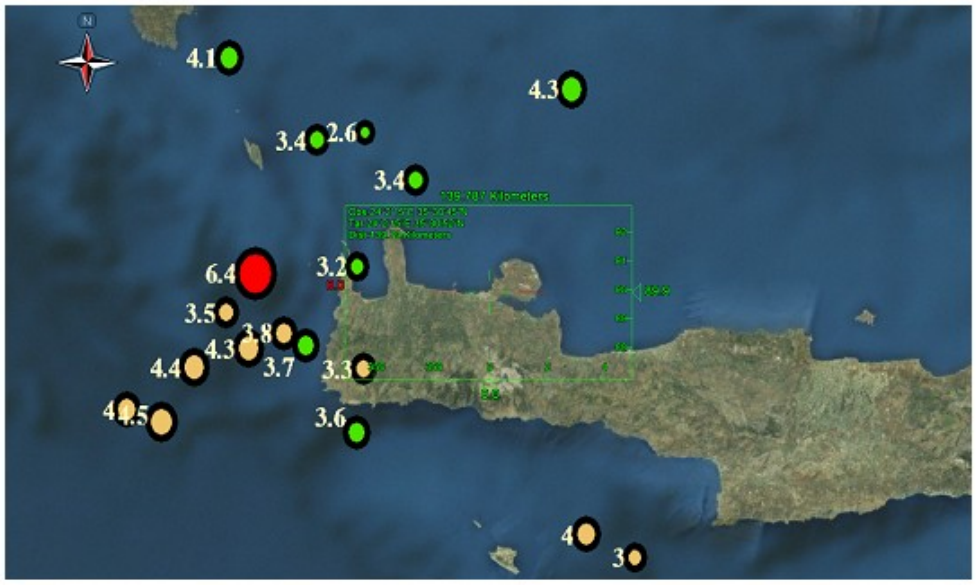

Figure 6.1. The region of interest. The earthquakes and their magnitude are depicted on the figure: Baseline events are denoted with green color, inspection events with yellow and the strong earthquake in denoted with red color

EARTHQUAKES AND THEIR GEOLOGICAL DETAILS. BASELINE AND INSPECTION PHASES.

Event	Date	Magnitude (M_w)	Latitude	Longitude	Depth (km)	Distance (km)
			Baseline Phase			
1	31/3/2013	4.3	36.03	24.30	70	62
2	11/4/2013	3.6	35.16	23.63	2	52
3	28/4/2013	3.4	35.80	23.81	2	36
4	22/5/2013	4.1	36.11	23.22	5	98
5	14/7/2013	2.6	35.92	23.65	9	55
6	23/7/2013	3.4	35.90	23.50	1	64
7	25/7/2013	3.7	35.38	23.47	20	55
8	8/8/2013	3.2	35.58	23.63	2	35
			Strong Earthquake			
	12/10/2013	**6.4**	**35.56**	**23.31**	**47**	**64**
			Inspection Phase Phase			
1	12/10/2013	4.3	35.37	23.29	50	70
2	13/10/2013	4.0	35.21	22.91	10	100
3	19/10/2013	4.5	35.18	23.02	60	97
4	29/11/2013	4.4	35.32	23.12	52	84
5	22/12/2013	3.8	35.41	23.40	23	60
6	2/1/2014	4.0	37.90	24.34	30	70
7	8/1/2014	3.3	35.32	23.65	2	39
8	8/1/2014	3.0	34.84	24.49	15	88
9	11/1/2014	3.5	35.46	23.22	2	72

Table 6.1. Earthquakes with their geological details. Baseline and inspection phases

6.3 Data analysis by ARX modeling

The vibration excitation-response signals (from both buildings) are modeled via scalar ARX models in the baseline phase (before the strong earthquake). The selected ARX models are then re-estimated in the inspection phase (after the strong earthquake). Damage detection is then realized by applying proper statistical hypothesis testing (see Eqs. 4.25 - 4.28 in chapter 4.3) using the estimated ARX models and their estimated parameters before and after the strong earthquake.

A. ARX Modeling of the Healthy Structure Dynamics

The acceleration signals recorded on the basement are currently considered as the excitations, while the acceleration recorded on the first and second floors are considered as the response signals. Both the East-West (EW) and North-South (NS) directions are analyzed for both buildings. The signals were initially recorded at 125 Hz, subsequently low-pass filtered at 25 Hz and then mean corrected. Figure 6.1 shows the excitation-response signals recorded at the old building for an event before the strong earthquake.

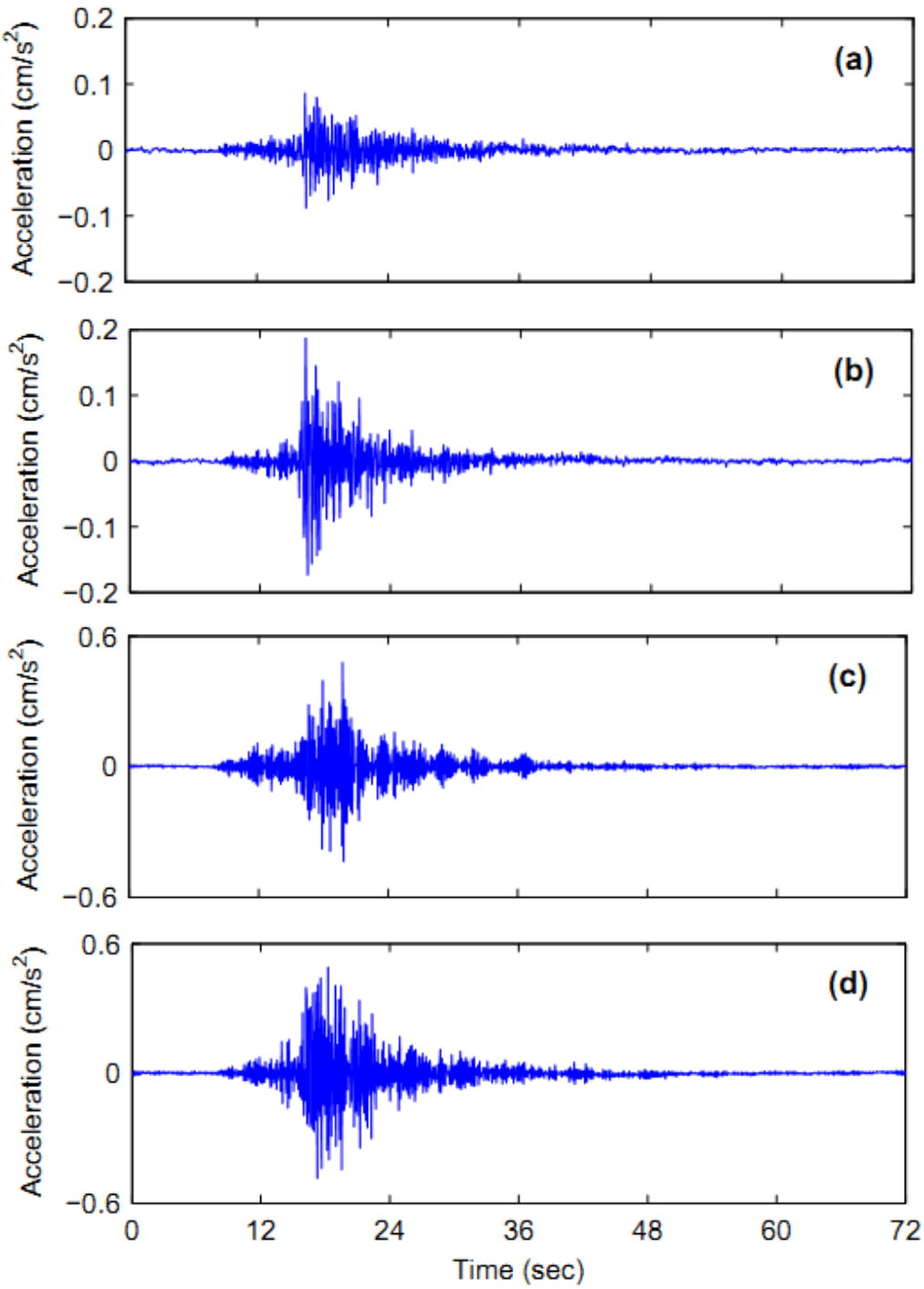

Figure 6.2. Excitation-response signals from the old building for an event before the strong earthquake: (a) East-West excitation (xew), (b) North-South excitation (xns), (c) first floor East-West response (y1ew), and (d) second floor North-South response (y2ns). (a,c) EW direction, (b,d) NS direction. Subscript denotes direction and superscript floor number.

Prior to ARX estimation, the excitation-response signals are scaled (devided by their standard deviation). The estimation results (old building, baseline phase, sixth event, xew=y1 EW signal pair) of ARX (na, na) models with increasing na order are presented in Figure 6.2. It is worth noting that the RSS criterion constantly reduces for increasing na order, figure 6.2(a). The BIC criterion suggests an ARX (38, 38) model, figure 6.2(b). Nevertheless, the frequency stabilization diagram presented in figure 6.2(c) suggests a higher na order for an effective “stabilization” of the system’s “modes”. Thus, the AR order was selected to na = 60 and a furher search on the X order nb lead to a final ARX (60, 20) model. The selected ARX (60, 20) model is also properly validated. Indeed, its predictive ability is judged as quite good figure 6.3(a), as the model-based residuals (black line) is characterized by much smaller (of order one) amplitude compared with the actual acceleration. In addition, the normalized autocorrelation function of the model-based residuals falls within the limits of statistical uncorrelatedness, figure 6.3(b). The selected models and estimation details are summarized in table 6.

SELECTED MODELS AND ESTIMATION DETAILS.

Building	Direction	Excitation	Response	Selected model	Number of estimated parameters
Old	East-West	x_{ew}	y^1_{ew}	ARX(60,20)	81
Old	North-South	x_{ns}	y^2_{ns}	ARX(62,22)	85
New	East-West	x_{ew}	y^1_{ew}	ARX(62,22)	85
New	North-South	x_{ns}	y^1_{ns}	ARX(64,24)	89

Table 6.2. Selected models

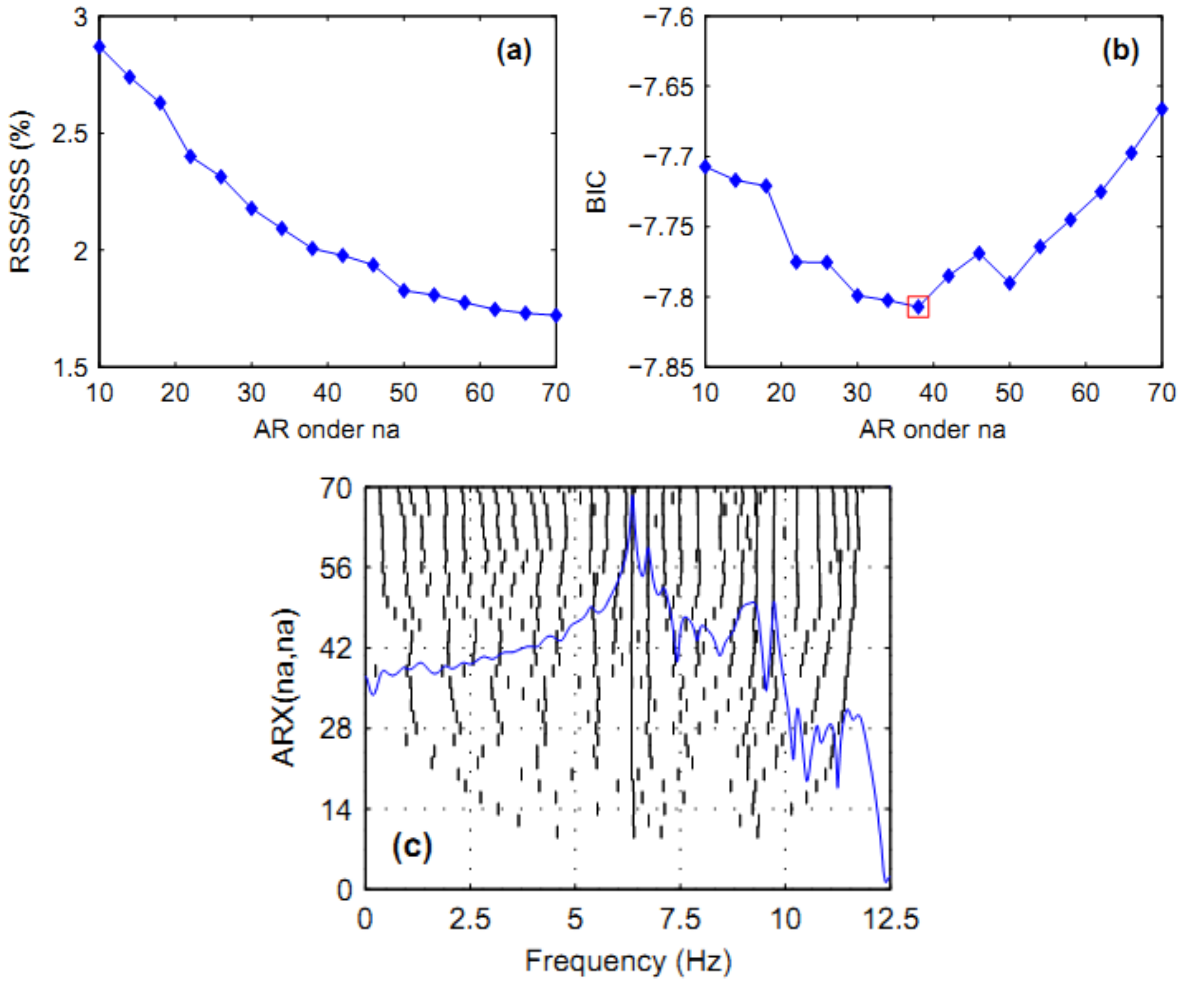

Figure 6.3. ARX identification results (old building, xew=y1ew signal pair, sixth event before the strong earthquake): (a) Percentage RSS/SSS, (b) BIC criterion (the square box indicates the criterion's minimum for na = 38), and (c) frequency stabilization diagram for various ARX (na; na) models [the blue line indicates the model-based FRF of the ARX (60, 60) model].

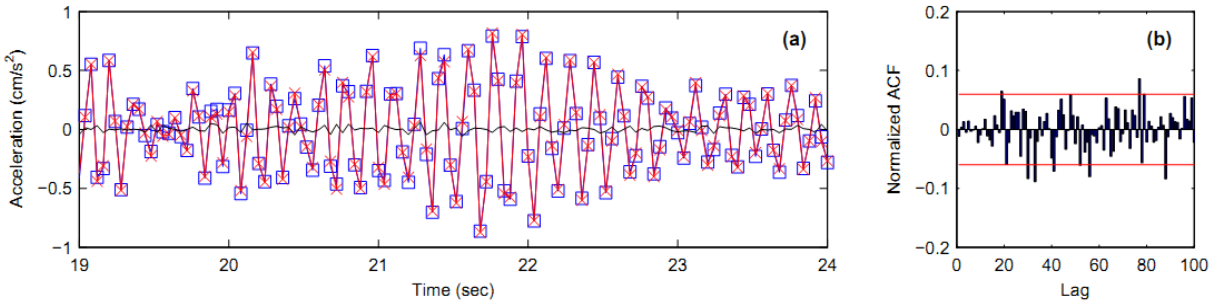

Figure 6.4. ARX (60, 20) validation: Actual response –□– and one-step-ahead model-based predictions –x–, (b) normalized autocorrelation function of the ARX (60, 20) model-based residuals (the horizontal lines indicate statistical significance at the α = 0.95 level).

B. Damage Detection in RC Concrete Buildings

In the present study, both buildings (old and new) of TEI of Crete, School of Applied Sciences located in Chania, Crete, Greece are investigated for potential damages due to the strong earthquake considered. Based on the first event of the baseline phase, two ARX models are identified - one for the EW and one for the NS direction - for each building, thus representingthe two structures in their healthy state in both directions (4 “test cases” in total). Then, for each test case the ARX models are re-estimated for all the remaining events within both the baseline and the inspection phases, and the characteristic quantity x_{θ}^{2} (see Equation 4.27 in chapter 4.3) based on the model’s AR parameters only, is evaluated. The AR parameters are only selected, as they fully characterize the structure’s dynamics and the evaluation of the quantity x_{θ}^{2} is thus expected to be less sensitive to noise and uncertainties.

By assuming that all the estimated ARX models corresponding to events of the baseline phase represent the structures intheir healthy state, it is expected for the characteristic quantity to present relatively small variations within the baseline phase. Nevertheless, since real structures under earthquake excitation are studied, these variations could be of higher magnitude asnoise and a number of uncertainties affect structural behavior. The limit (threshold) above of which a damaged is detected, is thus adjusted to a value slightly (typically 10%) greater than the maximum value of x_{θ}^{2} (values from the baseline phase). The results are all summarized and depicted in figure 6.4 for all “test cases”. A closer examination of figure 6.4 reveals thatthe characteristic quantity (blue bars) variates within the baseline phase. Nevertheless, these variations are expected due tonoise and various uncertainties affecting structural behavior. In addition, it is worth noting that the characteristic quantity values that correspond to the inspection phase (red bars) are all below the adjusted threshold (black horizontal line) except one event figure 6.4(b) (old building, NS direction).

All the rest x_{θ}^{2} values from the inspection phase are of similar magnitude with those obtained from the baseline phase. Thus, both buildings behave similarly before and after the strong earthquake, as the characteristic quantity values are almost all of similar magnitude for both the baseline and the inspection phase, and are below the adjusted threshold. Thus, it is concluded, that the strong earthquake did not cause damages to any of the buildings under study.

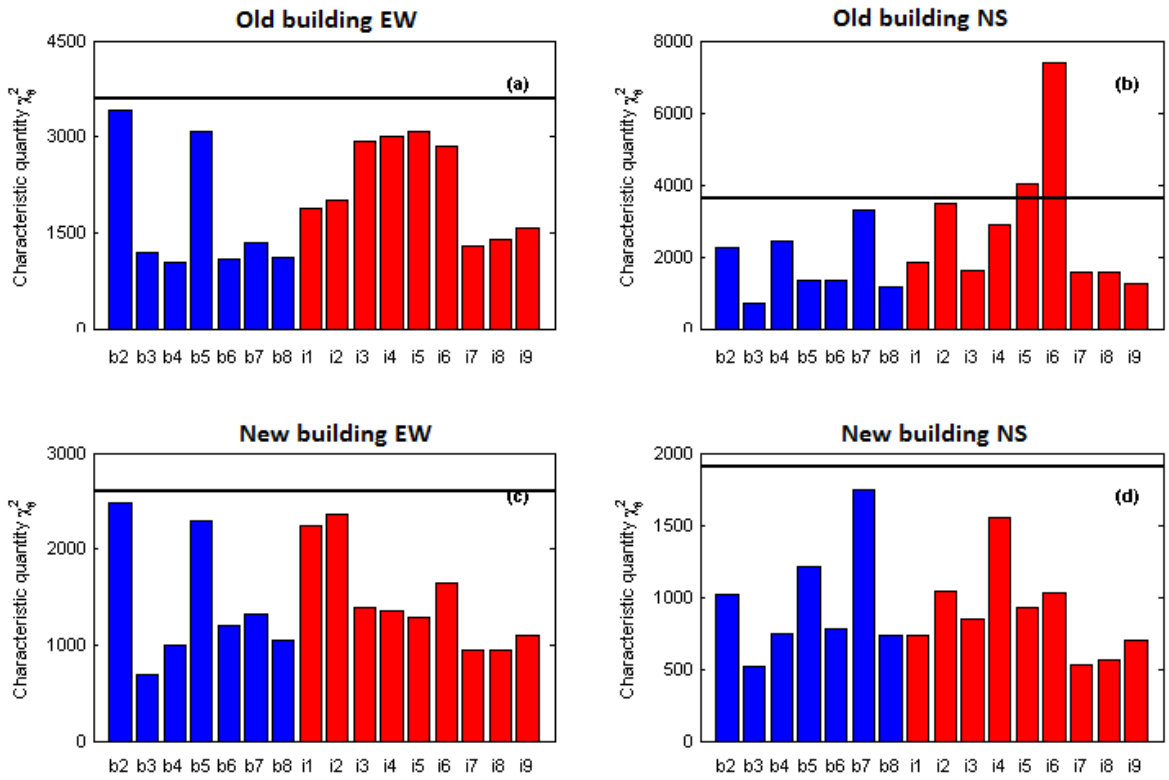

Figure 6.5. Damage detection results based on the characteristic quantity x_θ^2: (a) Old building EW direction, (b) old building NS direction, (c) new building EW direction and (d) new building NS direction.

6.4 Conclusions from parametric methodology

The problem of vibration-based damage detection in reinforced concrete buildings under real earthquakes based on a statistical time series method was investigated. The structural identification of the considered buildings was achieved based on AutoRegressive with eXogenous excitation (ARX) models, while damage detection was pursued after a strong earthquake through a statistical time series method. The results of the study indicated that ARX models adequately represent the structure's dynamics, while the damage detection scheme based on statistical time series methods indicated that the strong earthquake did not caused damages to the buildings under investigation. ARX model is linear in its parameters; such it is computationally efficient to estimate the model parameters, compared with other models like ARMAX, BJ, OE which are non linear in their parameters, and such computationally much more demanding. Although graphs of parametric FRF bodeplots indicate small frequency deviation before and after the major earthquake (see appendix F: the section of "Analysis of all ARX models") under a statistical analysis of the distribution of parameter vector estimator, this deviation remains in specific limits and such does not reveal structural damage on case study buildings.

Chapter 7. Discussion

7.1 Introduction

This chapter deals with the findings and results of previous chapters, from the key issues of the thesis, the case study results and the methodologies applied in recordings. Data results from the combination of DSP methods applied in chapter 5 and 6, are presented, along with the characteristics of instrumentation in chapter 3. Also DSP methods presented in previous chapter 4 are combined in order to create an algorithm for damage detection. At the end of this chapter, the aims and objectives referred in introduction chapter 1 are also discussed.

7.2 Cost effective wireless Structural Health Monitoring Network

There is an increasing demand to monitor the condition of infrastructures in order to maximize safety and security in the cities, especially at earthquake (EQ) prone areas. SHM systems are installed on bridges, highways, special structures and buildings in order to monitor the integrity and performance of the structures and nowadays towards detection and localization of damage. The cost of large scale implementation of SHM systems (many buildings in a metropolitan area) is quite high, even for wireless systems, and this is a significant drawback to overcome.

In this thesis, a wireless SHM sensor network (wSHMs) was designed and developed (chapter 3.1), that proves to be easy to install, more economical (concerning the implementation on many buildings) than the majority of wireless SHM systems and much more efficient than conventional wired SHM systems in terms of cost, installation, size, number of sensors, and ease of use. Key-features for wireless monitoring of the structural condition of buildings, namely, autonomy, continuous/real-time operation, data rate, resolution and synchronization, wireless error free connectivity and implementation cost have been analyzed and addressed in the design and configuration of the developed wSHMs. Hybrid networking combines a wireless sensor network with the exploitation of existing wire lines or wireless broadband connections and cloud technology.

The efficiency of the wSHMs was tested through a pilot comparative study of the operation in two neighboring buildings of different age in an earthquake prone area (Chania, Crete, Greece). The comparison was made against a far more expensive, high sensitivity, low level triggering, accelerometers network (chapter 3.2) installed in parallel using local intranet.

Small magnitude seismic events demand extremely sensitive accelerometers (sensitivity 10 μg, triggering threshold 200 μg) in order to be able to record. Thus, from the analysis of the measurements it is revealed that the wired system is able to record numerous tremors and weak seismic motions with peak of seismic acceleration of the order of 1 mg. To these events the developed wSHMs is insensitive, as its resolution is at 2 mg. On the other hand, such excitations do not affect the structural condition of buildings.

Strong motion events (with seismic acceleration on buildings higher than 16 mg) were recorded successfully by both wired and wireless SHM systems. The real performance of both sensor networks in the case of a strong earthquake (M 6.4) occurred close to Chania region on October 2013, demonstrated that the developed wSHMs is capable to record the acceleration caused by strong excitation, reveal the resonance frequencies and thus to monitor the structural health of the buildings being installed.

7.3 DSP methods for parametric and non-parametric modeling aiming to damage identification

The ultimate aim in Structural Health Monitoring (SHM) is to reveal possible structural damage in buildings and more generally in constructions. In this thesis, an optimized blend of digital signal processing methodologies were applied, tested, evaluated and combined on seismic accelaration data, collected by both the wired and the wireless structural health monitoring networks, deployed in two neighboring case study buildings of different age.

The installation took place in a nineteen years old three floor building and an adjacent seven years old three floor building. At each building accelerometers were deployed on ground floor, on the second floor and on the third floor, in order to record strong motion. The two buildings under SHM are the premises of Technological Educational Institute (TEI) of Crete at Chania, Crete. The island of Crete (Greece) is located at the south front of the Hellenic Arc where the subduction of the African Plate beneath the Eurasian plate is taking place, a region characterized by high seismicity. The broad region of study (south Hellenic arc) is a very actively seismic region which functions as a natural laboratory for earthquake engineering of this kind. Many seismic events analyzed in order to study the structural response of the case structures.

These real structure acceleration data were analyzed with non-parametric methods i.e., Frequency Response Function (FRF), Horizontal to Vertical Spectral Ratio (HVSR) and Wavelets in order to reveal possibly change of structural resonance frequencies.

The same data were analyzed by applying parametric system identification techniques (ARX, ARMAX) in order to reveal except the possible change in fundamental frequency, the dynamical properties of buildings under study that are strongly related with their stiffness (mode shapes, damping ratio). Similarities and differences between both method types were discussed in order to justify the necessity for combined implementation of DSP for SHM.

Key contribution of this study is that real structures are approximated as a system, and the escalating seismicity (considered input to this system) is correlated with system's global characteristics response and also with system's modal properties identified. Furthermore, strong seismic events which affected with severity the buildings under study analyzed to investigate if their global response, which includes specific modal characteristics for each kind of vibration, follows the same pattern as in the case of small earthquakes or if they create new and/or reveal hidden resonance frequencies which could probably be associated with the occurrence of structural damage.

7.3.1 FRF and HVSR indices of structural vulnerability

Initially (section 5) non-parametric method of FFT was applied on the acceleration recordings and the fundamental frequency of old and new building was studied, proposing an index that correlates the frequency deviation with the possible damage that each structure may already contain. The deviation frequency of fundamental frequency from the mean, was correlated with the age and the implied structural health age of each building. This increased vulnerability combined with the frequency deviation index could provide a fast but powerful method of damage detection through a non-parametric method of FFT.

In section 5.1 (and appendix C) it is revealed that old building exhibits higher deviation of fundamental frequency of the structure in relation to the new building. The same property applies to all floors of the old and the new building.

The approach to evaluate the vulnerability of a building, through the change of the HVSR amplitude between floors, is a novelty of this thesis. "HVSR change index" is presented to reveal higher structural vulnerability from floor to floor on a building at chapter 5.2 (more HVSR analyzed data are on Appendix D). By considering that the vertical ratio is almost the same from floor to floor, the main parameter that changes is the horizontal spectrum acceleration. As the horizontal acceleration increase from floor to floor, then also the differential inter-floor accelaration will increase, and thus also HVSR index will increase. As a result high differential building inter-floor acceleration could be depicted by HVSR index

change. Experimental data verify the above increase of HVSR index and especially in older buildings (with visible cracks in beams, damage and stress in their structure) a higher HVSR rise is observed compared to newer buildings without any visible damage.

Furthermore HVSR recordings of strong seismic motion are compared with HVSR recordings of ambient noise for each floor and each building of the case study (chapter 5.4 and appendix D). The similarities of HVSR recordings (under earthquake and ambient noise respectively) reveal the same analogy in HVSR spectrum. This enables a noise HVSR recording in a building to provide comparable information with an earthquake HVSR recording. This study presented an index which estimates the increase of HVSR amplitude from floor to floor (as we go up) and correlates this rate of change (increase or decrease) with the structural vulnerability of the structure.

The same SHM recordings analyzed by both methods (FFT and HVSR) under an earthquake excitation, can reveal resonance frequencies and their amplitude for the buildings under study, with great detail and efficiency in terms of ease of deployment, computation, cost and time. A sum many analyzed data (presented in Appendix C and D), indicate a correlation of frequency deviation index (proposed in chapter 5.1) with HVSR rise index (proposed in chapter 5.2). This correlation is addressed also in an another much older RC 2 floor building ("TEE" building located in Chania), damaged with multiple cracks on its structure, where also existence of higher “HVSR change index” is accompanied with wider “frequency deviation”.

The agreement between frequency deviation and HVSR index, suggests that if the methods are applied in parallel a more objective indication of structural vulnerability of a building can be achieved. The combination of these two techniques in the concrete buildings under study reveals a correlation between the values of frequency deviation index of the fundamental frequency of buildings with the maximum differential horizontal acceleration that can be observed from floor to floor at the specific buildings.

7.3.2 Application of wavelets families in SHM recordings

Wavelet theory (see section 2.3.7) was used to implement various wavelet families on specific seismological acceleration recordings (chapter 5.6). The study of different wavelet families reveals that wavelets transform results do not present big scale differences (from family to family), in terms of signal discretion and detection of specific features. Wavelets transform of an acceleration recording, with haar wavelet, but also with other wavelet

families, at “level 1” of detail, appears as noise. Next detail levels 4, 5, 6 clearly depict the signal of the earthquake recording. Then there is again noise on the next levels 7, 8, 9.

The same behavior is observed for all case study wavelets, with some wavelet families to add noise on higher detail levels. As wavelet family "coiflet" has completely different form from wavelets families "haar" or "db" (2) and "biorsplines", it would be expected the convolution of each family with the strong motion signal to present different results, i.e., the wavelets transform to be different. Nevertheless, the results reveal high similarities. Increase of signal resolution through the recording, is according to the threshold defined at each level in a wavelets transform. The de-noising limits of every detail level (on wavelets transform) determine the acceleration signal and efficiently remove noise contained (de-noising procedure).

Conclusively experimental analysis reveals that, wavelet transform could be used in SHM analysis as an independent non-parametric method in order to reveal frequency changes under a statistical manner, in cases where dynamic parameters of the system under study remain stable (lab conditions). But wavelet analysis in a non-parametric approach suffers from excitation effect, such input induce great scale changes in frequency-time plane.

7.3.3 ARX to ARMAX modeling

In order to proceed from indications to evidences for structural damage, parametric identification methods were added to the quiver, applied on the single-input single-output (SISO) seismic acceleration data for a frequency range 0-10.5 Hz of the concrete three floor buildings under study.

Keys points of this thesis parametric analysis are that time domain models use few parameters, there is the necessity of specific model selection and structure, optimum model order should also be selected, parameterization is based upon minimization of error residuals criterion and there is direct simulation and validation of the estimated model with the recording output data.

Pre-processing of the raw data performed mean removal, filtering and re-sampling at 18.5 Hz. The signal length is variable due to the fact that each seismic event has different data length. ARX and ARMAX models concurrently fitted to the acceleration data. Criteria for the optimum model order, like BIC, AIC, and RSS/SSS, applied to different estimated models, determine the minimum order required for the polynomial na, nb (ARX modeling) and na, nb,

nc (ARMAX modeling). For ARX modeling na=nb=62, for ARMAX model na=nb=nc=34 and for an optimized ARMAX model na=34 nb=32 nc=15 resulted.

In multidimensional parametric analysis every component has different bode plot, thus different structural modes (different fundamental frequency of each component). From the analysis results that ARMAX modeling requires much lower model order than ARX modeling. This can be explained from the fact that noise is being simulated with a polynomial nc parameter. The decrease of the model is of the order of nc. The disadvantage is that ARMAX modeling is much more inefficient computationally. It requires much more computational power and the results are the same as ARX. Thus ARX modeling proves to be more efficient for damage identification by parametric methods.

Studying the stabilization diagrams for each analysis, it is concluded that each estimated model is over determined, insomuch each model order could be much lower and simultaneously present system resonance frequencies or the specific modes contained in frequency spectrum. BIC and AIC have higher values in ARX models than in ARMAX models, although in ARMAX the parametric complexity is much higher, and it is constrained more than in ARX.

In one dimension analysis stabilization diagrams of ARX and ARMAX models, reveal the fundamental structural modes (resonances frequencies) at 5.5, 7.5, 9 Hz and many other lower amplitude structural modes in the frequency range from 0-10 Hz. In ARMAX stabilization diagrams, the plots separate the structural modes much more clearly, even for a very low order model. This is because ARMAX is modeling noise with a polynomial **nc** and thus from low order model there is the ability to distinguish resonance frequencies from noise effect.

Validation of results is applied through autocorrelation functions (ACF) of residuals between measured response recordings (raw data) and the ARX or ARMAX responses. The parametric modeling estimations are compared with the response data and the residuals of this comparison define the error of model estimation. ACF of residuals plots act as a model validation estimator. Comparison of raw data with parametric model results, reveals that both bode plots are almost similar (model estimates in detail the existing modes in the strong motion data). Moreover, a comparison of bode plots of ARX modeling with ARMAX modeling depicts high level of agreement between system's bode plots for both modeling processes.

Chapter 6 (and detailed analysis in Appendix G) presented the DSP for parametric damage identification. Parametric methods ARX and ARMAX applied on seismic acceleration time series recorded at the real scale buildings under study featuring different structural health. Each building is studied as a system with input (ground seismic excitation) and output (floor seismic response) in order to reveal specific modal parameters which are linked with the equation of motion. This methodological procedure is a different approach for damage detection that exploits small magnitude earthquakes to represent the different modes of building shaking under seismic excitation and the modal parameters of motion.

In parametric analysis (Appendix G) can be revealed that ARX modeling is characterized by lower complexity but while depicts high efficiency in terms of model fitting to the data. The ACF presents very low residuals without structure in them. The bode plot of the system contain the majority of the raw-data's frequency content from. Bode plots present with high accuracy the dynamic parameters of the system excitation-response for both SHM buildings.

The order of ARX modeling for old building appears to be higher than this for the new building (there is correlation with the frequency deviation). The order of each system's model denotes how many past values are needed in order to define the maximum of the system's hidden frequencies that exist in accelaration time series. It tends to be higher when a system is more unstable. This variance comes in agreement with the aforementioned increase of the HVSR index where in old building was higher than the newer, taking also into account that the change of the parameters of ARX model reveals a change in modal parameters of each system and also verifies the frequency deviation index (resulted from FRF) which is higher in the old than the new building.

Seismic influence on the buildings of TEI of Crete before a major earthquake and how these modal parameters changed during and after this event were studied. Initially one component (NS) was studied for the ground floor and the higher (3^{rd}) floor of each building in order to examine the way each building was shaking under seismic excitation before the strong earthquake. Then it was studied under the strong motion of the M 6.4 event seismic as well as for earthquakes that followed.

The same dynamic characteristics of a system create specific plot of bode-plot. In this context, the bode-plots before the major seismic event of M 6.4 were almost the same. This reveals that although different smaller earthquakes occurred prior the big one, and each of them had different influence on the system-building, the system's input-output always depicted almost the same transfer function. However, after the strong earthquake there is

change in this bode-plots of the system. Modal parameters of the old building present a change after this milestone event, whereas that of the new building, reveal smaller scale change. All seismic events analyzed after the M 6.4 earthquake have the same bode-plots but they differ from the bode-plots before the major event. Coherences diagrams reveal that both buildings structural integrity affected with severity. Coherence diagrams in correlation with the results of multi-component ARX modeling reveal that specific parametric methodology is damage sensitive and also is able to detect “dynamic parameters change” of the system.

Real world data include parameters and DoF, and overcome limitations of laboratory model in terms of simulation and accuracy. This is to say that natural (real scale) laboratory verifies or rejects well known and established damage identification methods though experimental analysis. The analysis, presented in the core text of the thesis, is one but very representative of the dozens of similar analyses that have been applied in order to verify the results statistical significance. The same analysis has been applied for more than 50 different seismic events that affected both buildings. The analysis reveals that big seismic event of magnitude M 6.4 has not affected both buildings under study. Although graphical bode-plots of both system-buildings reveal change in diagrams, after statistical analysis, such change in dynamical parameters of each system-building proves to be negligible.

Conclusively it is observed that HVSR change index agrees with the frequency deviation index and both are verified with ARX modeling for both buildings. Combination of a fine blend of non-parametric and parametric Digital Signal Processing methodologies can effectively contribute to reveal and estimate change of dynamical parameters of a system, under weak and strong seismic excitation. Furthermore, coherence diagrams are able to depict if there is a change in coherence of input-output relation for the SHM buildings, by studying different seismic events, and also to reveal which earthquakes may cause torsional modes in constructions.

On the other hand, every part of parametric analysis, every plot and testing model is absolutely necessary in order to define with accuracy the parameters for an effective parametric model. From the estimation of ARX model until ARMAX and ARMAX optimization, these procedures contribute to define the appropriate parameters and model for the last algorithm that applied in order to present the statistical FRFs plots. Parametric methods require much higher user expertise, but they have the capability to reveal information, which non-parametric method cannot.

7.4 Statistical time series analysis for SHM

Non parametric analysis of chapter 5 combined with parametric analysis of chapter 6 reveals that, statistical time series for SHM in real structures under earthquake excitation could function efficiently (damage detection, localization and quantification) under specific parameters. These parameters are addressed in appropriate data sets (excitation signals are required along with response signals). By this way input effect on the output is eliminated. Statistical model design imposes parametric analysis, where ARX model is strongly related with the dynamic parameters of the system. In chapter 5 it is presented that non-parametric FRF statistical analysis is inappropriate for acceleration recordings. Also the statistical decision could not reveal efficiently damage through FRF distribution. In contrast parametric statistical analysis through parametric FRF could efficiently reveal the dynamic properties of the case study system (chapter 6 and appendix G). Furthermore the statistical decision of the parameter vector distribution, could overpass limitations (in terms of different PSDs and FRFs in the same data sets-baseline or inspection phase events) and reveal with accuracy system transfer function distribution of dynamic parameters.

Advantages of statistical time series methods applied during this research could be addressed that are data based, inverse type (with high applicability), there is no requirement for finite element model or physical based model. Also the ability to reveal damage through specified structural parameters and without visual inspection or evidence is also important key-point. Disadvantages could be found in lower sensitivity than non-destructive damage identification methods (but where damage detection is focused on located areas of the structure), on the requirement of user expertise and also the limitation in localization of the damage.

7.5 Novel procedure of DSP methodologies to be applied for SHM

In this thesis, a novel procedure that combines a find blend of DSP methodologies is proposed and evaluated. A flow chart is presented (figure 7.1) that outlines the concept of this novel procedure. Initially non-parametric methods to determine the specific parameters of the recorded acceleration data, and prepare the data sets in appropriate form in order to apply, in following steps, parametric methodologies for damage identification in real structures.

Acceleration recordings (data sets), of excitation (input) and output (response) of a building, are filtered by applying specific low pass filters in order to remove higher frequency content and artificial noises. Then re-sampling of the data is taking place in order to maximize the

computation efficiency of the algorithm and the data analysis. Next step is ARX modeling. ARX model order from 0-100 is applied on the filtered and resampled data. Akaike, Bayesian and RSS/SSS criteria along with stabilization diagram define the optimum order of the ARX model (lower order that reveals all the hidden frequencies of the data set, in order to keep also the model complexity in low levels). Based on this defined model order, is applied the ARX parametric model. Parametric bode-plot (of the system) is designed and monitored. The validation of the modeled bode-plot is achieved by autocorrelation function of the residuals of the non-parametric FRF with the parametric FRF. Also 2nd validation of the parametric model is performed by cross correlation of the residuals with the input of the system (excitation). More bode-plots of scheduled or random time moments are added in the same data set of bode-plots.

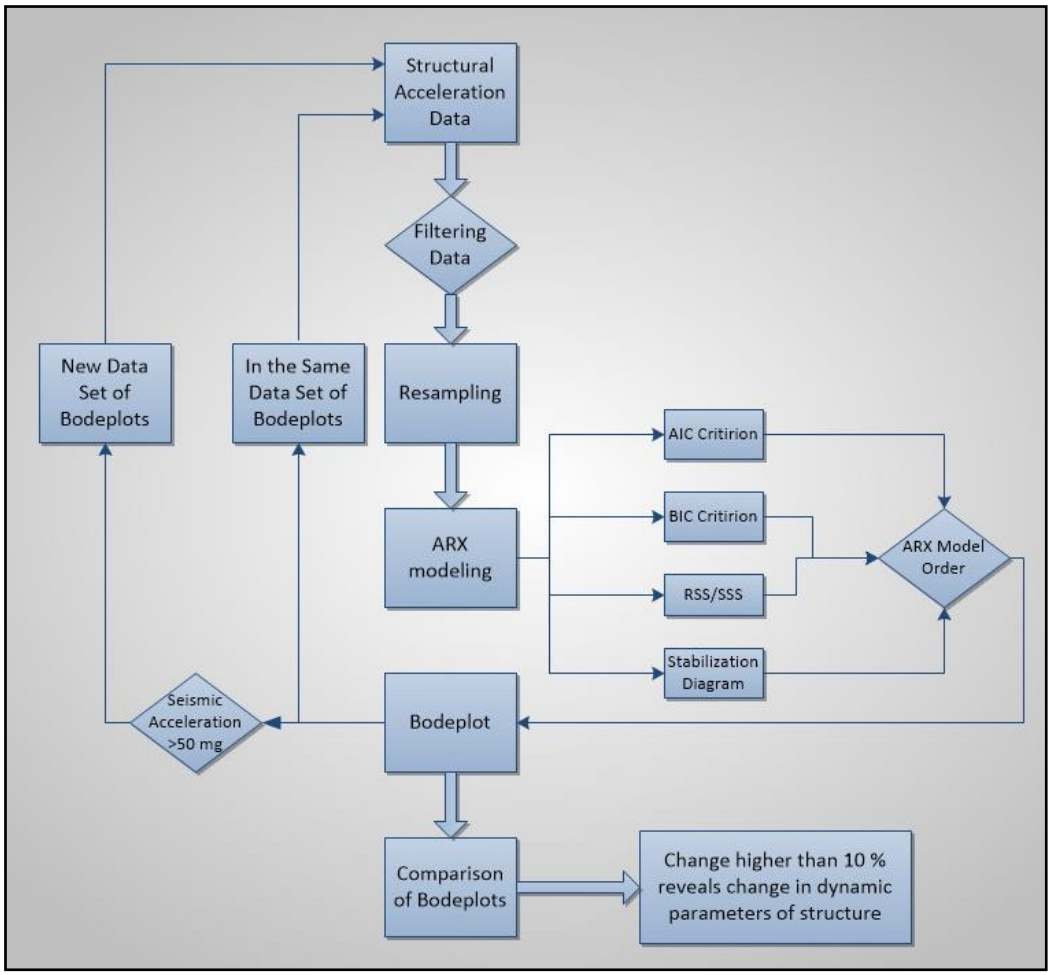

Figure 7.1. Proposed algorithm for SHM on real structures

These bode-plots should present almost the same distribution in amplitude and frequency content if there is no damage induced in the system. If there is a seismic acceleration of the building higher than a triggering level of 50 mg, then the bode-plots are stored in a new data

set of bode-plots. The new sum of bode-plots distribution is compared with the past one and the total sums of bode-plots (before and after) are correlated in order to present the state of dynamical parameters of the case study structures (if there is change or stability). There is a sum of bode-plots in order to be a statistical sample of bode-plots under excitation of different dynamical parameters. Thus, there is the ability to define limits and thresholds that bode-plots graphs could be (without indicate structural damage).

The novel DSP procedure overcomes the limitation of different dynamical parameters in real structure systems. Although different seismic events create different excitation and response on a building, studying the parametric FRF of an ARX model could indicate if the structure response with the same way, and/or if the modal parameters remain the same or there is change on them.

7.6 Novel map that correlates seismic activity with epicenter distance and structures seismic acceleration

A statistical analysis of seismicity effect from the broader region of southern Hellenic Arc is applied in order to reveal seismic acceleration on public buildings (university) according with the distance of each earthquake. High sensitivity accelerometers, record with great accuracy the seismic acceleration of buildings caused by small to large earthquakes, near and far away. Every seismic event is analyzed and studied in terms of magnitude, depth, and distance from the buildings under study and also seismic acceleration that is created in these specific buildings. The study reveals the correlation of magnitude due to distance and seismic acceleration and also the difference in seismic response of new and old building, from the ground floor to the higher floor, with the latter is more sensitive in seismic acceleration caused by earthquakes. Detailed description of the SHMs is on Pentaris et al. [209].

Date	Time (UTC)	Lat Degrees	Lon Degree	Depth (km)	Mw	Distance (km)	Direction	V 2OB	NS 2OB	EW 2 OB	V 3NB	NS 3NB	EW 3NB
20/12/2013	3:24:46	35.28	24.17	8	2.1	30	SE	90	100	110	70	110	120
25/12/2013	5:01:41	35.12	24.33	9.5	2.1	50	SE	150	160	200	60	120	110
23/12/2013	3:57:51	35.39	23.38	23.4	2.3	60	W	90	80	90	90	80	80
21/12/2013	13:16:28	35.03	24.59	20	3	90	SE	100	120	160	50	100	100
28/12/2013	0:01:45	35.08	23.73	2	3	65	SW	220	460	470	120	490	320
30/12/2013	22:26:43	35.35	23.42	30	3	57	SW	150	200	160	100	190	150
6/1/2014	16:48:51	35.29	23.58	2	3.1	47	SW	500	860	890	350	880	580
24/12/2013	4:19:57	35.1	26.17	2	3.1	220	E	220	110	60	140	100	180
8/1/2014	18:06:02	35.32	23.65	2	3.3	39	SW	1100	1600	1710	470	1680	950
27/12/2013	2:30:15	34.9	23.53	20	3.3	90	SW	140	120	170	60	110	140
6/1/2014	14:44:53	34.87	24.06	15	3.4	75	S	180	220	310	140	230	250
27/12/2013	1:27:51	36.11	22.82	2	3.5	130	NW	200	540	420	100	480	440
5/1/2014	6:40:34	35.5	23.34	5	3.6	60	W	100	110	200	80	120	200
24/12/2013	2:40:54	36.15	27.01	96	3.6	280	EEN	110	110	140	80	100	140
30/12/2013	8:37:41	35.4	26.2	5	3.6	220	E	90	130	150	80	160	140
9/1/2014	9:01:03	35.1	23.27	2	3.7	82	SW	170	150	180	180	230	190
15/12/2013	15:36:55	35.55	25.83	8	3.7	160	E	170	250	320	150	270	260
25/12/2013	7:53:18	34.85	24.09	8	3.7	80	S	180	230	310	110	220	195
22/12/2013	21:55:12	35.41	23.41	23.6	3.8	55	SW	300	460	520	230	500	540
22/12/2013	18:04:02	37.82	22.77	2	3.8	290	N	120	120	150	100	160	200
27/12/2013	16:59:53	34.78	27.45	10	3.8	320	EES	50	60	65	50	60	65
2/1/2014	5:29:21	34.9	24.34	30	4	70	SSE	400	1000	1400	440	960	1020
31/12/2013	6:29:09	35.1	23.2	30	4.1	87	SW	160	280	400	120	320	280
31/12/2013	15:06:17	34.55	25.28	49.5	4.3	150	SE	80	80	120	70	90	90
24/2/2014	4:41:20	34.66	24.12	12	4.5	85	S	400	800	1000	280	1120	1100
24/12/2013	3:32:50	34.82	26.29	15	4.8	210	EES	150	210	320	140	230	300

Table 7.1. Example of the rich database of earthquakes and corresponding structural seismic acceleration used in the analysis

On the previous table 7.1 is presented the time of seismic events, the geographical longitude and latitude epicenter in degrees, the depth and magnitude and the distance of the seismic epicenter from the buildings under study. In the column “V 2OB” is presented the vertical acceleration of the 2nd floor of the old building, NS is the north-south component and EW is the east-west component respectively. The same code is for the next three columns where “V 3NB” is the vertical component for the third floor in the new building of TEI etc. These data enable us to correlate the magnitude and the distance of an earthquake with the severity (seismic acceleration) that evolves in both new and old building of TEI.

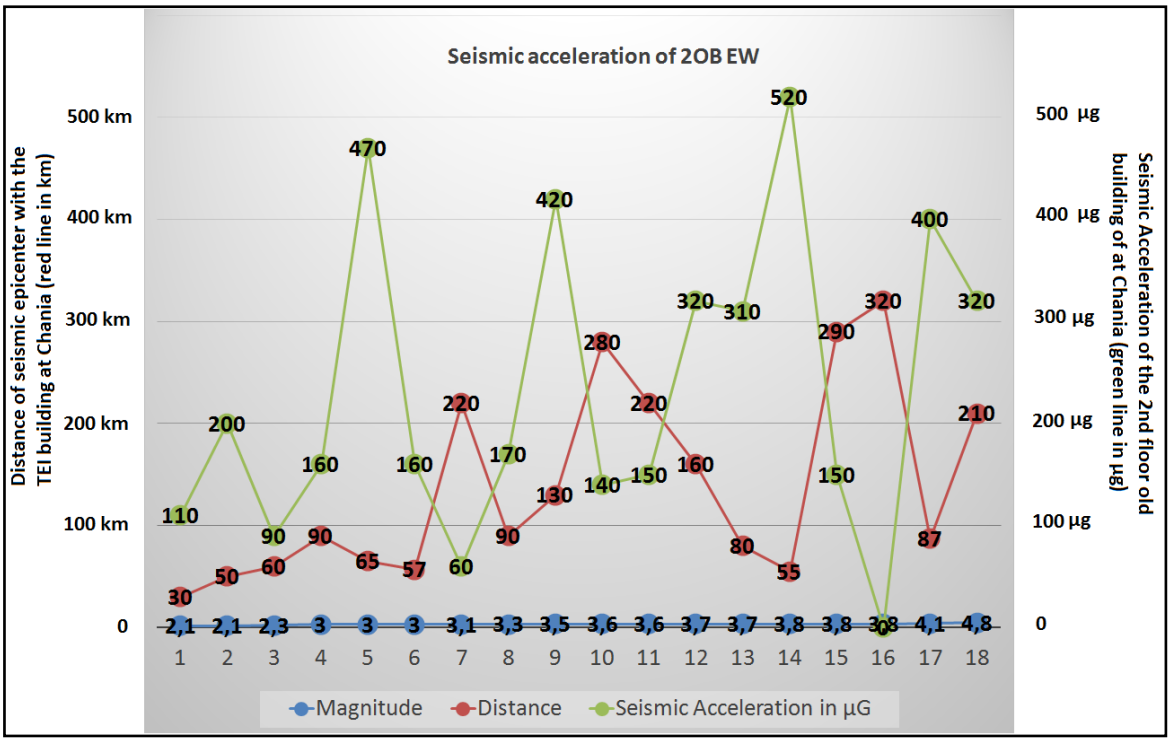

Figure 7.2. EW component of seismic acceleration (green) in relation with increasing EQ magnitude (blue) and EQ distance (red) recorded on the 2nd floor of the old building of TEI of Crete at Chania city.

Above graph (figure 7.2) presents the magnitude of earthquakes in relation with the correspondent distance from the building of TEI and the seismic acceleration of second floor in East-West component. The seismic acceleration that exists is in analogy with the magnitude and in reverse analogy of the distance. Every seismic event is analyzed and studied in terms of magnitude, depth, and distance from the buildings under study and also seismic acceleration that is created in these specific buildings. The study reveals the correlation of magnitude distance and seismic acceleration and also the difference in seismic response of new and old building, from the ground floor to the higher floor, with the latter to be more sensitive in seismic acceleration caused by earthquakes. Recording of seismicity in accordance with seismic acceleration in a building enables to study the impact of specific earthquake parameters to dedicated structures. Also there is the ability to monitor structure acceleration that exist on each floor and test if the differential acceleration from floor to floor remains within permissible limits or overpass them. Below figure 7.3 presents the map earthquake influence map according with table 7 data.

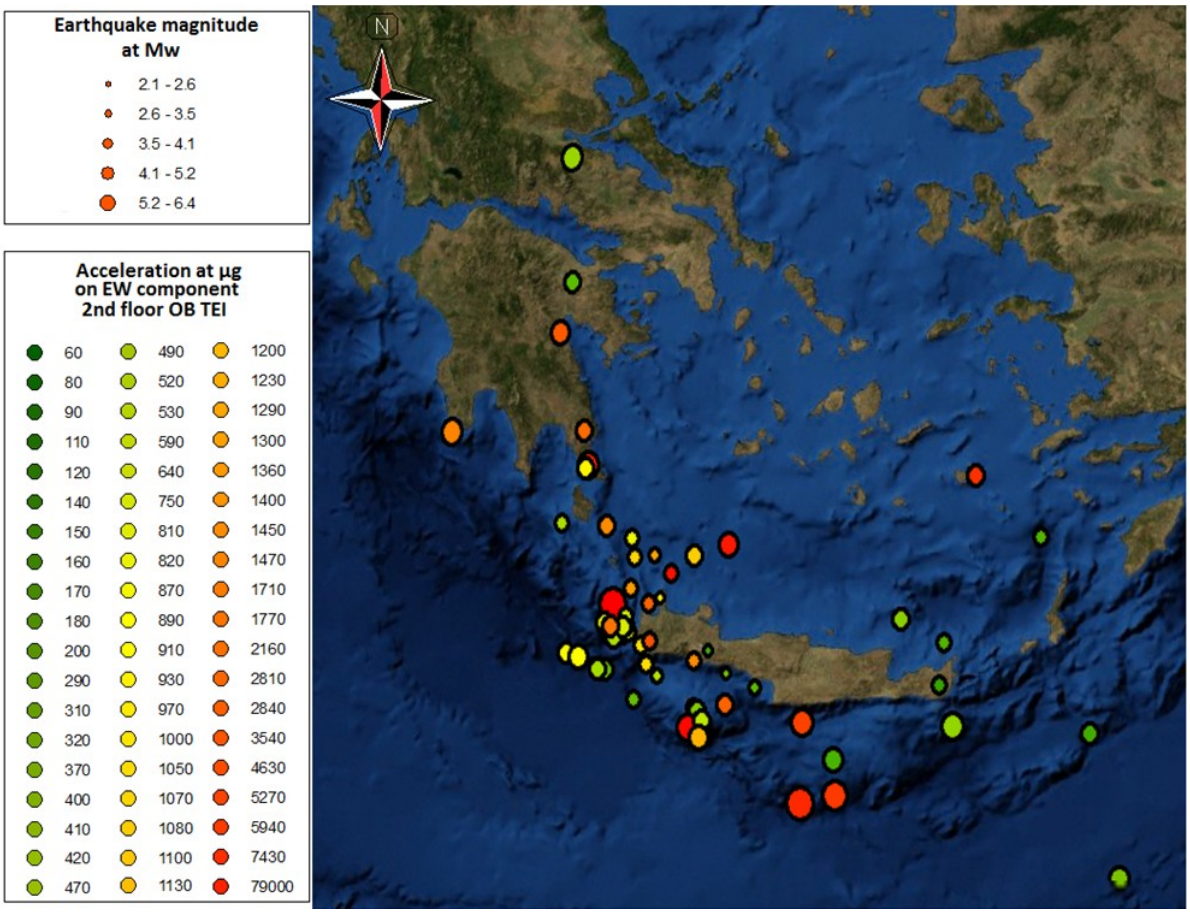

Figure 7.3. ***Earthquake influence map, by means of the EW component of seismic acceleration (color code from green-lower to red-higher), from the 2nd floor in the old building for year 2013 EQ epicenters having magnitudes (circle size) that affected the building located in Chania.***

The contribution of this study is that it applies statistical analysis that correlates the distance, depth and magnitude of earthquakes with the applied acceleration on each floor in specific concrete buildings. The statistical approach of association of seismic acceleration with distance and magnitude of earthquakes contributes to reveal the potential of vulnerability of the building in accordance with seismic parameters.

7.7 Comparison of real structures with artificial and laboratory models

Seismic acceleration measurements were made on real buildings and laboratory models. Results from vibration based measurements revealed that real structures differ completely from laboratory models in terms of excitation and response. Frequency coherence between input (excitation) and output (structural response) on real structures is very limited on a narrow frequency band (eg 0-10 Hz). This band could be enlarged when excitation magnitude is getting higher (eg 0-12 Hz) but still remains on this narrow frequency band. Other frequencies that could apply on input-excitation (eg 20-30 Hz) are completely disappeared on output-response of the case study buildings. In contrast artificial seismic acceleration that applied on laboratory models reveals that frequency coherence has completely different form. The frequency content of the output is analog with the frequency content of the input and the coherence is almost 1 for the whole spectrum. For excitation of 0-10 Hz the vibration response was 0-10 Hz, for excitation of 0-100 Hz the corresponding vibration response of the laboratory model was 0-100 Hz. This indicates that outcomes of non-parametric and/or parametric modeling of lab-models are completely different than the outcomes of real structures. Damage or fault detection on a lab model, under specific vibration excitation, could be clear and obvious, whereas the same damage on real structure could be hidden.

7.8 How much the aims and objectives have been achieved

Key questions discussed in introduction chapter 1 (section 1.2) were answered. Data analysis along with the processing results, presents that the aims and objectives addressed on chapter 1 have been achieved.

7.8.1 When a building or a structure is inadequate

In this thesis non-parametric methods namely power spectral densities, frequency response functions, coherences where combined with parametric methods (AR, ARX, ARMAX) in order to reveal possible damage from real structures and real vibration data of seismic responses. Statistical time series analysis's results (chapter 6.3), present that after a major earthquake shock that happened during the study period and affected with severity the building, there was no change in the dynamical behavior of the building. Results revealed that there was no change of the frequency response function of both case study and analyzed data were also verified from the bode plots of the systems (that were created in the procedure of parametric ARX modeling). Data collection included more than 20 low magnitude seismic events, before major earthquake and 15 small magnitude seismic events

after, that affected both buildings with accelerations from 0.4 mg up to 3 mg and occurred in a region up to 100km from the location of buildings. The specific results are correlated with the frequency deviation index that was proposed in chapter 5.1 and revealed that, in a structure which is affected from strong motion excitation, there is small change in FRF and this change is related with the fundamental frequency deviation in a small or larger scale (depended the severity of strong motion shock). This index combined also with a high HVSR rise index, could reveal high building internal drift (between floors) and such possible high introduced vulnerability of the structure.

7.8.2 How is it possible to identify this deficiency

The research of the thesis presents that application of parametric methods (ARX, ARMAX) and statistical time series analysis, could determined with high detail possible structural change in the dynamic properties of a structure through, parametric FRFs of the system, changes. Wavelet transform could contribute in damage identification when system-building excitation is stable, but in this case study research was inappropriate under seismic excitation. Also a structure could be characterized inadequate when there is high fundamental frequency deviation, which combined with high HVSR change index between floors, could identify structural damage and or high structural vulnerability.

7.8.3 What system is needed and what features should be that there is the ability to easily and cost-effectively monitor the structural condition of buildings

Expensive wired accelerometers were utilized for acceleration recordings able to record very low amplitude seismic acceleration. Also very cost effective wireless accelerometers were developed and applied, able to record strong motion excitation, caused by seismic acceleration on case study buildings. The necessary requirements are the sampling rate of the recordings to be in the frequency spectrum of vibration response of structures under study. Also the sensitivity of sensors should be able to capture and record the low level of accelerations (level of 2-10 mg). Wireless data communication supports the ability for extremely fast and relatively low cost deployment.

7.8.4 How could DSP techniques be combined in order to present a robust methodology to identify SHM faults in real structures

Non parametric methodologies such as PSD, FRFs and coherences could be computed, combined and correlated in order to define and determine specific characteristics and parameters of seismic acceleration recordings on case study structures (resonance

frequencies, coherence of input-output, fundamental frequency deviation between seismic events). These parameters determine the specifications of parametric methodologies applied in acceleration data (model order, stabilization diagrams, model order criteria) in order to reveal efficiently and with high accuracy autoregressive with exogenous input (ARX) FRF models (system bode-plots) and present the dynamic parameters of the structural system. These parametric FRFs are then studied by a statistical approach of parameter vector distribution, in order to indicate if this change-deviation could indicate structural damage.

Chapter 8. Conclusions – Future Work

8.1 Conclusions

In this thesis structural health monitoring has been investigated in detail, and a new developed wireless system has been applied with success. This work correlated state of the art SHM systems, developed and integrated them, and established with success and high recording detail, very affordable wSHMs in buildings. Technological combinations are deployed through wireless sensor networks and high accuracy, low power accelerometers. Furthermore in the frame of this thesis a hybrid-system of structural health monitoring was designed developed and parameterized comprising wired accelerometer of very high precision and accuracy and wireless accelerometer tremendously economical and flexible. The entire system operates as a network and record real-time seismic or man accelerations in buildings providing useful information on the safety of buildings under study. The data were analyzed-studied with advanced digital signal processing techniques to extract important information through the recordings. Within this project a new index was proposed, which measures the deviation of the fundamental frequency of buildings to assess the structural safety of a building. Implementation and evaluation of this index, in real structures, of different age, verified the proposed index.

Furthermore another one novel approach, which uses the method of HVSR in buildings and exhibits HVSR amplitude increasing from floor to floor. This index shows the increase of the spectral of horizontal acceleration related the vertical and correlates this increase from floor to floor with the increase of vulnerability at a building. These two indicators were combined and correlated showing that the respective proportions apply to buildings under study. Non-parametric methodologies applied on acceleration recordings. These methods did not revealed change in dynamical parameters of a structural system through a statistical manner of several events. Specific threshold is determined and upon this level there is indication of induced structural damaged on the case study system. Parametric methods also applied in acceleration data. The parsimony on data analysis and results presented as a very important issue. Data analysis presented the straight correlation of parametric bodeplots with the dynamic parameters, such parametric analysis enabled to reveal the state or change of dynamical parameters of case study buildings very effectively. The parametric bodeplots are also studied by the distribution of parameter vector. This distribution is a damage sensitive parameter which could address structural damage. The results indicated that there is no significant distribution on case study buildings after the major earthquake of 6.4 M.

8.2 Future work

The wireless structural health monitoring system that was designed programmed and installed in this project should be expanded to local regional and metropolital areas. Applications in a metropolitan scale will provide the facilite to monitor continuously the structural integrity of public and private buildings provide and alarm in case of damage detection.

More sensitive accelerometers will be studied, developed and evaluated on wireless SHM system in order to enable higher sensitivity on the acceleration recordings of the SHM network, with higher data rates and data analysis.

More sophisticated algorithms will be added in the programming part of wSHM network, that will be able to process and more computationally efficiently and fast, the recording data and provide reliable communication from the remote nodes to the central gateway.

Different communication protocols in the wireless data communication could be applied in the wSHM network in order to overcome limitations of zigbee protocol, but also to provide the ability of low power consumption and reliable data transmission.

Proposed HVSR index methodology will be studied and be expanded, in order to reveal additional characteristics in structures under study, through the study of ambient noise in buildings, and provide valuable information according their structural vulnerability. The specific method will be applied also in other type of constructions like bridges, tall buildings and heritage buildings.

The prototype map of structural seismic acceleration and statistical analysis, should be populated with more seismic events and regions (buildings) in order to characterize broader structural vulnerability maps. This proposed statistical approach of the earthquake influence on buildings needs to be expanded to cover the majority of the buildings of a city; eventually it would be possible to study the earthquake influence on urban areas and their vulnerability.

An investigation of the application and development of more parametric techniques through correlation and combination of existing parametric methods will reveal valuable information effectively and enable the application of SHM identification to more real structures.

Parametric analysis can be applied to other scientific fields (such as electromagnetism, magnetotellurics, and geosciences related with earthquakes) in order to model data, reveal non-linear characteristics and provide more efficient identification.

The methodology presented in this thesis is restricted to particular classes of buildings. The applicability of this parametric analysis and system identification offer potential for damage and fault detection, in other type of structures like bridges, tall buildings and steel framework constructions.

References

[1] A. Rytter, "Vibration Based Inspection of Civil Engineering Structures," Ph.D., Department of Building Technology and Structural Engineering, Aalborg, Denmark, 1993.

[2] W. Friederich, A. Brüstle, L. Küperkoch, T. Meier, and S. Lamara, "Focal mechanisms in the southern Aegean from temporary seismic networks – Implications for the regional stress field and ongoing deformation processes," *Solid Earth,* vol. 5, pp. 275-297, 2014.

[3] E. Daskalaki, G. A. Papadopoulos, K. Spiliotis, and C. Siettos, "Analysing the topology of seismicity in the Hellenic arc using complex networks," *Journal of Seismology,* vol. 18, pp. 37-46, 2014.

[4] A. A. Skarlatoudis, C. B. Papazachos, B. N. Margaris, C. Ventouzi, and I. Kalogeras, "Ground-motion prediction equations of intermediate-depth earthquakes in the Hellenic arc, southern Aegean subduction area," *Bulletin of the Seismological Society of America,* vol. 103, pp. 1952-1968, 2013.

[5] EL.STAT., "http://www.statistics.gr/," 2013.

[6] ArcGlobe, "www.esri.com," 2013.

[7] K. Worden, C. R. Farrar, G. Manson, and G. Park, "The fundamental axioms of structural health monitoring," *Proceedings of the Royal Society A: Mathematical, Physical and Engineering Science,* vol. 463, pp. 1639-1664, June 8, 2007.

[8] S. W. Doebling, C. R. Farrar, M. B. Prime, and D. Shevitz, "Damage identification and health monitoring of structural and mechanical systems from changes in their vibration characteristics: a literature review.," *Los Alamos National Laboratory report LA-13070-MS,* 1996.

[9] H. Kim and H. Melhem, "Damage detection of structures by wavelet analysis," *Engineering Structures,* vol. 26, pp. 347-362, 2004.

[10] H. Sohn, C. R. Farrar, F. M. Hemez, D. D. Shunk, D. W. Stinemates, B. R. Nadler*, et al.*, "{A review of structural health monitoring literature: 1996--2001}," *Los Alamos National Laboratory, Los Alamos, NM,* 2004.

[11] M. Gong, K. Toshihide, J. Sun, and L. Xie, "Application of ARX and RARX methods in structural parameter identification," presented at the 3rd International Conference on Information and Computing, Wuxi, Jiang Su, China, 4-6 July, 2010.

[12] N. Lin and C. Qun, "Structural health monitoring and damage detection using neural networks technique," presented at the 3rd International Conference on Intelligent System Design and Engineering Applications, ISDEA '13, Hong Kong, China, 16-18 January, 2013.

[13] A. Mojtahedi, M. A. Lotfollahi Yaghin, M. M. Ettefagh, Y. Hassanzadeh, and M. Fujikubo, "Detection of nonlinearity effects in structural integrity monitoring methods for offshore jacket-type structures based on principal component analysis," *Marine Structures,* vol. 33, pp. 100-119, 2013.

[14] M. Solís, M. Algaba, and P. Galvín, "Continuous wavelet analysis of mode shapes differences for damage detection," *Mechanical Systems and Signal Processing,* vol. 40, pp. 645-666, 2013.

[15] G. Jekikj and K. Morita, "System identification of structures for the purpose of structural health monitoring and damage detection," *Bulletin of the International Institute of Seismology and Earthquake Engineering,* vol. 47, pp. 91-96, 2013.

[16] Y. L. Xu, J. Zhang, J. Li, and X. M. Wang, "Stochastic damage detection method for building structures with parametric uncertainties," *Journal of Sound and Vibration,* vol. 330, pp. 4725-4737, 2011.

[17] J. Lee, "Identification of multiple cracks in a beam using natural frequencies," *Journal of Sound and Vibration,* vol. 320, pp. 482-490, 2009.

[18] Y. Goldfeld, "A direct identification procedure for assessment of stiffness distribution," *Engineering Structures,* vol. 31, pp. 1068-1076, 2009.

[19] O. S. Salawu, "Detection of structural damage through changes in frequency: A review," *Engineering Structures,* vol. 19, pp. 718-723, 1997.

[20] F. B. Sayyad and B. Kumar, "Identification of crack location and crack size in a simply supported beam by measurement of natural frequencies," *Journal of Vibration and Control,* vol. 18, pp. 183-190, February 1, 2012.

[21] Z. Mao and M. Todd, "Statistical modeling of frequency response function estimation for uncertainty quantification," *Mechanical Systems and Signal Processing,* vol. 38, pp. 333-345, 2013.

[22] M. Salehi, S. Ziaei-Rad, M. Ghayour, and M. A. Vaziri-Zanjani, "A frequency response based structural damage localization method using independent component analysis," *Journal of Mechanical Science and Technology,* vol. 27, pp. 609-619, 2013.

[23] A. Esfandiari, F. Bakhtiari-Nejad, and A. Rahai, "Theoretical and experimental structural damage diagnosis method using natural frequencies through an improved sensitivity equation," *International Journal of Mechanical Sciences,* 2013.

[24] Y. Goldfeld and D. Elias, "Using the exact element method and modal frequency changes to identify distributed damage in beams," *Engineering Structures,* vol. 51, pp. 60-72, 2013.

[25] B. Aygün and V. C. Gungor, "Wireless sensor networks for structure health monitoring: Recent advances and future research directions," *Sensor Review,* vol. 31, pp. 261-276, 2011.

[26] Jinping Ou and Hui Li, "Structural Health Monitoring in mainland China: Review and Future Trends," *Structural Health Monitoring,* vol. 9, pp. 219-231, May 1, 2010.

[27] M. M. R. Taha, A. Noureldin, J. L. Lucero, and T. J. Baca, "Wavelet Transform for Structural Health Monitoring: A Compendium of Uses and Features," *Structural Health Monitoring,* vol. 5, pp. 267-295, September 1, 2006.

[28] J. P. Lynch and K. J. Loh, "A Summary Review of Wireless Sensors and Sensor Networks for Structural Health Monitoring," *Shock and Vibration Digest, Sage Publications,* vol. 38, pp. 91-128, 2006.

[29] Z. Hou, M. Noori, and R. S. Amand, "Wavelet-based approach for structural damage detection," *Journal of Engineering Mechanics,* vol. 126, pp. 677-683, 2000.

[30] Z. Hou, A. Hera, and A. Shinde, "Wavelet-based structural health monitoring of earthquake excited structures," *Computer-Aided Civil and Infrastructure Engineering,* vol. 21, pp. 268-279, 2006.

[31] S. Xing, M. W. Halling, and Q. Meng, "Structural Pounding Detection by Using Wavelet Scalogram," *Advances in Acoustics and Vibration,* p. 10, 2012.

[32] A. El-Shafie, A. Noureldin, D. McGaughey, and A. Hussain, "Fast orthogonal search (FOS) versus fast Fourier transform (FFT) as spectral model estimations techniques applied for structural health monitoring (SHM)," *Structural and Multidisciplinary Optimization,* vol. 45, pp. 503-513, 2012.

[33] J. E. T. Penny, M. I. Friswell, and D. J. Inman, "Approximate frequency analysis in structural dynamics," *Mechanical Systems and Signal Processing,* vol. 27, pp. 370-378, 2012.

[34] S. D. Fassois and J. S. Sakellariou, "Time-series methods for fault detection and identification in vibrating structures," *Philosophical Transactions of the Royal Society A: Mathematical, Physical and Engineering Sciences,* vol. 365, pp. 411-448, February 15, 2007.

[35] R. Yan, R. X. Gao, and X. Chen, "Wavelets for fault diagnosis of rotary machines: A review with applications," *Signal Processing,* 2013.

[36] J. Chun and J. Chun, "Nonlinear filtering using the wavelet transform," *Signal Processing,* vol. 80, pp. 441-450, 2000.

[37] A. Pazos, M. J. Gonzalez, and G. Alguacil, "Non-linear filter, using the wavelet transform, applied to seismological records," *Journal of Seismology,* vol. 7, pp. 413-429, 2003.

[38] H. Zhang, C. Thurber, and C. Rowe, "Automatic P-wave arrival detection and picking with multiscale wavelet analysis for single-component recordings," *Bulletin of the Seismological Society of America,* vol. 93, pp. 1904-1912, 2003.

[39] S. Wang, Y. Dai, and F. Wang, "Seismic wavelet estimation via a system identification method," *Earthquake Science,* vol. 22, pp. 487-492, 2009.

[40] B. Xu, T. Zhang, G. Song, and H. Gu, "Active interface debonding detection of a concrete-filled steel tube with piezoelectric technologies using wavelet packet analysis," *Mechanical Systems and Signal Processing,* vol. 36, pp. 7-17, 2013.

[41] V. J. Filho, B. F. Guimarães, and I. J. Daniel, "Time-domain analysis of piezoelectric impedance-based structural health monitoring using multilevel wavelet decomposition," *Mechanical Systems and Signal Processing,* vol. 25, pp. 1550-1558, 2011.

[42] C. Wang, W.-X. Ren, Z.-C. Wang, and H.-P. Zhu, "Instantaneous frequency identification of time-varying structures by continuous wavelet transform," *Engineering Structures,* vol. 52, pp. 17-25, 2013.

[43] X.-L. Peng, H. Hao, Z.-X. Li, and K.-Q. Fan, "Experimental study on subsea pipeline bedding condition assessment using wavelet packet transform," *Engineering Structures,* vol. 48, pp. 81-97, 2013.

[44] X.-L. Peng, H. Hao, and Z.-X. Li, "Application of wavelet packet transform in subsea pipeline bedding condition assessment," *Engineering Structures,* vol. 39, pp. 50-65, 2012.

[45] M. Beenamol, S. Prabavathy, and J. Mohanalin, "Wavelet based seismic signal de-noising using Shannon and Tsallis entropy," *Computers & Mathematics with Applications,* vol. 64, pp. 3580-3593, 2012.

[46] M. Mucciarelli, P. Contri, G. Monachesi, G. Calvano, and M. Gallipoli, "An empirical method to assess the seismic vulnerability of existing buildings using the HVSR technique," *Pure and Applied Geophysics,* vol. 158, pp. 2635-2647, 2001.

[47] Triwulan, W. Utama, D. D. Warnana, and Sungkono, "Vulnerability index estimation for building and ground using microtremor," *The second International Seminar on applied Technology, Science and Arts* 2010.

[48] G. C. Luo, L. B. Liu, C. Qi, Q. F. Chen, and Y. P. Chen, "Structural response analysis of a reinforced concrete building based on excitation of microtremors and passing subway trains," *Chinese Journal of Geophysics (Acta Geophysica Sinica),* vol. 54, pp. 2708-2715, 2011.

[49] L.-L. Hong and W.-L. Hwang, "Empirical formula for fundamental vibration periods of reinforced concrete buildings in Taiwan," *Earthquake Engineering & Structural Dynamics,* vol. 29, pp. 327-337, 2000.

[50] S. D. Fassois, "Parametric Identification of Vibrating Structures," in *Encyclopedia of Vibration*, S. G. Braun, D. J. Ewins, and S. S. Rao, Eds., ed London: Academic Press, London, 2001.

[51] G. Cazzulani, S. Moschini, F. Resta, and F. Ripamonti, "A diagnostic logic for preventing structural failure in concrete displacing booms," *Automation in Construction,* 2013.

[52] C. Bao, H. Hao, and Z. X. Li, "Integrated ARMA model method for damage detection of subsea pipeline system," *Engineering Structures,* vol. 48, pp. 176-192, 2013.

[53] J. Cui, J. Zhang, L. Liu, Y. Zhao, K. Zhang, and G. Zhou, "Health diagnosis for aircraft based on the ARMA model," presented at the IEEE International Conference on Intelligent Computing and Integrated Systems, ICISS'10, Guilin, China, 22-24 October, 2010.

[54] S. D. Fassois, "MIMO LMS-ARMAX identification of vibrating structures-Part I: The method," *Mechanical Systems and Signal Processing,* vol. 15, pp. 723-735, 2001.

[55] A. Florakis, S. D. Fassois, and F. M. Hemez, "MIMO LMS-ARMAX identification of vibrating structures-Part II: A critical assessment," *Mechanical Systems and Signal Processing,* vol. 15, pp. 737-758, 2001.

[56] K. A. Petsounis and S. D. Fassois, "Parametric time-domain methods for the identification of vibrating structures-a critical comparison and assessment," *Mechanical Systems and Signal Processing,* vol. 15, pp. 1031-1060, 2001.

[57] Zhichun Yang and Le Wang, "Structural Damage Detection by Changes in Natural Frequencies," *Journal of Intelligent Material Systems and Structures,* vol. 21, pp. 309-319, February 1, 2010.

[58] X. Fang, H. Luo, and J. Tang, "Structural damage detection using neural network with learning rate improvement," *Computers and Structures,* vol. 83, pp. 2150-2161, 2005.

[59] A. Shi and X. H. Yu, "Structural damage detection using artificial neural networks and wavelet transform," presented at the Computational Intelligence for Measurement Systems and Applications (CIMSA), IEEE International Conference, Tianjin, 2012.

[60] S. Yaghmaei-Sabegh and H.-H. Tsang, "A new site classification approach based on neural networks," *Soil Dynamics and Earthquake Engineering,* vol. 31, pp. 974-981, 2011.

[61] P. D. Pastuszak, A. Muc, and M. Barski, "Methods of infrared non-destructive techniques: Review and experimental studies," *Key Engineering Materials,* vol. 542, pp. 131-141, 2013.

[62] Y. Goldfeld, "Identification of the stiffness distribution in statically indeterminate beams," *Journal of Sound and Vibration,* vol. 304, pp. 918-931, 2007.

[63] J. S. Lee, I. Y. Choi, and H. N. Cho, "Modeling and detection of damage using smeared crack model," *Engineering Structures,* vol. 26, pp. 267-278, 2004.

[64] M. N. Cerri and F. Vestroni, "Use of frequency change for damage identification in reinforced concrete beams," *JVC/Journal of Vibration and Control,* vol. 9, pp. 475-491, 2003.

[65] J. K. Sinha, M. I. Friswell, and S. Edwards, "Simplified models for the location of cracks in beam structures using measured vibration data," *Journal of Sound and Vibration,* vol. 251, pp. 13-38, 2002.

[66] W. X. Ren and G. De Roeck, "Structural damage identification using modal data. II: Test verification," *Journal of Structural Engineering,* vol. 128, pp. 96-104, 2002.

[67] J. M. Ndambi, J. Vantomme, and K. Harri, "Damage assessment in reinforced concrete beams using eigenfrequencies and mode shape derivatives," *Engineering Structures,* vol. 24, pp. 501-515, 2002.

[68] J. Brownjohn, A. De Stefano, Y.-L. Xu, H. Wenzel, and A. Aktan, "Vibration-based monitoring of civil infrastructure: challenges and successes," *Journal of Civil Structural Health Monitoring,* vol. 1, pp. 79-95, 2011.

[69] S. W. Doebling, C. R. Farrar, and M. B. Prime, "A summary review of vibration-based damage identification methods," *Shock and Vibration Digest,* vol. 30, pp. 91-105, 1998.

[70] M. G. Santoro and S. K. Kunnath, "Damage-based RC beam element for nonlinear structural analysis," *Engineering Structures,* vol. 49, pp. 733-742, 2013.

[71] F. J. Cara, J. Juan, E. Alarcón, E. Reynders, and G. De Roeck, "Modal contribution and state space order selection in operational modal analysis," *Mechanical Systems and Signal Processing,* vol. 38, pp. 276-298, 2013.

[72] C. Bao, H. Hao, and Z. Li, "Vibration-based structural health monitoring of offshore pipelines: Numerical and experimental study," *Structural Control and Health Monitoring,* vol. 20, pp. 769-788, 2013.

[73] N. Wu and Q. Wang, "Experimental studies on damage detection of beam structures with wavelet transform," *International Journal of Engineering Science,* vol. 49, pp. 253-261, 2011.

[74] T. R. Nuñez and R. L. Boroschek, "Modal properties of a high rise building under construction," presented at the 28th IMAC, A Conference on Structural Dynamics, Jacksonville, FL, United States,1-4 February, 2011.

[75] R. Garrido and A. Concha, "Parametric identification of seismically excited buildings using acceleration measurements," in *8th International Conference on Electrical Engineering, Computing Science and Automatic Control, IEEE*, Merida, Yucatan; Mexico, 2011.

[76] A. C. Altunişik, A. Bayraktar, B. Sevim, and Ş. Ateş, "Ambient vibration based seismic evaluation of isolated Gülburnu highway bridge," *Soil Dynamics and Earthquake Engineering,* vol. 31, pp. 1496-1510, 2011.

[77] B. Moaveni, X. He, J. P. Conte, and J. I. Restrepo, "Damage identification study of a seven-story full-scale building slice tested on the UCSD-NEES shake table," *Structural Safety,* vol. 32, pp. 347-356, 2010.

[78] H. Li, T. Yi, M. Gu, and L. Huo, "Evaluation of earthquake-induced structural damages by wavelet transform," *Progress in Natural Science,* vol. 19, pp. 461-470, 2009.

[79] Y. Lu and F. Gao, "A novel time-domain auto-regressive model for structural damage diagnosis," *Journal of Sound and Vibration,* vol. 283, pp. 1031-1049, 2005.

[80] Y. Okamoto, T. Akazawa, M. Yamada, Y. Onishi, and Y. Hayashi, "System identification of the vibration characteristics for a high-rise building using continuous seismic records," *AIJ Journal of Technology and Design,* vol. 19, pp. 59-64, 2013.

[81] Q. Mei and M. Gul, "An improved methodology for anomaly detection based on time series modeling," in *Proceedings of the 31st IMAC, conference on structural dynamics*, 2013, pp. 277-281.

[82] T. H. Yi, H. N. Li, and X. D. Zhang, "A modified monkey algorithm for optimal sensor placement in structural health monitoring," *Smart Materials and Structures,* vol. 21, 2012.

[83] Q. Fei, H. Zhou, X. Han, and J. Wang, "Structural health monitoring oriented stability and dynamic analysis of a long-span transmission tower-line system," *Engineering Failure Analysis,* vol. 20, pp. 80-87, 2012.

[84] T.-H. Yi, H.-N. Li, and M. Gu, "Optimal sensor placement for structural health monitoring based on multiple optimization strategies," *The Structural Design of Tall and Special Buildings,* vol. 20, pp. 881-900, 2011.

[85] H. S. Ulusoy, M. Q. Feng, and P. J. Fanning, "System identification of a building from multiple seismic records," *Earthquake Engineering & Structural Dynamics,* vol. 40, pp. 661-674, 2011.

[86] A. Pau, A. Greco, and F. Vestroni, "Numerical and experimental detection of concentrated damage in a parabolic arch by measured frequency variations," *Journal of Vibration and Control,* vol. 17, pp. 605-614, April 1 2011.

[87] M. Gul and F. N. Catbas, "Structural health monitoring and damage assessment using a novel time series analysis methodology with sensor clustering," *Journal of Sound and Vibration,* vol. 330, pp. 1196-1210, 2011.

[88] M. Bocca, L. M. Eriksson, A. Mahmood, R. Jäntti, and J. Kullaa, "A synchronized wireless sensor network for experimental modal analysis in structural health monitoring," *Computer-Aided Civil and Infrastructure Engineering,* vol. 26, pp. 483-499, 2011.

[89] J. M. Angeles-Cervantes and L. Alvarez-Icaza, "Identification of seismically excited buildings with two orthogonal horizontal components," *Journal of Vibration and Control,* vol. 17, pp. 881-901, May 1, 2011.

[90] A. Belleri, B. Moaveni, and J. I. Restrepo, "Damage assessment through structural identification of a three-story large-scale precast concrete structure," *Earthquake Engineering and Structural Dynamics,* vol. 43, pp. 61-76, 2014.

[91] T. Y. Hsu and C. H. Loh, "A frequency response function change method for damage localization and quantification in a shear building under ground excitation," *Earthquake Engineering and Structural Dynamics,* vol. 42, pp. 653-668, 2013.

[92] J.-H. Weng and C.-H. Loh, "Recursive subspace identification for on-line tracking of structural modal parameter," *Mechanical Systems and Signal Processing,* vol. 25, pp. 2923-2937, 2011.

[93] Y. Wang, S. Yuan, and L. Qiu, "Improved Wavelet-based Spatial Filter of Damage Imaging Method on Composite Structures," *Chinese Journal of Aeronautics,* vol. 24, pp. 665-672, 2011.

[94] M. D. Spiridonakos, A. G. Poulimenos, and S. D. Fassois, "Output-only identification and dynamic analysis of time-varying mechanical structures under random excitation: A comparative assessment of parametric methods," *Journal of Sound and Vibration,* vol. 329, pp. 768-785, 2010.

[95] M. D. Spiridonakos and S. D. Fassois, "Parametric identification of a time-varying structure based on vector vibration response measurements," *Mechanical Systems and Signal Processing,* vol. 23, pp. 2029-2048, 2009.

[96] A. G. Poulimenos and S. D. Fassois, "Output-only stochastic identification of a time-varying structure via functional series TARMA models," *Mechanical Systems and Signal Processing,* vol. 23, pp. 1180-1204, 2009.

[97] J. S. Sakellariou and S. D. Fassois, "Vibration based fault detection and identification in an aircraft skeleton structure via a stochastic functional model based method," *Mechanical Systems and Signal Processing,* vol. 22, pp. 557-573, 2008.

[98] D. D. Rizos, S. D. Fassois, Z. P. Marioli-Riga, and A. N. Karanika, "Vibration-based skin damage statistical detection and restoration assessment in a stiffened aircraft panel," *Mechanical Systems and Signal Processing,* vol. 22, pp. 315-337, 2008.

[99] M. Rucka and K. Wilde, "Application of continuous wavelet transform in vibration based damage detection method for beams and plates," *Journal of Sound and Vibration,* vol. 297, pp. 536-550, 11/6/ 2006.

[100] L. F. Ramos, G. De Roeck, P. B. Lourenço, and A. C. Costa, "Vibration based damage identification of masonry structures," presented at the International conference of structural analysis of historical constructions - "5th International Conference of Structural Analysis of Historical Constructions", New Delhi, 2006.

[101] L. F. Ramos, R. Aguilar, and P. B. Lourenço, "Operational modal analysis of historical constructions using commercial wireless platforms," *Structural Health Monitoring,* vol. 10, pp. 511-521, 2011.

[102] J.-H. Park, D.-D. Ho, K.-D. Nguyen, and J.-T. Kim, "Multi-scale hybrid sensor nodes for acceleration-impedance monitoring for steel structural connections," San Diego, California, USA, 2011.

[103] S. D. Fassois and J. S. Sakellariou, "Statistical Time Series Methods for SHM," in *Encyclopedia of Structural Health Monitoring.* , C. Boller, F.-K. Chang, and Y. Fujino, Eds., ed: John Wiley & Sons, 2009.

[104] J.-G. Han, W.-X. Ren, and Z.-S. Sun, "Wavelet packet based damage identification of beam structures," *International Journal of Solids and Structures,* vol. 42, pp. 6610-6627, 2005.

[105] M. J. Chae, H. S. Yoo, J. Y. Kim, and M. Y. Cho, "Development of a wireless sensor network system for suspension bridge health monitoring," *Automation in Construction,* vol. 21, pp. 237-252, 2012.

[106] S. Jang, S.-H. Sim, H. Jo, and J. B. F. Spencer, "Full-scale decentralized damage identification using wireless smart sensors," in *Sensors and Smart Structures Technologies for Civil, Mechanical, and Aerospace Systems* San Diego, California, USA, 2011.

[107] K.-V. Yuen and S.-C. Kuok, "Ambient interference in long-term monitoring of buildings," *Engineering Structures,* vol. 32, pp. 2379-2386, 2010.

[108] G. A. Prieto, J. F. Lawrence, A. I. Chung, and M. D. Kohler, "Impulse response of civil structures from ambient noise analysis," *Bulletin of the Seismological Society of America,* vol. 100, pp. 2322-2328, 2010.

[109] G. Maosheng, S. Jing, T. Kashima, and X. Lili, "Parameter identification of a 9-story building for earthquake damage detection," presented at the Image and Signal Processing (CISP), 3rd International Congress on, 2010.

[110] M. F. M. Zain, V. Krishnamurthy, E. Sazonov, M. Jamil, and I. M. Taib, "Performance Testing of Wireless Intelligent Sensor and Actuator Network (WISAN) on a Pre-Stressed Concrete Bridge," presented at the Proceedings of the 10th Wseas International Conference on

Mathematical methods, Computational Techniques, Non-linear Systems, Intelligent Systems, Corfu, Greece, October 26-28, 2008.

[111] D. Skolnik, Y. Lei, E. Yu, and J. W. Wallace, "Identification, Model Updating, and Response Prediction of an Instrumented 15-Story Steel-Frame Building," *Earthquake Spectra,* vol. 22, pp. 781-802, August 2006.

[112] R. Ditommaso, M. Mucciarelli, S. Parolai, and M. Picozzi, "Monitoring the structural dynamic response of a masonry tower: Comparing classical and time-frequency analyses," *Bulletin of Earthquake Engineering,* vol. 10, pp. 1221-1235, 2012.

[113] H. Jo, S.-H. Sim, K. A. Mechitov, R. Kim, J. Li, P. Moinzadeh*, et al.*, "Hybrid wireless smart sensor network for full-scale structural health monitoring of a cable-stayed bridge," San Diego, California, USA, 2011.

[114] G. Maosheng, T. Kashima, S. Jing, and X. Lili, "Identification and analysis of structural time-varying parameters using seismic response records," presented at the Natural Computation (ICNC), 2010 Sixth International Conference on, 2010.

[115] G. Maosheng, S. Jing, T. Kashima, and X. Lili, "Structural time-invariant modal parameters identification from seismic response data," presented at the Natural Computation (ICNC), Sixth International Conference on, 2010.

[116] S. Jang, H. Jo, S. Cho, K. Mechitov, J. A. Rice, S. H. Sim*, et al.*, "Structural health monitoring of a cable-stayed bridge using smart sensor technology: Deployment and evaluation," *Smart Structures and Systems,* vol. 6, pp. 439-459, 2010.

[117] K. Guler, E. Yuksel, and A. Kocak, "Estimation of the fundamental vibration period of existing RC buildings in Turkey utilizing ambient vibration records," *Journal of Earthquake Engineering,* vol. 12, pp. 140-150, 2008.

[118] J. F. Clinton, S. C. Bradford, T. H. Heaton, and J. Favela, "The observed wander of the natural frequencies in a structure," *Bulletin of the Seismological Society of America,* vol. 96, pp. 237-257, 2006.

[119] M. Çelebi, "Recorded earthquake responses from the integrated seismic monitoring network of the Atwood Building, Anchorage, Alaska," *Earthquake Spectra,* vol. 22, pp. 847-864, 2006.

[120] A. De Sortis, E. Antonacci, and F. Vestroni, "Dynamic identification of a masonry building using forced vibration tests," *Engineering Structures,* vol. 27, pp. 155-165, 2005.

[121] C.-H. Loh, J.-H. Weng, C.-H. Chen, and K.-C. Lu, "System identification of mid-story isolation building using both ambient and earthquake response data," *Structural Control and Health Monitoring,* vol. 20, pp. 139-155, 2013.

[122] A. Bagheri and S. Kourehli, "Damage detection of structures under earthquake excitation using discrete wavelet analysis," *Asian Journal of Civil Engineering,* vol. 14, pp. 289-304, 2013.

[123] R. Garrido and A. Concha, "Estimation of the parameters of structures using acceleration measurements," presented at the IFAC Proceedings Volumes, CINVESTAV, Departamento de Control Automático, 07360 D.F, Mexico 2012.

[124] Y. Dong, Y. Li, and M. Lai, "Structural damage detection using empirical-mode decomposition and vector autoregressive moving average model," *Soil Dynamics and Earthquake Engineering,* vol. 30, pp. 133-145, 2010.

[125] E. Peter Carden and J. M. W. Brownjohn, "ARMA modelled time-series classification for structural health monitoring of civil infrastructure," *Mechanical Systems and Signal Processing,* vol. 22, pp. 295-314, 2008.

[126] J. S. Sakellariou and S. D. Fassois, "Stochastic output error vibration-based damage detection and assessment in structures under earthquake excitation," *Journal of Sound and Vibration,* vol. 297, pp. 1048-1067, 2006.

[127] H. Liu, Z. Yang, and M. S. Gaulke, "Structural identification and finite element modeling of a 14-story office building using recorded data," *Engineering Structures,* vol. 27, pp. 463-473, 2005.

[128] C. C. Lin, L. L. Hong, J. M. Ueng, K. C. Wu, and C. E. Wang, "Parametric identification of asymmetric buildings from earthquake response records," *Smart Materials and Structures,* vol. 14, p. 850, 2005.

[129] C. Hellier, "Handbook of Nondestructive Evaluation," McGraw-Hill, Ed., ed, 2003.

[130] S. Cho, C.-B. Yun, J. P. Lynch, A. T. Zimmerman, J. B. F. Spencer, and T. Nagayama, "Smart Wireless Sensor Technology for Structural Health Monitoring of Civil Structures," *International Journal of Steel Structures,* vol. 8, pp. 267-275, 2008.

[131] L. Samantaray, M. Dash, and R. Panda, "A Review on Time-frequency, Time-scale and Scale-frequency domain signal analysis," *IETE Journal of Research,* vol. 51, pp. 287-293, 2005.

[132] B. F. Spencer Jr and S. Nagarajaiah, "State of the art of structural control," *Journal of Structural Engineering,* vol. 129, pp. 845-856, 2003.

[133] D. D. Ho, K. D. Nguyen, P. Y. Lee, D. S. Hong, S. Y. Lee, J. T. Kim*, et al.*, "Wireless structural health monitoring of cable-stayed bridge using Imote2-platformed smart sensors," in *Sensors and Smart Structures Technologies for Civil, Mechanical and Aerospace Systems, Proc. of SPIE*, 2012.

[134] Y. Uchimura, M. Takahashi, and T. Nasu, "Development of a time-synchronized wireless sensor network," *Electrical Engineering in Japan (English translation of Denki Gakkai Ronbunshi),* vol. 173, pp. 46-53, 2010.

[135] M. Ceriotti, L. Mottola, G. P. Picco, A. L. Murphy, Ş. Gună, M. Corrà*, et al.*, "Monitoring heritage buildings with wireless sensor networks: The Torre Aquila deployment," presented at the IPSN, San Fransisco, California, USA, April 15-18, 2009.

[136] Y. Wang, J. P. Lynch, and K. H. Law, "A wireless structural health monitoring system with multithreaded sensing devices: Design and validation," *Structure and Infrastructure Engineering,* vol. 3, pp. 103-120, 2007.

[137] K. Chintalapudi, T. Fu, J. Paek, N. Kothari, S. Rangwala, J. Caffrey*, et al.*, "Monitoring civil structures with a wireless sensor network," *IEEE Internet Computing,* vol. 10, pp. 26-34, 2006.

[138] N. Kurata, B. F. Spencer Jr, and M. Ruiz-Sandoval, "Risk monitoring of buildings with wireless sensor networks," *Structural Control and Health Monitoring,* vol. 12, pp. 315-327, 2005.

[139] H. Jo, S. H. Sim, T. Nagayama, and B. F. Spencer, "Development and Application of High-Sensitivity Wireless Smart Sensors for Decentralized Stochastic Modal Identification," *Journal of Engineering Mechanics,* vol. 138, pp. 683-694, 2012.

[140] E. Sazonov, V. Krishnamurthy, and R. Schilling, "Wireless Intelligent Sensor and Actuator Network - A Scalable Platform for Time-synchronous Applications of Structural Health Monitoring," *Structural Health Monitoring,* vol. 9, pp. 465-476, September 1, 2010.

[141] T. Harms, B. Banks, S. S. Sarvestani, and F. Bastianini, "Design and testing of a low-power wireless sensor network for structural health monitoring of bridges," in *Sensors and Smart Structures Technologies for Civil, Mechanical, and Aerospace Systems*, San Diego, CA, USA, 2009.

[142] J. P. Lynch, K. H. Law, A. S. Kiremidjian, E. Carryer, C. R. Farrar, H. Sohn*, et al.*, "Design and performance validation of a wireless sensing unit for structural monitoring applications," *Structural Engineering and Mechanics,* vol. 17, pp. 393-408, 2004.

[143] K. C. Lu and C. H. Loh, "Development of wireless sensing system for structural health monitoring," presented at the Earth and Space 2010: Engineering, Science, Construction,and Operations in Challenging Environments © 2010 ASCE, 2010.

[144] A. Araujo, J. Garcia-Palacios, J. Blesa, F. Tirado, E. Romero, A. Samartin*, et al.*, "Wireless Measurement System for Structural Health Monitoring With High Time-Synchronization Accuracy," *Instrumentation and Measurement, IEEE Transactions on,* vol. 61, pp. 801-810, 2012.

[145] S. Tadigadapa and K. Mateti, "Piezoelectric MEMS sensors: state-of-the-art and perspectives," *Measurement Science and Technology,* vol. 20, p. 092001, 2009.

[146] A. M. Madni and L. A. Wan, "Microelectromechanical systems (MEMS): an overview of current state-of-the-art," presented at the Aerospace Conference, 1998 IEEE, 1998.

[147] H. Jo, J. A. Rice, J. B. F. Spencer, and T. Nagayama, "Development of high-sensitivity accelerometer board for structural health monitoring," San Diego, CA, USA, 2010.

[148] K. I. K. Wang, Z. Salcic, M. R. Wilson, and K. M. Brook, "Miniaturized wireless sensor node for earthquake monitoring applications," presented at the Industrial Embedded Systems (SIES), 2012 7th IEEE International Symposium on, 2012.

[149] D. Waltenegus, C. Xiaojuan, and K. D. Mieso, "Modelling the energy cost of a fully operational wireless sensor network," *Telecommunication Systems,* vol. 44, pp. 3-15, 2010.

[150] L. Jin-Shyan, S. Yu-Wei, and S. Chung-Chou, "A Comparative Study of Wireless Protocols: Bluetooth, UWB, ZigBee, and Wi-Fi," presented at the Industrial Electronics Society, 2007. IECON 2007. 33rd Annual Conference of the IEEE, 2007.

[151] F. Sivrikaya and B. Yener, "Time synchronization in sensor networks: a survey," *Network, IEEE,* vol. 18, pp. 45-50, 2004.

[152] P. Jeongyeup, K. Chintalapudi, R. Govindan, J. Caffrey, and S. Masri, "A Wireless Sensor Network for Structural Health Monitoring: Performance and Experience," presented at the Embedded Networked Sensors, 2005. EmNetS-II. The Second IEEE Workshop on, 2005.

[153] S. Kim, "Wireless sensor networks for structural health monitoring," MSc, Electrical Engineering and Computer Sciences, University of California, Berkeley, 2005.

[154] F. L. Lewis, "Wireless Sensor Networks," *Smart Environments,* pp. 11-46, 2005.

[155] M. Z. A. Bhuiyan, W. Guojun, and C. Jiannong, "Sensor Placement with Multiple Objectives for Structural Health Monitoring in WSNs," presented at the High Performance Computing and Communication & 2012 IEEE 9th International Conference on Embedded Software and Systems (HPCC-ICESS), IEEE 14th International Conference on, 2012.

[156] P. Wang, Y. Yan, G. Y. Tian, O. Bouzid, and Z. Ding, "Investigation of wireless sensor networks for structural health monitoring," *Journal of Sensors,* vol. 12, 2012.

[157] A. Bilbao, D. Hoover, J. Rice, and J. Chapman, "Ultra-low power wireless sensing for long-term structural health monitoring," presented at the Sensors and Smart Structures Technologies for Civil, Mechanical, and Aerospace Systems, San Diego, California, USA, 2011.

[158] J. A. Rice, K. A. Mechitov, J. B. F. Spencer, and G. A. Agha, "Autonomous smart sensor network for full-scale structural health monitoring," presented at the Sensors and Smart Structures Technologies for Civil, Mechanical, and Aerospace Systems, San Diego, CA, USA, 2010.

[159] J. A. Rice and J. B. F. Spencer, "Flexible Smart Sensor Framework for Autonomous Full-scale Structural Health Monitoring," *Newmark Structural Engineering Laboratory Report Series 018,* 2009.

[160] J. C. Chin, J. M. Rautenberg, C. Y. T. Ma, S. Pujol, and D. K. Y. Yau, "An experimental low-cost, low-data-rate rapid structural assessment network," *IEEE Sensors Journal,* vol. 9, pp. 1361-1369, 2009.

[161] Y. Lei, A. S. Kiremidjian, K. K. Nair, J. P. Lynch, and K. H. Law, "Algorithms for time synchronization of wireless structural monitoring sensors," *Earthquake Engineering and Structural Dynamics,* vol. 34, pp. 555-573, 2005.

[162] S. Ganeriwal, R. Kumar, and M. B. Srivastava, "Timing-sync protocol for sensor networks," presented at the SenSys, Los Angeles, California , USA, 2003.

[163] J. Elson, L. Girod, and D. Estrin, "Fine-grained network time synchronization using reference broadcasts," *SIGOPS Oper. Syst. Rev.,* vol. 36, pp. 147-163, 2002.

[164] M. D. Lemmon, J. Ganguly, and L. Xia, "Model-based clock synchronization in networks with drifting clocks," presented at the Dependable Computing, 2000. Proceedings. 2000 Pacific Rim International Symposium on, 2000.

[165] P. Katsikogiannis, E. Zervas, and G. Kaltsas, "A wireless sensor network for building structural health monitoring and seismic detection," *Physica Status Solidi (C) Current Topics in Solid State Physics,* vol. 5, pp. 3834-3838, 2008.

[166] X. M. Sun, X. Feng, J. Zhou, and Z. C. Yan, "Sensor placement for structural damage detection with modal data," *Journal of Harbin Institute of Technology (New Series),* vol. 17, pp. 297-302, 2010.

[167] R. Morello, C. De Capua, and A. Meduri, "Remote monitoring of building structural integrity by a smart wireless sensor network," presented at the Instrumentation and Measurement Technology Conference (I2MTC), 2010 IEEE, 2010.

[168] Yuequan Bao, J. L. Beck, and Hui Li, "Compressive sampling for accelerometer signals in structural health monitoring," *Structural Health Monitoring,* vol. 10, pp. 235-246, May 1, 2011.

[169] T. Y. Hsu, S. K. Huang, K. C. Lu, and C. H. Loh, "A damage detection algorithm integrated with a wireless sensing system," *Journal of Physics: Conference Series,* vol. 305, 2011.

[170] J. G. Proakis and D. G. Manolakis, *Digital Signal Processing - Principles, Algorithms and Applications*: Prentice-Hall, 1996.

[171] L. Tan, *Digital Signal Processing - Fundamentals and Applications*: Elsevier, 2008.

[172] D. Stranneby and W. Walker, *Digital Signal Processing and Applications (Second Edition)*. Oxford: Newnes, 2004.

[173] J. D. Broesch, *Digital Signal Processing*. Burlington: Newnes, 2009.

[174] K. K. Sharma, S. D. Joshi, and S. Sharma, "Advances in shannon sampling theory," *Defence Science Journal,* vol. 63, pp. 41-45, 2013.

[175] A. Mertins, *Signal analysis : wavelets, filter banks, time-frequency transforms, and applications / Alfred Mertins*. Chichester, West Sussex, England ; New York :: J. Wiley, 1999.

[176] S. W. Smith, *The scientist and engineer's guide to digital signal processing*: California Technical Publishing, 1997.

[177] D. G. Manolakis and V. K. Ingle, *Applied Digital Signal Processing: Theory and Practice*: Cambridge University Press, 2011.

[178] S. Kaewarsa, "Signal processing techniques for power quality analysis: A review," *International Review on Modelling and Simulations,* vol. 5, pp. 596-608, 2012.

[179] C. R. Pinnegar and L. Mansinha, "Time-local Fourier analysis with a scalable, phase-modulated analyzing function: The S-transform with a complex window," *Signal Processing,* vol. 84, pp. 1167-1176, 2004.

[180] L. B. Almeida, "Fractional fourier transform and time-frequency representations," *IEEE Transactions on Signal Processing,* vol. 42, pp. 3084-3091, 1994.

[181] J. J. Shynk, "Frequency-domain and multirate adaptive filtering," *IEEE Signal Processing Magazine,* vol. 9, pp. 14-37, 1992.

[182] P. Duhamel and M. Vetterli, "Fast fourier-transforms - A tutorial review and a state-of the art," *Signal Processing,* vol. 19, pp. 259-299, 1990.

[183] M. Yoshimasa, "Introduction to the Bilinear Transformation Method," *Mathematics in Science and Engineering,* vol. Volume 174, pp. 5-46, 1984.

[184] P. Duhamel and M. Vetterli, "Fast fourier transforms: A tutorial review and a state of the art," *Signal Processing,* vol. 19, pp. 259-299, 1990.

[185] D. Gabor, "Theory of communication," *J.IEE,* vol. 93, pp. 429-457, 1946.

[186] S. Mallat, *A Wavelet Tour of Signal Processing, Third Edition: The Sparse Way*: Academic Press, 2008.

[187] M. Misiti, Y. Misiti, G. Oppenheim, and J.-M. Poggi, *Wavelets and their Applications*. London: ISTE Ltd, 2007.

[188] A. Haar, "Zur Theorie der orthogonalen Funktionensysteme," *Mathematische Annalen,* vol. 71, pp. 38-53, 1911.

[189] A. Mertins, "Signal Analysis: Wavelets, Filter Banks, Time-Frequency Transforms and Applications.," 1999.

[190] I. Daubechies, "Orthonormal bases of compactly supported wavelets," *Communications on Pure and Applied Mathematics,* vol. 41, pp. 909-996, 1988.

[191] J. Morlet, "Sampling Theory and Wave Propagation," *Issues in Acoustic Signal — Image Processing and Recognition,* vol. 1, pp. 233-261, 1983.

[192] J. Morlet, G. Arens, E. Fourgeau, and D. Giard, "Wave propagation and sampling theory - Part I. Complex signal and scattering in multilayered media," *GEOPHYSICS,* vol. 47, pp. 203-221, 1982.

[193] R. Shantha Selva Kumari, S. Bharathi, and V. Sadasivam, "Design of Optimal Discrete Wavelet for ECG Signal Using Orthogonal Filter Bank," presented at the Conference on Computational Intelligence and Multimedia Applications, 2007. International Conference on, 2007.

[194] GoogleEarth, ""Chania" 35°31'9.30"N, 24° 2'34.35"E Google Earth. ." 2012.

[195] X. Sun, Z. Yan, and D. Zhu, "Comparison of several methods for optimal sensor placement in structural health monitoring," *Advanced Materials Research,* vol. 250-253, pp. 3254-3257, 2011.

[196] H. Y. Guo, L. Zhang, L. L. Zhang, and J. X. Zhou, "Optimal placement of sensors for structural health monitoring using improved genetic algorithms," *Smart Materials and Structures,* vol. 13, pp. 528-534, 2004.

[197] A. F. Shakal and M.-J. Huang, "Strategies and criteria for the selection of buildings for instrumentation," in *Workshop on Strong-Motion Instrumentation of Structures*, Emeryville, California, 2001.

[198] M.-J. Huang and A. F. Shakal, "CSMIP building instrumentation measurement objectives and models," in *Workshop on Strong-Motion Instrumentation of Structures*, Emeryville, California, 2001.

[199] G. Yan, Z. Duan, and J. Ou, "Review on structural damage detection based on vibration data," *Journal of Earthquake Engineering and Engineering Vibration,* vol. 27, pp. 95-103, 2007.

[200] Reftek, "www.reftek.com," 2013.

[201] EMSC, "http://www.emsc-csem.org," 2013.

[202] D. Hoover, "Design, testing, and implementation of WiSeMote: A wireless sensor network for structural health monitoring," Master of Science, Electrical Engineering, Texas Tech University, Texas, 2012.

[203] J. Samuels, M. Reyer, S. Hurlebaus, S. Lucy, D. Woodcock, and J. Bracci, "Wireless sensor network to monitor an historic structure under rehabilitation," *Journal of Civil Structural Health Monitoring,* vol. 1, pp. 69-78, 2011.

[204] F. P. Pentaris, J. P. Makris, and F. Vallianatos, "Correlation of fast Fourier transform based Power Spectral densities and wavelet transform towards an novel index of main parameter dispersion," in *Proceedings of the 6th International Conference on Sensors and Signals (SENSIG '13)*, Lemesos, Cyprus, March 21-23, 2013, pp. 212-221.

[205] Libelium, "www.libelium.com," 2013.

[206] Digi, "http://www.digi.com/xbee/," 2013.

[207] AGGSoftware, "http://www.dataloggersuite.com/," 2013.

[208] F. P. Pentaris, J. Stonham, and J. P. Makris, "A cost effective wireless structural health monitoring network for buildings in earthquake zones," *Smart Materials and Structures,* vol. 23, p. 105010, 2014.

[209] F. P. Pentaris, J. Stonham, and J. P. Makris, "A review of the state-of-the-art of wireless SHM systems and an experimental set-up towards an improved design," presented at the IEEE EuroCon'13, Zagreb, 2013.

[210] L. Ljung, *System Identification: Theory for the User*, 2nd ed., 1999.

[211] T. S. Soderstrom and P. G. Stoica, *System Identification*: Prentice hall, 1989.

[212] K. Worden, "Structural fault detection using a novelty measure," *Journal of Sound and Vibration,* vol. 201, pp. 85-101, 1997.

[213] I. Papadopoulos, "Experimental and theoretical study of site amplification by usage of microtremors and field geophysical measurements " PhD, Dept. of Geology, University of Thessaloniki, Thessaloniki, 2013.

[214] Guralp, "http://www.guralp.com/," 2013.

[215] LennartzElectronicGmbH, "http://www.lennartz-electronic.de/," 2013.

[216] F. J. Chávez-García and J. Tejeda-Jácome, "Site response in Tecoman, Colima, Mexico—I: Comparison of results from different instruments and analysis techniques," *Soil Dynamics and Earthquake Engineering,* vol. 30, pp. 711-716, 2010.

[217] GEOPSY, "www.geopsy.org," 2013.

[218] G. Hloupis, I. Papadopoulos, J. P. Makris, and F. Vallianatos, "The South Aegean seismological network – HSNC," *Adv. Geosci.,* vol. 34, pp. 15-21, 2013.

Appendix A: Publications derived from this research

I. **F. P. Pentaris**, J.P. Makris, J. Stonham, and F. Vallianatos, "Principles in wireless building health monitoring systems", *Geophysical Research Abstracts*, Vol. 14, EGU2012-13239-1, 2012

II. **F. P. Pentaris** and J.P. Makris, "Combination of digital signal processing methods towards an improved analysis algorithm for structural health monitoring",*Geophysical Research Abstracts*, Vol. 15, EGU2013-9066-7, 2013

III. **F. P. Pentaris**, J. Stonham, J.P. Makris and F. Vallianatos, "Correlation of fast Fourier transform based Power Spectral densities and wavelet transform towards an novel index of main parameter dispersion " *WSEAS, Sensors and Signals, 21-23 March, Lemesos, Cyprus*, ISBN 978-1-61804-169-2, pp. 212-221, 2013

IV. **F. P. Pentaris**, J. Stonham and J.P. Makris, "A review of the state-of–the-art of wireless SHM systems and an experimental set-up towards an improved design*", IEEE, Region 8 Conference EuroCon 2013*, Zagreb, Croatia, 2013

V. **F. P. Pentaris**, J. Stonham, and J. P. Makris, "A novel approach of Structural Health Monitoring by the application of FFT and wavelet transform using an index of frequency dispersion," *NAUN-WSEAS, International Journal of Geology*, 2013.

VI. **F. P. Pentaris** and I. Papadopoulos, "A novel HVSR approach on structural heath monitoring for structural vulnerability assesement," *Geophysical Research Abstracts*, EGU2014-5347-3, vol. Vol. 16, 2014.

VII. **F. P. Pentaris** and G.N. Fouskitakis, "Parametric and Non-Parametric Vibration-Based Structural Identification under Earthquake Excitation," *Geophysical Research Abstracts*, EGU2014-7700-3, vol. 16, 2014.

VIII. **F. P. Pentaris** and J.P. Makris, "Statistics of Earthquake Influence on Buildings by means of Seismic Acceleration," *Geophysical Research Abstracts*, EGU2014-11567, vol. 16, 2014.

IX. **F. P. Pentaris**, G.N. Fouskitakis, J.S. Sakellariou and J.P. Makris "Vibration-Based Structural Health Monitoring of Concrete Structures Under Earthquake Excitation via Statistical Times Series Methods", *6th World Conference of the international association for structural control and monitoring (6WCSCM)*, Barcelona, July 15-17, 2014

X. **F. P. Pentaris,** "A novel Horizontal to Vertical Spectral Ratio approach in a wired Structural Health Monitoring system ", *Journal of Sensors and Sensor Systems*, vol. 3 pp. 145-165, 2014

XI. **F. P. Pentaris** and F. Vallianatos, "Application of HVSR on Reinforced Concrete Buildings," *in 2nd European Conference on Earthquake Engineering and Seismology*, Istanbul, Turkey, 2014

XII. **F. P. Pentaris**, J. Stonham, and J. P. Makris, "A cost effective wireless structural health monitoring network for buildings in earthquake zones," *IOP, Journal of Smart Materials and Structures*, vol. 23, p. 105010, 2014.

Appendix B: Programming of Waspmotes

The specific needs of project require programming for wireless multipoint-point communication, parametrizing of internal accelerometer sensitivity and sampling rate. Xbee modules require initialization in order to communicate with the same PAN id, sampling rate etc. Initially ready programs of libraries were tested.

"Wasp_pro_start_program_full_802_v1" program establishes wireless communication between the waspmote module and the gateway via xbee. The used protocol is 802.15.4 (xbee) and the mode this program works in is the API mode. The program builds a frame with the waspID and data. This frame is then sent wirelessly.

Main program structure:

```
// Include libraries
#include <WaspXBee802.h>
#include <WaspFrame.h>
// Declare global variables
packetXBee* packet;
char macHigh[10];
char macLow[11];
```

First the necessary libraries are included, and the global variables are declared. The created variables are the xbee packet, and the most- and least significant bits of the mac address of the xbee (respectively mackHigh and macLow).

```
void setup()
{ // 1. set up the XBee module
  xbee802.ON();
  // 2. Set up RTC and ACC
  delay(500);   RTC.ON();   ACC.ON();
 // 3. LEDs management
  Utils.setLED(LED0, LED_ON);
  Utils.setLED(LED1, LED_ON);
  delay(2000);
  Utils.setLED(LED0, LED_OFF);
  Utils.setLED(LED1, LED_OFF);
  for (int i=0;i<24;i++)
  {     Utils.blinkLEDs(125);   }
  // 4. Get the XBee MAC address
  xbee802.ON();
  delay(1000);
  xbee802.flush();
  // Get the XBee MAC address
  int counter = 0;
  while((xbee802.getOwnMac()!=0) && (counter<12))
  {     xbee802.getOwnMac();     counter++;   } // convert mac address from array to string
  Utils.hex2str(xbee802.sourceMacHigh, macHigh, 4);
  Utils.hex2str(xbee802.sourceMacLow,  macLow,  4);
  // 5. Print XBee module information
```

```
  USB.ON();
  USB.print("mac address:");
  USB.print(macHigh);
  USB.println(macLow);
  USB.OFF(); }
```

In the setup part, all the devices are initialized. The Xbee module, RTC clock and ACC are turned on, the leds are tested, and the MAC address of the Xbee module is loaded into the main program. The MAC address is then printed to the USB port.

```
void loop()
{
  // 6. Message composition
  // 6.1 Create new frame (No mote id)
  frame.createFrame(ASCII,"");
  // 6.2 Add frame fields
  frame.addSensor(SENSOR_MAC, macLow);
  frame.addSensor(SENSOR_ACC, ACC.getX(), ACC.getY(), ACC.getZ() );
  frame.addSensor(SENSOR_IN_TEMP, RTC.getTemperature());
  frame.addSensor(SENSOR_BAT, PWR.getBatteryLevel());
  // 6.3 Print frame
  //
Example:<=>
-----------------------------------------------------------------------------
#35690399##5#MAC:4066EF6B#ACC:-47;-26;1000#IN_TEMP:26.25#BAT:59#
  frame.showFrame();
```

In this part the API frame is built. To apply API frame, the waspmote frame library functions are needed. The functions frame.createFrame(), frame.addSensor(), frame.showFrame() are essential to create an API frame. (frame library includes details of parameters).

Next program from the Waspmote environment with wakeup interrupt that was tested is "ACC_05_inertial_wake_up_interrupt". Below is the schematic diagram of the code:

```
long previous = 0;
void setup()
{
  ACC.ON();
  USB.ON(); // starts using the serial port
  USB.println(F("ACC_05 example"));
}
```

Accelerometer and USB are initialized.

```
void loop()
{
  ACC.ON();
  USB.println(F("Accelerometer ON"));
  ACC.setIWU();
  USB.println("Inertial Wake-UP interrupt configured");
  USB.println("Go to sleep and wait Inertial Wake-UP interrupt");
  PWR.sleep(ALL_OFF);
  if( intFlag & ACC_INT )
  {
    // clear the accelerometer interrupt flag on the general interrupt vector
    intFlag &= ~(ACC_INT);
```

```
    ACC.unsetIWU();
    // read the acceleration source register
    delay(200);
    USB.ON();
    USB.println(F("+++++++++++++++++++++++++++++++++++++++++"));
    USB.println(F("++ Inertial Wake-UP interrupt detected ++"));
    USB.println(F("+++++++++++++++++++++++++++++++++++++++++"));
  }
  delay(2000);
}
```

The accelerometer is turned on, and the inertial wake up is set. Previous interruptions are cleared and the hardware interruption is attached to the pin. The waspmote is set in low power mode. If an interrupt occurs, the interrupt flag is cleared and the inertial wake-up is unset. After that a message is print to the USB port. Combination of the two previous programs into one program code.

```
// Include libraries
#include <WaspXBee802.h>
#include <WaspFrame.h>
#include <WaspRTC.h>
#include <WaspACC.h>
#include <stdlib.h>
// Declare global variables
packetXBee* packet;
char macHigh[10];char macLow[11];long previous = 0;
char* T = "T";char* comma = ",";char* dotcomma = ";";
char open[] = "{";char close[] = "}";char* newline = "\r\n";
char xval[] = "Xvalue";char yval[] = "Yvalue";char zval[] = "Zvalue";
char X,Y,Z
void setup()
{
    // 1. set up the XBee module
    xbee802.ON();
    // 2. Set up RTC and ACC
    delay(500);
    RTC.ON();      ACC.ON();
    // 3. LEDs management
    Utils.setLED(LED0, LED_ON);     Utils.setLED(LED1, LED_ON);     delay(2000);
    Utils.setLED(LED0, LED_OFF);    Utils.setLED(LED1, LED_OFF);
    for (int i=0;i<24;i++)
    {
      Utils.blinkLEDs(125);
    }
```

```
// 4. Get the XBee MAC address
    xbee802.ON();
    delay(1000);
    xbee802.flush();
    // Get the XBee MAC address
    int counter = 0;
    while((xbee802.getOwnMac()!=0) && (counter<12))
    {
      xbee802.getOwnMac();
      counter++;
```

```
    }

    // convert mac address from array to string
    Utils.hex2str(xbee802.sourceMacHigh, macHigh, 4);
    Utils.hex2str(xbee802.sourceMacLow,  macLow,  4);

}
```

First all the useful libraries are included and the global variables. Some arrays of chars are created to store certain words. We also use some characters in our code, they are all *char type. Further on in the setup loop the Xbee, RTC, accelerometer and LEDs are initialized. The xbee mac address is stored in the macLow and macHigh variables.

```
void loop()
{
    ACC.ON();
    ACC.setIWU();
    PWR.sleep(ALL_OFF);
    if( intFlag & ACC_INT )
      {
      intFlag &= ~(ACC_INT);
      for(int i = 0; i <20; i++)
        {
              // clear the accelerometer interrupt flag on the general interrupt vector
              ACC.unsetIWU();
              // read the acceleration source register
              USB.ON();
              // 6. Message composition
              // 6.1 Create new frame (No mote id)
              frame.createFrame(ASCII,"");
              frame.setFrameSize(1500);
              // 6.2 Add frame fields
              //Logging part
              frame.addSensor(SENSOR_STR, dotcomma);
              frame.addSensor(SENSOR_ACC, macLow);
              frame.addSensor(SENSOR_STR, dotcomma);
              frame.addSensor(SENSOR_ACC, ACC.getX());
              frame.addSensor(SENSOR_STR, dotcomma);
              frame.addSensor(SENSOR_ACC, ACC.getY());
              frame.addSensor(SENSOR_STR, dotcomma);
              frame.addSensor(SENSOR_ACC, ACC.getZ());
              frame.addSensor(SENSOR_STR, newline);
              frame.addSensor(SENSOR_STR, dotcomma);
              //Plotting part
              frame.addSensor(SENSOR_STR, open);
              frame.addSensor(SENSOR_STR, xval);
              frame.addSensor(SENSOR_ACC, macLow[7]);
              frame.addSensor(SENSOR_STR, comma);
              frame.addSensor(SENSOR_STR, T);
              frame.addSensor(SENSOR_STR, comma);
              frame.addSensor(SENSOR_ACC, ACC.getX());
              frame.addSensor(SENSOR_STR, close);
              frame.addSensor(SENSOR_STR, open);
              frame.addSensor(SENSOR_STR, yval);
              frame.addSensor(SENSOR_ACC, macLow[7]);
              frame.addSensor(SENSOR_STR, comma);
              frame.addSensor(SENSOR_STR, T);
```

```
                frame.addSensor(SENSOR_STR, comma);
                frame.addSensor(SENSOR_ACC, ACC.getY());
                frame.addSensor(SENSOR_STR, close);
                frame.addSensor(SENSOR_STR, open);
                frame.addSensor(SENSOR_STR, zval);
                frame.addSensor(SENSOR_ACC, macLow[7]);
                frame.addSensor(SENSOR_STR, comma);
                frame.addSensor(SENSOR_STR, T);
                frame.addSensor(SENSOR_STR, comma);
                frame.addSensor(SENSOR_ACC, ACC.getZ());
                frame.addSensor(SENSOR_STR, close);
                frame.addSensor(SENSOR_STR, dotcomma);
                frame.addSensor(SENSOR_STR, newline);
                // 6.3 Print frame
                // Example:  4066EF6B;-47;-26;1000
                frame.showFrame();
                ////////////////////////////////////////////////
                // 7. Send the packet
                ////////////////////////////////////////////////
                // 7.1 set packet to send
                packet=(packetXBee*); calloc(1,sizeof(packetXBee)); // memory allocation
                packet->mode=BROADCAST; // set Broadcast mode
                // 7.2 send the packet via the correct object depending on the protocol
                // turn XBee on
                xbee802.ON();
                // sets Destination parameters
                xbee802.setDestinationParams(packet,          "000000000000FFFF",          frame.buffer,
frame.length, MAC_TYPE);
                // send data
                xbee802.sendXBee(packet);
                // 7.3 free memory
                free(packet);  packet = NULL; delay(1);
        }
    }
}
```

The Waspmote is put in sleep mode. If an interrupt is detected, the interrupt flag is cleared, and the frame is created. With the function frame.createFrame() the ASCII frame structure is created. After that sensor values/characters/strings are added with the function frame.addSensor(). The function frame.showFrame is used to show the frame locally on the waspmote. When the total frame is created, it is sent wirelessly with xbee. To send the frame wirelessly, the function xbee802.setDestinationParams() is used. The data packet is selected, broadcast or unicast mode is set

AT mode

AT mode (transparent mode) is the default mode of the Xbee module. In AT mode the Xbee module acts as a serial line replacement. The data is sent wirelessly without a frame. There is no additional information sent with the data. In systems with more than one Waspmote, for example point to multipoint systems, it is nescessairy to send addional information with the data package to indentify the module from which the data has been sent.

API mode

API stands for Application Programming Interface. It is a frame-based method which allows the user to send or receive data via the radio's serial UART. All the data is packed in frames in order to establish a datastream without too much loss of data. It is a more safe option in comparison to the basic AT mode, which functions without these frames. The program for creating API xbee communication is quite computationally heavy, and it takes time to send one API frame. Experimentally it is determined the sending speed in API mode. To send one frame, about 1-2 seconds are needed. Such the maximum sample frequency at the gateway is 1-2 Hz. But in order to do Fast Fourrier Transformations on the data, a minimum sampling rate of 40 Hz is needed. The part of the frame that is filled with the measurements is called the payload. The payload contains maximum 100 bytes of data. Per 1 or 2 seconds, an API frames with their respectable payload are sent wirelessly. Each payload contains one measurement of the X, Y and Z axis. This means that the baudrate of the Waspmotes in API mode can be calculated as follows: 1-2Hz x 100 bytes = 100-200 baud = 800-1600 bps

Error rate AT mode

As stated earlier, the basic mode in which the Waspmote modules can work is the AT mode. In this mode, the xbee functions as a serial line replacement. This means that the data is not put in a frame, but the data is just sent over the air like if there would be a USB cable. This makes the communication much faster. Datasheet refers maximum transmition speed over USB at 115200 bps. This is quite fast. Assuming that the xbee in AT mode functions the same as an USB cable, it could be stated that data could be sent at this speed in AT mode. A little calculation:

- ⇨ 1 measurement = 20 bytes = 160 bits
- ⇨ Data rate of 1 kHz = 1000 measurements/ second = 160 000 bits / second

In AT mode it is possible to achieve a data rate more than 100 Hz. This is much faster than the data rate in API mode. However, the downside is that the data traffic is very chaotic. Since there are no frames, there is no possibility of identifying from which Waspmote a certain frame is sent. The data is unidentified, and if more than one Waspmote is sending at the same time, the data is mixed up because there is no indication of the beginning or the end of a certain measurement. To solve this, multiple solutions can be used:

- o Arbitrary system
- o Random delay of sending values
- o Manually program every Waspmote with ID
- o Use an array to store the measurements and print it afterwards:
  - Read out the the values of the array byte by byte with a for loop
  - Copy the array into a string and print the string

Use of array to store measurements

There are many ways to avoid collision of data packets. A random delay can be created to make the Waspmotes send at a different time. But maybe it is more useful to create a buffer where multiple measurements can be stored, for example an array. The array can be read out later and multiple measurements can be sent to the gateway in one time. In that way the sampling rate is faster. Another advantage of this technique is that the Waspmotes are not continuously sending data. There is a smaller chance that there will be collisions.

After the array is created, some kind of burst read is performed. The array is read out and written into a string. The string is then sent over the air. The string contains the identification of the Waspmote, and the measurement of the values of the X, Y and Z axis.

The principle is explained in the following code fragment:

```
      //Write ID and X, Y, Z measurement to string
      //Create suitable structure for writing to .csv file
      //String format: ID;X;Y;Z;
      z = sprintf(str,"%s",ID);
z += sprintf(str+z,"%c",semicolon);
      measurement = ACC.getX();
      z += sprintf(str+z,"%d",measurement);
z += sprintf(str+z,"%c",semicolon);
      measurement = ACC.getY();
      z += sprintf(str+z,"%d",measurement);
z += sprintf(str+z,"%c",semicolon);
      measurement = ACC.getZ();
      z += sprintf(str+z,"%d",measurement);
      z += sprintf(str+z,"%c\n",semicolon);
      //Print the string to USB
      USB.println(str);
          //Print the string + newline over the air in AT mode
      printString(str,0);
      printString("\r\n",0);
```

The main function that is used in this code fragment is the sprintf() function. This function takes a discrete string, integer or character and puts it into an array. The function requires three parameters. The first parameter is the name of the array at which the values/characters/strings will be printed to. In our case the array is called ‘str’. The second parameter is the format of the value/character/string. The format of the value/character/string we want to print into the array is defined by the sign that follows the ‘%’ sign. If a signed decimal integer value has to be printed into the array we write ‘%d’. If a character has to be printed into the array we write ‘%c’. There are multiple other formats that can be printed into the array. The third parameter is the name of the actual value/character/string that has to be printed into the array. The function has a return value. It

returns the number of bytes that are in the array. In the code fragment above the return value is stored in the variable ‘z’.

In the first line of the code, the ID of the Waspmote is printed into the array. The ID has the format ‘string’. It is printed at the first position of the array. The length of the array is returned and put into the variable ‘z’. In the next line of the code fragment, a semicolon character is written into the array at the position z+1. The new length of the array is returned and put into z. In the remaining lines of code the same principle is used. The X, Y and Z measurement are put into the array. The last character that is printed into the array is the newline character ‘\r\n’. After the array is filled, we use the normal print functions to print the array to USB or to the Xbee module.

The ID and the measurements form now one array of characters which can be printed like one packet. The output format looks like this:

C3;	38;	-105;	1006;

In the .csv file, this four parts of the array are distinguished from each other by the semicolon character. The newline character at the end of the array is an indication for excel to jump to a new line.

Final program code (First version)

The final code is based on the principle of storing the measurements in an array. The principle from 0 is applied and improved. The program is written for the AT mode of the Xbee. It has a stable frequency of 40Hz. In the program an array is created. In the array one ID and one X, Y and Z measurement are stored. The output looks like this:

C9;	37;	-104;	1005;

If a frequency of 40 Hz is applied and all five Waspmotes are used, there are no losses or errors at the gateway. All the necessary libraries are included. The constant ‘T_SAMPLE’ is defined after that. This constant is used for creating the stable 3.40Hz data output frequency.

```
#define T_SAMPLE 25
```

Next multiple variables are defined:

```
//Define variables
char *ID = "C3";
char* str;
int z;
int x_acc;int y_acc;int z_acc;
long timeShot1;long timeShot2;long timeShot3;long timeShot4;
```

In the variable ‘ID’ the ID of the particular Waspmote is stored. The ID has to be inserted manually in the program code, like in the example above. The ID consists of two characters, these two characters are the last two characters of the 16 bytes MAC address of the particular Waspmote. The next variable is the ‘str’ variable. ‘str ‘ is the array where the ID, and one X, Y and Z measurement are going to be stored. Later on the ‘str’ array is going to be printed to the output. In the ‘z’ variable the total length of the created string ‘str’ is stored. The integer variables ‘x_acc’, ‘y_acc’, ‘z_acc’ are used to store the X, Y and Z measurement of that particular moment. After that some timeshot variables are defined. With this timeshot variables some time intervals or delays can be measured. All this variables are defined globally. This means that they can be used in every part of the program, in the setup loop and in the main loop.The setup loop is written as below:

```
void setup(){
    USB.ON();
    //Set up the Xbee module to send in AT mode
    beginSerial(115200,0);
    Utils.setMuxSocket0();
    // Set up ACC
    ACC.ON();
    // Define the sampling rate of the accelerometer
    ACC.setSamplingRate(1000);
    // Set up Xbee module
    xbee802.ON();
    delay(1000);
    xbee802.flush(); }
```

First the USB.ON() function is used to initialise the USB functions. After that the Xbee socket 0 is activated to send serial data to the Xbee module. Next the accelerometer is initialised and the sampling rate of the accelerometer is set to 1000Hz. The last step is the initialisation of the Xbee module.

```
void loop(){
  ACC.ON();
  ACC.setIWU();
  //enter sleep mode and wait for interrupt
  PWR.sleep(ALL_OFF);
  if( intFlag & ACC_INT )
    {
    //clear the accelerometer interrupt flag on the general interrupt vector
    intFlag &= ~(ACC_INT);
    ACC.unsetIWU();
    xbee802.ON();
    for(int i=0;i < 1200; i++){
      timeShot1 = millis();
      str = (char*) calloc(50, sizeof(char));
      //Write ID and X, Y, Z measurement to array
      //Create suitable structure for writing to .csv file
      //String format: ID;X;Y;Z;
      x_acc = ACC.getX();      y_acc = ACC.getY();       z_acc = ACC.getZ();
      timeShot4 = millis();
z = sprintf(str,"%s;%d;%d;%d;",ID,x_acc,y_acc,z_acc);
      timeShot2 = millis();
      //Print the string to USB
      USB.println(str);
            //Print the string + newline over the air in AT mode
      printString(str,0);       printString("\r\n",0);
      free(str);       str = NULL;
      while((millis()-timeShot1)<T_SAMPLE);       timeShot3 = millis();
      }
    } }
```

The void loop starts with the enabling of the accelerometer. After that, the interrupt wake-up is set and the Waspmote goes to low power mode. If an interrupt is generated, the if-loop gets active. The interrupt wake-up flag is cleared and the Xbee module is put on. The for loop repeats itself 1200 times. In the for loop the actual measurements are done. The function 'millis()' measures the time in milliseconds since the program started. If the function 'millis()' is executed, the time in milliseconds is put in the 'timeShot1' variable. If we take another timeshot at the end of the loop, we can measure the total delay in the loop by taking the difference of the two timeshot variables.

After the 'timeShot1' variable the 'calloc' function is used to allocate and initialize the array 'str'. Next the actual measurements are done by using the ACC.getX(), ACC.getY() and ACC.getZ() functions. These functions return one measurement of the X, Y and Z axis. These measurements are then put in the variables 'x_acc', 'y_acc' and 'z_acc'. After that another timeshot is taken. Next the 'sprintf' function is used to put the ID and the measurements together in the 'str' array. The total length is returned by the 'sprintf' function and stored in the 'z'-variable. Another timeshot is taken. Then the 'str' array is printed to the USB port and the Xbee module with the functions 'USB.println()' and 'printString()'. The array is then cleared. The last step is creating a stable data rate. The while-loop at the end of the code is created for that purpose. The function 'millis()' checks the time at the end of the for-loop, and subtracts from it the time at the beginning of the for-loop. This time was stored in the 'timeShot1' variable. After this time is subtracted, it is compared to 'T_SAMPLE'. 'T_SAMPLE' was defined at the beginning of the code, it is a constant with the value '100'. In other words, if the time difference (in milliseconds) between the beginning and the end of the for-loop is smaller than 100ms, the while-loop repeats itself. When the time between the beginning and the end of the for-loop equals 100ms, the while-loop is exited. In that way the time to go through the for-loop is always 100ms. If one measurement is sent to the gateway every 100ms, we get a stable data rate of 10Hz.

Final program code (Second version)

After further testing of the program described above there are some limitations. Data are sent at a stable frequency of 40Hz, after an interrupt has been generated. The problem however is that in order to activate the interrupt pin of the system, a threshold value has to be exceeded. The default threshold value is quite insensitive. In this state, the interrupt is only generated if a value higher than 256 mg is generated only on the Z axis. This is not practical and the system is not able to measure low vibrations in that way. The default threshold value can be adjusted in the WaspACC library:

```
/*
 * setIWU (void) - sets the Inertial Wake-UP interrupt
 */
uint8_t WaspACC::setIWU(void)
{
        // clear the FF interrupt if active
        unsetIWU();
        // configure the different registers to
        // handle acceleration detection on the X, Y, or Z axis
        writeRegister(CTRL_REG3,0x00);
        writeRegister(INT1_THS,0x01);
        writeRegister(INT1_DURATION,0x00);
        writeRegister(INT1_CFG,0xAA);
        // attach the hardware interrupt to the pin
        enableInterrupts(ACC_INT);
        return flag;
}
```

In this library, the implementation of the function of the function 'setIWU' can be found. By default the register value 'INT1_THS' is set to 0x10. This value is the hexadecimal value for the decimal value 256 (mg). In the example above, the value is set to 0x01 (=16mg).The 'INT1_CFG' is a configuration value. A specific value indicates the conditions at which the interrupt pin has to be made high. For example, in the situation depicted above, the hexadecimal value 0xAA indicates that the interrupt pin has to be made high if the measured value at the X axis OR the Y axis OR the Z axis exceeds the 'INT1_THS' value. More information on this topic can be found in the accelerometer datasheet.

After these adjustments in the library were made, the system was tested again. The threshold was set to the most sensitive value, 16mg. An interrupt was generated if one of the axis measured a value that exceeded 16mg. This system worked better than the previous system, but the adjustments were insufficient. The little vibrations were still not measured. Besides the sensitivity problem of the interrupt, there was an extra problem. The interrupt function delayed the program a lot. Measurements presented how much time every instruction require. The interrupt function needed relatively lot of time.

After that it was concluded that it was better to leave the interrupt out of the program code, since it was not sensitive enough and it delayed the program too much. The program then ran in continuous mode. This was also not good because a huge amount of data was created in that way, and it was not clear when important events occurred. Another solution had to be found.

Solution for the problems described before:

```
void loop(){
  x_acc = ACC.getX();   y_acc = ACC.getY();   z_acc = ACC.getZ();
  if((x_acc < -8 || x_acc > 8) || (y_acc < -8 || y_acc > 8) ||
```

```
          (z_acc < 988 || z_acc > 1028))
   {      for(int i=0;i < 1200; i++){
     timeShot1 = millis();      str = (char*) calloc(50, sizeof(char));
     //Write ID and X, Y, Z measurement to array
     //Create suitable structure for writing to .csv file
     //String format: ID;X;Y;Z;          x_acc = ACC.getX();          y_acc = ACC.getY();          z_acc =
ACC.getZ();
           sprintf(str,"%s;%d;%d;%d;%lu;%lu",ID,x_acc,y_acc,z_acc,timeShot1,timeShot2);
     //Print the string to USB
     USB.println(str);
     //Print the string + newline over the air in AT mode
     printString(str,0);  printString("\r\n",0);   free(str);   str = NULL;   timeShot2 = millis();
     while((millis()-timeShot1)<T_SAMPLE);
     }   }
    //wait rest of time to fit sample rate}
```

Only the main loop of the code is displayed above, since the setup loop stays unchanged from the setup loop from the code in before. In the new code, the interrupt code is left out to save time. First, a measurement of the X, Y and Z axis is done. These measurements are stored in the variables ‘x_acc’, ‘y_acc’ and ‘z_acc’. After that an if-loop is inserted to replace the interrupt function. This if-loop tests the first measurements and checks if these measurements exceed the numbers described in the if-loop. In this example the if-loop is entered if the X value exceeds +8mg or -8mg OR if the Y value exceeds +8mg or -8mg OR if the Z axis exceeds 988mg or 1028mg. In the if-loop all the instructions for printing the data to the Xbee module are implemented. A for-loop is started. In the for-loop a new measurement is done and put in the string array as described above. The array is then printed to USB and to the Xbee module. In the while-loop is used to keep the steady frequency of 40Hz. After 1200 arrays are printed, the for-loop is exited. If the if-condition occurs again, the whole process is executed another one time.

Appendix C: Frequency Change Method Analysis

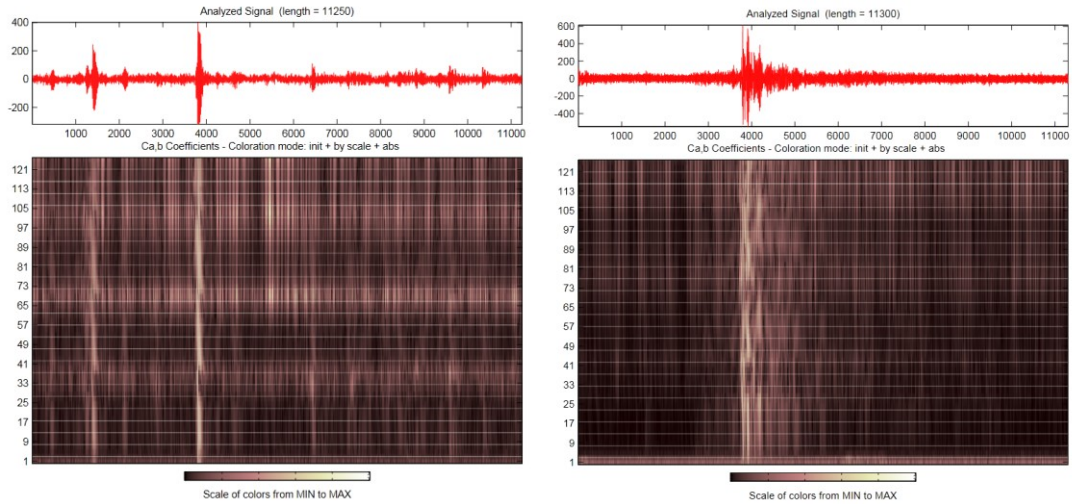

Figure C.1. 2012/11/23 02:08 UMT seismic event (left) and 2012/12/05 06:54 UMT seismic event (right), recorded at 3rd floor old building (3OB) accelerometer, North-South component (NS) A392 accelerometer, analyzed with Wavelet Transform, WV family db (level 2)

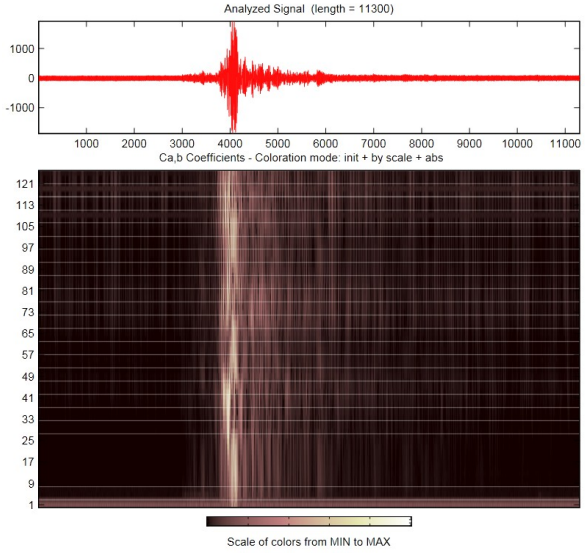

Figure C.2. 2013/01/05 02:04 UMT seismic event, recorded at 3rd floor old building (3OB) accelerometer, North-South component (NS) A392 accelerometer, analyzed with Wavelet Transform, WV family db (level 2)

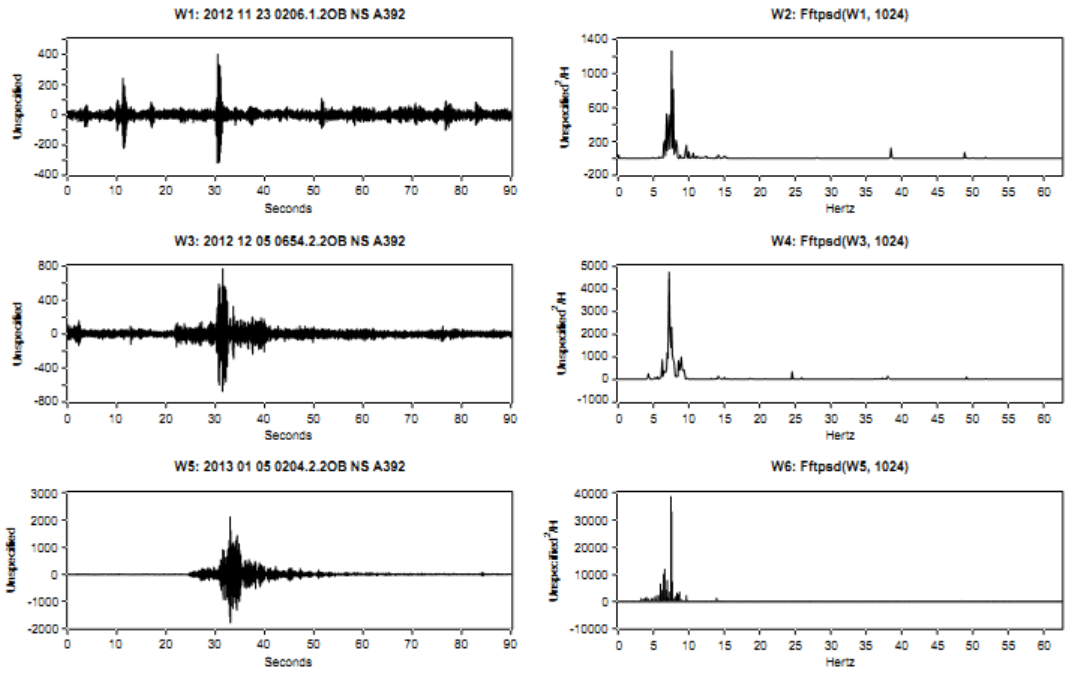

Figure C.3. FFT based PSD for the previous events (Figures 9. & Figure9.2)

The fundamental frequency of the old building can be revealed from figures C.1, C.2 & C.3 the accelerometer recordings have very clear spectrum and the fundamental frequency is fluctuating from 7.25Hz to 7.55Hz with a mean value (from a number of recordings) at 7.48Hz. Thus there is a frequency dispersion of 0.3Hz in fundamental frequency. Consequently, **Π**-index of the old building is calculated:

$$\mathbf{\Pi} \quad = 1 - \frac{f_{max} - f_{min}}{f_{mean}} = 1 - \frac{7.55 - 7.25}{7.48} = 1 - 0.04 = \ 0.96 \quad (9.1)$$

This value is lower than the value from the new building. It is expected because the old building it is anticipated to have lower structural stiffness and higher fundamental frequency deviation. It is also studied the resonance frequencies which appear in the vertical and in the East-West components for both buildings in the upper seismic events.

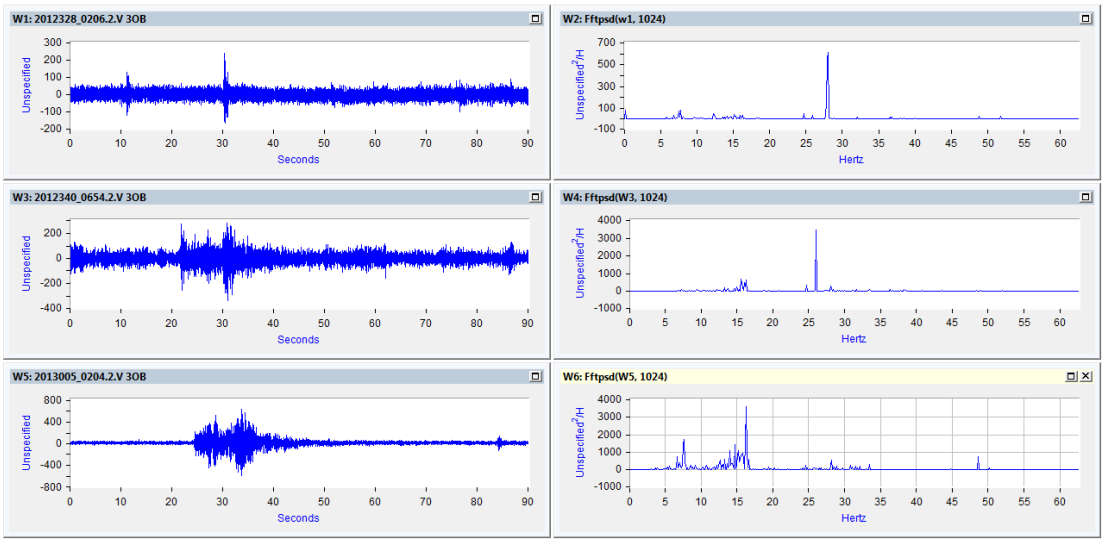

Figure C.4. FFT based PSDs for the previous events (up 2012/11/23 02:08 UMT, middle 2012/12/05 06:54 UMT and lower 2013/01/05 02:04 UMT) for the old building (Vertical component)

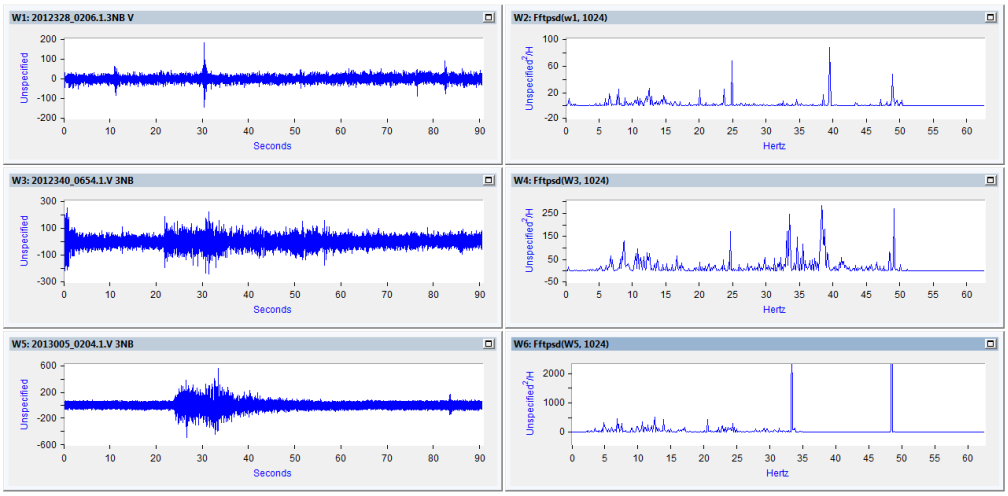

Figure C.5. FFT based PSDs for the previous events (up 2012/11/23 02:08 UMT, middle 2012/12/05 06:54 UMT and lower 2013/01/05 02:04 UMT) for the new building (Vertical component)

The seismic acceleration of the earthquake events, affect very low in the vertical components (for both buildings), although the same earthquakes have much higher magnitude in the two horizontal components. This results the resonance frequency of the structure to be unable to reveal. The peaks that present in the FFT spectrums are noises.

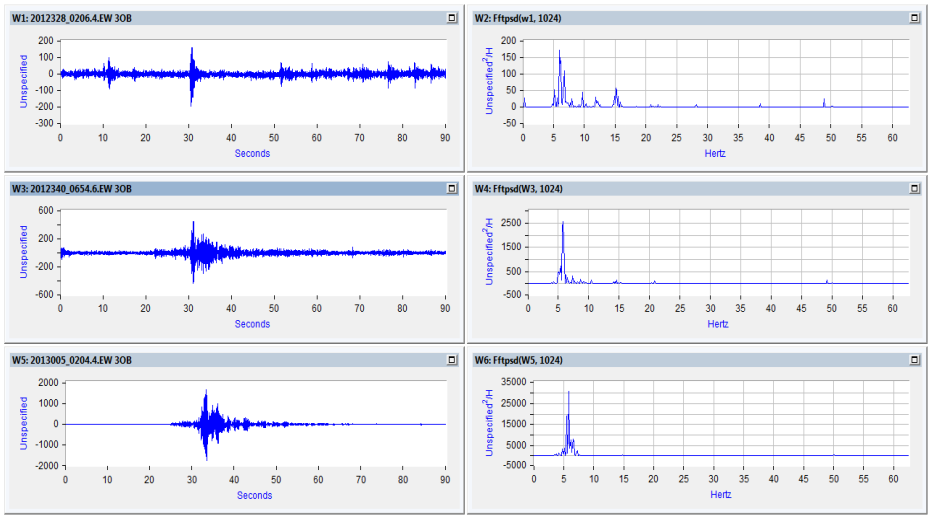

Figure C.6. FFT based PSDs for the previous events (up 2012/11/23 02:08 UMT, middle 2012/12/05 06:54 UMT and lower 2013/01/05 02:04 UMT) for the old building (East-West component)

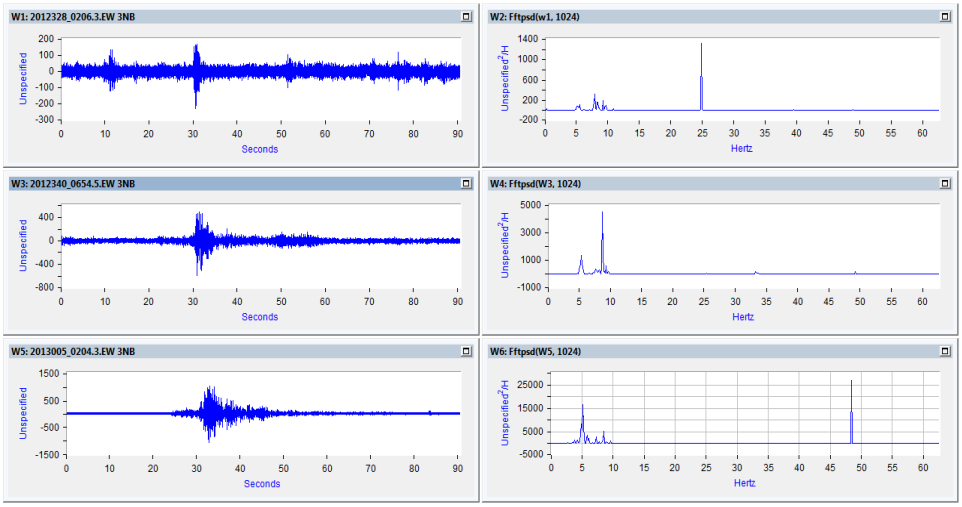

Figure C.7. FFT based PSDs for the previous events (up 2012/11/23 02:08 UMT, middle 2012/12/05 06:54 UMT and lower 2013/01/05 02:04 UMT) for the new building (East-West component)

Short Time Fourier Transform (STFT) is applied in recordings, in order to define and reveal the frequencies that appear for each earthquake with STFT and distinguish the differences from the Wavelet transform applied above. Figures C.8 and C.9 present spectrograms of East-West component at the 3rd floor of the old building and new building for the above seismic events dates.

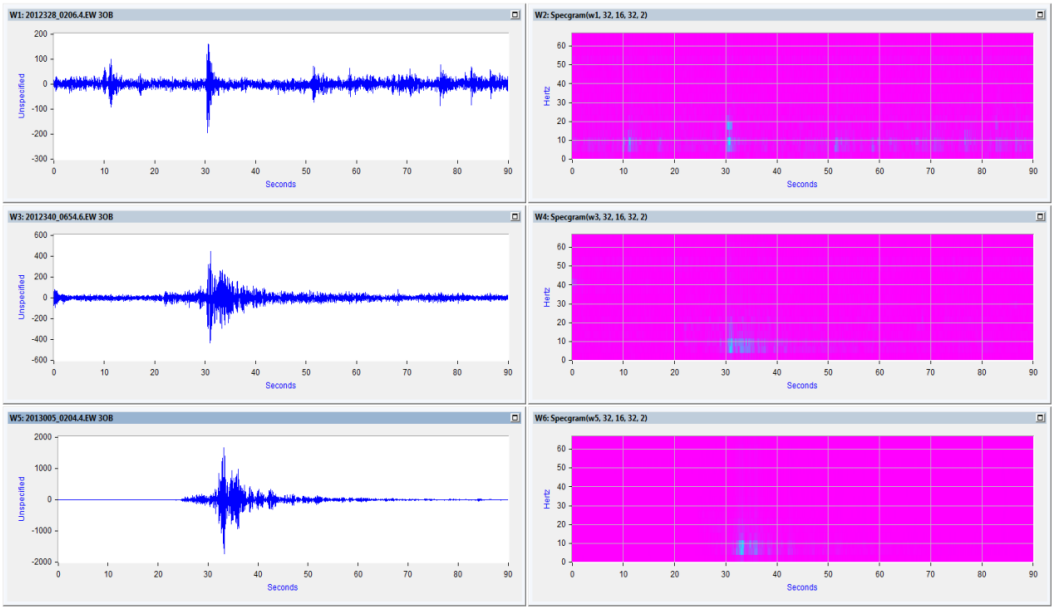

Figure C.8. Spectrogram for the previous events (up 2012/11/23 02:08 UMT, middle 2012/12/05 06:54 UMT and lower 2013/01/05 02:04 UMT) for the old building (East-West component)

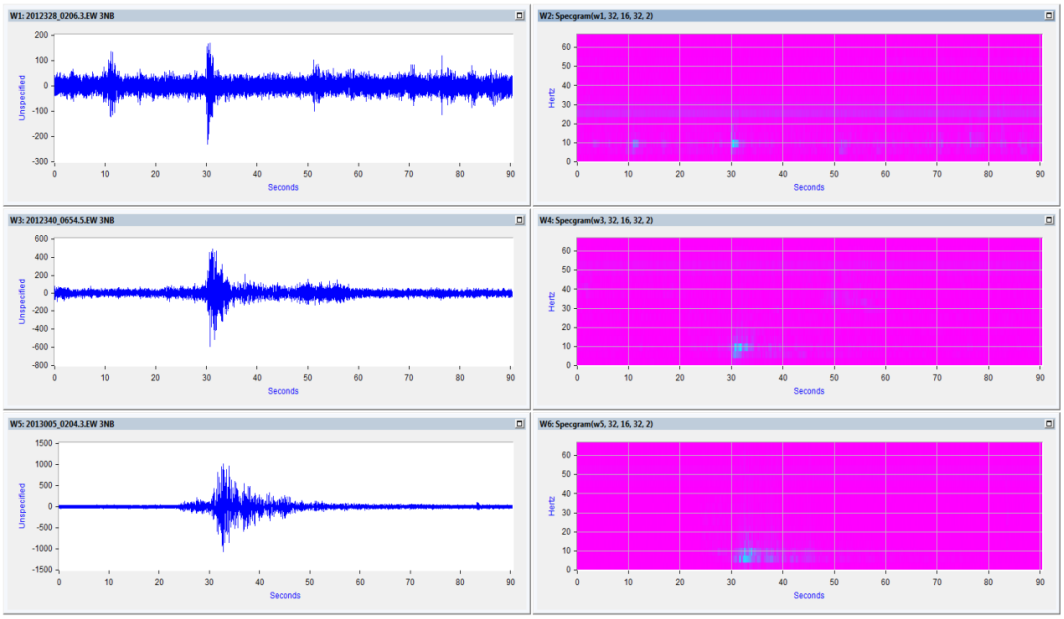

Figure C.9. Spectrogram for the previous events (up 2012/11/23 02:08 UMT, middle 2012/12/05 06:54 UMT and lower 2013/01/05 02:04 UMT) for the new building (East-West component)

STFT presents the frequency spectrum of each recording at the specific time that occurs, but the maximum resolution is limited by the length of the specific window that is used for STFT.

By wavelet transform there is the ability to reveal the coefficients of the specific wavelet that is used (in this study db2) in many scales (from the maximum frequency (125/2 Hz) until the minimum desired frequency) and study what signals are contained in experiment recordings, and when they occur, in great detail. In the figures C.1 & C.2 where data analysis is by wavelet transform, it is not revealed the Fourier transform of the signal (like STFT), but the coefficients that are produced by the wavelet transform of the signal with the specific wavelet. The analysis of both methods (wavelet and STFT) reveal that there is higher detail with the wavelet method, such the disturbances of the signals and the discontinuities are much more obvious with WT and also the resonance frequencies and the time that every frequency occurs, can be revealed with higher accuracy. From the above measurements (Figure C.6 & C.7) it is observed that at the east-west component the resonance frequency for the new building is:

$$\mathbf{\Pi} \quad = 1 - \frac{\mathrm{f_{max} - f_{min}}}{\mathrm{f_{mean}}} = 1 - \frac{5.25 - 5.20}{5.225} = 1 - 0.0095 = \ 0.9904 \qquad (9.2)$$

And also for the old building the resonance frequency for the old building is:

$$\mathbf{\Pi} \quad = 1 - \frac{\mathrm{f_{max} - f_{min}}}{\mathrm{f_{mean}}} = 1 - \frac{5.85 - 5.55}{5.76} = 1 - 0.052 = \ 0.948 \qquad (9.3)$$

The range of the **Π** index, in the east-west component, is very close to the range of the North-South component for the old and the new building respectively. This indicates that the frequency dispersion of the fundamental frequency is almost the same for the two horizontals components in both buildings.

Appendix D: HVSR Analysis

Figure D.1 presents broad region map of these four seismic events with code names 1(up left), 2(up right), 3(down left) and 4(down right).

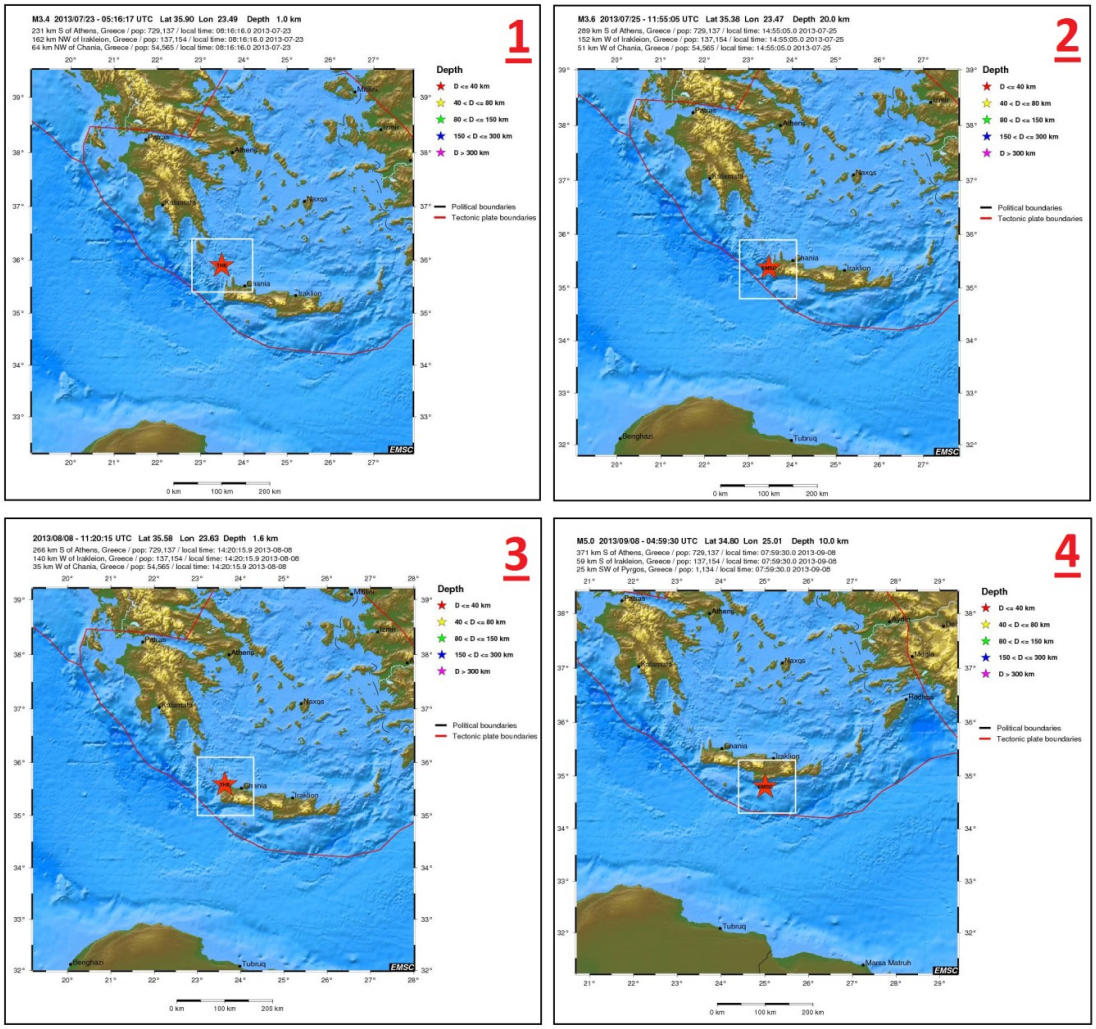

Figure D.1. Four seismic events with code names 1(up left), 2(up right), 3(down left) and 4(down right) [201]

Below figure D.2 presents the computation of HVSR for seismic event with code names 1(up left), 2(up right) of figure D.1. On figure D.2 HVSR plot graph with label A3OB is the recording of old building 3rd floor, HVSR plot graph with label B2OB is the recording of old building 2nd floor, HVSR plot graph with label C1OB is the recording of old building 1rst floor, HVSR plot graph with label D0OB is the recording of old building ground floor, HVSR plot graph with label ELOB is the recording of old building lower floor, HVSR plot graph with label F3OB is the recording of new building 3rd floor, HVSR plot graph with label G2OB is the

recording of new building 2nd floor, and HVSR plot graph with label HLOB is the recording of new building lower floor.

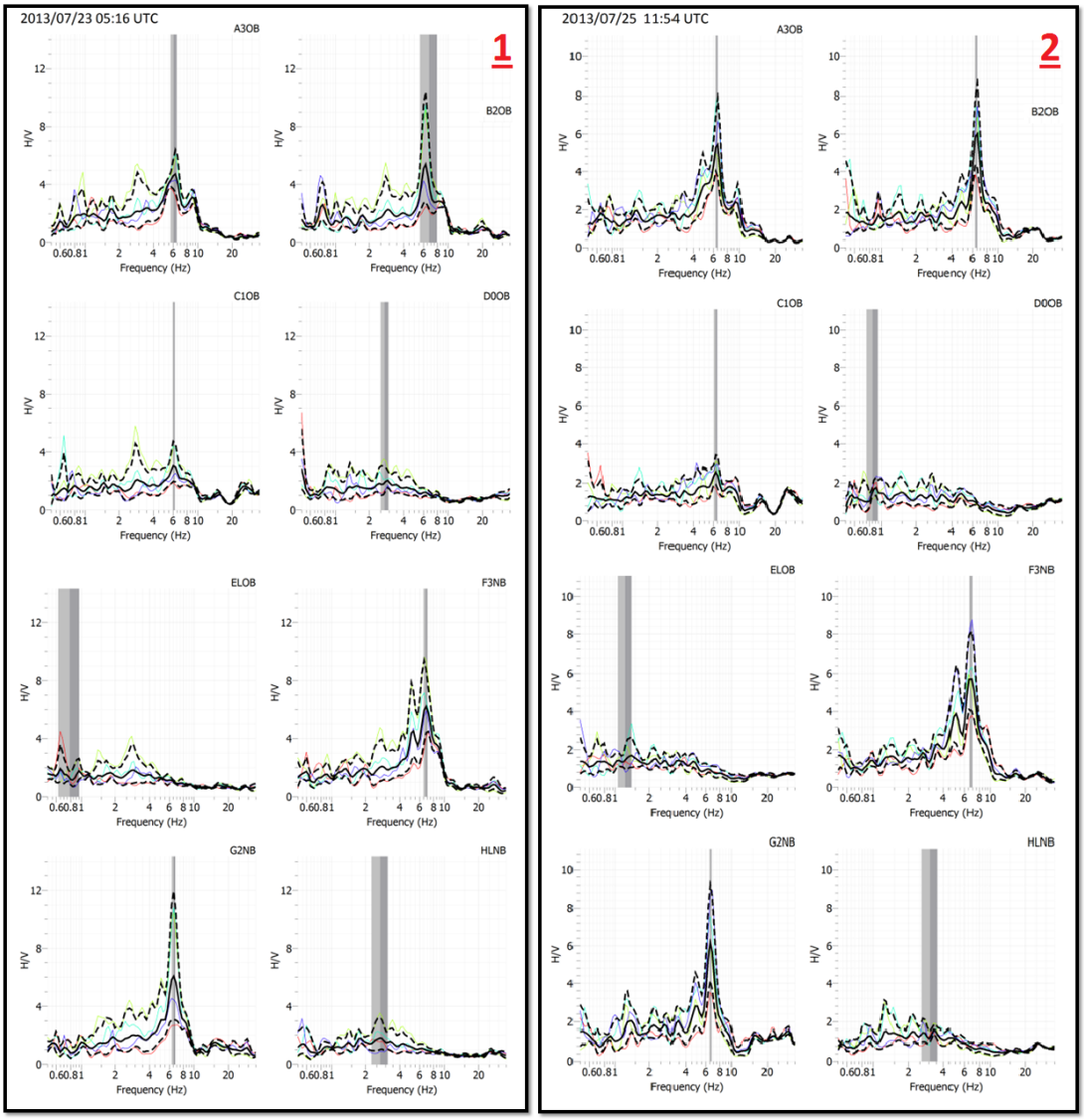

Figure D.2. HVSR analysis of seismic events with code names 1(left) and 2(right).

On figure D.3 are presented the computations of HVSR for seismic events with code names 3(down left), 4(down right) of figure D.1.

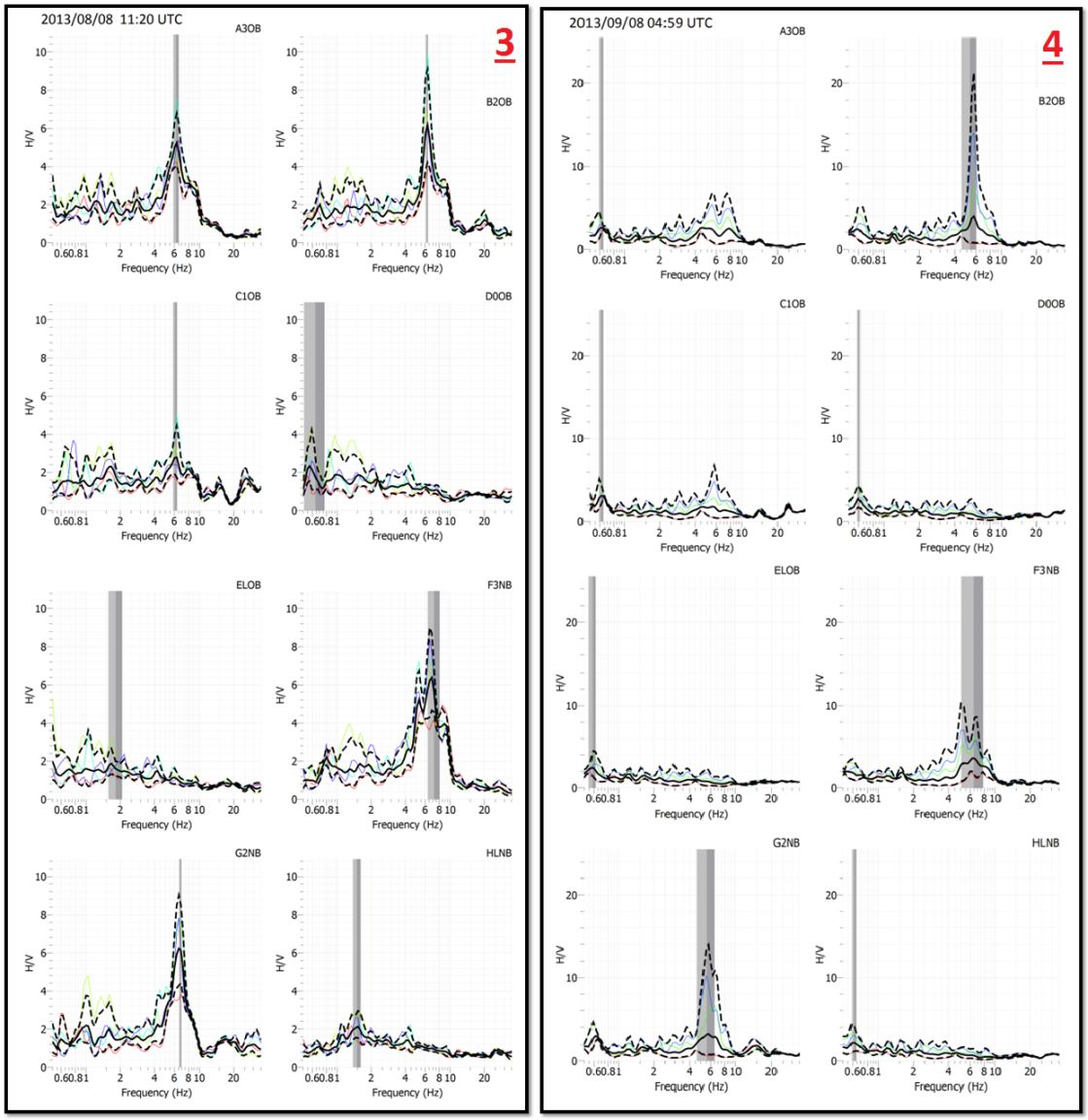

Figure D.3. HVSR analysis of seismic events with code names 3(left) and 4(right).

One hour time duration HVSR recordings of ambient noise during noon and midnight

It is going to present an HVSR recording of 30 minutes duration at noon (13:00 local time) in order to study the HVSR rise from floor to floor. Figure D.4 and D.5, present the HVSR recordings at noon and at night, on the old building of TEI with the presentation of, 25 seconds time duration windows, which are extended in the whole length of the recording.

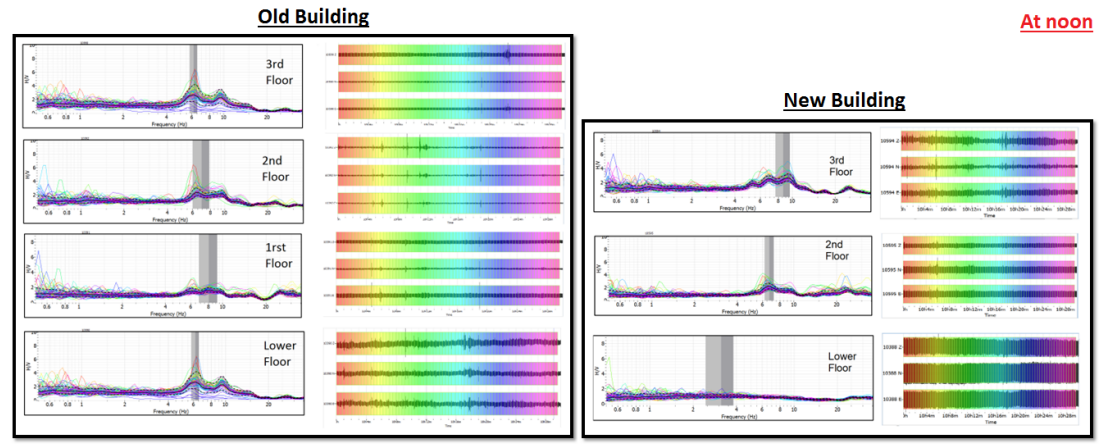

Figure D.4. Programmed 30 minutes HVSR recordings on 2013/05/08 10:00 UMT (2013/05/08 13:00 local time) on the old building of TEI. On the right is the presentation of 25 seconds time duration windows which are extended in the whole length of the recording.

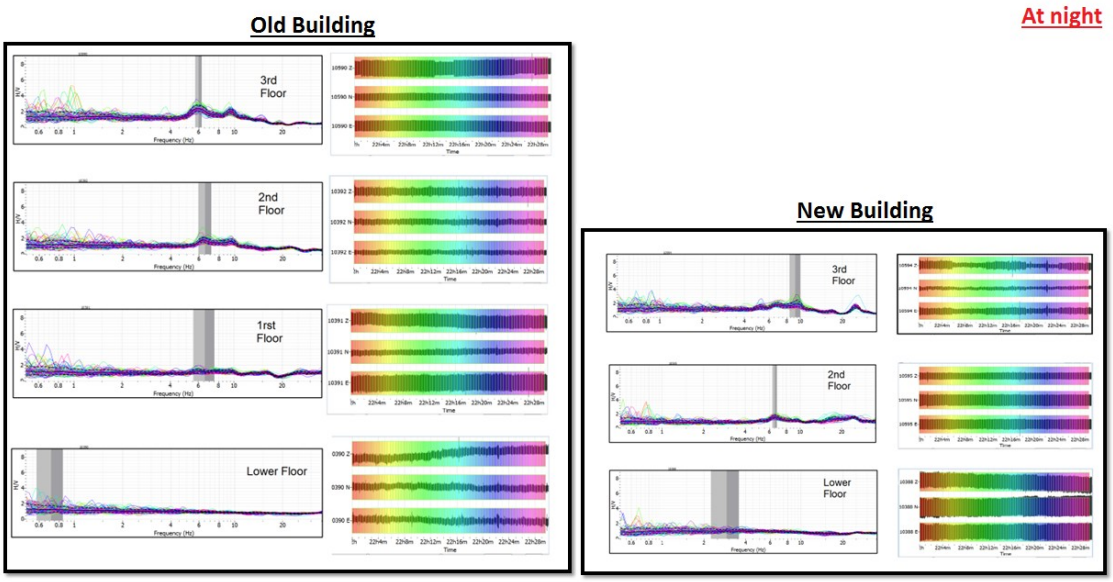

Figure D.5. Programmed 30 minutes HVSR recordings on 2013/05/07 22:00 UMT (2013/05/08 01:00 local time) on the old (left) and new (right) building of TEI. On the right is the presentation of 25 seconds time duration windows which are extended in the whole length of the recording.

On figure D.6, is presented the HVSR analysis of ambient noise, five months later for the old and the new building of TEI at Chania. The label of the HVSR plot graphs, is referred to the same floor and building, as with the figures D.2 and D.3.

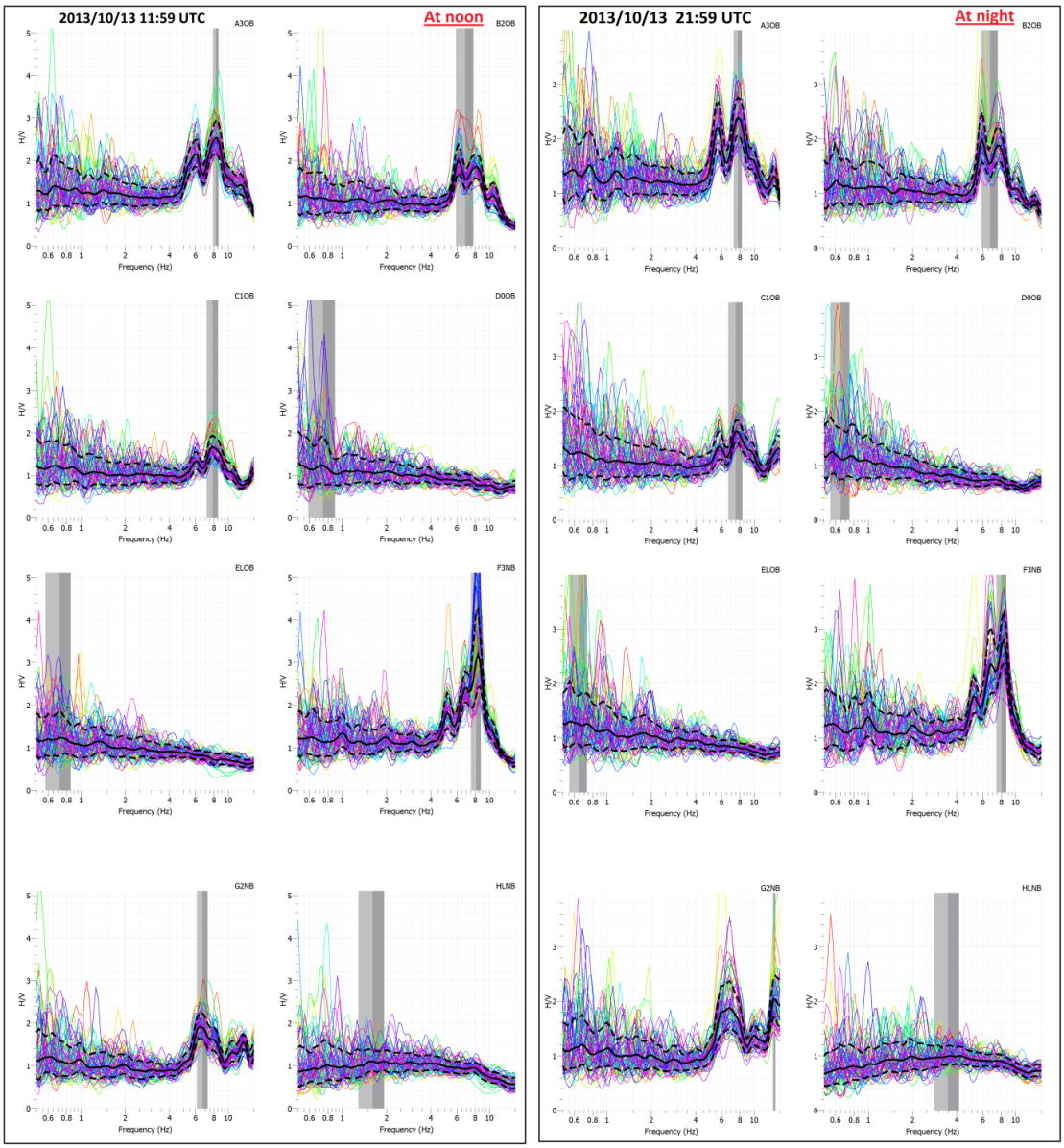

Figure D.6. HVSR analysis of ambient noise recording with time duration of 1 hour

Measurements with Lennartz seismometer.

In this section it is going to analyze HVSR measurements that were recorded in old and new building of TEI Chania and also in a public building located in the city of Chania "Technical chamber of Greece" (TEE). Below figure D.7 presents HVSR recordings for lower ground, first and second floor of the old building TEI. Length of time duration recording is on 10 minutes. The same time duration of acceleration recording is on figure 9.16 which presents HVSR recordings for outside and inside the building of TEI.

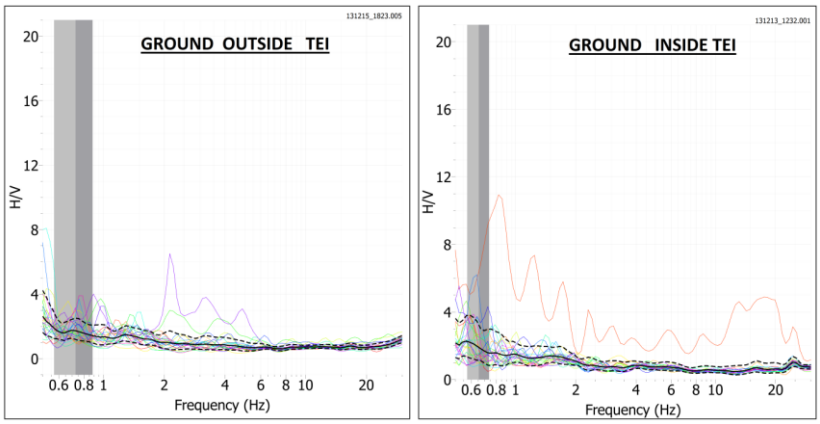

Figure D.7. HVSR plots of outside area (left figure) and inside building of TEI on the lower floor (right figure)

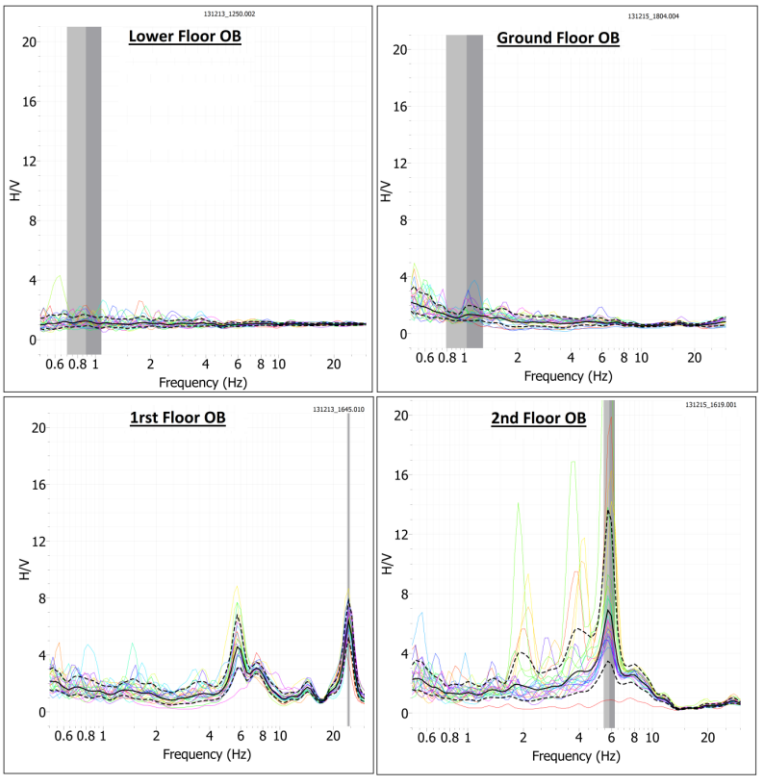

Figure D.8. HVSR plots of acceleration recordings for lower floor old building (up left figure), ground floor old building (up right figure), 1rst floor old building (down left figure) and 2nd floor old building (down right figure).

On figure D.8 is presented HVSR recordings for lower, ground and first floor of the new building TEI. Length of time duration recording is on 10 minutes. Figure 9.19 presents HVSR recordings for second and third floor of the new building TEI.

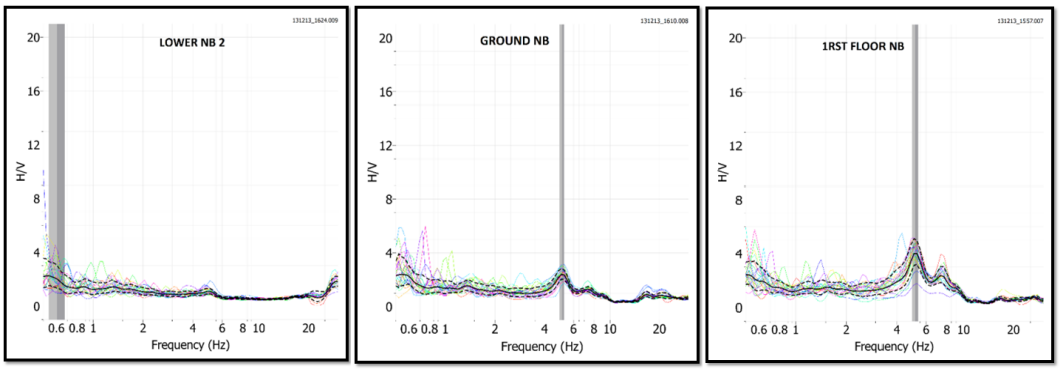

Figure D.9. HVSR plots of acceleration recordings for lower floor new building (left figure), ground floor new building (mid figure) and 1rst floor old building (right figure)

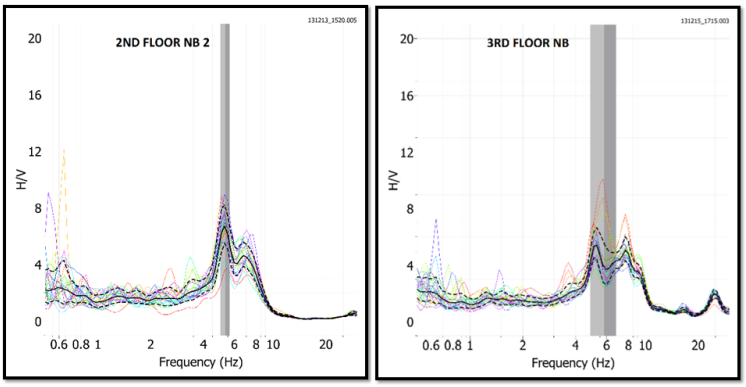

Figure D.10. HVSR plots of acceleration recordings for second floor new building (left figure), and third floor new building (right figure)

On this part of the study will be presented the HVSR from acceleration recordings of the TEE buidling located in the city of Chania. Figure D.11 presents the HVSR plots for the lower ,ground and first floor of the case study building.

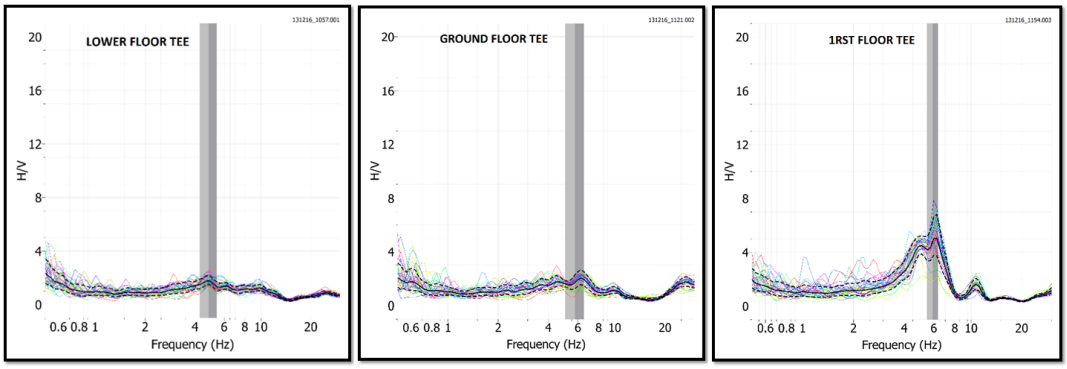

Figure D.11. HVSR plots of acceleration recordings for lower floor of TEE building (left figure), ground floor of TEE building (mid figure) and 1rst of TEE building (right figure)

Laboratory validation

The proposed approach is verified by results of laboratory model. On a metalic model (dexion) of dimansions 2 meter (height) 1,2m (length) 50cm (width) with four racks-levels have been placed four accelerometers reftek SMA 130, one on each level. The metallic columns of model is connected with the racks through screws. Two damage scenarios are applied in the specific case study. Initially there is no damage at all. All screws are absolute screwed. HVSR recordings of one hour time duration are applied in every level during day and night. The same HVSR recordings of one hour are applied also for the second scenario (damaged scenario). In this case study artificial damage has been introduced in the model through the relax of specific screws in the right corner of the third rack. The results of the data analysis reveal that HVSR rises as the damaged introduced to the system (as stiffness of model is reduced). This is also correlated with higher structural vulnerability of the model. The accelerometer sensors have specific maze which is added on the total maze of the rack-based model. Also they are stable related the metallic model. On figure D.12 is presented the photo of metallic dexion. Figures D.13 and D.14 present the HVSR analysis of ambient noise acceleration recording of the metallic model, for the undamaged scenario. Figures D.15 and D.16 present the increase of the maximum amplitude of the HVSR value, for the damaged scenario. Also on figures D.13, D.14, D.15 and D.16 the HVSR plot graphs with label “1_LEV” is the recording of 1rst (lower) rack of the metallic model, and respectively label “2_LEV” is the recording of the second rack, “3_LEV” the recording of the third rack and “4_LEV” the recording of the fourth (highest) rack.

Figure D.12. Metallic dexion model

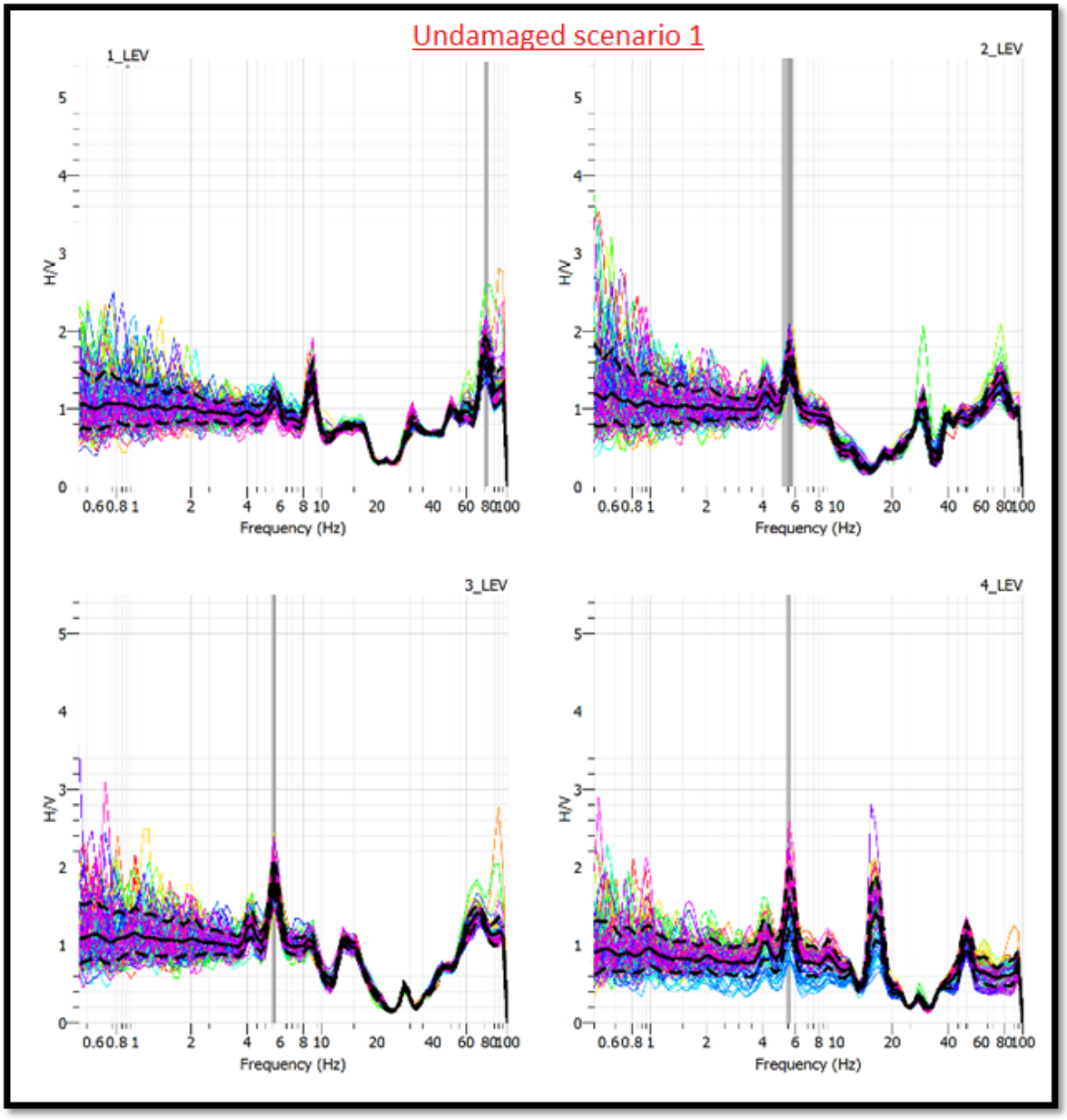

Figure D.13. HVSR analysis of ambient noise recording, for undamaged scenario 1 of the metallic model

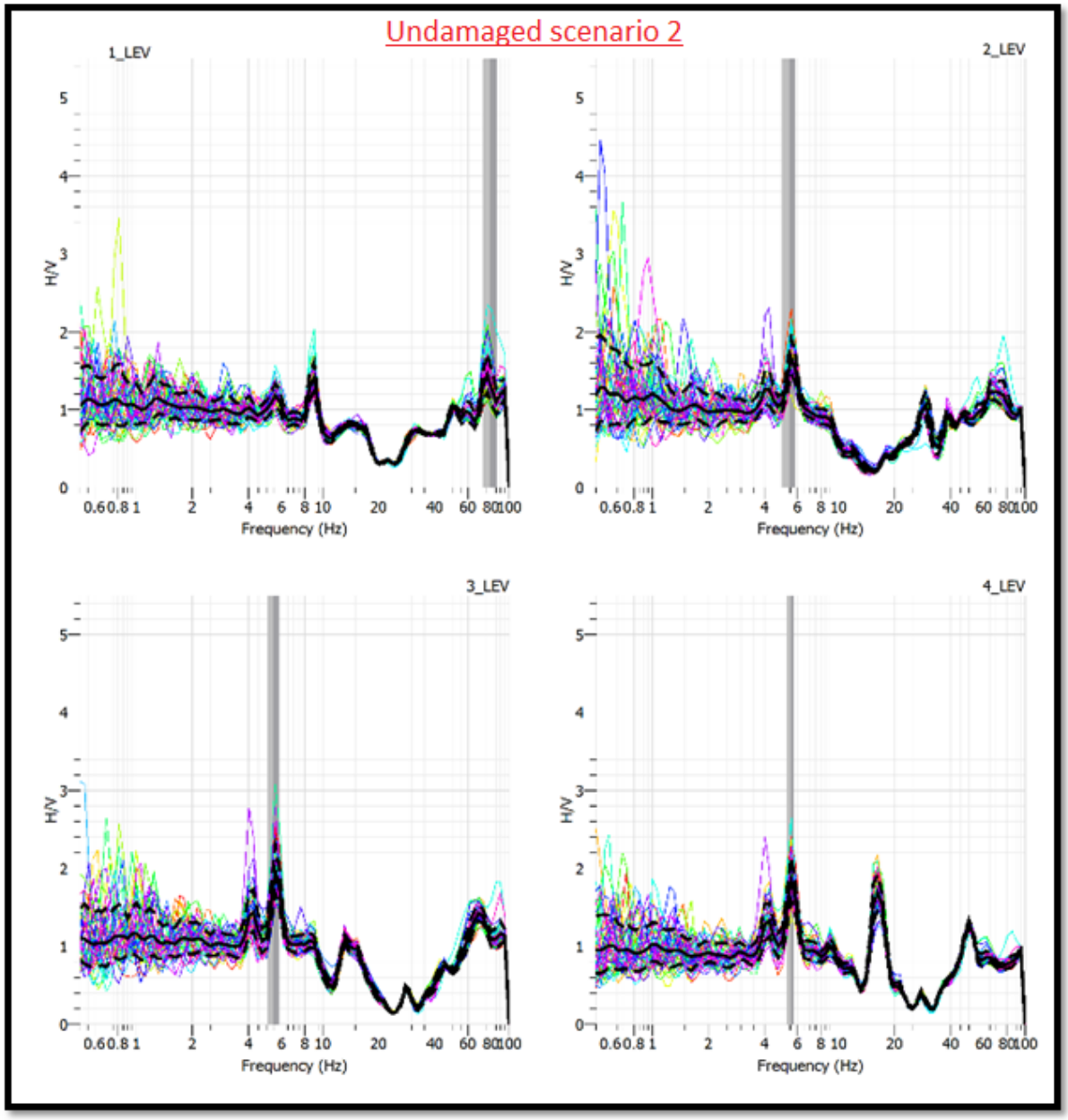

Figure D.14. HVSR analysis of ambient noise recording, for undamaged scenario 2 of the metallic model

Resonance frequencies (at 6 and 8 Hz) are almost stable and very close to the value of 2 for all levels. The HVSR rise is very low. The range of the values is from 1,5 until 2,5.

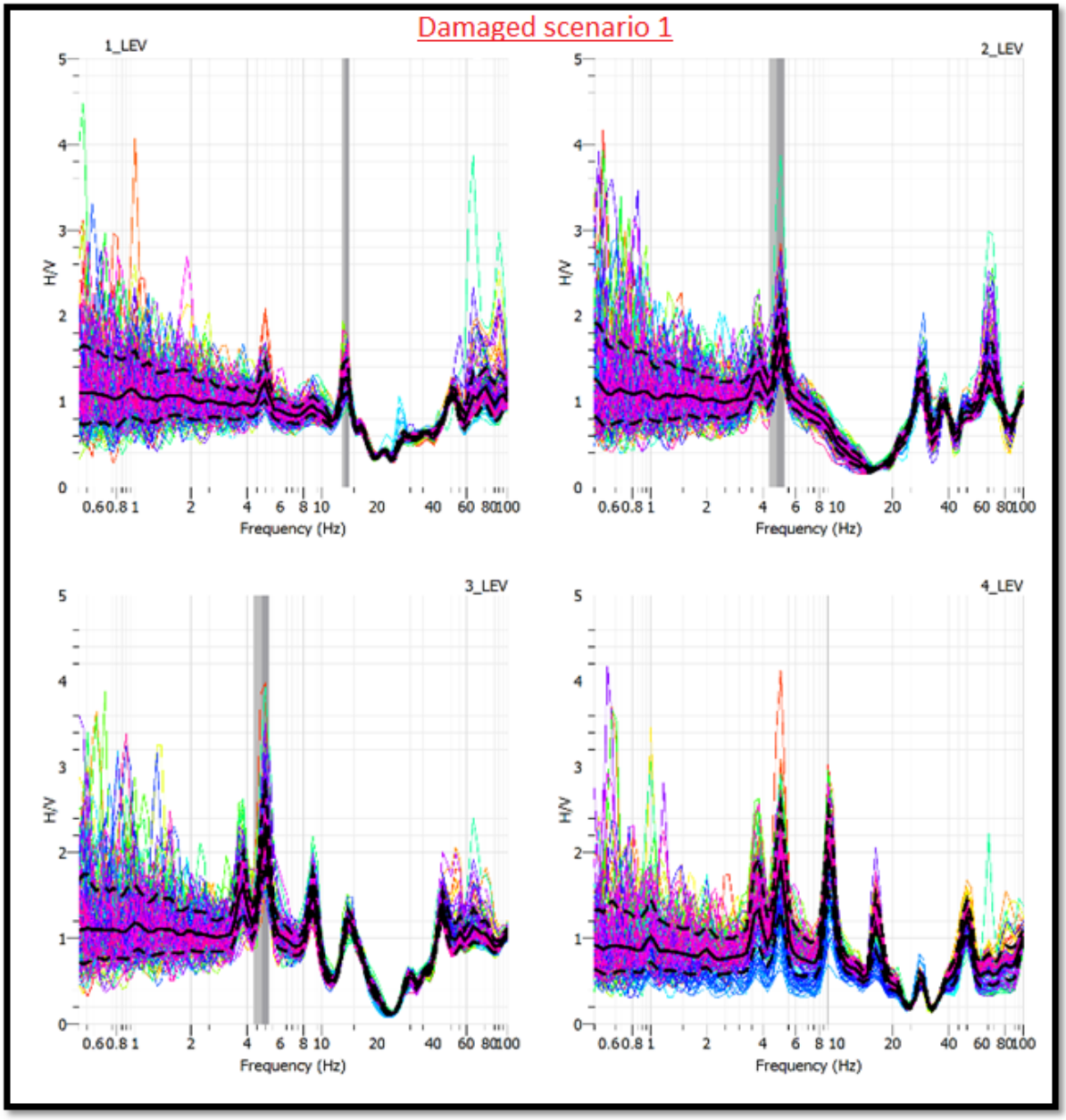

Figure D.15. HVSR analysis of ambient noise recording for damaged scenario 1 of the metallic model

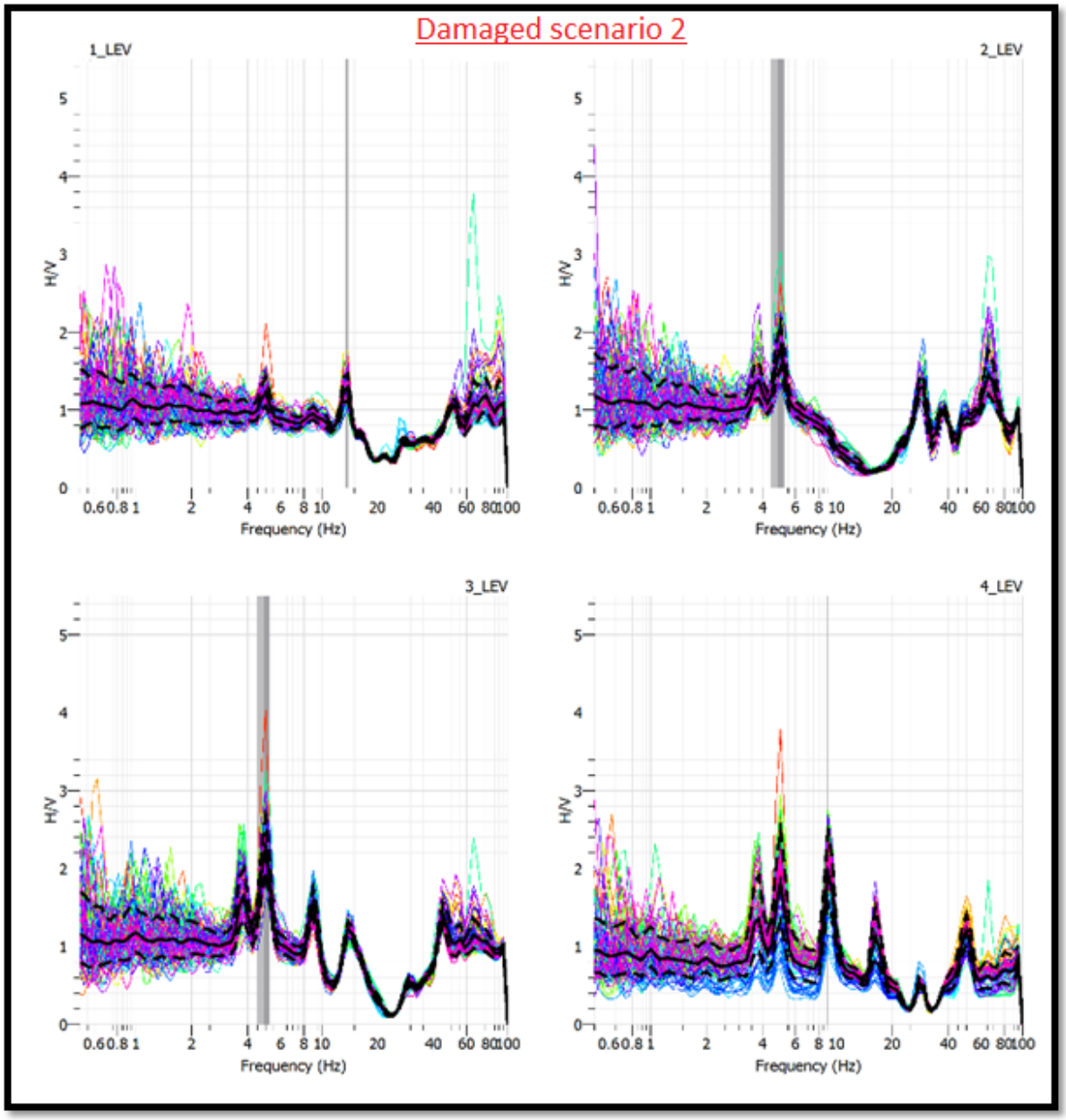

Figure D.16. HVSR analysis of ambient noise recording for damaged scenario 2 of the metallic model

Resonance frequencies have an HVSR range from 1.8 up to 3.5. Also there is frequency shift at all resonanse frequencies in damaged scenario related the undamaged scenario. At damaged scenarios, ambient noise creates HVSR rate much higher than in undamage scenario. Also the increase of the HVSR index fron level to level is higher in damage case than the undamaged.

Appendix E: PSD, FRF, Coherence Analysis

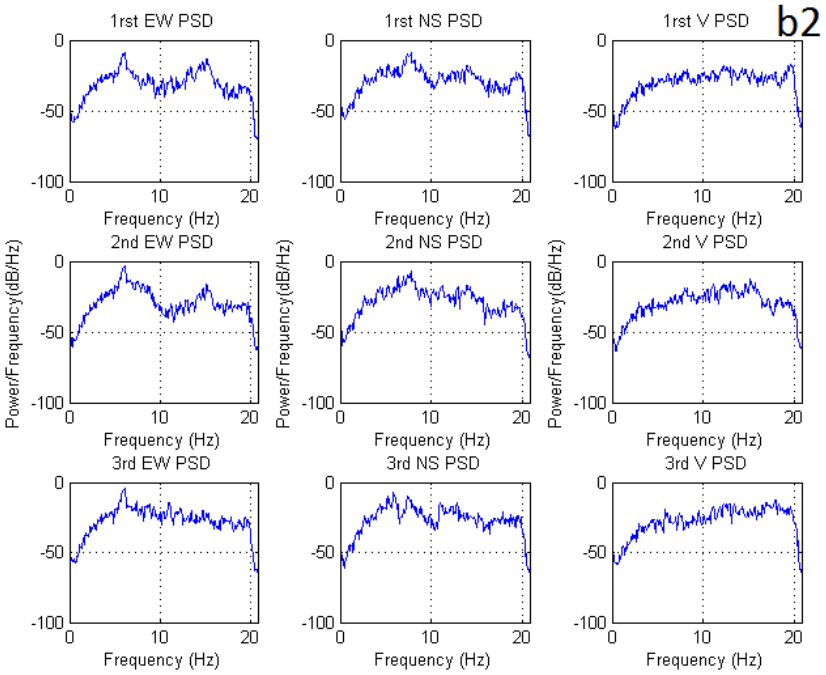

Figure E.1. PSDs of seismic event is with name code b2 from table 3.3 (31/03/2013 4.3M 62km)

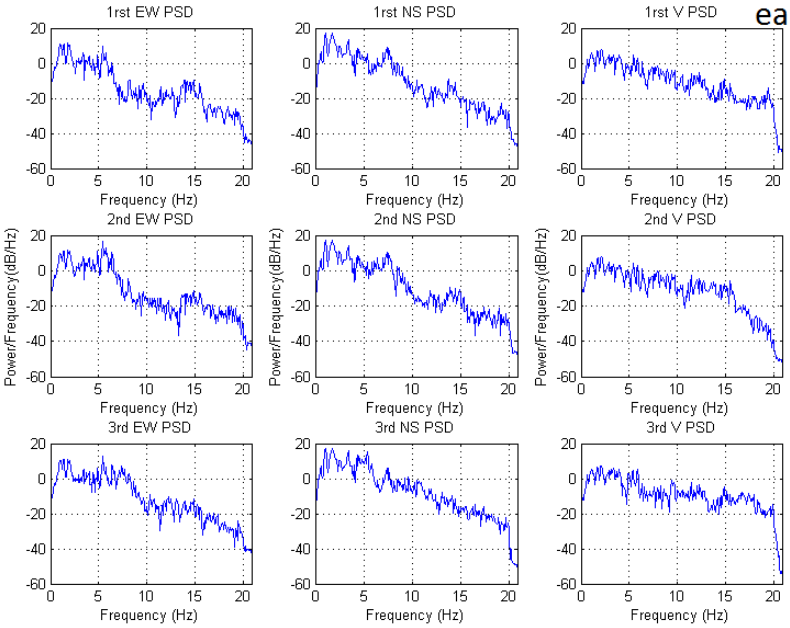

Figure E.2. PSDs of the strong motion seismic event with name code 13 from table 3.3 (12/10/2013 6.4M 65km)

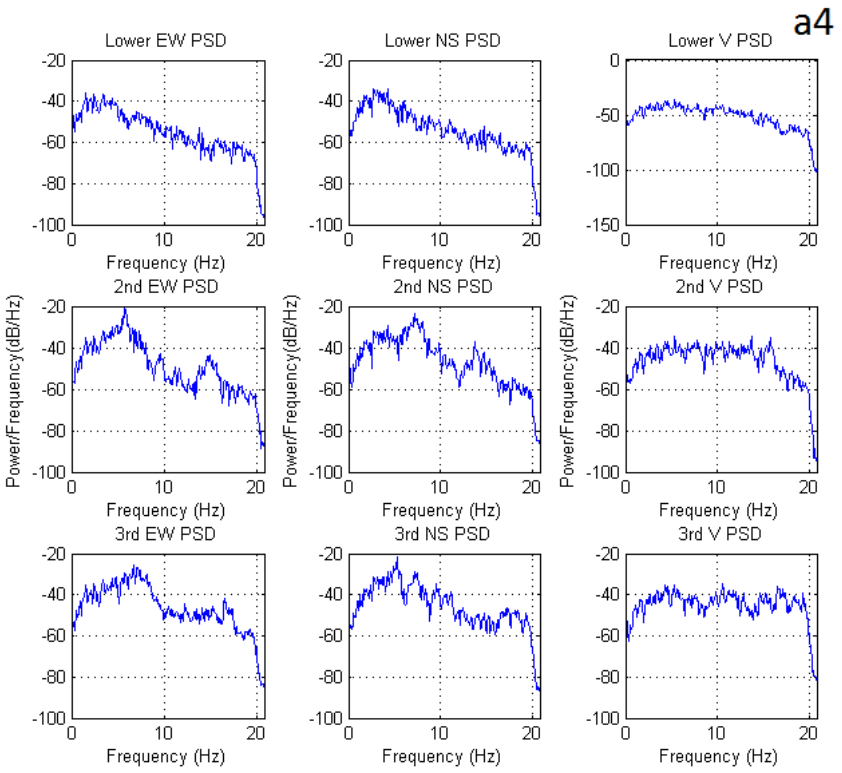

Figure E.3. PSD of seismic event with name code a4 from table 3.3 (22/12/2013 3.8M 60km)

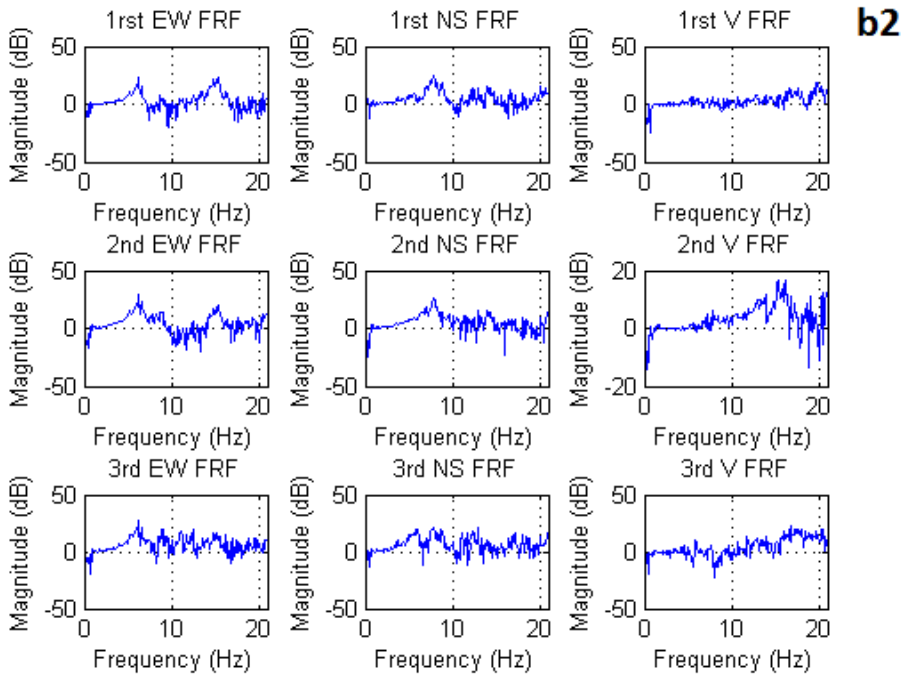

Figure E.4. FRFs of seismic event with name code b2 from table 3.3 (31/03/2013 4.3M 62km)

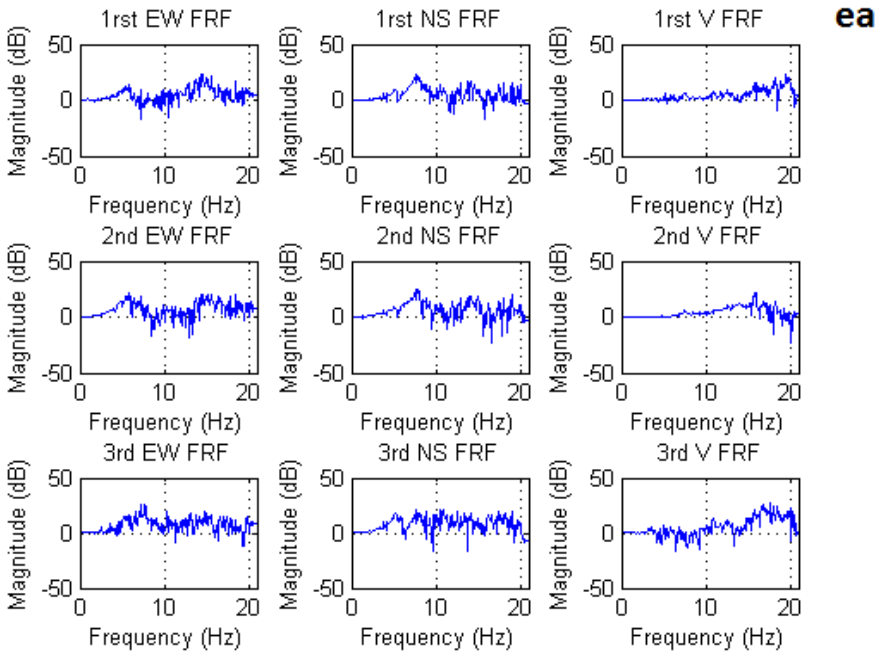

Figure E.5. FRFs of the strong motion seismic event with name code b13 from table 3.3 (12/10/2013 6.4M 65km)

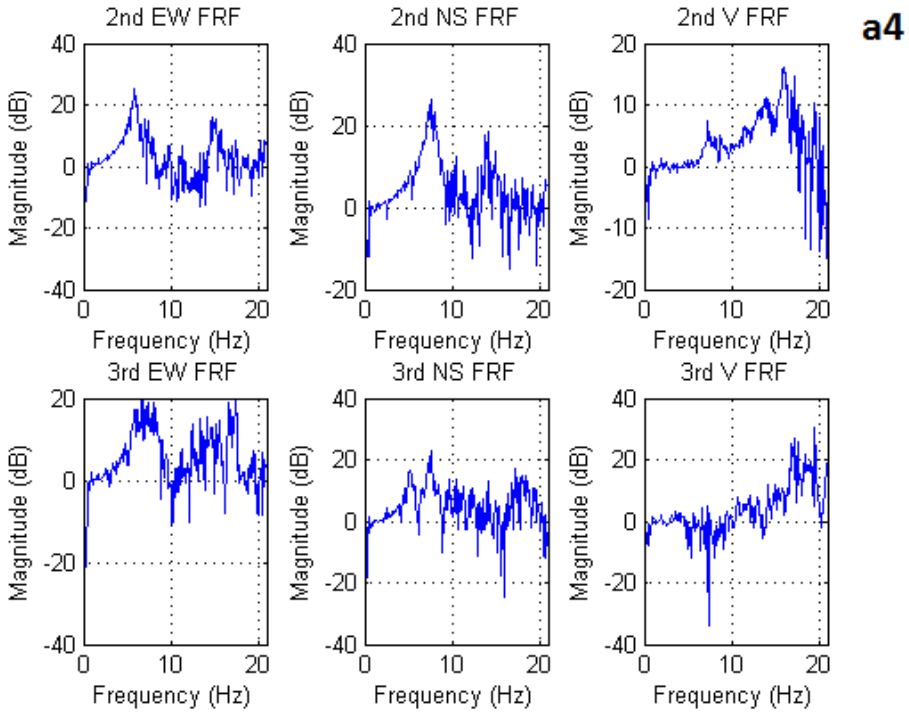

Figure E.6. FRFs of seismic event with name code a4 from table 3.3 (22/12/2013 3.8M 60km)

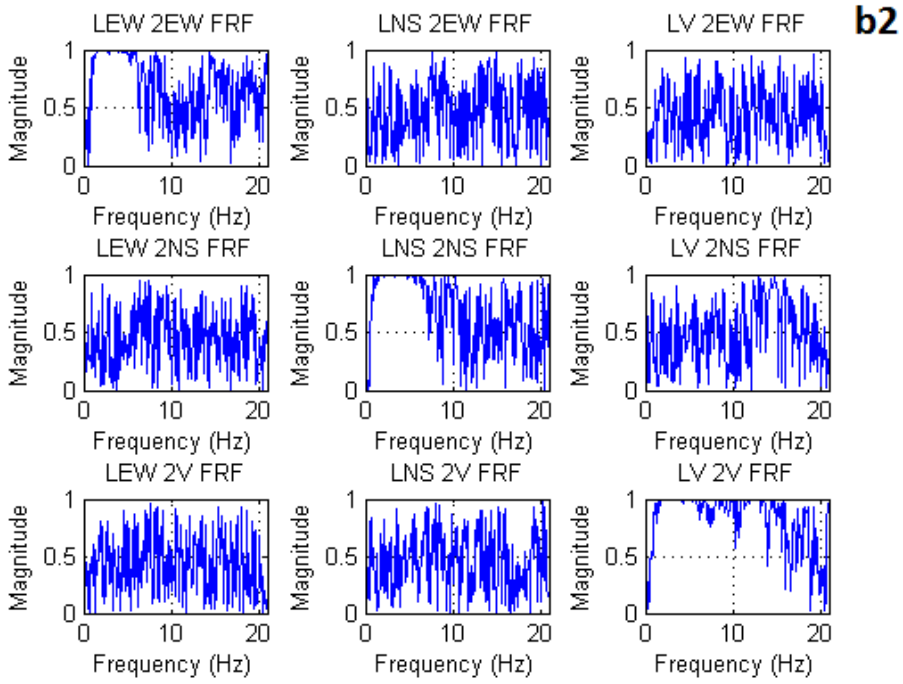

Figure E.7. Coherence diagrams of seismic event with name code b2 from table 3.3 (31/03/2013 4.3M 62km)

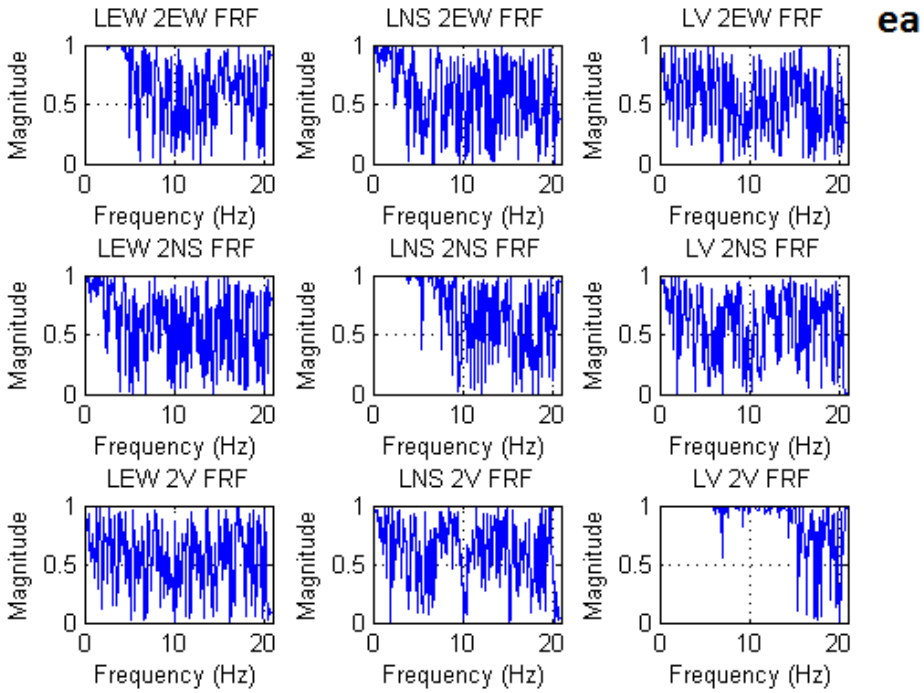

Figure E.8. Coherence diagrams of the seismic event with name code name code b13 from table 3.3 (12/10/2013 6.4M 65km)

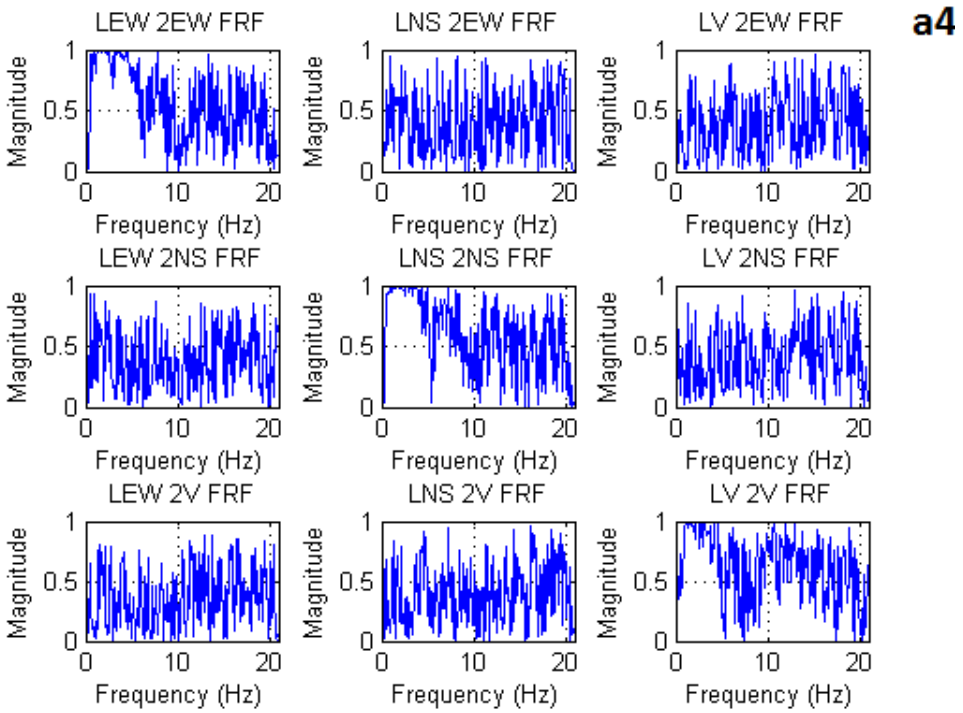

Figure E.9. Coherence diagrams of seismic event with name code a4 from table 3.3 (22/12/2013 3.8M 60km)

Appendix F: Wavelet Analysis

Daubechies Family Wavelet

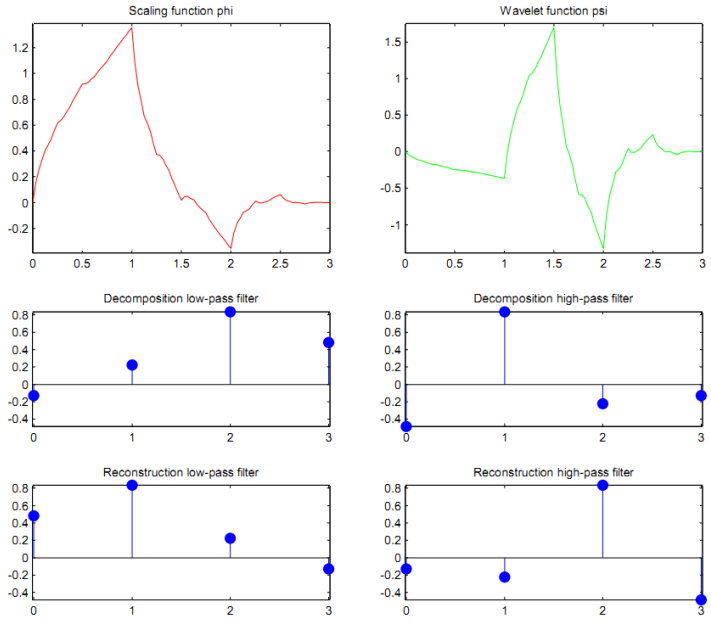

Figure F.1. DB wavelet (order of N is 2) scaling function phi and wavelet function psi. In the middle decomposition low and high pass filters and below the reconstruction low and high pass filters.

Mirror filter is used in order to go from one filter to the other (in a column), where mirror filter along with the multiplication by -1 for even values is applied in the row filters. Such all filters can be produced by one filter.

Characteristics of dbn wavelets is the orthogonality, which is related with the multirate analysis, the filters have a specific length of 2n, they are not symmetric and they contain n vanishing moments.

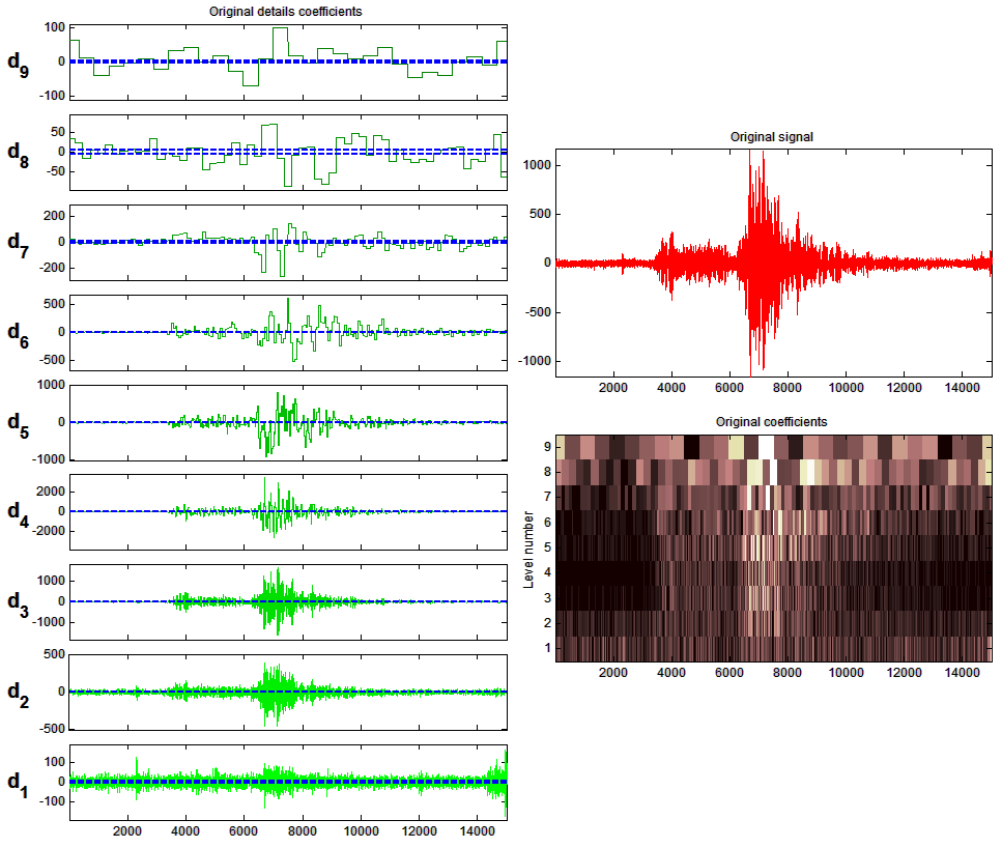

Figure F.2. DB N=2 wavelet original details coefficients (left), the original signal and the original coefficients (right).

On the above figure the wavelet coefficients from level 1-9 are presented (left side). The threshold is zero, and in the wavelet plane are revealed the original coefficients.

Specific thresholds are used in “detail” coefficients in order to de-noise the signal. In figure below there are two lines horizontal and dotted. The coefficients outside the two lines are presented in the new wavelet plane (thresholded coefficients) and everything is between these two lines minimized to zero (de-noise process). As a result the higher wavelet coefficients are presented.

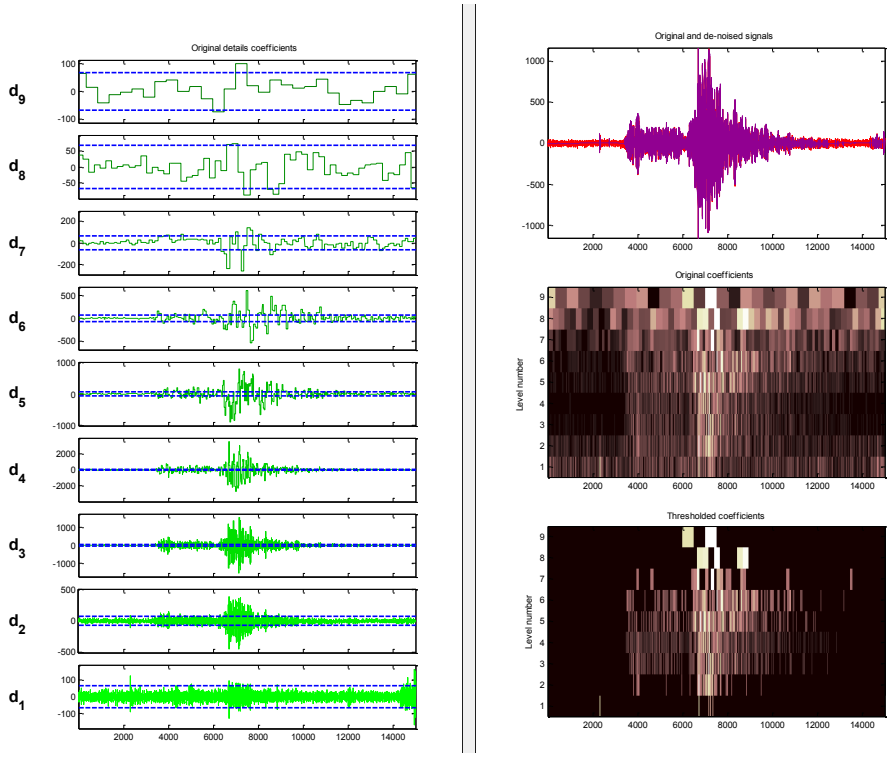

Figure F.3. DB N=2 wavelet original details coefficients (left), the original signal, the original coefficients and the thresholded coefficients (right)

In details d_1 the noise is presented in the whole length of the recording. The coefficient of the specific wavelet at this scale comes very close with the noise of the recording. That is the main reason that the threshold is adjusted in a level higher than the other levels. In levels d_2 also there is noise in the whole length of the recording but the signal of earthquake is now reveal much more clearly. Level d_2 until d_6 the signal of earthquake is presented in clear. Again in levels d_7 until d_9 the coefficients present also noise of the recording. There is a specific level d_4 where there is no need for threshold. There the pseudo-frequency of the coefficient comes closer to the fundamental frequency of the structure and the signal becomes maximum (it reveals exactly the recording of the excitation without any noise). The pseudo-frequency there, is 8 Hz.

Symlets Family Wavelet

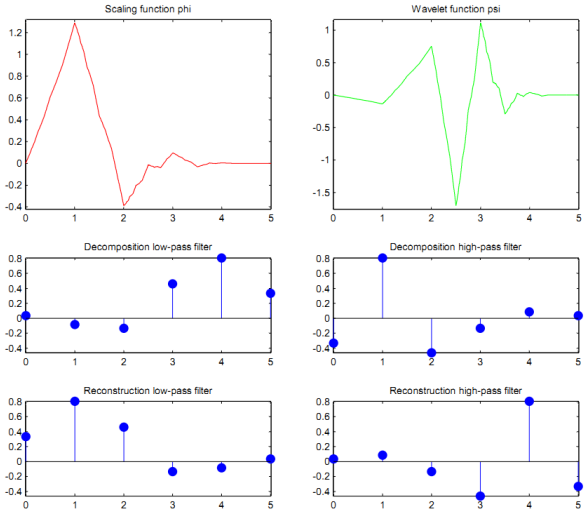

Figure F.4. Sym wavelet (order of N is 3) scaling function phi and wavelet function psi. In the middle decomposition low and high pass filters and below the reconstruction low and high pass filters.

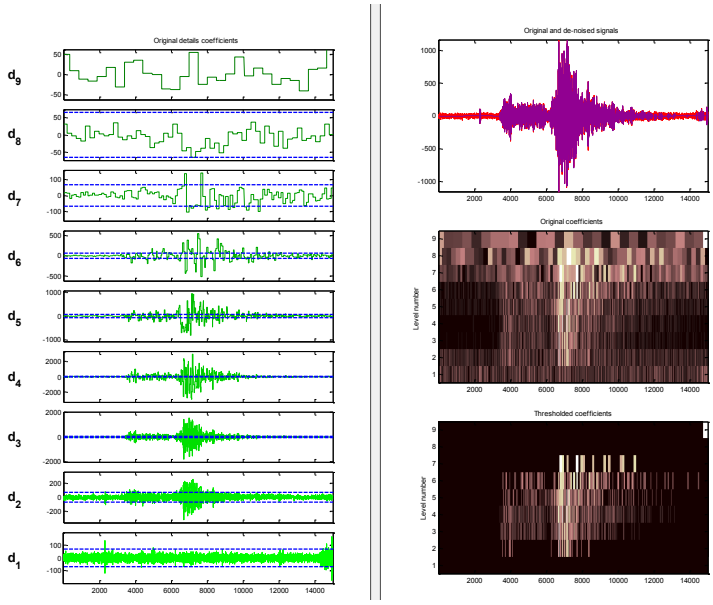

Figure F.5. Sym order N=3 wavelet original details coefficients (left), the original signal, the original coefficients and the thresholded coefficients (right)

In Symlet (3) de-noising it is used the same threshold in order to study what is the sensitivity of the specific wavelet related with the above (db2) in the signal de-noising of the recording.

Again level d_1 and d_2 present high noise in the whole length of the recording. In this wavelet family in level d_3 and d_4 the signal of earthquake is presented in clear. Again in levels d_5 until d_9 the coefficients present also noise of the recording. Instead of DB2 family in symlet the

specific levels d_3 and d_4 there is no need for threshold. There again the pseudo-frequency of the coefficient comes closer to the fundamental frequency of the structure and the signal becomes maximum (it reveals exactly the recording of the excitation without any noise). The pseudo-frequency there, is 8 Hz and also 16 Hz.

Coiflets Family Wavelet

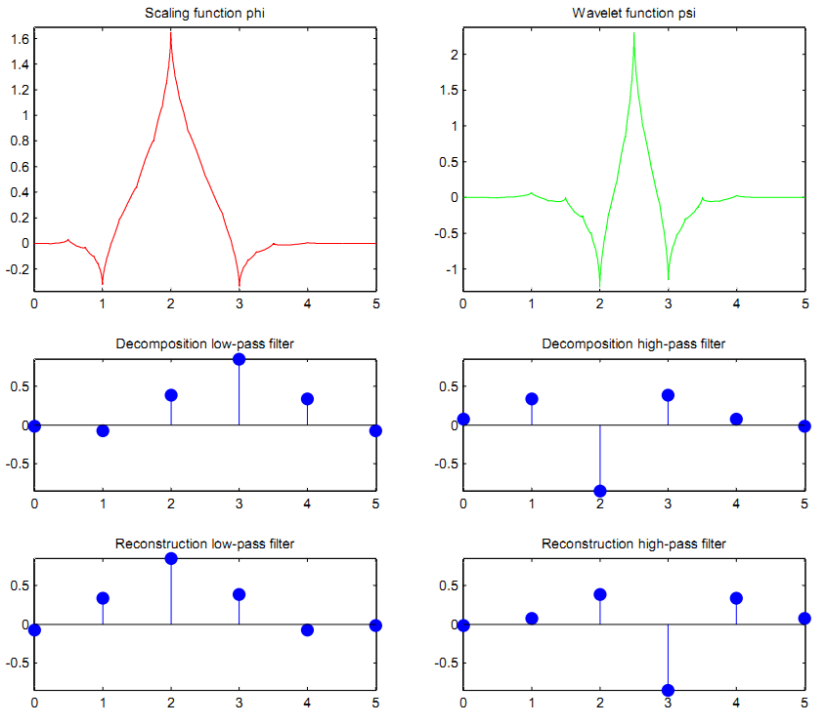

Figure F.6. Coiflets wavelet (order of N is 1) scaling function phi and wavelet function psi. In the middle decomposition low and high pass filters and below the reconstruction low and high pass filters.

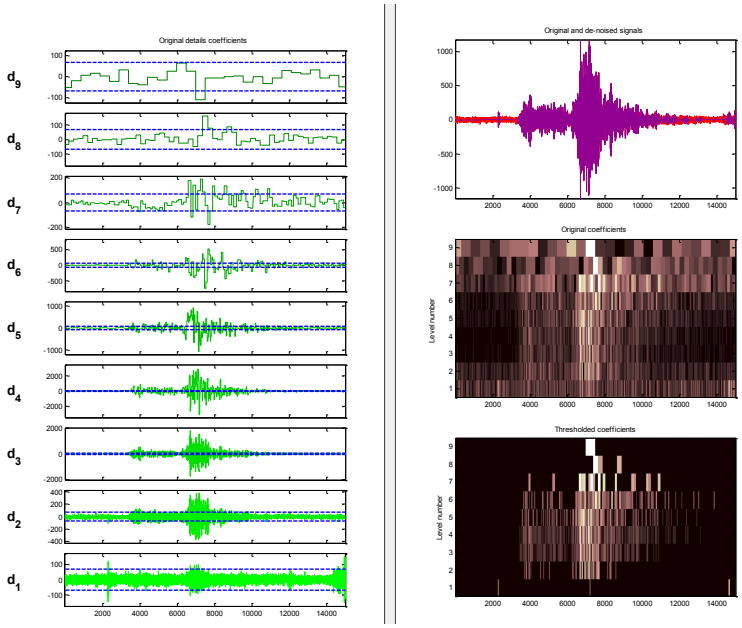

Figure F.7. Coiflets order N=1 wavelet original details coefficients (left), the original signal, the original coefficients and the thresholded coefficients (right).

In Coiflet (1) de-noising is also at the same threshold in order to study the sensitivity of the specific wavelet related with the above wavelets in the signal de-noising of that recording. The result of the wavelet transform comes very close with the previous wavelet family (symlets) in all levels.

Biorsplines Family Wavelet

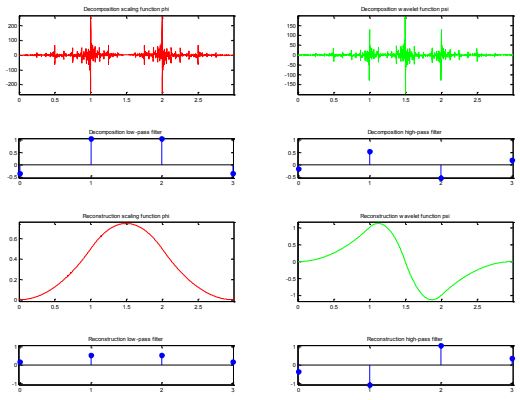

Figure F.8. Biorthogonal wavelet (order of N is 3.1) scaling function phi and wavelet function psi. In the middle decomposition low and high pass filters and below the reconstruction low and high pass filters.

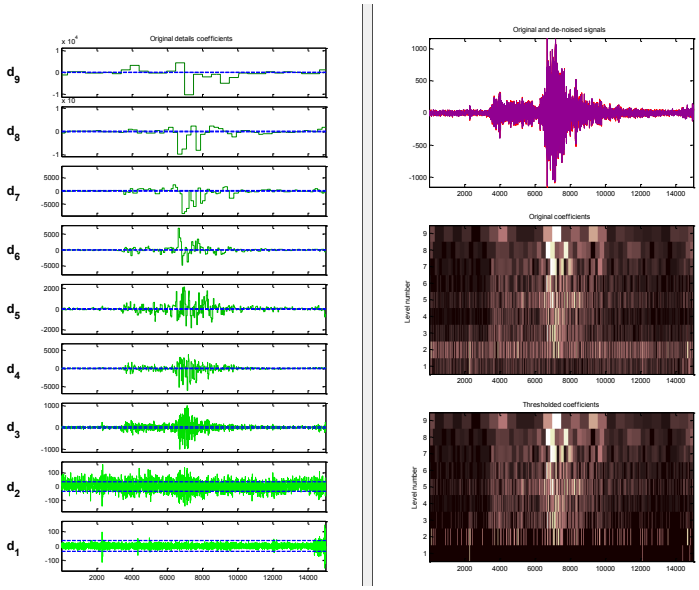

Figure F.9. Biorthogonal wavelet (order of N is 3.1) t original details coefficients (left), the original signal, the original coefficients and the thresholded coefficients (right).

With the specific family although the selected threshold is “penalize high” the denoising procedure presents very low efficiency. This indicates that the noise form comes very close to the shame of the selected wavelet family.

ReserveBior Family

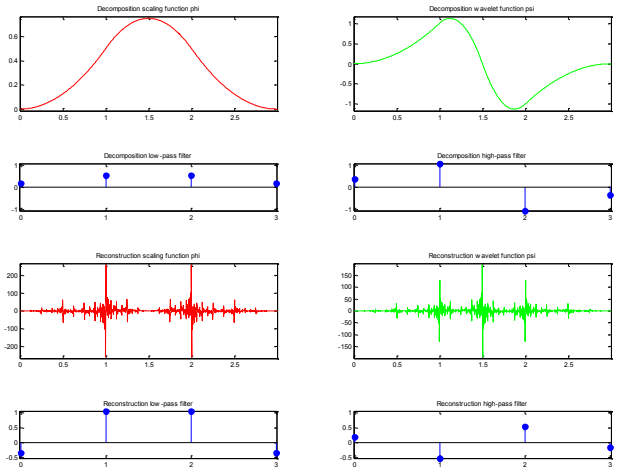

Figure F.10. ReserveBiorthogonal wavelet (order of N is 3.1) scaling function phi and wavelet function psi. In the middle decomposition low and high pass filters and below the reconstruction low and high pass filters.

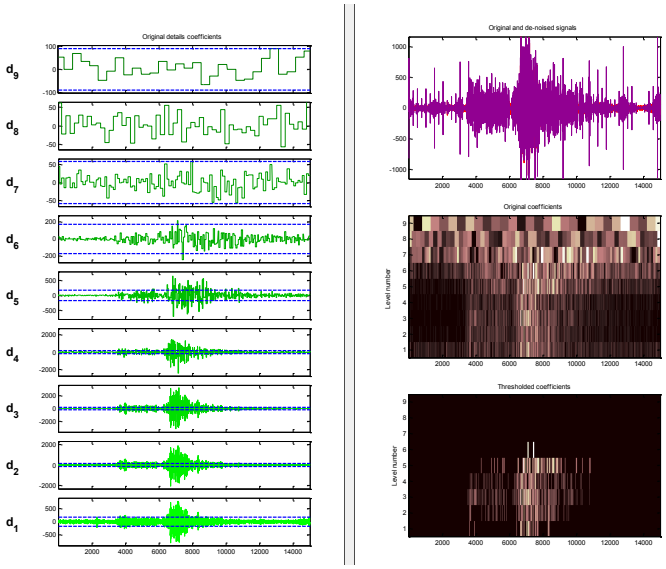

Figure F.11. Reserve Biorthogonal wavelet (order of N is 3.1) t original details coefficients (left), the original signal, the original coefficients and the thresholded coefficients (right).

It is observed that with selected threshold to be as above “penalize high” the de-noising procedure presents much more efficiency. This indicates that the signal form comes very close to the shape of the selected wavelet family. But in every level there is high presentation of noise.

Appendix G: Parametric Analysis

Below is presented the structure of parametric analysis on this appendix:

ARX analysis compared to AR analysis: PSDs and FRFs from different earthquakes are plotted in order to present input-excitation importance in data modeling. Study both input-output, elliminates the effect of different dynamical parameters of input to the system analysis.

Next step is one dimension modeling with ARX: One component of excitation response is studied (NS imput-NS output) in order to present the bodeplot of the system for this specific component.

Then one dimension modeling with ARMAX: NS input-NS output is studied in order to present the similarities-differences of ARX-ARMAX for the specific case study system-building (in terms of computation complexity, model order and frequencies presentation).

Next step is one dimension modeling with ARMAX and optimization of noise parameter: For specific model order of ARMAX (from previous section we defined na, nb ARMAX parameters), there is optimization of MA parameter nc (na, nb, nc, 1) in order to address ARMAX ability, to reveal system resonanse frequencies, with increased nc parameter.

Multidimensional modeling with ARX: After comparison of ARX with ARMAX, it is chosen ARX analysis. In this section there is comparison of previous one dimension analysis (NS input-NS output), with multidimensional analysis (NS input-EW output, NS input -Vertical output etc).

Frequency Coherence between component: Coherence between the same and different components of input-output is presented, in order to present the efficiency of one-dimension analysis due to multi-dimensional analysis.

Next step is multidimensional analysis with ARX in a cell: All recording data from earthquakes, are stored and analysed in a cell in order to being grouped and analyzed together.

At the end of this appendix is the graphical analysis of all ARX models: All case study low amplitude earthquakes, have been modeled by ARX and plotted on the same graph, for

old and new building of TEI, before and after the 6.4 M earthquakes. These reveal the deviation of parametric FRF bodeplots.

ARX analysis compared to AR analysis.

Below there is PSD analysis for the seismic event Table 3.3 (Chapter 3.3). Event "b" is earthquake with number 2 from Table 3.3, "c" event is number 3 and "d" event is earthquake number 4.

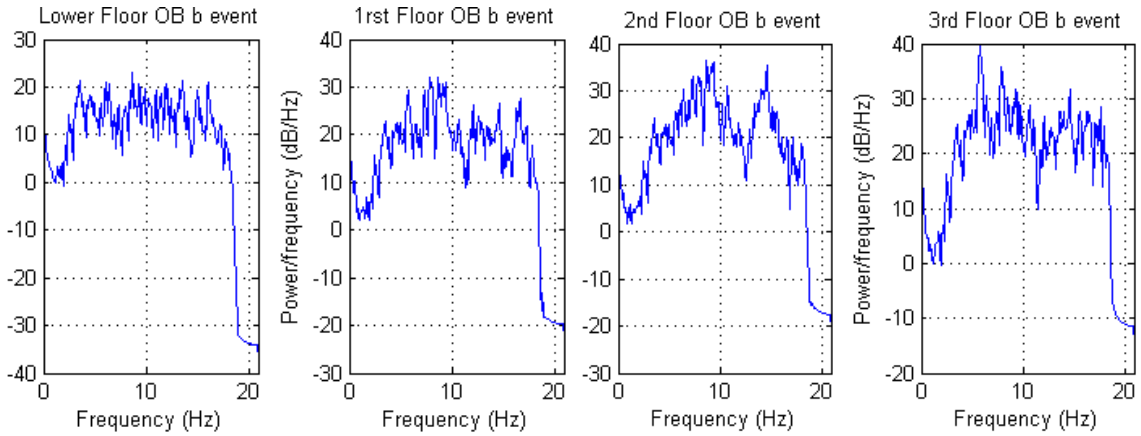

Figure G.1. Power Spectral Densities of b Seismic event.

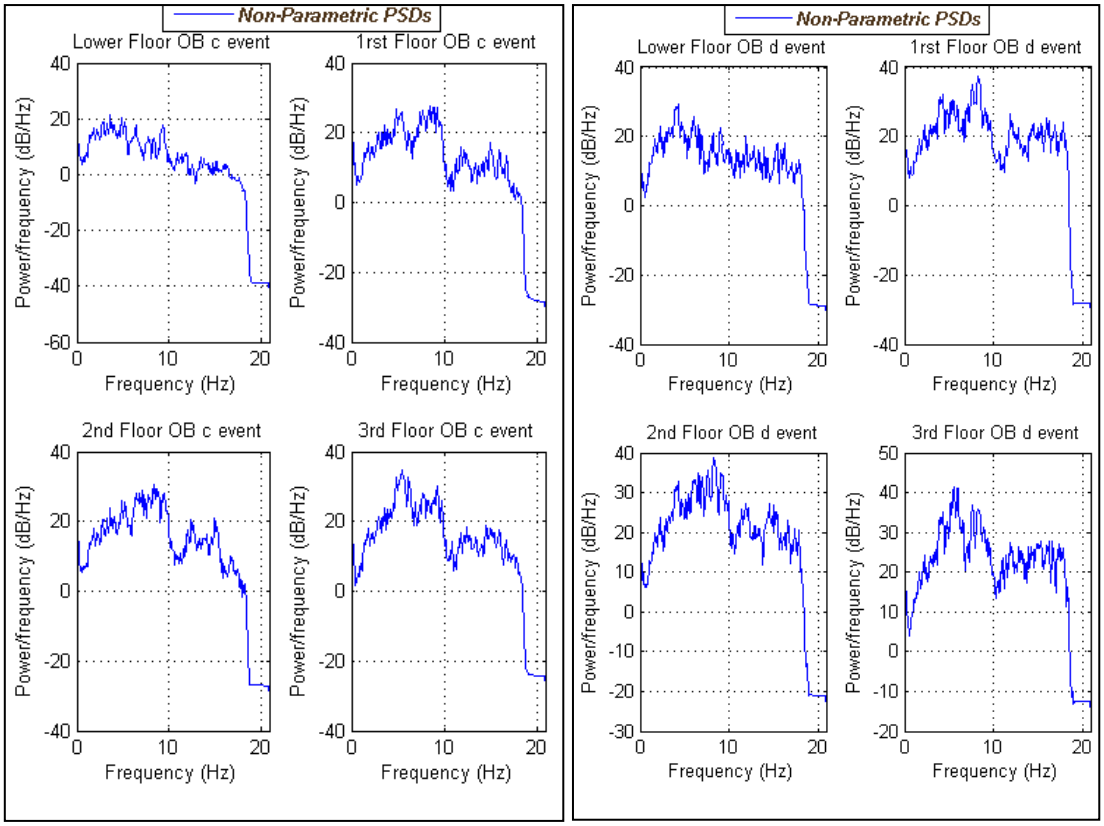

Figure G.2. Power Spectral Densities of c (left) and d (right) Seismic events.

Power spectral densities (PSDs) of seismic accelerations in old building of TEI reveal that in every earthquake the PSD and simultaneously the dynamic parameters of the excitation that affect building are different. The seismic acceleration is measured on the lower, first,second and third floor of the old building. The initial filtering is at 20 Hz, an acceptable frequency limit in order to study the response of buildings under seismic excitation.

FRF of "b", "c" and "d" seismic events.

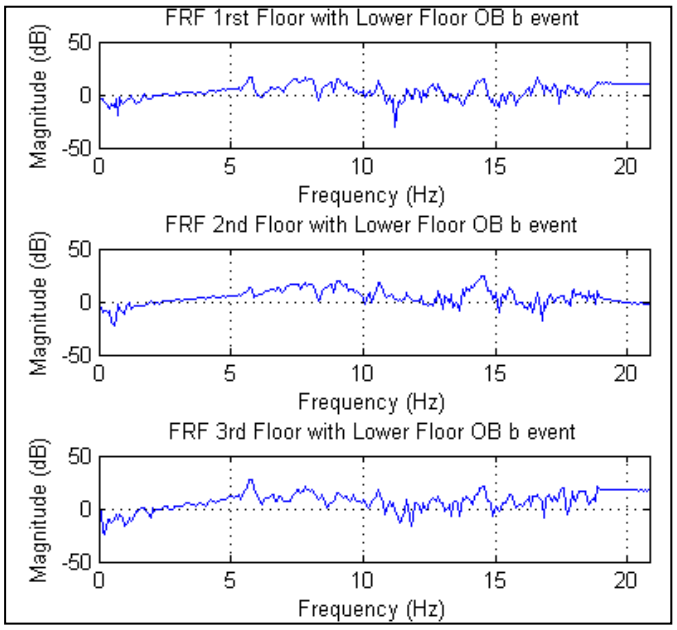

Figure G.3. Frequency Response Functions of seismic events b

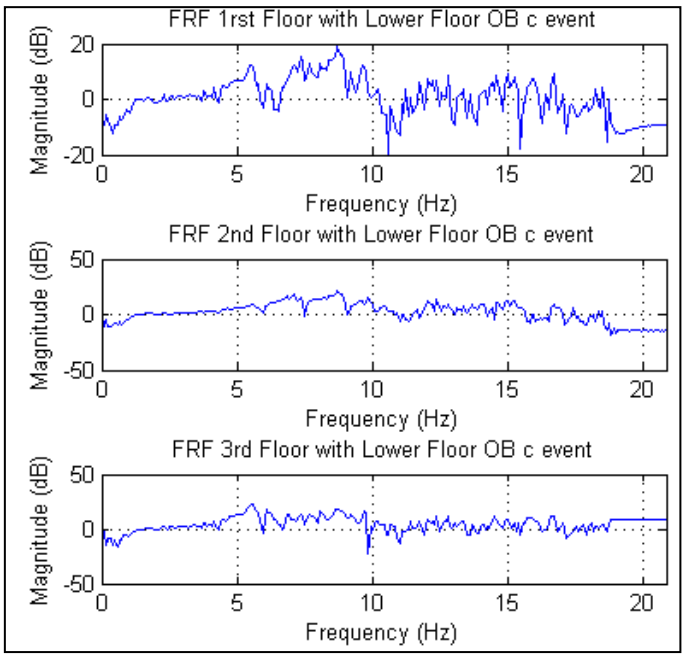

Figure G.4. FRF of c Seismic event.

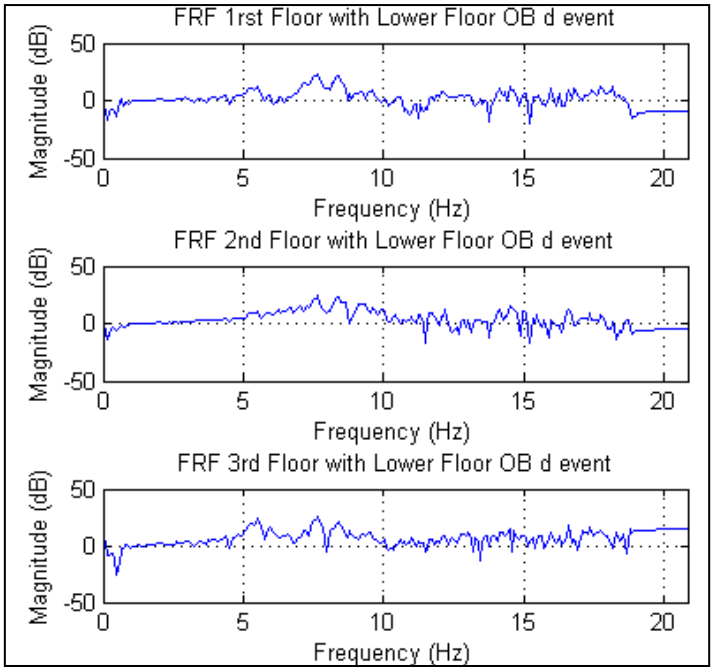

Figure G.5. FRF of d Seismic event.

The Frequency Response Functions (FRFs) for b, c and d seismic event. The FRFs of seismic accelerations in old building of TEI reveal that in every earthquake the FRF of input (excitation) related with the output (response) remains almost the same although the parameters of the excitation are different. Input is the lower floor and output is the 1rst, 2nd and 3rd floor respectively.

One dimension modeling with ARX (Event Select)

Initially acceleration recordings from specific events of the catalog of chapter 3.3 (raw data before and after earthquake of 6.4M) have been used. This is the primary stage of analysis where optimum order of ARX modeling will be selected according to specific criteria for these seismic events. Below is presented the procedure analysis of one seismic event (with code name f event). Event "f" is the earthquake on table 3.3 (chapter 3.3) with the number a1. The same analysis procedure has been done for more than 30 seismic events (with magnitude higher than 3.5 M and epicenter distance lower than 100 km from buildings) that affected both buildings in order to define the parameters that will be used for the statistical parametric analysis (parameter model, model order, components etc).

The events will be studied from one component in order to study the response of buildings in one dimension (NS input-NS output).

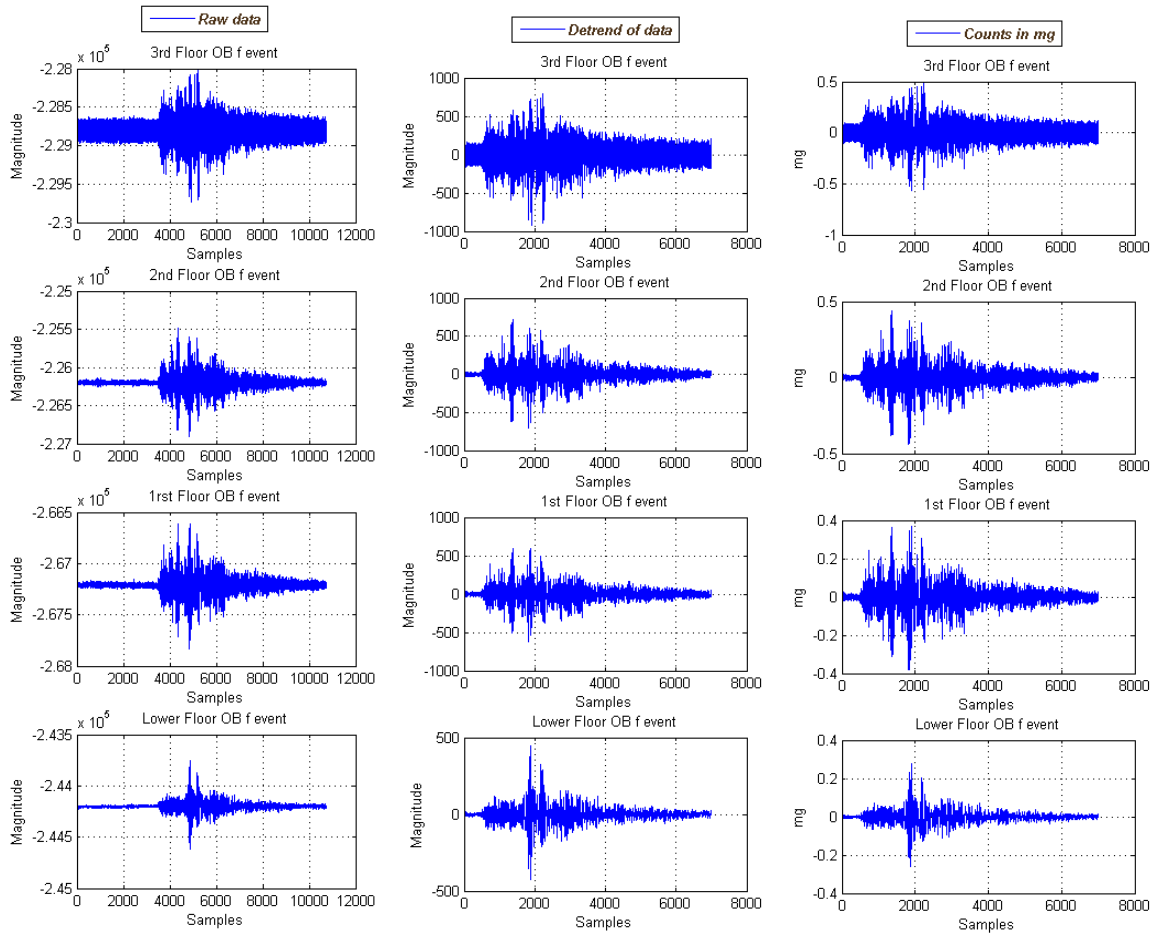

Figure G.6. Raw data(left), mean removal(mid) and transform in mg (right) of seismic event with codes f. Upper raw line refers on 3rd floor old building TEI, below refers to 2nd, under this is 1rst floor and at the bottom line is lower floor of the old building.

In raw data there is mean removal (de-trend of data) where mean and any trend in data is removed. Also data are transformed from counts to mg in order to illustrate the real recording acceleration of sensors. In above figure are presented acceleration recordings for every floor of the old building, without any process (left), with mean removal (mid) and with multiplication of counts with specific value (from datasheet of Reftek) in order to transfer accounts in mg. Seismic acceleration amplitude on each floor is presented clearly through above plots. As the floor is getting higher the amplitude also rises. The sampling rate of recordings is at 125 Hz, such 8000 samples have time duration of 64 seconds of acceleration recording.

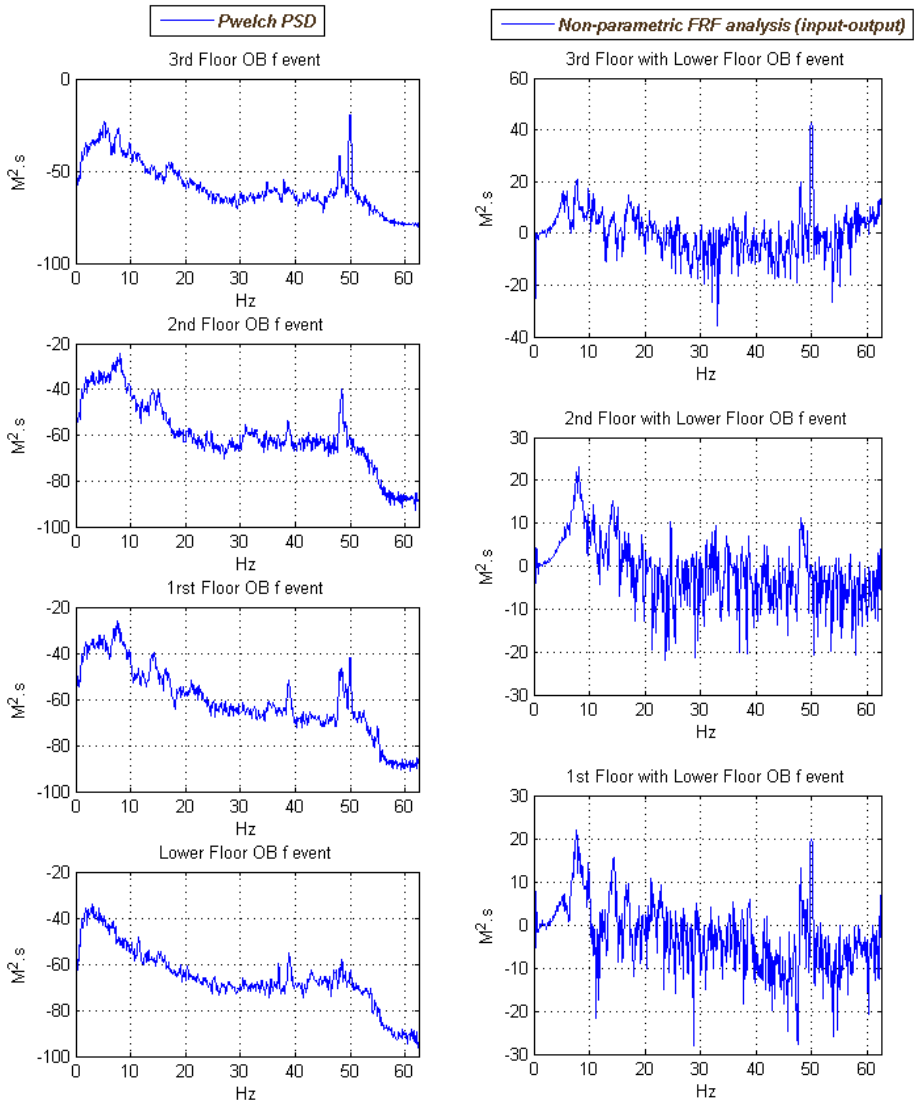

Figure G.7. PSDs (left) and non-parametric FRF (right) of seismic event with cofe f. Frequency range up to 62.5 Hz.

Power Spectral Densities and non-parametric Frequency Response Functions for the seismic events with name code f. Left plots present resonance frequencies on each floor. At 50 Hz is the noise from electric power network. Right plots reveal the frequency response functions on each floor related the lower floor. The resonance frequencies are more clearly than PSDs plots.

Filtering

Specific filters are applied based on the frequency spectrum that is interest. Theory refers that buildings present resonance frequencies under 10 Hz otherwise structures have very high stiffness. Analysis of frequency coherence between input and output (see figure below)

also verifies the previous theory. The coherence after 10 Hz is very low. This means that after 10 Hz the system (building) does not react or response on this frequency spectrum. Chebyshev filter is applied on data with 1 db ripple in pass band, starts at 18 Hz, 60 db falls at 19 Hz. In order to avoid spikes or disturbances at the filtered data, the filter curvature should be checked.

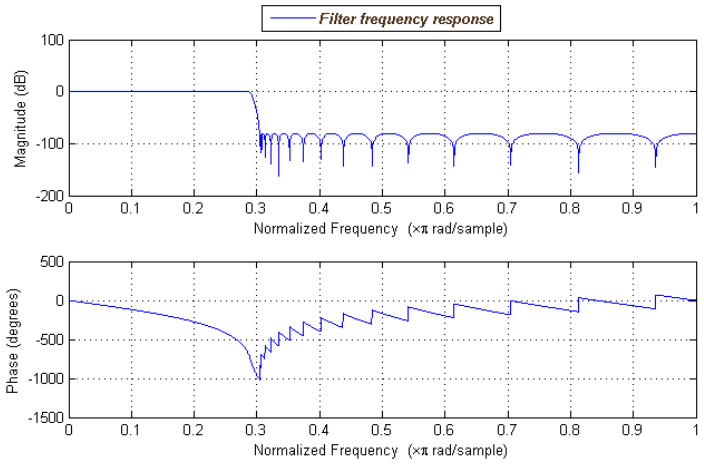

Figure G.8. Filter frequency response (magnitude up, phase down)

125 Hz is high amount of data. With filtering there is also re-sampling of the data in order to maximize the process power and minimize the process time of parametric modeling. Data are re-sampled at a value of 3. Data are re-sampled at a value of 3. In photo the normalized frequency is 62.5 Hz. The filter attenuates from 62.5/3.33=18,76 Hz.

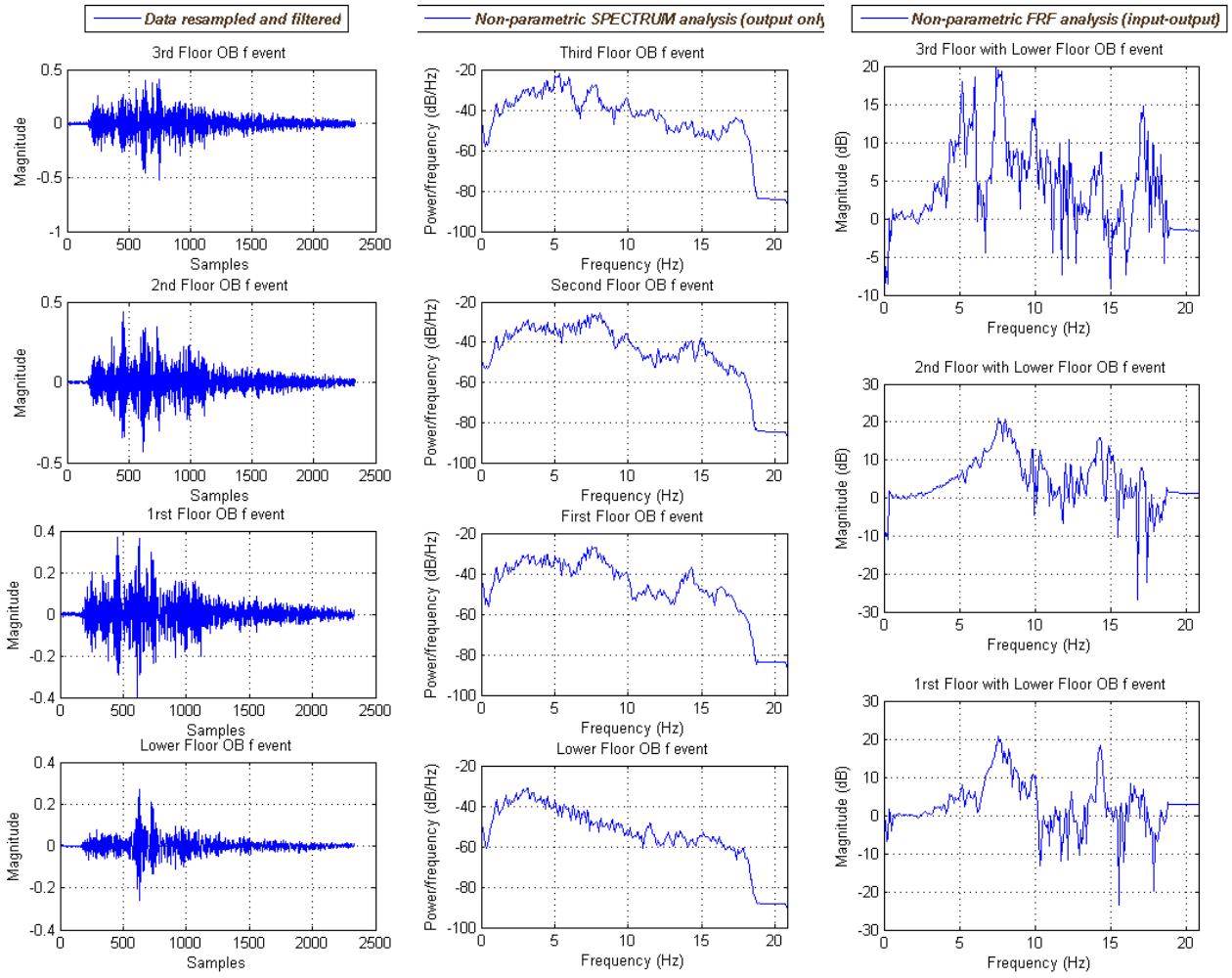

Figure G.9. Recording data filtered at 20 Hz (left acceleration waveforms, centre PSDs, right FRFs). Frequency range after filtering is up to 20 Hz.

Seismic data after re-sampling and filtering. Power spectral densities (mid) and FRFs (right). At this point it is tested if PSDs and FRF are similar with those before filtering and re-sampling in order to test if all important information has been kept and also if filter is the appropriate. By filtering, noise effect has been removed and the seismic acceleration that affected old building is presented much more clearly. The amplitude of the noise before the seismic wave P is much lower than before filtering. Also in PSDs noise spikes have been removed. At FRFs plots the fundamental frequency is presented in detail at 7,5 Hz. Until this point non-parametric analysis has been used in order to reshape and transform data to a specific form, appropriate for the specific requirements of parametric analysis.

Search for optimum model order

In this part of analysis input of data related with output of data will be processed in order to find model order of models ARX. The parameters are na of output, nb of input. The initial test will be from order 2 until 100 in order to cover a wide range of probable models and check the most appropriate in terms of fitness with the data and lower complexity. Also na and nb for this test.

Stabilization diagram is of great importance for the choice of model order. Stabilization diagram is a plot of model order (na) with the frequencies that are reveal on each order. The order is the number of DOF of the system and it is determinant for the model. More detailed, model order is the number of past values that each polynomial parameter computes for the ARX model. Model order defines how many past data the model will compute in order to create the specific model. In below diagram it is presented that an appropriate model order is around 60 where frequencies have been stabilized and almost every hidden frequency is revealed.

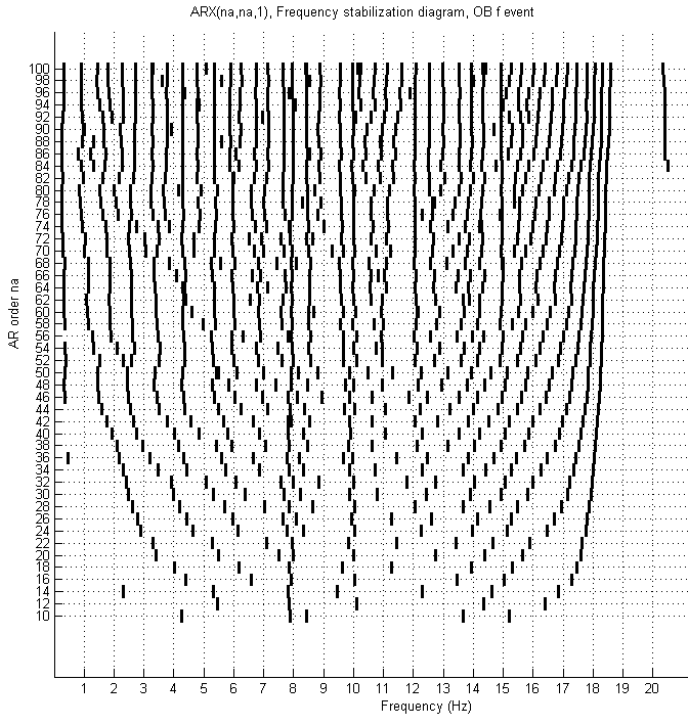

Figure G.10. Stabilization diagram of ARX modeling from 10-100 model order. Frequency range is up to 20 Hz (level of filtering)

BIC, AIC and RSS/SSS criteria

The choice of optimum order is based on specific criteria. Bayesian information criteria and Akaike information criteria are basic in model order selection. Both criteria favor the reveal of frequencies in the model but penalize the complexity of the model. This is a very important relation because they indicate the optimum model order (most frequencies that revealed) without increasing the model order (high model order is computational inefficient and also creates false frequencies. BIC penalizes complexity more than AIC.

RSS/SSS is the quotient of residuals square sum divide with the series sum of square. It presents the residual of the model in relation with the data of the event. As the model order increases the model fit better in the data so the RSS/SSS decreases.

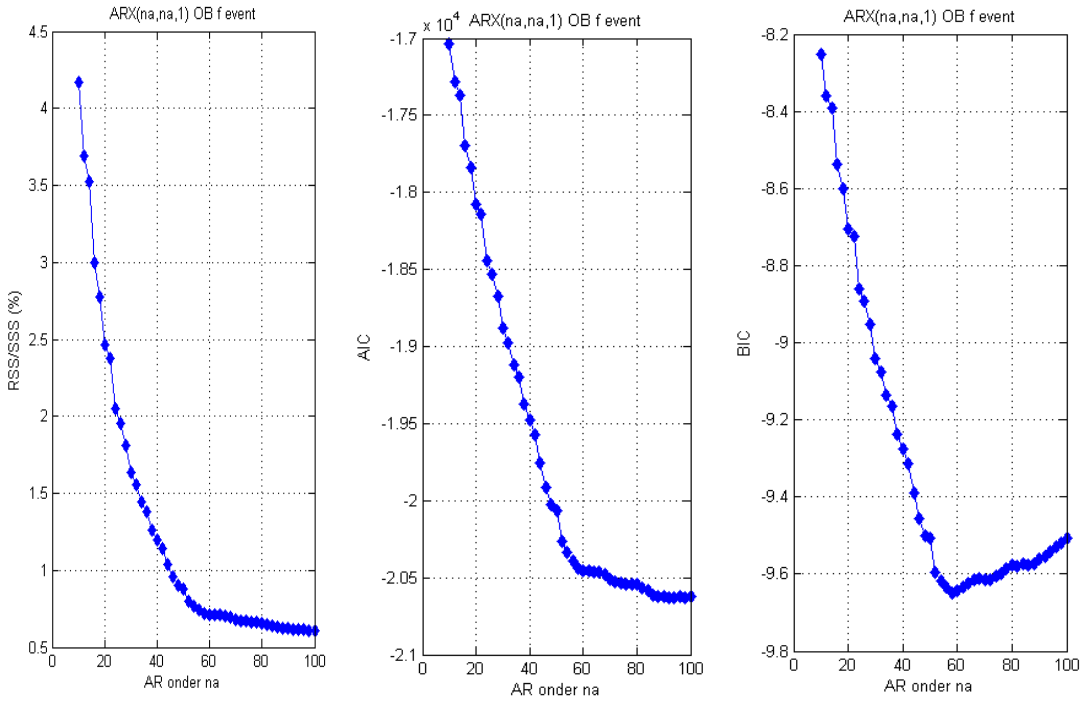

Figure G.11. Model order selection criteria (RSS/SSS, AIC and BIC).

Above figure presents G.11 the model order criteria namely RSS/SSS (at %), AIC and BIC. Order of 60 is also revealed as optimum model order.

Verification of the selected model by ACF of residuals between model and RAW data

Auto correlation function (ACF) of the residuals of model with data presents the residuals of the model with the data. Low ACF verifies the model. Low ACF means that the residuals between model and data is low , such there is not information that hasn't been include in the model and also the model simulates the data with the optimum way. High ACF or AFC with specific structure in the bands reveal that there is information (or frequencies) in residuals, such data that have been include in the model and as a result model is uncompleted.

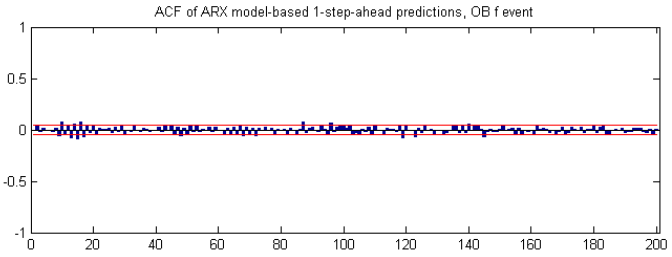

Figure G.12. Autocorrelation function of the "model to data" residuals

The ARX model with order of 62 that has been used in parametric analysis creates very low level residuals. The autocorrelation function of these residuals reveal that there is no information hidden on these residuals and also that every information has already been simulated by the model.

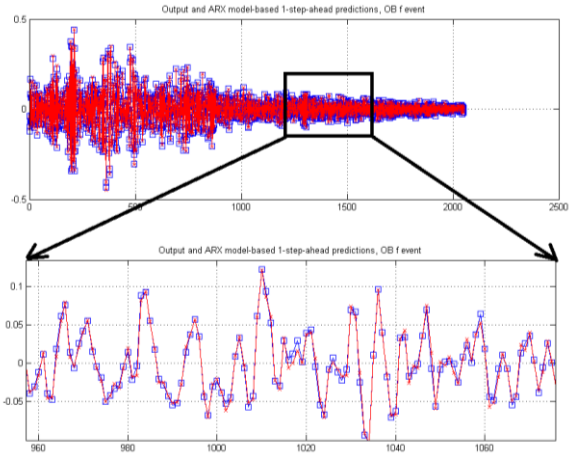

Figure G.13. Model fitting on the data waveform. Red color is the recording. Blue color is the designed ARX model.

Figure G.13 presents that model (blue squares) simulate almost exactly the seismic data of "f" event.

Bode plot of the system

At the end is the bode plot of the system. With the blue line is illustrated the bode plot of the data and with the red line the bode plot of the system (the building is tested as a system). The model (red line) is presented to simulate in very high grade the data. Figure presents two bode plots, non-parametric analysis (data FRF) with parametric analysis (system FRF).

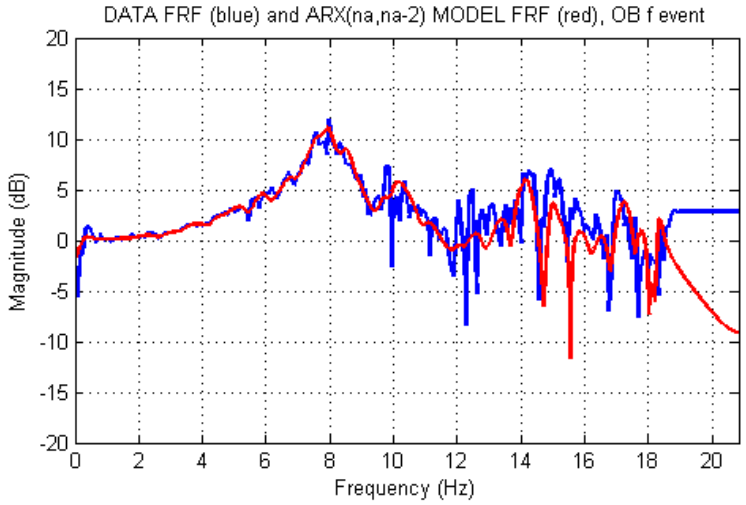

Figure G.14. Bode plot of the designed system model (red line) in comparison to raw data (blue line)

From coherences analysis has been presented that buildings have high frequency coherence until 10 Hz. This means that building response in the frequency range from 0-10 Hz. After this frequency there is no frequency coherence. Such although in bode-plots of data(blue line) with the bode-plot of the system (red line) there is difference in frequency higher than 10 Hz this is meaningless and has no effect in the performance of the model. The important is that designed ARX model simulates frequency spectrum from 0-10 Hz with significant success.

The two first resonance frequencies revealed from this bode plot also are presented as main frequencies from the very low level of order estimation in stabilization diagram. This shows that bode plot is a different form of frequency stabilization diagram and reverse that that stabilization diagram is an alternative form of system bode plot.

One dimension modeling with ARMAX

Filtering and re-sampling are required by ARMAX modeling. Noise is being modeled by a polynomial component nc. Model order will used na, nb and nc as the polynomial parameters of output, input and noise respectively. In this point na, nb and nc are studied as same.

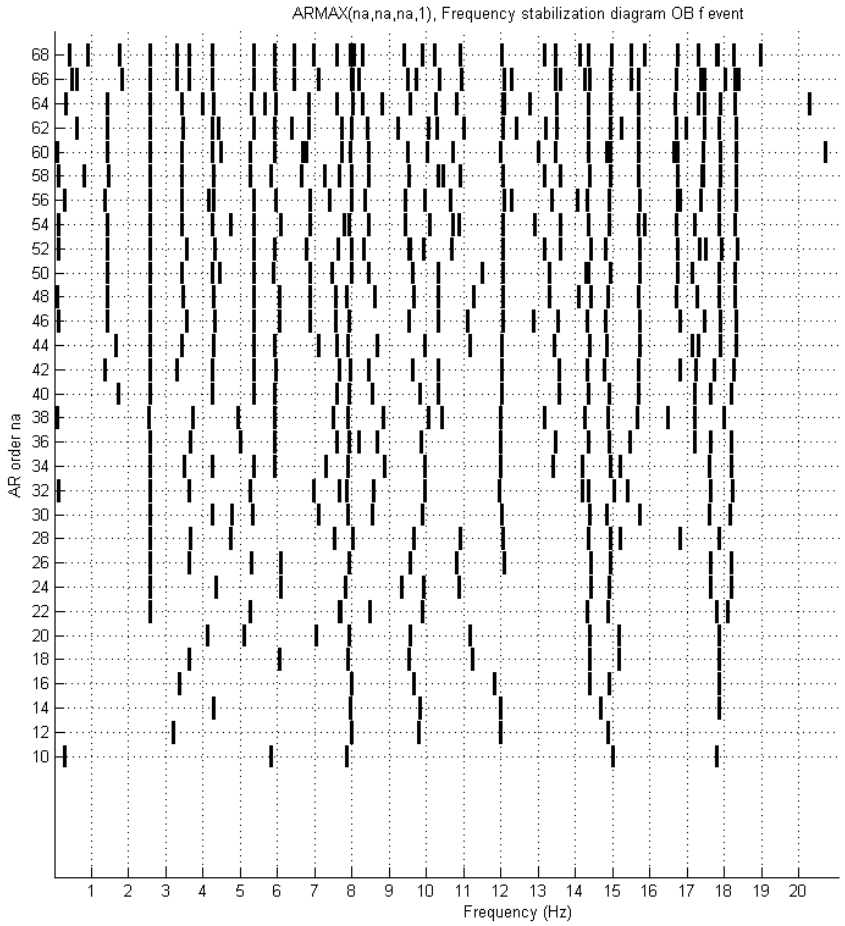

Figure G.15. Stabilization diagram of ARMAX modeling from 10-68 model order

By ARMAX stabilization diagram can be revealed that resonance frequencies can be detected through much lower model order. Modeling of noise with the polynomial nc contributes the model to be more effective in terms of model order but it is much more inefficient in computing requirements. Lower model order can be also explained from the moment that if the equation of ARMAX model na×y=nb×x+nc×e every term is divided by nc then there is an ARX equation with nc lower polynomial order.

BIC, AIC and RSS/SSS criteria

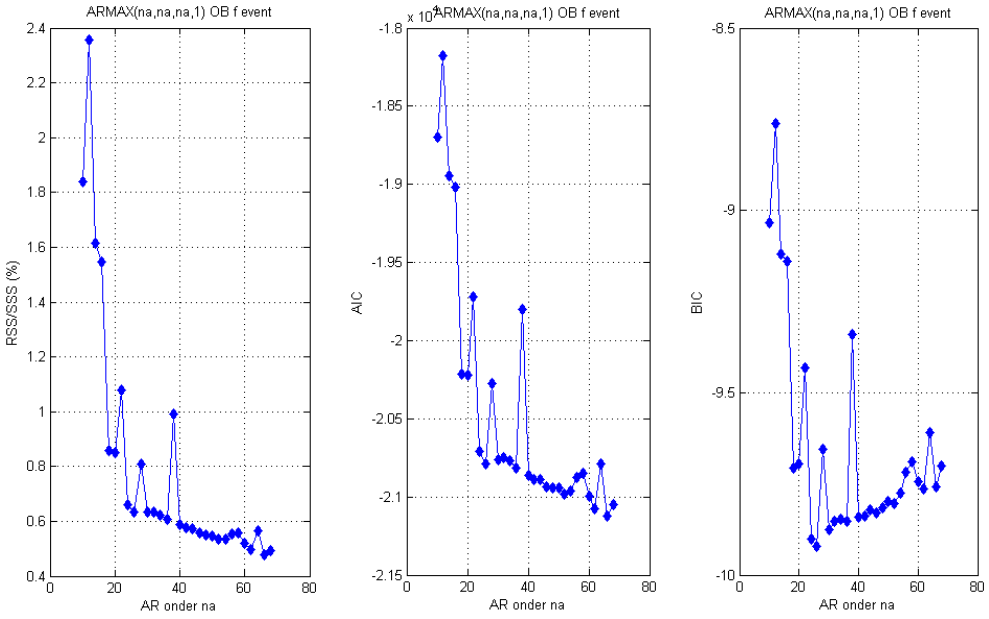

Figure G.16. Model order selection criteria (RSS/SSS, AIC and BIC)

Criteria present much lower optimum model order (order 24). From stabilization diagram it is presented that higher model order could reveal possible more frequencies (the stabilization diagram is a more stable). Such instead of 24 the model order is increased at 34, in order to increase the model order without increase significantly the model complexity. Verification of the selected model is applied by ACF of residuals between model and RAW data

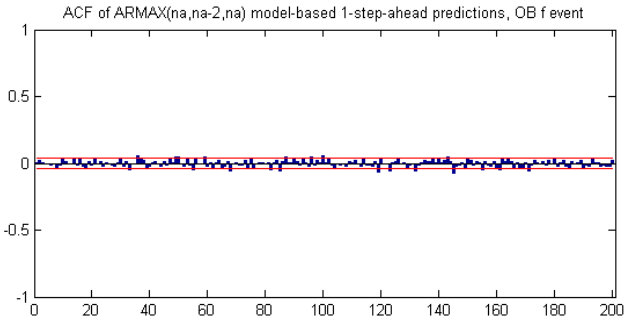

Figure G.17. Autocorrelation function of the "model to data" residuals of the ARMAX model with model order 34

ACF of model to data residuals show very effective model fitting with the seismic data.

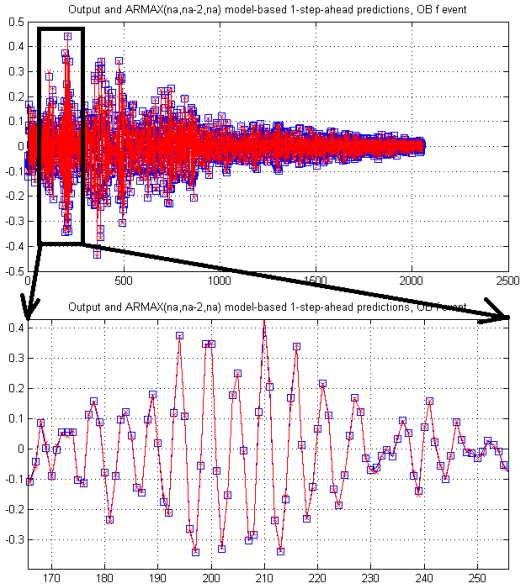

Figure G.18. Model fitting on the data waveform for the ARMAX(24,24,24,1) model

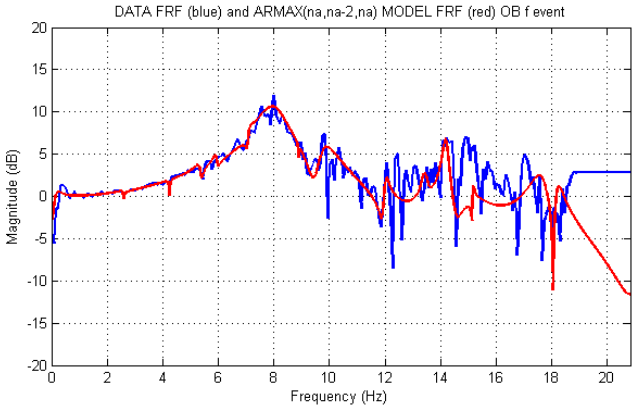

Figure G.19. Bode plot of the designed system model ARMAX (34,34,34,1) (red line) in comparison to raw data (blue line)

ARMAX bodeplot presents that ARMAX computes the same bodeplot with ARX analysis. From the moment that high order ARX requires much less computing power than lower order ARMAX model, it is suggested that ARX is more appropriate for the specific research.

One dimension modeling with ARMAX and optimization of noise parameter

The same steps as before but now the modeling is with extra search of ARMAX Moving Average nc parameter order. Before was found the optimum ARMAX order for each event with na, nb and nc equal. Now will test with na and nb stable (with the previous values) and search of the optimum nc in order to test if the new model will be better than previous ARMAX models.

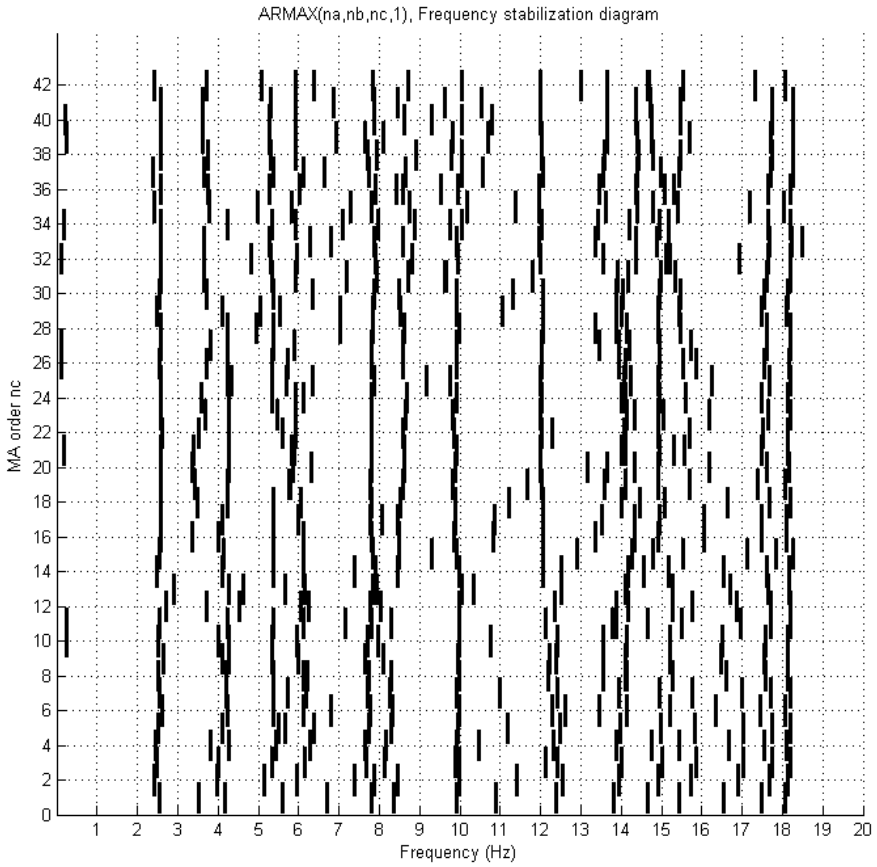

Figure G.20. Stabilization diagram of ARMAX (34,32,x,1) modeling with 1<x<42.

Polynomial of noise nc takes values from 1 until 42 in order to study the optimum order of the ARMAX model.

BIC, AIC and RSS/SSS criteria

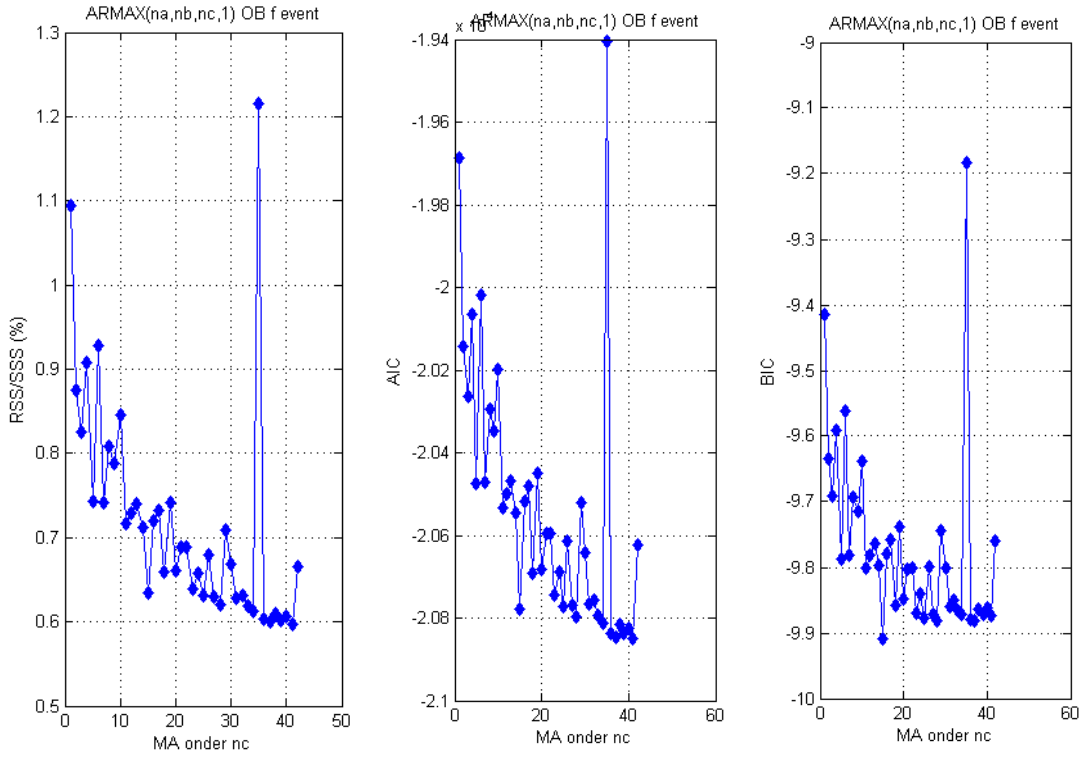

Figure G.21. Model order selection criteria (RSS/SSS, AIC and BIC) for the ARMAX (34,32,x,1) model, with 1<x<42

Verification of the selected model by ACF of residuals between model and RAW data

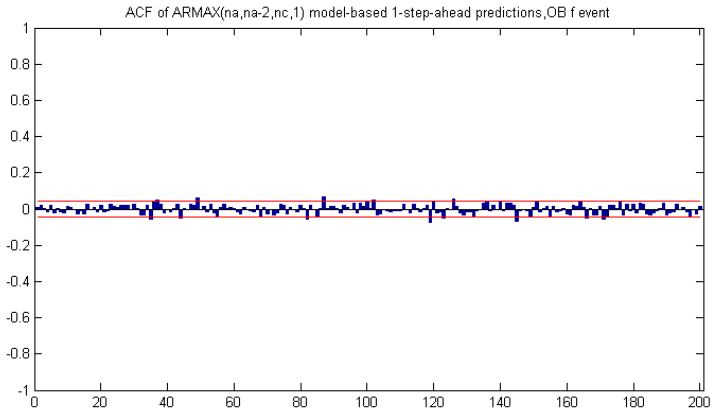

Figure G.22. Autocorrelation function of the "model to data" residuals for the ARMAX (34,32,15,1) model

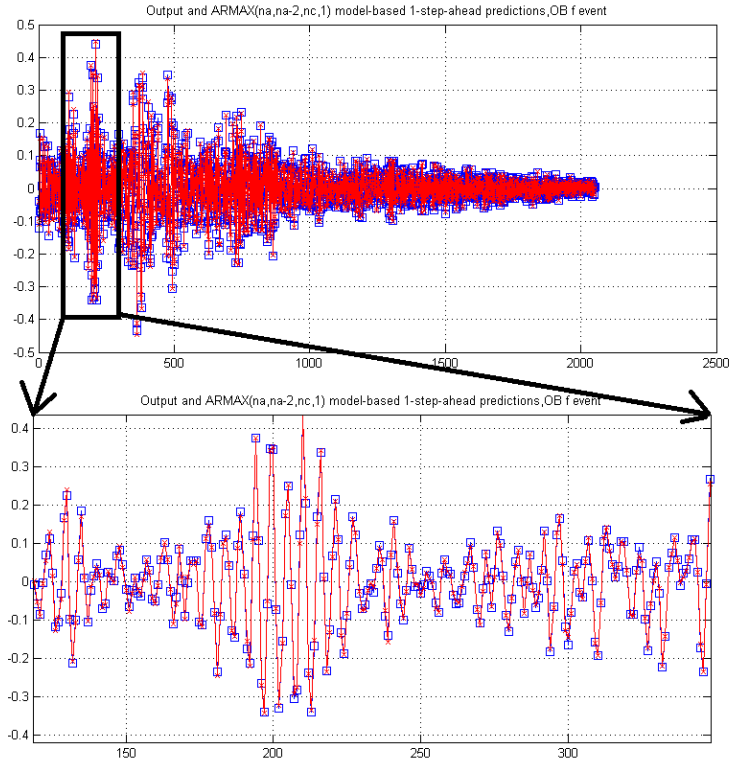

Figure G.23. ARMAX (34,32,15,1) model fitting on the data waveform

Bode plot of the system

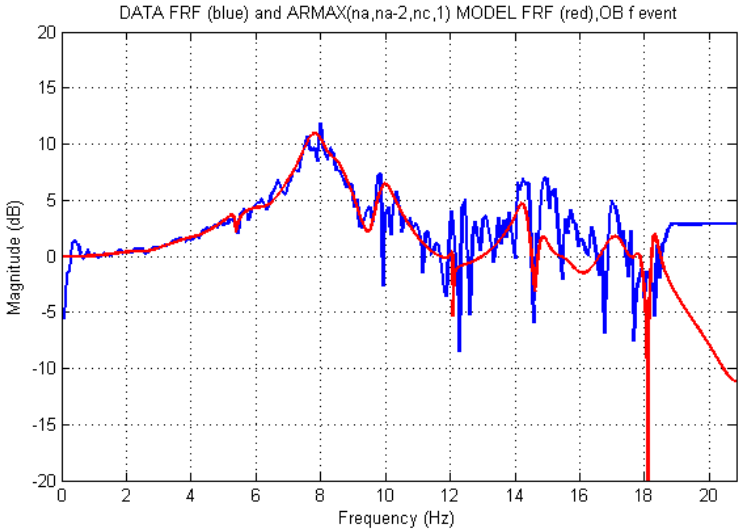

Figure G.24. Bode plot of the designed system model ARMAX (34,32,15,1) (red line) in comparison to raw data (blue line)

The bode plot of the 3rd test (namely ARMAX optimization) of the system (red line) with optimization of nc noise polynomial at the order of na=34, nb=32 & nc=15 has the same

characteristics with ARMAX model na=nb=nc=34 and also the same characteristics with ARX model order 60. ARMAX opt has small differences in details of the bode-plot (in some points it is little more sensitive compared with other to tests). Also second test (namely ARMAX) is has some small details more than ARX model, but these details are very small scale and do not affect the model performance at all. Each model of three test scenarios presents very high efficiency in simulating the real data of the seismic events.

Conclusively for the study of multidimensional modeling of both building it is selected ARX modeling due to the ability of powerful results in simulation and parametric modeling combined with very light computation requirements related the other two methodologies.

Multidimensional modeling with ARX

Previous analysis reveals that although ARMAX achieves with lower order optimum model fitting, it has the big disadvantage of computational requirements. Also ARX are similar powerful in optimum model selection although the order is higher. Both reasons indicate that ARX modeling will be used for the study.

Above analysis were on one component (North-South component). The analysis now is on every component (North-South, East-West, and Vertical).

Event select

More than 25 seismic events that occurred before the big seismic event of 6.4 M and also more than 15 seismic events that occurred after the seismic event have been analyzed with parametric methods in order to reveal possible changes in the frequency response functions of the systems. The analytical methodology follows the basic steps as above but now with multidimensional characteristics. Such for every seismic event there is analysis of 3 components namely North-South, East-West and vertical. Below are presented the steps of multidimensional analysis of one seismic event. Exactly the same methodology become for all seismic events of the catalog in chapter 4.3 (totally more than 40 seismic events).

Multidimensional recording (raw data)

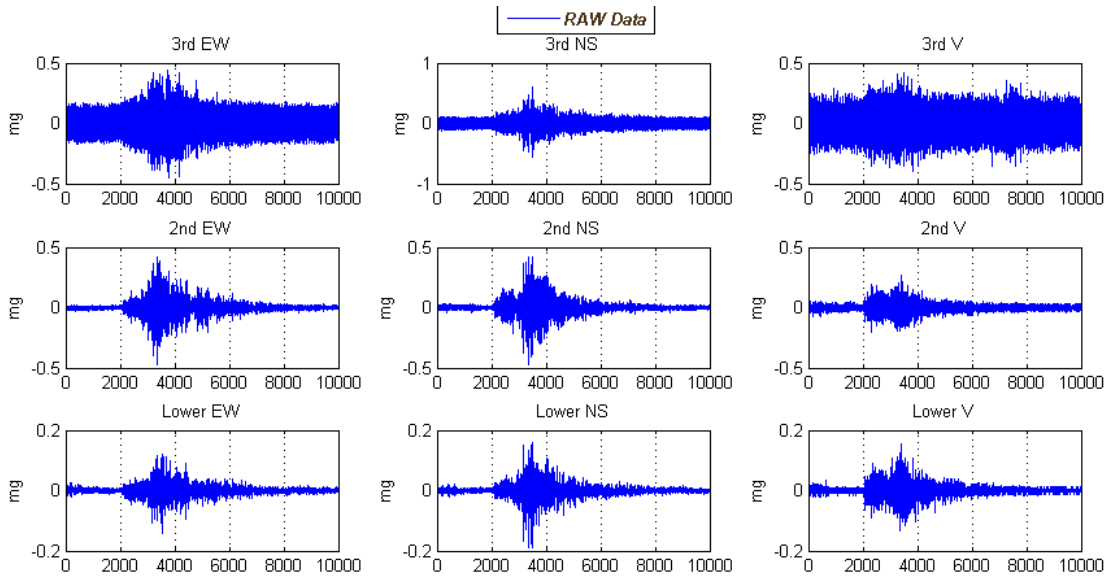

Figure G.25. Recording data with mean removal and transform in mg at all components on every floor. left column presents east-west component, mid column North-South and right is vertical component. Horizontal axe are the samples with sampling rate 125 Hz. Vertical axe is acceleration in mg.

Data have been transformed in mg and there is mean and trend removal as previous analysis (ARX analysis). On each column there is a specific component (et North-South) and in every line the specific floor of the building. In this data analysis presentation data are for seismic event with the number code 4 for the old building. The exact same analysis procedure has been applied also in new building and also in every other seismic event from code numbers 1-25 (see Raw data Chapter 4.3). The excitation is on the lower floor and the acceleration response is of the 2nd and 3rd floor respectively. Also it is obvious that on the 3rd floor the noise level is much higher than other two floors. This noise level is removed and does not affect the performance of non-parametric analysis (PSD, FRF and Coherence) and parametric analysis (ARX).

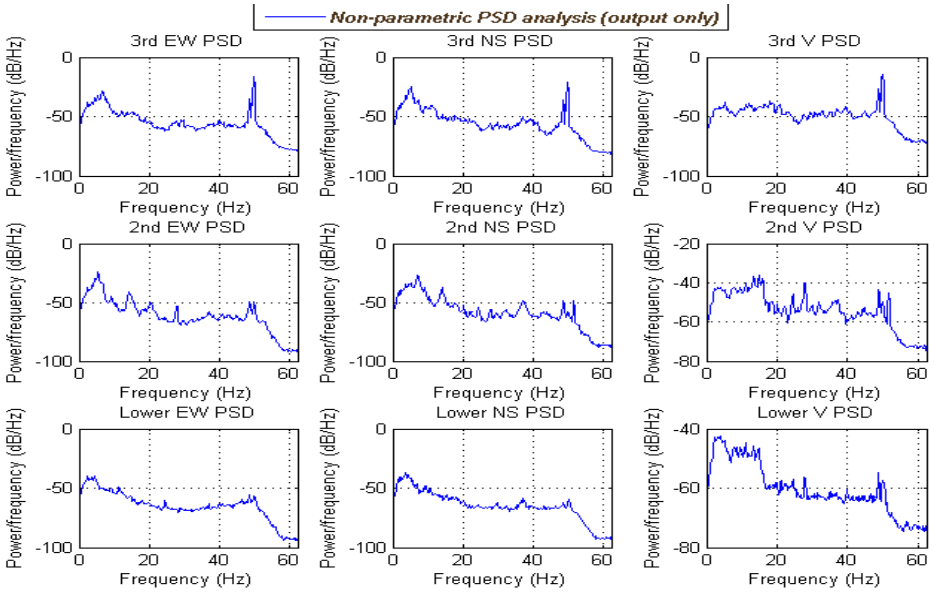

Figure G.26. Power spectral densities for every recording at every floor and component

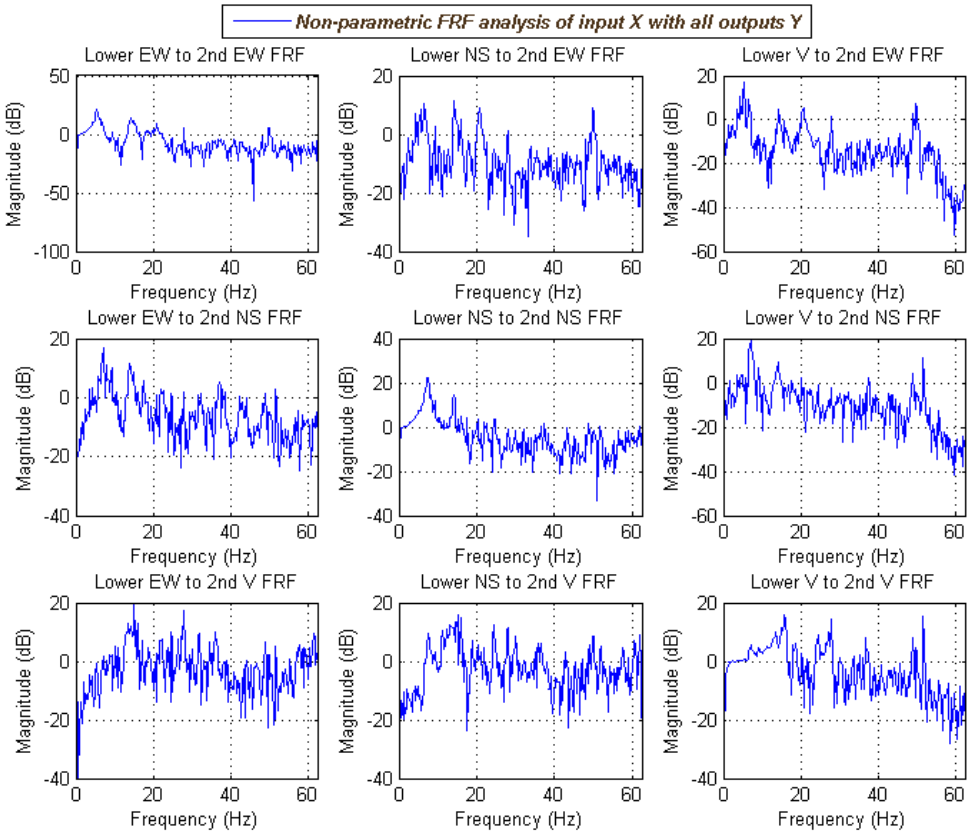

Figure G.27. Frequency response functions of every floor with the lower floor (for the same component)

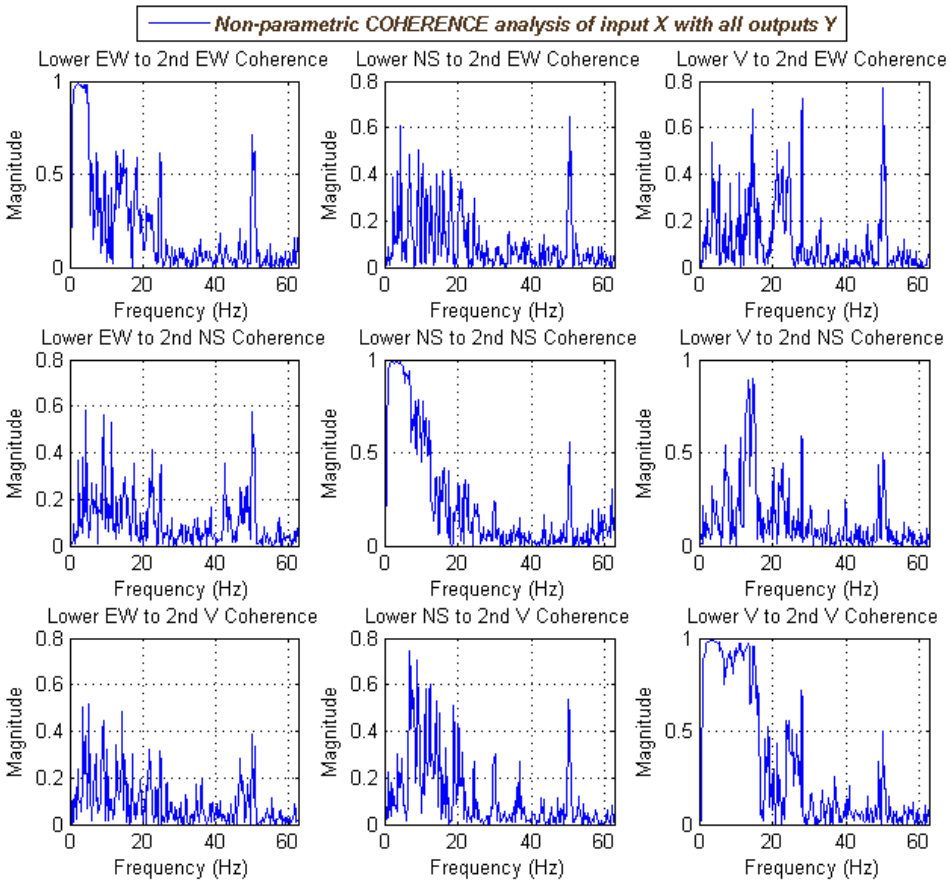

Figure G.28. Frequency coherences of every floor with the lower floor (for the same component)

PSDs, FRFs and frequency coherences non-parametric analysis for the multidimensional analysis of number code "4" seismic event for the old building. PSD plots present power spectral densities for each component (north0South, East-West and Vertical) for each floor (lower, 2nd, 3rd) of the old building. This enables us to study the effect of seismic acceleration and noise on each component at every floor of the building. Noise is also presented at 50 Hz (electricity network) and fundamental frequency is presented at every component at the same value. At the FRF plots it is selected to study the frequency response function of 2nd floor related to the lower floor. Every component of Lower floor (input-excitation) is correlated with every component of the 2nd floor (output-response) in order to reveal how each component of input react and effect each component of the output. FRF plots reveal that each component affects with much higher amplitude the same component at response (for example NS-input to NS-output) than the other components (NS-input to EW-output or NS-input to Vertical output). The same analogy is presented in coherences diagrams. The respective components are reinforced much more than other components of input-output.

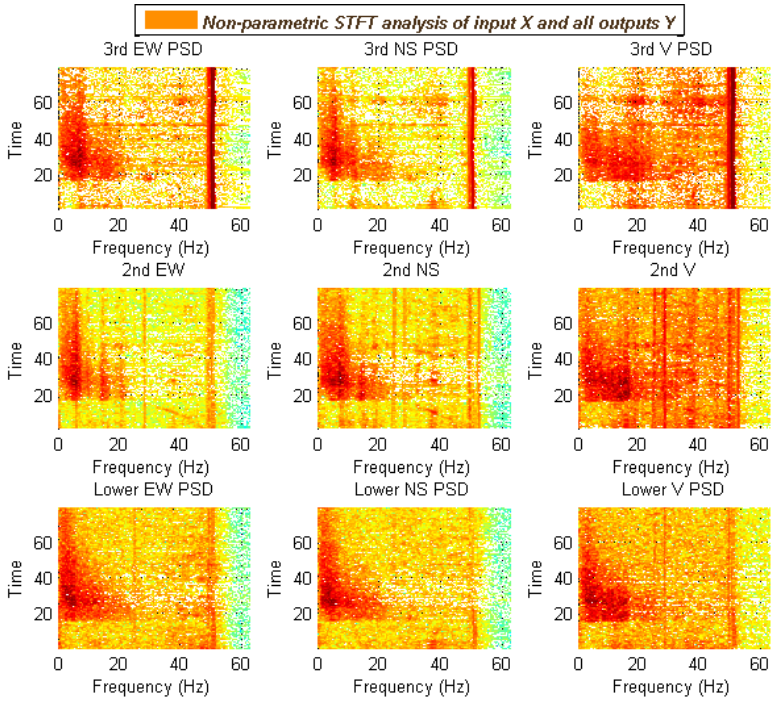

Short time Fourier transform for the above seismic data. Magnitude of seismic acceleration applied on each component and floor, related the specific time of occurrence is presented on each spectrogram.

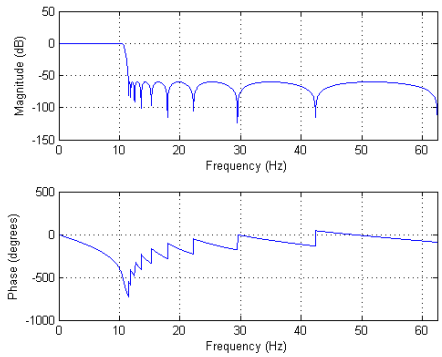

Figure G.29. Chebyshev filter frequency reqsponce (magnitude up, pahse down) with Low Pass filtering at 10.5 Hz

Filtering and re-sampling are again necessary in order to remove noise effect and reduce the quantity of data. After study of coherence frequency diagrams it is concluded that the appropriate frequency range is until the range of 10 Hz for the specific buildings. In precious analysis of ARX, ARMAX and ARMAX optimization, had been applied a filter until 20 Hz in order to study the possibility of resonance frequencies on that range and also the frequency response on that frequency range , although the frequency coherence between input and output there was very low. Figure presents the db attenuation and the phase (in degrees) of digital filter that is applied.

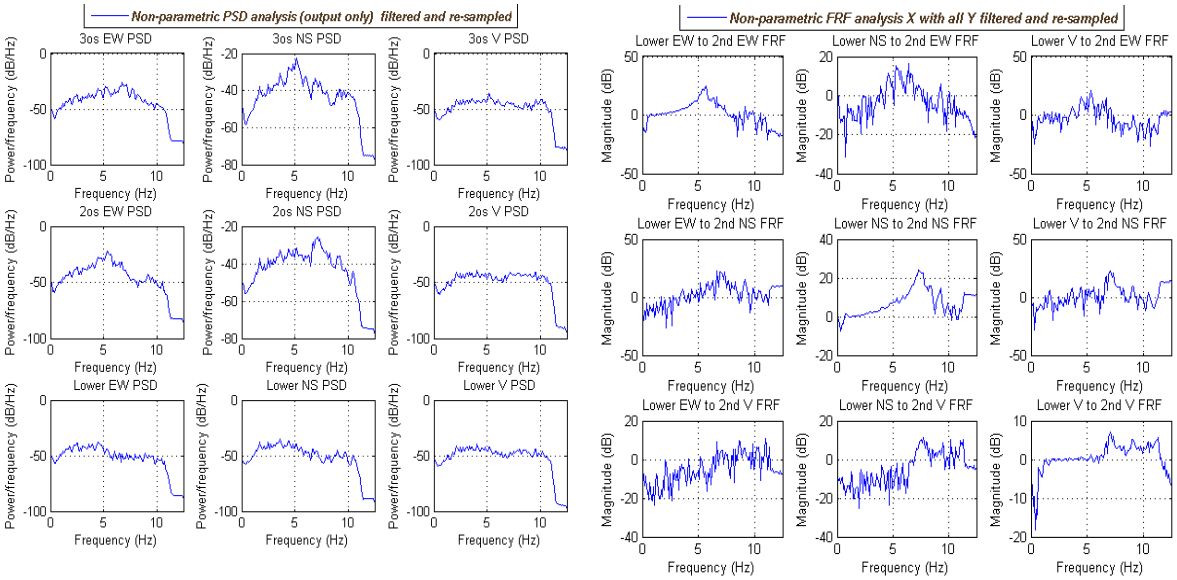

Figure G.30. PSD (left) and FRF (right) analysis of the filtered data. On PSD graphs (left side), up line is 3rd floor, mid is 2nd floor and lower line is lower floor of the old building TEI. FRF graphs (right side), up line is lower floor EW,NS & V components due to 2nd floor EW. Mid line is lower floor EW,NS & V components due to 2nd floor NS component, and lower line is lower floor EW,NS & V components due to Vertical component of 2nd floor.

PSDs and FRFs filtered and re-sampled at an order of 5. Data are re-sampled in lower order in order to minimize the amount of repeated information and such the amount of data, without lose valuable information, and maximize the power computation on autoregressive modeling.

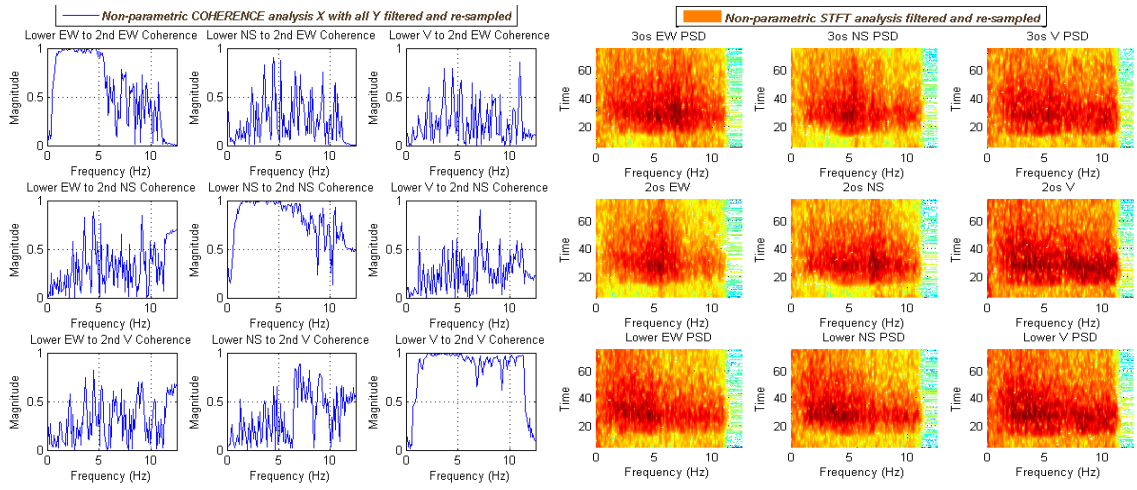

Figure G.31. Frequency coherence and STFT diagrams of the filtered data

PSD, FRF, Frequency coherence and STFT diagrams after filtering and re-sampling verify that all valuable information are included also after filtering without any valuable information losses.

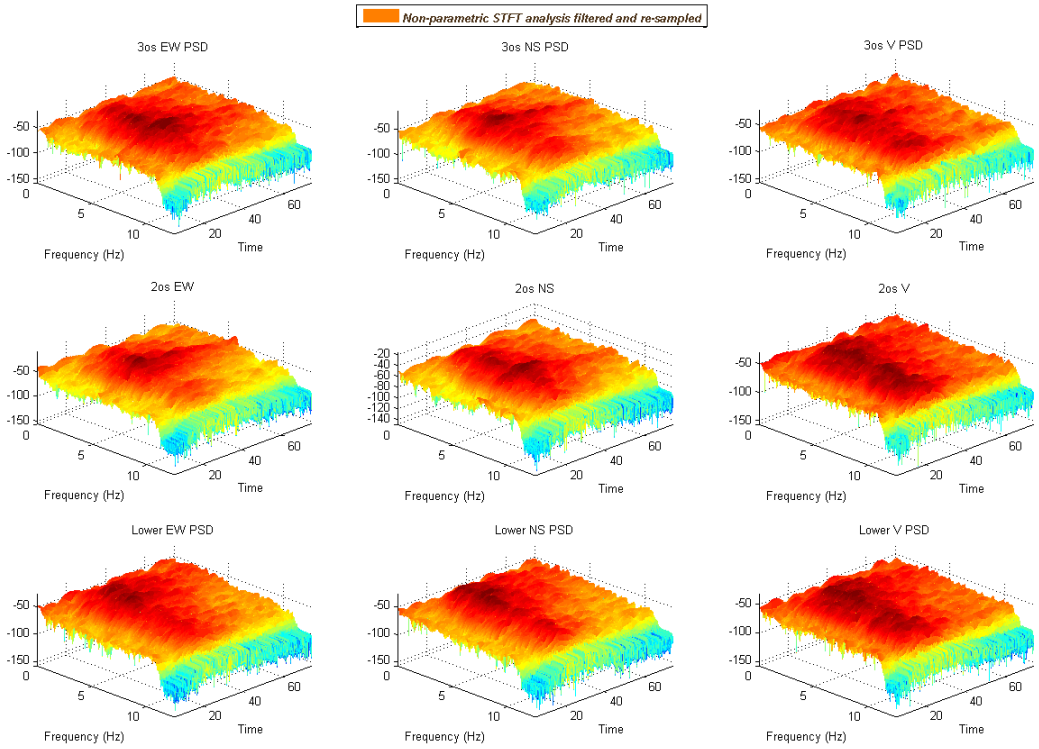

Figure G.32. 3D plots of the STFT data to reveal the amplitude of accelerations in time and space

3D plot of short time Fourier transform of seismic event with code 4 for the old building after low pass filtering at 10.5 Hz and re-sampling of 125 Hz at an order of 5. Darker areas reveal higher magnitude of acceleration (or higher acceleration) in these specific frequencies on specific times. The magnitude follows the pattern of accelerograph in figure of RAW data. When the S wave affect the structure (at the time of 30 seconds) the frequency effect almost on the whole frequency range of 10 Hz.

Search for optimum model order

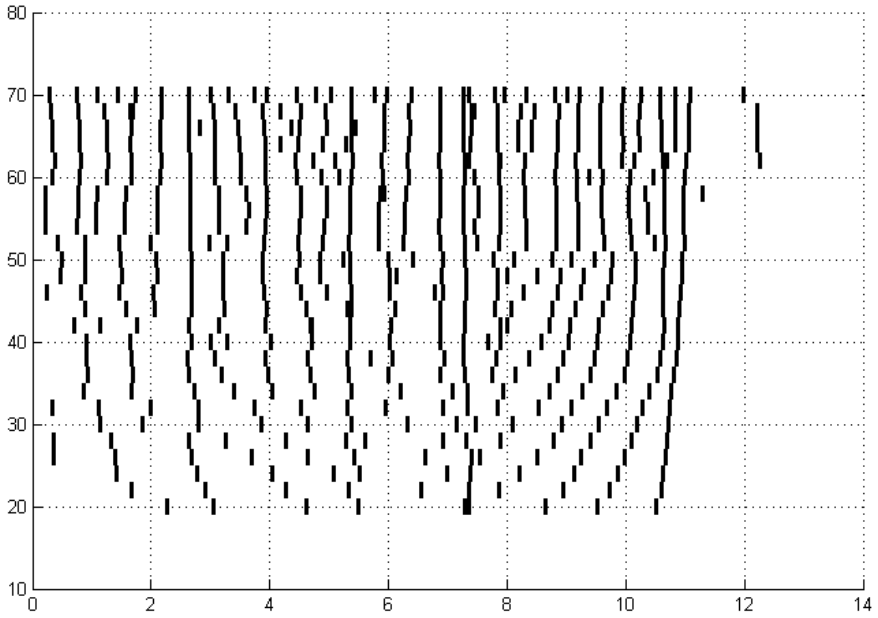

Figure G.33. Stabilization diagram of multi-component ARX modeling from 10-70 model order

BIC, AIC and RSS/SSS criteria

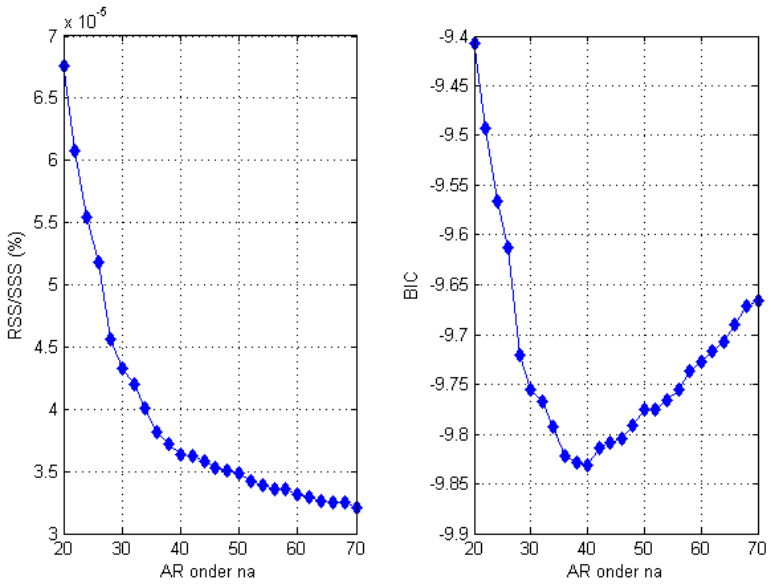

Figure G.34. Model order selection criteria (RSS/SSS and BIC)

Verification of the selected model by ACF of residuals between model and RAW data

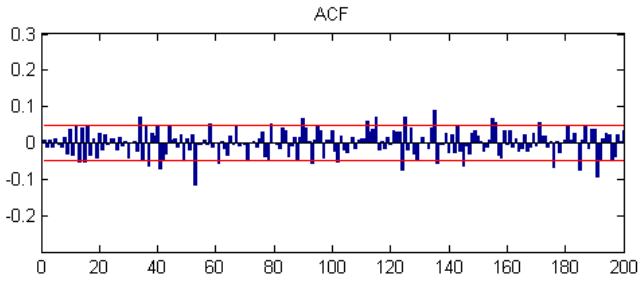

Figure G.35. Autocorrelation function of the "model to data" residuals of the designed ARX (40, 40, 1) model

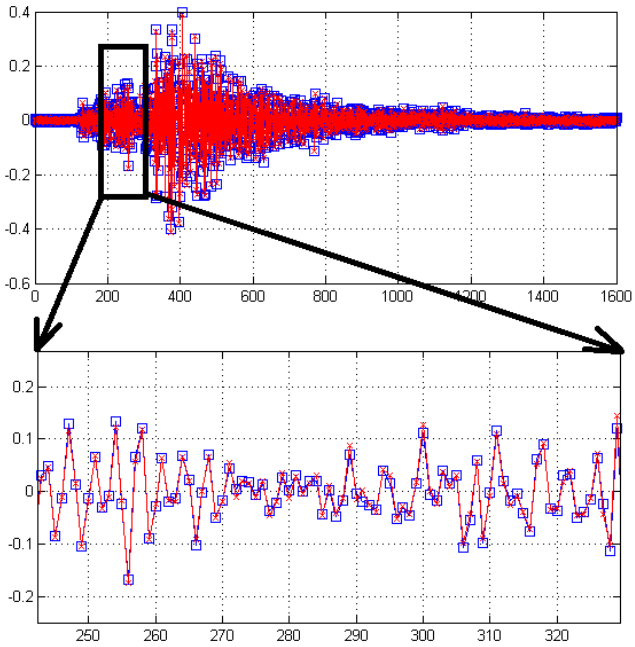

Figure G.36. ARX (40, 40, 1) model fitting on the data waveform

Bode plot of the system

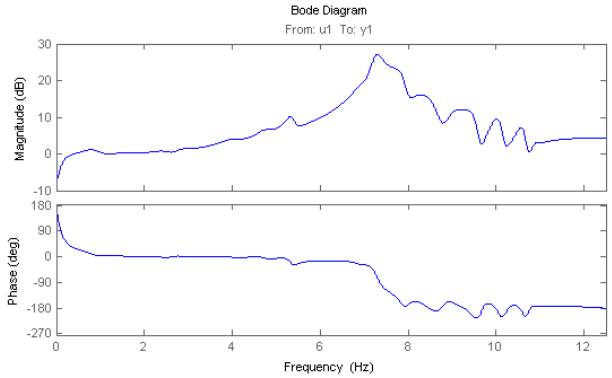

Figure G.37. Bode plot and phase of the designed system model ARX (40, 40, 1)

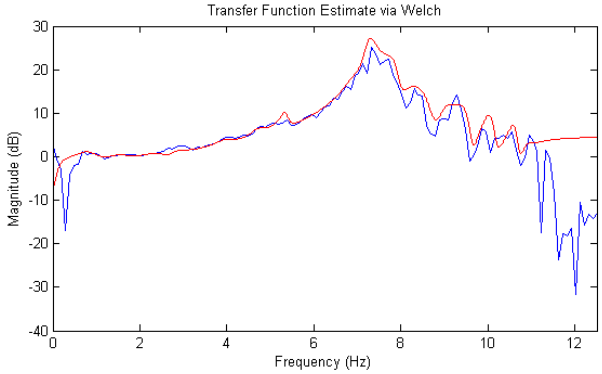

Figure G.38. Bode plot of the designed system model ARX (40, 40, 1)(red line) in comparison to raw data (blue line)

Frequency coherences between horizontal components

At this point will be demonstrated why seismic event of 6.4 affected the structural integrity of both buildings. Frequency coherence diagrams of the output (response) with the input (excitation) during earthquake 6.4 M will show what is the effect of excitation components on response components. Speaking more specifically, how North-South component of excitation (lower floor acceleration) affected or caused accelerations on North-South, East-West and vertical component of the responses (2nd and 3rd floor of the case study building). Also how East-West excitation component affected on North-South, East-West and vertical component of the responses. And also how Vertical component affected on North-South, East-West and vertical component of the responses. If there is correlation between those relations then there is twist and/or spin of the building, indicating high structural vulnerability and affect on dynamical parameters of the system (building as a system of transfer function of the building). Torsion modes affect with severity beams and plates of a concrete building providing possible micro-cracks and faults in the whole structure.

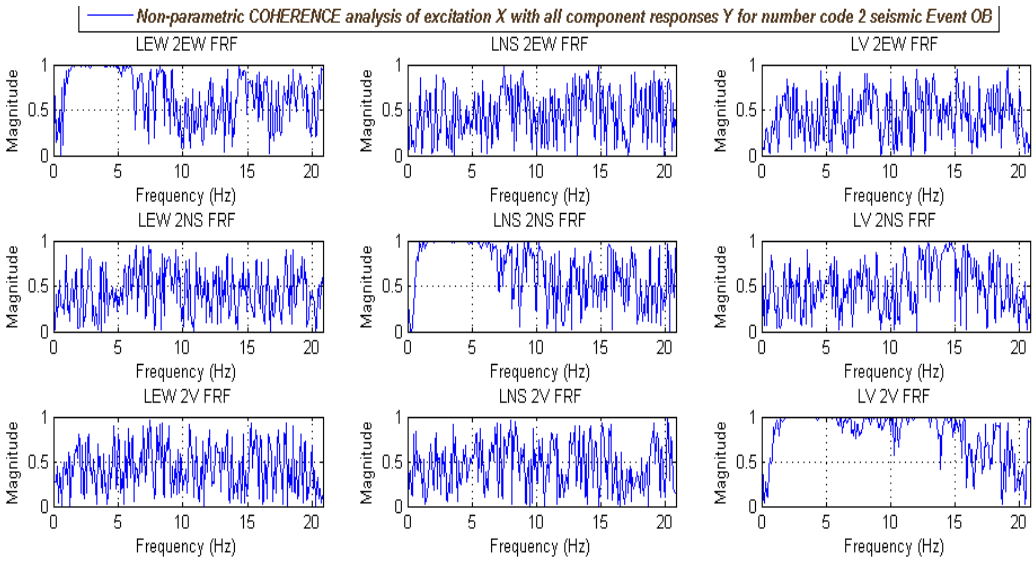

Figure G.39. Frequency coherence diagrams of excitation due to response for each component of input related to each component of output for seismic event code 2(before 6.4 M earthquake)

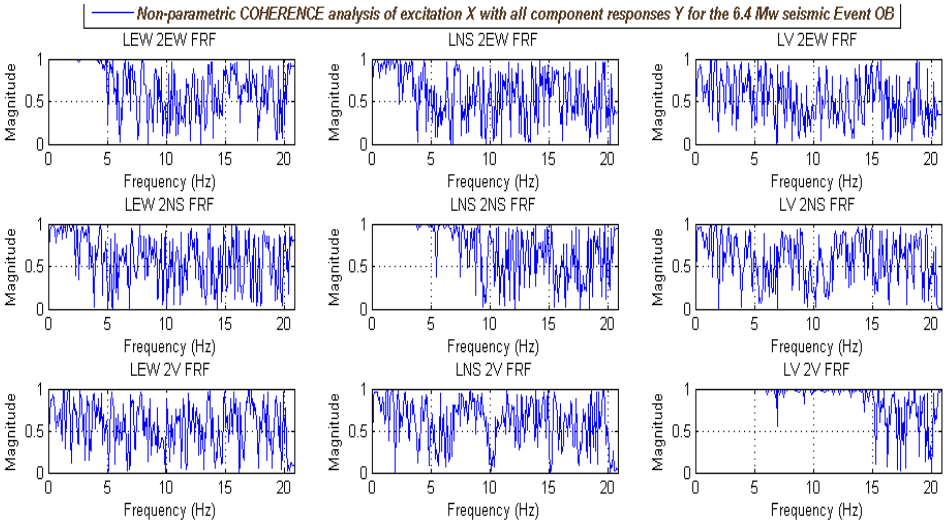

Figure G.40. Frequency coherence diagrams of excitation due to response for each component of input related to each component of output during seismic event of 6.4M

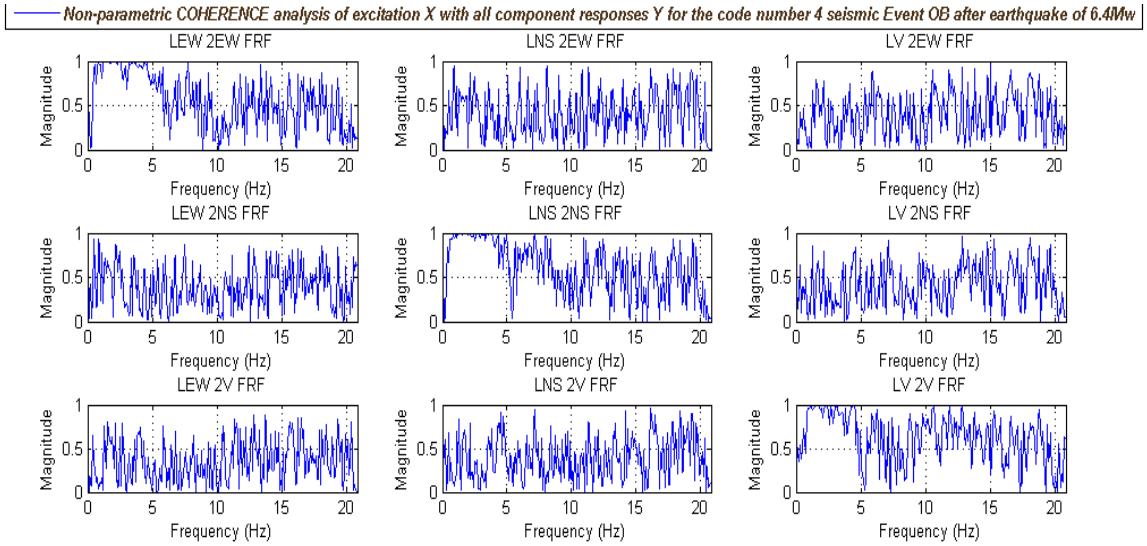

Figure G.41. Frequency coherence diagrams of excitation due to response for each component of input related to each component of output for seismic event code 4 (after 6.4 M earthquake)

Coherence between input (excitation) and output (response) before earthquake for New Building

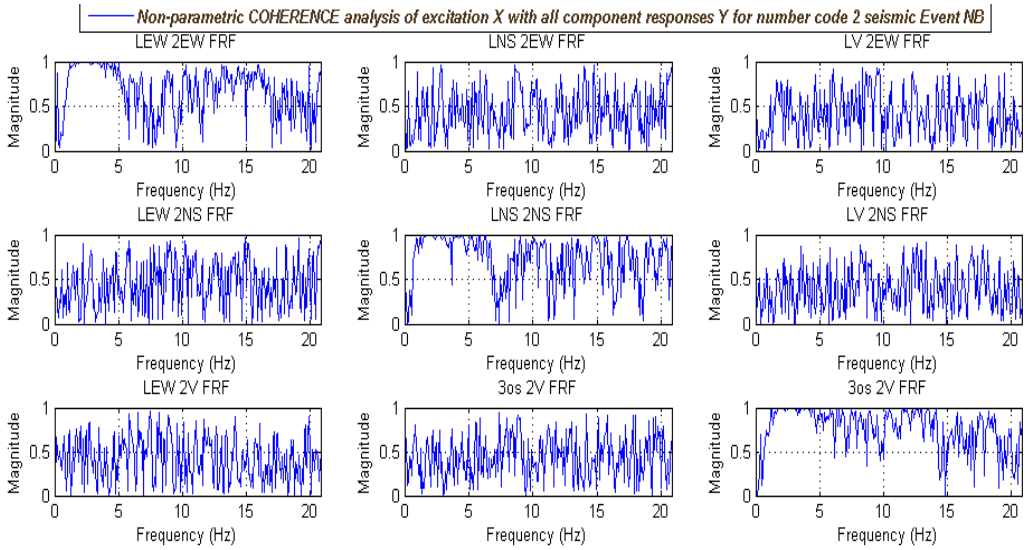

Figure G.42. Frequency coherence diagrams of excitation due to response for each component of input related to each component of output for seismic event code 2

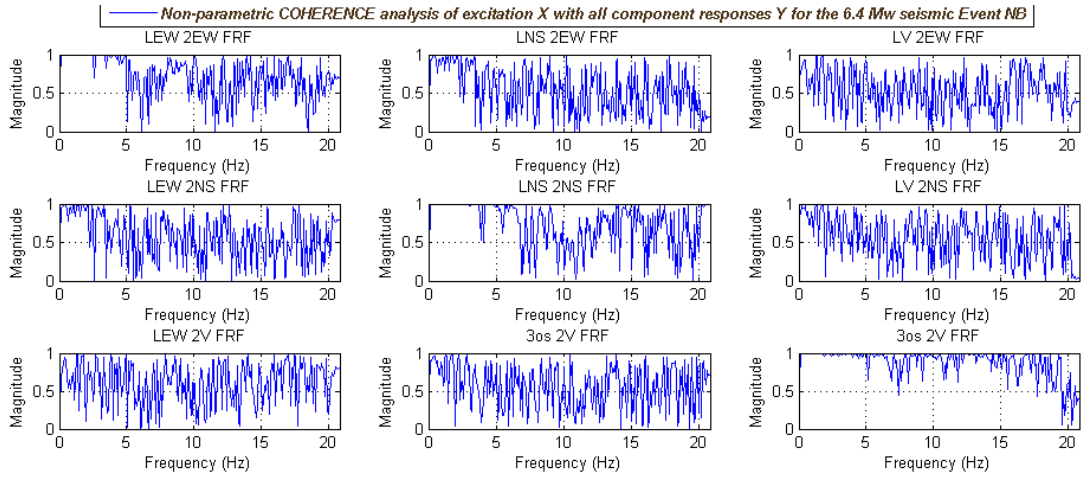

Figure G.43. Frequency coherence diagrams of excitation due to response for each component of input related to each component of output during seismic event of 6.4M

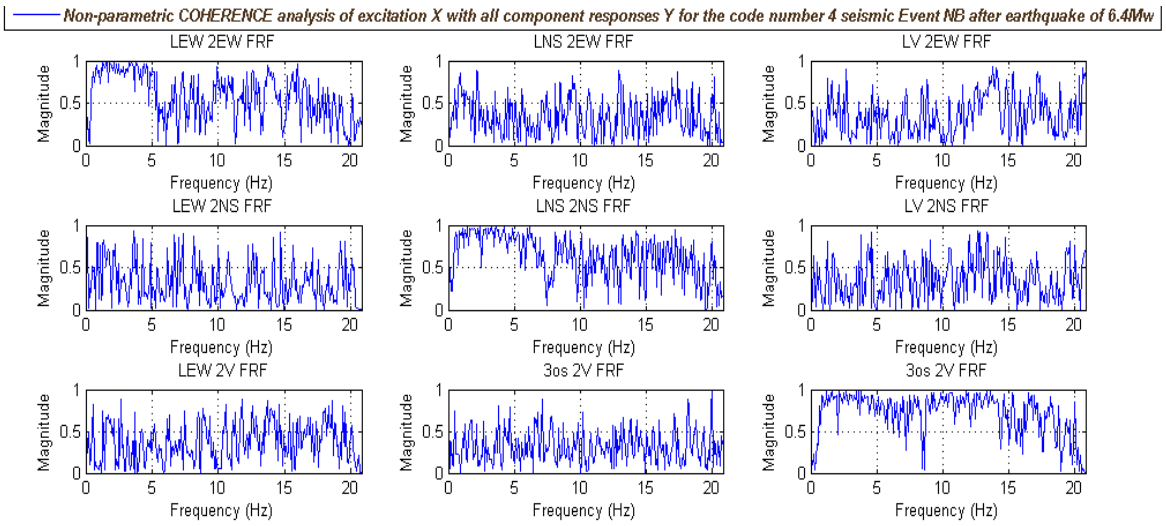

Figure G.44. Frequency coherence diagrams of excitation due to response for each component of input related to each component of output for seismic event code 4

Earthquake effected structural integrity of the OB and NB building. Frequency coherences diagrams reveal that earthquake of 6.4 M cause torsion on both old and new buildings. Similar specific tests repeated for more than 10 seismic events before and 10 seismic events after the earthquake of 6.4 M and revealed that coherence between different components existed only during 6.4 M earthquake. The structural characteristics of both buildings along with the dynamical parameters of both structures were affected. Below will be analyzed the bode plots of FRFs of the system (parametric analysis) in order to study it under a statistical manner. Also study how this change in coherence is correlated with the FRFs plots before and after the 6.4 M event.

Multidimensional modeling with ARX in a cell

All seismic events induced in a cell. In this cell specific model (ARX) with specific model order (40) is processed in order to produce bode plots of system for each seismic event. All models should have the same order in order to illustrate the same DOF of each excitation. The parameters are considered according with the previous analysis procedures of ARX, ARMAX and ARMAX opt modeling. Another one important parameter is that it is selected each component of the excitation (input) to be computed with the corresponding output (NS of input to NS of output). This is due to two reasons: **(a)** there is no coherence in other components (except the major earthquake) so any correlation of different direction component would be meaningful. **(b)** computing economy and presentation parsimony, otherwise the applied degree of freedom would be not 9 (as with current model) but 27 (in order every component of the system to be correlated with all other components.

Analysis of all ARX models

Plot of FRFs of bode plots before and after earthquake in Old Building

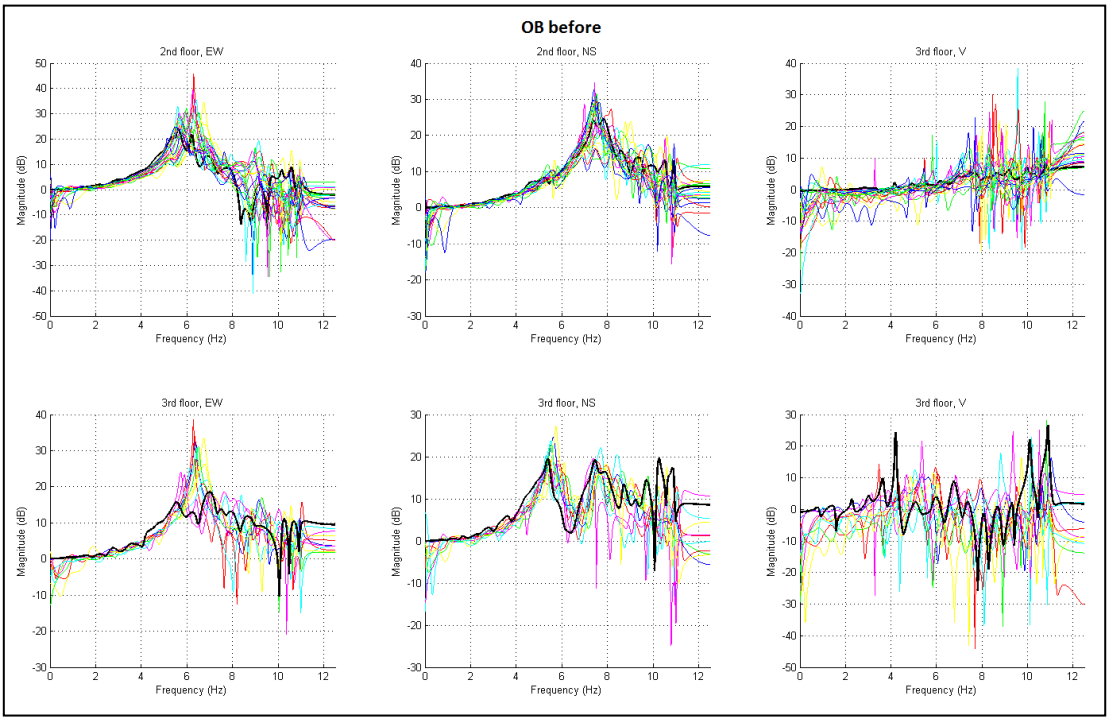

Figure G.45. Sum of bode plots for each floor and component for the old building before the earthquake (6.4M earthquake is indicated with bold black line)

Sum of bode plots for each floor and component for the old building before (up figure) and after (below figure) the earthquake (6.4M earthquake is indicated with bold black line.

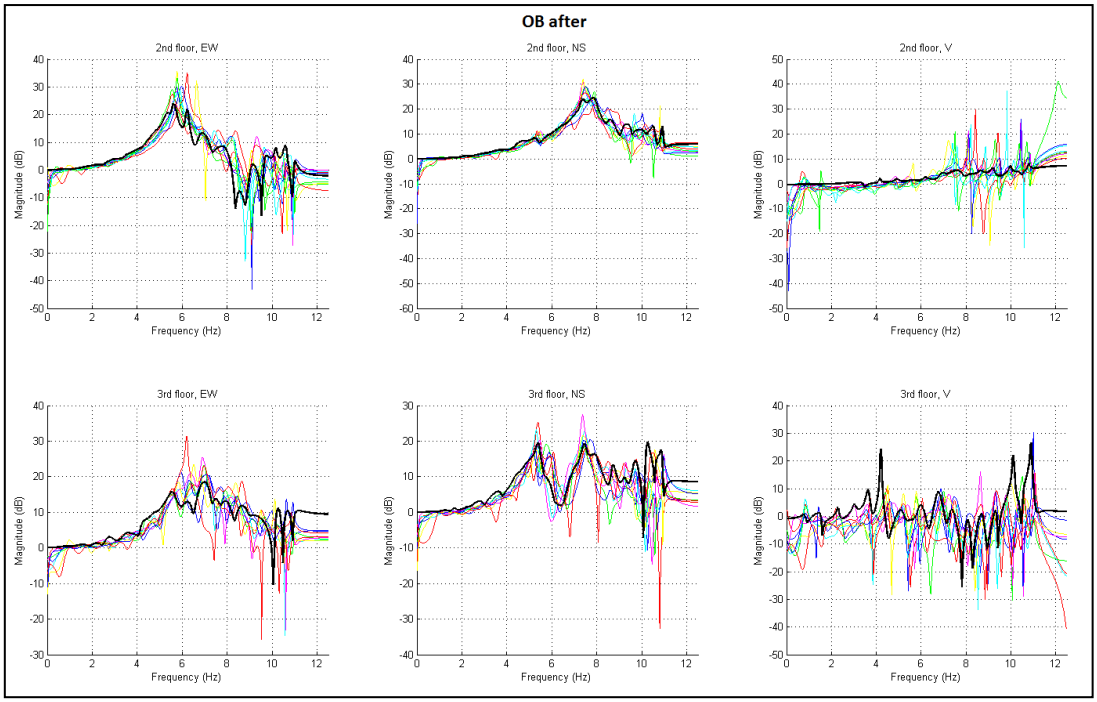

Figure G.46. Sum of bode plots for each floor and component for the old building after the earthquake (6.4M earthquake is indicated with bold black line)

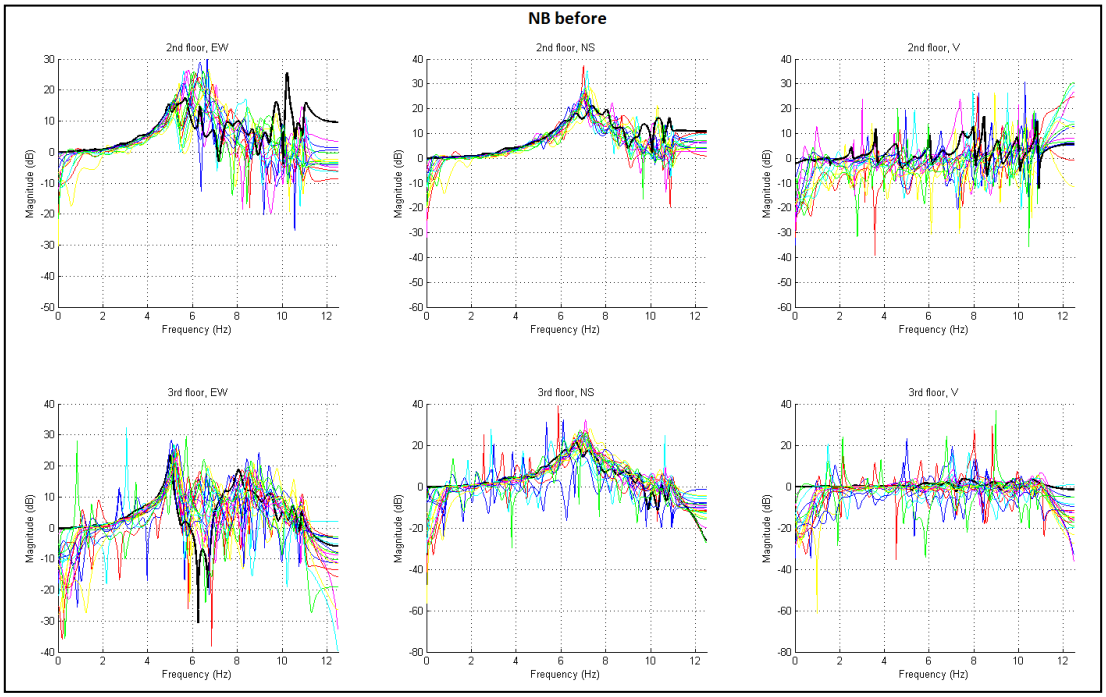

Figure G.47. Sum of bode plots for each floor and component for the new building before the earthquake (6.4M earthquake is indicated with bold black line)

Sum of bode plots for each floor and component for the new building before (up figure) and after (below figure) the earthquake (6.4M earthquake is indicated with bold black line)

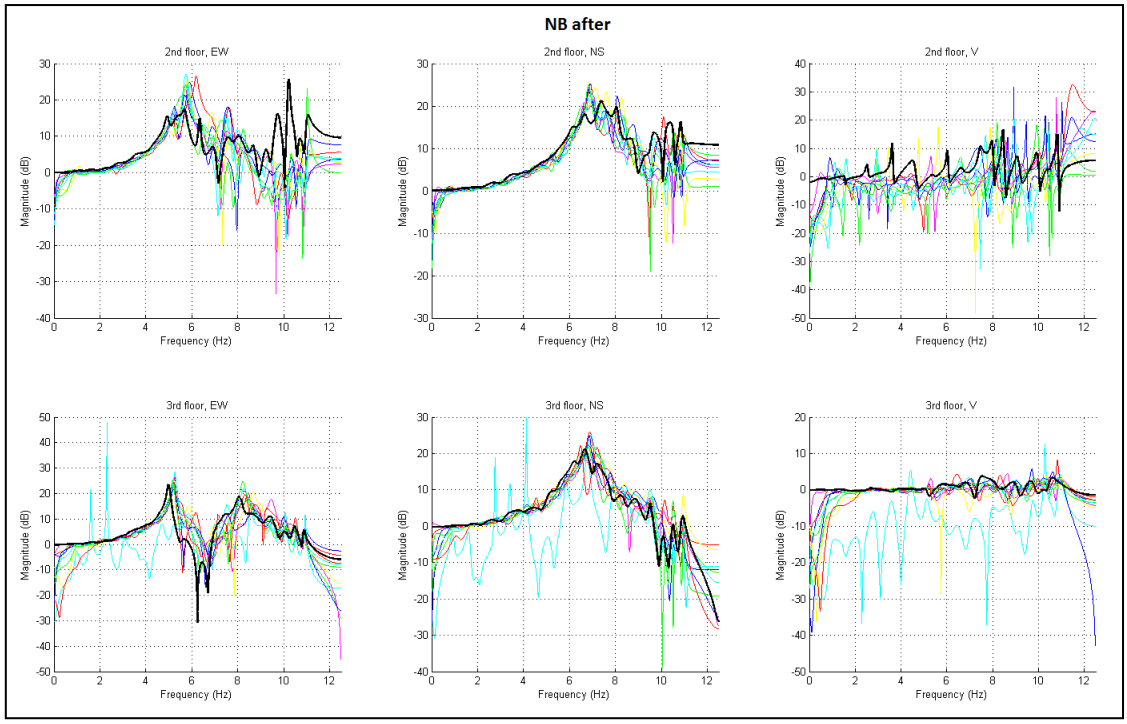

Figure G.48. Sum of bode plots for each floor and component for the new building after the earthquake (6.4M earthquake is indicated with bold black line)

Comparison of both plots with 6.4 M earthquake.

With the black bold line is the 6.4 M earthquake. It is in both diagrams, before and after 6.4 M earthquake, in order to compare the statistical range and amplitude of the earthquakes before and after due to a stable FRF graph of 6.4 M. Bode-plot diagrams present that before 6.4 M the bode plots have a specific deviation and amplitude, which is verified under a sum of bode plots. Also the bode plots after the 6.4 M have specific deviation and amplitude which is verified under a sum of bode plots. The critical point is that if it is compared a statistical sum of bodeplots, before and after the major earthquake, the diagrams are different. Such from the parametric FRF plots, there is change in FRF of the system after the 6.4 M earthquake, which implies change in dynamical parameters of the system (from the time that FRF is damage sensitive parameter). In chapter 6 there is analysis of the distribution of this parameter vector (parameter vector of the parametric FRF bodeplot) in order to check if the change of FRF bodeplots is significant and reveals change in dynamical parameters of the buildings.

Appendix H: Acceleration recordings before earthquake of 6.4 M

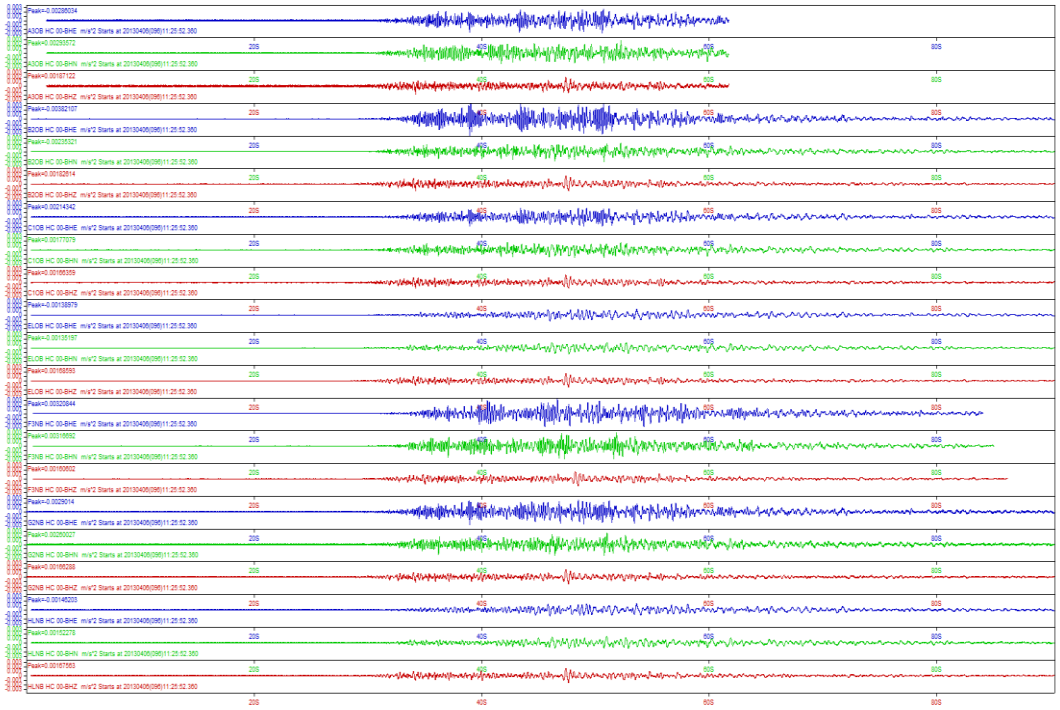

Figure H.1. Seismic acceleration recordings from 2013-04-06 11:26:22 UTC earthquake

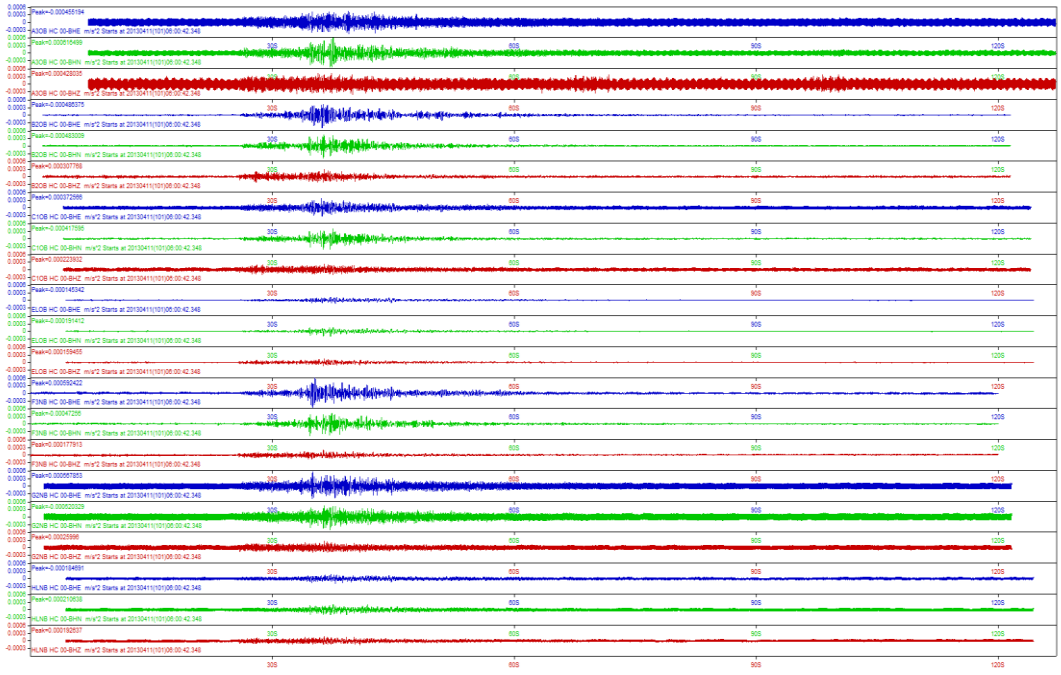

Figure H.2. Seismic acceleration recordings from 2014-04-28 00:43:04 UTC earthquake

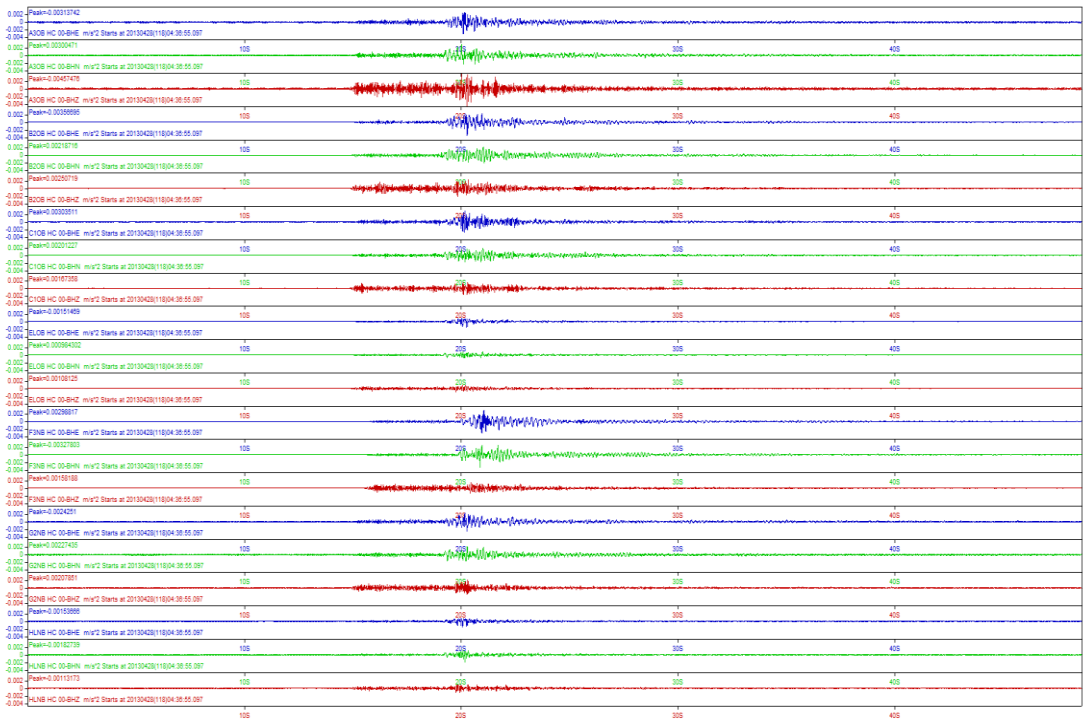

Figure H.3. Seismic acceleration recordings from 2014-04-28 04:37:25 UTC earthquake

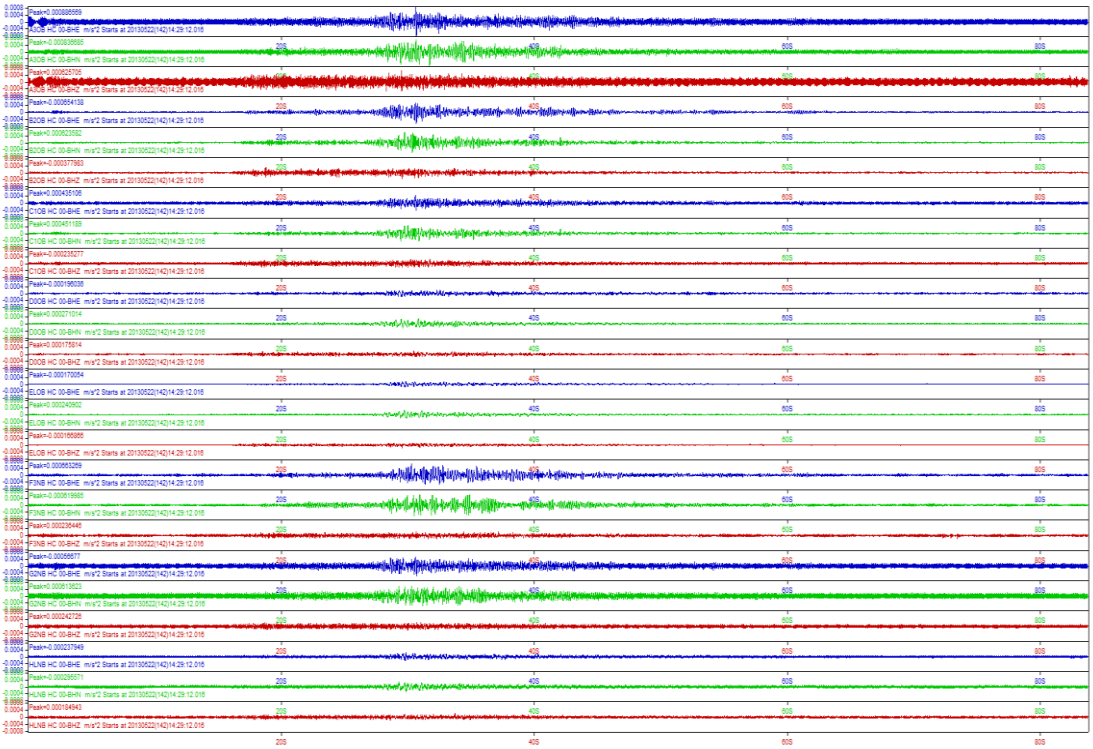

Figure H.4. Seismic acceleration recordings from 2014-05-22 14:29:42 UTC earthquake

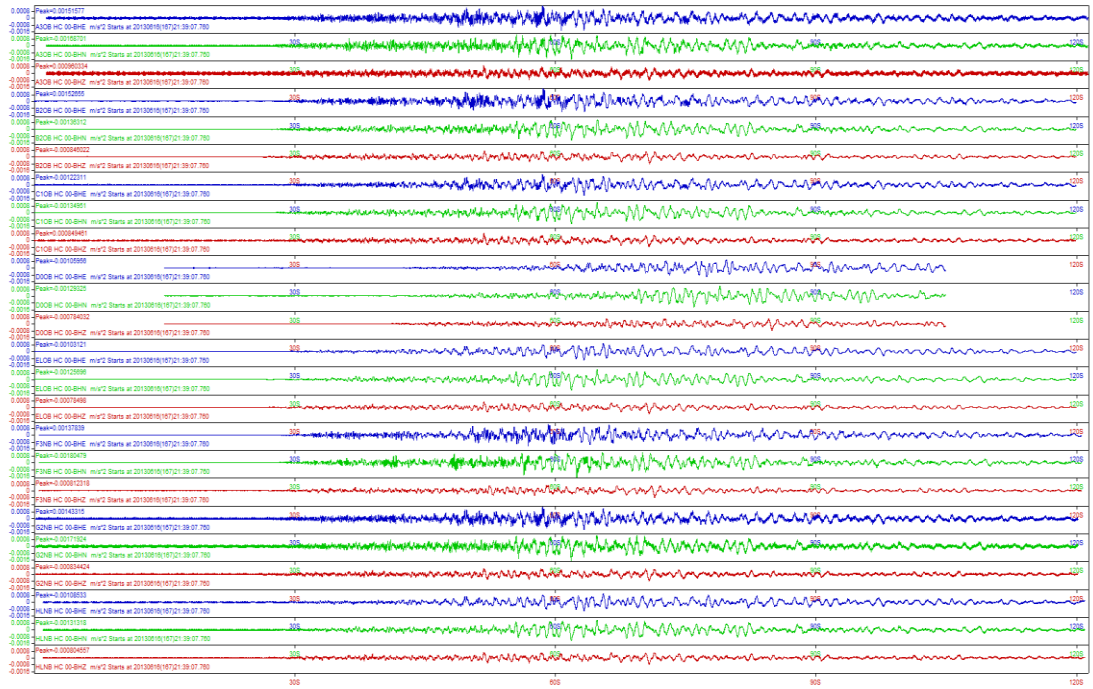

Figure H.5. Seismic acceleration recordings from 2014-06-16 21:39:37 UTC earthquake

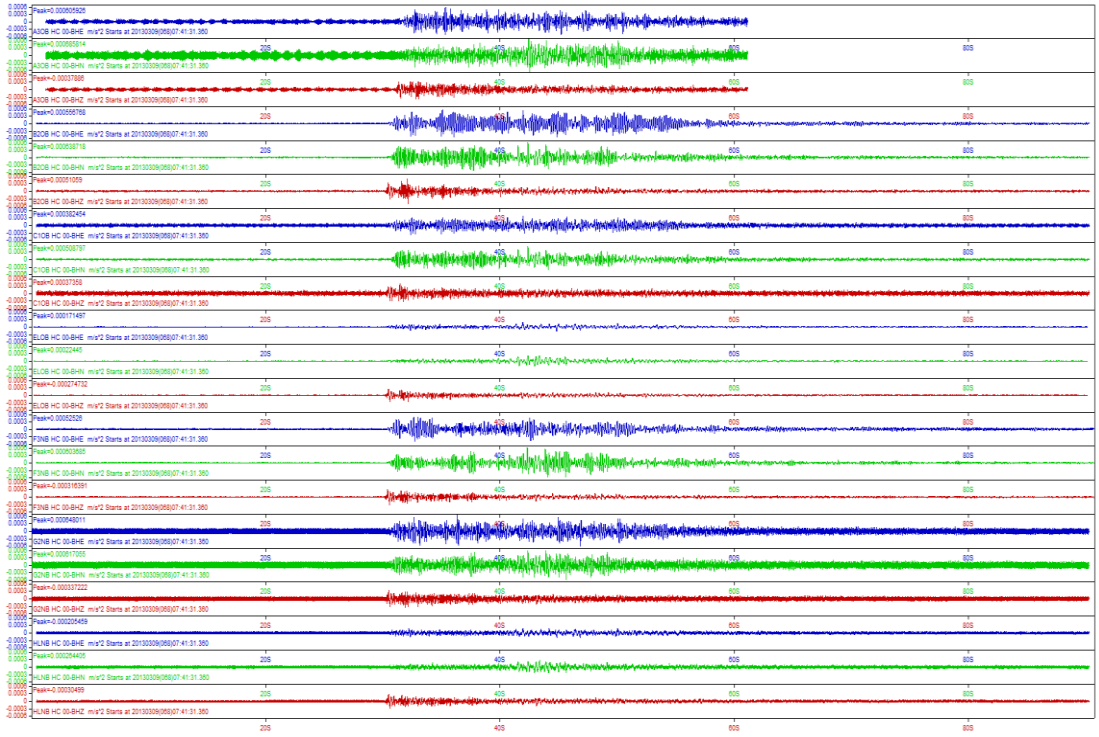

Figure H.6. Seismic acceleration recordings from 2013-09-09 07:42:01 UTC earthquake

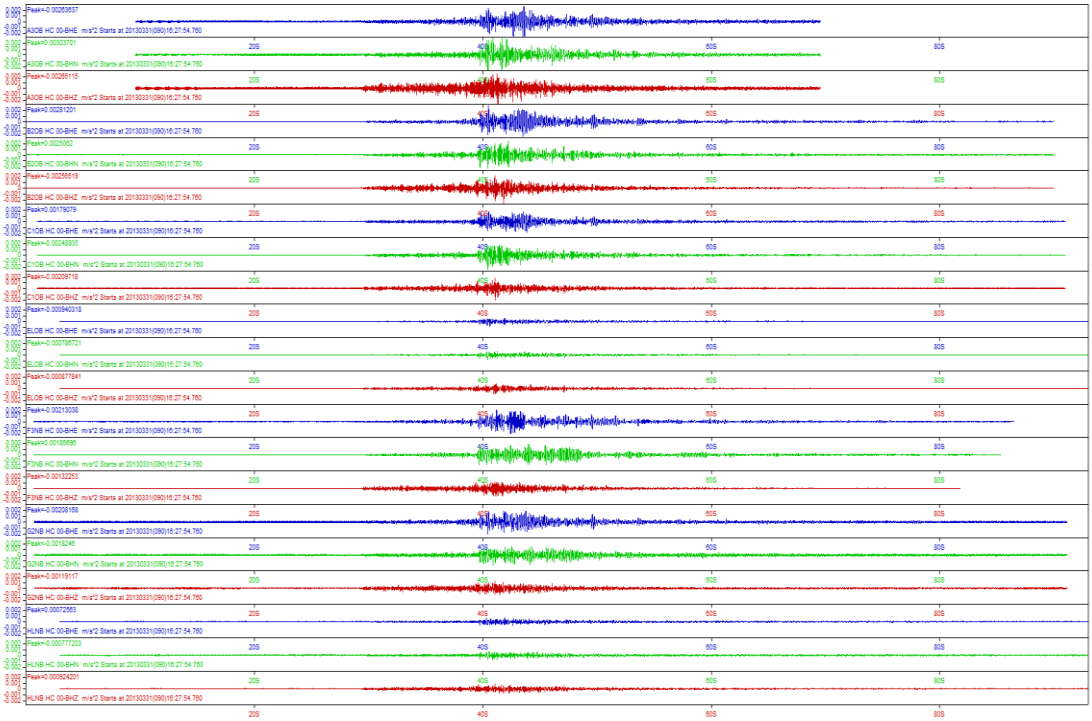

Figure H.7. Seismic acceleration recordings from 2014-03-31 16:28:24 UTC earthquake

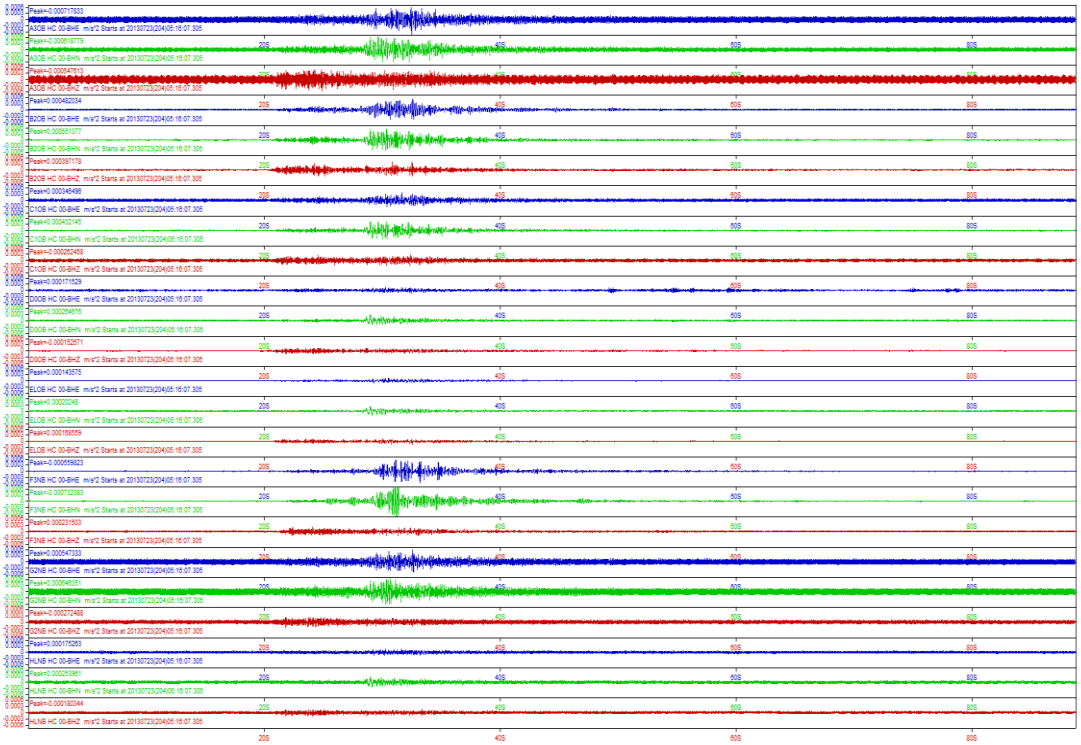

Figure H.8. Seismic acceleration recordings from 2014-07-23 05:16:37 UTC earthquake

Appendix I: Acceleration recordings after earthquake of 6.4 M

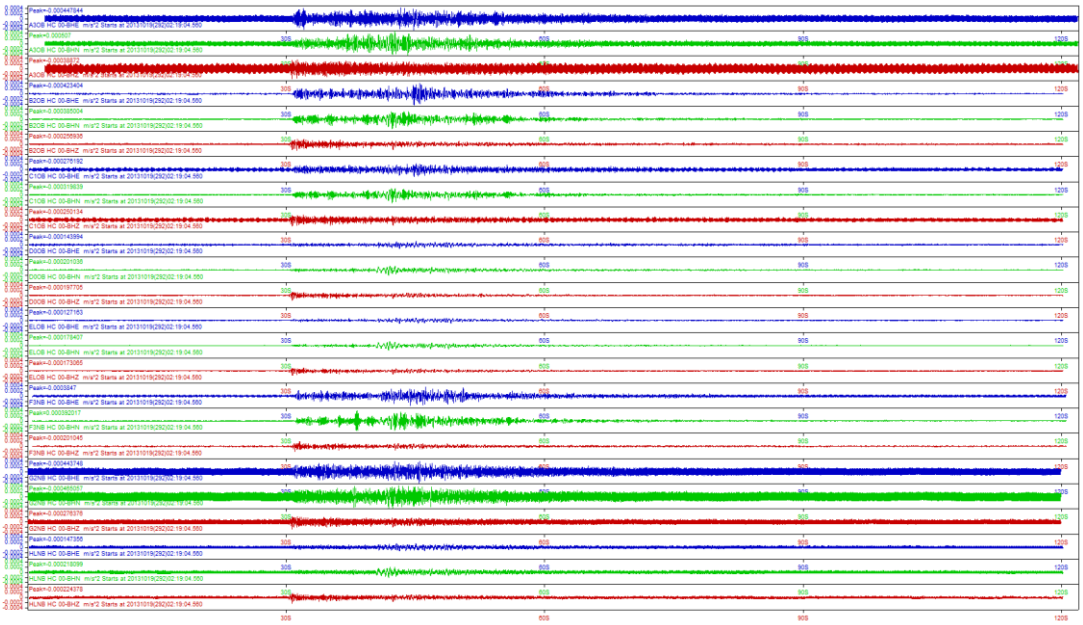

Figure I.1. Seismic acceleration recordings from 2013-10-19 02:19:34 UTC earthquake

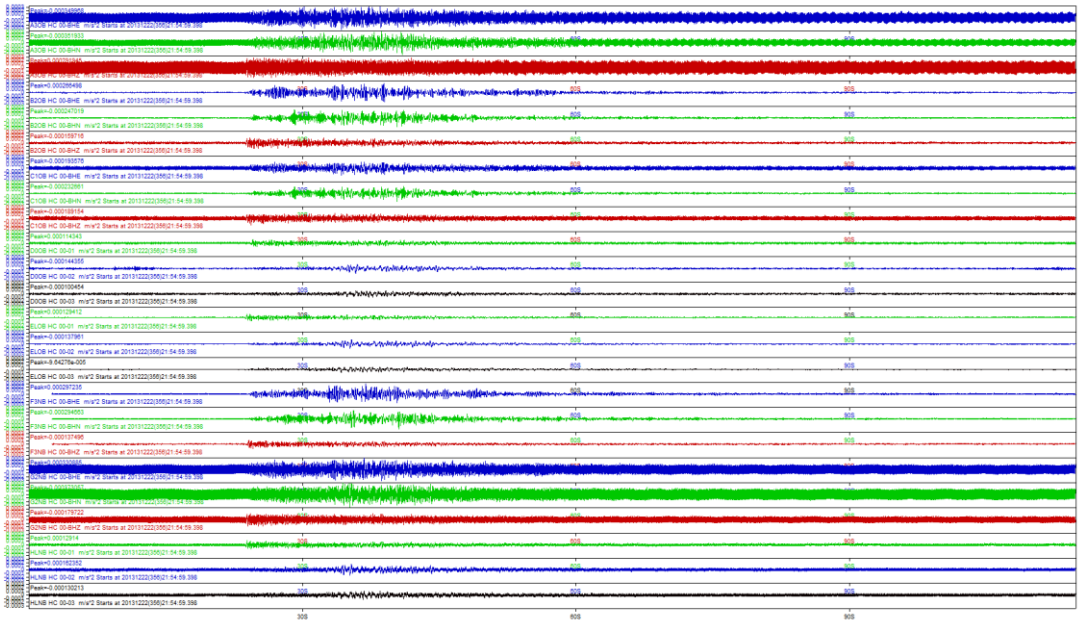

Figure I.2. Seismic acceleration recordings from 2013-12-22 21:55:29 UTC earthquake

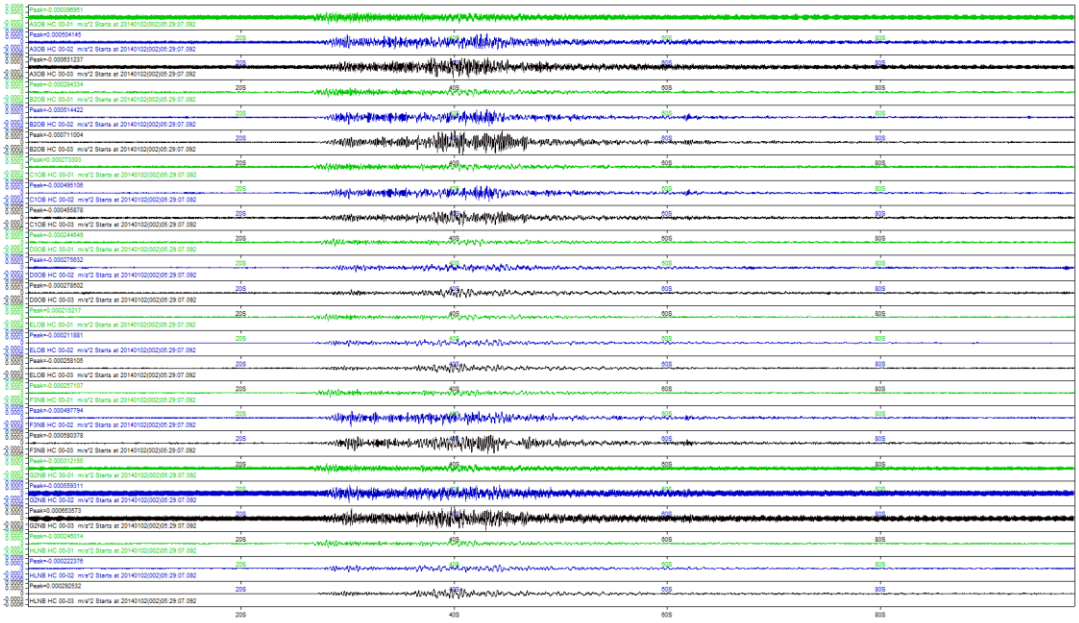

Figure I.3. Seismic acceleration recordings from 2014-01-02 05:29:07 UTC earthquake

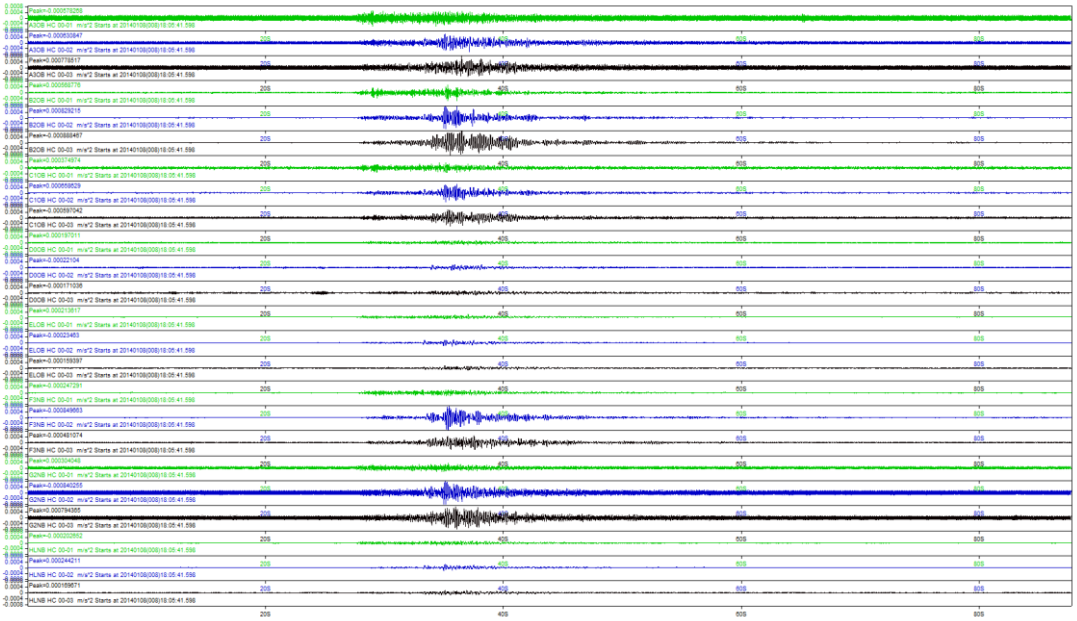

Figure I.4. Seismic acceleration recordings from 2014-01-08 18:06:11 UTC earthquake

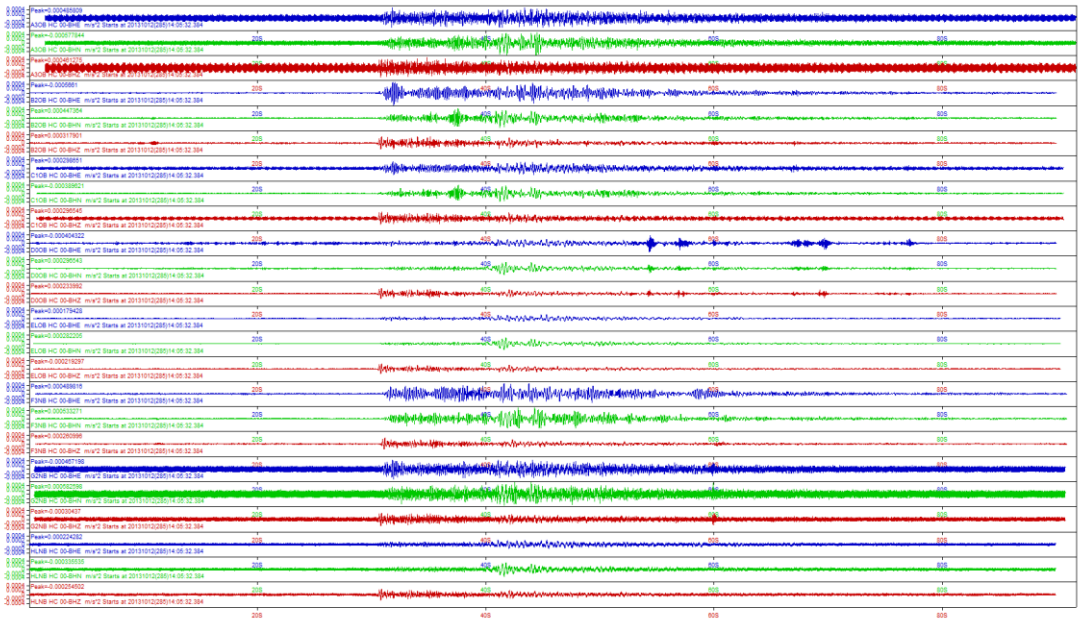

Figure I.5. Seismic acceleration recordings from 2013-10-12 14:06:02 UTC earthquake

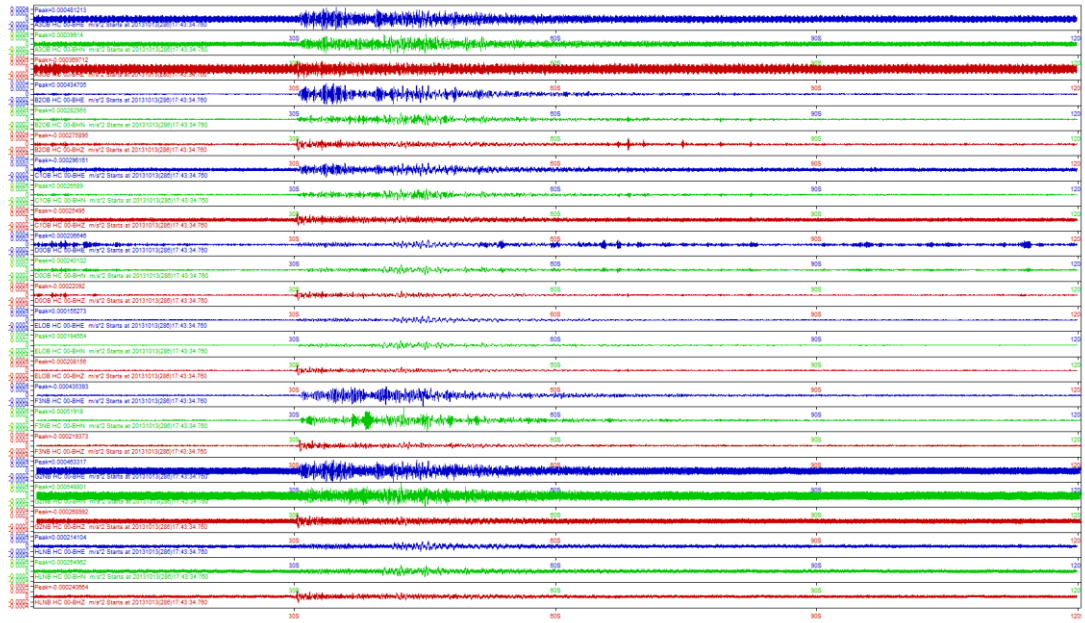

Figure I.6. Seismic acceleration recordings from 2013-10-13 17:44:04 UTC earthquake

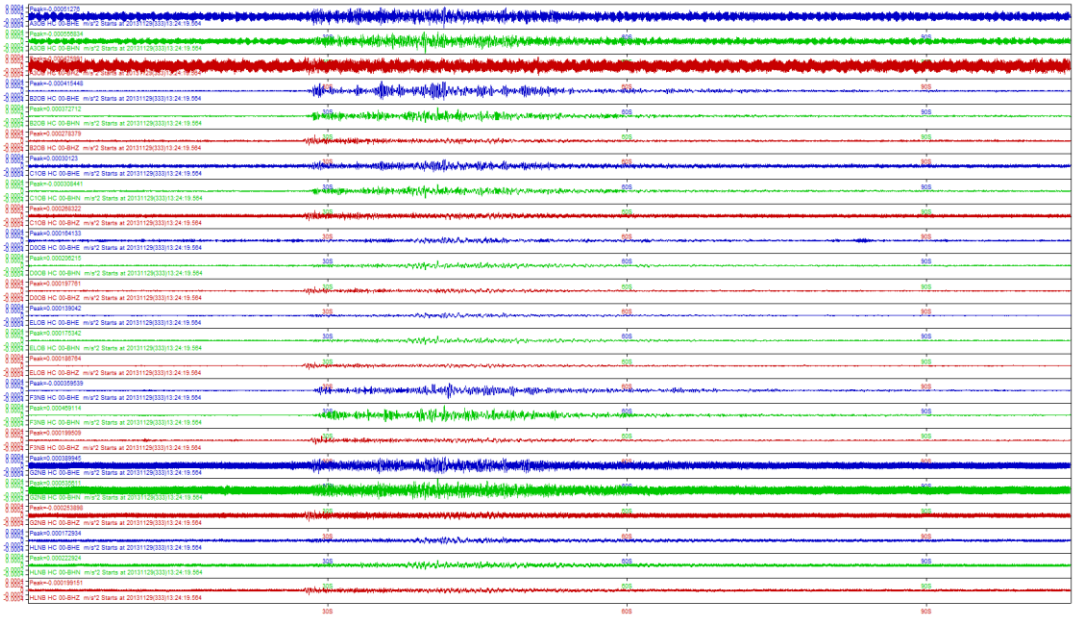

Figure I.7. Seismic acceleration recordings from 2013-11-29 13:24:49 UTC earthquake

Figure I.8. Seismic acceleration recordings from 2013-11-07 19:41:22 UTC earthquake

Appendix J: Ambient noise recordings

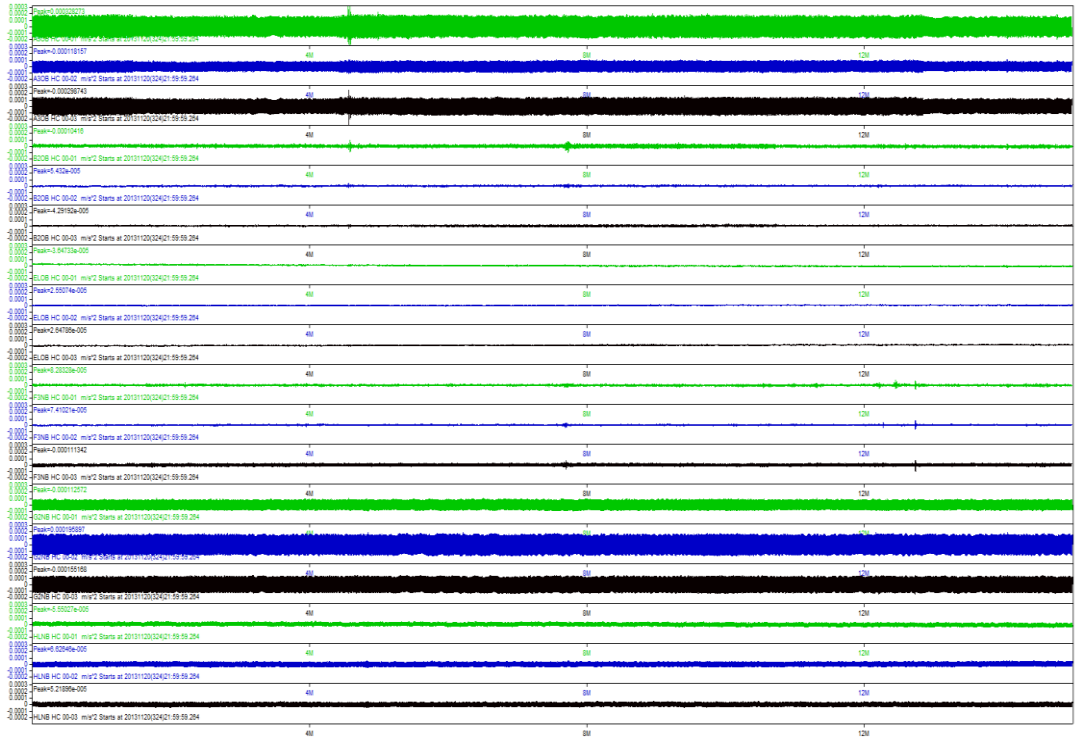

Figure J.1. 20 minutes ambient noise recording at 2013-11-20 21:59:59 UTC

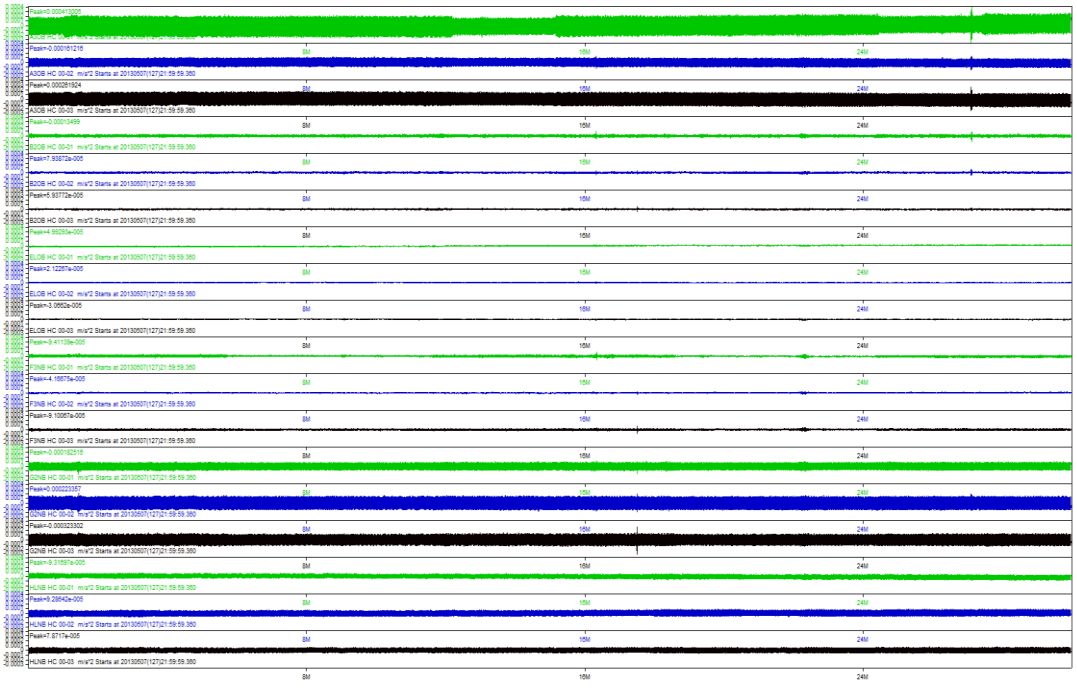

Figure J.2. 20 minutes ambient noise recording at 2013-05-07 21:59:59 UTC

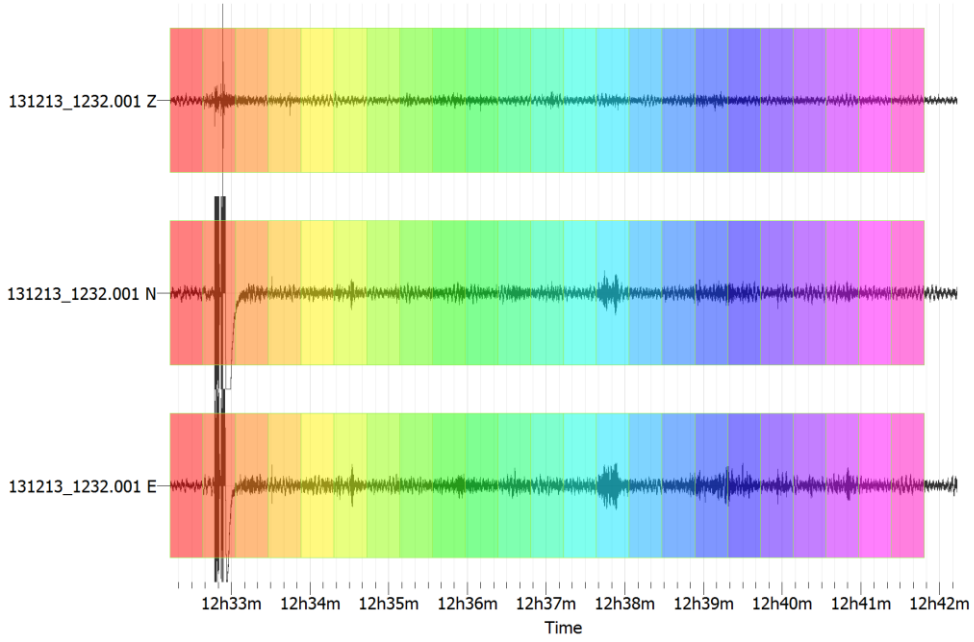

Figure J.3. 10 minutes ambient noise recording at 2013-12-13 12:33:00 UTC

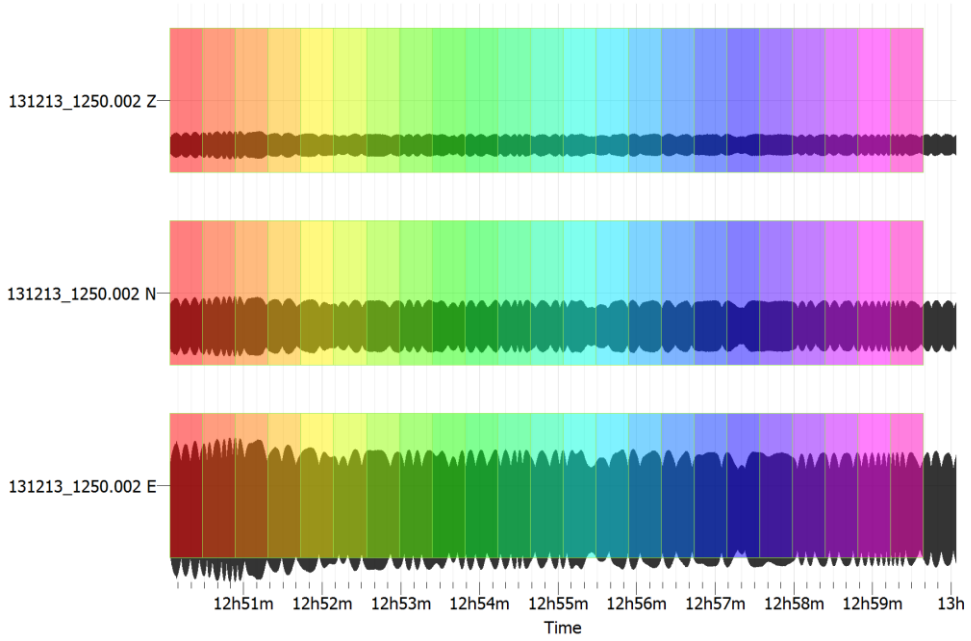

Figure J.4. 10 minutes ambient noise recording at 2013-12-13 12:51:00 UTC

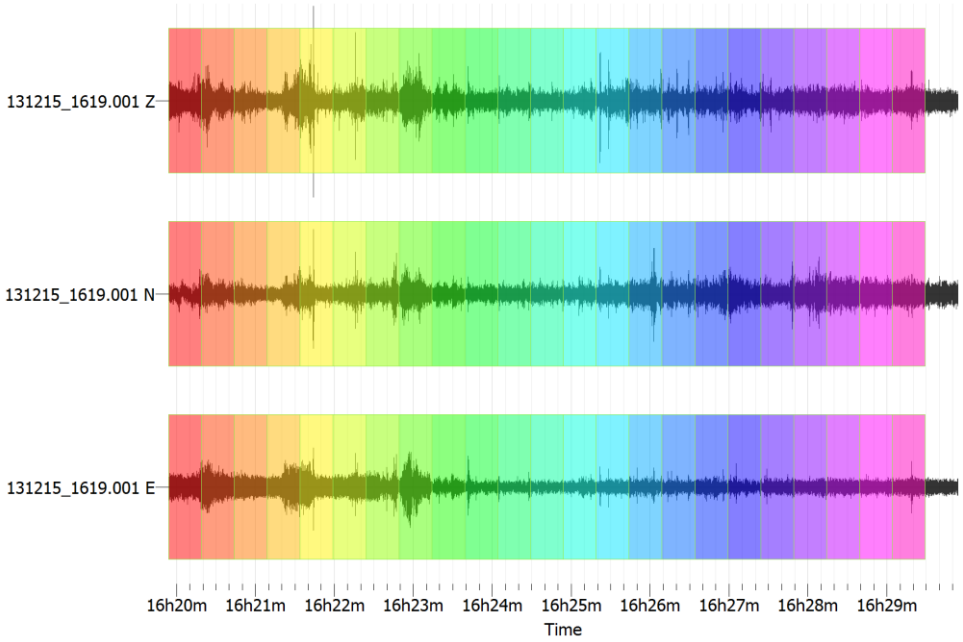

Figure J.5. 10 minutes ambient noise recording at 2013-12-15 16:19:00 UTC

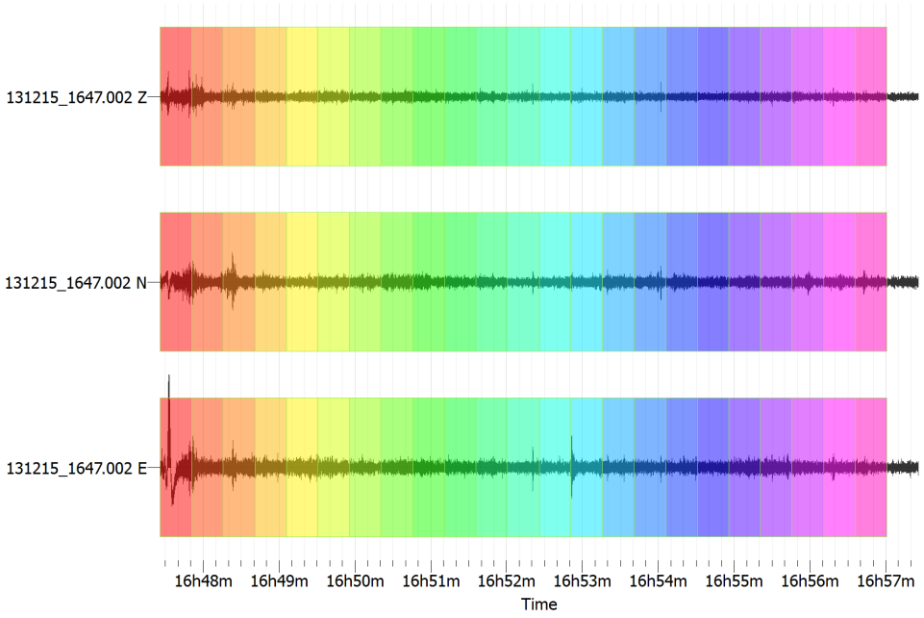

Figure J.6. 10 minutes ambient noise recording at 2013-12-15 16:47:00 UTC

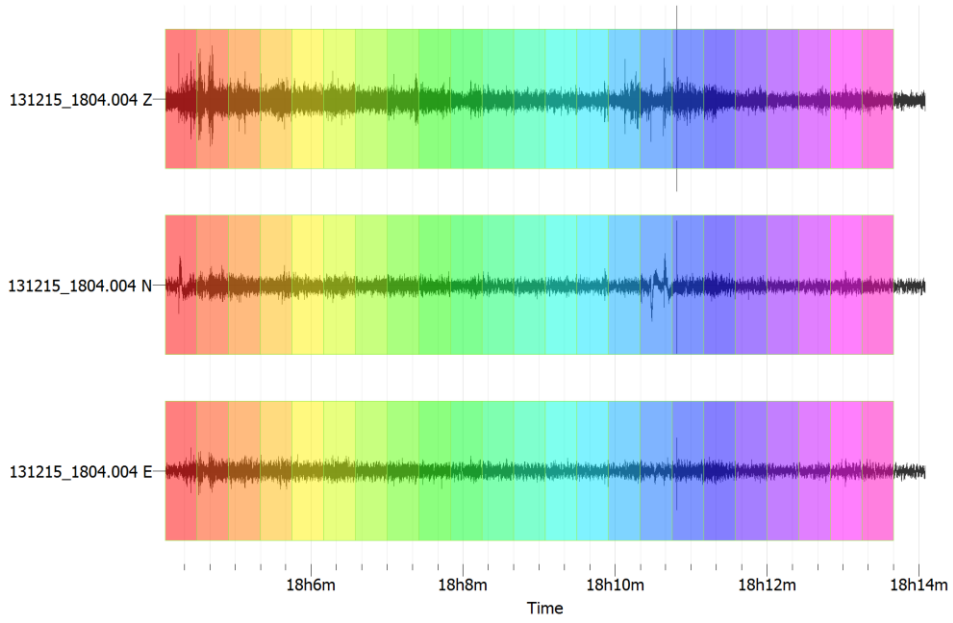

Figure J.7. 10 minutes ambient noise recording at 2013-12-15 18:04:00 UTC

Appendix K: Photos of instrumentation & installation

Figure K.1. Wired accelerometers

Figure K.2. Wireless accelerometers

Figure K.3. Instrumentation for ambient noise recordings

Appendix L: Analysis of seismic events with non-paramatric methods

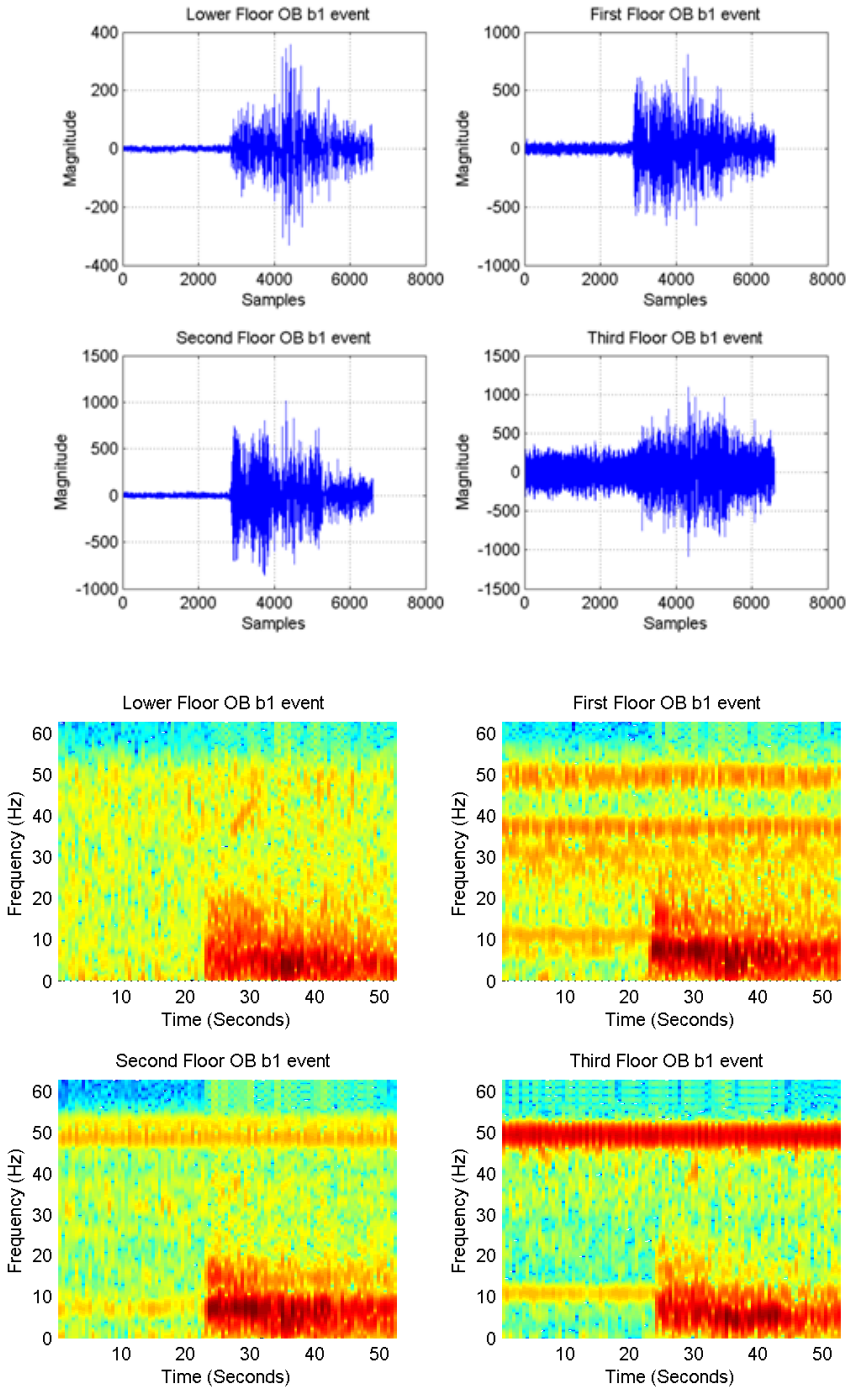

Figure L.1. For the earhquake with code name b1 (table 3.3) the acceleration recordings for lower, 1rst, 2nd & 3rd floor old buidling (up) and STFT (down)

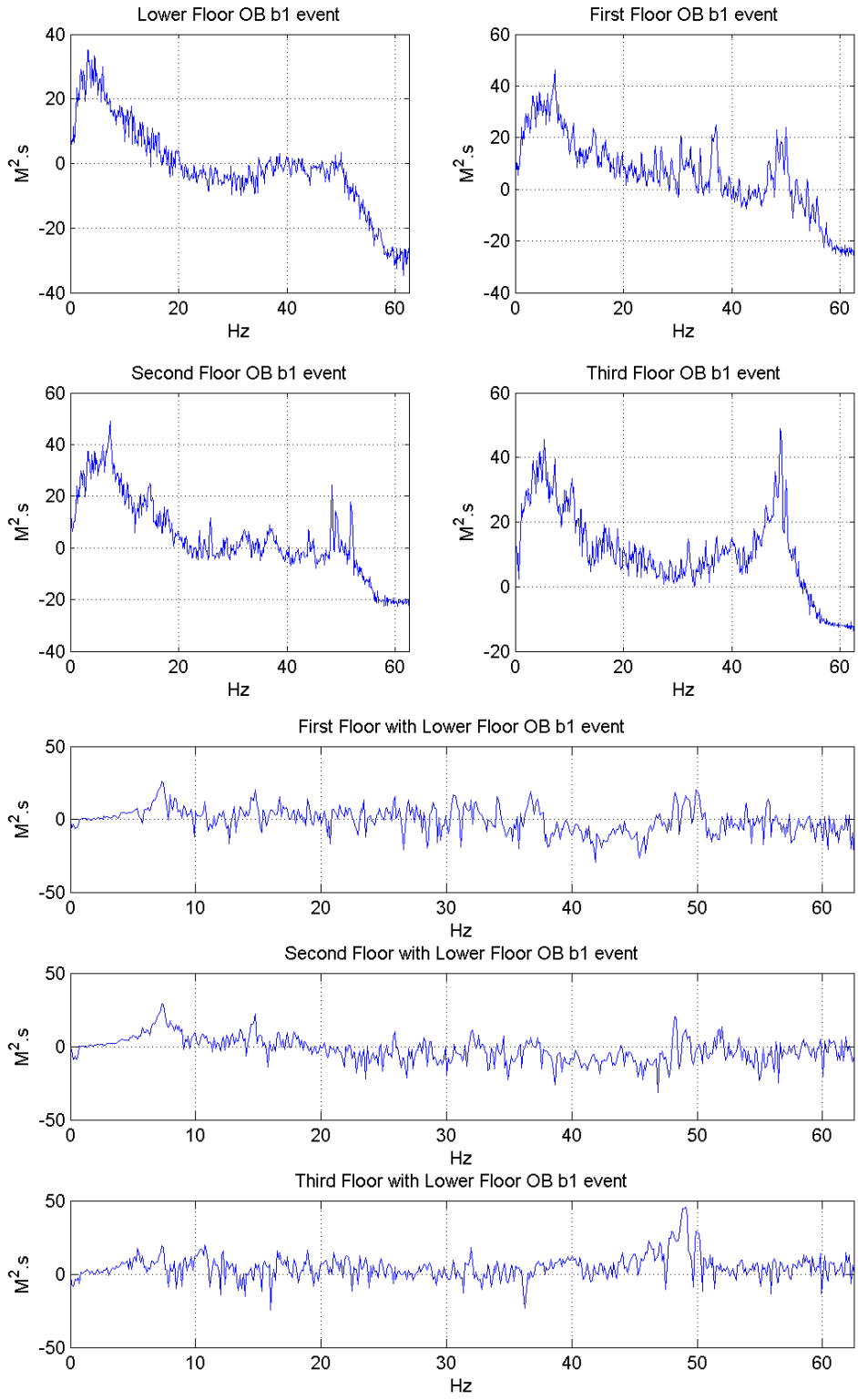

Figure L.2. For the earhquake with code name b1(table 3.3) the PSD for lower, 1rst, 2nd & 3rd floor old buidling (up) and FRF (down)

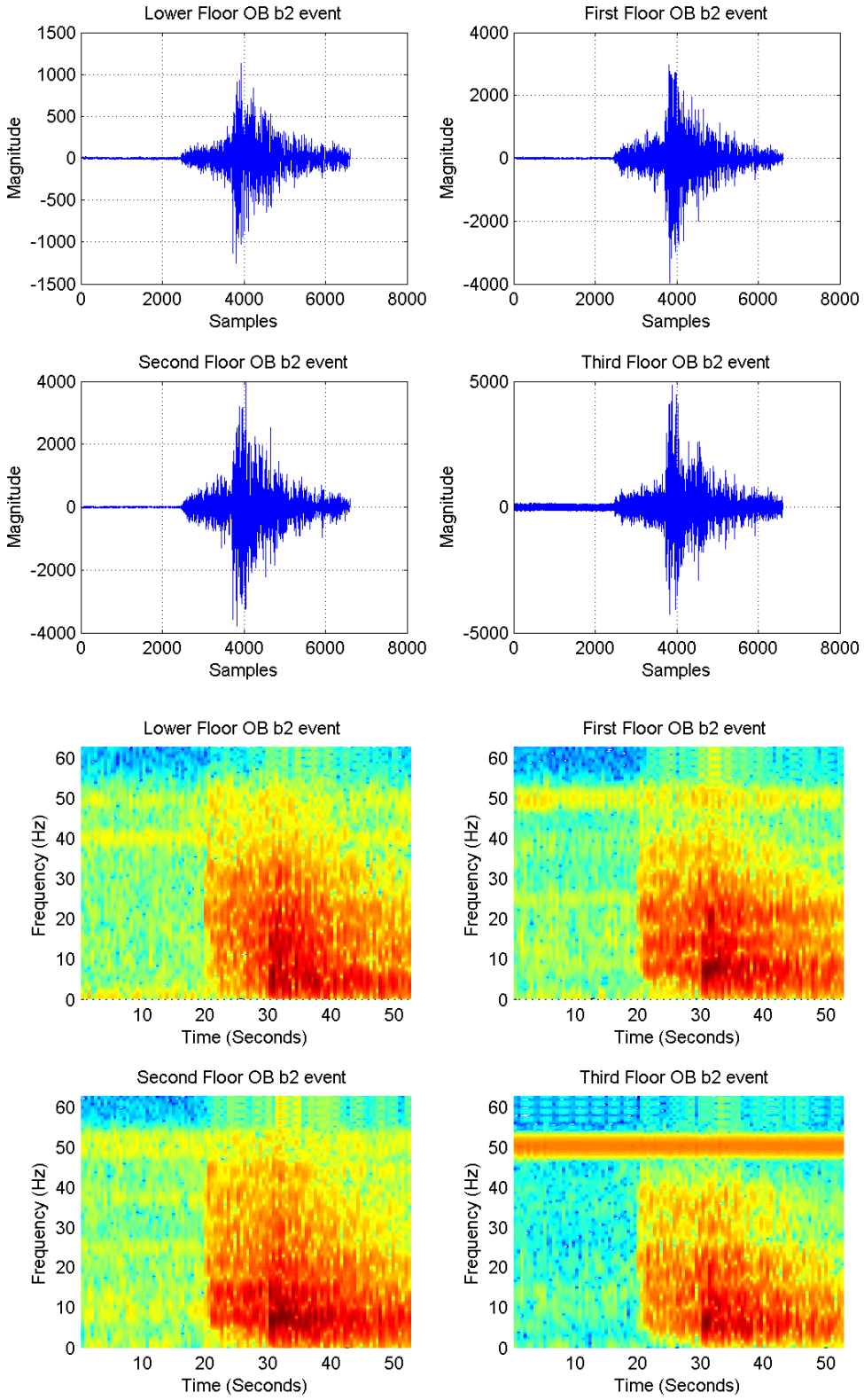

Figure L.3. For the earhquake with code name b2 (table 3.3) the acceleration recordings for lower, 1rst, 2nd & 3rd floor old buidling (up) and STFT (down)

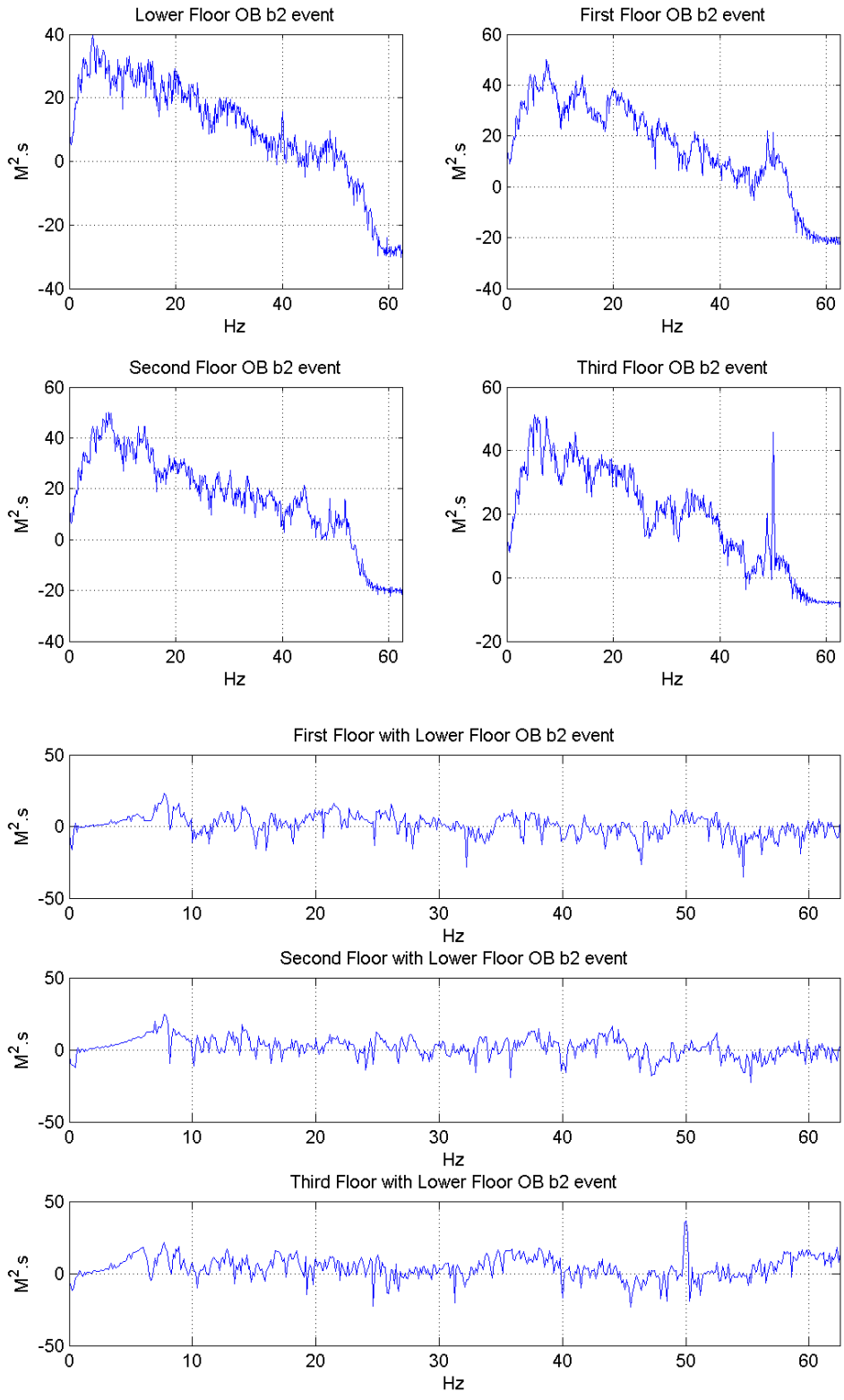

Figure L.4. For the earhquake with code name b2 (table 3.3) the PSD for lower, 1rst, 2nd & 3rd floor old buidling (up) and FRF (down)

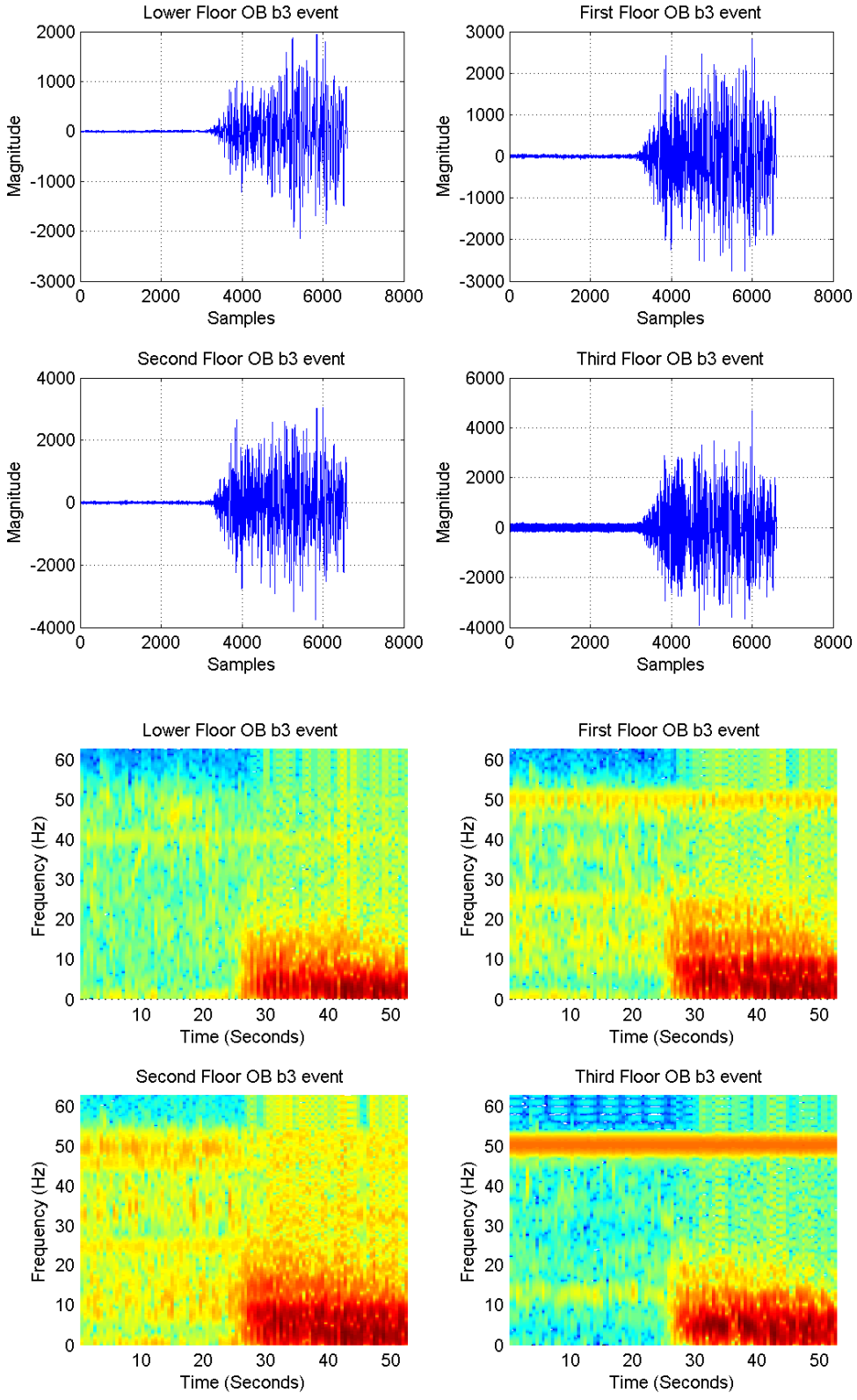

Figure L.5. For the earhquake with code name b3 (table 3.3) the acceleration recordings for lower, 1rst, 2nd & 3rd floor old buidling (up) and STFT (down)

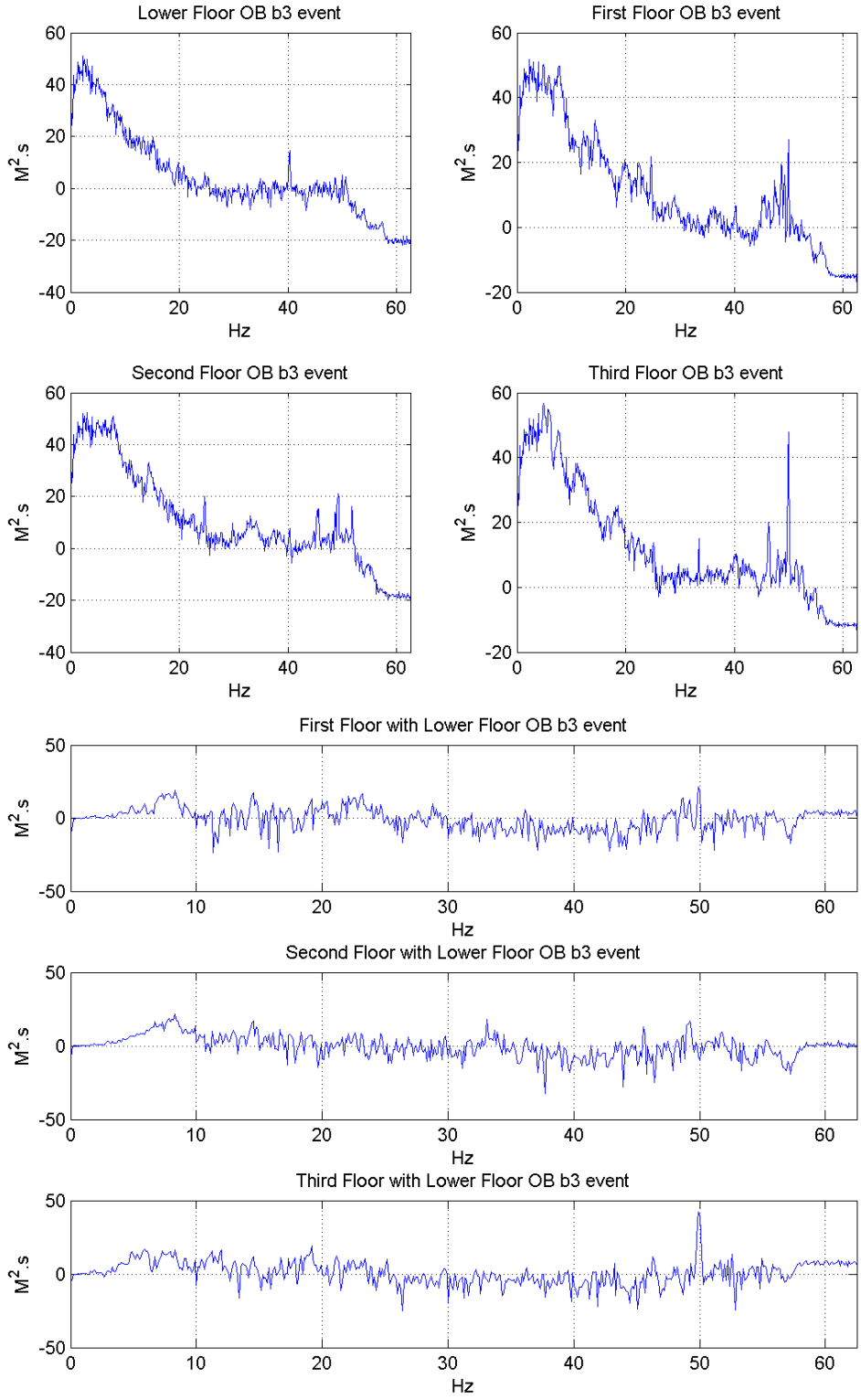

Figure L.6. For the earhquake with code name b3 (table 3.3) the PSD for lower, 1rst, 2nd & 3rd floor old buidling (up) and FRF (down)

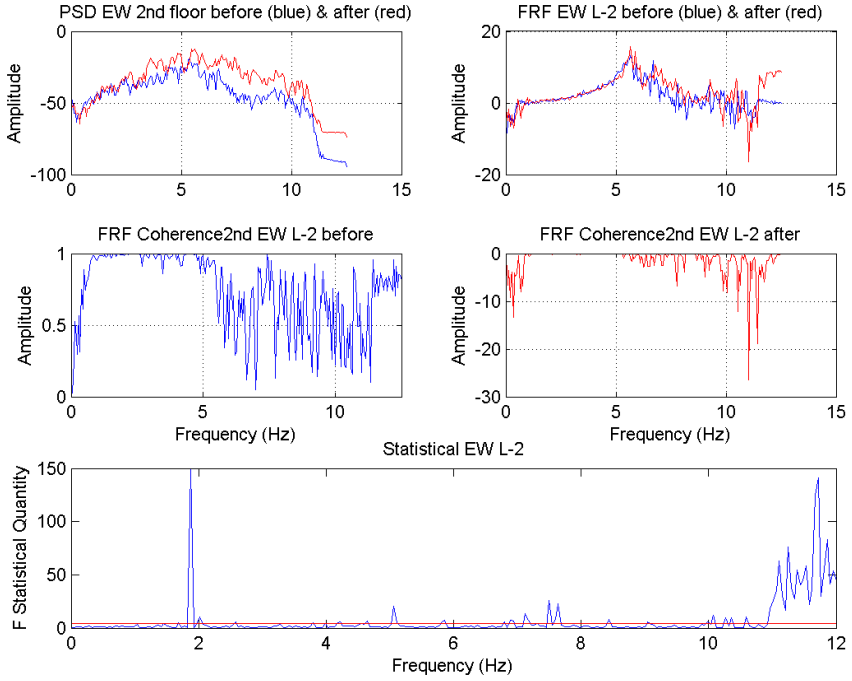

Figure L.7. ***Earhquakes with code names b4 & b5 (table 3.3). Comparison of PSD (up left), FRF (up right), FRF coherence diagrams (mid row left and right) and statistical analysis of FRF deviation (low graph) with "a risk level"(red line).***

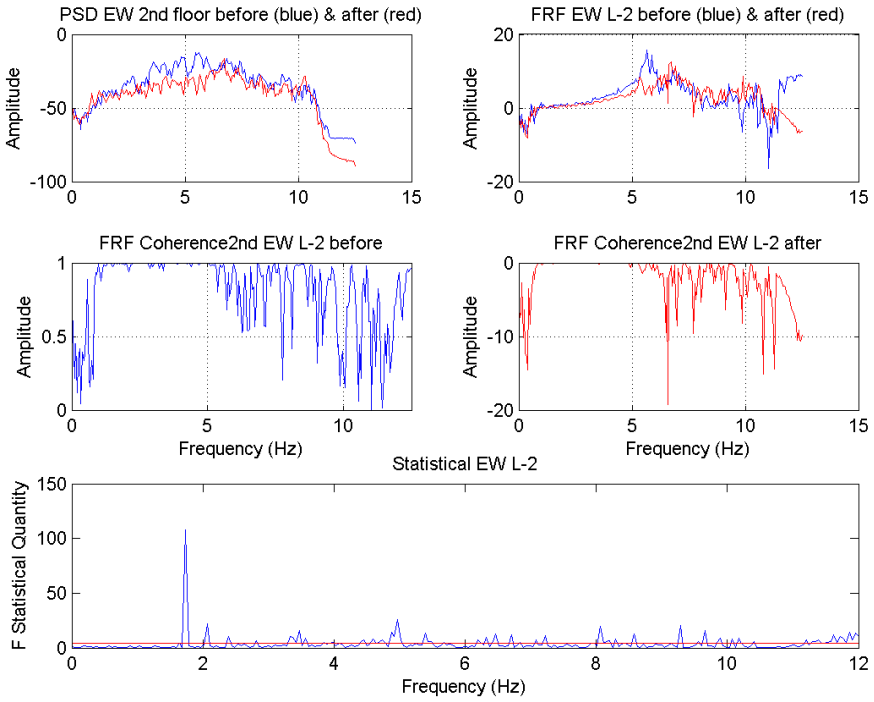

Figure L.8. Comparison of earhquake with code names b5 &b6 (table 3.3).

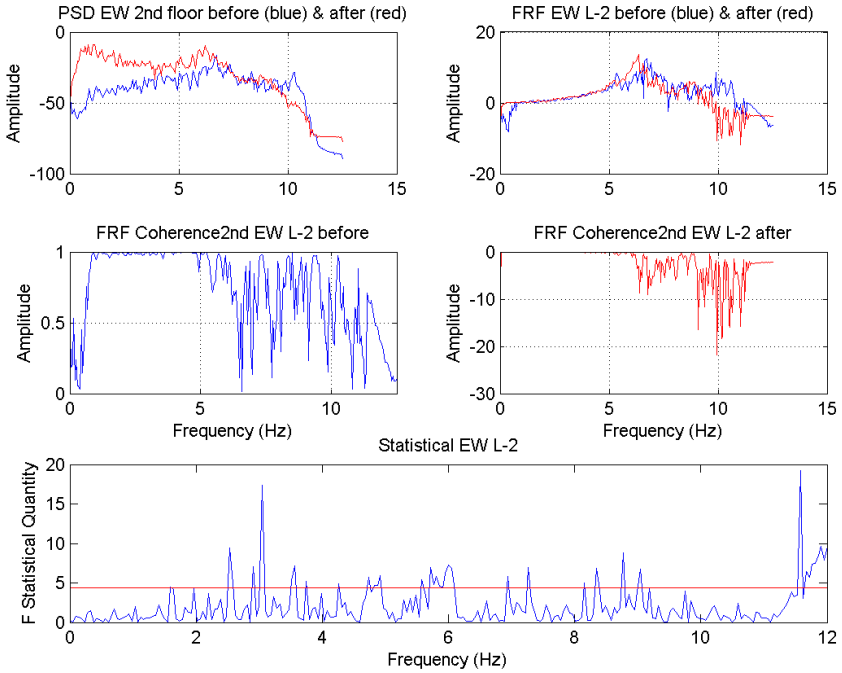

Figure L.9. Comparison of earhquake with code names b6 & b7 (table 3.3).

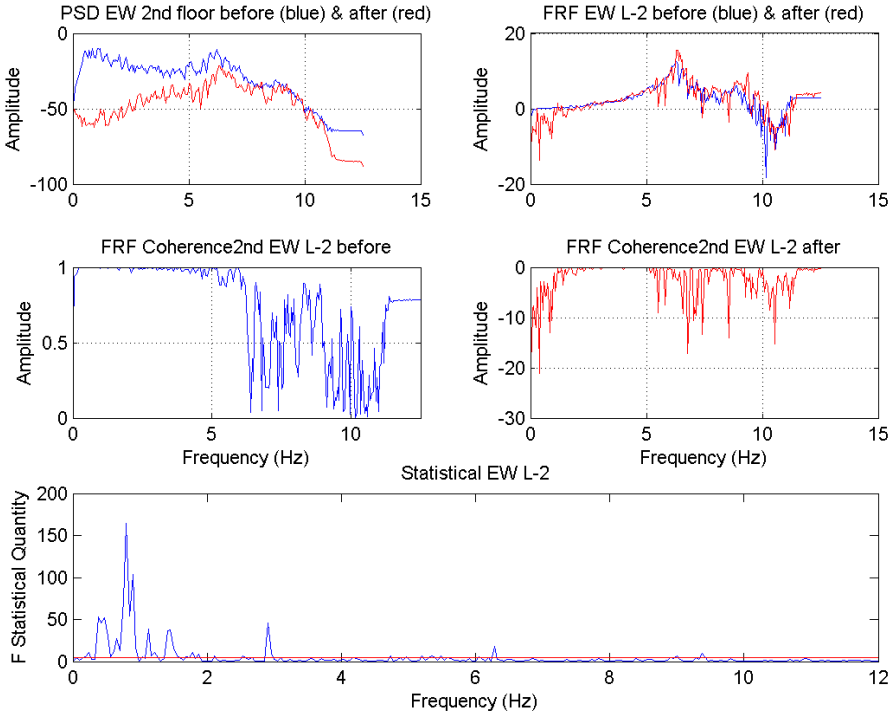

Figure L.10. Comparison of earhquake with code names b7 & b8 (table 3.3).

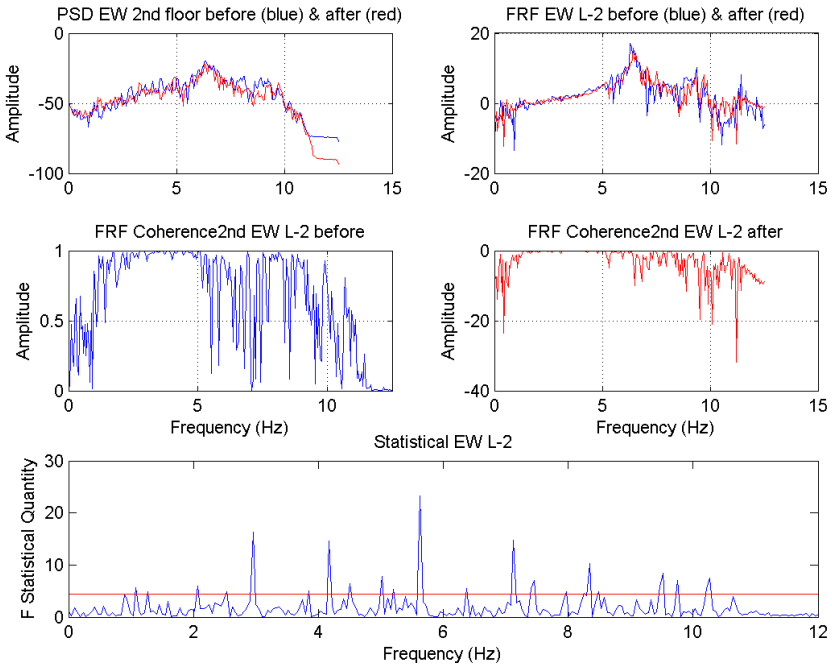

Figure L.11. Comparison of earhquake with code names b8 & b9 (table 3.3).

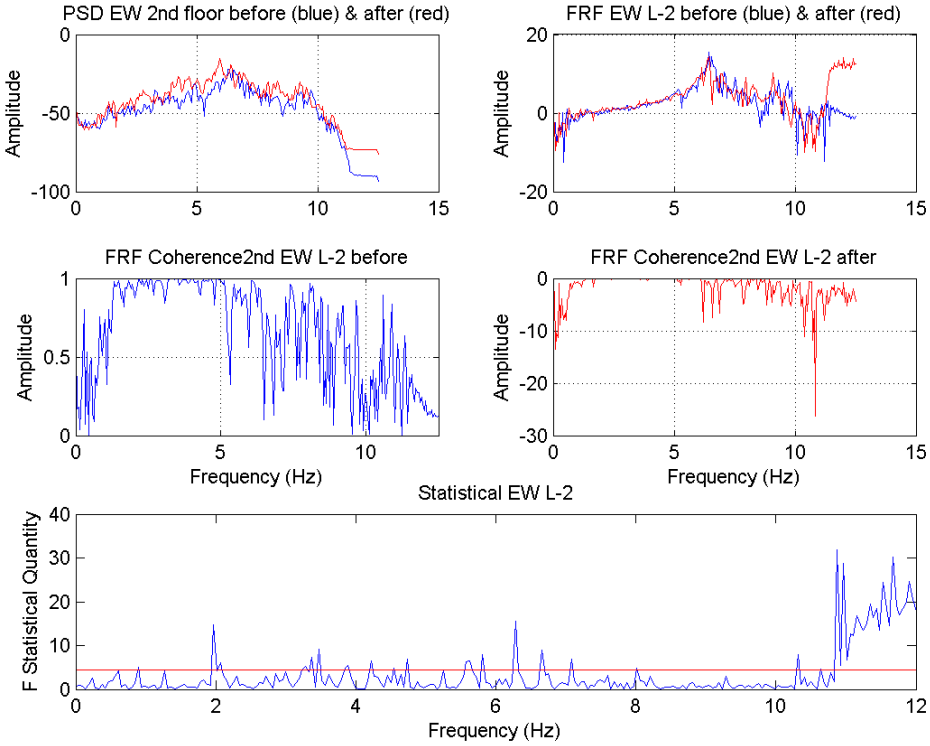

Figure L.12. Comparison of earhquake with code names b9 & b10 (table 3.3).

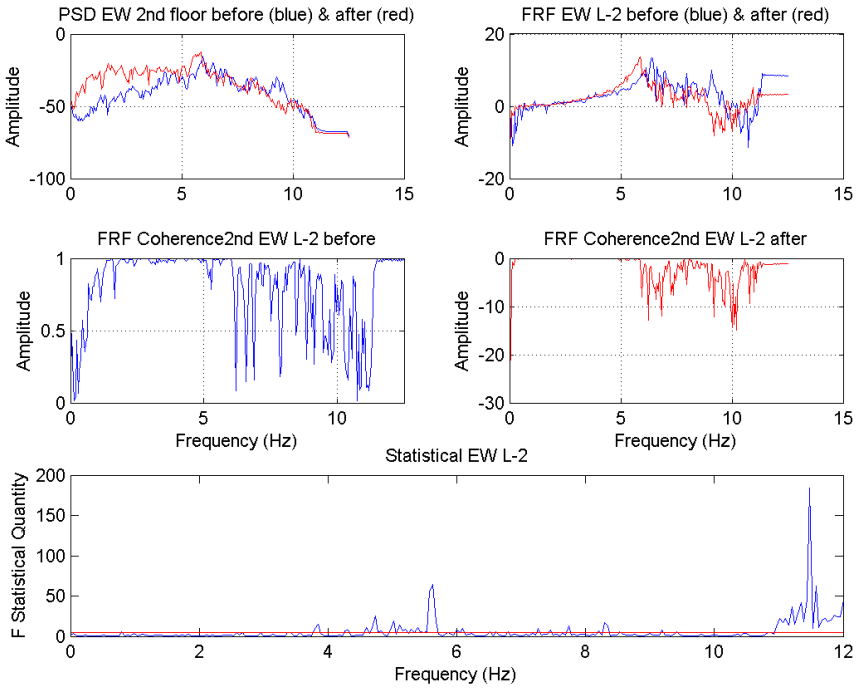

Figure L.13. Comparison of earhquake with code names b10 & b11 (table 3.3).

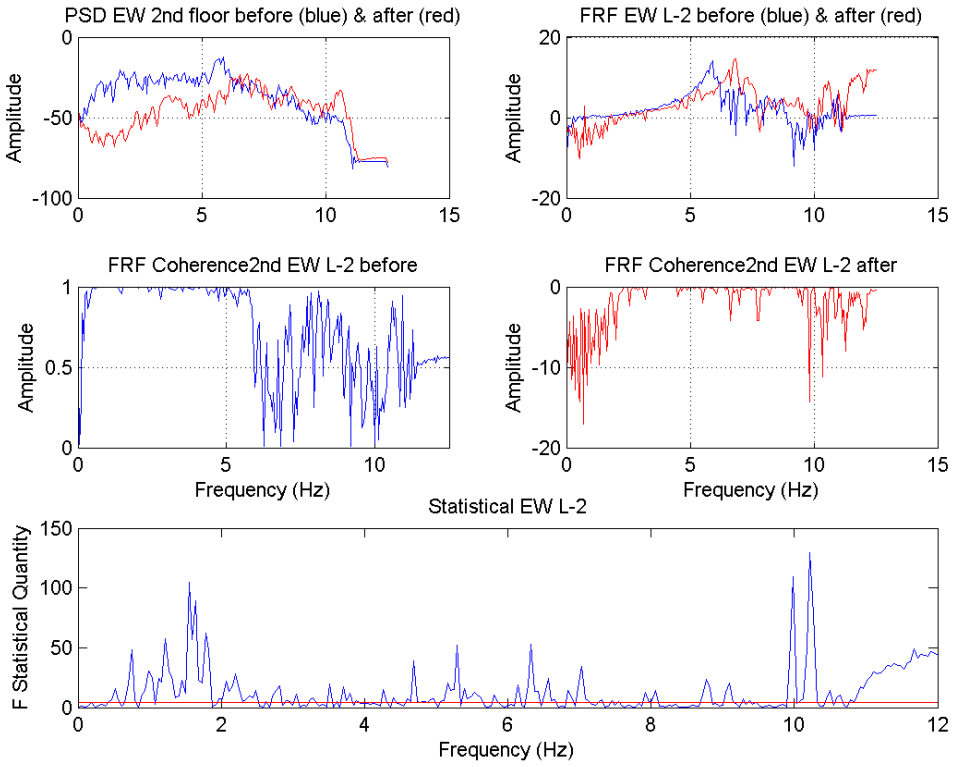

Figure L.14. Comparison of earhquake with code names b11 & b12 (table 3.3).

Appendix M: Analysis of seismic events with parametric methods

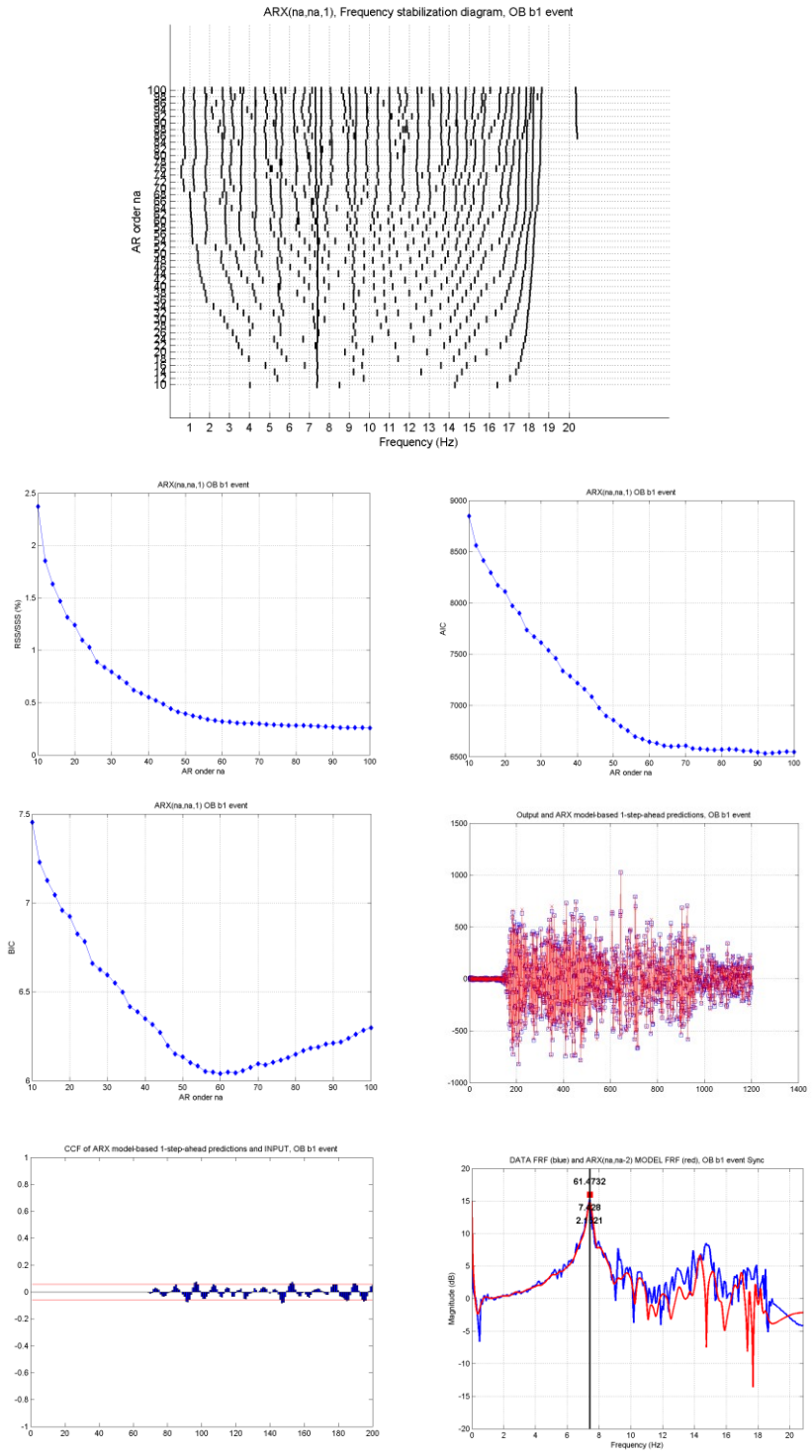

Figure M.1. Parametric analysis of earquake with code names b1 (table 3.3). Stabilization diagram(up), RSS/SSS, BIC & AIC critiria (mid) and bodeplot (down).

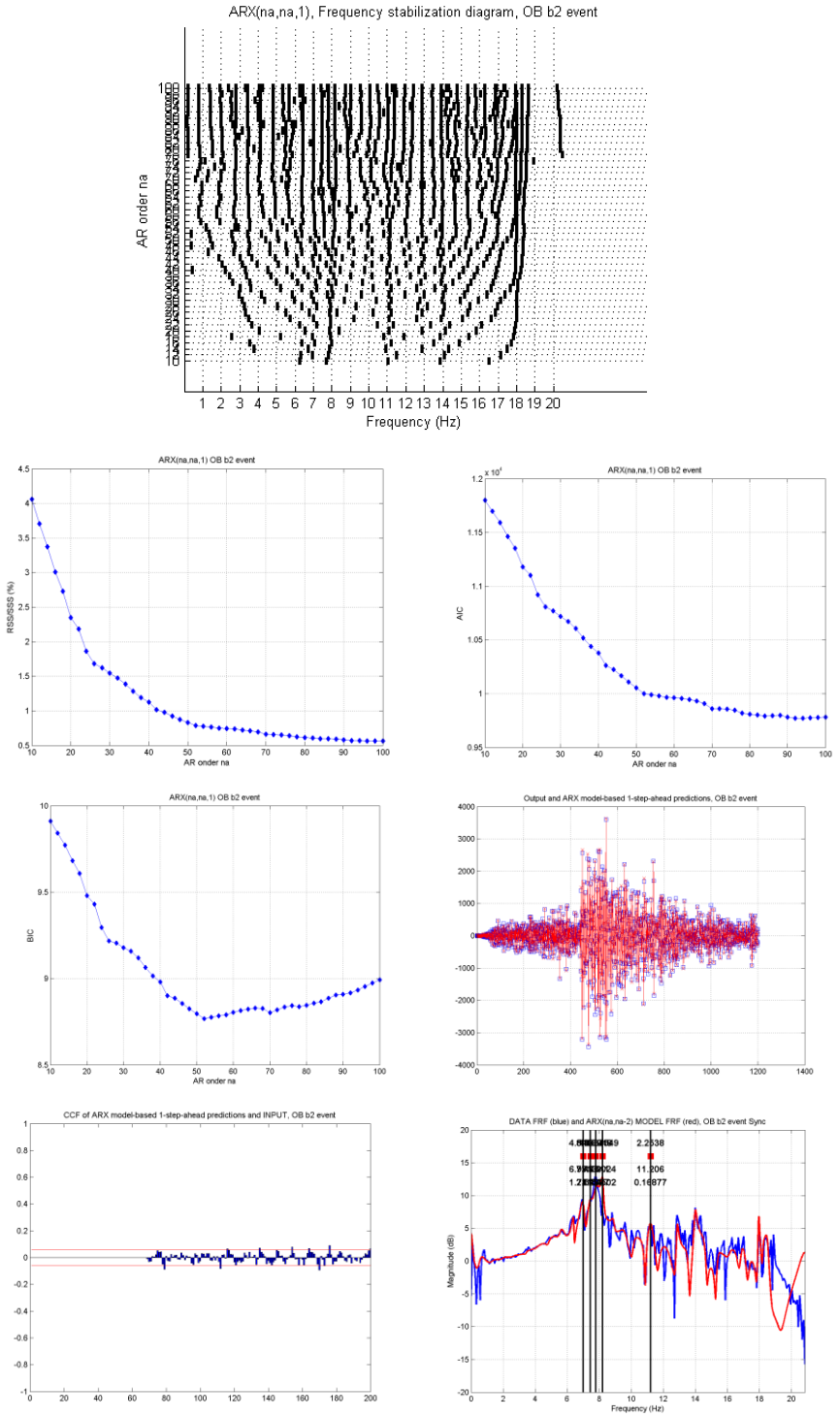

Figure M.2. Parametric analysis of earquake with code names b2 (table 3.3). Stabilization diagram(up), RSS/SSS, BIC & AIC critiria (mid) and bodeplot (down

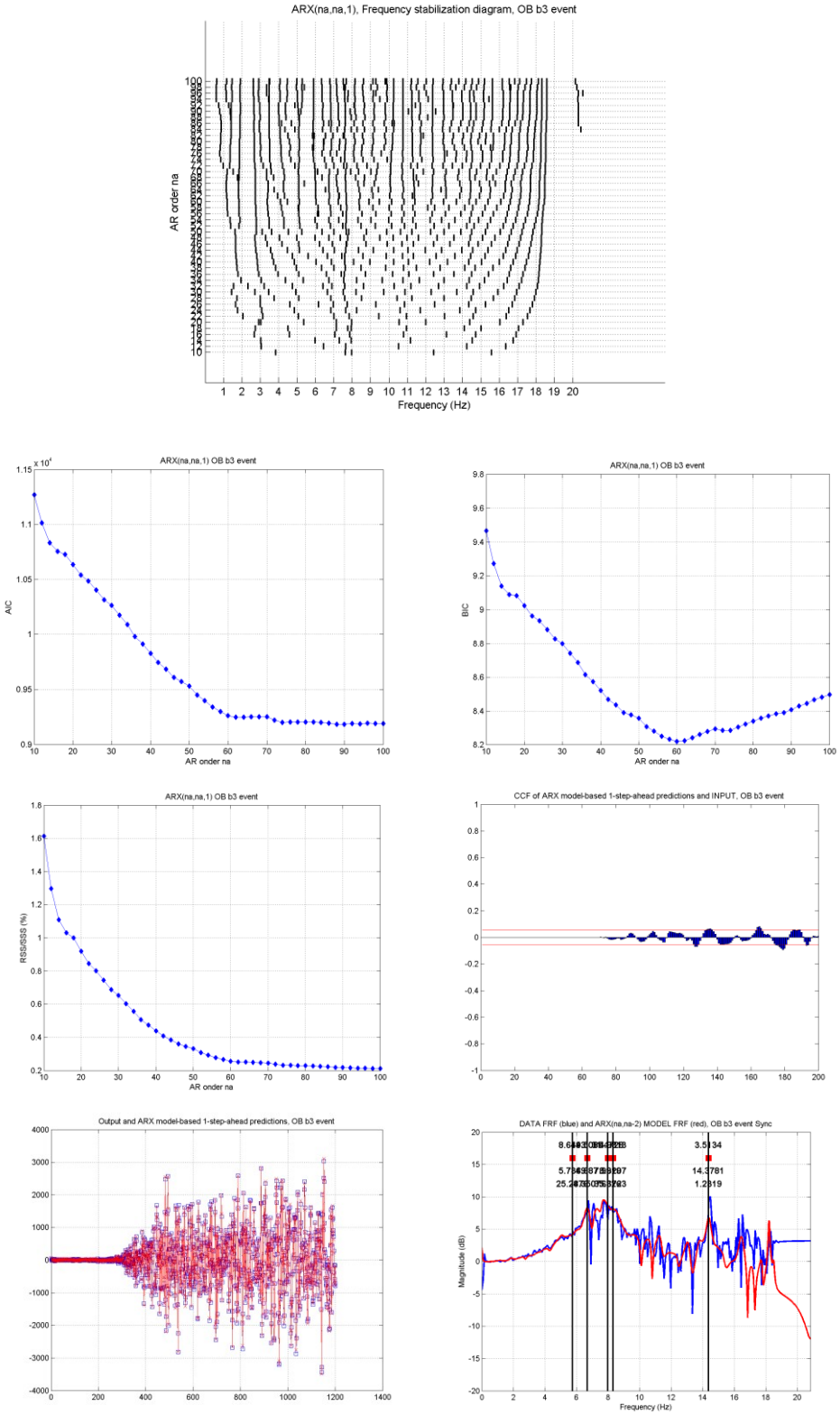

Figure M.3. Parametric analysis of earquake with code names b3 (table 3.3). Stabilization diagram(up), RSS/SSS, BIC & AIC critiria (mid) and bodeplot (down